New physics from a natural electroweak symmetry breaking

Nicolas Bizot

THÈSE

Pour obtenir le grade de

Docteur

Délivré par **l'université de Montpellier**

Préparée au sein de l'école doctorale **Information, Structures, Systèmes (I2S)**
Et de l'unité de recherche **Laboratoire Charles Coulomb(L2C)**

Spécialité : **Physique théorique**

Présentée par **Nicolas Bizot**

Fermionic extensions of the standard model and ultra-violet completions of composite Higgs models

Soutenue le 31 Octobre 2016 devant le jury composé de

Dr Michele Frigerio, Chargé de recherche CNRS, L2C Montpellier	Co-directeur de thèse
Dr Jean-Loïc Kneur, Directeur de recherche CNRS, L2C Montpellier	Directeur de thèse
Dr Marc Knecht, Directeur de recherche CNRS, CPT Marseille	Président du jury et Co-directeur de thèse
Pr Gerhard Buchalla, Professeur, LMU Munich	Rapporteur
Dr Francesco Riva, Chercheur, CERN Genève	Rapporteur
Dr Gregory Moreau, Maître de conférence, LPT Orsay	Examinateur
Dr Cyril Hugonie, Maître de conférence, LUPM Montpellier	Examinateur

Contents

List of Figures

List of Tables

9.2 The four-fermion couplings K_ϕ in the X-sector, and the associated one-loop two-point functions $\tilde{\Pi}^X_\phi(q^2)$. The latter are related to the two-point functions of the ψ-sector as follows: $\tilde{\Pi}^\psi_\phi(q^2) = \tilde{\Pi}_\phi(q^2, M^2_\psi, 2N)$ and $\tilde{\Pi}^X_\phi(q^2) = \tilde{\Pi}_\phi[q^2, M^2_X, (2N+1)(N-1)]$, where $\tilde{\Pi}_\phi(q^2, M^2_\psi, 2N)$ are defined in Table 8.2. We also give the expression of the mixed (one-loop) pseudoscalar-longitudinal axial correlator, as well as those of the couplings mixing the singlet scalars of the two sectors, σ_ψ and σ_X, and the singlet pseudoscalars η_ψ and η_X. The explicit calculation of the correlators $\tilde{\Pi}^X_\phi(q^2)$ is detailed in appendix H. 217

Abstract

Despite its impressive success, the standard model of particle physics does not account for every experimental observations. In addition, it has some theoretical puzzles in its formulation that seem to require more fundamental explanations. Then, instead of an ultra-violet complete theory, the standard model should rather be viewed as an effective description of a more fundamental theory and new physics should be introduced.

In this manuscript, we follow two different approaches of new physics. In the first one, we extend the standard model by only few new states assuming that the heavier states are decoupled from the electro-weak scale. This approach is mostly phenomenological as by hypothesis the extensions that we consider are a low energy manifestation of a more complete theory. We particularly focus on new fermions as they are a common prediction of a lot of well-motivated beyond the standard model theories. The main purpose is to study the effect of these new fermions in light of the recent Higgs couplings measurements.

The second approach has a more theoretical origin and is based on an ultra-violet complete theory. We focus on composite Higgs models that aim to solve one theoretical puzzle of the standard model that is the hierarchy problem of the electro-weak scale. While up to now, most of the works follow an effective approach to the composite dynamics, one goes further and consider UV realisations of composite Higgs models. These UV models being realised by a new strongly interacting sector made of new fundamental fermions, we study the non-perturbative dynamics within the Nambu and Jona-Lasinio framework. We derive for instance the spectrum of the lightest resonances which could be observed in a near future at the LHC or at some other colliders.

Résumé

Malgrès son impressionnant succès, le modèle standard de la physique des particules ne rend pas compte de toutes les observations exprimentales. De plus, des introgations théoriques intrinsques à sa formulation demeurent et requièrent des explications plus fondamentales. Par conséquent, au lieu d'être une théorie ultra-violette, le modèle standard devrait plutôt être vue comme une description effective, valide à basse énergie, d'une théorie plus fondamentale et de la nouvelle physique devrait être introduite.

Dans ce manuscrit, on considère deux approches pour introduire la nouvelle physique. Dans la première, on étend le modèle standard avec seulement quelques nouveaux états en assumant que les états plus lourds sont dcouplés de l'échelle électro-faible. Cette approche est principalement phénoménologique car par hypothèse, les extensions que l'on considère sont une manifestation à basse énergie d'une théorie plus complète. On se concentre en particulier sur de nouveaux fermions car ils sont une prédiction commune à un ensemble de théories au delà du modèle standard fortement motivés. L'objet principal de cette approche est d'étudier l'effet de ces nouveaux fermions à la lumière des mesures récentes des couplages du Higgs.

La seconde approche est plus théorique et est basée sur une théorie ultra-viollette. On se concentre sur les modèles de Higgs composite qui ont pour but de résoudre le problème de hiérarchie de l'échelle électro-faible. Alors que la plupart des travaux sur le Higgs composite suivent une approche effective de la dynamique fortement couplées, on fait un pas supplémentaire en étudiant des réalisations ultra-violette des modèles de Higgs composite. Ces modèles étant réalisés dans le cadre d'un nouveau secteur fortement couplé constitué de nouveaux fermions fondamentaux, on étudie la dynamique non-perturbative dans le cadre du modèle de Nambu et Jona-Lasinio. On dérive par exemple dans ce contexte le spectre des résonances les plus légères que l'on pourra peut-être observer dans un proche futur au LHC ou à d'autre collisionneurs.

Organisation of the manuscript

A lot of experimental and theoretical evidences call for beyond the Standard Model (SM) physics. The latter by itself is certainly not an ultra-violet (UV) complete model that can be extrapolated at any energy scale. Consequently it should rather be view as an effective theory valid up to a scale Λ_{SM}.

Two of the main options to address new physics above Λ_{SM} are: (i) to extend the SM with only few new states and (ii) to consider a well-motivated UV completion of the SM like for instance supersymmetry or composite Higgs models. In the first approach, the new states are assumed to be the lightest ones while other possible states are integrated out and are decoupled from the electroweak (EW) scale. This is a minimal and mostly phenomenological approach which can be viewed as a low energy manifestation of a more fundamental theory. The second approach is more theoretical and the purpose is to cure some shortcomings of the SM. For instance, composite Higgs models aim to solve the hierarchy problem.

The manuscript is organised as follow. In part I, we introduce the SM and consider some of its interesting features. The SM Lagrangian is introduced in chapter 1 while in chapters 2 and 3 we present QCD and the Nambu and Jona-Lasinio (NJL) model of QCD. The aim of this first part is to present the necessary background for the remaining of the manuscript. More precisely, in the first chapter we outline how new fermions, that will be considered in the next, can affect the SM predictions. In the second and third chapters, we present useful results related to QCD and to the NJL of QCD that will be latter relevant for the study of strongly coupled models.

In part II and III, we introduce new physics beyond the SM (BSM). The second part is devoted to the phenomenological approach of new physics mentioned above. In chapter 4 we consider the case where the SM is extended only with new fermions at the EW scale and we study their impact on the electroweak precision tests (EWPT) and on the Higgs couplings. Then, in chapter 5 we consider a Higgs sector extended by a second Higgs doublet and coupled to new fermions. We study again the EWPT as well as the Higgs couplings and we try at the same time to explain two LHC anomalies. These two chapters have in common the presence of new fermions which are a standard prediction of a lot of well-motivated BSM theories.

In part III, we rather follow the second and more theoretical approach to new physics. We focus on composite Higgs models (CHMs) as a solution of the hierarchy problem. We first review, from an effective point of view, the main ideas and properties of these models in chapter 6. Then, in chapter 7 we highlight the necessity to construct UV completions of composite Higgs models. We classify the minimal completions and isolate the most relevant and promising one. In chapter 8 and 9, we study in great details respectively the EW and the coloured sectors of this minimal UV completion while in chapter 10 we present some outlooks about the UV completions of CHMs. Finally, we present the conclusions of the manuscript in chapter 11.

Three papers are included in the manuscript [11–13], respectively in chapters 4, 5, 8 and 9. These papers contain the original work of the thesis. The material surrounding them, has for purpose to remind well known results present in the literature or details which are not included in the papers.

Part I

Aspects of the Standard Model

Chapter 1

Structure of the Standard Model

1.1 Qualitative introduction to the Standard Model

The beginning of the 20th century has seen the emergence of the two main pillars of modern physics, the quantum mechanics and the special relativity. These two theories have lead us in a territory where physics does not behave intuitively for us and follows different rules which are not familiar to our limited human perception.

As a classical example, when you walk towards a wall, if the wall is sufficiently solid, you know that there is no chance you cross it. This is a simple result of the laws of classical mechanics that we experience every days. However, in quantum mechanics there is a probability to cross the wall. This is the so-called tunnel effect which is responsible of the hydrogen fusion in the core of the Sun. If such a quantum mechanism was not present, two hydrogen nuclei should have more energy to overcome the Columbian repulsion and to fusion. In that case, the core temperature of the Sun should be higher and the burning of hydrogen would be faster. As a consequence, the life expectancy of the Sun would be reduced, the time necessary for the development of the life on Earth would be too short and we would not be there to study physics.

This simple example shows the importance of quantum mechanics and in general the relevance of a microscopic quantum and relativistic description of nature. Even if we don't see the consequences of the microscopic laws of nature in everyday life they are essential and condition our entire existence.

Our present knowledge of the microscopic laws of nature is now below the size of the nucleus. More precisely, we currently probe at the Large Hadrons Collider (LHC) the TeV scale that is a scale thousand times smaller than the size of the proton. The physics at this scale is commonly called particle physics. Within the framework of quantum fields theories which unify quantum mechanics and special relativity, in the last century a coherent model of particle physics has emerged until the complete construction of the standard model of particle physics. The latter is now the commonly accepted fundamental theory for the microscopic description of nature.

Let us briefly remind the historical construction of the SM. The development of particle physics is intimately related to the collider facilities to accelerate particles at high energy. More energetic collisions are able to probe lower scales and then the structure of matter has emerged more and more precisely with the increase of the accelerators energy. In the 1950-1960's, a lot of particles with various masses, life-time and decays was observed. At that time, these new states did not seem to constitute ordinary matter. The plethora of particles was in fact hiding a more fundamental structure which has been revealed after a detailed classification according to their properties. This classification had lead to the identification of quantum numbers associated to the different states and to an underlying symmetry constraining their interactions. The quantum numbers have been later identified with the quarks flavours and the observed particles with the hadrons. This was one of the first example outlining the importance of symmetries in particle physics. The hadrons are in fact made of quarks charged under a non-abelian gauge symmetry $SU(3)_c$ which predicts massless gauge bosons, the so-called gluons. This is the theory of quantum chromodynamics (QCD) which has been developed in the 1970's. Independently, the quantum electrodynamics (QED) has been developed in the 1940-1950's.

This theory is based on an abelian gauge symmetry $U(1)_{em}$ and predicts a massless gauge boson, the photon.

Beside the electromagnetic and strong interactions, also weak interactions was observed in β decays of nuclei and in muon decays. These decays was first explained by Fermi in the 1930's with four-fermions interactions. However such an operator has dimension 6 and the Fermi theory is an effective theory. The Fermi operator has strength $G_F \sim \mathcal{O}(1/\Lambda^2)$ where Λ is the scale where the new interaction should appear. This scale as we now know is the scale of the W and Z bosons and the four-fermion interactions postulated by Fermi come from the exchange of such boson. The latter have been discovered at SPS in 1984. A complete description of the weak interaction has then emerged in the 1960-1970's [14–17] where the electromagnetic and weak interactions was unified in a common framework called electroweak (EW) interactions and based on the gauge symmetry $SU(2)_L \times U(1)_Y$ in which the $U(1)_{em}$ symmetry is embedded. Contrary to the gluons and photon, the W and Z bosons are massive meaning that the EW symmetry is spontaneously broken at low energy. This breaking induces a mass for the W and Z bosons and in the SM, it is realised by the vacuum expectation value (vev) of a field, the Higgs field.

The SM, as described previously was finally completed and confirmed experimentally at LEP, Tevatron and the LHC. Precision measurements of the weak interactions have been done at LEP in the 1990's at an energy of $\sqrt{s} = 91$ GeV and up to 209 GeV. These measurements have confirmed the structure of the weak interactions and of the spontaneous breaking of the EW symmetry. In 1995, Tevatron discovered the last SM fermion that is the top quark by accelerating protons against anti-protons at an energy of $\sqrt{s} = 1.96$ TeV. Finally, the last missing piece of the SM, the so-called Higgs boson has been discovered [18, 19] recently in 2012 at the LHC in proton-proton collisions at $\sqrt{s} = 7 - 8$ TeV.

As we have seen, our current picture of nature is encoded in a coherent and very successful model that is the SM. The latter explains a lot of experimental results and is now tested at an unprecedent level of accuracy. As a spectacular example, the anomalous magnetic moment of the electron $[(g-2)_e/2]$ in QED is the most accurately verified prediction in the history of physics. The theoretical prediction is in agreement with the experimental measurement with a precision larger than one part in 10^{10}. However, despite its impressive success, the SM has intrinsically some shortcomings and missing pieces. It is a valid description at least up to the EW scale. Above this scale, we expect the presence of new physics which cure some SM problems. Then the SM should rather be viewed as an effective theory instead of a fundamental theory. It can not be extrapolated to any scale and the hope for BSM searches is that new physics belongs to the multi TeV range that is in an energy range accessible at present or next colliders.

In this preliminary chapter, we begin in section 1.2 by presenting the SM lagrangian. We will not follow the historical construction of this Lagrangian which has already been briefly detailed before but rather start from the gauge symmetry group of the SM and its field content. In this way, we present the main features of each sectors of the SM and highlight the places where new physics effects can manifest. In particular, we focus on the effect of possible new fermions as the latter will be discussed in part II of the manuscript. We also outline in sections 1.3 and 1.4, some important behaviours of the SM as the custodial symmetry of the Higgs sector and the gauge anomaly cancellation. These properties are crucial to construct any theory beyond the SM as either they are theoretically necessary for a self consistent theory or they are in well agreement with experimental measurements.

Finally, we present in section 1.5 the main limitations and shortcomings of the SM that call for new physics beyond the SM. In particular, in section 1.6 we focus on the hierarchy problem of the EW scale that is one of the main motivation for BSM physics like for instance the scenario of composite Higgs that will be presented in part III of the manuscript.

1.2 Structure of the standard model Lagrangian

In this section, we briefly present the SM Lagrangian. The aim is not to give a complete and detailed survey of the SM but rather to collect relevant formulas and conventions that will be useful in the next. We also outline the places where new physics can affect the SM predictions. The standard model of particle physics, the so called Glashow-Salam-Weinberg (GSW) [14–17] model, is a four-dimensional quantum field theory based on the Poincaré symmetry and the local (gauge) $SU(3)_c \times SU(2)_L \times U(1)_Y$ symmetry. The field content of the SM with the gauge quantum numbers of the different fields is given in table 1.1. The SM lagrangian can be written in a compact way as follows

$$\begin{aligned}\mathcal{L}_{SM} &= -\frac{1}{4}\sum_V V^{\mu\nu a}V^a_{\mu\nu} + i\sum_f \overline{f}_{L,Ri}\gamma^\mu D_\mu f_{L,Ri} + |D_\mu H|^2 \\ &\quad + \left(Y^u_{ij}\overline{q}_{Li}Hd_{Rj} + Y^d_{ij}\overline{q}_{Li}\tilde{H}u_{Rj} + Y^e_{ij}\bar{l}_{Li}He_{Rj} + h.c.\right) - V(H)\ , \end{aligned} \tag{1.2.1}$$

where the flavour structure is encoded by the indices $i, j = 1, 2, 3$. Note that after imposing the SM gauge symmetry, the above Lagrangian is the more general one with the field content of table 1.1.

The SM is a chiral gauge theory as the left and right-handed fermions do not transform in the same way under the gauge symmetry (see table 1.1). As a consequence, one can not write mass terms for the fermions since such terms require the two chiralities ie $m_f(\overline{f}_L f_R + h.c)$ and are manifestly not gauge invariant. In the same way, the gauge invariance forbids masses for the gauge bosons ie terms like $m_V V^\mu V_\mu$. However, experimentally we know that the fermions are massive as well as the W and Z bosons. Then one concludes that the EW symmetry should be broken. To introduce the EW symmetry breaking (EWSB) in the SM, let us consider the Higgs sector and in particular the Higgs potential

$$-V(H) = \mu^2 H^\dagger H - \lambda(H^\dagger H)^2\ , \tag{1.2.2}$$

where the Higgs doublet has four degrees of freedom which can be parametrised as $H = \begin{pmatrix} h_1 + ih_2 & h_3 + ih_4 \end{pmatrix}^T/\sqrt{2}$. The minimum of the Higgs potential is given by

$$\frac{\partial V(H)}{\partial H} = -\mu^2 H^\dagger + 2\lambda(H^\dagger H)H^\dagger = 0\ . \tag{1.2.3}$$

Field		$SU(3)_c \times SU(2)_L \times U(1)_Y$
quarks	$q_L = (u_L \quad d_L)$	$(3, 2, \frac{1}{6})$
($\times$ 3 generations)	u_R	$(3, 1, \frac{2}{3})$
	d_R	$(3, 1, -\frac{1}{3})$
leptons	$l_L = (\nu_L \quad e_L)$	$(1, 2, -\frac{1}{2})$
($\times$ 3 generations)	e_R	$(1, 1, -1)$
gluons	G^a_μ	$(8, 1, 0)$
W	$W^a_\mu = (W^+_\mu \quad W^0_\mu \quad W^-_\mu)$	$(1, 3, 0)$
B	B^0_μ	$(1, 1, 0)$
Higgs	$H = (H^+ \quad H^0)$	$(1, 2, \frac{1}{2})$

Table 1.1: The field content of the SM and the associated quantum numbers of the different fields under the gauge group $SU(3)_c \times SU(2)_L \times U(1)_Y$. The electric charges of the $SU(2)_L$-components are obtained from the relation $Q = \tau^3_L + Y$.

If μ^2 is negative, the two terms can not compensate each other and the minimum is located at the origin that is for vanishing field values ie $h_1 = h_2 = h_3 = h_4 = 0$. This is not the relevant case as the EW symmetry remains unbroken leading to massless gauge bosons and fermions. We then rather consider the broken phase where μ^2 is positive. In that case, the two terms compensate and the minima of the potential are located on the surface $H^\dagger H = (h_1^2 + h_2^2 + h_3^2 + h_4^2)/2 = \mu^2/(2\lambda)$. The minimisation condition of the potential is $v^2 = \mu^2/\lambda$ and the four degrees of freedom of the Higgs doublet can be arranged as follow

$$H = \begin{pmatrix} \varphi^+ \\ (h + v + i\varphi_Z)/\sqrt{2} \end{pmatrix} , \qquad H^\dagger = \begin{pmatrix} \varphi^- & (h + v - i\varphi_Z)/\sqrt{2} \end{pmatrix} . \tag{1.2.4}$$

Without loss of generality, using the $SU(2)_L$ symmetry the vev v has been taken real and in the lower component of the doublet $[h_3 = (v + h)/\sqrt{2}]$. Note that our normalisation with a square root of two corresponds to $v \simeq 246$ GeV. For our purpose, it will be simpler to study the SM in the unitary gauge where the Goldstone bosons φ^i are set to zero. In that case, from Eq. (1.2.2) we easily derive the tree-level mass and self-interactions of the Higgs boson

$$m_h^2 = 2\lambda v^2 , \qquad c_{hhh}^{SM} = -6\lambda v = -\frac{3m_h^2}{v} , \qquad c_{hhhh}^{SM} = -6\lambda = -\frac{3m_h^2}{v^2} . \tag{1.2.5}$$

Note that in order to trigger EWSB, we assumed that μ^2 is small, of the order of the EW scale ($\mu^2 \sim m_h^2$) and positive. However, there is no dynamical arguments behind this particular choice and the correct form of the Higgs potential is just imposed by hand in the SM, without dynamical explanations. This feature may seem unsatisfactory and several BSM theories attempt to give a dynamical explanation of the mechanism of EWSB (see sections 1.6 and 6.4 in the general case and in the composite Higgs context respectively).

Now we have seen that the vev v of the Higgs boson breaks the EW symmetry, let us consider the consequences for the gauge bosons by considering the kinetic term of the Higgs doublet

$$\mathcal{L}_{SM}^H = |D_\mu H|^2 = (D_\mu H)^\dagger (D^\mu H) . \tag{1.2.6}$$

Developing the covariant derivatives, we obtain in the unitary gauge

$$\begin{aligned} \mathcal{L}_{SM}^H &= \left| \left(\partial_\mu - igW_\mu^i \tau^i - ig' Y B_\mu\right) H \right|^2 \\ &= \left| \begin{pmatrix} \partial_\mu - i\frac{g}{2}W_\mu^3 - i\frac{g'}{2}B_\mu & -i\frac{g}{2}(W_\mu^1 - iW_\mu^2) \\ -i\frac{g}{2}(W_\mu^1 + iW_\mu^2) & \partial_\mu + i\frac{g}{2}W_\mu^3 - i\frac{g'}{2}B_\mu \end{pmatrix} \begin{pmatrix} 0 \\ \frac{v+h}{\sqrt{2}} \end{pmatrix} \right|^2 \\ &= \frac{1}{2}(\partial^\mu h)(\partial_\mu h) + \frac{g^2}{8}\left[(W_\mu^1)^2 + (W_\mu^2)^2 + \left(\frac{g'}{g}B_\mu - W_\mu^3\right)^2 \right] (v + h)^2 , \end{aligned} \tag{1.2.7}$$

The Higgs h is well canonically normalised and one immediately recognize the mass terms associate with the three massive gauge bosons. The mixing between B_μ and W_μ^3 leads to one massive combination as it can checked from the following mixing matrix which has determinant equal to zero

$$\mathcal{L}_{SM}^H = \frac{v^2}{8} \begin{pmatrix} B_\mu & W_\mu^3 \end{pmatrix} \begin{pmatrix} g'^2 & -g'g \\ -g'g & g^2 \end{pmatrix} \begin{pmatrix} B_\mu \\ W_\mu^3 \end{pmatrix} + \cdots \tag{1.2.8}$$

The mass eigenstates are obtained by a rotation

$$\begin{aligned} Z_\mu &= c_w W_\mu^3 - s_w B_\mu , & B_\mu &= c_w A_\mu - s_w Z_\mu , \\ A_\mu &= s_w W_\mu^3 + c_w B_\mu , & W_\mu^3 &= c_w Z_\mu + s_w A_\mu , \end{aligned} \tag{1.2.9}$$

where A_μ is the massless state while Z_μ the massive one and the Weinberg angle controlling the mixing is defined by

$$\cos\theta_w \equiv c_w = \frac{g}{\sqrt{g^2 + g'^2}} , \qquad \sin\theta_w \equiv s_w = \frac{g'}{\sqrt{g^2 + g'^2}} . \tag{1.2.10}$$

For the two remaining massive bosons, the mass eigenstates are defined by

$$W_\mu^\pm = \frac{1}{\sqrt{2}}(W_\mu^1 \mp i W_\mu^2) \ , \tag{1.2.11}$$

such that $W_\mu^\pm$ have a definite EM charge. The W and Z masses are obtained from Eq. (1.2.7), and given by

$$M_W = \frac{gv}{2} \ , \qquad M_Z = \sqrt{g^2+g'^2}\frac{v}{2} = \frac{M_W}{c_w} > M_Z \ . \tag{1.2.12}$$

The Golstone bosons $\varphi^\pm$ and φ_Z have been eaten respectively by the $W^\pm$ and Z bosons which aquire in this way a non-zero mass (a longitudinal component). This is the famous Brout-Englert-Higgs mechanism [20–25]. For the Higgs couplings to W and Z bosons we have

$$c_{hVV}^{SM} = 2\frac{M_V^2}{v} \ , \qquad c_{hhVV}^{SM} = 2\frac{M_V^2}{v^2} \ , \qquad V = W, Z \ . \tag{1.2.13}$$

Let us make some comments at this point. In general, with an extended Higgs sector like in a two Hggs doublet model (2HDM) discussed in chapter 5, the Higgs couplings to W and Z bosons may deviate from the above SM prediction. However, the deviations can not be too large as the Higgs couplings are now measured with accuracy (see appendix C). Then, in a 2HDM we should remain close to an alignment limit where the Higgs couplings are SM-like. In the same way, in composite Higgs model the scale of the chiral Lagrangian f is constrained to be larger than around 1 TeV in order for the Higgs couplings to SM gauge bosons to be SM-like (see section 6.2).

One can directly write the covariant derivative in the physical basis as follows

$$D_\mu H = \left[\partial_\mu - \frac{ig}{\sqrt{2}}(\tau^+ W_\mu^+ + \tau^- W_\mu^-) - \frac{ig}{c_w}(\tau^3 - Q s_w^2) Z_\mu - ieQA_\mu\right] H \ , \tag{1.2.14}$$

where $\tau^\pm = \tau^1 \pm i\tau^2$ and we identify the EM charge operator Q and the EM gauge coupling e

$$Q = \tau^3 + Y \ , \qquad e = g s_w = g' c_w \ . \tag{1.2.15}$$

Looking at the gauge transformation of the Higgs vev

$$\langle H\rangle \to e^{i\alpha^i\tau^i} e^{i\alpha_Y Y}\langle H\rangle = \langle H\rangle + \frac{i}{2}\begin{pmatrix}\alpha^3+\alpha_Y & \alpha^1 - i\alpha^2 \\ \alpha^1 + i\alpha^2 & -\alpha^3+\alpha_Y\end{pmatrix}\begin{pmatrix}0\\ \frac{v}{\sqrt{2}}\end{pmatrix} + \cdots \ , \tag{1.2.16}$$

one sees that only one combination of generators is invariant. This combination corresponds to $\alpha^3 = \alpha_Y$ and $\alpha^1 = \alpha^2 = 0$ that is to the EM charge generator $Q = \tau^3 + Y$ of Eq. (1.2.15). The latter is associated with the $U(1)_{em}$ group such that the EM is not broken by the Higgs vev which is in agreement with the presence of the massless photon A_μ.

We now turn to the kinetic terms of the SM gauge bosons.

$$\mathcal{L}_{SM}^{gauge} = -\frac{1}{4}\sum_V V^{\mu\nu a} V_{\mu\nu}^a = -\frac{1}{4}G^{\mu\nu a}G_{\mu\nu}^a - \frac{1}{4}W^{\mu\nu i}W_{\mu\nu}^i - \frac{1}{4}B^{\mu\nu}B_{\mu\nu} \ . \tag{1.2.17}$$

The field strength tensors explicitly read

$$B_{\mu\nu} = \partial_\mu B_\nu - \partial_\nu B_\mu \ , \qquad W_{\mu\nu}^i = \partial_\mu W_\nu^i - \partial_\nu W_\mu^i + g\epsilon^{ijk}W_{\mu j}W_{\mu k} \ , \tag{1.2.18}$$

$$G_{\mu\nu}^a = \partial_\mu G_\nu^a - \partial_\nu G_\mu^a + g_s f^{abc} G_{\mu b} G_{\mu c} \ . \tag{1.2.19}$$

Using Eqs. (1.2.9) and (1.2.11) one easily gets the kinetic terms, trilinear and quartic interactions between the physical gauge bosons (see for e.g [26]). Note that when we will introduce new physics, as we will not extend the SM gauge group, this sector will remain completely SM-like.

For the Yukawa sector of the SM which is responsible of the SM fermions masses and couplings to the Higgs boson h, the relevant lagrangian is

$$\mathcal{L}_{SM}^{Yukawa} = -Y_{ij}^{d}\overline{q}_{Li}Hd_{Rj} - Y_{ij}^{u}\overline{q}_{Li}\tilde{H}u_{Rj} - Y_{ij}^{e}\overline{l}_{Li}He_{Rj} + h.c. \tag{1.2.20}$$

where the doublet $\tilde{H} = i\sigma^2 H^* = ((h+v-i\phi_Z)/\sqrt{2} \quad -\phi^-)$ transforms like H under $SU(2)_L$, that is, it is a doublet and not a 2^* like $H^\dagger$. The Yukawa matrices $Y_{ij}^{u,d,e}$ are not diagonal in all generality. After EWSB, we obtain in the unitary gauge

$$\mathcal{L}_{SM}^{Yukawa} = -\frac{(h+v)}{\sqrt{2}}\left[Y_{ij}^{d}\overline{d}_{Li}d_{Rj} + Y_{ij}^{d}\overline{u}_{Li}u_{Rj} + Y_{ij}^{e}\overline{e}_{Li}e_{Rj} + h.c.\right] \ . \tag{1.2.21}$$

The physical masses are obtained by going to the mass basis, that is, by diagonalising the Yukawa matrices and rotating the fields. For example, the up quark Yukawa matrix is diagonalised as follows $Y_u = U_u M_u K_u^\dagger$ where the U_u, K_u matrices are unitary and $M_u = diag(\lambda_u, \lambda_c, \lambda_t)$. The down quark and charged lepton Yukawa matrices are diagonalised in the same way. Now by changing the basis of the left and right-handed fermions, $u_L \to U_u u_L$, $u_R \to K_u u_R$ and similarly for the down quarks and charged leptons, it removes the U and K matrices from the Yukawa terms leaving only the diagonalised Yukawa matrices $M_{u,d,e}$. However, the combination $U_u^\dagger U_d$ is physical because it reappears in the charged currents (see below). The masses and Higgs couplings to fermions are then

$$m_f = \frac{\lambda_f v}{\sqrt{2}} \ , \qquad\qquad c_{h\overline{f}f} = -\frac{m_f}{v} \ . \tag{1.2.22}$$

Let us make two comments on the Yukawa sector of the SM. First, there is no right-handed neutrinos ν_R and then no Yukawa coupling Y^ν such that the neutrinos remain massless after EWSB. This is in contradiction with the experimental observation that the different flavours of neutrinos oscillate during their propagation. We will return to this issue in section 1.5 where we will present some possibilities to generate a tiny mass for the neutrinos. Second, there is no tree-level flavour changing neutral currents (FCNC) in the SM Yukawa sector as the Higgs couplings are diagonalised at the same time with the masses. This is an important feature of the SM because in general in BSM theories with an extended Higgs sector, the Higgs may couple to two different flavours. In that case, we have a clear signal of new physics as it is discussed in chapter 5 in the context of a 2HDM with lepton flavour violating (LFV) $h\tau\mu$ couplings. Note that flavour changing neutral currents may also be induced by the presence of new fermions mixing with the SM ones, as discussed in chapter 4.

The last piece of the SM is the kinetic term of the SM fermions

$$\mathcal{L}_{SM}^{kin} = i\sum_f \overline{f}_{L,Ri}\gamma^\mu D_\mu f_{L,Ri} \ . \tag{1.2.23}$$

The sum stands for all of the SM fermions multiplets and the index $i = 1,2,3$ stands for the three generation of SM fermions. This term contains the covariant derivative of the fermions which is defined similarly to the Higgs doublet as follows

$$\begin{aligned} D_\mu f &= \left(\partial_\mu - ig_s T^a G_\mu^a - ig\tau^i W_\mu^a - ig' Y B_\mu\right) f \\ &\left[\partial_\mu - ig_s T^a G_\mu^a - \frac{ig}{\sqrt{2}}(\tau^+ W_\mu^+ + \tau^- W_\mu^-) - ieQA_\mu - i\frac{g}{c_w}(\tau^3 - Qs_w^2)Z_\mu\right] f \ . \end{aligned} \tag{1.2.24}$$

For the leptons (l_L and e_R) which are uncoloured fermions, the covariant derivative does not contain the term with gluons. In the same way, for the right-handed fermions (u_R, d_R and e_R) which are $SU(2)_L$ singlets, the W bosons are not present in the covariant derivative. As it can be seen from Eq. (1.2.23), the gauge boson interactions do not mix families in the original flavour basis. However, this feature is altered when going to the mass basis. More precisely, rotating the fermions fields, the neutral currents associated to A_μ and Z_μ (or equivalently B_μ and W_μ^3) are unaffected since they do not mix up and down fermions. In that case we have

$$\mathcal{L}_{SM}^{NC} = \sum_f \frac{g}{c_w}\overline{f}\gamma^\mu(g_V^f - g_A^f\gamma_5)f + eQ_f\overline{f}\gamma^\mu f \ , \tag{1.2.25}$$

where the flavour contractions are diagonal and the vector and axial-vector couplings of the Z boson are defined by

$$g_V^f = \frac{1}{2} I_f^3 - Q_f s_w^2 \ , \qquad\qquad g_A^f = \frac{1}{2} I_f^3 \ . \tag{1.2.26}$$

The factor I_f^3 is the third component of the weak isospin. As a consequence of the above discussion, there is no tree-level FCNC associated to the Z boson in the SM. This feature is tested experimentally with a high precision and then when one adds new fermions mixing with the SM ones, one should be careful to not induce too large tree-level FCNC between the SM fermions. In addition, one should also be careful to not generate large deviations in the Z boson couplings. As the couplings of the third generation are less constrained, if new fermions mix with the SM ones, they can mainly mix with them. In that case, as discussed in chapter 4, the SM couplings of the third generation can be affected in a significant way by the presence of new fermions and tree-level FCNC between the new fermions an the third generation are present. The charged currents associated with $W_\mu^\pm$ are sensitive to the flavour rotation as they mix up and down fermions

$$\mathcal{L}_{SM}^{CC} = \frac{g}{\sqrt{2}} \left[W_\mu^+ \overline{u}_L V_{CKM} \gamma^\mu d_L + W_\mu^+ \overline{e}_L \gamma^\mu \nu_L + h.c. \right] \ . \tag{1.2.27}$$

Indeed, going to the mass basis, the charged currents are not flavour diagonal and the Cabibbo-Kobayashi-Maskawa (CKM) matrix [27, 28] is defined by $V_{CKM} \equiv U_u^\dagger U_d$. The CKM matrix is a complex unitary matrix and thus has nine degrees of freedom. However some phases can be set to zero by rotating independently the SM quarks fields leading to only four physical degrees of freedom: three angles and one phase δ. Additionally, as for the Z couplings, new fermions mixing with the SM ones can affect the W couplings. As the third generation sector is less constrained, it is simpler to mix new fermions with this generation. Anyway, when we add new fermions even if they mix only with the third generation, the unitarity of the CKM matrix which is tested experimentally is spoiled and constrain new physics.

Note that in the SM, there is no equivalent of the CKM matrix in the leptonic sector as there are no Yukawa couplings associated to the neutrinos. Then ν_L can be rotated freely to absorb the matrix U_e of the charged fermions. If we add Yukawa couplings in the neutral lepton sector (see section 1.5), the charged currents involving the leptons contain a flavour matrix, the so-called Pontecorvo-Maki-Nakagawa-Sakata (PMNS) matrix [29–31].

1.3 Custodial symmetry

Let us now discuss an important feature of the SM, that is, the custodial symmetry $SU(2)_{cus}$. The Higgs sector of the SM possesses an accidental global symmetry larger than the $SU(2)_L \times U(1)_Y$ local symmetry. In term of the four degrees of freedom h_i $(i = 1, \cdots, 4)$, the potential of Eq. (1.2.2) can be rewritten as

$$-V(H) = -\lambda (H^\dagger H - \frac{v^2}{2})^2 = -\frac{\lambda}{2} (h_1^2 + h_2^2 + h_3^2 + h_4^2 - v^2)^2 \ , \tag{1.3.1}$$

where we used the minimisation condition $\mu^2 = \lambda v^2$ and the fact that the potential is defined up to a constant term. The SM Higgs potential of Eq. (1.3.1) is invariant under an $SO(4)$ global symmetry under which the quadruplet (h_1, h_2, h_3, h_4) transforms in the fundamental representation. The $SO(4)$ symmetry has six generators which is two times the number of generators in $SU(2)_L$. When H gets a vev after EWSB [$\langle h_3 \rangle = v$ and $\langle h_1 \rangle = \langle h_2 \rangle = \langle h_4 \rangle = 0$], the $SO(4)$ symmetry is spontaneously broken down to $SO(3)$. Thus there is three unbroken global symmetry directions in the SM Higgs potential instead of one (local) associated to $U(1)_{em}$. The $SO(4)$ symmetry is isomorphic to $SU(2)_L \times SU(2)_R$ and the unbroken $SO(3)$ symmetry is equivalent to $SU(2)_{L+R} \equiv SU(2)_{cus}$ such that, after EWSB, the SM Higgs potential possesses a global custodial invariance under the $SU(2)_{cus}$ symmetry.

Let us examine more deeply the $SO(4)$ global invariance of the SM Higgs sector by defining the following bi-doublet

$$\Phi = \frac{1}{\sqrt{2}}\begin{pmatrix}\tilde{H} & H\end{pmatrix} = \frac{1}{\sqrt{2}}\begin{pmatrix}\phi^{0*} & \phi^{+} \\ -\phi^{-} & \phi^{0}\end{pmatrix} . \tag{1.3.2}$$

The SM Higgs potential can be rewritten as follow

$$-V(\Phi) = \mu^2 Tr[\Phi^\dagger\Phi] - \lambda(Tr[\Phi^\dagger\Phi])^2 . \tag{1.3.3}$$

Of course, the above potential is still locally invariant under $SU(2)_L \times U(1)_Y$ as it can be checked from the following transformations

$$\underline{SU(2)_L \times U(1)_Y}: \quad \Phi \to L\Phi \ \exp(i\alpha_Y \tau_R^3) , \qquad L = \exp(i\alpha_L^i \tau_L^i) , \tag{1.3.4}$$

where the hypercharge operator has been replaced by the third generator of $SU(2)_R$. In addition, one can check that the potential is also invariant under the global $SU(2)_L \times SU(2)_R$ transformations defined as follow

$$\underline{SU(2)_L \times SU(2)_R}: \quad \Phi \to L\Phi R^\dagger , \qquad L, R = \exp(i\alpha_{L,R}^i \ \tau_{L,R}^i) . \tag{1.3.5}$$

Then, Φ is a quadruplet of $SO(4)$ or equivalently a bi-doublet of $SU(2)_L \times SU(2)_R$. After EWSB, the Higgs field acquires a vev and as a consequence $\langle\Phi\rangle$ takes the following form

$$\langle\Phi\rangle = \frac{1}{2}\begin{pmatrix} v & 0 \\ 0 & v\end{pmatrix} . \tag{1.3.6}$$

This vev transforms as follows under the global symmetries $L\langle\Phi\rangle \neq \langle\Phi\rangle$ and $\langle\Phi\rangle R^\dagger \neq \langle\Phi\rangle$ such that $SU(2)_L \times SU(2)_R$ is spontaneously broken. However, the diagonal transformation ($V = L = R$) leads to $V\langle\Phi\rangle V^\dagger = \langle\Phi\rangle$ such that $SU(2)_{L+R} \equiv SU(2)_{cus}$ remains unbroken while $SU(2)_{L-R}$ is broken. Looking at Eqs. (1.3.4) and (1.3.5), one easily identifies the embedding of the SM gauge group inside $SU(2)_L \times SU(2)_R$, that is, the hypercharge generator corresponds to $Y = \tau_R^3$ while the embedding of $SU(2)_L$ is obvious. After EWSB, the EM charge operator is then $Q = Y + \tau_L^3 = \tau_R^3 + \tau_L^3$ in agreement with the unbroken custodial symmetry $SU(2)_{R+L}$.

Let us now look at the other sectors of the SM. The kinetic part of the Higgs sector can be written as

$$\mathcal{L}_{SM}^H = Tr[(D_\mu\Phi)^\dagger D^\mu\Phi] , \qquad D_\mu\Phi = (\partial_\mu - igW_\mu^i\tau_L^i - ig'B_\mu\tau_R^3)\Phi . \tag{1.3.7}$$

The latter term, has a custodial invariance in the limit where $g' = 0$ ($s_w = 0$). Indeed, in that case

$$D_\mu\Phi = (\partial_\mu - igW_\mu)\Phi \to (\partial_\mu - igU_L W_\mu U_L^\dagger)U_L\Phi U_R^\dagger = U_L(D_\mu\Phi)U_R^\dagger , \tag{1.3.8}$$

where we have used the notation $W_\mu = W_\mu^i\tau_L^i \to U_L W_\mu U_L^\dagger$. Then, the kinetic term in Eq. (1.3.7) is only approximatively invariant under $SU(2)_L \times SU(2)_R$ as $g' \neq 0$ is small. As a consequence, in the SM the custodial symmetry is explicitly broken by the gauging of the hypercharge. This breaking is a tree-level effect and it determines the ratio between the W and Z bosons masses or equivalently the relative strength of the weak and EM gauge couplings

$$\frac{M_W^2}{M_Z^2} = \frac{g^2}{g^2 + g'^2} = c_w^2 . \tag{1.3.9}$$

When $g' = 0$ ($c_w = 1$) the W and Z masses are equal as there is no mixing between W_μ^3 and B_μ. Taking into account the tree-level breaking of the custodial symmetry due to the hypercharge, we define the ρ parameter as

$$\rho \equiv \frac{M_W^2}{M_Z^2 c_w^2} . \tag{1.3.10}$$

In the SM, the tree-level prediction is $\rho_0 = 1$. This is really particular to the SM because in general [1] with an extended Higgs sector one has $\rho_0 \neq 1$.

We now turn to the SM loop contributions to the ρ parameter. It can be useful to define the parameter $T = (\rho - 1)/\alpha$ where

$$T = \frac{1}{\alpha}\left[\frac{\Pi_{WW}(0)}{M_W^2} - \frac{\Pi_{ZZ}(0)}{M_Z^2}\right] = \frac{1}{\alpha c_w^2}\left[\frac{\Pi_{33}(0) - \Pi_{WW}(0)}{M_Z^2}\right] . \tag{1.3.11}$$

The $\Pi's$ are the vacuum polarisation amplitudes of the SM gauge boson. The above definitions are in agreement with the tree-level SM prediction for which $\Pi_{WW}^{tree}(0) = M_W^2$ and $\Pi_{ZZ}^{tree}(0) = M_Z^2$ such that $T_0 = 0$ and $\rho_0 = 1$. Note that the pure one-loop gauge contribution (see figure 1.1) vanishes as the kinetic term of the SM gauge bosons respect $SU(2)_L \times SU(2)_R$. However, the one-loop Higgs-gauge diagrams and the pure Higgs diagrams (see figure 1.2) contribute to the T parameter in the limit where $g' \neq 0$. They are then one-loop manifestations of the breaking by the hypercharge of the custodial symmetry.

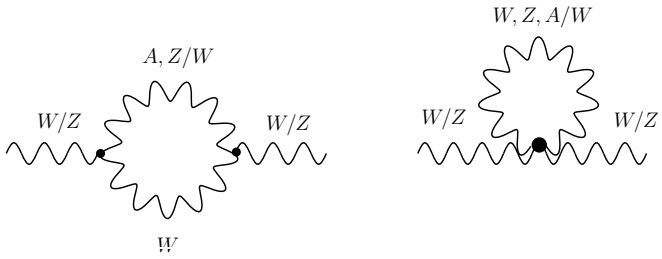

Figure 1.1: One-loop diagrams involving the SM gauge bosons and contributing separately to $\Pi_{WW,ZZ}$ but not to the T parameter.

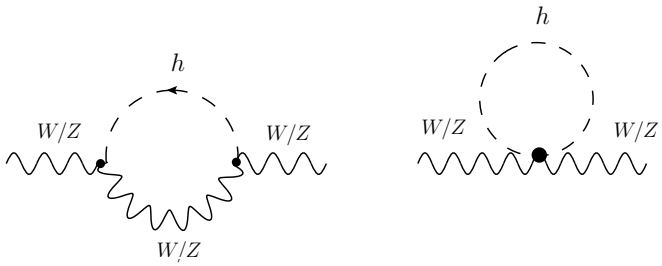

Figure 1.2: One-loop diagrams involving the SM gauge bosons and the Higgs (left) and only the Higgs (right). These diagrams give a logarithmic contribution $\sim \ln m_h^2$ to the T parameter.

We now look at the fermionic sector of the SM. One can group the up and down quarks u_R and d_R into a right-handed doublet such that

$$q_L = \begin{pmatrix} u_L \\ d_L \end{pmatrix} \to L\, q_L \ , \qquad q_R = \begin{pmatrix} u_R \\ d_R \end{pmatrix} \to R\, q_R \ . \tag{1.3.12}$$

We can do the same thing for the leptons but in that case one needs to add a right-handed neutrinos ν_R (see section 1.5). Let us restrict to the quark sector for the example. Assuming that we have the same Yukawa coupling for the up and down quarks, one can form an invariant under $SU(2)_L \times SU(2)_R$ as follows

$$\mathcal{L}_{yuk} = -\lambda \bar{q}_L \Phi q_R + h.c. = -\lambda \bar{q}_L \begin{pmatrix} \tilde{H} & H \end{pmatrix} \begin{pmatrix} u_R \\ d_R \end{pmatrix} . \tag{1.3.13}$$

Then the difference $(\lambda_u - \lambda_d)$ breaks the custodial symmetry. As the top-bottom quarks have the larger difference in mass, their contribution to the T parameter will be the dominant one and we

[1] Among the particular cases that predict $\rho_0 = 1$ (without a tuning of the scalar vevs), there are theories with an arbitrary number of doublets with $Y = \pm 1/2$ and/or with an arbitrary number of singlet with $Y = 0$.

can neglect the other light quarks and leptons. It was the main indication of the top mass before its discovery at Tevatron. Note that for the Higgs (see e.g. Ref. [32]), the contributions to the T parameter are only logarithmically sensitive to the Higgs mass ($\sim \ln m_h^2$). Then the constraints were smaller compare to the top for which the T parameter is quadratically ($\sim m_t^2$) sensitive (see subsection 1.6). Finally, the kinetic term of the SM fermions is invariant under $SU(2)_L \times SU(2)_R$ such that there is no contribution to T from this sector.

Let us finish this section by some comments on new physics. Generally, the parameter $\Delta T = T - T^{SM}$ is used to constraint new physics, that is, the T parameter where the SM contributions have been removed. ΔT is precisely measured (see appendix C) such that it brings important constraints on new physics. Looking at new physics, it is important to understand if the model has a custodial limit in order to control the corrections to ΔT. This limit can be identified following a similar procedure as we presented for the SM. As a classical example, extensions with VL fermions interacting only with the SM gauge bosons have a custodial symmetry as the left and right-handed contributions ΔT cancelled each other. However, when we depart from this pure VL limit and add some Yukawa couplings $\lambda_i \neq 0$, possibly dangerous contributions to ΔT appear. One can control them by taking sufficiently small Yukawa couplings (or in some cases with a particular pattern of the Yukawa couplings) and then a nice feature of VL fermions is that one can always stay close to a custodial limit. Finally, in addition to the T parameter, there is other parameters that constraint new physics. The most relevant one is the S parameter as it is discussed in appendixC.

1.4 Gauge anomaly cancellation

As we have seen, the SM is based on a gauge symmetry $SU(3)_c \times SU(2)_L \times U(1)_Y$ which is spontaneously broken by the Higgs vev v down to $SU(3)_c \times U(1)_{em}$. The SM Lagrangian is the more general renormalisable one after imposing the gauge invariance. Indeed, all of the possible gauge invariant operators of dimension $d \leqslant 4$ constructed with the field content of table 1.1 are present [2]. However, the interactions in the SM Lagrangian are tree-level interactions such that the gauge invariance is insured at least at the classical level. There is no insurance that the gauge symmetry remains exact at the quantum level or in other words that the radiative corrections do not spoil the gauge invariance. This is a crucial question because in a theoretically consistent theory, the gauge symmetry should be exact at all orders.

It can be shown that the anomalous contributions breaking the gauge symmetry may only come from loops of fermions. More precisely, one can restrict to triangle loops of fermions with gauge currents at the external legs. Indeed, if these diagrams are non-anomalous, all of the other diagrams will also be non-anomalous. In QED and QCD, there is no such anomalous contributions as these theories are vector-like (VL), that is, the left and right-handed fermions couple in the same way to the gauge fields. In that case, as we will see the gauge invariance once imposed in the Lagrangian is insured at the quantum level. On the contrary, the SM is not a VL theory but rather a chiral theory where the left and right-handed fermions do not couple in the same way to the $SU(2)_L \times U(1)_Y$ gauge bosons and consequently, anomalous diagrams are possibly present.

Let us first consider a simplest case where the gauge symmetry contains only one gauge group. The gauge currents are $J_\mu^a = \sum_\psi \overline{\psi}_i (T_R^a)_{ij} \gamma_\mu \psi_j$ and fermions ψ can be left-handed or right-handed. The generators T_R^a are in an arbitrary representation R of the gauge symmetry. The anomalous contribution , that is, the contribution to the divergence $(\partial^\mu J_\mu^a)$ can be calculated from the two diagrams of figure 1.3 where the second diagram comes from the exchange of two external currents. The trace over the generators can always be written as a sum of symmetric and antisymmetric tensors as follow

$$Tr[T_R^a T_R^b T_R^c] = \frac{1}{2} Tr[[T_R^a, T_R^b] T_R^c] + \frac{1}{2} Tr[\{T_R^a, T_R^b\} T_R^c] = \frac{i}{2} f^{abc} C(R) + \frac{1}{4} d_R^{abc} \ . \tag{1.4.1}$$

The contribution proportional to f^{abc} gives the difference between the two loops and is UV divergent

[2] Up to the QCD θ term (see sections 1.5 and 2.1).

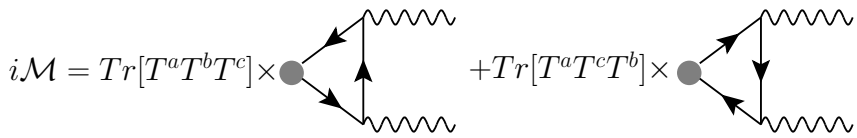

Figure 1.3: Flavour structure of the two anomalous triangle diagrams.

(see Ref. [26]). However, this part can be removed through renormalisation without violating gauge invariance and then does not contribute to the gauge anomalies. The remaining part proportional to d_R^{abc} contributes to the anomaly. The totally symmetric tensor $d_R^{abc} = 2Tr[\{T_R^a, T_R^b\}T_R^c] = A(R)d^{abc}$ and then we have for the divergence

$$\begin{aligned} \partial^\rho J_\rho^a &= \left(\sum_{left} d_{R_\ell}^{abc} - \sum_{right} d_{R_r}^{abc}\right) \frac{g^2}{64\pi^2}\frac{1}{2}\epsilon^{\mu\nu\alpha\beta}F_{\mu\nu}^b F_{\alpha\beta}^c \\ &= \left(\sum_{left} A(R_\ell) - \sum_{right} A(R_r)\right) \frac{g^2}{128\pi^2} d^{abc}\epsilon^{\mu\nu\alpha\beta}F_{\mu\nu}^b F_{\alpha\beta}^c \ , \end{aligned} \tag{1.4.2}$$

where g is the gauge coupling, the sums run over left and right-handed fermions and $A(R_{l,r})$ are the corresponding anomaly coefficients. An important point is that the left and right-handed fermions contribute with a different sign [3]. The currents J_μ^a are gauge currents such that the divergence $\partial^\mu J_\mu^a$ should be equal to zero. There are two possibilities (i) the anomaly coefficients $A(R_{l,r})$ are zero or (ii) there is a cancellation between the left and right-handed contributions. The first possibility occurs when the fermions are in real or pseudo-real representations [it is the case for $SO(N)$ [4] and $Sp(2N)$ gauge symmetries but not always for $SU(N)$]. One concludes that there are no $SU(2)_L^3$ gauge anomalies in the SM because $SU(2) \cong Sp(2)$. The second possibility is less trivial and require a cancellation between the different fermionic contributions. Let us consider QED and QCD first. As mentioned above, the anomaly cancellation is trivial in these VL theories. Indeed, the left-handed f_L and right-handed f_R fermions have the same quantum numbers leading to the same anomaly coefficient ie $A(f_L) = A(f_R)$ and the cancellation of the anomalies is

$$\underline{\text{QED, QCD}}: \qquad \sum_{left} A(R_\ell) - \sum_{right} A(R_r) = \sum_f [A(f_L) - A(f_R)] \equiv 0 \ . \tag{1.4.3}$$

Then in the SM there is no gauge anomalies associated to $SU(3)_c^3$. On the contrary, in chiral gauge theories, we have in general $A(f_L) \neq A(f_R)$ and the cancellation is not so simple.

We have seen how the cancellation of the gauge anomalies occurs when the gauge symmetry contains only one symmetry group. Let us now consider the full SM gauge symmetry. The first thing is to identify the possible anomalous diagrams. We have three currents J_μ^{QCD}, J_μ^{weak} and J_μ^Y associated with the three gauge symmetries of the SM respectively $SU(3)_c$, $SU(2)_L$ and $U(1)_Y$. As already mentioned, there are no cubic $SU(2)_L^3$ and $SU(3)_c^3$ anomalies. One can also exclude diagrams involving one generator of $SU(2)_L$ or $SU(3)_c$ because the anomaly coefficients in that cases vanish as

[3] A simple way to see that, is to consider only left-handed fermions by taking the charge conjugate of the right-handed fermions. Let us for example consider two fermions with opposite chiralities but transforming in the same gauge representation R ie $f_L \sim f_R \sim R$ and $f_R^c \sim \overline{R}$. As $A(\overline{R}) = -A(R)$, the charge conjugate fermion f_R^c which is equivalent to the right-handed fermions f_R contributes with a minus sign compared to the left-handed one f_L.

[4] Up to complex Spinorial representations of $SO(N)$.

they are proportional to $Tr[\tau^i]$ or $Tr[T^a]$. Consequently the diagrams

$$\begin{aligned} &SU(2)_L - U(1)_Y^2 \ , \quad SU(3)_c - U(1)_Y^2 \ , \quad SU(3)_c - SU(2)_L - U(1)_Y \ , \\ &SU(3)_c - SU(2)_L^2 \ , \quad SU(3)_c - SU(2)_L^2 \ , \quad SU(3)_c^2 - SU(2)_L \ , \end{aligned} \tag{1.4.4}$$

do not contain any gauge anomalies. In addition, we should also consider diagrams involving the graviton. There is obviously no gauge anomalies in $SU(2)_L - grav^2$ and $SU(3)_c - grav^2$. The remaining four possible anomalous diagrams are the $U(1)_Y^3$, $U(1)_Y - SU(2)_L^2$, $U(1)_Y - SU(3)_c^2$ and $U(1)_Y - grav^2$ (see figure 1.4).

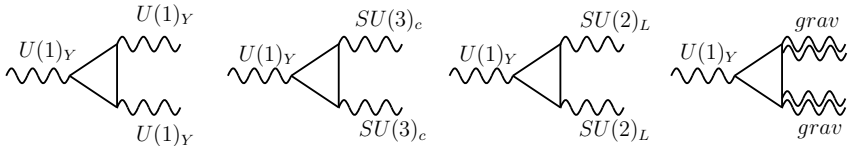

Figure 1.4: The four triangle diagrams that receive non-trivial anomalous contributions in the SM. From the left to the right: the cubic hypercharge anomaly, the weak isospin anomaly, the coloured anomaly and the gravitational anomaly.

Note that all of these diagrams involve the hypercharge current. The contributions from the SM fermions to each of these diagrams are the following. For the cubic hypercharge anomaly, all of the SM fermions contribute and we have

$$\begin{aligned} \underline{U(1)_Y^3}: \quad 2Tr[Y\{Y,Y\}] &= 4Tr[Y^3] = 4\left(\sum_{left} Y_\ell^3 - \sum_{right} Y_r^3\right) \\ &= 4\left[N_c(N_w Y_q^3 - Y_u^3 - Y_d^3) + N_w Y_l^3 - Y_e^3\right] = 0 \ , \end{aligned} \tag{1.4.5}$$

where the last equality has been obtained by replacing the hypercharges listed in table 1.1 and by the replacements $N_c = 3$ and $N_w = 2$. Indeed, the weak doublets contribute with a multiplicity factor N_w while the coloured triplet with a factor N_c.

For the weak isospin anomaly we have

$$\begin{aligned} \underline{SU(2)_L^2 - U(1)_Y}: \quad 2Tr[\tau^i\{\tau^j,Y\}] &= 4Tr[Y]Tr[\tau^i\tau^j] \\ &= 2\delta^{ij}\left(\sum_{\substack{\text{left} \\ \text{non-singlets}}} Y_\ell - \sum_{\substack{\text{non-singlets} \\ \text{coloured}}} Y_r\right) \\ &= 2\delta^{ij}\left[N_c Y_q + Y_l\right] = 0 \ . \end{aligned} \tag{1.4.6}$$

This time only the SM weak doublets which are charged under $SU(2)_L$ contribute to the anomaly. For the coloured anomaly we have

$$\begin{aligned} \underline{SU(3)_c^2 - U(1)_Y}: \quad 2Tr[T^a\{T^b,Y\}] &= 4Tr[Y]Tr[T^aT^b] \\ &= 2\delta^{ab}\left(\sum_{\substack{\text{left} \\ \text{coloured}}} Y_\ell - \sum_{\substack{\text{right} \\ \text{coloured}}} Y_r\right) \\ &= 2\delta^{ab}\left[N_w Y_q - Y_u - Y_d\right] = 0 \ , \end{aligned} \tag{1.4.7}$$

and obviously, only the quarks charged under $SU(3)_c$ contribute. Finally, for the gravitational anomaly all the SM fermions contribute and we have

$$\begin{aligned} \underline{grav^2 - U(1)_Y}: \quad Tr[Y] &= \left(\sum_{left} Y_\ell - \sum_{right} Y_r\right) \\ &= \left[N_w N_c Y_q + N_w Y_l - N_c Y_u - N_c Y_d - Y_e\right] = 0 \ . \end{aligned} \tag{1.4.8}$$

The amazing thing is that all of the gauge anomalies are cancelled in the SM, and the cancellation occurs in a rather non-trivial way between the quarks and leptons. The anomaly cancellation is valid for every generations of fermions independently (as we implicitly assumed) and consequently the number of generations is not fixed from this point of view.

Finally, let us finish this section by some comments on BSM theories. When new fermions are added to the SM, the four anomalies cancellation conditions should remain exact. The latter requirement constrains the possible theoretically self-consistent fermionic extensions of the SM as discussed in chapter 4. There are few cases where the anomaly cancellation is trivial. For instance, vector-like fermions automatically respect the anomaly cancellation conditions as the left and right-handed fermions have the same quantum numbers under the SM gauge group ie $f_L \sim f_R \sim (R_c, R_w, Y)$. Another classical case comes from a SM gauge singlet $N_R \sim (1, 1, 0)$ (see section 1.5) which obviously does not contribute to the anomalous diagrams. This situation generalises to fermions in real or pseudo-real representations of $SU(3)_c$ and $SU(2)_L$ with zero hypercharge that is fermions transforming as $(R_c, R_w, 0)$ with $\overline{R}_{c,w} = R_{c,w}$ or $\overline{R}_{c,w} = R^*_{c,w}$. A well know example of this kind is a weak triplet $\Sigma_R \sim (1, 3, 0)$.

1.5 Motivations to go beyond the SM

In this section, we outline some of the main limitations of the SM as despite its success, it has some shortcomings and missing pieces. In particular, we highlight the problems that can be addressed in the phenomenological extensions of the SM that will be presented in part II.

First, an important experimental observation is the evidence for dark matter (DM), a weakly interacting form of matter, in our universe (for a review see for e.g. [33]). Its existence seems to be an unavoidable necessity to explain anomalies observed at several scales in the universe. However, the SM does not contain any dark matter candidate and BSM physics should be invoked to provide such a candidate. We do not focus on the DM problem in the next but rather only mention the fermionic DM candidates appearing in the classification of chapter 4. These DM candidates can be an additional motivation for the studied phenomenological models.

Another experimental evidence of new physics, is the domination of matter over anti-matter in our universe. To reproduce this asymmetry one needs a mechanism of baryogenesis which requires among other things a source of CP violation. The only such source in the SM is the phase δ of the CKM matrix but the latter is generally not enough to explain baryogenesis. Again, we do not focus on this problem but introducing CP violating new physics is an interesting feature which can provide additional motivations for new physics. For instance, in chapter 4, some of the studied fermionic extensions of the SM posses CP violation phases. In addition, in a 2HDM (see chapter 5) there is in general a CP violating phase associated with one of the two doublets.

Let us now turn to more theoretical puzzles of the SM. The EM and weak interactions are unified in the SM into a common framework based on the $SU(2)_L \times U(1)_Y$ gauge group which is broken by the Higgs vev down to the EM gauge group $U(1)_{em}$. This unification may seem incomplete as it is based on two distinct symmetry groups. Then it is natural to try to unify the EW and strong interactions into a single gauge group leading to a so-called Grand Unified Theory (GUT). Indeed, using the renormalization group equations (RGEs) of the SM, the three SM gauge couplings can be extrapolated to high energies where they seem to converge. However, the unification is not perfect in the SM. This can be interpreted as the indication that new physics is needed to modify the running of the gauge couplings and make them unify.

Next, in the QCD Lagrangian, a term of the form $\theta_{QCD}\epsilon_{\mu\nu\rho\sigma}G^{\mu\nu a}G_a^{\rho\sigma}$ is allowed by gauge invariance. This term breaks the CP symmetry and the parameter θ_{QCD} is the QCD vacuum angle. Its value is expected to be of order 1. However, upper bounds on the electric dipole moment of the neutron translate into an upper bound on θ_{QCD} of about 10^{-10}. This is called the strong CP problem. A solution to this problem is provided by the Peccei-Quinn mechanism [34, 35] which involves a new BSM field, the axion.

Another theoretical puzzle comes from the "large" numbers of parameters (19 parameters without giving mass to the neutrinos) in the SM. In this respect, the latter can then be seen as an incomplete

theory of the EW, strong and Yukawa interactions. Theoretically, it could be attractive to reduce this number with a UV complete and more predictive model. Most of the parameters belong to the fermionic sector (9 Yukawa couplings and 4 CKM parameters) of the SM and there is a large hierarchy between them. The latter can be explained by a flavour symmetry but there is no convincing theory of flavour yet. This is the so-called flavour puzzle of the SM. For example, the Yukawa couplings of the SM fermions run from $\lambda_e \sim \mathcal{O}(10^{-9})$ for the electron to $\lambda_t \sim \mathcal{O}(1)$ for the top quark. A similar hierarchy is present in the CKM matrix where the entries vary from $\mathcal{O}(1)$ to $\mathcal{O}(10^{-3})$. Then, the hierarchy in the parameters of the SM turns out to be "accidental" and this feature points in favour of the SM being an effective model of a more fundamental theory.

Finally, there is also the evidence of neutrinos oscillations which implies a non-zero mass for at least two of the three SM neutrinos. This is certainly the most robust evidence of BSM physics because in the SM there is no right-handed ν_R and consequently the neutrinos are massless at the renormalisable level. Note that in the SM the cancellation of the gauge anomalies does not require the presence of ν_R (see subsection 1.4) and then in its first formulation the SM does not contain such a field. On the contrary, as already mentioned, the custodial symmetry point in favour of a right-handed neutrinos such that one can form an $SU(2)_R$ doublet $\begin{pmatrix}\nu_R & e_R\end{pmatrix}^T$. The simple solution to the neutrinos masses is to extend the SM with three right-handed neutrinos coupled to the Higgs field through a Yukawa term of the following form

$$\mathcal{L}_\nu = -Y^\nu_{ij}\bar{l}_{Li}\tilde{H}\nu_{Rj} + h.c. \tag{1.5.1}$$

In this way, the neutrinos become massive and there is a non-trivial PMNS matrix in the charged-currents of the lepton sector. However, the Yukawa couplings in the mass-basis that is the couplings in $M_\nu = diag(\lambda_{\nu_1}, \lambda_{\nu_2}, \lambda_{\nu_3})$ are extremely small, very far from the other Yukawa couplings which already spread over several orders of magnitude. Then it could be interesting to have a mechanism that insures a non-zero but tiny masses for the neutrinos. To that end, let us first consider the lowest-dimensional SM gauge invariant operator generating a mass for the neutrinos

$$\mathcal{L}_{d=5} = -\frac{c_{ij}}{\Lambda_\nu}(\bar{l}_{Li}\ \tilde{H})(H\ l_{Li})\ . \tag{1.5.2}$$

This operator has dimension equal to five and quite remarkably, it is the only gauge invariant operator with this dimension. If we want to reproduce the tiny neutrino masses let say $m_\nu \sim 0.1$ eV for simplicity, for a coupling $c_{ij} \sim \mathcal{O}(1)$, one needs a very large scale of the order of $\Lambda_\nu \sim 10^{15}$ GeV. In this hypothesis, the new physicsΛ_ν is really far from the energy range currently accessible at colliders. There are several possibilities to generate the above operator from the exchange of a state with a mass of the order of Λ_ν. Let us consider the simplest one that is as before a right-handed neutrino. In all generality, in addition to the Yukawa term of Eq. (1.5.1), there is also the possibility to have a Majorana mass term which is not forbidden by the EW symmetry as $\nu_R \sim (1, 1, 0)$ is an EW singlet (sometimes referred as sterile neutrino). The relevant lagrangian is

$$\mathcal{L}_\nu = -Y^\nu_{ij}\bar{l}_{Li}\tilde{H}\nu_{Rj} - iM_{ij}\nu^c_{Ri}\nu_{Rj} + h.c. \tag{1.5.3}$$

If neutrinos have any quantum number, such Majorana mass term is forbidden and only a Dirac mass is allowed. For example, the most natural quantum number for right-handed neutrinos is the lepton number. After EWSB, the Lagrangian in Eq. (1.5.3) leads to the following mass matrix

$$\mathcal{M}_\nu = \begin{pmatrix} 0 & m \\ m & M \end{pmatrix}\ , \qquad m_{1,2} = \sqrt{m^2 + \frac{M^2}{4}} \pm \frac{M}{2}\ . \tag{1.5.4}$$

Note that for simplicity, we have considered only one generation but it is straightforward to generalise to the three SM families. In the limit where $M \gg m$, on has for the two mass eigenstates $m_{heavy} \simeq M$ and $m_{light} \simeq m^2/M \ll m_{heavy}$ where the heavy neutrinos mostly comes from the singlet ν_R while the light neutrinos from the doublet ν_L. Indeed, the mixing angle is of the order of $m/M \ll 1$. As an example, if one takes the Dirac mass at the EW scale $m \simeq 100$ GeV and the Majorana mass very high

$M \simeq 10^{14}$ GeV one obtains $m_{light} \simeq 0.1$ eV. The above mechanism may explain the lightness of the neutrinos, it is called (type I) see-saw mechanism: as M goes up, m goes down to keep m_{light} fixed.

One can extend the above mechanism by considering weak triplets $\Sigma_R \sim (1,3,0)$ instead of weak singlet, this is the so-called type III see-saw mechanism. With one new fermionic state, the type I and III see-saw are the only possibilities to generate the effective operator in Eq. (1.5.2) [5]. One can also realise the see-saw mechanism with several Majorana multiplets. Finally, there also exist more complicated scheme like the inverse see-saw mechanism where several singlet ν_R realise an approximate lepton number symmetry $U(1)_L$ that insure the smallness of the neutrino mass by a cancellation between several contributions. In that case, the lightness of the neutrinos is realised for a naturally small coupling in Eq. (1.5.2) instead of for a high scale Λ_ν and consequently, the heavy neutrinos can be lighter. Some of these possibilities are presented in chapter 4 in the context of the Higgs couplings.

1.6 Hierarchy problem

We now focus to another SM problem which has not been addressed before. This is one of the most important theoretical shortcoming of the SM, the so-called hierarchy problem of the EW scale. The latter is the main motivation for composite Higgs models that will be presented in part III of the manuscript. This problem has triggered a lot of theoretical efforts as contrary to other experimental or theoretical evidences that call for BSM physics at an undetermined scale (see section 1.5), the solution of the hierarchy problem should be close to the EW scale.

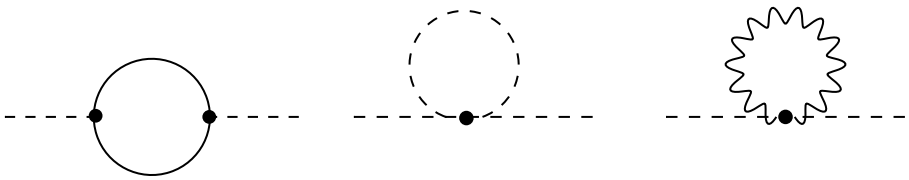

Figure 1.5: Diagrams quadratically divergent. From the left to the right, one-loop diagram involving fermions, scalars and spin one fields.

The hierarchy problem is intrinsically related to the only operator in the SM Lagrangian with a non-dimensionless coupling ie $\mu^2 H^\dagger H$. This coupling controls the Higgs mass as the SM tree-level prediction is $m_h^2 = 2\mu^2/\lambda$. However, the latter tree-level prediction receives loop corrections. For instance, the one-loop self energy coming from a Dirac fermion is given by

$$\Pi^f_{hh}(0) = -2\lambda_f^2 \int \frac{d^4k}{(2\pi)^4} \left[\frac{1}{k^2 - m_f^2} + \frac{2m_f^2}{(k^2 - m_f^2)^2} \right] , \tag{1.6.1}$$

which is divergent. More precisely, if we regularise the divergent integral with a cut-off Λ, we see that the first term is quadratically divergent. Indeed, counting the dominant contribution to the integral, $\Pi^f_{hh}(0)$ behaves like $\int d^4k\ k^2/k^4 \sim \int dk\ k \sim \Lambda^2$. In the same way, the other diagrams of figure 1.5 are all quadratically divergent. On the contrary, the diagrams of figure 1.6 that also induce radiative corrections to the Higgs mass are only logarithmically divergent as $\int d^4k\ 1/k^4 \sim \int dk\ 1/k \sim \ln \Lambda$. Note that we work in the broken phase ($\langle H \rangle \neq 0$) where the SM fermions are massive but the same reasoning should hold in the unbroken phase because the radiative corrections to the Higgs mass come in fact from the radiative corrections to μ^2.

If we consider only the SM which is a perfectly defined renormalisable theory, the quadratic divergences are absorbed by the renormalisation procedure. The physical Higgs mass is given by

$$m_h^2\big|_{phys} = m_h^2 + \delta m_h^2 , \tag{1.6.2}$$

[5] Note that there is also the possibility to add a scalar multiplet $\Delta \sim (1,3,1)$ to generate the $d = 5$ operator. This is the so-called type II seesaw mechanism.

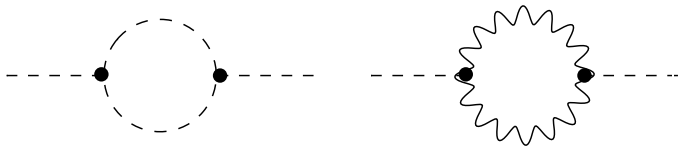

Figure 1.6: Diagrams logarithmically divergent.

where m_h^2 is the tree-level mass squared while δm_h^2 are the radiative corrections. These radiative corrections come from loops of SM particles such that δm_h^2 is of the order of the heavy SM particles like e.g. the top quark mass. Then, after renormalisation, the quadratic divergences translate into a sensitivity in the mass of the heavy SM particles. The physical Higgs mass is given by the sum of the tree-level and loops contributions but the latter are of the same order, that is, of the order of the EW scale and then $m_h^2|_{phys}$ is naturally of the order of the EW scale.

Up to now, we have considered only the SM, assuming implicitly that there is no new physics. However, from section 1.5, we believe that the SM is an effective theory and that new physics should appear at a higher scale Λ_{NP}. Let us explore the consequence of the presence of new physics on the radiative corrections to the Higgs mass. If the SM is an effective theory and at a higher scale, new physics with new heavy states are present, the latter will contribute to the radiative corrections to the Higgs mass [6]. More precisely, in that case the physical Higgs mass is given by

$$m_h^2\big|_{phys} = m_h^2 + \delta m_h^2\big|_{SM} + \delta m_h^2\big|_{NP} \ , \tag{1.6.3}$$

where the radiative corrections have been divided into those coming from the SM particles and those from the new heavy states. As mentioned above, after renormalisation $\delta m_h^2\big|_{SM}$ is of the order of the EW scale. However, $\delta m_h^2\big|_{NP}$ is of the order of the mass scale of the new heavy states and there should be a cancellation between $\delta m_h^2|_{SM}$ and $\delta m_h^2|_{NP}$ such that the physical Higgs mass stays at the EW scale. In general this cancellation is highly unnatural. To fix the ideas, let us for instance consider that new physics appears at $\Lambda_\nu \sim 10^{15}$ GeV. Then the cancellation should be between $\Lambda_{EW}^2 \sim (10^2$ GeV$)^2$ and $\Lambda_\nu^2 \sim (10^{15}$ GeV$)^2$ which corresponds to a very precise cancellation of one part in 10^{26}.

That is the hierarchy problem: in presence of new physics with new heavy states, the Higgs is naturally of the order of Λ_{NP}, more precisely of the order of the masses of the new heavy states. The presence of a new scale tends to destabilise Λ_{EW} and to push it toward the new physics scale A large fine-tuning is then necessary to precisely adjust the Higgs mass with its physical value. In addition, this fine-tunning should be done at every orders in perturbation theory. This is technically possible but it appears highly unnatural. In the sequel, we present some solutions that allow to have naturally a Higgs mass at the EW scale or in other words, solutions that allow to stabilise the gap between the EW scale and the new physics scale.

Before turning to solutions of the hierarchy problem, it is instructive to consider the radiative corrections to other particles than scalars. For instance, the one-loop self-energy of the photon in QED receives contributions from fermions which are similar to the ones of the first diagram of figure 1.5. Consequently, these radiative corrections are a priori quadratically divergent. However, there is no hierarchy problem in QED because, provided that the theory is regularised in a gauge invariant way, the divergence is in fact only logarithmic and absorbed after renormalisation in the running of the gauge coupling. Then, there is a symmetry principle, the gauge symmetry that enforces the photon to remain massless. The same feature happens in the SM but it is a bit more complicated as the gauge symmetry is non-abelian and spontaneously broken.

In a similar way, radiative corrections for instance to the electron mass in QED are a priori linearly divergent. This is less dramatic than quadratic divergences but such linear divergence would still lead

[6] Note that, one of the first scale that we can think of is the Planck scale where the general relativity should be replace by a quantum theory. However, in that case we have no way to evaluate the contribution to the Higgs mass from loops of gravitons.

to unacceptable fine-tuning in order to arrive at the physical electron mass. However, the detailed calculation gives $\delta m_e \sim m_e \ln \Lambda$. Then even if Λ is very high, no large fine-tunning is necessary. This is a consequence of the chiral symmetry. Indeed, if the tree-level fermions masses are zero, there is an exact global symmetry (see section 2.2) such that any radiative corrections should be proportional to the tree-level mass itself and vanishes in the chiral limit. The linear divergence then becomes a logarithmic divergence and the chiral symmetry protects the fermions masses from large radiative corrections.

As we have seen, the masses of fermions and gauge bosons are protected from large radiative correction by symmetries, respectively the gauge and the chiral symmetry. It is natural to ask if the Higgs mass could be protected in a similar way. In fact, interesting solutions to the hierarchy problem are based on a new symmetry that protects the Higgs mass. These solutions invoke new physics at a scale close to the EW one in order to avoid large fine-tuning cancellations between the scale of new physics, where the solution to the hierarchy problem arrives and the EW scale. This is the strongest argument in favour of BSM physics at the TeV scale, that is, new physics possibly accessible at colliders such as the LHC or its successors. There are two main dynamical options to solve the Hierarchy problem (*i*) supersymmetry or (*ii*) a shift symmetry as in composite Higgs models. Let us explain a bit these two possibilities.

In the first one, if the supersymmetry is exact, the radiative corrections to the Higgs mass are zero. This is due to the particular relations imposed by the supersymmetry between the couplings of the SM particles and their superpartners which lead to a cancellation between the SM contributions and the superpartners contributions. However, we know that supersymmetry should be broken as superpartners have not been observed yet. Then, the cancellation is not perfect and the Higgs mass is of the order of the mass splitting between the SM and the superpartners particles. If this mass difference is sufficiently small, there is no large fine-tunning and the Higgs is naturally at the EW scale. On the contrary, if the superpartners masses are decoupled from the EW scale, the fine-tunning becomes more and more important with the increase of the mass splitting. Then, supersymetry can addressed the hierarchy problem provided that it scale is close to the EW one. Note that, the largest couplings to the Higgs are associated to the top quark and then also to its partners such that, we expect relatively light supersymetric (scalar) top partners to further suppress their radiative contributions.

The second option to solve the hierarchy problem is a shift symmetry. In that case, the Higgs appears as a pseudo Nambu Goldstone boson (pNGB) associated to the spontaneous breaking of a global symmetry. If this shift symmetry would be exact, the Higgs would be a Nambu Goldstone boson (NGB), that is, a massless particle. As it is not the case, there are explicit breaking sources that induce radiatively a mass for the Higgs. As a consequence, the Higgs mass is loop-induced and of the order of the explicit breaking coupling times the scale f of the pNGBs. If one decouples the new physics from the EW scale by increasing f, one then reintroduces a fine-tunning in the Higgs mass. Consequently, a shift symmetry can address the hierarchy problem but again, the new physics scale f should be close to the EW one, that is close to v. The parameter $\xi \equiv v^2/f^2$ parametrises most of the deviations compare to the SM predictions. It should be small in order to have a SM-like Higgs as experimentally observed but not too small in order to limit the tunning in the Higgs mass. One realisation of the above mechanism happens in composite Higgs models where the relevant source of explicit breaking comes from the top quark such that, to further reduce the tunning, in general relatively light (fermionic) top partners are expected [36]. The composite Higgs solution to the hierarchy problem is discussed in more details in chapter 6. As an interesting remark, the above mechanism already happens in QCD (pions are pNGBs) and it is quite reasonable to think that it can hold also at the EW scale.

Let us make some comments on the two above solutions to the hierarchy problem. One can take the point of view that the motivation for supersymmetry is not mainly the hierarchy problem but rather the fact that the maximal external symmetry leading to a non-trivial theory in a four-dimensional space-time is provided by the supersymmetric algebra. Then, supersymmetry could be realised at a higher scale and could have nothing to do with the hierarchy problem. The latter being just one among several interesting features of supersymmetric theories. On the contrary, composite Higgs

models are designed to solve the hierarchy problem and without this feature, it remains no strong motivations for these models.

Finally, let us comment on alternative possibilities for the hierarchy problem. First, there is the possibility that no new physics are present up to the Planck scale in which a yet unknown mechanism protects the Higgs mass from large radiative corrections from the Planck scale physics itself. This scenario postpone the solution of the hierarchy problem to the Planck scale but the hypothetic solution can still be dynamical.

Another scenario could be that the Higgs mass is simply unnatural and we should accept an enormous fine-tuning.

As a last possibility, the Higgs mass is maybe not a fundamental parameter but instead dictated by environment principle, this is the so-called anthropic principle. In that case, the physical Higgs mass takes the particular observed value otherwise the physics would be such that our universe would not suitable for life. This kind of anthropic scenario can take place in the context of a multiverse where all of the possible values of m_h exist but depending on the latter, only few universes are suitable for life.

The two last possibilities, the unaturalness and the anthropic principle, are less satisfactory solutions to the hierarchy problem. Indeed, they are not dynamical solutions and further, they can not be tested soon and maybe we will never be able to probe them. Anyway, we can not discard such possibilities but as long as there is no way to test them, it is better interesting to focus on dynamical solutions. Note that all of the three above alternatives (Planck scale solution, unaturalness and anthropic solution) would greatly reduce the expectations for new physics at the TeV scale. Maybe, we are currently probing a scale where there is no new physics and we should wait more to find BSM physics. In any case, these very speculative ideas demonstrate the relevance of the hierarchy problem and the need to further investigate it.

A Some group theory formulas

In this appendix, we fix the notations and normalisations of the generators of a Lie algebra. These conventions will be particularly useful in the remaining of the manuscript. We consider generators T^a_R in a representation R. In practise, we will not consider exceptional groups and restrict to $SU(N)$, $SO(N)$ and $Sp(2N)$.

For the fundamental representation $R = F$ we have $T^a_F \equiv T^a$ while for the adjoint $R = G$ we have $(T^a_G)^{bc} = if^{bac}$ where f^{bac} are the structure constant of the group. Important relations for the generators are the commutation relations that determine the structure of the Lie algebra and the trace of two generators that determines the normalisation of the latter. They are given by

$$[T^a_R, T^b_R] = if^{abc}T^c_R \ , \qquad Tr[T^a_R T^b_R] = C(R)\delta^{ab} \ . \tag{A.1}$$

Our normalisation for the generators of the fundamental representation is $C(F) = 1/2$. This choice fixes the Dynkin indices $C(R)$ of all of the other representations. From Eqs. (A.1), we determine the structure constants

$$f^{abc} = \frac{-i}{C(R)} Tr\left[[T^a_R, T^b_R]T^c_R\right] \ , \tag{A.2}$$

where it is easy to check with the cyclic property of the trace that f^{abc} is completely antisymmetric. Another important constant is the Casimir $C_2(R)$ which is defined by

$$T^a_R \cdot T^a_R = C_2(R)\mathbb{1} \ , \qquad d(R)C_2(R) = d(G)C(R) \ . \tag{A.3}$$

For each representations R, it is linked to the Dynkin index by the dimension of the representation $d(R)$ and the one of the adjoint $d(G)$. For instance, for $SU(N)$ we have $C_2(G) = N = C(G)$ and then $C_2(F) = (N^2-1)/(2N)$. The last important quantity that we will encounter is the anomaly coefficient. It is defined by

$$2Tr\left[T^a_R\{T^b_R, T^c_R\}\right] = A(R)d^{abc} \equiv d^{abc}_R \ . \tag{A.4}$$

Again, it is easy to check with the cyclic properties of the trace that the tensor d^{abc} is completely symmetric. For real and pseudo-real representations, the anomaly coefficient are all equal to zero. Then there is no anomaly coefficients in $SO(N)$ [7] and $Sp(2N)$ while for $SU(N)$ we have $A(R) = -A(\overline{R})$ [8]. The above normalisation of the fundamental representation leads to $A(F) = 1$. Finally, let us define the following anti-commutation relations

$$\{T^a_R, T^b_R\} = \alpha \mathbb{1}_R \delta^{ab} + \beta d^{abc}_R T^c_R \ . \tag{A.6}$$

Using Eqs.(A.4) and (A.1) we find that $\alpha = 2C(R)/d(R)$ and $\beta = 1/[2C(R)]$ such that

$$\{T^a_R, T^b_R\} = 2C(R)\frac{\mathbb{1}_R}{d(R)}\delta^{ab} + \frac{1}{2C(R)} d^{abc}_R T^c_R \ . \tag{A.7}$$

Then the product of two generators can be decomposed as

$$T^a_R T^b_R = \frac{1}{2}\{T^a_R, T^b_R\} + \frac{1}{2}[T^a_R, T^b_R] = \frac{C(R)}{d(R)}\mathbb{1}_R\delta^{ab} + \frac{1}{2}h^{abc}_R T^c_R \ , \tag{A.8}$$

where $h^{abc}_R = d^{abc}_R/[2C(R)] + if^{abc}$ which translates for the fundamental representation into $h^{abc} = d^{abc} + if^{abc}$.

[7] Up to possible complex Spinorial representations.

[8] Indeed, the generators of $\overline{R}$ are $-T^{a*}_R$. Replacing this generators in Eq. (A.4) we get

$$A(\overline{R})d^{abc} \equiv 2Tr\left[T^a_{\overline{R}}\{T^b_{\overline{R}}, T^c_{\overline{R}}\}\right] = -2Tr\left[T^{a*}_R\{T^{b*}_R, T^{c*}_R\}\right] = -A(R)d^{abc} \ , \tag{A.5}$$

where the last equality has been obtained using the hermicianity of the generators and the cyclic property of the trace.

Chapter 2

A strongly coupled theory: QCD

In the precedent chapter, we have presented the SM Lagrangian and some of its limitations that call for BSM physics. We have introduced in particular the hierarchy problem and mentioned one of its possible solution happening in composite Higgs models. These composite models will be considered in part III of the manuscript. They are strongly coupled at low energy and then in order to become more familiar with this kind of theories, let us now consider in details the QCD part of the SM and in particular its strongly coupled regime. Indeed, QCD is the only known strongly coupled theory in nature such that it is an interesting starting point before turning to composite Higgs models. In this spirit, we outline the interesting features of QCD that will be relevant in the composite Higgs context. We start by considering the gauge symmetry of QCD in section 2.1. Next, in section 2.2 we present the global symmetries of QCD and finally, in sections 2.3, 2.4 and 2.5 we consider interesting features related to the non-perturbative dynamics like the 't Hooft anomaly matching, the QCD sum rules and the gauging of the electromagnetism.

2.1 QCD as a gauge theory of strong interactions

Let us first remind the main properties of QCD as an $SU(3)_c$ gauge theory. The matter fields charged under QCD are the so-called quarks q which are triplets of $SU(3)_c$ and appear in six different flavours $q = \{u, d, s, c, b, t\}$ with masses m_q. The free quark Lagrangian is then

$$\mathcal{L}_{\text{free quarks}} = \sum_q \overline{q}(i\gamma^\mu \partial_\mu - m_q)q \ , \tag{2.1.1}$$

where the sum runs over all flavours of quarks q and an implicit contraction over colour indices is understood ie $\overline{q}q = \overline{q}_i \delta_{ij} q_j$. The QCD Lagrangian can be derived from the free quark Lagrangian by applying the gauge principle with respect to the colour gauge group $SU(3)_c$. The quarks fields transform in the fundamental representation of $SU(3)_c$ as follow

$$q(x) \to q'(x) = e^{i\Theta_a(x)T_c^a} q(x) \equiv U(x)q(x) \ . \tag{2.1.2}$$

The eight matrices $T_c^a \equiv \lambda_c^a/2$ are the generators of $SU(3)_c$ (the subscript c refer to colour) and λ_c^a are the Gell-Man matrices

$$\lambda_c^1 = \begin{pmatrix} 0 & 1 & 0 \\ 1 & 0 & 0 \\ 0 & 0 & 0 \end{pmatrix} \ , \qquad \lambda_c^2 = \begin{pmatrix} 0 & -i & 0 \\ i & 0 & 0 \\ 0 & 0 & 0 \end{pmatrix} \ , \qquad \lambda_c^3 = \begin{pmatrix} 1 & 0 & 0 \\ 0 & -1 & 0 \\ 0 & 0 & 0 \end{pmatrix} \ , \tag{2.1.3}$$

$$\lambda_c^4 = \begin{pmatrix} 0 & 0 & 1 \\ 0 & 0 & 0 \\ 1 & 0 & 0 \end{pmatrix} \ , \qquad \lambda_c^5 = \begin{pmatrix} 0 & 0 & -i \\ 0 & 0 & 0 \\ i & 0 & 0 \end{pmatrix} \ , \qquad \lambda_c^6 = \begin{pmatrix} 0 & 0 & 0 \\ 0 & 0 & 1 \\ 0 & 1 & 0 \end{pmatrix} \ , \tag{2.1.4}$$

$$\lambda_c^7 = \begin{pmatrix} 0 & 0 & 0 \\ 0 & 0 & -i \\ 0 & i & 0 \end{pmatrix} \ , \qquad \lambda_c^8 = \frac{1}{\sqrt{3}} \begin{pmatrix} 1 & 0 & 0 \\ 0 & 1 & 0 \\ 0 & 0 & -2 \end{pmatrix} \ . \tag{2.1.5}$$

The convention for the normalisation of the generators is $Tr[T_c^a T_c^b] = \delta^{ab}/2$ (see appendix A). The anti-quark fields transform as $\overline{q}(x) \to \overline{q}(x)U^\dagger(x)$ and consequently, from Eq. (2.1.2) we see that the mass term of the free quarks Lagrangian is gauge invariant but not the kinetic term because of the partial derivative. In order to maintain the invariance under local transformations, one needs to introduce the gluons fields. They transform as

$$G^\mu \equiv G_a^\mu T_c^a \to G'^\mu = UG^\mu U^\dagger - \frac{i}{g_s}\partial^\mu U U^\dagger \ . \tag{2.1.6}$$

The partial derivative $\partial_\mu q$ is then replaced by the covariant derivative $D_\mu q \equiv (\partial_\mu - ig_s G_\mu)q$ which by construction transforms as the quark field. Note that the gauge interactions are flavour independent (diagonal in the flavour space) which means that the gluons couple in the same way to each flavour of quark.

The kinetic term of the gluons involves the field strength tensor $G_{\mu\nu}$

$$G_{\mu\nu} \equiv G_{\mu\nu}^a T_c^a = \partial_\mu G_\nu - \partial_\nu G_\mu + ig_s[G_\mu, G_\nu] \ , \tag{2.1.7}$$

where $G_{\mu\nu}^a$ is defined in Eq. (1.2.19). As follows from Eq. (2.1.6), $G^{\mu\nu} \to UG^{\mu\nu}U^\dagger$ and the QCD Lagrangian locally invariant under $SU(3)_c$ is

$$\mathcal{L}_{QCD} = \sum_q \overline{q}(i\gamma^\mu D_\mu - m_q)q - \frac{1}{2}Tr[G_{\mu\nu}G^{\mu\nu}] = \sum_q \overline{q}(i\gamma^\mu D_\mu - m_q)q - \frac{1}{4}G_{\mu\nu}^a G_a^{\mu\nu} \ , \tag{2.1.8}$$

where the trace is in the colour space. Let us note that the gauge invariance allows in addition a term of the form

$$\mathcal{L}_\theta = \frac{g_s^2}{64\pi^2}\theta \ \varepsilon_{\mu\nu\rho\sigma}G_a^{\mu\nu}G^{\rho\sigma a} = \frac{g_s^2}{32\pi^2}\theta \ \varepsilon_{\mu\nu\rho\sigma}Tr[G^{\mu\nu}G^{\rho\sigma}] \ . \tag{2.1.9}$$

This is the so-called θ term of QCD which implies an explicit breaking of the discrete symmetries P and CP. However, θ is experimentally constrained to be extremely small (see section 1.5) and consequently, QCD is separately invariant under the discrete symmetries C, P and T.

Finally, let us note that from the above gauge theory and the value of the current [1] masses [see Eq. (2.2.1)], one can compute the running of the strong coupling constant $\alpha_s(\mu) = g_s^2(\mu)/(4\pi)$. The result is that QCD is asymptotically free ($g_s \to 0$) in the UV and becomes strongly coupled in the IR. In the remaining of this chapter, we will focus on the strongly coupled phase, that is, the low energy regime of QCD.

2.2 The chiral symmetry

In addition to its local invariance, the QCD Lagrangian of Eq. (2.1.8) also exhibits a global invariance under the chiral symmetry group $SU(N)_L \times SU(N)_R \times U(1)_L \times U(1)_R$ where N stands for the number of flavours. As we will see, this chiral symmetry is approximatively respected only by the light quarks that is for the two and three flavours cases where $N = 2$ and $N = 3$. The aim of this section is to introduce the chiral symmetry as well as its explicit breaking by the current masses. We will also present briefly the axial $U(1)_A$ anomaly and finally the spontaneous breaking of the chiral symmetry.

2.2.1 Global symmetries of QCD

Let us start by introducing the global symmetries of QCD. As already mentioned above, all flavours of quarks behaves equally with respect to the $SU(3)_c$ gauge theory and the only distinction between them comes from their masses. Looking at the current masses, we can separate the different flavours in two categories: the light quarks (u, d, s) for which the masses are well below 1 GeV (roughly the

[1] The term current masses refers to the masses involved in the divergence of the currents (see Eq. (2.2.27) for instance) while the constituent masses are the dynamical masses generated after the spontaneous breaking of the chiral symmetry. For example, the current mass of the up quark is of the order of few MeV and the corresponding constituent mass is of the order of 300 MeV $\sim \Lambda_{QCD}$.

QCD scale of condensation Λ_{QCD}) and the heavy quarks (c, b, t) for which the masses are around 1 GeV or even well above. Then we have the following picture

$$\begin{pmatrix} m_u \simeq 2-3 \text{ MeV} \\ m_d \simeq 4-6 \text{ MeV} \\ m_s \simeq 80-130 \text{ MeV} \end{pmatrix} \ll 1 \text{ GeV} < \begin{pmatrix} m_c \simeq 1.3 \text{ GeV} \\ m_b \simeq 4 \text{ GeV} \\ m_t \simeq 170 \text{ GeV} \end{pmatrix} . \tag{2.2.1}$$

Let us first consider the QCD Lagrangian without mass terms

$$\mathcal{L}^0_{QCD} = \sum_q (\overline{q}_L i\gamma^\mu D_\mu q_L + \overline{q}_R i\gamma^\mu D_\mu q_R) - \frac{1}{4} G^{\mu\nu}_a G^a_{\mu\nu} . \tag{2.2.2}$$

We will come back to the issue of the masses in the subsection 2.2.2. Note that to highlight the global symmetries of QCD, we have written the Lagrangian $\mathcal{L}^0_{QCD}$ in term of left and right-handed fields ($q_{R,L} = P_{R,L}\ q$ and $\overline{q}_{R,L} = \overline{q}\ P_{L,R}$). In all generality, we have the following decompositions

$$\overline{q}\ \Gamma q = \begin{cases} \overline{q}_R \Gamma q_R + \overline{q}_L \Gamma q_L & \text{for } \Gamma = \{\gamma^\mu, \gamma^\mu\gamma_5\} \\ \overline{q}_R \Gamma q_L + \overline{q}_L \Gamma q_R & \text{for } \Gamma = \{\mathbb{1}, \gamma_5, \sigma^{\mu\nu}\} \end{cases} , \tag{2.2.3}$$

where the Γ matrix stands for the 16 independent Dirac contractions. From the Lagrangian of Eq. (2.2.2) it is easy to check the invariance under the global symmetry $SU(N)_L \times SU(N)_R \times U(1)_L \times U(1)_R$. Indeed, the $SU(N)_L$ and $SU(N)_R$ transformations are defined as

$$\underline{SU(N)_{L,R}}: \qquad \Psi_{L,R} \to U_{L,R}\ \Psi_{L,R} = \exp\left(i \sum_{a=1}^{N^2-1} \alpha^a_{L,R} T^a \right) \Psi_{L,R} , \tag{2.2.4}$$

where the matrices T^a are the generators of $SU(N)$ and Ψ is a flavour multiplet with N components ie $\Psi = (u, d, s, \cdots)^T$. For the two flavour case ($N = 2$), $\Psi = (u, d)^T$ and $T^a = \sigma^a/2$ where σ^a are the usual Pauli matrices while for the three flavours case ($N = 3$), $\Psi = (u, d, s)^T$ and $T^a = \lambda^a/2$ where λ^a are the Gell-Mann matrices listed in section 2.1. In the same way, for the $U(1)_L$ and $U(1)_R$ transformations we have

$$\underline{U(1)_L}: \quad \Psi_L \to e^{i\alpha_L}\Psi_L , \quad \Psi_R \to \Psi_R , \qquad \underline{U(1)_R}: \quad \Psi_R \to e^{i\alpha_R}\Psi_R , \quad \Psi_L \to \Psi_L , \tag{2.2.5}$$

where the exponentials implicitly contain an identity in the flavour space ie $\mathbb{1}_N$ and not the generator of $U(N)$ normalised as $T^0 = \mathbb{1}_N/\sqrt{2N}$. This normalisation leads to entire $U(1)$-charges for the quarks fields (see table 2.1). In terms of the flavour multiplet Ψ, the Lagrangian of Eq. (2.2.2) can be rewritten as follow

$$\mathcal{L}^0_{QCD} = \overline{\Psi} i\gamma^\mu D_\mu \Psi - \frac{1}{4} G^{\mu\nu}_a G^a_{\mu\nu} = (\overline{\Psi}_L i\gamma^\mu D_\mu \Psi_L + \overline{\Psi}_R i\gamma^\mu D_\mu \Psi_R) - \frac{1}{4} G^{\mu\nu}_a G^a_{\mu\nu} . \tag{2.2.6}$$

Note that, to look at the global invariance of the Lagrangian in Eq. (2.2.2), it can be useful to define transformations directly on the fields Ψ and not on its left and right-handed parts. Indeed, as we will see these symmetries are the relevant ones in the low energy regime where the chiral symmetry is spontaneously broken. From Eq. (2.2.4), one defines the vector and axial transformations as follow

$$\underline{SU(N)_V}: \qquad \Psi \equiv \begin{pmatrix} \Psi_L \\ \Psi_R \end{pmatrix} \to \begin{pmatrix} e^{i\alpha^a_L T^a}\Psi_L \\ e^{i\alpha^a_L T^a}\Psi_R \end{pmatrix} = U_V\ \Psi = \exp\left(i \sum_{a=1}^{N^2-1} \alpha^a_V T^a \right) \Psi , \tag{2.2.7}$$

$$\underline{SU(N)_A}: \qquad \Psi \to \begin{pmatrix} e^{i\alpha^a_L T^a}\Psi_L \\ e^{-i\alpha^a_L T^a}\Psi_R \end{pmatrix} = U_A\ \Psi = \exp\left(i \sum_{a=1}^{N^2-1} \alpha^a_A T^a \gamma_5 \right) \Psi . \tag{2.2.8}$$

The vector $SU(N)_V$ transformations corresponds to $\alpha^a_L = \alpha^a_R \equiv \alpha^a_V$ while the axial $SU(N)_A$ transformation corresponds to $\alpha^a_L = -\alpha^a_R \equiv \alpha^a_A$. Then the transformations $SU(N)_L \times SU(N)_R$ are equivalent

to $SU(N)_V \times SU(N)_A$. Similarly, the $U(1)_L \times U(1)_R$ transformations are equivalent to $U(1)_V \times U(1)_A$ which are defined as follow

$$\underline{U(1)_V}: \qquad \Psi \to e^{i\alpha_V}\Psi \ , \qquad\qquad \underline{U(1)_A}: \qquad \Psi \to e^{i\alpha_A\gamma_5}\Psi \ . \tag{2.2.9}$$

At low energy, the $SU(N)_V \times U(1)_V$ symmetry remains [2] unbroken while $SU(N)_A \equiv [SU(N)_L \times SU(N)_R]/SU(N)_V$ is spontaneously broken. Note that $U(1)_A$ is explicitly broken by the gauge anomaly (see subsection 2.2.4) and should not be considered as a symmetry of QCD. Transformations of the quark fields under $U(1)_A$ induce a shift of θ in Eq. (2.1.9). From Eqs. (2.2.5) and (2.2.9) we obtain the $U(1)$-charges of the left and right-handed quark fields. They are listed in table 2.1.

	$U(1)_L$	$U(1)_R$	$U(1)_V$
q_L	1	0	1
q_R	0	1	1
$\overline{q}_L$	-1	0	-1
$\overline{q}_R$	0	-1	-1

Table 2.1: The $U(1)$-charges of the left and right-handed quarks.

2.2.2 Explicit breaking by the quark current masses

We now consider the issue of the quark current masses by adding an additional mass term of the form $m\overline{\Psi}\Psi = m(\overline{\Psi}_R\Psi_L + \overline{\Psi}_L\Psi_R)$ in Eq. (2.2.6). For simplicity we first consider that all flavours of quarks have a same current mass m. This mass term is not a chiral invariant as it mixes the left and right-handed chiralities. More precisely, one can check that $\overline{\Psi}\Psi$ respects the vector symmetries but breaks the axial ones. Indeed, the infinitesimal transformation of the mass term under $SU(N)_A$ is

$$\underline{SU(N)_A}: \qquad \overline{\Psi}\Psi \to \overline{\Psi}\Psi + 2i\alpha_A^a\ \overline{\Psi}\gamma_5 T^a\Psi = \overline{\Psi}\Psi + 2\sqrt{2N}\alpha_A^a P^a \ , \tag{2.2.10}$$

where P^a is the non-singlet pseudo-scalar densities defined in Eq. (2.2.28). Then, the chiral symmetry is approximatively realised when a small explicit breaking mass is present as it is the case for the quarks $q = u, d$ and s for which $m_q \ll \Lambda_{QCD}$. This feature justify to restrict to the $N = 2$ and $N = 3$ cases where the chiral symmetry is a good approximation.

We now consider the more realistic case where the current quark masses are different. The relevant Lagrangian encoding the explicit breaking is

$$\mathcal{L}_M = -\overline{\Psi}\mathcal{M}\Psi = -(\overline{\Psi}_R\mathcal{M}\Psi_L + \overline{\Psi}_L\mathcal{M}\Psi_R) \ , \qquad \mathcal{M} = \begin{pmatrix} m_u & 0 & 0 \\ 0 & m_d & 0 \\ 0 & 0 & m_s \end{pmatrix} \ , \tag{2.2.11}$$

where $\mathcal{M}$ is the current quark mass matrix in the three flavours case. The restriction to the two flavour case is obtained by taking $m_s = 0$. The Lagrangian in Eq. (2.2.11) transforms as follow under the $SU(N)_A$

$$\underline{SU(N)_A}: \qquad \overline{\Psi}\mathcal{M}\Psi \to \overline{\Psi}\mathcal{M}\Psi + i\alpha_A^a\ \overline{\Psi}\gamma_5\{\mathcal{M}T^a, T^a\mathcal{M}\}\Psi \ . \tag{2.2.12}$$

The transformation under $SU(1)_V$ is obtained by replacing the anti-commutator by a commutator. Then, $\mathcal{L}_M$ explicitly breaks the axial symmetries as before but it also breaks $SU(N)_V$ if $\mathcal{M}$ is not proportional to the identity matrix, that is, for different current masses. On the contrary, the $U(1)_V$ symmetry remains unbroken in any case insuring the conservation of the number of quarks. Note that the explicit breaking of $SU(2)_V$ is smaller compared to the one of $SU(3)_V$ as $m_u \simeq m_d \ll m_s$.

[2] Up to explicit breaking terms.

Let us make some comments on CHMs. In these cases, explicit breaking mass terms can a priori be present. However, as no resonance has been observed yet, it is not relevant to enter in the details by considering different current masses and we will always consider a diagonal mass matrix $\mathcal{M} = m\mathbb{1}$ (see chapter 9) such that the vector symmetries are not explicitly broken.

2.2.3 Noether theorem, currents and densities

In this subsection, we remind the Noether theorem and then derive the currents and densities of QCD. The Noether theorem connects the continuous global symmetries of a dynamical system to the conserved quantities ie the constants of motion. Let us start with a Lagrangian $\mathcal{L}$ depending on n independent fields Φ_i and their first partial derivatives $\partial_\mu \Phi_i$

$$\mathcal{L} = \mathcal{L}(\Phi_i, \partial_\mu \Phi_i) \ , \qquad\qquad i = 1 \cdots n \ . \tag{2.2.13}$$

From the above Lagrangian, we obtain n equations of motion through the Euler-Lagrange equation

$$\frac{\partial \mathcal{L}}{\partial \Phi_i} - \partial_\mu \frac{\partial \mathcal{L}}{\partial \partial_\mu \Phi_i} = 0 \ . \tag{2.2.14}$$

We assume that the Lagrangian of Eq. (2.2.13) is invariant under a continuous global symmetry. In order to identify the Noether currents associated with this symmetry, we promote it to a local symmetry. In that case, the fields Φ_i transform as follow

$$\Phi_i(x) \to \Phi_i'(x) = \Phi_i(x) + \delta\Phi_i(x) = \Phi_i(x) + i\varepsilon_a(x) F_{ai}[\Phi(x)] \ , \tag{2.2.15}$$

where $\Phi(x)$ denotes collectively all the fields $\Phi_i(x)$ and the higher order ε terms have been neglected. The variation of the Lagrangian under the local transformation is

$$\begin{aligned} \delta\mathcal{L} &= \mathcal{L}(\Phi', \partial_\mu \Phi') - \mathcal{L}(\Phi, \partial_\mu \Phi) = \frac{\partial \mathcal{L}}{\partial \Phi_i}\delta\Phi_i + \frac{\partial \mathcal{L}}{\partial \partial_\mu \Phi_i}\partial_\mu \delta\Phi_i \\ &= \varepsilon_a \left(i\frac{\partial \mathcal{L}}{\partial \Phi_i} F_{ai} + i\frac{\partial \mathcal{L}}{\partial \partial_\mu \Phi_i}\partial_\mu F_{ai} \right) + \partial_\mu \varepsilon_a \left(i\frac{\partial}{\partial \partial_\mu \Phi_i} F_{ai} \right) \\ &\equiv -\varepsilon_a \ \partial_\mu J_a^\mu - \partial_\mu \varepsilon_a \ J_a^\mu \ , \end{aligned} \tag{2.2.16}$$

From the above equation, we define the current corresponding to the transformation of Eq. (2.2.15) as well as its divergence

$$J_a^\mu = i\frac{\partial \mathcal{L}}{\partial \partial_\mu \Phi_i} F_{ai} \ , \qquad\qquad \partial_\mu J_a^\mu = i\frac{\partial \mathcal{L}}{\partial \Phi_i} F_{ai} + i\frac{\partial \mathcal{L}}{\partial \partial_\mu \Phi_i}\partial_\mu F_{ai} \ . \tag{2.2.17}$$

One can check using the Euler-Lagrange equation that taking the divergence of J_a^μ, one obtain the above result. From the last line of Eq. (2.2.16) we obtain more useful definitions of the current and its divergence

$$J_a^\mu = -\frac{\partial \delta\mathcal{L}}{\partial \partial_\mu \varepsilon_a} \ , \qquad\qquad \partial_\mu J_a^\mu = -\frac{\partial \delta\mathcal{L}}{\partial \varepsilon_a} \ , \tag{2.2.18}$$

which can then be computed in general from $\delta\mathcal{L}$. To derive the above relations, we assumed the transformation to be local. However, the Lagrangian of Eq. (2.2.13) is only globally invariant by hypothesis. Then $\partial_\mu \varepsilon_a = 0$ and from Eq. (2.2.16) we have $\delta\mathcal{L} = -\varepsilon_a \partial_\mu J_a^\mu = 0$ which means that the current J_a^μ is conserved. For a conserved current, the charge is time independent ($Q_a(t) = Q_a$) and defined in general as

$$Q_a(t) = \int d^3x J_a^0(t, \vec{x}) \ . \tag{2.2.19}$$

We now derive the currents of QCD and their divergences from Eq. (2.2.18). Let us first consider the case with zero current quarks masses. The variation of the Lagrangian $\mathcal{L}_{QCD}^0$ of Eq. (2.2.2) under the transformations $SU(N)_L \times SU(N)_R \times U(1)_L \times U(1)_R$ is

$$\delta\mathcal{L}_{QCD}^0 = -\overline{q}_R \left(\sum_{a=1}^{8} \partial_\mu \alpha_R^a T^a + \partial_\mu \alpha_R \right) \gamma^\mu q_R + (L \leftrightarrow R) \ . \tag{2.2.20}$$

From the above relation and Eq. (2.2.18) we then derive the following currents

$$L^\mu_a = -\frac{\partial\delta\mathcal{L}^0_{QCD}}{\partial\partial_\mu\alpha^a_L} = (\overline{q}_L\gamma^\mu T^a q_L)\ , \qquad R^\mu_a = -\frac{\partial\delta\mathcal{L}^0_{QCD}}{\partial\partial_\mu\alpha^a_R} = (\overline{q}_R\gamma^\mu T^a q_R)\ , \tag{2.2.21}$$

$$L^\mu = -\frac{\partial\delta\mathcal{L}^0_{QCD}}{\partial\partial_\mu\alpha_L} = (\overline{q}_L\gamma^\mu q_L)\ , \qquad R^\mu = -\frac{\partial\delta\mathcal{L}^0_{QCD}}{\partial\partial_\mu\alpha_R} = (\overline{q}_R\gamma^\mu q_R)\ , \tag{2.2.22}$$

while the corresponding divergences are zero because we do not consider explicit breaking by the quark masses ie $\delta\mathcal{L}^0_{QCD} = 0$. For the non-singlet vector and axial-vector currents one has from the above equations

$$V^{\mu a} = R^{\mu a} + L^{\mu a} = (\overline{q}\gamma^\mu T^a q)\ , \qquad A^{\mu a} = R^{\mu a} - L^{\mu a} = (\overline{q}\gamma^\mu\gamma_5 T^a q)\ , \tag{2.2.23}$$

and similarly for the singlet currents replacing the generators T^a by the identity matrix. Note that the divergence of A^μ is in fact different from zero, even in the chiral limit, due to the axial anomaly. This feature will be addressed in subsection 2.2.4. Note also that we can check the above relations directly from Eq. (2.2.18) and

$$\delta\mathcal{L}^0_{QCD} = -\overline{q}\gamma^\mu\left(\sum_{a=1}^{8}\partial_\mu\alpha^a_V T^a + \partial_\mu\alpha_V\right)q - \overline{q}\gamma^\mu\gamma_5\left(\sum_{a=1}^{8}\partial_\mu\alpha^a_A T^a + \partial_\mu\alpha_A\right)q\ . \tag{2.2.24}$$

We now consider the mass term of Eq.(2.2.11). The variation of $\mathcal{L}_M$ under the left and right-handed transformation is given by

$$\begin{aligned}\delta\mathcal{L}_M &= i\left[\overline{q}_R\left(\sum_{a=1}^{8}\alpha^a_R T^a + \alpha_R\right)\mathcal{M}q_L - \overline{q}_R\mathcal{M}\left(\sum_{a=1}^{8}\alpha^a_L T^a + \alpha_L\right)q_L + (R\leftrightarrow L)\right] \\ &= i\left[\sum_{a=1}^{8}\alpha^a_R\left(\overline{q}_R T^a\mathcal{M}q_L - \overline{q}_L\mathcal{M}T^a q_R\right) + \alpha_R\left(\overline{q}_R\mathcal{M}q_L - \overline{q}_L\mathcal{M}q_R\right) + (R\leftrightarrow L)\right]\ ,\end{aligned} \tag{2.2.25}$$

As $\delta\mathcal{L}_M$ depends only on $\alpha^a_R, \alpha^a_L, \cdots$ and not on their derivatives, the currents are the same than before. However the divergences receive a non-zero contribution from $\delta\mathcal{L}_M$. For instance, for the non-singlet currents we have

$$\begin{aligned}\partial_\mu L^{\mu a} &= -\frac{\partial\delta\mathcal{L}_M}{\partial\alpha^a_L} = -i\left(\overline{q}_L T^a\mathcal{M}q_R - \overline{q}_R\mathcal{M}T^a q_L\right)\ , \\ \partial_\mu R^{\mu a} &= -\frac{\partial\delta\mathcal{L}_M}{\partial\alpha^a_R} = -i\left(\overline{q}_R T^a\mathcal{M}q_L - \overline{q}_L\mathcal{M}T^a q_R\right)\ ,\end{aligned} \tag{2.2.26}$$

and similarly for the singlet currents replacing the generators T^a by the identity matrix. The corresponding divergences for the vector and axial currents are

$$\begin{aligned}\partial_\mu V^{\mu a} &= -i\overline{q}_R[T^a,\mathcal{M}]q_L - i\overline{q}_L[T^a,\mathcal{M}]q_R = i\overline{q}[\mathcal{M},T^a]q\ , \\ \partial_\mu A^{\mu a} &= i\overline{q}_L\{T^a,\mathcal{M}\}q_R - i\overline{q}_R\{T^a,\mathcal{M}\}q_L = i\overline{q}\gamma_5\{T^a,\mathcal{M}\}q\ , \\ \partial_\mu A^{\mu} &= 2i\overline{q}\gamma_5\mathcal{M}q + \frac{g_s^2 N}{32\pi^2}\epsilon_{\mu\nu\rho\sigma}G^{\mu\nu}_a G^{\rho\sigma}_a\ ,\end{aligned} \tag{2.2.27}$$

where the $U(1)_A$ anomaly, discussed in subsection 2.2.4, has also been taken into account in the last line and the $U(1)_V$-current is conserved such that $\partial_\mu V^\mu = 0$. Then we explicitly check the results of subsection 2.2.2: the axial symmetries are explicitly broken by the quark masses as $\partial_\mu A^{\mu a}$ and $\partial_\mu A^\mu$ [3] become non-zero when $\mathcal{M}\neq 0$ and the $SU(N)_V$ symmetry is explicitly broken when $\mathcal{M}$ is not proportional to the identity matrix that is when the current quark masses are different. More precisely, the broken currents $V^{\mu a}$ are the ones corresponding to $[\mathcal{M},T^a]\neq 0$. Then in the two flavours

[3] Up to the anomaly.

case where $m_u \simeq m_d$ is a good approximation, one can consider that all of the vector currents are conserved. On the other hand, in the three flavours case where $m_u \simeq m_d < m_s$, only the currents with diagonal generators ($a = 3, 8$) and the currents with generators of the two flavours sector ($a = 1, 2$) are unbroken.

To summarise the various approximate global symmetries of the strong interactions, we have for the realistic three flavours case

- In the limit of massless quarks commonly called chiral limit, the sixteen currents L^a_μ and R^a_μ or alternatively V^a_μ and A^a_μ are conserved. This is also true for V_μ while the singlet axial-vector current A_μ has an anomaly.

- The individual flavour currents $\overline{u}\gamma^\mu u$, $\overline{d}\gamma^\mu d$ and $\overline{s}\gamma^\mu s$ (V^μ being the sum of these currents) are always conserved for any values of the quark masses. This feature reflects the fact that the strong interactions are flavour independent and that the quark mass matrix $\mathcal{M}$ is diagonal.

- The axial currents A^a_μ and A_μ have a non-zero divergence due to the current quark masses $m_q \neq 0$ (in addition to the anomaly for the singlet).

- In the case of equal masses $m_u = m_d = m_s$, the eight vector currents V^a_μ are conserved as $[T^a, \mathbb{1}] = 0$ while the eight axial-vector currents A^a_μ are not conserved as $\{T^a, \mathbb{1}\} = 2T^a$.

- In the case where $m_u = m_d \neq m_s$, the $SU(3)_V$ flavour symmetry reduces to the $SU(2)_V$ isospin symmetry. The latter symmetry is explicitly broken by $m_u \neq m_d$ but this effect is small compare to the breaking of $SU(3)_V$.

For latter use, we define the scalar and pseudo-scalar [4] singlet and non-singlet densities

$$S^0 = (\overline{q}T^0 q)\ , \qquad P^0 = (\overline{q}i\gamma_5 T^0 q)\ , \qquad S^a = (\overline{q}T^a q)\ , \qquad P^a = (\overline{q}i\gamma_5 T^a q)\ . \tag{2.2.28}$$

We now derive the equal-time commutation relations involving the charges and the currents (densities). Let us first consider the following commutation relation $[ab, cd] = a\{b, c\}d - ac\{b, d\} + \{a, c\}db - c\{a, d\}b$, from which we obtain

$$\begin{aligned} \int d^3\vec{x}\ [\overline{\Psi}(t,\vec{x})\Gamma_1 F_1 \Psi(t,\vec{x}),\ \overline{\Psi}(t,\vec{y})\Gamma_2 F_2 \Psi(t,\vec{y})] \\ = \overline{\Psi}(t,\vec{y})\big[\Gamma_1\gamma^0\Gamma_2 F_1 F_2 - \Gamma_2\gamma^0\Gamma_1 F_2 F_1\big]\Psi(t,\vec{y})\ , \end{aligned} \tag{2.2.29}$$

where Γ stands for any Dirac matrices of Eq. (2.2.3) and F is a flavour contraction. We have also used the equal-time anti-commutation relations of the quark fields

$$\{\Psi_{\alpha i}(t,\vec{x}), \Psi^\dagger_{\beta j}(t,\vec{y})\} = \delta^3(\vec{x}-\vec{y})\delta_{\alpha\beta}\delta_{ij}\ , \qquad \{\Psi_{\alpha i}(t,\vec{x}), \Psi_{\beta j}(t,\vec{y})\} = 0\ . \tag{2.2.30}$$

From Eq. (2.2.30), we derive for instance the commutation relation between the axial charge and the vector current

$$\begin{aligned} [Q^a_A(t), V^{\mu b}(t,\vec{y})] &= \int d^3\vec{x}\ [A^{0a}(t,\vec{x}), V^{\mu b}(t,\vec{y})] \\ &= \int d^3\vec{x}\ [\overline{q}(t,\vec{x})\gamma^0\gamma_5 T^a q(t,\vec{x}), \overline{q}(t,\vec{y})\gamma^\mu T^b q(t,\vec{y})] \\ &= \overline{q}(t,\vec{y})\gamma^\mu\gamma_5[T^a, T^b]q(t,\vec{y}) = if^{abc}A^{\mu c}(t,\vec{y})\ , \end{aligned} \tag{2.2.31}$$

where we have used the commutation relation between the generators $[T^a, T^b] = if^{abc}T^c$. Note that the commutation relation $[Q^a_A(t), A^{\mu b}(t,\vec{y})]$ can be obtained from the above equation by replacing the

[4] Note that the factor i in the pseudo-scalar density P^a insures its hermitianity that is $(P^a)^\dagger = P^a$ and similarly for the singlet density P^0.

axial current $A^{\mu c}$ by the vector current $V^{\mu c}$ in the left-hand side. In the same way, the commutation relation between the axial charge and the scalar density is given by

$$\begin{aligned}[Q_A^a(t), S^b(t,\vec{y})] &= \int d^3\vec{x}\ [A^{0a}(t,\vec{x}), S^b(t,\vec{y})] = i\ \bar{q}(t,\vec{y}) i\gamma_5 \{T^a, T^b\} q(t,\vec{y}) \\ &= i\left[\sqrt{\frac{2}{N}} P^0(t,\vec{y})\delta^{ab} + d^{abc} P^c(t,\vec{y})\right] . \end{aligned} \tag{2.2.32}$$

The commutator $[Q^a(t), P^b(t,\vec{y})]$ can be obtained from the above relation by replacing the pseudo-scalar densities P^0 and P^a by the scalar densities S^0 and S^a. Similarly, one can obtain all of the commutations relations between the charges and the currents or densities. We just have listed here the ones involving the axial non-singlet charge Q_A^a as they will be relevant in the next. For a more complete list see e.g. Ref. [37].

The above commutation relations are useful for instance to derive the sum rules that we will be presented in subsection 2.4 in the QCD case and in subsection 8.1.4 in the composite Higgs context. In addition, from the example of QCD, one can check the expressions of the currents and densities in another theory than QCD e.g. in the case of UV completions of CHMs.

2.2.4 U(1) axial anomaly

As already mentioned above, the $U(1)_A$ symmetry is not a symmetry of QCD. Indeed, this symmetry is anomalous and its divergence is non-zero even in the chiral limit. One has

$$\partial^\mu A_\mu = 2\ \bar{q} i\gamma_5 \mathcal{M} q + \frac{g_s^2}{32\pi^2} Tr[\mathbb{1}_N] Tr[\{T_c^a, T_c^b\}] \epsilon^{\mu\nu\rho\sigma} G^a_{\mu\nu} G^b_{\rho\sigma} . \tag{2.2.33}$$

The trace $Tr[\{T_c^a, T_c^b\}]$ comes from the quark couplings to gluons while the trace $Tr[\mathbb{1}_N]$ from the flavour. This flavour trace is in fact weighted by the axial charge of the left and right-handed quarks. Explicitly the relevant factor in the divergence is $[Q_A(q_L) - Q_A(q_R)] = 2 \neq 0$ (see figure 2.1) where the two chiralities contribute with a relative sign as mentioned in section 1.4. Then it is easy to see

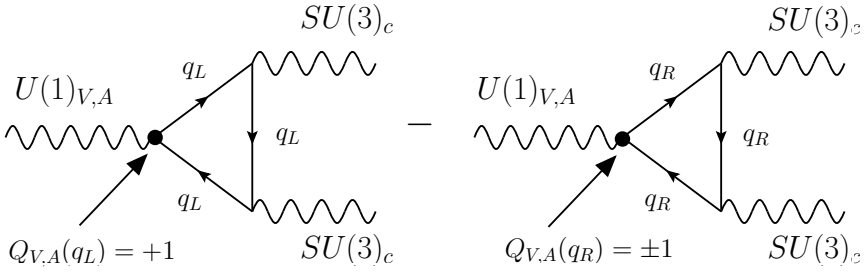

Figure 2.1: Contribution of the left-handed and right-handed quarks to the axial U(1) anomaly.

that $U(1)_V$ is non-anomalous as the flavour trace involves $[Q_V(q_L) - Q_V(q_R)] = 0$. In the same way, for $SU(N)_{V,A}$ the trace in the flavour space is $Tr[T^a] = 0$ and these symmetries are not anomalous. Writing explicitly the traces, the divergence of Eq. (2.2.33) becomes

$$\partial^\mu A_\mu = 2\ \bar{q} i\gamma_5 \mathcal{M} q + \frac{g_s^2}{32\pi^2} N \epsilon^{\mu\nu\rho\sigma} G^a_{\mu\nu} G^b_{\rho\sigma} . \tag{2.2.34}$$

Note that $\partial^\mu A_\mu$ is proportional to the number of Dirac fermions N present in the theory and in the large N_c limit, the anomaly cancel as $g_s \sim 1/\sqrt{N_c}$ [5].

This $U(1)$ anomaly is an important feature of QCD. For instance, it is responsible of the much larger mass of the η' compare to the other Goldstone bosons. In the same way, anomalous symmetries are an important feature in the UV completions of CHMs.

[5] The cancellation of the axial anomaly in the large N_c limit comes from the independence of the Dynkin index with respect to N_c. This feature is valid for the fundamental representation as $C(F) = 1/2$ but it can be modified with higher dimensional representations for which the Dynkin index depends on N_c (see section 9.1).

2.2.5 Spontaneous breaking of the chiral symmetry

As we have seen in the precedent subsections, the QCD Lagrangian possesses a global invariance under the chiral group $SU(N)_L \times SU(N)_R \times U(1)_V$ or equivalently under $SU(N)_V \times SU(N)_A \times U(1)_V$. However, at low energy the QCD spectrum does not reflect all of these symmetries. Indeed, the resonances organised in multiplets of $SU(N)_V$ rather than in multiplets of $SU(N)_L \times SU(N)_R$. For instance, in the three flavour case, the lightest pseudo-scalar mesons organised into an octet $(\pi^\pm, \pi^0, K^0, \overline{K}^0, K^\pm, \eta)$ and a singlet η' of $SU(3)_V$. In the two flavours case, the octet reduces to the triplet of pions $(\pi^\pm, \pi^0)$. Then, at low energy the chiral symmetry is spontaneously broken. This breaking occurs below the scale of condensation $\Lambda_{QCD} \simeq 1$ GeV where the colour confines and $SU(3)_c$-singlet resonances form. The spontaneous breaking is due to non-zero order parameters, that is, to parameters with a non-zero vacuum expectation value. In QCD, one of the most relevant order parameter is the two fermions condensate $\langle \overline{q}q \rangle$. The latter transforms with respect to the chiral symmetry like the explicit breaking term presented in subsection 2.2.2. However, it is not an explicit breaking term such that the condensate $\langle \overline{q}q \rangle$ spontaneously breaks the axial $SU(N)_A$ symmetry.

According to the Golstone theorem, the QCD spectrum contains $(N^2 - 1)$ pNGBs. For $N = 3$, they correspond to the pseudo-scalar octet mentioned above and for $N = 2$ to the triplet of pions. Note that these pseudo-scalar are not exact NGBs as a consequence of the current masses which explicitly break the chiral symmetry. Of course, in this respect the pions are the lightest pNGBs as the associated current masses are $m_{u,d}$ while for the other pNGBs are also associated to m_s. An important feature of the spontaneous breaking is that the pNGBs belonging to the the coset space $SU(N)_A \equiv SU(N)_L \times SU(N)_R / SU(N)_V$ couple to the broken currents, that is, to the axial currents A^a_μ

$$\langle 0 | J^{\mu a} | G^b(p) \rangle = i p^\mu F_G \delta^{ab} \ , \tag{2.2.35}$$

where F_G is the decay constant of the pNGBs G^a and it is also an order parameter. When $SU(N)_V$ is explicitly broken, the above picture is slightly modified as there are several Goldstone decay constants. For instance, in the $N = 2$ case we have in a good approximation only one decay constant that is F_π while in the three flavours case we have F_π and F_K.

Finally, let us now make some further comments on the above pattern of symmetry breaking. First, QCD belongs to the particular class of vector-like theories. Indeed, the latter are asymptotically free and confining gauge theories with a set of N Dirac fermions transforming under a representation of the gauge group, in such a way that it is possible to make all fermions massive in a gauge invariant way. Moreover, the Vafa-Witten theorem [38] states that: *"in any vector-like theory with massless fermions and vanishing vacuum angles, the subgroup H_m of the flavour group G_F that corresponds to the remaining global symmetry when all fermions flavours are given identical gauge invariant masses, cannot be spontaneously broken."* According to this theorem, one can infer that if G_F is spontaneously broken toward some subgroup H_F, then $H_m \subseteq H_F$. In vector-like theories, H_m corresponds to the maximal subgroup of G_F and consequently there is only three possible pattern of symmetry breaking: $G_F = SU(N) \times SU(N)'$ and $H_F = H_m = SU(N)_V$; $G_F = SU(2N)$ and $H_F = SO(2N)$ (real case) or $H_F = Sp(2N)$ (pseudo-real case). QCD corresponds to the first case [6] and as a result, the chiral $SU(N)_L \times SU(N)_R$ symmetry should be spontaneously broken down to $SU(N)_V$ and not to another subgroup.

2.3 't Hooft anomaly matching

The Vafa-Witten theorem restricts the chiral symmetry of QCD to be spontaneously broken to its diagonal subgroup $SU(N)_V \times U(1)_V$. However, this is not a proof that the breaking occurs as the theory could in principle remains in an unbroken phase. Of course we know that it is not the case as all of the hadrons organised into multiplets of $SU(N)_V$ and not of $SU(N)_L \times SU(N)_R$. Anyway, it is interesting to find a way to demonstrate that the breaking occurs. First because we will better

[6] In the chiral limit where the fundamental quarks have no current mass.

understand QCD itself and second because if we have such arguments, we can apply them to other strongly coupled theories like CHMs.

As pointed out by 't Hooft [39], the global anomalies present in the UV theory should match with the ones in the IR theory. In other words, the global anomalies generated before condensation by the fundamental quarks have to be the same than the ones generated by the composite resonances. Then we have conditions, the so called 't Hooft anomaly matching conditions that link the UV theory and the IR theory or equivalently the dynamical degrees of freedom at high energy (quarks) to the ones at low energy (hadrons). These conditions, as we will see, may be helpful to prove that the spontaneous breaking occurs.

The 't Hooft anomaly matching conditions use the fact that the three-point functions of the Noether currents (global currents) receive anomalous contributions from the massless fundamental quarks [40–42] in the UV. These anomalous contributions imply that the corresponding three-point functions have very specific physical singularities at zero momentum transfer [39,43,44]. According to the Coleman-Grossman theorem, this kind of singularities can only be produced by (i) massless spin 1/2 fermions (ii) massless scalars (NGBs) (see figure 2.2). Below the confinement scale, if the global symmetry is not spontaneously broken, the first option is excluded and the theory should produce massless spin 1/2 bound states (baryons). These fermionic bound states will occurs in multiplet of the unbroken global symmetry, and their multiplicities have to be such as to exactly reproduce the coefficients of the anomalies in the three-point functions. If it is not possible to saturate the anomalies with only massless spin 1/2 bound states then massless spin zero bound states coupled to the Noether currents are required. These massless scalars correspond of course to NGBs meaning that the global symmetry is spontaneously broken. Note that if the anomaly matching conditions can be satisfied by massless baryons, the spontaneous breaking is not a necessity but it can not be excluded either. Note also that a crucial point assumed above is that the theory confines otherwise the matching is trivial. We discuss below the 't Hooft anomaly matching in the QCD case and refer to subsections 8.1.2 and 9.1.1 for a discussion in the context of the minimal UV completion of composite Higgs model.

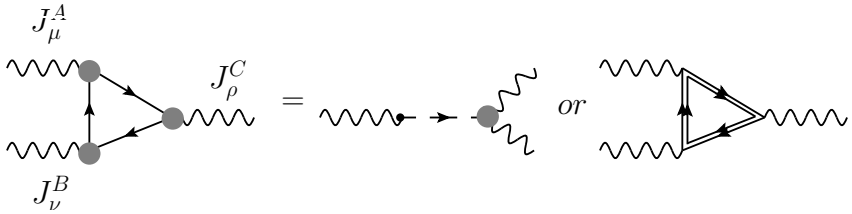

Figure 2.2: Graphical illustration of the Coleman-Grossman theorem: the anomalous contributions to the three point function $\langle J^A_\mu J^B_\nu J^C_\rho \rangle$ and induced by the massless fundamental quarks in the UV can be produced in the IR either by massless scalar or massless spin 1/2 baryons.

In QCD, the left and right-handed quarks transform as follow under the chiral symmetry $SU(N)_L \times SU(N)_R \times U(1)_V$: $q_L \sim (N,1,1)$ and $q_R \sim (1,N,1)$ while a generic spin 1/2 baryon transforms as (l,r,y). The five anomalous diagrams are $SU(N)^3_{L,R}$, $SU(N)^2_{L,R} \times U(1)_V$ and $U(1)^3_V$. The other triangle diagrams involving the remaining combinations of currents do not enter in the anomaly matching as the traces over flavour are trivially zero in these cases ie $Tr[T^a_R] = 0$. Let us consider first the $SU(N)^3_L$ cubic anomaly. The anomaly matching condition is

$$\begin{aligned} \underline{SU(N)^3_L}: \quad \sum_{l,r,y} N(l,r,y)d(r)A(l) &= \sum_{l,r,y>0} N(l,r,y)d(r)A(l) + \sum_{l,r,y<0} N(l,r,y)d(r)A(l) \\ &= \sum_{l,r,y>0} \ell(l,r,y)d(r)A(l) = cte \ , \end{aligned} \tag{2.3.1}$$

where $d(r)$ is the dimension of the representation r (the number of spin 1/2 fermions in the representation l with $U(1)_V$-charge y) and $A(l)$ is the anomaly coefficient associated with the representation l. The latter is given by $2Tr[T^a_{R_l}\{T^b_{R_l}, T^c_{R_l}\}] = A(R_l)d^{abc}$ (see section A) where $T^a_{R_l}$ stands for the generators of $SU(N)_L$ in the representation R_l. In the last equality of Eq. (2.3.1) we have defined

$\ell(l,r,y) \equiv N(l,r,y) - N(\bar{l},\bar{r},-y)$ which stands for the number of spins 1/2 (fermions minus anti-fermions). We have also used $d(\bar{r}) = d(r)$ and $A(\bar{l}) = -A(l)$. In the same way, for the other anomalies we have

$$\underline{SU(N)_R^3}: \qquad \sum_{l,r,y>0} l(l,r,y)d(l)A(r) = cte\ , \tag{2.3.2}$$

$$\underline{SU(N)_L^2 \times U(1)_V}: \qquad \sum_{l,r,y>0} l(l,r,y)C(l)d(r)y = cte\ , \tag{2.3.3}$$

$$\underline{SU(N)_R^2 \times U(1)_V}: \qquad \sum_{l,r,y>0} l(l,r,y)C(r)d(l)y = cte\ , \tag{2.3.4}$$

$$\underline{U(1)_V^3}: \qquad \sum_{l,r,y>0} l(l,r,y)d(l)d(r)y^3 = cte\ , \tag{2.3.5}$$

In the case of $N_c = 3$, the baryons contain three quarks [7] (or antiquarks). We do not consider

(r,l)	$d(r,l)$	$C(r,l)$	$A(r,l)$
$\bullet$	1	0	0
$\square$	N	1/2	1
$\square\square$	$\frac{N(N+1)}{2}$	$\frac{N+2}{2}$	$N+4$
$\begin{smallmatrix}\square\\\square\end{smallmatrix}$	$\frac{N(N-1)}{2}$	$\frac{N-2}{2}$	$N-4$
$\square\square\square$	$\frac{N(N+1)(N+2)}{6}$	$\frac{(N+2)(N+3)}{4}$	$\frac{(N+3)(N+6)}{2}$
$\begin{smallmatrix}\square\\\square\\\square\end{smallmatrix}$	$\frac{N(N-1)(N-2)}{6}$	$\frac{(N-2)(N-3)}{4}$	$\frac{(N-3)(N-6)}{2}$
$\begin{smallmatrix}\square\square\\\square\end{smallmatrix}$	$\frac{N(N^2-1)}{3}$	$\frac{(N^2-3)}{2}$	N^2-9

Table 2.2: The dimensions $d(r,l)$, Dynkin index $C(r,l)$ and anomaly coefficients $A(r,l)$ of the lowest representations of $SU(N)_{r,l}$ involved in the 't Hooft anomaly matching conditions for QCD. The coefficients $C(r,l)$ and $A(r,l)$ are defined in chapter 5.3.3. For the conjugate representations $(\bar{r},\bar{l})$ we have $d(\bar{r},\bar{l}) = d(r,l)$, $C(\bar{r},\bar{l}) = C(r,l)$ and $A(\bar{r},\bar{l}) = -A(r,l)$.

exotic states with more than three quarks for simplicity. It can be justified by the maximal attractive channel (MAC) hypothesis [45] as exotic states like pentaquarks are less likely to form. Then there is only few possibilities for the baryons representations which are listed below

$$\ell(l,r,y) = \Big\{ \ell_{1+}(\square\square\square,\bullet,3),\ \ell_{1-}(\begin{smallmatrix}\square\\\square\\\square\end{smallmatrix},\bullet,3),\ \ell_3(\begin{smallmatrix}\square\square\\\square\end{smallmatrix},\bullet,3),\ \ell_{2+}(\square,\square\square,3),\ +\ell_{2-}(\square,\begin{smallmatrix}\square\\\square\end{smallmatrix},3), \tag{2.3.6}$$
$$+\ell_{4+}(\square\square,\square,3),\ +\ell_{4-}(\begin{smallmatrix}\square\\\square\end{smallmatrix},\square,3),\ \ell_{5+}(\bullet,\square\square\square,3),\ +\ell_{5-}(\bullet,\begin{smallmatrix}\square\\\square\\\square\end{smallmatrix},3),\ +\ell_6(\bullet,\begin{smallmatrix}\square\square\\\square\end{smallmatrix},3)\Big\}\ .$$

We now insert the baryons of Eq. (2.3.6) in the five above matching conditions. The contribution of the fundamental quarks is trivial. For instance, for the cubic $SU(N)_L^3$ anomaly, only the left-handed quarks contribute. As they are in the fundamental representation of $SU(N)_L$, the anomaly coefficient is simply equal to $A(l=\square) = 1$ and their multiplicity is N_c. For the spin 1/2 bound states, only the baryons charged under $SU(N)_L$ contribute, such that their multiplicity is ℓ_i where $i = 1\pm, 2\pm, 3, 4\pm$

[7] Note that a theory with $N_c \neq 3$ can be studied as well with the 't Hooft anomaly matching conditions. However, the baryons with the lowest number of quarks are made of $N_c \neq 3$ quarks in that case such that the details of the matching are completely different.

and their corresponding anomaly coefficients are listed in table 2.2 . Then we have

$$\underline{SU(N)_L^3:} \quad N_c = \ell_{1\pm}\frac{(N\pm3)(N\pm6)}{2} - \ell_{2\pm}\frac{N(N\pm1)}{2} + \ell_3(N^2-9) + \ell_{4\pm}N(N\pm4)\ , \tag{2.3.7}$$

where the minus signs stand for the right-handed baryons. In the same way, for the cubic $SU(N)_R^3$ anomaly we have

$$\underline{SU(N)_R^3:} \quad -N_c = -\ell_{2\pm}N(N\pm4) + \ell_{4\pm}\frac{N(N\pm1)}{2} - \ell_{5\pm}\frac{(N\pm3)(N\pm6)}{2} - \ell_6(N^2-9)\ , \tag{2.3.8}$$

where this time only the baryons charges under $SU(N)_R$ contribute, that is, the baryons with multiplicity $\ell_{2\pm}, \ell_{4\pm}, \ell_{5\pm}$ and ℓ_6. For the $SU(N)_L^2 \times U(1)_V$ anomaly, the anomaly coefficient decomposes into the product of the $U(1)_V$ charge times the Dynkin index of $SU(N)_L$

$$\underline{SU(N)_L^2 \times U(1)_V:} \quad \frac{N_c}{2} = 3\left[\ell_{1\pm}\frac{(N\pm2)(N\pm3)}{4} - \ell_{2\pm}\frac{N(N\pm1)}{4} + \ell_3\frac{(N^2-3)}{2} + \ell_{4\pm}\frac{N(N\pm2)}{2}\right]. \tag{2.3.9}$$

Similarly for the $SU(N)_R^2 \times U(1)_V$ anomaly we have

$$\underline{SU(N)_R^2 \times U(1)_V}: -\frac{N_c}{2} = 3\left[-\ell_{2\pm}\frac{N(N\pm2)}{2} + \ell_{4\pm}\frac{N(N\pm1)}{4} - \ell_{5\pm}\frac{(N\pm2)(N\pm3)}{4} - \ell_6\frac{(N^2-3)}{2}\right]. \tag{2.3.10}$$

Finally, for the cubic $U(1)_V^3$ anomaly, the anomaly coefficients are the cube of the $U(1)_V$ charges and the multiplicities of the baryons correspond to l_i times the dimensions of the representations

$$\underline{U(1)_V^3:} \quad 0 = 3^3\left[\ell_{1\pm}\frac{N(N\pm1)(N\pm2)}{6} - \ell_{2\pm}\frac{N^2(N\pm1)}{2} + \ell_3\frac{N(N^2-1)}{3} + \ell_{4\pm}\frac{N^2(N\pm1)}{2} - \ell_{5\pm}\frac{N(N\pm1)(N\pm2)}{6} - \ell_6\frac{N(N^2\pm1)}{3}\right]. \tag{2.3.11}$$

The zero on the right-hand side of the precedent equation comes from the cancellation between the left and right-handed quarks contributions: $1^3 \times N_c - 1^3 \times N_c = 0$. In fact, this cancellation is expected as only the n-point functions with an odd numbers of axial-vector currents receive anomalous contributions like for instance VVA or AAA while VVV has no anomalous contributions (see section 1.4). The last condition in Eq. (2.3.11) leads to $l_{1\pm} = l_{5\pm}$, $l_{2\pm} = l_{4\pm}$ and $l_3 = l_6$ and only two independent conditions remain

$$\begin{cases} 3 = l_{1\pm}\dfrac{(N\pm3)(N\pm6)}{2} + l_{2\pm}\dfrac{N(N\pm7)}{2} + l_3(N^2-9)\ , \\ 1 = l_{1\pm}\dfrac{(N\pm2)(N\pm3)}{2} + l_{2\pm}\dfrac{N(N\pm3)}{2} + l_3(N^2-3)\ , \end{cases} \tag{2.3.12}$$

In general, for an arbitrary number of flavours N, there are solutions to the precedent system of equations. However, the cases where N is a multiple of 3 are particular. Indeed, in that cases there is no solution and the global symmetry has to be spontaneously broken.

In the two flavours case, however there is a family of solutions as ℓ_{1-} is not present (empty representation), ℓ_{2-} transforms as ℓ_3 as well as ℓ_{4-} transforms as ℓ_6. Then Eq. (2.3.12) becomes

$$\begin{cases} 3 = l_{1+}\dfrac{(N+3)(N+6)}{2} + l_{2\pm}\dfrac{N(N\pm7)}{2} + l_3(N^2-9)\ , \\ 1 = l_{1+}\dfrac{(N+2)(N+3)}{2} + l_{2\pm}\dfrac{N(N\pm3)}{2} + l_3(N^2-3)\ , \end{cases} \tag{2.3.13}$$

and a family of solutions is

$$\ell_{1+} = c_1 \ , \qquad \ell_{2+} = 2 + 5c_2 \ , \qquad \ell_{2-} = 6 + 7c_1 + 17c_2 \ , \qquad \ell_3 = -3 - 3c_1 - 8c_2 \ , \tag{2.3.14}$$

where $c_{1,2}$ are integer numbers.

We have prove that in the realistic and physical case with three flavours of quarks, the chiral symmetry of QCD should be spontaneously broken. However, there is no such proof in the two flavours case and in general for the N-flavours cases. Note that there are some additional arguments, the so-called Appelquist-Carazzone decoupling conditions [46], that allow to demonstrate that the spontaneous breaking occurs in the $N = 2$ case. However, these conditions are less rigorous than the 't Hooft anomaly matching conditions and in practise we will not consider them.

2.4 QCD sum rules

In this section, we derive the QCD sum rules: the well-known Weinberg sum rules [47] but also the scalar sum rules of QCD. These sum rules allow to relate different strong quantities and are then useful to constrain the QCD spectrum. Let us first define in all generality some relevant two points functions. The scalar non-singlet correlatoris defined by

$$i \int d^4x e^{ip\cdot x} \langle 0|T\{S^a(x)S^b(0)\}|0\rangle = \Pi_S(p^2)\delta^{ab} \ , \tag{2.4.1}$$

where we have extracted the flavour tensor structure δ^{ab}. For the non-singlet pseudo-scalar correlator $\Pi_P(p^2)$, we have a similar relation replacing the scalar densities S^a by the pseudo-scalar ones P^a while the singlet correlators Π_{S^0} and Π_{P^0} are obtained by replacing the non-singlet densities by the singlet ones which are S^0 and P^0. In the next, we just present the non-singlet correlators as the extension to the singlet correlators is straightforward. The vector two-points functions are defined by

$$i \int d^4x e^{ip\cdot x} \langle 0|T\{V^a_\mu(x)V^b_\nu(0)\}|0\rangle = [\Pi_V(p^2)(p_\mu p_\nu - \eta_{\mu\nu}p^2) + \Pi^L_V(p^2)p_\mu p_\nu]\delta^{ab} \ , \tag{2.4.2}$$

while the axial correlators $\Pi_A(p^2)$ and $\Pi^L_A(p^2)$ are obtained in a similar way replacing the vector currents V^a_μ by the axial-vector currents A^a_μ. The Lorentz tensor structure in Eq. (2.4.2) can be understand as follows. We have only a simple set of tensors at our disposal, that is, $\{p^\mu, \eta^{\mu\nu}, \epsilon^{\mu\nu\rho\sigma}\}$. Then, the only two independent and non-zero tensors with two uncontracted indices that can be constructed are: $p^\mu p^\nu$ and $\eta^{\mu\nu}$ ($\epsilon^{\mu\nu\rho\sigma}p_\rho p_\sigma = 0$). The two orthogonal combinations of these tensors are $T^{\mu\nu} = (\eta^{\mu\nu} - p^\mu p^\nu/p^2)$ and $L^{\mu\nu} = p^\mu p^\nu/p^2$. They are projectors meaning that $T^{\mu\rho}T^\nu_\rho = T^{\mu\nu}$, $L^{\mu\rho}L^\nu_\rho = L^{\mu\nu}$ and $T^{\mu\rho}L^\nu_\rho = 0$. This decomposition in transverse and longitudinal parts is relevant because when the vector (axial) current is conserved we have $\partial_\mu V^{\mu a} = 0$ ($\partial_\mu A^{\mu a} = 0$) and then $p_\mu \Pi^{\mu\nu}_{V(A)}(p^2) = 0$. Consequently, in that case there is no longitudinal part $[\Pi^L_{V(A)}(p^2) = 0]$ in the two points functions as $T^{\mu\nu}p_\mu = 0$ but $L^{\mu\nu}p_\mu \neq 0$. Note that, in Eqs. (2.4.2) we rather extracted $-p^2T^{\mu\nu}$ and $p^2L^{\mu\nu}$. As we will see in the next, this is useful to have a simpler pole structure for the two point functions.

The two last correlators [8] that we consider are the axial-pseudoscalar and vector-scalar two points functions. For the axial-pseudoscalar correlator we have

$$i \int d^4x e^{ip\cdot x} \langle 0|T\{A^a_\mu(x)P^b(0)\}|0\rangle = \Pi_{AP}(p^2)\delta^{ab}ip^\mu \ . \tag{2.4.3}$$

The equivalent relation for $\Pi_{VS}(p^2)$ is straightforward. When the vector current V^a_μ is conserved, $\Pi_{VS}(q^2) = 0$ while Π_{AP} is different from zero. Note that, as QCD respect parity, the correlators

[8] Note that in principle we can do the same thing for the correlators involving the tensor densities. For example, the tensor structure of the vector-tensor $[\Pi^{\mu\nu\rho}_{VT}(p^2)]$ and axial-tensor $[\Pi^{\mu\nu\rho}_{AT}(p^2)]$ correlators can only contain the following tensors: $p^\mu p^\nu p^\rho, g^{\mu\nu}p^\rho, g^{\mu\rho}p^\nu, g^{\nu\rho}p^\nu$ and $\epsilon^{\mu\nu\rho\sigma}p^\sigma$ where the indices $\mu\nu$ are attached to the tensor density. The antisymmetry of the latter restricts the precedent set to two possibilities: $(g^{\mu\rho}p^\nu - g^{\nu\rho}p^\mu)$ and $\epsilon^{\mu\nu\rho\sigma}p_\sigma$. The first one is associated with VT and the second with AT. In the same way, one finds that TS and TA are zero as there is no antisymmetric tensor with only two uncontracted indices.

PS, AV, VP and AS are zero.

We now turn to the derivation of the sum rules. After the spontaneous breaking of the chiral symmetry, the following matrix elements $\langle 0|[Q_A^a, \theta]|0\rangle$ are interesting as they can be order parameters that is, quantities which becomes non zero when the symmetry is spontaneously broken [9]. Indeed, the axial charges are spontaneously broken and respect $Q_A^a|0\rangle \neq 0$. Let us first consider the possibility $\theta = T\{V_\mu^b(x), A_\nu^c(0)\}$. We obtain

$$\begin{aligned}\langle 0|[Q_A^a, T\{V_\mu^b(x)A_\nu^c(0)\}]|0\rangle &= \langle 0|T\{[Q_A^a, V_\mu^b(x)]A_\nu^c(0) + V_\mu^b(x)[Q_A^a, A_\nu^c(0)]\}|0\rangle \\ &= if^{acd}\langle 0|T\{V_\mu^b(x)V_\nu^d(0)\}]|0\rangle - if^{adb}\langle 0|T\{A_\mu^d(x)A_\nu^c(0)\}]|0\rangle \ , \end{aligned} \tag{2.4.4}$$

where we have used the commutation relations of subsection 2.2.3. Taking the Fourrier transformation [see Eq. (2.4.2)] we obtain

$$i\int d^4x e^{iq.x}\langle 0|[Q_A^a, T\{V_\mu^b(x)A_\nu^c(0)\}]|0\rangle = (q_\mu q_\nu - q^2 g_{\mu\nu})f^{acb}[\Pi_V(q^2) - \Pi_A(q^2)] \neq 0 \ , \tag{2.4.5}$$

where we have assumed to be in the chiral limit such that the longitudinal parts are absent. Then the parameter $\Pi_{V-A}(q^2) \equiv [\Pi_V(q^2) - \Pi_A(q^2)]$ is an order parameter of the spontaneous breaking of the global symmetry. In the same way, we can construct the order parameters involving the scalar and pseudo-scalar densities. For instance

$$i\int d^4x e^{iq.x}\langle 0|[Q_A^a, T\{S^b(x)P^c(0)\}]|0\rangle = d^{abc}[\Pi_S(q^2) - \Pi_P(q^2)] \neq 0 \ , \tag{2.4.6}$$

such that $\Pi_{S-P}(q^2) \equiv [\Pi_S(q^2) - \Pi_P(q^2)]$ is an order parameter [10]. Similarly, Π_{S^0-P} and Π_{S-P^0} are order parameters.

There is other combinations of two point functions which are order parameters like for instance Π_{AP}

$$i\int d^4x e^{iq.x}\langle 0|[Q_A^a, T\{A_\mu^b(x)S^0(0)\}]|0\rangle = i\sqrt{2/N}\delta^{ab}q_\mu\Pi_{AP}(q^2) \ , \tag{2.4.7}$$

However, as a consequence of the Ward identity there is no associated sum rule as the latter correlator is entirely saturated by the Goldstone boson pole

$$\Pi_{AP}(q^2) = \frac{1}{q^2}\frac{\langle S^0\rangle}{\sqrt{N}} \ . \tag{2.4.8}$$

Finally, let us note that when the chiral symmetry is explicitly broken, the notion of order parameters disappear but one can still derive sum rules [11]. For simplicity, we restrict to the chiral case in the next.

As $\Pi_{V-A}, \Pi_{S-P}, \Pi_{S^0-P}$ and Π_{S-P^0} [12] are order parameters of the spontaneous symmetry breaking, they behave smoothly at short distances ($Q^2 \equiv -q^2 > 0$). We have

$$\lim_{Q^2\to+\infty}(Q^2)^2\Pi_{V-A}(-Q^2) = 0 \ , \qquad \lim_{Q^2\to+\infty}Q^2\Pi_{S-P}(-Q^2) = 0 \ , \tag{2.4.9}$$

while Π_{S^0-P} and Π_{S-P^0} behave like Π_{S-P}. These short distance properties can be infer from the operator product expansion (OPE) which gives the behaviour at short distance, for instance of a matrix element of the following form $\langle 0|AB|0\rangle$.

Let us consider for example the vector and axial correlators $\Pi_V(-Q^2)$ and $\Pi_A(-Q^2)$. The OPE is the following

[9] Matrix elements involving the axial $U(1)_A$ charge like $\langle 0|[Q_A, \theta]|0\rangle$ can not be used to derive order parameters as $U(1)_A$ is an anomalous symmetry.

[10] In fact, that is the case only if $d^{abc} \neq 0$. Then, in the two flavours case where $SU(2) \cong Sp(2)$, there is no anomaly coefficient and $\Pi_{S-P}(q^2)$ is not an order parameter.

[11] For instance, when the chiral symmetry is explicitly broken by the current quark masses, one can derive sum rules from $\Pi_V + \Pi_V^L - \Pi_A - \Pi_A^L$ instead of from Π_{V-A} in the chiral limit.

[12] $\Pi_{S^0-P^0}$ is also an order parameter and just a combination of the three other correlators.

- $\Pi_V^{PT}(-Q^2) = \Pi_A^{PT}(-Q^2)$, $\mathcal{O}(Q^0)$,
- $m^2 \mathbb{1}/Q^2$, $\mathcal{O}(Q^{-2})$,
- $m\langle\overline{\Psi}\Psi\rangle/Q^4$, $\langle G^{\mu\nu}G_{\mu\nu}\rangle/Q^4$, $\mathcal{O}(Q^{-4})$,
- $\langle(\overline{\Psi}\Gamma\Psi)(\overline{\Psi}\Gamma'\Psi)\rangle/Q^6$, $m\langle\overline{\Psi}\sigma^{\mu\nu}T^a\Psi G^a_{\mu\nu}\rangle/Q^6$, $f^{abc}\langle G^{\mu a}_{\nu}G^{\nu b}_{\rho}G^{\rho c}_{\mu}\rangle/Q^6$, $\mathcal{O}(Q^{-6})$.

The contribution from perturbation theory is the same for the axial and vector correlators as the global symmetry is not broken perturbatively (the fundamental theory does not feel the spontaneous symmetry breaking). The same feature holds for the gluonic condensate which is a chiral singlet and then contributes in the same way to the axial and vector correlators. Consequently, in the chiral limit ($m = 0$), $\Pi_{V-A}(-Q^2) \sim \mathcal{O}(Q^{-6})$ which leads to the short distance properties of Eq. (2.4.9). Similarly for the scalar and pseudo-scalar correlators we have for instance for the non-singlets $\Pi_S^{PT} = \Pi_P^{PT}$ which is now of order $\mathcal{O}(Q^2)$ due to the pole structure in Eq. (2.4.13) [$\Pi_{V,A}$ have dimension zero while $\Pi_{S,P}$ dimension two.]. Then, as the OPE starts at $\mathcal{O}(Q^2)$, the first non-zero contribution to Π_{S-P} in the chiral limit is at the order Q^{-4} and $\Pi_{S-P}(-Q^2) \sim \mathcal{O}(Q^{-4})$. From the short distance properties of Eq. (2.4.9), we deduce the following convergent spectral sum rules

$$\int_0^\infty dt\ \mathrm{Im}\Pi_{\mathrm{V-A}}(\mathrm{t}) = 0\ , \qquad \int_0^\infty \mathrm{dt\ t\ Im}\Pi_{\mathrm{V-A}}(\mathrm{t}) = 0\ , \tag{2.4.10}$$

$$\int_0^\infty dt\ \mathrm{Im}\Pi_{\mathrm{S-P}}(\mathrm{t}) = 0\ , \qquad \int_0^\infty \mathrm{dt\ t\ Im}\Pi_{\mathrm{S^0-P}}(\mathrm{t}) = 0\ , \qquad \int_0^\infty \mathrm{dt\ t\ Im}\Pi_{\mathrm{S-P^0}}(\mathrm{t}) = 0\ , \tag{2.4.11}$$

where $t = Q^2$ and the sum rule associated to Π_{S-P} is not present in the two flavours case as discussed before. The sum rules of Eq. (2.4.10) are called Weinberg sum rules (WSR) while those in Eq. (2.4.11) are the scalar sum rules of QCD. Assuming that the correlators are saturated by an infinite set of narrow resonances (large N_c limit), the correlators take the form

$$\Pi_V(q^2) = -\sum_V \frac{f_V^2 M_V^2}{q^2 - M_V^2}\ , \qquad \Pi_A(q^2) = -\frac{F_G^2}{q^2} - \sum_A \frac{f_A^2 M_A^2}{q^2 - M_A^2}\ , \tag{2.4.12}$$

$$\Pi_S(q^2) = -\sum_S \frac{G_S^2}{q^2 - M_S^2}\ , \qquad \Pi_P(q^2) = -\frac{G_G^2}{q^2} - \sum_P \frac{G_P^2}{q^2 - M_P^2}\ , \tag{2.4.13}$$

where V and A are non-singlet vector and axial vector resonances while S and P are non-singlet scalar and pseudo-scalar resonances. For the singlet correlators, similar relations hold replacing the non-singlet resonances by singlets ones. In addition to the infinite sums of narrow resonances, there is also the contribution of the massless Golstone bosons G^a in Π_P and Π_A. In the non-chiral limit, they becomes massive and the Goldstone pole moves from $q^2 = 0$ to $q^2 = M_G^2 \neq 0$. In addition, this pole migrates from the transverse part to the longitudinal part of the axial correlator. The above pole structures will be important when we will compute the decay constants ($F_G, f_V, f_A, \cdots$) and the scalar constants ($G_S, G_P, \cdots$) in the context of NJL model. To be complete and for latter use, we also give the form of the axial-pseudoscalar correlator which is entirely saturated by the Goldstone boson pole in the chiral limit

$$\Pi_{AP}(q^2) = -\frac{F_G G_G}{q^2} - \sum_P \frac{F_P G_P}{q^2 - M_P^2}\ . \tag{2.4.14}$$

The spectral densities associated with the above correlators, for instance for the vector and axial-vector channels are given by

$$\rho_V(t) = \mathrm{Im}\Pi_{\mathrm{V}}(\mathrm{t}) = \sum_{\mathrm{V}} \mathrm{f_V^2 M_V^2}\delta(\mathrm{t} - \mathrm{M_V^2})\ , \qquad \rho_{\mathrm{A}}(\mathrm{t}) = \mathrm{Im}\Pi_{\mathrm{A}}(\mathrm{t}) = \mathrm{F_G^2}\delta(\mathrm{t}) + \sum_{\mathrm{A}} \mathrm{f_A^2 M_A^2}\delta(\mathrm{t} - \mathrm{M_A^2})\ , \tag{2.4.15}$$

where the delta functions come from the simple pole structure in the narrow width approximation. Similar relations hold for the scalar and pseudo-scalar densities. Using the Cauchy theorem one has for Π_{V-A}

$$\begin{aligned}\Pi_{V-A}(-Q^2) &= \frac{1}{\pi}\int_{S_0}^{\infty} ds \frac{\rho_V(s)-\rho_A(s)}{s+Q^2} \\ &\sim \frac{1}{Q^2}\frac{1}{\pi}\int_{S_0}^{\infty} dt\ [\rho_V(s)-\rho_A(s)] - \frac{1}{Q^4}\frac{1}{\pi}\int_{S_0}^{\infty} ds\ s\ [\rho_V(s)-\rho_A(s)] + \mathcal{O}(Q^{-6})\end{aligned} \tag{2.4.16}$$

As $\Pi_{V-A} \sim \mathcal{O}(Q^{-6})$, the first two integrals should vanish. Then using the spectral densities in Eq. (2.4.15), one obtains for the two Weinberg sum rules

$$\underline{1^{rst}\text{WSR}}: \quad f_V^2 M_V^2 - f_A^2 M_A^2 - F_G^2 = 0\ , \qquad \underline{2^{nd}\ \text{WSR}}: \quad f_V^2 M_V^4 - f_A^2 M_A^4 = 0\ . \tag{2.4.17}$$

We have assumed that the correlators are saturated by the first resonances such that only the first therm of the infinite sums of narrow resonances is present. One can follows the same procedure for the scalar sum rules, one obtains

$$\underline{S-P}: \quad G_S^2 - G_P^2 = 0\ , \qquad \underline{S^0-P}: \quad G_\sigma^2 - G_P^2 = 0\ , \qquad \underline{S-P^0}: \quad G_S^2 - G_G^2 = 0\ . \tag{2.4.18}$$

Let us make some comments about the above sum rules. The latter are interesting as they give informations about the QCD spectrum in the spin one sector as well as in the spin zero sector. Then, it is relevant to look at the realisation of the sum rules in the context of the NJL model. In this way, from the exact relation in Eqs. (2.4.10) and (2.4.11), one can estimate the validity of the NJL approximation. In addition, the narrow width approximation and the saturation by the lightest resonances leading to Eqs. (2.4.17) and (2.4.18), also gives important informations related to the lightest resonances. These features are discussed in details in section 8.2.7 in the the context of the minimal UV completion of a CHM.

2.5 QCD coupling to the electromagnetism

Up to now, we have only considered QCD in isolation. However, the quarks are electrically charged and $U(1)_{em}$ is embedded inside the chiral symmetry. Then gauging the electromagnetism induces a new source of explicit breaking. There is two main effects of turning on the electromagnetic coupling. First, the charged pNGB will acquire a new contributions to their masses from loops of photons and second, some pNGB will get anomalous couplings to two photons

Let us first present the embedding of $U(1)_{em}$ inside the chiral symmetry. As the electromagnetism is an unbroken gauge symmetry, it should be contained in $U(N)_V$. For the two and three flavours cases we respectively have

$$Q = \tau^3 + \frac{1}{3}\tau^0 = \begin{pmatrix} 2/3 & 0 \\ 0 & -1/3 \end{pmatrix}\ , \qquad Q = T^3 + \frac{1}{\sqrt{3}}T^8 = \begin{pmatrix} 2/3 & 0 & 0 \\ 0 & -1/3 & 0 \\ 0 & 0 & -1/3 \end{pmatrix}\ , \tag{2.5.1}$$

where in the three flavours case, the generators $T^{3,8} = \lambda^{3,8}/2$ are given in section 2.1. Note that the EM charge operator Q is always a combination of diagonal generators.

2.5.1 Radiative corrections to the pion mass

We now consider the first main consequence of gauging the electromagnetism that is the radiative contributions to the masses of the pNGBs [13] . Let us consider the most general possibility. We gauge

[13] Note that in principle, other states than pNGBs are charged under EM and receive radiative corrections. However these corrections can not be calculated in a simple way as it is possible for the pNGBs. In addition, one can argue that pNGBs are the lightest states in the spectrum and the radiative corrections are more important in that case compare to the other resonances.

the following generator $T^{\mathcal{W}} = T^W + T^{\hat{W}}$ which is a combination of unbroken generators T^W and broken generators $T^{\hat{W}}$. The radiative contribution to the masses of the pNGBs $G^{\hat{A}}$ from the above gauging (see subsection 8.1.5) is

$$\Delta M^2_{G^{\hat{A}}} = -\frac{3}{4\pi F_G^2}\frac{g_{\mathcal{W}}^2}{4\pi}\int_0^\infty dQ^2 Q^2 \Pi_{V-A}(Q^2)\left[\sum_{\hat{B}}(f^{\hat{A}W\hat{B}})^2 - \sum_{B}(f^{\hat{A}\hat{W}B})^2\right] , \tag{2.5.2}$$

where according to the Witten inequality, the term $-Q^2\Pi_{V-A}(Q^2)$ is positive. Then the sign of $\Delta M^2_{G^{\hat{A}}}$ is completely determined by the factor on the right-hand side of Eq. (2.5.2), that is by the embedding of $U(1)_{em}$ inside the chiral symmetry. As the EM is not spontaneously broken we have $T^{\mathcal{W}} = T^W$ and $f^{\hat{A}\hat{W}B} = 0$ such that the radiative EM contribution is positive ie $\Delta M_G^2 \geq 0$ and it does not destabilise the QCD potential.

For simplicity, we now restrict to the two flavour case where the pNGBs are $(\pi^0, \pi^\pm)$. The extension to the three flavour case is straightforward. Obviously, only $\pi^\pm$ receive a radiative contribution as they are charged under $U(1)_{em}$. The non-zero group theory factor in Eq. (2.5.2) is given by

$$\sum_{\hat{B}}(f^{\hat{A}W\hat{B}})^2 \equiv \sum_{\hat{B}}\Big(2i\ Tr[T^W[T^{\hat{A}}, T^{\hat{B}}]\Big)^2 = \sum_a \big(2i\ Tr[Q[\tau^\pm, \tau^a]\big)^2 = 1 , \tag{2.5.3}$$

where $\tau^\pm = (\tau^1 \pm i\tau^2)/\sqrt{2}$ corresponds to the generators associated with $\pi^\mp$ [$\pi^+ \sim \overline{\Psi}\tau^-\Psi = (\overline{d}u)/\sqrt{2}$ and $\pi^- \sim \overline{\Psi}\tau^+\Psi = (\overline{u}d)/\sqrt{2}$] and Q is the EM charge operator of Eq. (2.5.1). Then we obtain

$$\Delta M^2_{\pi^\pm} = -\frac{3\alpha}{4\pi F_\pi^2}\int_0^\infty dQ^2 Q^2 \Pi_{V-A}(Q^2) . \tag{2.5.4}$$

We can do the same thing in the three flavours case and compute the radiative contribution to the masses of the pNGBs $K^\pm$. In that case, the relevant generators are $\lambda_4^\pm/2$ (see subsection 3.2.4) [14] and the decay constant F_π should be replaced by F_K. As π^0 receives no EM radiative contribution to its mass, Eq. (2.5.4) gives in fact the difference between the charged and neutral pions masses ie $\Delta M^2_{\pi^\pm} = M^2_{\pi^\pm} - M^2_{\pi^0}$.

We now evaluate quantitatively $\Delta M^2_{\pi^\pm}$. Assuming that the correlator Π_{V-A} is saturated by the first resonances (see section 2.4) we have

$$-Q^2\Pi_{V-A}(Q^2) = F_\pi^2 + Q^2\frac{f_A^2 M_A^2}{Q^2+M_A^2} - Q^2\frac{f_V^2 M_V^2}{Q^2+M_V^2} , \tag{2.5.5}$$

where the vectors V and axial vectors A are the spin-one mesons associated with the generators $\tau^\pm$. Let us for the moment evaluate the integral up to $Q^2 = \Lambda^2$

$$\begin{aligned} -\int_0^{\Lambda^2} dQ^2 Q^2 \Pi_{V-A}(Q^2) \quad &= \quad (F_\pi^2 + f_A^2 M_A^2 - f_V^2 M_V^2)\Lambda^2 + f_V^2 M_V^4 \ln\frac{\Lambda^2+M_V^2}{M_V^2} \\ &\quad - f_A^2 M_A^4 \ln\frac{\Lambda^2+M_A^2}{M_A^2} . \end{aligned} \tag{2.5.6}$$

Using the first and second Weinberg sum rules in Eq. (2.4.17) we obtain

$$-\int_0^\infty dQ^2 Q^2 \Pi_{V-A}(Q^2) \simeq f_V^2 M_V^4 \ln\frac{M_A^2(\Lambda^2+M_V^2)}{M_V^2(\Lambda^2+M_A^2)} \underset{\Lambda^2\to\infty}{\longrightarrow} f_V^2 M_V^4 \ln\frac{M_A^2}{M_V^2} , \tag{2.5.7}$$

Now using the Weinberg mass relation $M_A \simeq \sqrt{2}M_V$ which leads in conjunction with the WSRs to $f_A \simeq f_V/2$ and $f_V M_V \simeq \sqrt{2}F_\pi$ we have

$$-\int_0^\infty dQ^2 Q^2 \Pi_{V-A}(Q^2) \simeq 2F_\pi^2 M_V^2 \ln 2 . \tag{2.5.8}$$

[14] Note that the group theory factor attached to $\pi^\pm$ is of course the same in the two and three flavours cases despite the fact that in the first case the generators are the Pauli matrices and in the second case the Gell-Mann matrices.

Inserting this result in Eq. (2.5.4) we obtain for the pion mass difference [48]

$$\Delta M^2_{\pi^\pm} \simeq \frac{3\ln 2}{2\pi}\alpha M_V^2 \simeq 5.0 \text{ MeV} , \tag{2.5.9}$$

which is in good agreement with the experimental value of 4.6 MeV.

Finally, let us comment on the possible applications for BSM theories. As we will see, in the context of CHMs, we have pNGBs charged under the SM gauge group and the latter is embedded inside the unbroken global symmetry such that as in QCD, the potential is not destabilises by the gauging. The radiative corrections are more or less important depending on the pNGB under consideration. Indeed, the pNGBs of the EW sector get radiative corrections from the gauging of $SU(2)_L \times U(1)_Y$ while the coloured pNGBs from $SU(3)_c \times U(1)_Y$. In general the radiative corrections to the coloured pNGBs are more important than the ones in the EW sector. In addition, the potential of the EW sector needs to be destabilised, in order to break the EW symmetry, by the introduction of linear couplings between the top quark and the new strong sector (see section 6.4) such that the computation of the radiative corrections alone is not relevant. When it is possible to evaluate these radiative corrections, it is more correct to compute the integral in Eq. (2.5.6) instead of to saturate the correlator Π_{V-A} with the lightest resonances. This is done in section 9.2 for the minimal UV completion of a CHM.

2.5.2 π^0 decay in two photons

We now turn to the second issue of gauging the electromagnetism that is the presence of anomalous couplings between the pNGBs and two photons. As we have seen in section 2.3, some three-point functions involving the Noether currents receive anomalous contributions. More precisely, only the diagrams with an odd number of axial currents are anomalous. Restricting to triangle diagrams, the anomalous diagrams are VVA and AAA. Let us consider VVA, the axial current couples to one pNGB according to Eq. (2.2.35) and the two vector currents can be chosen to correspond to $U(1)_{em}$ such that we obtain an anomalous coupling between a pNGB and two photons. In all generality, such anomalous coupling is given by the following Wess-Zumino-Witten effective [49–51] Lagrangian

$$\mathcal{L}^{WZW} = -\frac{g_{\mathcal{W}}^2}{64\pi^2}\frac{d_c}{F_G}\epsilon_{\mu\nu\rho\sigma}\mathcal{W}^{\mu\nu}\mathcal{W}^{\rho\sigma}\sum_{\hat{A}} d^{WW\hat{A}}G^{\hat{A}} + \cdots \tag{2.5.10}$$

The index $\hat{A}$ corresponds to the axial currents while the indices W to a combination of vector currents. Note that, in general the gauge bosons $\mathcal{W}^{\mu\nu}$ associated with the vector currents can be associated with broken and unbroken generators ie they are not always vector bosons.

For the coupling to two photons, the anomaly coefficient is $d^{QQa} = 4Tr[Q^2T^a]$ where Q^2 is diagonal and then T^a has to be diagonal as well that is τ^0 and τ^3 in the case of two flavours (τ^3 corresponds to the π^0 while τ^0 corresponds to another neutral state). In the three flavours case, T^a corresponds to T^0, T^3 or T^8 (T^3 corresponds to the π^0 while T^0 and T^8 correspond to the η^0 and η^8). Let us begin for simplicity by the two flavours case and then generalise to the three flavour case. The anomaly coefficient associated to the π^0 is given by $d^{QQ3} = 2(Q_u^2 - Q_d^2) = 2/3$ [15] and then

$$\mathcal{L}^{WZW} = -\frac{\alpha}{8\pi F_\pi}\epsilon_{\mu\nu\rho\sigma}F^{\mu\nu}F^{\rho\sigma}\pi^0 + \cdots \tag{2.5.11}$$

where we have used $N_c = 3$ and $\mathcal{W}^{\mu\nu} = F^{\mu\nu}$. Using the results of Ref. [11] (see equation B.10) and the value $F_\pi = 92$ MeV for the pion decay constant, we obtain for the decay width $\pi^0 \to \gamma\gamma$

$$\Gamma(\pi^0 \to \gamma\gamma) = \frac{\alpha^2}{64\pi^3}\frac{M_{\pi^0}^3}{F_\pi^2} = \frac{\alpha^2}{64\pi^3}\frac{M_{\pi^0}^3}{F_\pi^2}N_c^2(Q_u^2 - Q_d^2)^2 \simeq 7.8 \text{ eV} , \tag{2.5.12}$$

which is in good agreement with the experimental value. Note that the second equality, obtained from the calculation of the triangular loop (with up and down quarks running inside) is in agreement with the result obtained from the WZW term as $Q_u = 2/3$ and $Q_d = -1/3$.

[15] This result remains of course valid in the three flavours case.

Let us make a final comment on the two flavours case. As we have seen, only the axial-vector currents with diagonal generators have anomalous couplings with the EM. As a consequence, the divergences of these currents have a contribution from the anomaly. Following Eq. (2.2.33), the divergence $\partial_\mu A^{\mu 3}$ in Eq. (2.2.27) becomes

$$\begin{aligned} \partial_\mu A^{\mu 3} &= 2i\ \bar{q}\gamma_5 T^3 \mathcal{M} q + \frac{e^2}{64\pi^2} N_c\ d^{QQ3} \epsilon_{\mu\nu\rho\sigma} F^{\mu\nu} F^{\rho\sigma} \\ &= 2i\ \bar{q}\gamma_5 T^3 \mathcal{M} q + \frac{e^2}{32\pi^2} \epsilon_{\mu\nu\rho\sigma} F^{\mu\nu} F^{\rho\sigma}\ , \end{aligned} \tag{2.5.13}$$

and then the WZW Lagrangian is in fact a consequence of the above divergence and of the couplings between the axial-vector currents and the pNGBs.

Let us now generalise briefly to the three flavours case. In that case, in addition to the π^0, there are two other pNGBs, the η_0 and η_8. However, these states mix because of the difference between the strange mass and the up and down masses (see e.g. section 3.2.4). The two resulting mass eigenstates are the η and η' [16]. Then, the picture is a bit more complicated. The derivation of the WZW terms associated to η_0 and η_8 follows essentially the same steps than before but to compute the decay widths we must consider the physical linear combinations η and η' and then another parameter that is the mixing angle $\theta_{\eta\eta'}$ is involved.

The anomalous couplings of the neutral pNGBs to two photons are then an interesting way to test QCD and to measure some of its parameters (for instance F_π). In the same way, in composite Higgs models there is anomalous couplings between the pNGBs and the SM gauge bosons. These couplings are important as they offer production and decay modes for the pNGBs and then a possible way to observe experimentally these composite resonances.

[16] Taking into account the breaking of the isospin $SU(2)_V$ symmetry, the π^0 should also mixes with the η_0 and η_8. However, this mixing can be neglected in first approximation as the explicit breaking of $SU(2)_V$ is small.

Chapter 3

Nambu and Jona-Lasinio model of QCD

In its weakly coupled regime, at high energy (large momentum transfer), QCD is a well-defined and computable theory. This is due to the property of asymptotic freedom that QCD exhibits at short distances. In other words, the coupling between quarks and gluons becomes small in this regime and the perturbation theory can be trusted. However, this nice property does not remain true at low energy (small momentum transfer) as at large distances, QCD becomes strongly coupled and the usual perturbative expansion breaks down. Then despite the UV theory at our disposal, one can not easily extract informations of its low energy regime. One possibility is based on a numerical approach where QCD is promoted to a lattice gauge theory. However, this is a very dedicated and as it is not the aim of this manuscript, we will not further discuss this possibility. Thus we are lead to the conclusion that we need a simplified description of QCD in its strongly coupled regime, we need a simpler Lagrangian which still encodes the more important features of QCD. In this way, we will be able to study the features which have been isolated as relevant.

The simplified model that we will present in this chapter is the NJL model [52, 53]. The latter allows to make non-perturbative computations as it based on an expansion in the number of colours. The small parameter that insures the convergence of the expansion is $1/N_c$ [54, 55]. Historically, The NJL was first developed as a pre-QCD theory for nucleons and only later reinterpreted as a theory with quarks as degrees of freedom. The NJL model is a useful description of QCD at low energy as it captures the observed QCD symmetries. In particular, it encodes one of the most important symmetry, that is, the chiral symmetry introduced in section 2.2. The latter is primordial to understand the lightest hadrons of the QCD spectrum. One important thing is that in addition to the chiral symmetry, the NJL model also reproduces the dynamical breaking of this symmetry by the formation of a non-zero quarks condensate $\langle \overline{q}q \rangle$. The special role of the NGBs is also explicitly present in the model.

In the NJL, one argues that the interaction between quarks and antiquarks, which comes from complicated processes exchanging gluons with a strong coupling constant, is attractive. This interaction leads to a condensation of a quark-antiquark pair in the vacuum which breaks the chiral symmetry and leads to the emergence of the Goldstone modes. In this picture, only the quarks are degrees of freedom, the gluons are froze out and the NJL Lagrangian only contains four-fermions [1] interactions. This is similar to the Fermi theory of weak interactions where the W and Z bosons are integrated out at low energy due to their large masses. In the NJL, the gluons are supposed to acquire a dynamical masses leading to effective interactions between quarks.

Despite the above nice features of the NJL model, it has some shortcomings. The interaction between quarks is assumed to be point-like as the gluons are froze out. Then the NJL is not a renormalisable theory but rather an effective theory for which a regularisation scheme should be specified. The regularisation scheme allows to deal with improper integrals that arrive as a consequence of the non-renormalisability. It specifies the length scale of the theory and can be expressed as a cut-off Λ which cut in momenta the divergent integrals. This cut-off can be regarded as a crude implemen-

[1] Up to the 't Hooft term which is e.g. a six-point interaction in the case of three flavours as we will see in the next.

tation of the asymptotic freedom of QCD: the interactions between quarks are suppressed at large momentum transfer which simulates the behaviour of the running coupling constant of QCD. Another important shortcoming of the NJL comes from the fact that it do not include the confinement of the quarks which is also one of the main features of QCD. However, in many cases of interest where we are below the threshold for producing free quarks, the issue of the confinement is not important and the chiral symmetry is the more relevant aspect.

This chapter aims to remind the basic features of the NJL model of QCD (see e.g. Refs. [56, 57]). The objective is to introduce the non-perturbative techniques of calculations used in the NJL as they will serve latter when we will study the case of an UV completion of a composite Higgs model. In section 3.1, we construct in all generality the four-fermion interactions of the NJL Lagrangian as well as the 't Hooft term encoding the explicit breaking of the $U(1)_A$ axial anomaly. Next, in section 3.2 we specialise to the case of QCD with two and three flavours. The two flavours case is discussed in some details. For instance, the gap equation giving rise to the dynamical mass acquire by the quarks is derived as well as the masses of the mesonic resonances (spin 0 and spin 1). We also discuss the computation of the Goldstone decay constant and of other strong parameters. Finally, we generalise to the more realistic and complicated case with three flavours pointing the main differences compare to the two flavours case.

3.1 Construction of the NJL Lagrangian

We start by the construction of the NJL Lagrangian which is by definition supposed to be a simplified description of the gauge Lagrangian of Eq. (2.1.8). As mention above, the NJL Lagrangian contain only the quark fields as dynamical degrees of freedom. Then the interactions are at the non-renormalisable level as there is no interacting terms between quarks with a dimension ≤ 4.

The NJL Lagrangian is constructed from the operators of lowest dimension. Thus the operators of interest are mainly four-fermions interactions (dimension 6 operators). The latter have to be invariant under the chiral symmetry (see section 2.2.1) but also respect the underlying gauge symmetry $SU(3)_c$ and the discrete symmetries of QCD, that is, C, P and T. The four-fermions interactions respecting the chiral symmetry are derived in subsection 3.1.1. They generally also respect accidentally the axial $U(1)_A$ symmetry. Then in addition to the four fermions interactions, one needs an operator that explicitly breaks $U(1)_A$. We refer to this operator as the 't Hooft term and it is derived in subsection 3.1.2.

3.1.1 Four-fermions interactions

In this subsection, we derive the four-fermions interactions of the NJL Lagrangian. We postpone the derivation of the 't Hooft term parametrising tthe $U(1)_A$ anomaly to subsection 3.1.2. The vector and axial-vector transformations of the flavour multiplet Ψ are listed in Eqs. (2.2.7), (2.2.8) and (2.2.9). Let us consider the bilinears $(\overline{\Psi}\Gamma F\Psi)$ where Γ is one of the sixteen Dirac contraction and $F = \{T^0, T^a\}$ is a flavour contraction. There is ten independent fermionic bilinears of the form

$$\overline{\Psi}\Gamma T^a\Psi = \begin{cases} \overline{\Psi}_R\Gamma T^a\Psi_R + \overline{\Psi}_L\Gamma T^a\Psi_L & \text{for } \Gamma = \{\gamma^\mu, \gamma^\mu\gamma_5\} \\ \overline{\Psi}_R\Gamma T^a\Psi_L + \overline{\Psi}_L\Gamma T^a\Psi_R & \text{for } \Gamma = \{\mathbb{1}, \mathrm{i}\gamma_5, \sigma^{\mu\nu}\} \end{cases} \tag{3.1.1}$$

and similarly for the singlet channels replacing T^a by T^0. These bilinears have the same quantum numbers than the physical mesonic resonances and we will refer to them as the scalar ($\Gamma = \mathbb{1}$), pseudo-scalar ($\Gamma = i\gamma_5$), vector($\Gamma = \gamma^\mu$), axial-vector ($\Gamma = \gamma^\mu\gamma_5$) and tensor ($\Gamma = \sigma^{\mu\nu}$) non-singlet ($T^a$) or singlet ($T^0$) channels.

Let us first consider the scalar and pseudo-scalar channels. The four possible operators invariant under the Lorentz symmetry as well as the discrete symmetries of QCD transform as follow under the

axial $SU(N)_A$ symmetry

$$\left(\overline{\Psi}T^0\Psi\right)^2 \rightarrow \left(\overline{\Psi}T^0\Psi\right)^2 + 2\alpha_a\sqrt{\frac{2}{N}}S^0P^a \tag{3.1.2}$$

$$\left(\overline{\Psi}i\gamma_5T^0\Psi\right)^2 \rightarrow \left(\overline{\Psi}i\gamma_5T^0\Psi\right)^2 - 2\alpha_a\sqrt{\frac{2}{N}}S^aP^0 \tag{3.1.3}$$

$$\left(\overline{\Psi}T^a\Psi\right)^2 \rightarrow \left(\overline{\Psi}T^a\Psi\right)^2 + 2\alpha_a\sqrt{\frac{2}{N}}S^aP^0 + 2\alpha_a d^{abc}S^bP^c \tag{3.1.4}$$

$$\left(\overline{\Psi}i\gamma_5T^a\Psi\right)^2 \rightarrow \left(\overline{\Psi}i\gamma_5T^a\Psi\right)^2 - 2\alpha_a\sqrt{\frac{2}{N}}S^0P^a - 2\alpha_a d^{abc}S^bP^c \tag{3.1.5}$$

Then in general, the only combination invariant under $SU(N)_A$ is

$$\left(\overline{\Psi}T^A\Psi\right)^2 + \left(\overline{\Psi}i\gamma_5T^A\Psi\right)^2 \ , \qquad N \geq 3 \ , \tag{3.1.6}$$

where for simplicity, we have defined the matrices T^A which are the generators of $U(N)$. One can check that the operator in Eq. (3.1.6) is also invariant under $SU(N)_V$, $U(1)_A$ as well as under $U(1)_V$. In fact, the invariance under $U(1)_V$ is trivial for all of the bilinears in Eq. (3.1.1). Note that, the case $N = 2$ is particular as the symmetric constants d^{abc} are equal to zero for $SU(2)$. Therefore, in that case there are two invariant operators

$$\left(\overline{\Psi}T^a\Psi\right)^2 + \left(\overline{\Psi}i\gamma_5T^0\Psi\right)^2 \ , \qquad \left(\overline{\Psi}T^0\Psi\right)^2 + \left(\overline{\Psi}i\gamma_5T^a\Psi\right)^2 \ , \qquad N = 2 \ , \tag{3.1.7}$$

which are also invariant under $SU(2)_V$ but explicitly breaks $U(1)_A$. We will come back latter to this specificity of the $N = 2$ case as it is directly related to the 't Hooft term. Repeating the same procedure for the the spin one channels, one finds the three following chiral invariant (including under $U(1)_A$) operators

$$\left(\overline{\Psi}\gamma^\mu T^0\Psi\right)^2 \ , \qquad \left(\overline{\Psi}\gamma^\mu\gamma_5T^0\Psi\right)^2 \ , \qquad \left(\overline{\Psi}\gamma^\mu T^a\Psi\right)^2 + \left(\overline{\Psi}\gamma^\mu\gamma_5T^a\Psi\right)^2 \ , \qquad \forall N \tag{3.1.8}$$

Finally, for the tensor bilinears [58], the transformations are the same compare to the spin zero bilinears. We obtain one invariant operator in the general case

$$\left(\overline{\Psi}T^A\sigma^{\mu\nu}\Psi\right)^2 + \left(\overline{\Psi}i\gamma_5\sigma^{\mu\nu}T^A\Psi\right)^2 \ , \qquad N \geq 3 \ , \tag{3.1.9}$$

and two invariant operators in the particular case with two flavours

$$\left(\overline{\Psi}\sigma^{\mu\nu}T^a\Psi\right)^2 + \left(\overline{\Psi}i\gamma_5\sigma^{\mu\nu}T^0\Psi\right)^2 \ , \quad \left(\overline{\Psi}\sigma^{\mu\nu}T^0\Psi\right)^2 + \left(\overline{\Psi}i\gamma_5\sigma^{\mu\nu}T^a\Psi\right)^2 \ , \qquad N = 2 \ , \tag{3.1.10}$$

where $\gamma_5\sigma_{\mu\nu} = i\epsilon_{\mu\nu\alpha\beta}\sigma^{\alpha\beta}/2$ is the dual tensor of $\sigma_{\mu\nu}$. Again, for $N \geq 3$, the tensor operators are accidentally invariant under $U(1)_A$ while for the special case of $N = 2$ the axial $U(1)_A$ symmetry is already explicitly broken by the four-fermions tensor interactions.

From the above discussion, the NJL Lagrangian compatible with the chiral symmetry takes the following form

$$\begin{aligned}\mathcal{L}_{NJL} \ = \ & G_S[\left(\overline{\Psi}T^A\Psi\right)^2 + \left(\overline{\Psi}i\gamma_5T^A\Psi\right)^2] + G_T[\left(\overline{\Psi}T^A\sigma^{\mu\nu}\Psi\right)^2 + \left(\overline{\Psi}i\gamma_5\sigma^{\mu\nu}T^A\Psi\right)^2] \\ & + G_V[\left(\overline{\Psi}\gamma^\mu T^a\Psi\right)^2 + \left(\overline{\Psi}\gamma^\mu\gamma_5T^a\Psi\right)^2] + G'_V\left(\overline{\Psi}\gamma^\mu T^0\Psi\right)^2 \\ & + G''_V\left(\overline{\Psi}\gamma^\mu\gamma_5T^0\Psi\right)^2 \ .\end{aligned} \tag{3.1.11}$$

The above Lagrangian is invariant under the chiral symmetry but also under $U(1)_A$ such that, even for the particular $N = 2$ case, we postpone the parametrisation of the $U(1)_A$ explicit breaking in the 't Hooft terms to the following subsection. Let us comment further on the NJL Lagrangian. There are five independent couplings G_i which have dimension -2 and can be parametrised as $G_i \sim \left(\frac{g_i}{\Lambda}\right)^2$. The scale Λ is a reference scale that we chose to be the cut-off of the NJL model (see section 3.2). It

is a free parameter of the NJL model. To fix the ideas, one can crudely interpret Λ as the dynamical mass acquire by the gluons and g_i as their coupling to the quarks. As the number of colours N_c and the number of flavours N are fixed, there are six free parameters (if we do not consider the $U(1)_A$ anomaly) in the NJL model: the cut-off Λ and the five couplings G_i. However, as we will see in subsection 3.2.3, under the hypothesis that the four-fermions interactions are generated from an $SU(3)_c$ current-current operator, it is possible to relate all of the four-fermions couplings G_i. In this way, the model contains only two free parameters: one four-fermion coupling and the cut-off Λ. In addition, we will not consider the tensor channels for simplicity. The latter have been investigated in Ref. [58]. This simplification can be justify in the current-current hypothesis which gives $G_T = 0$.

Note that, to derive the NJL Lagrangian in Eq. (3.1.11), we implicitly restricted to colour singlet bilinears because due to the confinement, coloured bilinears do not correspond to physical mesons. However, operators with coloured bilinears are involved in the calculation of the baryonic masses as they correspond to diquarks channels. We will briefly discuss this possibility in chapter 10.

We now present another way to derive the NJL Lagrangian. In the above procedure, the fermions was in reducible representations of $SU(N)_V \times SU(N)_A$. As a consequence, it was not trivial to impose the chiral symmetry. Instead of vector and axial symmetries, it can be easier to consider left and right-handed symmetries for which Ψ_L and Ψ_R transform in irreducible representations. Under $SU(N)_L \times SU(N)_R$ we have

$$\Psi^a_L \sim (N_L, 0) \ , \qquad \Psi^a_R \sim (0, N_R) \ . \tag{3.1.12}$$

and the relevant bilinears transform as

$$\overline{\Psi}_L \Gamma \Psi_R \ \sim (\overline{N}_L, N_R) \ , \qquad \overline{\Psi}_R \Gamma \Psi_L \ \sim (N_L, \overline{N}_R) \ , \qquad \Gamma = \{\mathbb{1}, \sigma^{\mu\nu}\} \ , \tag{3.1.13}$$

$$\overline{\Psi}_L \gamma^\mu \Psi_L \ \sim (\overline{N}_L \times N_L, 0) \ , \qquad \overline{\Psi}_R \gamma^\mu \Psi_R \ \sim (0, \overline{N}_R \times N_R) \ . \tag{3.1.14}$$

Then, considering for instance the spin zero bilinears of Eq. (3.1.13) we have

$$(\overline{\Psi}_{La} \Psi^b_R)(\overline{\Psi}_{Rc} \Psi^d_L) \sim (\overline{N}_L, N_R) \times (N_L, \overline{N}_R) = (1_R, 1_L) + \cdots \tag{3.1.15}$$

while $(\overline{\Psi}_{aL,R} \Psi^b_{R,L})(\overline{\Psi}_{cL,R} \Psi^d_{R,L})$ does not contain a singlet contraction [2]. The singlet contraction is obviously

$$\begin{aligned} [(\overline{\Psi}_{La} \Psi^b_R)(\overline{\Psi}_{Rc} \Psi^d_L) + h.c.] \delta^a_d \delta^c_b &= 2[(\overline{\Psi}_R T^0 \Psi_L)(\overline{\Psi}_L T^0 \Psi_R) + (\overline{\Psi}_R T^a \Psi_L)(\overline{\Psi}_L T^a \Psi_R) + h.c.] \\ &= (S^0 + iP^0)(S^0 - iP^0) + (S^a + iP^a)(S^a - iP^a) \\ &= S^A S^A + P^A P^A \ , \end{aligned} \tag{3.1.16}$$

where we have used the general flavour decomposition

$$(\overline{\Psi}_a \Gamma \Psi^b) = 2(T^0)^b_a (\overline{\Psi} T^0 \Gamma \Psi) + 2(T^a)^b_a (\overline{\Psi} T^a \Gamma \Psi) \ . \tag{3.1.17}$$

The operator in Eq. (3.1.16) is the same than the one in Eq. (3.1.6). Of course, one can do the same thing to derive the vector and tensor operators but also to derive the 't Hooft term as we now see.

3.1.2 Parametrisation of the U(1) axial anomaly

Following the procedure of the precedent subsection, we now construct the 't Hooft term respecting the chiral symmetry $SU(N)_V \times SU(N)_A \times U(1)_V$ but explicitly breaking $U(1)_A$. From table 2.1, it is easy to see that an operator with a larger or smaller number of left-handed fields (Ψ_L or $\overline{\Psi}_R$) compare to the right-handed ones (Ψ_R or $\overline{\Psi}_L$) explicitly breaks the axial $U(1)_A$. Then the minimal operators of this kind contains only scalar or tensor bilinears of the form

$$(\overline{\Psi}_{L,R} \Gamma \Psi_{R,L}) = (\overline{\Psi} \Gamma P_{R,L} \Psi) \ , \qquad \Gamma = \{\mathbb{1}, \sigma^{\mu\nu}\} \ . \tag{3.1.18}$$

[2] Up to the particular case of $N = 2$ where $\overline{2} = 2^*$ (see subsection 3.1.2)

Consequently, the 't Hooft terms contribute only to the spin-zero and tensor channels but not to the spin one channels. To construct the minimal chiral invariants with the bilinears of Eq. (3.1.18) only, we can take N replicas of them as the product of N fundamental representations gives a singlet in $SU(N)$. For instance, the 't Hooft term involving only the scalar bilinears is

$$\begin{aligned}\mathcal{L}_{U(1)} &= H\epsilon^{a_1\cdots a_N}\epsilon_{b_1\cdots b_N}[(\overline{\Psi}_{La_1}\Psi^{b_1}_R)\cdots(\overline{\Psi}_{La_N}\Psi^{b_N}_R)+h.c.] \\ &= H\epsilon^{a_1\cdots a_N}\epsilon_{b_1\cdots b_N}[(\overline{\Psi}_{a_1}P_R\Psi^{b_1})\cdots(\overline{\Psi}_{a_N}P_R\Psi^{b_N})+(P_R\to P_L)]\ ,\end{aligned} \tag{3.1.19}$$

where the flavour singlet contraction is obtained with two invariant tensors of $SU(N)$ which are $\epsilon_{a_1\cdots a_N}$ and $\epsilon^{a_1\cdots a_N}$ and $(P_R\to P_L)$ insures that Parity is respected. In the same way, one can construct 't Hooft terms involving the tensor bilinears. They are obtained by replacing an even number of scalar bilinears by tensor bilinears in Eq. (3.1.19) that is

$$(\overline{\Psi}_aP_{R,L}\Psi^b)(\overline{\Psi}_cP_{R,L}\Psi^d)\to(\overline{\Psi}_a\sigma^{\mu\nu}P_{R,L}\Psi^b)(\overline{\Psi}_c\sigma_{\mu\nu}P_{R,L}\Psi^d) \tag{3.1.20}$$

Note that, the above 't Hooft terms should be reduced to four-fermions interactions in order to make NJL calculations (see subsection 3.2.4). This is done by closing a sufficient number of loops ie by replacing the bilinears by their corresponding condensates. As the condensate $\langle\overline{\Psi}\sigma^{\mu\nu}\Psi\rangle=0$ (otherwise the Lorentz symmetry is broken), only the 't Hooft terms with a maximum of two tensor bilinears contribute in the NJL approximation. Then, for N free we have only two different $U(1)_A$ breaking terms relevant in the NJL approximation. However, we do not consider further the possibility to have tensor modes in the 't Hooft terms as we already not considered them in the four-fermions interactions.

We now rewrite the 't Hooft term of Eq. (3.1.19) in the physical basis where the bilinears have the same quantum numbers than the physical resonances. To that end, we use the following decomposition of the epsilon product

$$\epsilon^{a_1\cdots a_N}\epsilon_{b_1\cdots b_N}=\begin{vmatrix}\delta^{a_1}_{b_1} & \cdots & \delta^{a_1}_{b_N}\\ \vdots & \ddots & \vdots\\ \delta^{a_N}_{b_1} & \cdots & \delta^{a_N}_{b_N}\end{vmatrix}\ , \tag{3.1.21}$$

and the flavour decomposition of the bilinear in Eq. (3.1.17). Let us restrict to the relevant cases where $N=2$ and $N=3$. The extension to larger N can be useful for BSM strongly coupled theory and is straightforward. The 't Hooft term of Eq. (3.1.19) contains $2N$ fermions, that is, it is a four-fermions interaction for $N=2$ and a six-points interaction for $N=3$. Let us begin by the two flavour case where the 't Hooft term is

$$\begin{aligned}\mathcal{L}_{U(1)}(N=2) &= H\epsilon^{ab}\epsilon_{cd}[(\overline{\Psi}_aP_R\Psi^c)(\overline{\Psi}_bP_R\Psi^d)+(P_R\to P_L)] \\ &= H[(\overline{\Psi}_aP_R\Psi^a)(\overline{\Psi}_bP_R\Psi^b)-(\overline{\Psi}_aP_R\Psi^b)(\overline{\Psi}_bP_R\Psi^a)+(P_R\to P_L)]\ ,\end{aligned} \tag{3.1.22}$$

and we have used in the second line the flavour contraction of Eq. (3.1.21) that reduced in that case to $\epsilon^{ab}\epsilon_{cd}=\delta^a_c\delta^b_d-\delta^a_d\delta^b_c$. Using the flavour decomposition of Eq. (3.1.17), the latter operator reduces to

$$\mathcal{L}_{U(1)}(N=2)=\frac{H}{2}\left[(\overline{\Psi}T^0\Psi)^2+(\overline{\Psi}i\gamma_5T^a\Psi)^2-(\overline{\Psi}i\gamma_5T^0\Psi)^2+(\overline{\Psi}T^a\Psi)^2\right]\ . \tag{3.1.23}$$

Then, combining the above equation with Eq. (3.1.11), we get the two independent four-fermions interactions of Eq. (3.1.7) that respect $SU(N)_V\times SU(N)_A\times U(1)_V$ but break $U(1)_A$. We now turn to the three flavours case where the 't Hooft terms is

$$\mathcal{L}_{U(1)}(N=3)=H\epsilon^{abc}\epsilon_{def}[(\overline{\Psi}_aP_R\Psi^d)(\overline{\Psi}_bP_R\Psi^e)(\overline{\Psi}_cP_R\Psi^f)+(P_R\to P_L)] \tag{3.1.24}$$

The flavour contraction reduces to

$$\epsilon^{abc}\epsilon_{def}=\delta^a_d\delta^b_e\delta^c_f+\delta^a_e\delta^b_f\delta^c_d+\delta^a_f\delta^b_d\delta^c_e-\delta^a_d\delta^b_f\delta^c_e-\delta^a_f\delta^b_e\delta^c_d-\delta^a_e\delta^b_d\delta^c_f\ , \tag{3.1.25}$$

and the 't Hooft term in the physical basis reads

$$\mathcal{L}_{U(1)}(N=3)=\frac{H}{6}D_{ABC}\left[\frac{1}{3}(\overline{\Psi}T^A\Psi)(\overline{\Psi}T^B\Psi)(\overline{\Psi}T^C\Psi)-(\overline{\Psi}T^Ai\gamma_5\Psi)(\overline{\Psi}T^Bi\gamma_5\Psi)(\overline{\Psi}T^C\Psi)\right]\ , \tag{3.1.26}$$

where the totally symmetric coefficient is given by

$$D^{ABC} = \begin{cases} d^{abc} & \text{for } \mathrm{a,b,c} = \{1,\cdots,8\} \\ -\frac{1}{\sqrt{6}} & \text{for } \mathrm{A}=0,\ \mathrm{B}=\mathrm{C}=\{1,\cdots,8\} \\ \frac{2}{\sqrt{3}} & \text{for } \mathrm{A}=\mathrm{B}=\mathrm{C}=0\ , \end{cases} \tag{3.1.27}$$

and $d^{abc} = Tr[T^a\{T^b, T^c\}]$ is the completely symmetric tensor of $SU(3)$.

3.2 NJL model with two and three flavours

In the precedent section, we have constructed the NJL four-fermions interactions invariant under the chiral symmetry as well as the 't Hooft term parametrising the breaking of the $U(1)_A$ symmetry. We are now able to make calculations in the NJL model starting from Eqs. (3.1.11) and Eq. (3.1.19). We first consider in some details the simpler case with two flavours ($N = 2$). In that case, we present in subsection 3.2.1 the dynamical breaking of the chiral symmetry which leads to the emergence of a non-zero constituent mass M for the fermions. Then, in subsections 3.2.2 we compute in the NJL framework, the masses of the spin zero and spin one resonances as well as the Goldstone decay constants F_G. In the sequel, in subsection 3.2.3, we start from an $SU(3)_c$ current-current operator and generate using Fiez transformations the NJL four-fermions interactions. In this way, we obtain a phenomenological link between all the four-fermions coupling constant. Finally, in subsection 3.2.4 we consider the more involved case with three flavours ($N = 3$) where we briefly outline the main differences compare to the two flavours case.

3.2.1 Dynamical breaking of the chiral symmetry

Let us first consider the spin-zero sector, that is, the Lagrangian

$$\mathcal{L}^0_{NJL} = m\left(\overline{\Psi}\Psi\right) + K_\sigma\left[\left(\overline{\Psi}\tau^0\Psi\right)^2 + \left(\overline{\Psi}i\gamma_5\tau^a\Psi\right)^2\right] + K_S\left[\left(\overline{\Psi}\tau^0 i\gamma_5\Psi\right)^2 - \left(\overline{\Psi}\tau^a\Psi\right)^2\right]\ , \tag{3.2.1}$$

where we have defined the more convenient couplings $K_\sigma = K_\pi = (G_S + H/2)$, $K_S = K_\eta = (G_S - H/2)$ and in addition to the four-fermions interactions, we have introduced an explicit breaking mass term m which corresponds to the current masses of the up and down quarks. For simplicity, we neglect the isospin violation such that $m = m_u = m_d$ (see section 2.2.2).

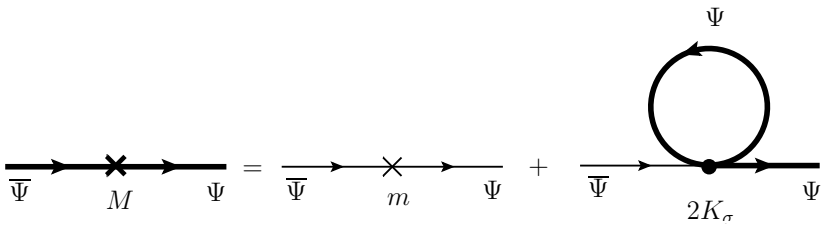

Figure 3.1: Graphical illustration of the gap equation (Bethe-Salpeter equation) in the NJL approximation with no explicit breaking of the $SU(N)_V$ symmetry. Thick and thin lines represent dressed and bare quark propagators, respectively. On the right-hand side of the equation, the contribution of the explicit breaking mass term m and the one of the four fermion interaction associated to the singlet scalar channel σ.

The Dyson equation which allows to compute the dynamical mass acquired by the fundamental quarks due to the strong interactions is depicted in figure 3.1. This equation is self-consistent as the dynamical mass M is present on both sides of the equality. We have

$$-iM = -im + (-1)2i\widehat{G}_S Tr[\tau^0\tau^0]N_c \int \frac{d^4k}{(2\pi)^4}\frac{iTr[\not{k} + M]}{k^2 - M^2}\ , \tag{3.2.2}$$

where M is the constituent mass of the quarks ($M = M_u = M_d$) and the factor N_c comes from the trace over colour. Note that only the scalar singlet operator (σ-channel) contributes to the above gap equation as for the others, the flavour and/or Dirac traces are zero. Replacing explicitly the Dirac and flavour traces, the gap equation reduces to

$$1 - \frac{m}{M} - 4K_\sigma N_c \tilde{A}_0(M^2) = 0 \ , \tag{3.2.3}$$

where we have defined the one-loop function

$$\tilde{A}_0(M^2) = i \int_0^\Lambda \frac{d^4k}{(2\pi)^4} \frac{1}{k^2 - M^2} = \frac{\Lambda^2}{16\pi^2} \left[1 - \frac{M^2}{\Lambda^2} \ln \frac{\Lambda^2 + M^2}{M^2} \right] \ . \tag{3.2.4}$$

The latter integral has been regularised [3] with a cut-off Λ. This cut-off is part of the NJL model and is a free parameter. From Eq. (3.2.3), one can see that in the chiral limit ($m = 0$), there is a critical value

$$G_{crit} = \frac{4\pi^2}{N_c \Lambda^2} \ , \tag{3.2.5}$$

above which a non-zero dynamical mass develops.

3.2.2 Masses of the resonances and pion decay constant

The masses of the physical resonances are obtained at first order in $1/N_c$, from the Schwinger-Dyson equation depicted in figure 3.2. The latter resums in a geometrical series the dominant large-N_c diagrams contributing to the two point function with the appropriate quantum numbers. In the scalar and pseudo-scalar cases, the resumed two point function is

$$\overline{\Pi}_\phi(p^2) = \frac{\tilde{\Pi}_\phi(p^2)}{1 - 2K_\phi \tilde{\Pi}_\phi(p^2)} \ , \tag{3.2.6}$$

where K_ϕ is the four-fermion coupling attached to the resonance ϕ and $\tilde{\Pi}_\phi$ is the corresponding one-loop two point function. The latter are explicitly computed in appendix B. The masses of the resonances are given by the poles of the resumed correlator, that is by

$$1 - 2K_\phi \tilde{\Pi}_\phi(p^2 = M_\phi^2) = 0 \ , \qquad p^2 = M_\phi^2 \ , \tag{3.2.7}$$

For instance, for the pseudo-scalar non-singlet channel we have

$$1 - 2K_\pi 2N_c \left[\tilde{A}_0(M^2) - \frac{M_\pi^2}{2} \tilde{B}_0(M_\pi^2, M^2) \right] = \frac{m}{M} + 2N_c K_\pi \tilde{B}_0(M_\pi^2, M^2) M_\pi^2 = 0 \ , \tag{3.2.8}$$

where we have used the gap equation in the second equality. One obtains for the pions mass

$$M_\pi^2 = -\frac{m}{M} \frac{1}{2N_c K_\pi \tilde{B}_0(M_\pi^2, M^2)} \ . \tag{3.2.9}$$

Then one explicitly checks that in the chiral limit ($m = 0$), the pions are massless ie NGBs. An important point is that the pion mass M_π is contained also in the left side of Eq. (3.2.9) such that one has to solve the above equation to obtain the physical mass. Similarly, for the singlet scalar σ, one obtains

$$M_\sigma^2 = 4M^2 - \frac{m}{M} \frac{1}{2N_c K_\sigma \tilde{B}_0(M_\sigma^2, M^2)} \ . \tag{3.2.10}$$

In the chiral limit, the σ mass is proportional to the gap equation and we have the well-known relation $M_\sigma = 2M$.

[3] Other regularisation are possible, see e.g [56].

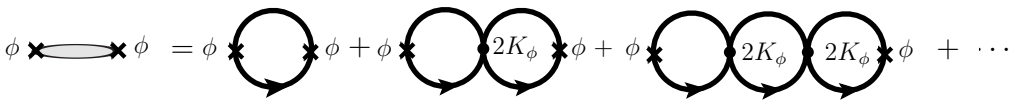

Figure 3.2: Graphical illustration of Schwinger-Dyson equation that resums the leading $1/N_c$ graphs and corresponds to a mesonic two-point correlator $\overline{\Pi}_\phi$.

For the scalar non-singlet S^a and the the pseudo-scalar singlet η masses, we respectively have

$$M_S^2 = 4M^2 - \frac{1}{2N_c K_S \tilde{B}_0(M_S^2, M^2)} \left[\frac{m}{M} + 4N_c H \tilde{A}_0(M^2)\right] , \tag{3.2.11}$$

$$M_\eta^2 = -\frac{1}{2N_c K_\eta \tilde{B}_0(M_\eta^2, M^2)} \left[\frac{m}{M} + 4N_c H \tilde{A}_0(M^2)\right] . \tag{3.2.12}$$

In the chiral limit and when the 't Hooft term coupling is set to zero, the η is massless. Then, one sees that H parametrises the explicit breaking of the axial $U(1)_A$ symmetry by giving a non-zero mass to the pseudo-scalar singlet even in the chiral limit. Neglecting the dependence in the masses of the resonances of the $\tilde{B}_0$ functions, one obtains the following interesting relations

$$M_\sigma^2 = M_\pi^2 + 4M^2 , \qquad M_S^2 = M_\eta^2 + 4M^2. \tag{3.2.13}$$

We now turn to the spin one resonances. The relevant four-fermion interactions are

$$\mathcal{L}^1_{NJL} = -G_V \left[\left(\overline{\Psi}\gamma^\mu \tau^a \Psi\right)^2 + \left(\overline{\Psi}\gamma^\mu\gamma_5 \tau^a \Psi\right)^2\right] - G'_V \left(\overline{\Psi}\gamma^\mu \tau^0 \Psi\right)^2 - G''_V \left(\overline{\Psi}\gamma^\mu\gamma_5 \tau^0 \Psi\right)^2 , \tag{3.2.14}$$

where the minus sign convention is necessary to obtain positive masses squared for a positive coupling. The resumed two-point functions associated with the non-singlet channels are given by

$$-p^2 \overline{\Pi}_{V,A}(p^2) = \frac{\tilde{\Pi}_{V/A}(p^2)}{1 - 2K_{V/A}\tilde{\Pi}_{V/A}(p^2)} , \qquad p^2 \overline{\Pi}^L_A(p^2) = \frac{\tilde{\Pi}^L_A(p^2)}{1 - 2K_A \tilde{\Pi}^L_A(p^2)} , \tag{3.2.15}$$

where $K_V = K_A = G_V$ Similar relations hold for the singlet channels replacing the couplings $K_{V/A}$ respectively by $K_v = G'_V$ and $K_a = G''_V$. The masses are obtained from the poles of the transverse correlators. For the vector non-singlets one obtains

$$M_V^2 = \frac{-3}{4N_c K_V \tilde{B}_0(M_V^2, M^2)} + 2M^2 \frac{\tilde{B}_0^0(M^2)}{\tilde{B}_0(M_V^2, M^2)} - 2M^2 , \tag{3.2.16}$$

The mass of the vector singlet v^μ is obtained in a similar way by replacing in the above equation $K_V = G_V$ by $K_v = G'_V$ and $\tilde{B}_0(M_V^2, M^2)$ by $\tilde{B}_0(M_v^2, M^2)$. Similarly for the axial-vector channel

$$M_A^2 = \frac{-3}{4N_c K_A \tilde{B}_0(M_A^2, M^2)} + 2M^2 \frac{\tilde{B}_0^0(M^2)}{\tilde{B}_0(M_A^2, M^2)} + 4M^2 , \tag{3.2.17}$$

The mass of the axial-vector singlet a^μ is obtained in a similar way by replacing in the above equation $K_A = G_V$ by $K_a = G''_V$ and $\tilde{B}_0(M_A^2, M^2)$ by $\tilde{B}_0(M_a^2, M^2)$. If one neglects the dependences of the $\tilde{B}_0$ functions, one has

$$M_A^2 = M_V^2 + 6M^2 . \tag{3.2.18}$$

Finally, let us consider the pion decay constant F_π. In the chiral limit, the pion pole is in the transverse correlator [see Eq. (2.4.12)] such that

$$F_\pi^2 = \lim_{p^2 \to 0} [-p^2 \overline{\Pi}_A(p^2)] = \frac{\tilde{\Pi}_A(0)}{1 - 2K_A \tilde{\Pi}_A(0)} = \frac{\tilde{F}_\pi^2}{1 - 2K_A \tilde{F}_\pi^2} = g_A(0) \tilde{F}_\pi^2 , \tag{3.2.19}$$

where $\tilde{F}_\pi$ is the one-loop pion decay constant defined by

$$\tilde{F}_\pi^2 \equiv \tilde{\Pi}_A(0) = -4N_c M^2 \tilde{B}_0^0(M^2) = \tilde{\Pi}_A^L(0) \ , \tag{3.2.20}$$

and the factor $g_A(p^2)$ is defined by

$$g_A(p^2) = \Big[1 - 2K_A \tilde{\Pi}_A^L(p^2)\Big]^{-1} \ . \tag{3.2.21}$$

Similarly, from Eqs. (2.4.12) and (2.4.13) one can extract $f_{V,A}$ and $G_{\sigma,S,\eta,\eta}$. When there is an explicit breaking mass m, the Goldstone boson pole is in the longitudinal correlator such that

$$F_\pi^2 = \lim_{p^2 \to M_\pi^2} [p^2 \overline{\Pi}_A^L(p^2)] = \frac{\tilde{\Pi}_A^L(M_\pi^2)}{1 - 2K_A \tilde{\Pi}_A^L(M_\pi^2)} = g_A(M_\pi^2) \tilde{\Pi}_A^L(M_\pi^2) \ . \tag{3.2.22}$$

Let us make few comments about the above derivations. First, we did not consider the mixing between the axial longitudinal and pseudo-scalar channels. Indeed, in that case Eq. (3.2.6) generalises to a matrix form

$$\overline{\mathbf{\Pi}}_\pi(p^2) = [\mathbb{1} - 2\mathbf{K}_\pi \tilde{\mathbf{\Pi}}_\pi(p^2)]^{-1} \tilde{\mathbf{\Pi}}_\pi(p^2) \ , \tag{3.2.23}$$

where

$$\mathbf{K}_\pi = \begin{pmatrix} K_\pi & 0 \\ 0 & K_A \end{pmatrix} \ , \qquad \tilde{\mathbf{\Pi}}_\pi(p^2) = \begin{pmatrix} \tilde{\Pi}_P(p^2) & \sqrt{p^2}\tilde{\Pi}_{AP}(p^2) \\ \sqrt{p^2}\tilde{\Pi}_{AP}(p^2) & \tilde{\Pi}_A^L(p^2) \end{pmatrix} \ . \tag{3.2.24}$$

The mass is given by a generalisation of Eq. (3.2.7)

$$\det[\mathbb{1} - 2\mathbf{K}_\pi \tilde{\mathbf{\Pi}}_\pi(p^2)] \ , \qquad p^2 = M_\pi^2 \ . \tag{3.2.25}$$

From the above equations, one obtains for the pion mass

$$M_\pi^2 = -g_A^{-1}(M_\pi^2) \frac{m}{M} \frac{1}{2N_c K_\pi \tilde{B}_0(M_\pi^2, M^2)} \ , \tag{3.2.26}$$

such that, there is an additional factor $g_A^{-1}(M_\pi^2)$ coming from the axial-pseudoscalar mixing. In the same ay, one obtains for the η mass

$$M_\eta^2 = -g_a^{-1}(M_\eta^2) \frac{1}{2N_c K_\eta \tilde{B}_0(M_\eta^2, M^2)} \left[\frac{m}{M} + 4N_c H \tilde{A}_0(M^2)\right] \ , \tag{3.2.27}$$

where the factor $g_a(p^2)$ is defined similarly to the one in Eq. (3.2.21) replacing the non-singlet coupling K_A by the singlet one K_a, that is, $g_a(p^2) = [1 - 2K_a \tilde{\Pi}_A^L(p^2)]$.

Note that we have considered only the resumed correlators $\overline{\Pi}_\phi$ in order to extract the masses of the resonances but also the associated decay constants. One can also consider the T-matrix $\overline{T}_\phi$ (see appendix H) which gives the coupling $g_{\phi\overline{\Psi}\Psi}$ between the resonance and the fundamental quarks. All of this points are discussed in more details in chapter 8 as the objective here is just to give a first glimpse of the NJL techniques in the context of QCD.

3.2.3 Current-current hypothesis

In the precedent subsection, we have derived the masses of the physical mesonic resonances using the techniques of the NJL model. These masses depends on the four-fermions coupling constants G_i. If we put aside the tensor modes, there are four different couplings: G_S, G_V, G'_V and G''_V. In addition, there is also the cut-off of the NJL model Λ and the coupling H of the 't Hooft term. Then it can be useful for phenomenological reasons to reduce the number of free parameters. One way to do that is to assume that the strong dynamics generates mainly a coloured current-current operator of the following form

$$\begin{aligned} \mathcal{L}_{NJL}^c &= G_c \left(\overline{\Psi}\gamma^\mu T_c^a \Psi\right)\left(\overline{\Psi}\gamma_\mu T_c^a \Psi\right) \\ &= G_c \ \overline{\Psi}_{\alpha i a}\Psi_{\beta j b}\overline{\Psi}_{\gamma k c}\Psi_{\delta l d} \ (\gamma^\mu)_{\alpha\beta}(\gamma_\mu)_{\gamma\delta} \ (\mathbb{1})_{ab}(\mathbb{1})_{cd} \ (T_c^a)_{ij}(T_c^a)_{kl} \ . \end{aligned} \tag{3.2.28}$$

Using Fierz transformations, one can rewrite the above operator in term of coloured singlet and in particular in term of the NJL four-fermion operators in Eq. (3.1.11). To that end, let us consider the Fierz transformations attached to the Dirac [59], flavours and colours contractions in the quark-antiquark channel $[(\overline{q}_1 q_2)(\overline{q}_3 q_4) \to (\overline{q}_1 q_4)(\overline{q}_3 q_2)]$. These transformations are

$$\begin{pmatrix} \left(T^0\right)_{ij}\left(T^0\right)_{kl} \\ \sum_a \left(T^a\right)_{ij}\left(T^a\right)_{kl} \end{pmatrix} = \begin{pmatrix} \frac{1}{N} & \frac{1}{N} \\ \frac{N^2-1}{N} & -\frac{1}{N} \end{pmatrix} \begin{pmatrix} \left(T^0\right)_{il}\left(T^0\right)_{kj} \\ \sum_a \left(T^a\right)_{il}\left(T^a\right)_{kj} \end{pmatrix} , \tag{3.2.29}$$

$$\begin{pmatrix} (\mathbb{1})_{ij}(\mathbb{1})_{kl} \\ (i\gamma_5)_{ij}(i\gamma_5)_{kl} \\ (\gamma^\mu)_{ij}(\gamma_\mu)_{kl} \\ (\gamma^\mu\gamma_5)_{ij}(\gamma_\mu\gamma_5)_{kl} \\ (\sigma^{\mu\nu})_{ij}(\sigma_{\mu\nu})_{kl} \end{pmatrix} = \begin{pmatrix} \frac{1}{4} & -\frac{1}{4} & \frac{1}{4} & -\frac{1}{4} & \frac{1}{8} \\ -\frac{1}{4} & \frac{1}{4} & \frac{1}{4} & -\frac{1}{4} & -\frac{1}{8} \\ 1 & 1 & -\frac{1}{2} & -\frac{1}{2} & 0 \\ -1 & -1 & -\frac{1}{2} & -\frac{1}{2} & 0 \\ 3 & -3 & 0 & 0 & -\frac{1}{2} \end{pmatrix} \begin{pmatrix} (\mathbb{1})_{il}(\mathbb{1})_{kj} \\ (i\gamma_5)_{il}(i\gamma_5)_{kj} \\ (\gamma^\mu)_{il}(\gamma_\mu)_{kj} \\ (\gamma^\mu\gamma_5)_{il}(\gamma_\mu\gamma_5)_{kj} \\ (\sigma^{\mu\nu})_{il}(\sigma_{\mu\nu})_{kj} \end{pmatrix} . \tag{3.2.30}$$

For general properties of Fierz transformations we refer to appendix I. The relevant transformations for our present purpose are

$$\begin{aligned} (\gamma^\mu)_{\alpha\beta}(\gamma_\mu)_{\gamma\delta} &= (\mathbb{1})_{\alpha\delta}(\mathbb{1})_{\gamma\beta} + (i\gamma_5)_{\alpha\delta}(i\gamma_5)_{\gamma\beta} - \frac{1}{2}(\gamma^\mu)_{\alpha\delta}(\gamma_\mu)_{\gamma\beta} \\ &\quad -\frac{1}{2}(\gamma^\mu\gamma_5)_{\alpha\delta}(\gamma_\mu\gamma_5)_{\gamma\beta} , \end{aligned} \tag{3.2.31}$$

$$(\mathbb{1})_{ab}(\mathbb{1})_{cd} = 2(T^0)_{ad}(T^0)_{cb} + 2(T^a)_{ad}(T^a)_{cb} , \tag{3.2.32}$$

$$(T^a_c)_{ij}(T^a_c)_{kl} = \frac{N_c^2-1}{2N_c^2}(\mathbb{1})_{il}(\mathbb{1})_{kj} - \frac{1}{N_c}(T^a_c)_{il}(T^a_c)_{kj} , \tag{3.2.33}$$

for the Lorentz, flavour and colour indices respectively. On immediately see that, starting from a current-current operator, the latter does not contain tensor modes which justify a posteriori that we have not considered them previously. The current-current operator of Eq. (3.2.28) rewrites

$$\begin{aligned} \mathcal{L}^c_{NJL} &= \frac{N_c^2-1}{2N_c^2} 2G_c \Big\{ (\Psi T^0\Psi)^2 + (\Psi T^a\Psi)^2 + (\Psi T^0 i\gamma_5\Psi)^2 + (\Psi T^a i\gamma_5\Psi)^2 - \frac{1}{2}(\Psi T^0\gamma^\mu\Psi)^2 \\ &\quad -\frac{1}{2}(\Psi T^a\gamma^\mu\Psi)^2 - \frac{1}{2}(\Psi T^0\gamma^\mu\gamma_5\Psi)^2 - \frac{1}{2}(\Psi T^a\gamma^\mu\gamma_5\Psi)^2 \Big\} , \end{aligned} \tag{3.2.34}$$

where we have omitted the coloured octet contractions which do not contribute to the mesonic modes [4]. Comparing the above equation with Eq. (3.1.11), we find that

$$G_S = G_c\frac{N_c^2-1}{N_c^2} = \frac{8}{9}G_c , \qquad G_S = -2G_V , \qquad G_V = G'_V = G''_V , \qquad G_T = 0 . \tag{3.2.35}$$

Then, in the hypothesis that the strong dynamics generates mainly the current-current operator od Eq. (3.2.28), there is only one independent four-fermion coupling that we can choose to be G_S. Note that these phenomenological relations between the four-fermion couplings lead to quite reasonable results compare the more general case where the couplings are not related [60]. An important point is that, when we will study the UV completions of CHMs, we will also use for phenomenological reasons the current-current hypothesis (see chapters 8 and 9)

[4] In addition, these channels are not supposed to be attractive from the point of view of the maximal attractive channel (see subsection 10.2.1).

For completeness, we also give the Fierz transformations in the quark-quark channel $[(\overline{q}_1 q_2)(\overline{q}_3 q_4) \to (\overline{q}_1 \overline{q}_3)(q_4 q_2)]$

$$\begin{pmatrix} (\mathbb{1})_{ij}\,(\mathbb{1})_{kl} \\ (i\gamma_5)_{ij}\,(i\gamma_5)_{kl} \\ (\gamma^\mu)_{ij}\,(\gamma_\mu)_{kl} \\ (\gamma^\mu\gamma_5)_{ij}\,(\gamma_\mu\gamma_5)_{kl} \\ (\sigma^{\mu\nu})_{ij}\,(\sigma_{\mu\nu})_{kl} \end{pmatrix} = \begin{pmatrix} -\frac{1}{4} & -\frac{1}{4} & \frac{1}{4} & -\frac{1}{4} & -\frac{1}{8} \\ -\frac{1}{4} & \frac{1}{4} & \frac{1}{4} & -\frac{1}{4} & \frac{1}{8} \\ 1 & 1 & -\frac{1}{2} & -\frac{1}{2} & 0 \\ 1 & 1 & \frac{1}{2} & \frac{1}{2} & 0 \\ -3 & 3 & 0 & 0 & -\frac{1}{2} \end{pmatrix} \begin{pmatrix} (i\gamma_5 C)_{ik}\,(Ci\gamma_5)_{lj} \\ (C)_{ik}\,(C)_{lj} \\ (\gamma^\mu\gamma_5 C)_{ik}\,(C\gamma_\mu\gamma_5)_{lj} \\ (\gamma^\mu C)_{ik}\,(C\gamma_\mu)_{lj} \\ (\sigma^{\mu\nu} C)_{ik}\,(C\sigma_{\mu\nu})_{lj} \end{pmatrix} \tag{3.2.36}$$

$$\begin{pmatrix} \left(T^0\right)_{ij}\left(T^0\right)_{kl} \\ \sum\limits_a \left(T^a\right)_{ij}\left(T^a\right)_{kl} \end{pmatrix} = \begin{pmatrix} \frac{1}{N} & -\frac{1}{N} \\ \frac{N-1}{N} & -\frac{N+1}{N} \end{pmatrix} \begin{pmatrix} \sum\limits_a \left(T_s^a\right)_{ik}\left(T_s^a\right)_{jl} \\ \sum\limits_a \left(T_A^a\right)_{ik}\left(T_A^a\right)_{jl} \end{pmatrix} \tag{3.2.37}$$

respectively for the Dirac and flavour or colour contractions. In some cases, these relations are useful to rewrite the current-current operator in coloured channels. For instance, the computation of the baryonic masses in the NJL necessitates as a first step to compute the diquark masses. The latter are obtained as usual from the Bethe-Salpether equation where the coupling is one of those attached to four-fermion interactions with coloured bilinears. Then, the Fierz transformations in the quark-quark channel allow to reduce the number of free parameters in the baryonic sector and even to relate these couplings to the mesonic sector. This is discussed briefly in subsection 10.2.1 in the QCD context and also in the CHM context.

3.2.4 Generalisation to the three three flavours case

Let us now turn to the more realistic case with three flavours of quarks. Our goal is not to present this case in details but rather to outline the main differences compare to the two flavours case (see e.g. Refs. [60,61]). First, with three flavours, the Fierz transformations are the same than in the two flavours case [see Eq. (3.2.32)] such that at the level of the four-fermions interactions, there are no differences.

The only changes arrive in the explicit breaking terms. More precisely, at the Lagrangian level the two differences are: (i) the current mass term which is not proportional to the identity matrix [see Eq. (2.2.11)] and (ii) the 't Hooft term which is a six-point interaction [see Eq.(ref't Hooft term three flavours)].

The first point leads to an explicit breaking of the vector $SU(3)_V$ symmetry down to $SU(2)_V$. Then we expect $M_u = M_d \neq M_s$ and all of the flavour traces are modified. Indeed, the one-loop functions appearing in the gap equation involve the following flavour traces

$$Tr[\mathcal{M}T^0] = \frac{1}{\sqrt{6}}(M_u + M_d + M_s) = \frac{1}{\sqrt{6}}(2M_u + M_s)\ , \qquad Tr[\mathcal{M}T^3] = \frac{1}{2}(M_u - M_d) = 0\ , \tag{3.2.38}$$

$$Tr[\mathcal{M}T^8] = \frac{1}{2\sqrt{3}}(M_u + M_d - 2M_s) = \frac{1}{\sqrt{3}}(M_u - M_s)\ , \tag{3.2.39}$$

where the second equalities are valid when $SU(2)_V$ is an exact symmetry, that is, for $M_u = M_d$. The traces involving all of the other (non-diagonal) generators are zero. Note that, in this subsection, the mass matrix $\mathcal{M}$ contains the dynamical masses $M_{u,d,s}$ and not only the current masses $m_{u,d,s}$. As a consequence, the σ-channel associated to T^0 contributes to the gap equation but also the S^8-channel associated to T^8. This is a result of the mixing between this two channels and we will come back latter to this point.

In a similar way, the flavour traces of the one-loop two point functions $\tilde{\Pi}_i$ are modified. To properly define these two-point functions, we need to define a more convenient basis for the $SU(N)$ generators

$$T_1^\pm = \frac{1}{\sqrt{2}}(T^1 \pm iT^2)\ , \qquad T_4^\pm = \frac{1}{\sqrt{2}}(T^4 \pm iT^5)\ , \qquad T_6^\pm = \frac{1}{\sqrt{2}}(T^6 \pm iT^7)\ , \tag{3.2.40}$$

while the diagonal generators remain the same. In this new basis, the resonances associated to the above generators have definite EM charges such that we identify the mass eigenstates [5]. A change of basis was not necessary in the two flavours case because there is no breaking of the vector$SU(2)_V$ symmetry such that all of the resonances in a multiplet of $SU(2)_V$ have the same masses and we can work independently in any basis. I the above basis, the relevant and non-zero traces involved in the one-loop two point functions are

$$Tr[T^0\mathcal{M}T^0\mathcal{M}] = \frac{1}{6}(M_u^2+M_d^2+M_s^2) = \frac{1}{6}(2M_u^2+M_s^2)\ , \tag{3.2.41}$$

$$Tr[T^3\mathcal{M}T^3\mathcal{M}] = \frac{1}{4}(M_u^2+M_d^2) = \frac{1}{2}M_u^2\ , \tag{3.2.42}$$

$$Tr[T^8\mathcal{M}T^8\mathcal{M}] = \frac{1}{12}(M_u^2+M_d^2-2M_s^2) = \frac{1}{6}(M_u^2-M_s^2)\ , \tag{3.2.43}$$

$$Tr[T_1^+\mathcal{M}T_1^-\mathcal{M}] = \frac{1}{2}M_uM_d = \frac{1}{2}M_u^2\ , \tag{3.2.44}$$

$$Tr[T_4^+\mathcal{M}T_4^-\mathcal{M}] = \frac{1}{2}M_uM_s\ , \tag{3.2.45}$$

$$Tr[T_6^+\mathcal{M}T_6^-\mathcal{M}] = \frac{1}{2}M_dM_s = \frac{1}{2}M_uM_s\ , \tag{3.2.46}$$

where again, the second equalities are valid when $SU(2)_V$ is not broken. In addition, there is also the trace involving the T^0 and T^8 generators

$$Tr[T^0\mathcal{M}T^8\mathcal{M}] = \frac{1}{2\sqrt{18}}(M_u^2+M_d^2-2M_s^2) = \frac{1}{\sqrt{18}}(M_u^2-M_s^2)\ , \tag{3.2.47}$$

while $Tr[T^0\mathcal{M}T^3\mathcal{M}] = (M_u^2-M_d^2)/(2\sqrt{6})$ and $Tr[T^3\mathcal{M}T^8\mathcal{M}] = (M_u^2-M_d^2)/(4\sqrt{3})$ vanish due to the $SU(2)_V$ symmetry ie $M_u = M_d$. Then, there is a mixing between the resonances attached to the generators T^0 and T^8 [6]. In the limit where $M_u = M_s = M$, all of the above traces are either equal to zero or to $M^2/2$ in agreement with the two flavours case. Note that in the channels $T_4^\pm$ and $T_6^\pm$, a further complication comes from the fact that there are two fundamental fermions with different masses running at the same time in the loop. This is not the case for $T_1^\pm$ and T^3 which are associated to the $SU(2)_V$ subgroup. Note that the kinetic parts of the one-loop two point functions (see appendix B) do not involve $\mathcal{M}$ and are then not modified compare to the two flavours case.

Let us now turn to the second point which is related to the 't Hooft term. The latter induces new effective contributions to the four-fermions interactions. Indeed, some of the six-point interactions of Eq. (3.1.26) contribute to the Schwinger-Dyson equation as well as to the Bethe-Salpeter equation. More precisely, the first operator $D_{abc}(\overline{\Psi}T^a\Psi)(\overline{\Psi}T^b\Psi)(\overline{\Psi}T^c\Psi)$ brings new contributions to the gap equation as one can close two loops (instead of one in the case of four-fermion interactions). From the above discussion, only a part of this operator contributes, that is, the part with two non-zero traces of the form $Tr[\mathcal{M}T^a]$. Taking into account all of the symmetry factors coming from the closure of the loops, one obtains [60]

$$\begin{cases} M_u = m_u - \langle\overline{u}u\rangle(G_S + H\langle\overline{s}s\rangle) = M_d\ , \\ M_s = m_s - \langle\overline{u}u\rangle G_S - H\langle\overline{u}u\rangle^2\ , \end{cases} \tag{3.2.48}$$

where we have also taken into account the breaking of $SU(3)_V$ ie $m_s \neq m_u = m_d$. As a result, there is a system of two coupled gap equations, one for the up and down quarks and one for the strange quark. This is illustrated in figure 3.3. Note that, in the limit where the coupling of the 't Hoft term is set to zero ($H = 0$), the two gap equations are decoupled.

[5] Up to the mixing in the $T^0 - T^8$ sector (see below).

[6] If $SU(2)_V$ is explicitly broken as a consequence of $m_u \neq m_d$, there is a mixing between the sectors T^0, T^3 and T^8 as it can be seen from Eq. (3.2.38)

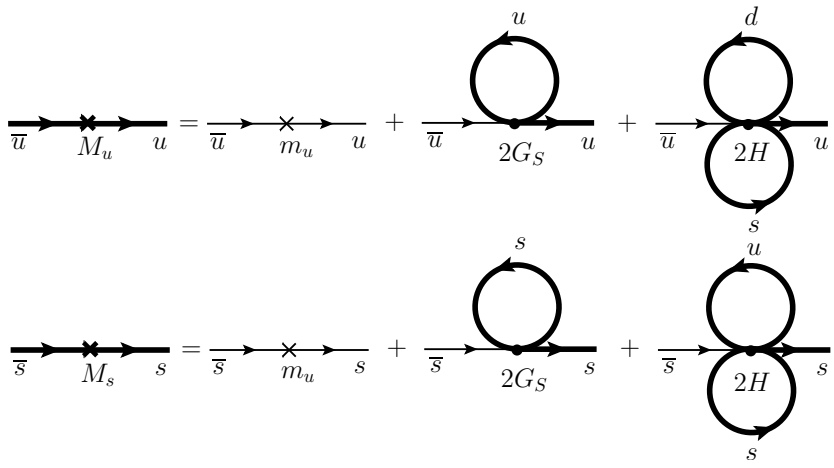

Figure 3.3: Graphical illustration of the two gap equations ($M_u = M_d$ and M_u) in the NJL approximation with three flavours. Thick and thin lines represent dressed and bare quark propagators, respectively. On the right-hand side of the equation, the contribution of the explicit breaking mass term m_q, the one of the four fermion interaction (G_S) and the one coming from the six-point 't Hooft interaction ($2H$).

Similarly, there are new contributions to the masses of the resonances which come from the 't Hooft term. These contributions arrive from new effective four-fermion interactions which are obtained by closing one loop in the two operators of Eq. (3.1.26). One has [60]

$$\begin{aligned}
K^S_{ab} &= G_S - Hc_{ab} \ , & T^a &= (T^b)^\dagger \ , \\
K^P_{ab} &= G_S + Hc_{ab} \ , & T^a &= (T_b)^\dagger \ , \\
K^V_{ab} &= \begin{cases} -(G_V + G'_V + G''_V) \ , \\ -G_V \ , \end{cases} & \begin{aligned} T^a &= T^b = T^0 \ , \\ T^a &= (T^b)^\dagger \ (a,b \neq 0) \ , \end{aligned} \\
K^A_{ab} &= \begin{cases} -(G_V + G'_V - G''_V) \ , \\ -G_V \ , \end{cases} & \begin{aligned} T^a &= T^b = T^0 \ , \\ T^a &= (T^b)^\dagger \ (a,b \neq 0) \ , \end{aligned}
\end{aligned} \tag{3.2.49}$$

respectively for the scalar (K^S_{ab}), pseudo-scalar (K^P_{ab}), vector (K^V_{ab}) and axial-vector (K^A_{ab}) channels. The coefficient c_{ab} is given by

$$c_{ab} = \begin{cases} \langle \overline{s}s \rangle \ , & a = 1^\pm, b = 1^\mp; \ a = b = 3 \ , \\ \langle \overline{u}u \rangle \ , & a = 4^\pm, b = 4^\mp; \ a = 6^\pm, b = 6^\mp \ , \\ \frac{4}{3}\langle \overline{u}u \rangle - \frac{1}{3}\langle \overline{s}s \rangle \ , & a = b = 8 \ , \\ -\frac{4}{3}\langle \overline{u}u \rangle - \frac{2}{3}\langle \overline{s}s \rangle \ , & a = b = 0 \ , \\ \frac{\sqrt{2}}{3}\langle \overline{u}u \rangle - \frac{\sqrt{2}}{3}\langle \overline{s}s \rangle \ , & a = 0, b = 8 \ , \\ 0 \ , & \text{all others} \ . \end{cases} \tag{3.2.50}$$

The 't Hooft term contributes only to the scalar and pseudo-scalar couplings (see subsection 3.1.2) with factors of the form $H[\alpha\langle \overline{u}u \rangle + \beta\langle \overline{s}s \rangle]$ where α, β are some combinatoric factors. This is a consequence of closing one loop in the operators of Eq. (3.1.26).

One can compute the masses of the resonances from Eq. (3.2.6), the effective four-fermions couplings above and the generalised (with the new flavour traces listed above) expressions of the one-loop two point functions $\tilde{\Pi}_i$. Note that, in some cases there are two mass eigenstates in the loop such that $\tilde{\Pi}_i(p^2) = \tilde{\Pi}_i(p^2, M_u^2, M_s^2)$ and the $\tilde{B}_0$ function should also be generalised in a similar way. As mentioned above, we do not present the details of the computations and refer to Ref. [60].

Finally, the last complication comes from the mixing in the $T^0 - T^8$ sector. Indeed, in that case, the four-fermions couplings and the one-loop two point functions take the following matrix form

$$\mathbf{K}^{S/P}_{08} = \begin{pmatrix} K^{S/P}_{00} & K^{S/P}_{08} \\ K^{S/P}_{80} & K^{S/P}_{88} \end{pmatrix} \ , \qquad \tilde{\mathbf{\Pi}}_{08} = \begin{pmatrix} \tilde{\Pi}^{00}_{S/P}(p^2, M^2_{u,s}) & \tilde{\Pi}^{08}_{S/P}(p^2, M^2_{u,s}) \\ \tilde{\Pi}^{80}_{S/P}(p^2, M^2_{u,s}) & \tilde{\Pi}^{88}_{S/P}(p^2, M^2_{u,s}) \end{pmatrix} \ , \tag{3.2.51}$$

in the scalar and pseudo-scalar sectors [7]. For simplicity, we have neglected in the above equation, the axial pseudo-scalar mixing (see comments in subsection 3.2.2). The physical masses M_i, are obtained from $\det[\mathbb{1} - 2\mathbf{K}_{08}^{S/P}\tilde{\mathbf{\Pi}}_{08}(p^2 = M_i^2)] = 0$ which is a generalisation of Eq. (3.2.7) in the matrix case. For instance, the mixing in the $\eta_0 - \eta_8$ sector is parametrised by the angle $\theta_{\eta\eta'}$

$$\begin{pmatrix} \eta \\ \eta' \end{pmatrix} = \begin{pmatrix} \cos\theta_{\eta\eta'} & -\sin\theta_{\eta\eta'} \\ \sin\theta_{\eta\eta'} & \cos\theta_{\eta\eta'} \end{pmatrix} \begin{pmatrix} \eta_8 \\ \eta_0 \end{pmatrix} . \tag{3.2.52}$$

One can compute this angle in the NJL (see e.g. Ref. [60]). This is relevant in the context of the η, η' decays in two photons (see subsection 2.5.2).

Finally, let us comment on new physics. In CHMs, the 't Hooft term connects the EW (from which the Higgs emerges) and the coloured (containing top partners) sector in such a way that there is a mixing between some resonances of the two sectors which have the same quantum numbers. However, this mixing is less involved than the one in QCD because it has nothing to do with the flavour symmetry in CHMs. More precisely, in CHMs the mixing arrives as a result of an effective four-fermion interaction between the two sectors. In other words, the coupling matrix in Eq. (3.2.51) has off-diagonal elements while matrix containing the one-loop two point functions is diagonal (see section 9.2.5). The QCD case is then a relevant starting point to understand the mixing bewteen the scalar and pseudo-scalar resonances of the CHMs.

[7] In the vector and axial-vector channels, the coupling matrix is diagonal as there are no contributions from the 't Hooft term. However, there is a mixing between the resonances associated to T^0 and T^8 as the matrix of one-loop two point functions contains off-diagonal elements as a result of the flavour trace.

B One-loop two point functions with Dirac fermions in the large-N_c approximation

In this appendix, we compute explicitly the one-loop two point functions involved in the derivations of subsection 3.2.2, that is, we compute the correlators relevant for the NJL model of QCD when no explicit breaking of $SU(N)_V$ is present. In the NJL approximation, the one-loop two point functions are estimated from the exchange of fermions with a dynamical mass M. The following computations stand for the QCD case with N flavours of Dirac fermions in the fundamental representation of colour. The generalisation to other gauge representations is straightforward while the equivalent computations with Weyl fermions instead of Dirac ones is not so obvious and reported in appendix H. According to section 2.4, the general [8] expression of the one-loop two-point functions $\tilde{\Pi}_i(p^2, M^2)$ is given by

$$\begin{aligned} i\tilde{\Pi}^{ab}_{\alpha\beta}(p^2, M^2) &= (-1)N_c\, Tr[T^a T^b] \int \frac{d^4k}{(2\pi)^4} \frac{Tr[i(\not{p}\ \not{k} + M) i\Gamma_\alpha i(\not{k} + M) i\Gamma_\beta]}{[(p+k)^2 - M^2][k^2 - M^2]} \\ &\equiv i\tilde{\Pi}_{\alpha\beta}(p^2, M^2)\delta^{ab} \ , \end{aligned} \tag{B.1}$$

where we have assumed that only one fermion with mass M runs in the loop (see comments below). The matrix Γ stands for the Dirac contractions [see Eq. (2.2.3)] while the factor N_c and $Tr[T^a T^b] = \delta^{ab}/2$ correspond respectively to the colour and flavour traces. In the next we consider only the one-loop functions involving the Dirac contractions $\Gamma = \{\mathbb{1}, i\gamma_5, \gamma^\mu, \gamma^\mu\gamma_5\}$. Indeed, we do not consider the tensor modes for simplicity but also because the latter are not induced by the current-current operator of subsection 3.2.3). Note that the flavour and Dirac tensor structures of the one-loop two point functions are already discussed in section 2.4. In the next, we do not consider the flavour tensor structure such that our expressions are valid both for the singlet and non-singlet channels.

Let us begin by the spin zero channels. The scalar two point function $\tilde{\Pi}_S(p^2, M^2)$ corresponds to $\Gamma_\alpha = \Gamma_\beta = \mathbb{1}$ such that

$$\begin{aligned} \tilde{\Pi}_S(p^2, M^2) &= 2iN_c \int \frac{d^4k}{(2\pi)^4} \frac{(p+k)\cdot k + M^2}{[(p+k)^2 - M^2][k^2 - M^2]} \\ &= 2iN_c \int \frac{d^4k}{(2\pi)^4} \frac{1}{2} \frac{[(p+k)^2 - M^2] + [k^2 - M^2] - (p^2 - 4M^2)}{[(p+k)^2 - M^2][k^2 - M^2]} \\ &= 2N_c \left[\tilde{A}_0(M^2) - \frac{1}{2}(p^2 - 4M^2)\tilde{B}_0(p^2, M^2) \right] \ , \end{aligned} \tag{B.2}$$

where $\tilde{A}_0(M^2)$ is defined in Eq. (3.2.4) while $\tilde{B}_0(p^2, M^2)$ corresponds to

$$\tilde{B}_0(p^2, M^2) \equiv i \int_0^\Lambda \frac{d^4k}{(2\pi)^4} \frac{1}{[(p+k)^2 - M^2][k^2 - M^2]} \ . \tag{B.3}$$

We refer to appendix G for the expression of the $\tilde{B}_0$ function after the integration over momenta. As it can be seen from Eq. (B.2), the Dirac trace divides in two non-zero parts: one involving the massive parts of the propagators ($\sim M^2 Tr[\Gamma_\alpha\Gamma_\beta]$) and the other one involving the two kinetic parts ($\sim Tr[(\not{p} + \not{k})\Gamma_\alpha\ \not{k}\Gamma_\beta]$). The same behaviour is valid for $\tilde{\Pi}_{P,V,S}$ while for $\tilde{\Pi}_{AP}$, the non-zero traces involve the product of the kinetic and massive parts of the propagators ($\sim M\ Tr[(\not{p} + \not{k})\Gamma_\alpha\Gamma_\beta + \Gamma_\alpha\ \not{k}\Gamma_\beta]$).

Similarly, for the pseudoscalar two point function $\tilde{\Pi}_P(p^2, M^2)$ for which $\Gamma_\alpha = \Gamma_\beta = i\gamma_5$, we have

$$\tilde{\Pi}_P(p^2, M^2) = 2iN_c \int \frac{d^4k}{(2\pi)^4} \frac{(p+k)\cdot k - M^2}{[(p+k)^2 - M^2][k^2 - M^2]} = 2N_c \left[\tilde{A}_0(M^2) - \frac{p^2}{2}\tilde{B}_0(p^2, M^2) \right] \ . \tag{B.4}$$

[8] The axial-pseudoscalar correlator is defined slightly differently [see Eq. (2.4.3)].

Let us now turn to the spin one channels, that is to $\tilde{\Pi}_V$ and $\tilde{\Pi}_A$. The vector and axial traces give respectively

$$\int \frac{d^4k}{(2\pi)^4} \frac{Tr[\gamma^\mu(\not{p}+\not{k}+M)\gamma^\nu(\not{k}+M)]}{[(p+k)^2-M^2][k^2-M^2]} = \int \frac{d^4k}{(2\pi)^4} \frac{Tr[\gamma^\mu(\not{p}+\not{k})\gamma^\nu \not{k} + M^2\gamma^\mu\gamma^\nu]}{[(p+k)^2-M^2][k^2-M^2]}$$
$$= \frac{4}{3}T^{\mu\nu}\left[-2\tilde{A}_0(M^2) + (p^2+2M^2)\tilde{B}_0(p^2,M^2)\right] , \tag{B.5}$$

$$\int \frac{d^4k}{(2\pi)^4} \frac{Tr[\gamma^\mu\gamma_5(\not{p}+\not{k}+M)\gamma^\nu\gamma_5(\not{k}+M)]}{[(p+k)^2-M^2][k^2-M^2]} = \int \frac{d^4k}{(2\pi)^4} \frac{Tr[\gamma^\mu(\not{p}+\not{k})\gamma^\nu \not{k} - M^2\gamma^\mu\gamma^\nu]}{[(p+k)^2-M^2][k^2-M^2]}$$
$$= \frac{4}{3}T^{\mu\nu}\left[-2\tilde{A}_0(M^2) + (p^2-42M^2)\tilde{B}_0(p^2,M^2)\right] - 8M^2L^{\mu\nu}\tilde{B}_0(p^2,M^2) , \tag{B.6}$$

where the transverse and longitudinal tensor are defined in section 2.4. Note that, to derive the above relations, we have used the following tensorial reduction

$$\tilde{B}^\mu(p^2,M^2) \equiv i\int \frac{d^4k}{(2\pi)^4} \frac{k^\mu}{[(p+k)^2-M^2][k^2-M^2]} = p^\mu \tilde{B}_1(p^2,M^2) = -p^\mu \frac{\tilde{B}_0(p^2,M^2)}{2} , \tag{B.7}$$

where in the last equality, we have used $p_\mu \tilde{B}^\mu = -p^2\tilde{B}_0/2 = p^2\tilde{B}_1$. Similarly,

$$\tilde{B}^{\mu\nu}(p^2,M^2) \equiv i\int \frac{d^4k}{(2\pi)^4} \frac{k^\mu k^\nu}{[(p+k)^2-M^2][k^2-M^2]} \tag{B.8}$$
$$= g^{\mu\nu}\tilde{B}_{00}(p^2,M^2) + p^\mu p^\nu B_{11}(p^2,M^2)$$
$$= \frac{1}{3}\left[\frac{1}{2}\tilde{A}_0(M^2) - \frac{1}{4}(p^2-4M^2)\tilde{B}_0(p^2,M^2)\right] g^{\mu\nu} + \frac{1}{3}\left[\tilde{A}_0(M^2) + (p^2-M^2)\tilde{B}_0(p^2,M^2)\right]\frac{p^\mu p^\nu}{p^2} ,$$

where the last equality has been obtained from $g^{\mu\nu}\tilde{B}_{\mu\nu} = 4\tilde{B}_0 + p^2\tilde{B}_{11} = \tilde{A}_0 + M^2\tilde{B}_0$ and $p^\mu\tilde{B}_{\mu\nu} = [\tilde{A}_0 + p^2\tilde{B}_0/2]p_\nu/2 = [\tilde{B}_{00} + p^2\tilde{B}_{11}]p_\nu$. From the above relations, one obtains for the vector and axial-vector one-loop correlators

$$\tilde{\Pi}_V^{\mu\nu}(p^2,M^2) = \tilde{\Pi}_V(p^2,M^2)T^{\mu\nu} = \frac{2}{3}N_c T^{\mu\nu}\left[-2M^2\tilde{B}_0^0(M^2) + (p^2+2M^2)\tilde{B}_0(p^2,M^2)\right] , \tag{B.9}$$

$$\begin{aligned}\tilde{\Pi}_A^{\mu\nu}(p^2,M^2) &= \tilde{\Pi}_A(p^2,M^2)T^{\mu\nu} + \tilde{\Pi}_A^L(p^2,M^2)L^{\mu\nu} \\ &= \frac{2}{3}T^{\mu\nu}\left[-2M^2\tilde{B}_0^0(M^2) + (p^2-4M^2)\tilde{B}_0(p^2,M^2)\right] - 4M^2L^{\mu\nu}\tilde{B}_0(p^2,M^2) .\end{aligned} \tag{B.10}$$

One should notice two important points in the above equations. First, in order to preserve the current conservation, we have replace $\tilde{A}_0(M^2)$ by $M^2\tilde{B}_0^0(M^2) \equiv M^2\tilde{B}_0(0,M^2)$ such that $\tilde{\Pi}_{V,A}^{\mu\nu}(0,M^2) = 0$ [9]. Second, the one-loop axial correlator contains a non-zero longitudinal part even when the axial symmetry is not explicitly broken. This is a very specific feature of the NJL model where the dynamical mass M acts like an explicit breaking term. This does not remain true for the resumed correlator $\overline{\Pi}_A^L(p^2)$ which is equal to zero in the chiral limit (see subsection 3.2.2), in agreement with the current conservation. These two points are discussed in more details in subsection 8.2.4.

Finally, the last one-loop function that we consider is the axial-pseudoscalar correlator $\tilde{\Pi}_{AP}$. In that case, according to the definition in Eq. (2.4.3) we have

$$\begin{aligned}\tilde{\Pi}_{AP}^\mu(p^2,M^2) &\equiv \tilde{\Pi}_{AP}(p^2,M^2)p^\mu = \frac{N_c}{2}\int \frac{d^4k}{(2\pi)^4} \frac{Tr[(\not{p}\not{k}+M)\gamma^\mu\gamma_5(\not{k}+M)i\gamma_5]}{[(p+k)^2-M^2][k^2-M^2]} \\ &= -i\frac{N_c}{2}\int \frac{d^4k}{(2\pi)^4} \frac{Tr[(\not{p}\not{k}+M)\gamma^\mu(\not{k}-M)]}{[(p+k)^2-M^2][k^2-M^2]} \\ &= -2N_cM\tilde{B}_0(p^2,M^2)\sqrt{p^2}p^\mu .\end{aligned} \tag{B.11}$$

[9] Remember that both the vector and the axial currents are conserved in the chiral limit even if the axial symmetry is spontaneously broken.

All of the above results, valid for one massive fermion, can be generalised to the case of two fermions with a different masses running in the loop. That is relevant e.g. in the case of the NJL model of QCD with tree-flavours. Indeed, as discussed in subsection 3.2.4, some channels involve the up quark (or the down quark) and the strange quark at the same time ($M_u = M_d \neq M_s$). Moreover, this is also relevant for the diquarks channels in CHMs as the latter involve one EW and one coloured fermion which have a different mass ie $M_\psi \neq M_X$ (see subsection 10.2.1). However, in this generalised case, the expressions of the one-loop two point functions are more involved to derive and not really telling. Let us just mention that $\tilde{\Pi}_V^L(p^2, M_1^2, M_2^2)$ and $\tilde{\Pi}_{VS}(p^2, M_1^2, M_2^2)$ become non-zero when $M_1 \neq M_2$.

Finally, if one compares the above two-points functions with the ones of appendix H, there is an additional factor two in the present Dirac case. This is due to the fact that in QCD we have N Dirac fermions, that is, N left-handed and N right-handed Weyl fermions instead of only N left-handed fermions in the CHM of chapters 8 and 9. As the normalisation of the flavour generators is the same in the two cases while the Lorentz traces are different, the Dirac and Weyl one-loop two point functions differ by a factor of two.

Part II

Phenomenological extensions of the SM

In the precedent part of the manuscript, we have reviewed some interesting aspects of the SM. We have seen in particular that the presence of BSM physics is needed to account for some experimental facts and theoretical puzzles that the SM does not explain. Let us now turn to the introduction of new physics. There are two main options to address new physics: (i) to extend the SM with only few new states and (ii) to consider a well-motivated UV complete model. In this part of the manuscript, we follow the first phenomenological approach to new physics, that is, we extend the SM only with few new states at the EW scale. These states can be seen as the low energy manifestation of a more complete UV model where the other states are heavy and can be decoupled from the low energy theory. However, we are agnostic of the UV theory and this approach is largely model independent. The second approach which is more theoretically motivated and by definition model dependent will be presented in part III where the focus will be on CHMs.

The main feature of the extensions that we consider in chapters 4 and 5 is the presence of new fermions coupled to the Higgs boson. There are several interesting points to consider new fermions instead of scalar or spin one particles. Indeed, some solutions to the hierarchy problem predict the presence of new fermions (see section 1.6 and also 6.3) close to the EW scale. That is the case e.g. in composite Higgs models where the breaking of the EW symmetry is mainly driven by the presence of relatively light top partners. In addition, most of the scenarios addressing the issue of the neutrinos masses require the presence of new fermionic states. Furthermore, the SM field content (see table 1.1) is already mainly fermionic such that, new fermions represent a natural extension of the SM. They can give for instance an explanation of the observed flavour structure of the SM. Finally, even if we do not address these questions, some fermions can be interesting DM candidates and some fermionic extensions can bring new sources of CP violation as required for baryogenesis.

New fermions were already studied in the past from the point of view of the EWPT like the Z boson couplings and the S and T parameters. As some Higgs couplings are now measured and will be measured with more and more accuracy in the near future, it is relevant to study the impact of these new fermions on the Higgs couplings in conjunction with the EWPT constraints. Then, the aim is to have a clear picture of what BSM models with new fermions are still allowed with the additional constraints coming from the Higgs couplings measurements. For instance, the classical example of a fourth generation in its simplest form is now ruled out by the Higgs couplings measurements. Let us mention that other studies undertook the study of fermionic extensions affecting the Higgs couplings but the latter have considered only few cases and are not as exhaustive as the one in chapter 4.

There may be alternative phenomenological motivations than the Higgs couplings to study fermionic extensions of the SM. We list below some possibilities. First, one can try to explain some experimental anomalies with new fermions. For instance, Refs. [62, 63] try to explain the $(g-2)_\mu$ anomaly. They classify the fermionic but also scalar and vector extensions that give a contribution to the anomalous magnetic moment of the muon. In the same spirit, Ref. [64] consider the possibility that the discrepancy between the SM prediction and the experimental measurement in the right-handed couplings $Z\bar{b}_R b_R$ (see appendix C.3) is due to the presence of new physics. They study the impact of new fermions but also new scalars and spin one particles. Another motivation is to look for generic dark matter candidates as it is done e.g. in Refs. [6, 65, 66]. In general, the above analysis do not restrict to new fermions but also consider new scalars and spin one particles. Then, it can be interesting for a future work to do an exhaustive classification of the scalar and spin one extensions that affect the Higgs couplings. However, one should note that scalar and spin one extensions at the EW scale are less trivial than fermionic extensions. Indeed, it is not easy to separate the spin zero and spin one states from an UV theory. The masses of new scalars particles are not protected from large radiative corrections (see section 1.6) and the introduction of such particles worsen the naturalness of the EW scale. For instance, new scalars can be bounds states of a new strongly interacting sector that condensates. In this way the radiative corrections are naturally cut at the condensation scale. Similarly, for a theoretically self-consistent theory with spin one particles, one should precise the origin of the new states, that is, if they are gauge bosons of a new spontaneously broken gauge symmetry or if the are bound states of a new strongly interacting sector. This UV origin constrains the couplings of the spin one states. In addition, contrary to new fermions, the structure of the SM can be widely affected by spin zero and spin one particles because the Higgs sector can be extended as well as the SM gauge

symmetry.

Let us comment a bit more on scalar extensions. In a lot of well-motivated BSM theory like e.g. supersymmetry, there is an extended Higgs sector. The most simple possibilities with respect to the T parameter are new scalar singlets or doublet with respective hypercharges $Y = 0, \pm 1/2$ (see section 1.3). Then, an interesting possibility is an extension with a second Higgs doublet and in addition to consider the effect of new fermions. These kind of models can be seen as a natural continuation of the extensions mentioned above. In particular, we already now that a Higgs doublet exists such that a second one is a natural possibility that will be considered in chapter 5.

This second part of the manuscript is organised as follow. We first discuss the fermionic extensions that couple to the SM Higgs doublet in chapter 4. In that case, the new fields content is purely fermionic and we mainly study the effects of new fermions on the EWPT as well as on the Higgs couplings. We make use of the results of chapter 1, e.g. the classification of the SM fermionic extensions is mostly based on the requirement that the SM gauge anomalies are cancelled, we highlight the fermionic extensions with a custodial symmetry protecting the T parameter and we relate some extensions to well-motivated BSM theories like SUSY or composite Higgs models. We also outline the deviations that appear in the Higgs and Z boson couplings to the SM fermions. Then in chapter 5, we present a more complicated case where the Higgs sector is extended with a second Higgs doublet and new fermions are also introduced. This chapter can be seen as a enlargement of the precedent framework. We do not classify all of the possible extensions as the fermionic extensions coupled to the SM Higgs doublet are the same than the ones with two Higgs doublets. Consequently, we rather focus on VL fermions which represent a well-motivated possibility of new fermions. The discussion is mostly driven by the possibility to reproduce two LHC anomalies: the LFV decay $h \to \tau\mu$ and the diphoton excess at 750 GeV. The second anomaly has now disappeared but as we will see, our framework is general enough to be interesting in a generalised context.

Chapter 4

Fermionic extensions of the standard model

In this chapter, we present a detailed analysis of the fermionic extensions of the SM that coupled to the Higgs boson. Indeed, when the Large Hadron Collider began its data taking, possible extensions of the Standard Model at the TeV scale were already severely constrained: electroweak precision measurements accurately confirmed the structure of the gauge sector [67–69], a number of flavour violating observables showed no significant deviation from the SM predictions [70, 71], all direct searches of non-standard particles at LEP and Tevatron gave null results [68, 72, 73]. After the first run of the LHC, the lower bounds on the masses of new particles increased substantially [74, 75]. The crucial discovery of the Higgs boson [18, 76] and the measurement of some of its properties [77–79] supported the minimal realisation of electroweak symmetry breaking , as predicted by the SM. Thus, the room for SM extensions further compressed.

In this phase, it is essential to reassess the possibilities still open for non-standard physics close to the TeV scale. As already mentioned above, in this chapter we focus on new spin-1/2 degrees of freedom. In particular, we will assume that the scalar and gauge sector is the SM one, with one standard Higgs doublet. In general, additional dynamics in the EWSB sector may well be present, including corrections to the Higgs boson couplings to the electroweak gauge bosons, as well as additional scalar or vector states: here we do not consider these possibilities, assuming that such dynamics takes place at sufficiently higher scale, or it is sufficiently weakly coupled to the SM. In other words, we will study effective field theories containing the SM degrees of freedom plus additional fermions only, being agnostic on the ultraviolet completion at higher energy.

When wondering what fundamental fermions exist in Nature, one may notice that the fermion field content of the SM appears whimsical in some respects. Each fermion family is a set of five chiral multiplets, l_L, e_R, q_L, u_R and d_R, whose gauge quantum numbers are not explained within the SM, with the remarkable property to be anomaly-free (see section 1.4). The number of families, three, is unexplained too. All SM fermions are massless before EWSB and, when the Higgs develops a vacuum expectation value, they acquire a mass proportional to their Yukawa coupling to the Higgs doublet. The structure of the Yukawa coupling matrices is not determined by the SM symmetries either (see section 1.5). Of course, some of these issues may find a convincing interpretation in very high energy extensions of the SM, such as grand unification or flavour theories, but in this chapter we will take a phenomenological point of view and centre on the TeV scale only.

Additional chiral fermions that are massless before EWSB are definitely worth to look for, as their mass is bound to the TeV scale; the classical example of a chiral fourth family, with the same field content as the SM ones, was ruled out long ago [80], but we will show that more exotic possibilities exist. On the other hand, chiral fermions that transform in a real representation or form vector-like pairs, with respect to the SM gauge group, can acquire a mass before EWSB. While in general such mass can be much larger than the EW scale, in a number of well-motivated extensions of the SM there are new, fermionic degrees of freedom close to the TeV scale. Here are some familiar examples:

- Non-zero neutrino masses may be generated through the mixing with heavier fermions, typically sterile neutrinos. The latter may have a mass close to the EW scale. However very different

scenarios are possible, spanning from the eV scale to the grand unification scale.

- The dark matter energy density may be carried by new, weakly interacting fermions. If thermally produced, their mass should be close to the EW scale.

- If the quantum stability of the EW scale is guaranteed by supersymmetry broken at the TeV scale, the SM gauge bosons shall be accompanied by gauginos, and the scalar bosons by higgsinos.

- If the weak scale is stabilised by dimensional transmutation, via a new strongly-coupled sector that condenses at the TeV scale, a number of composite spin-1/2 resonances may be present in the low energy spectrum. For example, in the scenario of partial compositeness [81, 82], the SM chiral fermions, or at least the heaviest ones, are accompanied by vector-like composite partners with the same gauge quantum numbers.

Given the diversity of phenomenological and theoretical motivations, and the wide-ranging discovery reach of the LHC, in section 4.1 we undergo a classification of the fermionic extensions of the SM, as general as possible. Theoretical consistency requires the absence of gauge anomalies. In addition, all new fermions should acquire a large mass to comply with null direct searches. As we want to explore the new constraints that materialised after the Higgs discovery, we limit ourselves to those fermions that interact with the Higgs doublet via Yukawa couplings. We provide the full list of SM extensions with these properties, formed by up to four new chiral multiplets, and comment on larger sets of new fermions. We note in passing that there may be alternative phenomenological motivations to study fermions that do not interact with the Higgs, for example to avoid the flavour problem altogether, or to look for generic dark matter candidates; some complementary classifications along this line can be found e.g. in Refs. [6, 65, 66].

The rest of the chapter is dedicated to the phenomenology of the fermionic SM extensions, in particular to identify the regions of parameters that survive to three broad classes of constraints: (i) EW precision tests; (ii) collider direct searches; (iii) Higgs boson couplings. Our purpose is to provide a comprehensive, comparative description of all possible sets of fermions, that are presently allowed and may have an observable effect at the second run of the LHC. Such analysis has several limitations that one should keep in mind:

- We compute only the leading order corrections to the Higgs and gauge boson couplings due to the extra fermions, and we roughly extract the collider bounds on their masses and couplings from the available experimental papers. A precision analysis would require a dedicated study for each given set of new fermions (and it is already available for several specific cases).

- We assume that the new fermions do not mix with the first and second SM families, in order to avoid the strong constraints coming from flavour observables (tree-level flavour changing neutral currents are absent). Indeed, the mixing with the third family is sufficient to characterise the corrections to the EW and Higgs observables, that are our main subject of interest. In addition, the Higgs couplings to the light families are presently unconstrained. Note that the mixing with the third family can still induce flavour violating processes at one loop, especially in B-meson decays or oscillations, when the top or bottom quarks mix with new fermions. However, the corrections are suppressed with respect to the SM by the masses of the new fermions and their mixing with the SM ones. The constraints are typically mild, but in some cases may be complementary to those discussed in this chapter, see e.g. Refs. [83–85].

- The new fermions are not supposed to form an ultraviolet complete theory, consistent up to a scale much larger than the TeV. Therefore, we do not impose constraints coming from the coupling evolution at high energies, such as vacuum stability, absence of Landau poles, or gauge unification. We have no pretension to determine the full theory.

- We do not restrict the possible SM extensions using cosmological considerations, that rely in most cases on specific assumptions on the early Universe evolution. For example, we do not impose bounds on the relic abundance of the new fermions, based on the assumption of an initial thermal abundance.

As a matter of fact, these points can be addressed only in a model-dependent manner. In specific, well-motivated scenarios, it would be worth to perform more precise computations and include additional constraints from the other sectors of the theory.

In section 4.2 we discuss purely chiral sets of fermions, that is, fermions that are massless before EWSB. Fermions with an EW-invariant mass, that is, either a Majorana or a vector-like mass term, are discussed in section 4.3, if they are colourless, and in section 4.4, if they are coloured. With a little abuse of terminology, we will call 'leptons' all the colourless fermions, even when they do not mix with the SM leptons, and 'quarks' all the coloured ones, even when they do not transform in the fundamental representation of the colour group $SU(3)_c$. Finally, in section 4.5 we recapitulate the most interesting results of our analysis.

For each sets of new fermions, we were confronted with the need to compute EW precision observables and Higgs couplings. Thus, we took the opportunity to collect all the relevant formulas in the appendices, that generalise well-known results to the case of a generic fermionic extension of the SM. In appendix C, we present the fermion-gauge boson couplings, the corrections to the S and T parameters, as well as to the $Zf\bar{f}$ vertex. In appendix D, we discuss the fermion-Higgs boson couplings, both the tree-level and the loop-induced ones, and we briefly summarise the present experimental constraints on the Higgs couplings.

4.1 Minimal fermionic extensions of the SM

Let us consider the extension of the SM by additional fermions, classified according to their transformation under the SM gauge group $SU(3)_c \times SU(2)_w \times U(1)_Y$, whose irreducible representations can be denoted by (R_c, R_w, Y). The SM extension is defined by the most general renormalizable Lagrangian involving the SM fields and a given set of extra chiral fermion multiplets.

We wish each set of new fermions (i) to be phenomenologically viable, (ii) to be theoretically self-consistent, *and* (iii) to modify the Higgs couplings. This leads to the following series of requirements:

(i) *No massless fermions after EWSB, except for the three SM neutrinos and gauge singlets.* Indeed, massless fermions are phenomenologically forbidden, unless they have no colour ($R_c = 1$), no electric charge ($Q = T_3 + Y = 0$), and no coupling to the Z-boson ($T_3 - \tan^2\theta_w Y = 0$). The latter two conditions imply $Y = T_3 = 0$. These conditions would allow for a massless neutral component in the chiral multiplet $(1, R_w, 0)$ with R_w odd, however the gauge symmetries permit a Majorana mass term for such a multiplet.

(ii) *No SM gauge anomalies.* The fermionic extensions of the SM under consideration are intended as effective theories valid up to the multi-TeV scale, therefore they should cancel all SM anomalies self-consistently. (Extra fermions much heavier than the EW scale play no role in the anomaly cancellation, since they form vector-like pairs with respect to the SM gauge group.) Since the SM field content is anomaly-free by itself, the anomaly-cancellation conditions must be imposed on the set of new fermions only.

As we require the absence of massless coloured states, the new fermions form a (reducible) real representation of $SU(3)_c$, therefore the $SU(3)_c$-cubic anomaly is automatically vanishing. Denoting the new fermion representations by (R_{ci}, R_{wi}, Y_i), for $i = 1, \ldots, n$, the remaining anomaly-cancellation conditions read

$$\begin{array}{rcl} SU(3)_c - SU(3)_c - U(1)_Y & : & \sum_{i=1}^n N_{wi} C(R_{ci}) Y_i = 0 \,, \\ SU(2)_w - SU(2)_w - U(1)_Y & : & \sum_{i=1}^n N_{ci} C(R_{wi}) Y_i = 0 \,, \\ U(1)_Y - U(1)_Y - U(1)_Y & : & \sum_{i=1}^n N_{ci} N_{wi} Y_i^3 = 0 \,, \\ grav - grav - U(1)_Y & : & \sum_{i=1}^n N_{ci} N_{wi} Y_i = 0 \,, \end{array} \tag{4.1.1}$$

where $N_w \equiv \dim(R_w)$, $N_c \equiv \dim(R_c)$ – this notation is redundant for $SU(2)$ but not for $SU(3)$ – and the index $C(R)$ of a given representation is defined by $\mathrm{Tr}(T_R^a T_R^b) = C(R)\delta_{ab}$, with the index of the fundamental conventionally normalised to $C(N) = 1/2$ for $SU(N)$. In the case of $SU(2)$ one has $C(R_w) = N_w(N_w^2-1)/12$. In the case of $SU(3)$ each representation R_c is characterised by

two integer Dynkin labels (a_1, a_2) with $a_i \geq 0$, and one has $N_c = (1+a_1)(1+a_2)(1+a_1/2+a_2/2)$ and $C(R_c) = N_c(a_1^2 + 3a_1 + a_1a_2 + 3a_2 + a_2^2)/24$.

Additionally, the $SU(2)_w$ gauge group has a global anomaly, that cancels only when the sum $\sum_{i=1}^{n} N_{ci}C(R_{wi})$ is an integer number [86]. Note that $C(R_w)$ is half-integer for $N_w = 2 + 4n$, $n = 0, 1, 2, \ldots$, and integer in all other cases. As for the previous anomalies, this condition must be satisfied by the fermions below the multi-TeV scale. (Heavier fermions, decoupled from the EW scale, necessarily give an integer contribution to the sum: only an even number of multiplets with N_w even can acquire a vector-like mass.)

(iii) *Non-zero corrections to the Higgs boson couplings.* This corresponds to consider only new fermions with a Yukawa coupling to the SM Higgs doublet. More precisely, any subset of new fermions that satisfies the requirements (i) and (ii) by itself – any subset with no massless states nor anomalies – should have a non-zero Yukawa coupling to the Higgs. Otherwise, such subset would interact with the SM only through gauge interactions; strictly speaking, it can still affect the Higgs boson couplings at the two-loop level, but here we neglect such small effects.

We stress that the three requirements above are independent, in the sense that none is automatically implied by the others. In particular: vector-like fermions are automatically massive and anomaly-free, but they may not couple to the Higgs doublet; chiral fermions that have non-zero masses, such as an extra family of quarks, can be anomalous; an anomaly-free set of fermions, such as zero-hypercharge fermions, may contain some massless components.

In the following we classify the sets of n chiral fermions that satisfy the requirements (i), (ii) and (iii), for $n = 1, 2, 3, 4$, and we briefly comment on larger sets. For convenience, we will mark with the symbol $\square$ each viable set that is identified.

4.1.1 One multiplet

If we add to the SM only one new chiral fermion $\psi \sim (R_c, R_w, Y)$, the only possibility to avoid massless states with non-zero SM gauge charges is the presence of a Majorana mass term $m_\psi \psi\psi$, that requires $R_c = \overline{R_c}$, $Y = 0$ and N_w odd. Such multiplet is anomaly-free. The additional requirement to couple to the Higgs doublet, $H \sim (1, 2, 1/2)$, restricts the possibilities to $R_c = 1$ and $R_w = 1$ or 3, that is,

$$\square \qquad N \sim (1, 1, 0) \qquad \text{or} \qquad \Sigma \sim (1, 3, 0)\ . \tag{4.1.2}$$

In both cases a Yukawa coupling is allowed among the new fermion, H and the SM lepton doublet $l \sim (1, 2, -1/2)$.

Since N (Σ) forms by itself a self-consistent extension of the SM that modifies the Higgs couplings, n replicas of N (and/or Σ) also define a set of new fermions satisfying all our criteria. We will analyse their phenomenology in section 4.3.1. Of course, there may also be consistent sets of n new fermions that are partly formed by replicas of N or Σ, and partly by different multiplets, as we will see in the following sections.

4.1.2 Two multiplets

Let us classify the possible pairs of chiral fermions ψ_1 and ψ_2 that can be added consistently to the SM and that modify the Higgs couplings. The fermion ψ_1 can satisfy all requirements without ψ_2 only if it transforms as $(1, 1, 0)$ or $(1, 3, 0)$, as shown in section 4.1.1. In this case the three obvious possibilities are

$$\square \qquad N_1 + N_2\ , \qquad \Sigma_1 + \Sigma_2\ , \qquad N + \Sigma\ . \tag{4.1.3}$$

For all other representations, a coupling between ψ_1 and ψ_2 is necessary: either there is a vector-like mass term $m_{12}\psi_1\psi_2$, or a Yukawa coupling $\psi_1\psi_2 H(\tilde{H})$. The latter possibility leads to an inconsistent mass spectrum: one has $N_{w1} = N_{w2} + 1$ (or vice versa) and the unbalanced component of ψ_1 has $T_3 \neq 0$, therefore it cannot be massless. Then, either ψ_1 admits a Majorana mass term or it couples to a SM fermion too. One can check that, in both cases, either another unwanted massless state is left, or a SM neutrino acquires a large mass too. An alternative way to exclude the case of the

ψ_{L1}	ψ_{L2}	coupling to
$E \sim (1,1,-1)$	$E^c \sim (1,1,+1)$	l, e^c
$L \sim (1,2,-\frac{1}{2})$	$L^c \sim (1,2,+\frac{1}{2})$	l, e^c
$\Lambda \sim (1,2,-\frac{3}{2})$	$\Lambda^c \sim (1,2,+\frac{3}{2})$	e^c
$\Delta \sim (1,3,-1)$	$\Delta^c \sim (1,3,+1)$	l
$T \sim (3,1,+\frac{2}{3})$	$T^c \sim (\overline{3},1,-\frac{2}{3})$	q, u^c
$B \sim (3,1,-\frac{1}{3})$	$B^c \sim (\overline{3},1,+\frac{1}{3})$	q, d^c
$X_T \sim (3,2,+\frac{7}{6})$	$X_T^c \sim (\overline{3},2,-\frac{7}{6})$	u^c
$Q \sim (3,2,+\frac{1}{6})$	$Q^c \sim (\overline{3},2,-\frac{1}{6})$	q, d^c, u^c
$Y_B \sim (3,2,-\frac{5}{6})$	$Y_B^c \sim (\overline{3},2,+\frac{5}{6})$	d^c
$X_Q \sim (3,3,+\frac{2}{3})$	$X_Q^c \sim (\overline{3},3,-\frac{2}{3})$	q
$Y_Q \sim (3,3,-\frac{1}{3})$	$Y_Q^c \sim (\overline{3},3,+\frac{1}{3})$	q

Table 4.1: Vector-like pairs of left-handed chiral fermions, that provide a consistent extension of the SM and modify the Higgs boson couplings.

Yukawa coupling $\psi_1\psi_2 H(\tilde{H})$ is to solve the anomaly system (4.1.1) for $n = 2$: one obtains $N_{c1} = N_{c2}$, $C(R_{c1}) = C(R_{c2})$, $R_{w1} = R_{w2}$ and $Y_1 = -Y_2$. Thus, we conclude that the two chiral fermions should form a vector-like pair,

$$\square \qquad \psi_1 \sim (R_c, R_w, Y) \ , \qquad \psi_2 \sim (\overline{R_c}, R_w, -Y) \ . \tag{4.1.4}$$

In order to modify the Higgs couplings, at least one among ψ_1 and ψ_2 should have a Yukawa coupling with a SM fermion and the Higgs doublet. We take conventionally all chiral fermions to be left-handed. A SM family is formed by $l \sim (1,2,-1/2)$, $e^c \sim (1,1,1)$, $q \sim (3,2,1/6)$, $u^c \sim (\bar{3},1,-2/3)$, and $d^c \sim (\bar{3},1,1/3)$. In order to have a Yukawa coupling with these representations, the new fermions should transform under $SU(3)_c$ either as singlets or triplets. The former mix with SM leptons and can be called vector-like leptons (VLLs), the latter mix with SM quarks, hence the name vector-like quarks (VLQs). Under $SU(2)_w$ they can transform as singlets, doublets or triplets. All possible vector-like fermions with a Yukawa coupling to the SM fermions are listed in Table 4.1.

To analyse the phenomenology of vector-like fermion multiplets, it is useful to name the components with different electric charge Q. The possible components of the VLLs have charges $Q(N) = 0$, $Q(E) = -1$ and $Q(F) = -2$. Then, the self-conjugate leptons N and Σ and the four VLLs can be written as

$$N, \quad \Sigma = \begin{pmatrix} E^c \\ N \\ E \end{pmatrix} ; \quad E, \quad L = \begin{pmatrix} N \\ E \end{pmatrix} , \quad \Lambda = \begin{pmatrix} E \\ F \end{pmatrix} , \quad \Delta = \begin{pmatrix} N \\ E \\ F \end{pmatrix} \ . \tag{4.1.5}$$

After EWSB, N, E and E^c can mix with the SM leptons ν, e and e^c, respectively, while F does not mix with the SM. We will discuss the phenomenology of these VLLs in section 4.3.2.

The possible components of the VLQs have charges $Q(X) = 5/3$, $Q(T) = 2/3$, $Q(B) = -1/3$ and $Q(Y) = -4/3$. They are embedded in seven possible VLQ multiplets,

$$T, \quad B, \quad X_T = \begin{pmatrix} X \\ T \end{pmatrix} , \quad Q = \begin{pmatrix} T \\ B \end{pmatrix} , \quad Y_B = \begin{pmatrix} B \\ Y \end{pmatrix} , \quad X_Q = \begin{pmatrix} X \\ T \\ B \end{pmatrix} , \quad Y_Q = \begin{pmatrix} T \\ B \\ Y \end{pmatrix} \ . \tag{4.1.6}$$

After EWSB, T, T^c, B and B^c can mix with the SM quarks t, t^c, b and b^c, respectively. On the contrary, the components X, Y and their conjugate do not mix with the SM. We will discuss the phenomenology of these VLQs in section 4.4.1.

4.1.3 Three multiplets

Let us classify the possible sets of three chiral fermions $\psi_{1,2,3}$ that can be added to the SM consistently with the requirements of section 4.1. Of course, there is the trivial possibility to combine smaller sets that are already consistent on their own:

- ☐ Three copies of $N \sim (1,1,0)$ and/or of $\Sigma \sim (1,3,0)$.
- ☐ A vector-like fermion from Table 4.1 plus one copy of N or Σ. As the latter couples to the SM lepton doublet l, there may be a non-trivial interplay with the VLLs E, L and Δ, that also couple to l. We will discuss this case in section 4.3.4.

To explore all the other possibilities, note that there are two patterns for the colour representations of $\psi_{1,2,3}$, that guarantee the absence of massless coloured states:

- $R_{c1} = \overline{R_{c1}}$ plus a vector-like pair $R_{c2} = \overline{R_{c3}} \neq R_{c1}$. The only choice allowing for couplings to the Higgs is $R_{c1} = 1$ and $R_{c2} = 3$. In this case the two subsets ψ_1 and $\psi_{2,3}$ do not interact with each other, therefore each should be a consistent extension of the SM by itself, reducing to the trivial possibilities already listed above.
- $R_{c1} = R_{c2} = \overline{R_{c3}}$. These can be either real or complex representations. One may have considered three real representations of $SU(3)_c$ not all equal to each other; in this case, however, it is not possible to allow Yukawa couplings to the Higgs and to give a mass to all coloured components, at the same time.

In the only non-trivial case, $R_{c1} = R_{c2} = \overline{R_{c3}}$ or permutations, the anomaly conditions in Eq. (4.1.1) reduce to

$$\begin{cases} N_{w1}^3 Y_1 + N_{w2}^3 Y_2 + N_{w3}^3 Y_3 = 0 \ , \\ N_{w1} Y_1 + N_{w2} Y_2 + N_{w3} Y_3 = 0 \ , \\ N_{w1} Y_1^3 + N_{w2} Y_2^3 + N_{w3} Y_3^3 = 0 \ . \end{cases} \tag{4.1.7}$$

The possible solutions of this system (with N_{wi} positive integers) are

(a) $Y_i = 0$ and N_{wi} arbitrary, for $i = 1,2,3$.

(b) $Y_1 = 0$ with N_{w1} arbitrary, $Y_2 = -Y_3 \neq 0$ with $N_{w2} = N_{w3}$, or permutations.

(c) For any pair of integer numbers $n, m \geq 0$,

$$\begin{cases} N_{w1} = 1 + n \ , & N_{w2} = 2 + n + m \ , & N_{w3} = 3 + 2n + m \ , \\ Y_1 \neq 0 \text{ arbitrary}, & Y_2 = -Y_1 \dfrac{N_{w1}(N_{w3}^2 - N_{w1}^2)}{N_{w2}(N_{w3}^2 - N_{w2}^2)} \ , & Y_3 = Y_1 \dfrac{N_{w1}}{N_{w3}} \dfrac{N_{w2}^2 - N_{w1}^2}{N_{w3}^2 - N_{w2}^2} \ , \end{cases} \tag{4.1.8}$$

or permutations.

Let us consider these solutions in turn, to analyse whether they can satisfy the other requirements of section 4.1.

(a) In order to couple to the Higgs boson, one needs $R_{ci} = 1$ and $R_{wi} = 1$ or 3 for $i = 1,2,3$, that is three copies of N or Σ: a trivial possibility already considered.

(b) Suppose first that ψ_2 and ψ_3 form a vector-like pair, that is, $R_{c1} = R_{c2} = \overline{R_{c3}}$. But, to avoid unpaired complex representations of $SU(3)_c$, one needs R_{c1} to be real. Barring the trivial cases where ψ_1 and $\psi_{2,3}$ form self-consistent extensions of the SM separately, the necessary condition to modify the Higgs couplings is to allow for a Yukawa coupling between ψ_1 and $\psi_{2,3}$. This leads to

☐ $$\psi_1 \sim (R_c, R_w, 0) \ , \quad \psi_2 \sim (R_c, R_w \pm 1, \frac{1}{2}) \ , \quad \psi_3 \sim (R_c, R_w \pm 1, -\frac{1}{2}) \ , \quad R_c = \overline{R_c} \ . \tag{4.1.9}$$

The choice of R_w is arbitrary up to the $SU(2)_w$ global anomaly: for $N_w = 2 + 4n$, one needs N_c to be even. The colourless case $R_c = 1$ will be discussed in section 4.3.4. The coloured case $R_c = 8, 27, \ldots$ will be discussed in section 4.4.3.

Next, suppose that ψ_2 and ψ_3 do not form a vector-like pair, that is, a complex representation $R_{c1} = \overline{R_{c2}} = \overline{R_{c3}}$. In order to have the same number of colour-conjugate representations one needs $N_{w1} = 2N_{w2}$. A Yukawa coupling is also needed among ψ_1 and $\psi_{2,3}$ to provide masses, so the only possibility is

$$\square \qquad \psi_1 \sim (R_c, 2, 0) \ , \quad \psi_2 \sim (\overline{R_c}, 1, \frac{1}{2}) \ , \quad \psi_3 \sim (\overline{R_c}, 1, -\frac{1}{2}) \ , \quad R_c \neq \overline{R_c} \ . \tag{4.1.10}$$

The $SU(2)_w$ global anomaly further requires that N_c must be even. Note that this is the minimal, consistent set of chiral fermions that has no vector-like mass terms, rather it acquires a mass from the Yukawa couplings only. The phenomenology of purely chiral fermions is discussed in section 4.2.

(c) For $(n, m) \neq (0, 0)$, one has $N_{w3} \geq 4$. Then, ψ_3 does not couple to the SM nor to ψ_1, and even the possible Yukawa coupling to ψ_2 cannot provide a mass to all the N_{w3} components of ψ_3. Therefore, let us take $(n, m) = (0, 0)$, that implies

$$\psi_1 \sim (R_c, 1, Y) \ , \quad \psi_2 \sim (R_c, 2, -\frac{4}{5}Y) \ , \quad \psi_3 \sim (\overline{R_c}, 3, \frac{1}{5}Y) \ . \tag{4.1.11}$$

By requiring an equal number of components with opposite electric charge, one finds $Y = \pm 1/2$ or $Y = \pm 1/6$. In both cases one can check that some components of the new fermions remain massless, therefore no consistent SM extension of this type exists.

4.1.4 Four multiplets

In the previous sections we derived the list of all the consistent sets of n new chiral fermions, with $n \leq 3$, discussing in detail how to implement the requirements of section 4.1. Here we provide the complete list for $n = 4$, without displaying the lengthy and involved analysis needed to prove this result.

First of all, there are a number of possibilities to combine smaller subsets of new fermions that are already consistent by themselves. It is worth to list them for bookkeeping and to point out those combinations with special phenomenological relevance:

- ☐ Four copies of N and/or Σ.
- ☐ Two copies of N and/or Σ plus a vector-like fermion from Table 4.1. In particular, the set (N, Σ, L, L^c) corresponds to the neutralinos and charginos of the minimal supersymmetric SM: bino, wino and the two higgsinos. This case is discussed in section 4.3.4.
- ☐ Two vector-like fermions Ψ_1 and Ψ_2 from Table 4.1. A non-trivial interplay occurs when Ψ_1 and Ψ_2 couple both to a given SM fermion, as indicated in the last column of Table 4.1, and/or when there is a Yukawa coupling between Ψ_1 and Ψ_2: this happens for E or Δ with L or Λ; T or X_Q with X_T or Q; B or Y_Q with Q or Y_B. In models of partial compositeness, a SM fermion acquires its mass by mixing with two vector-like composite fermions, with the same quantum numbers as the SM left- and right-handed components: Q and T for the top quark, Q and B for the bottom quark, L and E for the tau lepton. This case is discussed in section 4.3.3 for leptons and 4.4.2 for quarks.
- ☐ One copy of N or Σ and a set of three fermions from Eq. (4.1.9) or Eq. (4.1.10). A non-trivial interplay occurs in the case $(1, 3, 0) + (1, 5, 0) + (1, 4, 1/2) + (1, 4, -1/2)$, discussed in section 4.3.4.

Let us come to the consistent sets of four fermions that are not the union of two smaller self-consistent sets. We found that non-trivial solutions are possible only when the four colour representations R_{ci} are all equal or conjugate to each other. After all requirements of section 4.1 are taken into account, only two possible patterns emerge:

- For arbitrary R_c and R_w, a viable set of four multiplets is provided by

  $$\square \qquad (R_c, R_w - 1, 0) + (R_c, R_w + 1, 0) + (\overline{R_c}, R_w, 1/2) + (\overline{R_c}, R_w, -1/2) \ , \tag{4.1.12}$$

  with one exception: if N_w is odd, then either $C(R_w - 1)$ or $C(R_w + 1)$ is half-integer, therefore one needs N_c even to cancel the global $SU(2)_w$ anomaly.

  The case $R_c = 1$ can be described as two Majorana leptons plus a vector-like lepton (see section 4.3.4). The case $R_c = \overline{R_c} \neq 1$ is the analogue for coloured fermions (section 4.4.3). Finally, the case $R_c \neq \overline{R_c}$ is purely chiral, with no masses before EWSB (section 4.2).

- For arbitrary R_c, R_w and Y, a viable set of four multiplets is

  $$\square \qquad (R_c, R_w, Y) + (\overline{R_c}, R_w, -Y) + (R_c, R_w + 1, Y - 1/2) + (\overline{R_c}, R_w + 1, -Y + 1/2) \ . \tag{4.1.13}$$

  For the first time we encounter a pattern where the hypercharges of the new fermions are not determined uniquely.

  The case $R_c = 1$ corresponds to two VLLs (section 4.3.3), except when $Y = 0$ with N_w odd, or $Y = 1/2$ with N_w even: then, one has two Majorana leptons plus one VLL (section 4.3.4). The case $R_c \neq 1$ corresponds to two VLQs (section 4.4.2), except when $R_c = \overline{R_c}$ and $Y = 0$ with N_w odd, or $Y = 1/2$ with N_w even: then, one has two Majorana quarks plus one VLQ (section 4.4.3).

We found that all other sets of four multiplets relevant for Higgs couplings are not viable: either some component remains massless, or a gauge anomaly is present.

4.1.5 Larger sets of new fermions

We do not attempt a general classification for $n \geq 5$ new chiral fermions. On the one hand, the general principles and the different phenomenological possibilities are already well illustrated by more minimal sets of fermions. On the other hand, a detailed analysis is worth only in the context of a specific, well-motivated theory beyond the SM. Here we shall mention some prominent examples that have been extensively studied, to situate them in the context of our classification.

- We have shown that there are two sets of purely chiral fermions, displayed in Eq. (4.1.10) and in Eq. (4.1.12), formed by three and four multiplets, respectively. The more traditional chiral extension of the SM is a fourth family, formed by the five multiplets q'_L, t'_R, b'_R, l'_L and τ'_R. It was already excluded at the time of LEP, because the Z invisible width forbids a fourth massless neutrino, but it could be rescued adding a sixth multiplet, a sterile neutrino ν'_R. It is by now excluded by the measurement of the Higgs boson couplings [87], as we will review at the end of section 4.2.

- The minimal supersymmetric extensions of the SM predicts fermionic partners for the gauge bosons and for the two Higgs doublets. This amounts to five chiral multiplets: a bino $\sim (1, 1, 0)$, a wino $\sim (1, 3, 0)$, two higgsinos $\sim (1, 2, \pm 1/2)$ and a gluino $\sim (8, 1, 0)$. The latter does not enter in our classification, since it does not couple to the Higgs doublet. Concerning the other four multiplets, supersymmetry restricts the possible couplings among them and to the SM, therefore it corresponds to a special case in the parameter space of the SM extension by the set (N, Σ, L, L^c). We will briefly discuss the related phenomenology in section 4.3.4. Of course, our purely fermionic extension of the SM corresponds to the limit where the scalar supersymmetric partners are significantly heavier than neutralinos and charginos.

- Another scenario addressing the hierarchy problem is compositeness. An effective way to couple the SM fermions to a composite Higgs doublet amounts to a partial fermion compositeness: each SM chiral fermion mixes with a composite vector-like fermion with the same quantum numbers. Thus, to induce a Yukawa coupling among two SM fermions and the composite Higgs one needs two vector-like fermions. Therefore, a SM extension by four chiral multiplets is suitable to study this mechanism for one SM Yukawa coupling at a time. Indeed, partial compositeness corresponds to a special subspace of parameters, because the symmetries of composite models restrict the couplings of the new fermions and of the SM ones. We will briefly discuss the phenomenology of τ-compositeness in section 4.3.4 and the case of b and t-compositeness in section 4.4.2. Of course, realistic models of partial compositeness require more than two vector-like fermions, e.g. to induce the Yukawa couplings of all the heavy, third family fermions. The interplay between the Higgs and composite vector-like fermions is studied in detail e.g. in Refs. [88–92].

4.2 Phenomenology of new chiral fermions

In this section we study purely chiral sets of new fermions, that is to say, one cannot write any fermion mass term before EWSB, thus their masses are generated by the Higgs vev only. These sets do not contain vector-like pairs of chiral multiplets, that would admit a Dirac mass, nor multiplets in the representations $(R_c, R_w, 0)$ with $R_c = \overline{R_c}$ and R_w odd, that would admit a Majorana mass. A purely chiral set, consistent with the requirements of section 4.1, constitutes a new fermion 'family', very much analogue to the three SM families.

We identified two classes of purely chiral sets, formed by three and four multiplets respectively, displayed in Eq. (4.1.10) and Eq. (4.1.12). We will discuss the phenomenology of these two classes in some detail. In the last part of the section, we will investigate whether larger chiral sets of fermions may be compatible with present Higgs data.

- ***Three chiral multiplets.*** The only consistent 'family' formed by three chiral multiplets is

$$\psi_{1L} \sim (R_c, 2, 0) \ , \quad \psi_{2R} \sim \left(R_c, 1, \frac{1}{2}\right) \ , \quad \psi_{3R} \sim \left(R_c, 1, -\frac{1}{2}\right) \ , \quad R_c \neq \overline{R_c} \ , N_c \text{ even} \ , \tag{4.2.1}$$

the smallest viable representation being $R_c = 6$. The Yukawa interactions are

$$-\mathcal{L}_Y = \lambda_{12} \overline{\psi_{1L}} \tilde{H} \psi_{2R} + \lambda_{13} \overline{\psi_{1L}} H \psi_{3R} + h.c. \ . \tag{4.2.2}$$

Here and in the rest of the chapter we do not display the obvious kinetic terms, that must be added for each new fermion. After EWSB one is left with two mass eigenstates F_{12} and F_{13} in the same colour representation R_c, with charge $Q = \pm 1/2$ and mass $m_{12} = \lambda_{12} v/\sqrt{2}$ and $m_{13} = \lambda_{13} v/\sqrt{2}$, respectively.

The lightest new fermion is stable and forms hadrons with exotic charges, that are constrained to be heavier than several hundreds of GeVs. Indeed, the searches for R-hadrons [5, 93] assume the existence of a stable stop or sbottom (scalar with $R_c = 3$), or of a stable gluino (fermion with $R_c = 8$). In the latter case one finds $m_{R_c=8} \gtrsim 1320$ GeV [94], and we expect a similar (stronger) bound for $R_c = 6$ (larger colour representations), as these fermions are pair-produced through their coupling to gluons. To roughly estimate the limit on a stable sextet, we rescale the gluino bound by computing the ratio between the sextet and octet production cross section at tree level. Taking into account the different colour contractions and the interference of the s, t and u-channel, we obtain a lower bound $m_{R_c=6} \gtrsim 1400$ GeV. Further discussions and references on the constraints on R-hadrons can be found e.g. in Refs. [6, 95]. This limit from direct searches already leads to some tension with the perturbativity upper bound, $m_{12,13} \ll (4\pi) v/\sqrt{2} \simeq 2.2$ TeV.

The contribution of $F_{12,13}$ to the oblique parameters reads

$$S \simeq \frac{N_c}{6\pi} \ , \qquad T \simeq \frac{N_c}{16\pi s_w^2 c_w^2 m_Z^2} \left(m_{12}^2 + m_{13}^2 - 2 \frac{m_{12}^2 m_{13}^2}{m_{12}^2 - m_{13}^2} \ln \frac{m_{12}^2}{m_{13}^2} \right) \ . \tag{4.2.3}$$

Note that for $(m_{12} - m_{13}) \to 0$ one finds $T \propto (m_{12} - m_{13})^2$, because in the degenerate limit the custodial symmetry is restored: for $\lambda_{12} = \lambda_{23}$ Eq. (4.2.2) has a global $SU(2)_R$ symmetry with ψ_{2R} and ψ_{3R} transforming as a doublet. The value of S can lie within the 3σ ellipse, but only if $N_c = 6$ and $T \simeq 0.3$ at the same time (see figure C.2). This can be achieved for $(m_{12} + m_{13})/2 \simeq 1500$ GeV and $(m_{12} - m_{13}) \simeq 50$ GeV. Thus, this 'family' of new fermions is marginally compatible with direct searches and EW precision tests.

After the Higgs discovery, however, one can definitely exclude such a set of new fermions. As they are heavier than the Higgs boson and do not mix with the SM fermions, the Higgs decay width at tree-level are unchanged. However, a huge deviation occurs in the loop-induced Higgs coupling to gluons,

$$R_{gg} \equiv \frac{\sigma(gg \to h)}{\sigma_{SM}(gg \to h)} \simeq [1 + 4C(R_c)]^2 \ . \tag{4.2.4}$$

where we have taken the limit $m_t^2, m_{12}^2, m_{13}^2 \gg m_h^2/4$ in the loop form factor (see appendix D.2). Even the smallest possible colour representation has $C(6) = 5/2$, leading to a huge $R_{gg} = 121$, totally incompatible with LHC data.

• ***Four chiral multiplets.*** Let us move to the only consistent 'family' formed by four chiral multiplets,

$$\psi_{1L} \sim (R_c, R_w - 1, 0), \quad \psi_{2L} \sim (R_c, R_w + 1, 0), \quad \psi_{3R} \sim \left(R_c, R_w, \frac{1}{2}\right), \quad \psi_{4R} \sim \left(R_c, R_w, -\frac{1}{2}\right), \tag{4.2.5}$$

with $R_c \neq \overline{R_c}$ to prevent vector-like or Majorana mass terms, and with N_c even if N_w is odd, to prevent a global $SU(2)_w$ anomaly. The allowed Yukawa interactions are

$$-\mathcal{L}_Y = \lambda_{13}\overline{\psi_{1L}}\tilde{H}\psi_{3R} + \lambda_{14}\overline{\psi_{1L}}H\psi_{4R} + \lambda_{23}\overline{\psi_{2L}}\tilde{H}\psi_{3R} + \lambda_{24}\overline{\psi_{2L}}H\psi_{4R} + h.c. \ . \tag{4.2.6}$$

where the explicit $SU(2)_w$ contractions are defined in Eq. (D.4). After EWSB the components of $\psi_{1,2L}$ combine with those of $\psi_{3,4R}$ to forms $2N_w$ mass eigenstates: one with charge $Q = N_w/2$; two mixed states with $Q = N_w/2 - 1, \ldots, -N_w/2 + 1$; one with $Q = -N_w/2$. As they have (half-)integer charges, they do not mix with the SM quarks and the lightest state is stable and hadronises, with collider bounds above 1 TeV, analogue to those discussed above. The discussion of oblique parameters is also similar to the previous case: one can be marginally consistent with data, by choosing the parameters to realise an approximate custodial protection.

The way to definitely exclude this set of chiral fermions is, once again, their contribution to the Higgs boson coupling to gluons. Note that each of the $2N_w$ mass eigenstates belongs to the same colour representation R_c and must be (much) heavier than the top quark, therefore one finds

$$R_{gg} \simeq [1 + 2(2N_w)C(R_c)]^2 \ . \tag{4.2.7}$$

Even in the minimal case with $N_w = 2$ and $C(3) = 1/2$, one finds a very large $R_{gg} \simeq 25$, incompatible with the LHC Higgs data.

• ***Larger sets of chiral multiplets.*** Let us ask the question whether we can exclude any set of purely chiral fermions, even when it is formed by more than four multiplets. Indeed, the Higgs coupling to gluons implies that any new chiral fermion should be colourless, because even the minimal set of chiral coloured fermions, formed by a weak doublet and two weak singlets with $R_c = 3$, leads to a large $R_{gg}^{min} \simeq 9$. This is not compatible with the range currently allowed by global fits, $0.5 \lesssim R_{gg} \lesssim 1.8$ at 99 % C.L. [96] (see appendix D.3 for details). In particular, in this way one can exclude [87] a fourth SM family, formed by the six multiplets q'_L, t'_R, b'_R, l'_L, τ'_R and ν'_R. Recall that the sterile neutrino is required to avoid an additional massless neutrino, that is forbidden by the Z invisible width; then this set of fermions is not purely chiral, but one may invoke a lepton number symmetry to forbid the sterile neutrino Majorana mass. Let us remark that coloured chiral fermions may be allowed in the case of extended Higgs sectors, not considered in the present chapter. For example, adding an Higgs

triplet, it is possible to rescue the fourth family [97]. Another example is provided by coloured chiral fermions receiving their mass from a second Higgs doublet [98].

Coming to colourless chiral fermions, some of the mass eigenstates are necessarily charged and thus contribute to the Higgs width to photons as

$$R_{\gamma\gamma} = \frac{\left|\mathcal{A}^{\gamma\gamma}_{SM} + A^{\gamma\gamma}_{new}\right|^2}{\left|\mathcal{A}^{\gamma\gamma}_{SM}\right|^2} \,, \qquad A^{\gamma\gamma}_{new} \simeq \frac{4}{3}\sum_k Q_k^2 \,, \tag{4.2.8}$$

where $R_{\gamma\gamma}$ is defined in Eq. (D.41), the SM amplitude is $\mathcal{A}^{\gamma\gamma}_{SM} \simeq -6.5$ and the sum runs over the new fermion mass eigenstates. Note that, to derive Eq. (4.2.8) from Eqs. (D.21) and (D.22), we took (i) $2m_i \gg m_h$, that is accurate enough, even though the lower bounds on heavy charged lepton masses are weaker than those on coloured particles; (ii) Higgs-fermion couplings $y_i = m_i/v$ and $\tilde{y}_i = 0$, that is the case for purely chiral fermions, because their mass matrices are proportional to the Higgs vev v, see Eq. (D.6). Note also that the result is independent from potential mixing between the new fermions and the SM leptons. The presently allowed range is $0.5 \lesssim R_{\gamma\gamma} \lesssim 1.9$ at 99 % C.L. [96]. For n chiral multiplets (R_{wi}, Y_i), one finds

$$\mathcal{A}^{\gamma\gamma}_{new} \simeq \frac{2}{3}\sum_{i=1}^{n}\sum_{k=1}^{N_{wi}} Q_k^2 = \frac{2}{3}\sum_{i=1}^{n}\frac{N_{wi}(N_{wi}^2 + 12Y_i^2 - 1)}{12} \,. \tag{4.2.9}$$

We added an overall factor 1/2 to take into account that each massive fermion is formed by two chiral components. Equivalently, one may take the sum only over fermions of a given chirality. For example, a minimal set is formed by a weak doublet 2_L of hypercharge Y paired with two weak singlets $(1+1)_R$, giving a contribution $\mathcal{A}^{\gamma\gamma}_{new} = 2(1+4Y^2)/3 \geq 2/3$. The next-to-minimal set $(2+2)_L$ paired with $(1+1+1+1)_R$ implies $A^{\gamma\gamma}_{new} > 4/3$, that is still allowed by the present constraint on $R_{\gamma\gamma}$, while for example $(3+2)_L$ gives already $A^{\gamma\gamma}_{new} > 10/3$, that is almost excluded. Since the SM amplitude has opposite sign w.r.t. the one of new fermions, one can also envisage the contrived possibility of a large $A^{\gamma\gamma}_{new} \sim -2\mathcal{A}^{\gamma\gamma}_{SM} \simeq 13$.

This shows that there are purely chiral sets of n fermions that satisfy the $\gamma\gamma$ constraint. However, we have also shown before that no set exists for $n \leq 4$, that satisfies the consistency requirements of section 4.1. It is non-trivial to check whether purely chiral sets with $n > 4$ could be consistent. Consider for example the case of two weak doublets plus four weak singlets. In order for all components to receive a mass from the Yukawa couplings to the Higgs doublet, the hypercharges must be chosen as

$$(2, Y_1) \,, \quad (2, Y_2) \,, \quad \left(1, -Y_1 + \frac{1}{2}\right) \,, \quad \left(1, -Y_1 - \frac{1}{2}\right) \,, \quad \left(1, -Y_2 + \frac{1}{2}\right) \,, \quad \left(1, -Y_2 - \frac{1}{2}\right) \,, \tag{4.2.10}$$

in the convention where all multiplets have the same chirality. The absence of anomalies requires Eq. (4.1.1) to hold, and this leads to $Y_1 = -Y_2 \equiv Y$. As a consequence, three vector-like mass terms are allowed and such set of fermions does not qualify as purely chiral.

At this point one should recall that, in this chapter, we took the point of view that all mass terms and interactions allowed by the gauge symmetries are present. In alternative, one can easily introduce some global symmetry to forbid possible vector-like mass terms, thus imposing by hand that a given set of fermions is chiral. For example in Eq. (4.2.10) take a $U(1)$ symmetry with charge $+1$ for doublets and -1 for singlets. If one takes this point of view, the set of fermions in Eq. (4.2.10) qualifies as the minimal still viable set of purely chiral fermions. Indeed, besides being consistent with all the requirements of section 4.1, it can be compatible with direct searches, EW precision tests, and constraints from the Higgs couplings.

Concerning direct collider searches, as the new leptons have charges $Q = Y \pm 1/2$, they do not mix with the SM leptons (except for $|Y| = 1/2$ or $3/2$) and the lightest state is stable. There are severe bounds on the number density of such charged relics [6], but they depend on cosmological assumptions: e.g. for a reheating temperature below their mass, they were never produced in the early Universe. Limits on heavy stable leptons are of the order of a few hundreds of GeVs, and are

$\|Q\|$	1/3	2/3	1	2	3	4	5	6	7	8
bound in GeVs	200	480	574	685	752	793	796	781	757	715

Table 4.2: The 95 % C.L. lower bounds on the mass of heavy stable leptons, from the CMS collaboration [5]. The production is assumed to occur through the Drell-Yan process only. Limits are obtained for $SU(2)_w$ singlets, but they remain similar in general [6]. The ATLAS collaboration obtains comparable but less stringent limits in the range $2 \leq |Q| \leq 6$ [7]. For larger values of Q see Ref. [8].

displayed in Table 4.2 for some representative values of Q. For a review on heavy stable particles see Ref. [95].

The contributions to the S and T parameters of a fermion 'family' formed by one doublet and two singlets are given in Eqs. (C.24) and (C.25). In the present case we have two such 'families' with $N_c = 1$ and opposite hypercharges $\pm Y$, and one can easily lie within the 3σ ellipse of Fig. 10. For example in the custodial limit where the two mass eigenstates of each 'family' are degenerate, one finds $T \simeq 0$ and $S \simeq 0.1$. Concerning the Higgs couplings, one finds $\mathcal{A}^{\gamma\gamma}_{new} = 4(1+4Y^2)/3$, that lies in the allowed range of $R_{\gamma\gamma}$ for $|Y| \lesssim 0.3$ and $1.4 \lesssim |Y| \lesssim 1.6$.

Finally, it is interesting to compare Eq. (4.2.9) with the analogue amplitude for the Higgs boson coupling to γZ. For n chiral multiplets (R_{wi}, Y_i), one finds

$$\mathcal{A}^{\gamma Z}_{new} \simeq \frac{2}{3}\sum_{i=1}^{n}\sum_{k=1}^{N_{wi}} Q_k \frac{T_{3k} - s_w^2 Q_k}{c_w^2} = \frac{2}{3}\sum_{i=1}^{n} \frac{N_{wi}(N_{wi}^2 - 12Y_i^2\tan^2\theta_w - 1)}{12} \,, \tag{4.2.11}$$

where we used Eq. (D.31) particularised to the case of chiral fermions, in the same way we did above for the $\gamma\gamma$ case. Note that, when summing over the mass eigenstates of equal charge Q, the mixing matrices disappear from the Z couplings in Eq. (C.6), therefore one reduces to a sum over the interaction eigenstates. For example, the set in Eq. (4.2.10) gives $\mathcal{A}^{\gamma Z}_{new} \simeq 2\left[1 - \left(1+8Y^2\right)\tan^2\theta_w\right]/3$.

4.3 Phenomenology of non-chiral leptons

In this section we discuss new colourless fermions, which admit either a Majorana or a vector-like mass term before EWSB.

4.3.1 Majorana leptons

Let us consider leptons that admit a Majorana mass term. The latter requires a vanishing hypercharge, $Y = 0$. The two possibilities relevant for the Higgs couplings are sterile neutrinos $N \sim (1,1,0)$, and weak triplets $\Sigma \sim (1,3,0)$.

• ***Sterile neutrinos.*** In the case of one sterile neutrino, the SM Lagrangian is extended to $\mathcal{L} = \mathcal{L}_{SM} + \mathcal{L}_N$, where

$$\mathcal{L}_N = -\overline{l_{L\alpha}}\lambda_{N\alpha}\tilde{H}N_R - \frac{1}{2}\overline{N_R^c}M_N N_R + h.c. \,. \tag{4.3.1}$$

Only one linear combination ν_L of the three active neutrinos $\nu_{L\alpha}$ couples to N_R, and since we are not concerned with flavour issues we will drop the index α in the following. After EWSB, ν_L and N_R^c mix and combine into two Majorana fermions ν_l and ν_h with definite masses, $m_{\nu_l} \leq m_{\nu_h}$; active neutrino mass searches imply $m_{\nu_l} \lesssim 1$ eV. If one takes the limit $m_{\nu_l} \ll m_h$, the type I seesaw mechanism is realised: $m_{\nu_l} \simeq \lambda_N^2 v^2/(2M_N)$ and $m_{\nu_h} \simeq M_N$. The Higgs boson couplings to $\nu_l\nu_l$ and $\nu_h\nu_h$ are proportional to m_{ν_l}/v, and the coupling to $\nu_l\nu_h$ is proportional to $\sqrt{m_{\nu_l}m_{\nu_h}}/v$, leading to a negligibly small decay width, $\Gamma(h \to \nu_l\nu_h) < m_h^2/(8\pi v^2)m_{\nu_l} \lesssim 10^{-8}$ MeV. Also, one can check that the decay widths of the Z-boson receive negligible corrections, always proportional to m_{ν_l}/v. For m_{ν_h} above

the EW scale, one can compute the ν_h contribution to the S and T parameters, that turns out to be suppressed by the tiny ratio m_{ν_l}/m_{ν_h}.

In the case of two or more sterile neutrinos N_i, in most of the parameter space the arguments above apply to each N_i separately: either the Majorana mass M_i is as small as the eV scale, or the active-sterile mixing $\theta_i \equiv \lambda_{N_i}(v/\sqrt{2})/M_{N_i}$ is suppressed, $|\theta_i^2 M_{N_i}| \sim m_{\nu_l} \lesssim 1$ eV. In either case the corrections to the Higgs and Z/W-boson couplings are tiny. The only exception occurs when much larger θ_i are tuned among each other, in order for the N_i contributions to the light neutrino mass to cancel. Consider for simplicity two sterile neutrinos $N_{1,2}$. At leading order in the mixing angles θ_i one has

$$m_{\nu_l} \simeq |\theta_1^2 M_{N_1} + \theta_2^2 M_{N_2}| \lesssim 1 \text{ eV} \ . \tag{4.3.2}$$

The two summands have a physical relative phase, therefore they can be orders of magnitude larger than m_{ν_l}, if there is a strong cancellation between the two: the active-sterile mixing can be large, no matter how large the sterile masses $m_{\nu_{h1,2}}$ are. Even though this scenario requires a severe tuning of parameters to lead to observable effects, it may be justified by some symmetry. For example, in the so-called inverse seesaw model [99–101] (see also Ref. [102]), the lepton number symmetry $U(1)_L$ is broken by a small mass parameter, and the cancellation occurs naturally in the limit where this parameter goes to zero. Therefore, it is worth to analyse the phenomenological consequences of a large active-sterile mixing: both Higgs couplings and EW gauge boson couplings can be significantly modified.

Consider first the neutrino mass eigenstates ν_l, ν_{h1}, ν_{h2} in the regime $m_{\nu_l} \ll m_{\nu_{h1,2}} \ll m_h, m_Z$. One finds that the decay widths of the Higgs boson can be significantly modified, in particular $\Gamma(h \to \nu_l \nu_{hi}) \simeq m_h m_{\nu_{hi}}^2 |\theta_i|^2/(8\pi v^2)$ and $\Gamma(h \to \nu_{hi}\nu_{hi}) \simeq m_h m_{\nu_{hi}}^2 |\theta_i|^4/(4\pi v^2)$. These rates can be easily as large as the total SM Higgs width, $\Gamma_h^{SM} \simeq 4$ MeV, therefore the LHC experiments already constrain θ_i and $m_{\nu_{hi}}$. Note that both invisible and visible decay channels are affected, since $\nu_{h1,2}$ decay not only into light neutrinos, but also into SM particles e.g. via virtual W-bosons. Detailed analyses of the parameter space and of various constraints can be found e.g. in Refs. [103–107]. Note that the Z-boson invisible width Γ_Z^{inv}, that is measured at the few per mil level, is not significantly affected for $m_{\nu_{h1,2}} \lesssim 1$ MeV, with $\nu_{h1,2}$ decaying mostly invisibly into three ν_l: even in the presence of large mixing, only the active components of $\nu_{l,h1,h2}$ couple to the Z-boson, and one recovers the SM value of Γ_Z^{inv} once the sum over all neutrino pairs is taken. On the contrary, for larger $m_{\nu_{h1,2}}$ the heavy neutrinos mediate visible Z-decays, therefore Γ_Z^{inv} is depleted and a significant upper bound applies on $|\theta_i|$.

Consider next the complementary regime $m_h, m_Z \lesssim m_{\nu_{h1,2}}$. In this case the Higgs and Z decay width are not modified, but a significant active neutrino fraction in $\nu_{h1,2}$ can still have observable consequences. Direct searches of EW scale sterile neutrinos through their mixing with active neutrinos have been performed e.g. by ATLAS [108,109] and CMS [110,111]. Here we would like to point out that the EW precision parameters S and T can also receive important corrections, that constrain the masses and mixing of the sterile neutrinos. To understand this quite surprising fact, that is generally overlooked, it is convenient to write the 3×3 neutrino mass matrix in the basis $(\nu_L, N_{R1}^c, N_{R2}^c)$ as

$$\mathcal{M}_\nu = U^* diag(m_{\nu_l}, m_{\nu_{h1}}, m_{\nu_{h2}}) U^\dagger \ , \tag{4.3.3}$$

with U unitary and subject to the constraint $0 = (\mathcal{M}_\nu)_{11} \simeq U_{12}^{*2} m_{\nu_{h1}} + U_{13}^{*2} m_{\nu_{h2}}$, where we neglected the tiny m_{ν_l}. Then, the active neutrino fractions U_{1i} contained in the mass eigenstates can be parametrized in full generality as follows: $U_{13} = \theta$ taken to be real, $U_{12} = i\theta/\sqrt{r_h}$ with $r_h \equiv m_{\nu_{h1}}/m_{\nu_{h2}}$ and $|U_{11}|^2 = 1 - \theta^2(1+r_h)/r_h$. The 3σ lower bound on Γ_Z^{inv} implies $\theta^2(1+r_h)/r_h \lesssim 0.015$. We computed T and S using the formulas in appendix C, as a function of θ, r_h and $r_Z \equiv m_Z/m_{\nu_{h2}}$, neglecting the mass of the SM leptons and including a symmetry factor $1/2$ for loops of Majorana fermions. Here

we report the result in some physically interesting limits:

$$
\begin{aligned}
&(a)\ m_{\nu_{h2}} = m_{\nu_{h1}} \gg m_Z: \quad T \simeq \frac{\theta^4}{4\pi s_w^2 c_w^2}\frac{m_{\nu_{h2}}^2}{m_Z^2}\ , \quad S \simeq \frac{2\theta^2}{9\pi}\left(4 + 3\log\frac{m_{\nu_{h2}}^2}{m_Z^2}\right); \\
&(b)\ m_{\nu_{h2}} \gg m_{\nu_{h1}} = m_Z: \quad T \simeq \frac{\theta^4}{8\pi s_w^2 c_w^2}\frac{m_{\nu_{h2}}^2}{m_Z^2}\left(3 - \log\frac{m_{\nu_{h2}}^2}{m_Z^2}\right), \quad S \simeq \frac{\theta^2}{4\pi}\frac{m_{\nu_{h2}}}{m_Z}\ .
\end{aligned}
\tag{4.3.4}
$$

In case (a), taking the maximal allowed value $\theta^2_{max} \simeq 0.007$, the correction to T grows quadratically with the sterile neutrino mass: requiring to remain in the 3σ ellipse in the $S-T$ plane (see Fig. 10), one finds the upper bound $m_{\nu_{h2}} \lesssim 8.5$ TeV. This sensitivity to very large scales is due to the significant fraction of the active neutrino in the heavy states; note that this non-decoupling effect requires a strong tuning among the two sterile neutrino parameters. In case (b), the active fraction in the heaviest sterile neutrino is rather $\theta^2_{max} \simeq 0.015(m_Z/m_{\nu_{h2}})$, therefore T grows only logarithmically with $m_{\nu_{h2}}$, while S remains constant: one remains in the ellipse for $m_{\nu_{h2}}$ as large as the Planck scale.

• ***Weak triplets with zero hypercharge.*** In the case of a weak triplet $\Sigma_R \sim (1,3,0)$, the SM Lagrangian is extended by

$$
\mathcal{L}_{\Sigma_R} = -\sqrt{\frac{2}{3}}\overline{l_{L\alpha}}\lambda_{\Sigma\alpha}\Sigma_R\tilde{H} - \frac{1}{2}\mathrm{Tr}\left(\overline{\Sigma_R^c}M_\Sigma\Sigma_R\right) + h.c.\ , \tag{4.3.5}
$$

where we adopted the matrix notation

$$
\Sigma_R \equiv \sqrt{2}\Sigma_R^a\tau^a = \frac{1}{\sqrt{2}}\begin{pmatrix} \Sigma_R^3 & \Sigma_R^1 - i\Sigma_R^2 \\ \Sigma_R^1 + i\Sigma_R^2 & -\Sigma_R^3 \end{pmatrix} \equiv \begin{pmatrix} \frac{1}{\sqrt{2}}\Sigma_R^0 & -\Sigma_R^+ \\ \Sigma_R^- & -\frac{1}{\sqrt{2}}\Sigma_R^0 \end{pmatrix} \tag{4.3.6}
$$

and we normalised the triplet Yukawa coupling according to appendix D.1. After EWSB, the neutral component Σ_R^0 and a linear combination of active neutrinos combine into two Majorana fermions ν and Σ_0, in complete analogy to the case of ν_l and ν_h discussed above. As usual, we will consider only the mixing with the third lepton family, taking $\lambda_{\Sigma e,\Sigma\mu} = 0$ and $\lambda_{\Sigma\tau} \equiv \lambda_\Sigma$. Indeed, flavour changing neutral current processes such as $\mu \to e\gamma$ or $\mu \to 3e$ are strongly constrained [112, 113]. In the limit $\lambda_\Sigma v \ll M_\Sigma$ one realises the so-called type III seesaw mechanism: $m_\nu \simeq \lambda_\Sigma^2 v^2/(6M_\Sigma)$ and $m_{\Sigma_0} \simeq M_\Sigma$. The charged components $(\Sigma_R^+)^c$ and Σ_R^- mix with the SM charged leptons τ_L and τ_R respectively, to form the mass eigenstates τ and Σ^-. Then, three real parameters – the Yukawa coupling λ_Σ, the mass M_Σ and the SM tau Yukawa coupling λ_τ – determine the mass of four physical states, m_ν and M_{Σ^0} in the neutral sector, m_τ and M_{Σ^-} in the charged sector. The mixing angles for neutrinos and left-handed charged leptons are suppressed by $\sqrt{m_\nu/M_{\Sigma^0}}$; the mixing of right-handed charged leptons receives an additional suppression by m_τ/M_{Σ^-}.

The couplings of Σ_0 to the Z and Higgs bosons are exactly the same as the couplings of ν_h discussed above. In particular, for vanishing m_ν all Z and Higgs couplings reduce to their SM values, therefore the corrections are negligibly small. At tree level, $M_{\Sigma^-} - M_{\Sigma^0}$ also vanishes with m_ν, however it is well-known that at one loop weak interactions induce a mass split, $M_{\Sigma^-} - M_{\Sigma^0} \simeq 170$ MeV (see e.g. Ref. [65]). Neglecting the tiny mixing angles, the only heavy lepton couplings are $Z\Sigma^+\Sigma^-$ and $W^+\Sigma^-\Sigma^0$; other mixing-suppressed couplings are relevant for Σ-decays [114]. The contribution of Σ to the EW precision parameters S and T is vanishingly small, as EWSB is felt only through the mixing angles and through the loop-induced mass splitting among the Σ-components, and both are very small.

Coming to direct searches, LEP looked for new charged leptons pair produced and decaying to $W\nu$, setting a lower bound $M_{\Sigma^-} \gtrsim 100$ GeV [115]. At the LHC heavy leptons are mostly pair-produced via $Z^*/\gamma^* \to \Sigma^+\Sigma^-$ and $W^{\pm *} \to \Sigma^\pm\Sigma^0$. The fraction of Σ that decays into each lepton flavour, $b_\alpha = \theta_\alpha/(\theta_e + \theta_\mu + \theta_\tau)$, characterises the final state. CMS [116] considered either $b_e = b_\mu = b_\tau = 1/3$, $b_e = 1$ or $b_\mu = 1$, obtaining constraints in the range $M_\Sigma \geq 180 - 210$ GeV. The most stringent constraint comes from ATLAS [117], with $M_\Sigma \geq 325$ GeV for $b_e = 1$ and $M_\Sigma \geq 400$ GeV for $b_\mu = 1$.

We expect a weaker bound in the case $b_\tau = 1$, that we assumed above. Other decay channels relevant for Σ searches at the LHC are discussed in Ref. [114], including displaced vertexes, as Σ becomes long-living in the limit of very small mixing.

In the case of two or more lepton triplets Σ_i, the phenomenology is similar, except when the mixing between the SM leptons and the new leptons is not suppressed. As in the case of sterile neutrinos, this is possible only by severely tuning the Yukawa couplings of the various Σ_i to keep m_ν small. In the case of two triplets, the neutrino mass matrix is diagonalised as in Eq. (4.3.3), while the charge lepton mass matrix can be written as $M_e = U_L diag(m_\tau, M_{\Sigma_1}, M_{\Sigma_2}) U_R^\dagger$. Neglecting m_ν and m_τ, the left-hand mixing matrix U_L coincides with the neutrino mixing matrix up to a $\sqrt{2}$ factor: $(U_L)_{13} \simeq \sqrt{2}\theta$, $(U_L)_{12} \simeq i\sqrt{2}\theta/\sqrt{r_h}$ and $|(U_L)_{11}|^2 \simeq 1 - 2\theta^2(1+r_h)/r_h$, with $r_h = M_{\Sigma_1}/M_{\Sigma_2}$, while the mixing angles in U_R are further suppressed by m_τ/M_{Σ_i}. When θ is large, the corrections to S and T may become significant as already discussed for sterile neutrinos. In addition, the new charged leptons, that are necessarily above the EW scale, could contribute significantly to $h \to \gamma\gamma, \gamma Z$. Before computing these corrections, one should notice that a strong upper bound on the mixing comes from the Z coupling to $\tau^+\tau^-$. The LEP measurement of $\Gamma(Z \to \tau^+\tau^-)$ [69] implies $2\theta^2(1+r_h)/r_h \lesssim 0.004$ at 3σ.

Let us describe in some detail the main corrections to $R_{\gamma\gamma}$ and $R_{\gamma Z}$, defined by Eq. (D.41). Similar analytic approximations could be used for the models analysed in the next sections as well. For the diphoton channel, using the results of Appendix D.2 one finds

$$\begin{aligned} R_{\gamma\gamma} &\simeq \frac{\left|\mathcal{A}^{\gamma\gamma}_{SM} + (|(U_L)_{11}|^2 - 1) A_{1/2}(\tau_\tau) + |(U_L)_{12}|^2 A_{1/2}(\tau_{\Sigma_1}) + |(U_L)_{13}|^2 A_{1/2}(\tau_{\Sigma_2})\right|^2}{\left|\mathcal{A}^{\gamma\gamma}_{SM}\right|^2} \\ &\simeq \frac{\left|\mathcal{A}^{\gamma\gamma}_{SM} + 2\theta^2 \frac{1+r_h}{r_h} A_{1/2}(\tau_{\Sigma_k})\right|^2}{\left|\mathcal{A}^{\gamma\gamma}_{SM}\right|^2} \simeq 1 - 4\theta^2 \frac{1+r_h}{r_h} \frac{A_{1/2}(\tau_{\Sigma_k})}{\left|\mathcal{A}^{\gamma\gamma}_{SM}\right|} \gtrsim 0.998 \,, \end{aligned} \tag{4.3.7}$$

where we took the maximal allowed values for the mixing angle and the form factor, $A_{1/2}(\tau_{\Sigma_k}) \simeq 1.5$ for $M_{\Sigma_k} \simeq 100$ GeV. Note that $R_{\gamma\gamma} \simeq \mu_{\gamma\gamma}$, because the Higgs production rate and the total Higgs width are not significantly modified with respect to the SM. Thus the diphoton signal strength can be slightly reduced (the fermionic part of the amplitude slightly increases and interferes destructively with the W-loops), but only at a few permil level. For the γZ channel the new physics contribution can be written as $\mathcal{A}^{\gamma Z}_{new} = \mathcal{A}^{\gamma Z}_{\Sigma,diag} + \mathcal{A}^{\gamma Z}_{\Sigma,off-diag}$. Using the results of Appendix D.2, the loops involving a single mass eigenstate give

$$\begin{aligned} \mathcal{A}^{\gamma Z}_{\Sigma,diag} &\simeq \left[\left(|(U_L)_{11}|^2 - 1\right) \frac{1 - 4s_w^2}{4c_w^2} A_{1/2}(\tau_\tau, \lambda_\tau) \right. \\ &+ \left. |(U_L)_{12}|^2 A_{1/2}(\tau_{\Sigma_1}, \lambda_{\Sigma_1}) + |(U_L)_{13}|^2 A_{1/2}(\tau_{\Sigma_2}, \lambda_{\Sigma_2}) \right] , \end{aligned} \tag{4.3.8}$$

where we took the Z couplings to the interaction eigenstates, thus neglecting corrections of higher order in the small mixing. The loops involving two mass eigenstates give

$$\begin{aligned} \mathcal{A}^{\gamma Z}_{\Sigma,off-diag} \simeq -\sum_{k=2,3} \frac{|(U_L)_{11}|^2 |(U_L)_{1k}|^2}{4c_w^2} \times \\ \times \left[\frac{M_{\Sigma_k} + m_\tau}{\sqrt{m_\tau M_{\Sigma_k}}} A_{1/2}(\tau_\tau, \lambda_\tau, \tau_{\Sigma_k}, \lambda_{\Sigma_k}) - i \frac{M_{\Sigma_k} - m_\tau}{\sqrt{m_\tau M_{\Sigma_k}}} B_{1/2}(\tau_\tau, \lambda_\tau, \tau_{\Sigma_k}, \lambda_{\Sigma_k}) \right] . \end{aligned} \tag{4.3.9}$$

Retaining only terms of order θ^2 and neglecting m_τ/M_{Σ_k}, the rate relative to the SM can be written as

$$R_{\gamma Z} \simeq 1 - 4\theta^2 \frac{1+r_h}{r_h} \frac{A_{1/2}(\tau_{\Sigma_k}, \lambda_{\Sigma_k}) - \frac{1}{4c_w^2} \sqrt{\frac{M_{\Sigma_k}}{m_\tau}} A_{1/2}(\tau_\tau, \lambda_\tau, \tau_{\Sigma_k}, \lambda_{\Sigma_k})}{\left|\mathcal{A}^{\gamma Z}_{SM}\right|} . \tag{4.3.10}$$

We neglected the $B_{1/2}$ term, as it interferes only with the very small imaginary part of the SM amplitude. The diagonal and off-diagonal form factors have comparable size, $A_{1/2}(\tau_{\Sigma_k}, \lambda_{\Sigma_k}) \simeq 1.3$ and $\sqrt{M_{\Sigma_k}/m_\tau} A_{1/2}(\tau_\tau, \lambda_\tau, \tau_{\Sigma_k}, \lambda_{\Sigma_k}) \simeq 1$, where we took the large M_{Σ_k} limit. Replacing the maximal allowed value for the mixing, we find $R_{\gamma Z} \gtrsim 0.998$, with a suppression at the few permil level, of the same order as for $R_{\gamma\gamma}$.

Finally, let us note that, with two or more sterile neutrinos N_i (or triplets Σ_i) the CP symmetry can be broken. In general, the Higgs couplings to the fermion mass eigenstates are not real, and the off-diagonal couplings of the Z-boson can be complex as well. This does not modify any of the above results, because the CP violating effects vanish in the limit $m_{\nu_l}/m_{\nu_{hk}} \to 0$ (and $m_\tau/m_{\Sigma_k} \to 0$ in the triplet case), therefore they are subleading.

4.3.2 One vector-like lepton

Let us consider the addition to the SM of one vector-like lepton (VLL). The four different possibilities are a weak singlet E, a weak doublet L or Λ, a weak triplet Δ, whose charges are displayed in Table 4.1. As usual, we restrict ourself to mixing with the third SM family, i.e. with τ and ν_τ. The SM Lagrangian is extended by

$$-\mathcal{L}_\psi = \lambda_\psi \overline{l_L} H \psi_R + M_\psi \overline{\psi_L} \psi_R + h.c. \ , \quad \psi = E, \Delta \ , \tag{4.3.11}$$

$$-\mathcal{L}_\psi = \lambda_\psi \overline{\psi_L} H(\tilde{H}) \tau_R + M_\psi \overline{\psi_L} \psi_R + h.c. \ , \quad \psi = L(\Lambda) \ , \tag{4.3.12}$$

where the $SU(2)_w$ contractions are understood (see appendix D.1 for details). In the case of E (L) one could write an additional mass term $m_E \overline{E_L} \tau_R$ ($m_L \overline{l_L} L_R$), but such term can be removed by choosing conveniently the basis for the two fields E_R and τ_R (l_L and L_L), that have identical charges. Thus, in each case there are only two real parameters: the vector-like mass M_ψ and the Yukawa coupling λ_ψ; the mixing among the new leptons and the SM ones vanishes for vanishing λ_ψ. There is no CP violation.

The components of each multiplet ψ are listed in Eq. (4.1.5). The doubly-charged component F does not mix as there is no SM counterpart with $Q = 2$, therefore $m_F^2 = M_\psi^2$. The $Q = 1$ component E mixes with the SM τ to form the two physical mass eigenstates τ' and τ. The mass matrix is given by

$$\mathcal{M}_e = \begin{pmatrix} \lambda_\tau \frac{v}{\sqrt{2}} & \kappa_\psi \lambda_\psi \frac{v}{\sqrt{2}} \\ 0 & M_\psi \end{pmatrix} \ , \ \psi = E, \Delta \ , \quad \mathcal{M}_e = \begin{pmatrix} \lambda_\tau \frac{v}{\sqrt{2}} & 0 \\ \kappa_\psi \lambda_\psi \frac{v}{\sqrt{2}} & M_\psi \end{pmatrix} \ , \ \psi = L, \Lambda \ . \tag{4.3.13}$$

The $SU(2)_w$ Clebsch-Gordan coefficient κ_ψ is equal to one, except in the triplet case, $\kappa_\Delta = \sqrt{1/3}$. The rotation to the mass basis can be parametrized as

$$\mathcal{M}_e = V_L \begin{pmatrix} m_\tau & 0 \\ 0 & m_{\tau'} \end{pmatrix} V_R^T \ , \quad V_{L,R} = \begin{pmatrix} c_{L,R} & s_{L,R} \\ -s_{L,R} & c_{L,R} \end{pmatrix} \ . \tag{4.3.14}$$

The triangular mass matrix structure of Eq. (4.3.13) implies some strict relations among the mixing angles and the mass eigenvalues. For the case of L and Λ, one finds

$$\tan\theta_L = \frac{m_\tau}{m_{\tau'}} \tan\theta_R \ll \tan\theta_R \ , \quad s_L = \frac{m_\tau}{M_\psi} s_R \ , \quad c_L = \frac{m_{\tau'}}{M_\psi} c_R \ . \tag{4.3.15}$$

For the case of E and Δ, the same relations hold with $L \leftrightarrow R$. Note that direct searches of charged leptons at LEP [115] require $m_{\tau'} \gtrsim 100$ GeV , therefore one angle is at least two orders of magnitude smaller than the other. In the following we will refer only to the dominant mixing angle θ_ψ for each ψ, dropping the subscript L, R on (co)sines. Note that $m_{\tau'}^2 \simeq M_\psi^2/c_\psi^2 \geq M_\psi^2$. The neutral component N does not mix with the SM neutrino ν_τ in the case of L. In the case of Δ there is mixing in the neutral sector, described by

$$\mathcal{M}_\nu = \begin{pmatrix} \sqrt{\frac{1}{3}} \lambda_\Delta v \\ M_\Delta \end{pmatrix} = U_L \begin{pmatrix} 0 \\ m_{\nu'} \end{pmatrix} \ , \quad U_L = \begin{pmatrix} \widetilde{c} & \widetilde{s} \\ -\widetilde{s} & \widetilde{c} \end{pmatrix} \ , \tag{4.3.16}$$

with $\widetilde{s}^2 \simeq 2s_\Delta^2/(1+s_\Delta^2) \geq s_\Delta^2$. One neutrino remains massless, while the second acquires a mass $m_{\nu'}^2 \simeq (1+s_\Delta^2)m_{\tau'}^2 \geq m_{\tau'}^2$. In summary, the tree-level spectrum of heavy leptons satisfies

$$\begin{aligned} &M_E \leq m_{\tau'} \quad (\psi = E)\ , && m_F = M_\Delta \leq m_{\tau'} \leq m_{\nu'} \quad (\psi = \Delta)\ , \\ &m_{\nu'} = M_L \leq m_{\tau'} \quad (\psi = L)\ , && m_F = M_\Lambda \leq m_{\tau'} \quad (\psi = \Lambda)\ . \end{aligned} \tag{4.3.17}$$

with the mass splitting controlled by the mixing, $\Delta m^2(\psi) \sim s_\psi^2 M_\psi^2$.

Let us briefly discuss the collider bounds on M_ψ. In first approximation one can neglect the mass splitting. It is possible to recast some LHC multi-lepton searches to put bounds on VLLs. The limits on M_ψ strongly depend on the SM generation that couples to the heavy leptons. For couplings only to the third one and for the doublet L, Ref. [118] reports $M_L \gtrsim 280$ GeV, while the LEP limit remains more constraining in the case of the singlet E, $M_E \gtrsim 100$ GeV. For the exotic doublet Λ with a doubly-charged component, Ref. [119] reports $M_\Lambda \gtrsim 320$ GeV. To the best of our knowledge, no similar analysis is available for the triplet Δ. We expect a bound comparable or slightly stronger than to the one for Λ. These bounds only apply for promptly decaying particles. We will only consider this possibility, because heavy leptons become long-lived ($c\tau \gtrsim 1m$) for a tiny mixing $s_\psi \simeq 10^{-8} - 10^{-9}$, and the mixing suppresses all the deviations from the SM that we are interested in. More details on the collider phenomenology of Λ and Δ can be found in Refs. [120] and [121, 122], respectively.

It is mandatory to require that the Yukawa coupling λ_ψ lies in the perturbative regime, $|\lambda_\psi| \ll 4\pi$. This consistency requirement translates into an upper bound on the product of the heavy lepton mass and the mixing angle,

$$|\lambda_\psi| \simeq \left| \frac{\sqrt{2}}{\kappa_\psi} \frac{m_{\tau'}}{v} s_\psi \right| \ll 4\pi\ . \tag{4.3.18}$$

The perturbativity constraint on the SM Yukawa coupling λ_τ is satisfied a fortiori. The non-zero couplings of the physical Higgs boson to the charged mass eigenstates, using the convention of Eq. (D.5), are given by

$$y_{\tau\tau} = c_\psi^2 \frac{m_\tau}{v}\ , \quad y_{\tau'\tau'} = s_\psi^2 \frac{m_{\tau'}}{v}\ , \quad y_{\tau\tau'} = c_\psi s_\psi \frac{m_\tau + m_{\tau'}}{2v}\ , \quad \widetilde{y}_{\tau\tau'} = \pm c_\psi s_\psi \frac{m_{\tau'} - m_\tau}{2vi}\ . \tag{4.3.19}$$

where the plus (minus) sign holds in the case of E and Δ (L and Λ). In the case of Δ, there are also non-zero couplings to neutral leptons,

$$y_{\nu'\nu'} = \widetilde{s}^2 \frac{m_{\nu'}}{v}\ , \quad y_{\nu\nu'} = \widetilde{c}\widetilde{s} \frac{m_{\nu'}}{2v}\ , \quad \widetilde{y}_{\nu\nu'} = \widetilde{c}\widetilde{s} \frac{m_{\nu'}}{2vi}\ . \tag{4.3.20}$$

Important constraints come from the Z-decays into SM leptons. The couplings of the fermion mass eigenstates to the Z are defined in Eq. (C.6). The couplings to the SM leptons τ_L, $\nu_{\tau L}$ and τ_R are modified if they mix with new leptons with a different weak isospin T_3. Neglecting (m_τ/m_Z)-corrections, at tree level one finds

$$R(Z \to \tau^+\tau^-) \simeq \frac{(g_{\tau\tau}^V)^2 + (g_{\tau\tau}^A)^2}{(g_{\tau\tau}^{V,SM})^2 + (g_{\tau\tau}^{A,SM})^2}\ , \tag{4.3.21}$$

where $g_{\tau\tau}^{V,A}$ receive a correction of order s_ψ^2 with respect to the SM. The experimentally allowed range given in Eq. (C.28) implies an upper bound on the mixing angle, for any VLL: we find $s_{E,\Delta} \lesssim 6.0 \cdot 10^{-2}$ and $s_{L,\Lambda} \lesssim 6.7 \cdot 10^{-2}$. In addition, in the case of Δ there is a correction to the Z-coupling to neutrinos, and thus to the Z-invisible width,

$$R(Z \to inv) \simeq \frac{2}{3} + \frac{1}{3} \frac{(g_{\nu\nu}^V)^2 + (g_{\nu\nu}^A)^2}{(g_{\nu\nu}^{V,SM})^2 + (g_{\nu\nu}^{A,SM})^2}\ . \tag{4.3.22}$$

The couplings $g_{\nu\nu}^{V,A}$ receive a correction of order $\tilde{s}^2$, that leads to a comparable limit $s_\Delta \lesssim 8.2 \cdot 10^{-2}$. Extracting the couplings of $W_\mu^\pm$, W_μ^3 and B_μ from Eq. (C.4), one can calculate the S and T parameters with the general formulas in appendix C.2. We find, at leading order in the mixing angle,

$$T \simeq \frac{1}{16\pi c_w^2 s_w^2} s_\psi^4 \left(a_\psi^T \frac{m_{\tau'}^2}{m_Z^2} \right)\ , \qquad S \simeq \frac{1}{6\pi} s_\psi^2 \left(a_\psi^S + b_\psi^S \log \frac{m_{\tau'}^2}{m_Z^2} \right)\ , \tag{4.3.23}$$

where a_ψ^T, a_ψ^S and b_ψ^S are numerical coefficients of order one. Taking into account the upper bound $s_\psi \lesssim 0.06$ from $Z \to \tau^+\tau^-$, as well as the perturbativity bound from Eq. (4.3.18), $(m_{\tau'}/m_Z)s_\psi \lesssim 10$, we checked that S and T always lie in the allowed ellipse of Fig. 10.

Coming to the Higgs boson signals, we first recall that all the dominant Higgs production channels at the LHC are not affected by the new leptons, as they leave the Higgs couplings to gluons and quarks unchanged. The total Higgs width also receives negligible corrections, as new leptons affect only the partial widths $\Gamma(h \to \alpha)$, for $\alpha = \tau^+\tau^-, \gamma\gamma, \gamma Z$. Therefore the Higgs signal is given by the ratio of partial widths in the model w.r.t. the SM, $\mu_\alpha \simeq R_\alpha$. The tree-level Higgs decays are directly controlled by the couplings in Eq. (4.3.19) and Eq. (4.3.20), in particular

$$R_{\tau\tau} = (1 - s_\psi^2)^2 \gtrsim 0.99 \ , \tag{4.3.24}$$

where we used the bound from $Z \to \tau^+\tau^-$. There is also the marginal possibility that the new leptons are lighter than the Higgs boson, thus opening the channels $h \to \tau\tau'$ and $h \to \nu\nu'$. However, direct searches seem to allow the singlet E only to be sufficiently light. Using equation (D.7) and neglecting $m_\tau/m_{\tau'}$, we find

$$\Gamma(h \to \tau^+\tau'^-) \simeq \frac{c_E^2 s_E^2 m_{\tau'}^2}{16\pi v^2} m_h \left(1 - \frac{m_{\tau'}^2}{m_h^2}\right)^2 \lesssim 0.2 \text{ MeV} \ . \tag{4.3.25}$$

Note that both the couplings $y_{\tau\tau'}$ and $\tilde{y}_{\tau\tau'}$ contribute equally to the decay width, see Eq. (4.3.19). We maximised the product $s_E^2 m_{\tau'}^2$ by taking $s_E = 6 \cdot 10^{-2}$ and $m_{\tau'} = 100$ GeV. As the SM total Higgs width is $\Gamma_h \simeq 4.1$ MeV, an enhancement of order 5% may be possible. Note that experimental searches at the LHC concentrated on $h \to \tau\tau$ [123,124], $\tau\mu$ [125,126] and $\mu\mu$ [127,128]. These channels are suppressed due to the small masses of the SM leptons, in contrast with the Higgs decays into a SM lepton plus a heavy lepton. It would be interesting to perform a dedicated search for this channel.

For the photon-photon channel we find

$$R_{\gamma\gamma} = \frac{\left|\mathcal{A}_{SM}^{\gamma\gamma} + s_\psi^2 \left[A_{1/2}(\tau_{\tau'}) - A_{1/2}(\tau_\tau)\right]\right|^2}{\left|\mathcal{A}_{SM}^{\gamma\gamma}\right|^2} \simeq 1 - 2s_\psi^2 \frac{A_{1/2}(\tau_{\tau'})}{\left|\mathcal{A}_{SM}^{\gamma\gamma}\right|} \ , \tag{4.3.26}$$

where the form factors are defined in appendix D.2. The addition of a VLL amounts to an additional τ'-loop and a modified τ-loop, that interfere destructively with the W-loops. Maximising the mixing and choosing $m_{\tau'} = 100$ GeV (the form factor decreases for larger masses), we find $\delta R_{\gamma\gamma} \simeq -1.9 \cdot 10^{-3}$, a permil reduction of the signal strength. For the γZ channel the relevant Z couplings, $g^{V,A}_{\tau\tau,\tau\tau',\tau'\tau'}$, receive corrections of order s_ψ^2 relatively to their unmixed values, as follows from Eq. (C.6). At leading order in the small mixing and neglecting m_τ, we find

$$R_{\gamma Z} \simeq 1 + 2s_\psi^2 \frac{\left(T_{E,\psi}^3 + s_w^2\right) A_{1/2}(\tau_{\tau'}, \lambda_{\tau'}) \pm \frac{1}{4}\sqrt{\frac{m_{\tau'}}{m_\tau}} A_{1/2}\left(\tau_\tau, \lambda_\tau, \tau_{\tau'}, \lambda_{\tau'}\right)}{c_w^2 \left|\mathcal{A}_{SM}^{\gamma Z}\right|} \ , \tag{4.3.27}$$

where $T_{E,\psi}^3$ is the isospin of the $Q = -1$ component of the multiplet ψ, and the plus (minus) sign in front of the off-diagonal term corresponds to the case $\psi = L$ ($\psi = E, \Lambda, \Delta$). As a consequence, the diagonal and off-diagonal terms always interfere destructively. The relative magnitude of the form factors is given below Eq. (4.3.10). The size of the correction change depending on the VLL under consideration, but it is always very small. The maximal deviation is obtained for Λ, with $\delta R_{\gamma Z} \simeq 1.3 \cdot 10^{-3}$.

4.3.3 Two vector-like leptons (including τ compositeness)

Let us consider a SM extension by two VLLs. They may couple to each other by a Yukawa interaction or not.

• ***Two VLLs not coupled to each other.*** In this case, each VLL must be a consistent extension of the SM by itself, therefore it should have the quantum numbers of E, L, Λ or Δ,

that are displayed in Table 4.1. The six possible pairs of VLLs decoupled from each other are $(\psi,\psi')=(E,E'),(L,L'),(\Lambda,\Lambda'),(\Delta,\Delta'),(E,\Delta)$ and(L,Λ). In the first four cases the additional mass term $\psi\psi'$ can be rotated away without loss of generality. The phenomenological effects are a trivial sum of those discussed in section 4.3.2 for a single VLL, with one noticeable exception.

When L and Λ have the same Yukawa coupling to the SM and the same mass, the Lagrangian

$$-\mathcal{L}_{L,\Lambda}=\frac{\lambda_\psi}{\sqrt{2}}\left(\overline{L_L}\quad\overline{\Lambda_L}\right)\begin{pmatrix}H\\ \tilde{H}\end{pmatrix}\tau_R+M_\psi\left(\overline{L_L}\quad\overline{\Lambda_L}\right)\begin{pmatrix}L_R\\ \Lambda_R\end{pmatrix}+h.c. \tag{4.3.28}$$

preserves a global $SU(2)_L\times SU(2)_R$ symmetry. In this custodial limit the corrections to the T parameter vanish, and those to the coupling $Z\tau_R\tau_R$ vanish as well [129]. This is the smallest set of tau custodians [130, 131]. A linear combination of the charge-one components of L and Λ, $\tau''\equiv(E^{(L)}-E^{(\Lambda)})/\sqrt{2}$, does not mix. The orthogonal combination, $E\equiv(E^{(L)}+E^{(\Lambda)})/\sqrt{2}$, mixes with the SM exactly as shown in Eqs. (4.3.13)-(4.3.15), to form the mass eigenstates τ' and τ. The spectrum reads $m_{\tau''}=m_N=m_F=M_\psi\leq m_{\tau'}\simeq M_\psi/c_R$. As discussed in section 4.3.2, direct searches already require all these states to be heavier than the Higgs boson. Thanks to the custodial symmetry, the Z couplings to leptons do not constrain the right-handed mixing s_R between τ and τ': one has $\delta g^R_{\tau\tau}=0$ and $\delta g^L_{\tau\tau}=s_L^2/2=(m_\tau/M_\psi)^2 s_R^2/2$, that is negligibly small. The $Z\nu\bar{\nu}$ coupling is SM-like as well. The T parameter is almost SM-like as no additional sources of custodial breaking are introduced, and the correction to the S parameter is within the experimental range.

The most stringent constraint on s_R comes from $R_{\tau\tau}\simeq(1-s_R^2)^2$. Using the 3σ lower bound $R_{\tau\tau}\gtrsim 0.2$ (see Table 4), one finds $s_R\lesssim 0.7$. Indeed, the mixing can be large and reduce significantly the $h\tau\tau$ coupling. As a consequence, the total Higgs width may be slightly reduced and, correspondingly, the signal strength for the other Higgs decay channels, defined in Eq. (D.40), may augment by a factor $\Gamma_h^{SM}/\Gamma_h\lesssim 1.04$. The deviation in the $\gamma\gamma$ channel has the same form as in Eq. (4.3.26): imposing the constraint from $h\to\tau\tau$, one finds a lower bound $\mu_{\gamma\gamma}\gtrsim 0.86$, that is close to the present experimental sensitivity. Coming to the γZ channel, the loop involving both τ and τ' vanishes when one neglects the tiny left-handed mixing s_L, because the custodial symmetry imposes $g^R_{\tau\tau'}=0$. Then, Eq. (4.3.27) reduces to

$$R_{\gamma Z}\simeq 1+2s_R^2\tan^2\theta_w\frac{A_{1/2}(\tau_{\tau'},\lambda_{\tau'})}{|\mathcal{A}^{\gamma Z}_{SM}|}\ , \tag{4.3.29}$$

with a maximal correction $\delta\mu_{\gamma Z}\simeq 0.12$. In the near future the increasing experimental precision on $\mu_{\tau\tau}$ can further constrain or eventually determine the mixing parameter s_R in this custodial limit.

• ***Two VLLs coupled to each other, not mixing with the SM fermions.*** Next, we have to discuss the case of two VLLs coupled through a Yukawa interaction. The most general assignment for their four chiral components is

$$\psi_{1L},\psi_{1R}\sim(1,R_w,Y)\ ,\qquad \psi_{2L},\psi_{2R}\sim(1,R_w+1,Y+\frac{1}{2})\ , \tag{4.3.30}$$

with the Lagrangian

$$-\mathcal{L}_{\psi_1\psi_2}=\lambda_{12}\overline{\psi_{1L}}\tilde{H}\psi_{2R}+\lambda_{21}\overline{\psi_{2L}}H\psi_{1R}+M_1\overline{\psi_{1L}}\psi_{1R}+M_2\overline{\psi_{2L}}\psi_{2R}+h.c.\ . \tag{4.3.31}$$

The four phases of λ_{12}, λ_{21}, M_1 and M_2 cannot be all rotated away: one phase is physical and allows for CP violation. In the special case $Y=0$ ($Y+1/2=0$) and R_w odd (even), one should add Majorana mass terms for $\psi_{1L,R}$ ($\psi_{2L,R}$): we postpone to section 4.3.4 the discussion of sets formed by one VLL plus Majorana leptons. For a few other values of R_w and Y, displayed in Eq. (4.3.41), interaction terms between $\psi_{1,2}$ and the SM leptons are allowed and should be added to the Lagrangian. We discuss first the no-mixing case and postpone to the end of this section the discussion of the mixing with the SM. In the absence of mixing, the lightest new lepton ψ_{light} is stable, at least at the renormalizable level. If Y is an integer multiple of $1/2$, ψ_{light} may decay into a SM lepton through some higher dimensional operator. For all other values of Y, this state is absolutely stable and it has non-zero electric charge. Collider searches put a lower bound on the mass of stable heavy leptons as a function of their charge

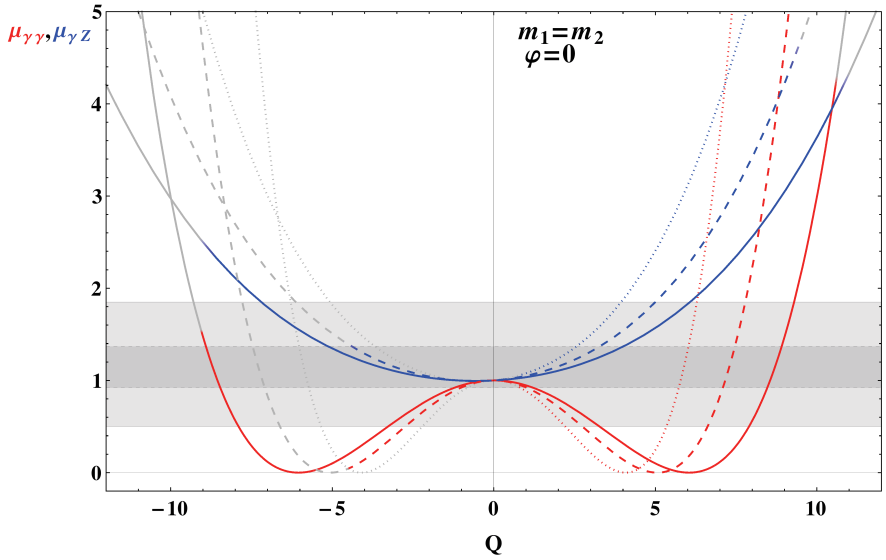

Figure 4.1: Signal strengths $\mu_{\gamma\gamma}$ (red) and $\mu_{\gamma Z}$ (blue) in the case of two VLLs $\psi_1 \sim (1,1,Q)$ and $\psi_2 \sim (1,2,Q+1/2)$, as a function of Q. We chose the following mass matrix parameters, defined by Eq. (4.3.33): $m_1 = m_2 = 800$ GeV, $\varphi = 0$, and three values for the relevant mixing angle, $\theta_L - \theta_R = \pi/8$ (dotted), $\pi/10$ (dashed), $\pi/12$ (solid). The grey parts of the curves are excluded by S and T, see Eq. (4.3.36). The shaded horizontal band is the presently allowed range for $\mu_{\gamma\gamma}$ at 1σ (dark) and 3σ (light).

Q, see the discussion in section 4.2 and the limits in Table 4.2. The effect of the set of fermions in Eq. (4.3.30) on $h \to \gamma\gamma$ was studied e.g. in Ref. [132].

Let us begin by analysing the case $R_w = 1$. There is one state with $Q = Y + 1$ and mass M_2, and two states with $Q = Y$ that mix, with mass matrix

$$\mathcal{M}_Y = \begin{pmatrix} M_1 & m_{12} \\ m_{21} & M_2 \end{pmatrix} , \qquad m_{12} = \frac{\lambda_{12} v}{\sqrt{2}} , \quad m_{21} = \frac{\lambda_{21} v}{\sqrt{2}} . \tag{4.3.32}$$

As $\mathcal{M}_Y$ is the most general 2×2 matrix, it is useful to parametrize it in terms of the five physical parameters,

$$\mathcal{M}_Y = U_L \begin{pmatrix} m_1 & 0 \\ 0 & m_2 \end{pmatrix} U_R^\dagger, \quad U_L = \begin{pmatrix} c_L & s_L \\ -s_L & c_L \end{pmatrix} \begin{pmatrix} e^{i\varphi} & 0 \\ 0 & 1 \end{pmatrix} , \quad U_R = \begin{pmatrix} c_R & s_R \\ -s_R & c_R \end{pmatrix} , \tag{4.3.33}$$

where $m_{1,2}$ are the real and positive masses of the eigenstates $f_{1,2}$, the mixing angles θ_L and θ_R vary between 0 and $\pi/2$, and the CP violating phase φ varies between 0 and 2π. The only restriction comes from the perturbativity of the Yukawa couplings,

$$|\lambda_{12}| = \frac{\sqrt{2}|m_2 s_L c_R - m_1 e^{i\varphi} c_L s_R|}{v} \ll 4\pi , \quad |\lambda_{21}| = \frac{\sqrt{2}|m_2 c_L s_R - m_1 e^{i\varphi} s_L c_R|}{v} \ll 4\pi . \tag{4.3.34}$$

These relations imply e.g. an upper bound on the masses for fixed values of the mixing angles. Vice versa, as the masses become larger and larger, the mixing angles vanish and the new fermions decouple from the EW scale.

The Higgs boson couplings to $f_{1,2}$ are directly obtained from Eq. (D.5). Taking for illustration the limit where f_1 and f_2 are mass-degenerate, one has $|M_1| = |M_2| \equiv M$, $|m_{12}| = |m_{21}| \equiv \mu$ and $m_1 = m_2 = \sqrt{M^2 + \mu^2} \equiv m_\psi$. In this case the contribution to the amplitude for $h \to \gamma\gamma$ is

$$\mathcal{A}^{\gamma\gamma}_{f_1,f_2} = 2Q^2 F(\theta_L, \theta_R, \varphi)\, A_{1/2}(\tau_\psi) , \qquad F(\theta_L, \theta_R, \varphi) = s_L^2 c_R^2 + c_L^2 s_R^2 - 2 c_L s_L c_R s_R \cos\varphi . \tag{4.3.35}$$

The CP-odd contribution vanishes because $\tilde{y}_{11} = -\tilde{y}_{22}$ in the degenerate limit. The perturbativity conditions in Eq. (4.3.34) reduce to $F(\theta_L, \theta_R, \pi) \ll 8\pi^2 v^2/m_\psi^2$. The interference with the SM is destructive as $\mathcal{A}^{\gamma\gamma}_{f_1,f_2} \geq 0$. There are two allowed regions of parameters:

(i) A SM-like region for small Q: the smallness of the charge ensures a small, negative departure from the SM.

(ii) A cancellation region at large Q: for $Q^2 \simeq 4.8/F(\theta_L, \theta_R, \varphi)$, the rate is accidentally close to the SM as $\mathcal{A}^{\gamma\gamma}_{f_1,f_2} \simeq -2\mathcal{A}^{\gamma\gamma}_{SM}$.

This behaviour is illustrated in Fig. 4.1 for the CP conserving case $\varphi = 0$, where $F(\theta_L, \theta_R, 0) = \sin^2(\theta_L - \theta_R)$. Indeed the amplitude grows from $\varphi = 0$ to $\varphi = \pi$, as $F(\theta_L, \theta_R, \pi) = \sin^2(\theta_L + \theta_R)$. Further constraints on the parameters come from the EW precision tests. In the limit $m_\psi \gg m_Z$ we find

$$\begin{aligned} S &\simeq \frac{1}{6\pi}\left[F\left(\theta_L, \theta_R, \varphi\right) + 4\left(Q + \frac{1}{2}\right)\ln\frac{m_\psi^2}{M^2}\right] , \\ T &\simeq \frac{1}{8\pi s_w^2 c_w^2 m_Z^2}\left[m_\psi^2 - 3M^2 + \frac{2M^4}{m_\psi^2 - M^2}\ln\frac{m_\psi^2}{M^2}\right] , \end{aligned} \tag{4.3.36}$$

where M is the mass of the unmixed state with $Q = Y + 1$. Therefore, for fixed values of the mixing parameters, S and T constrain the charge Q, as illustrated in Fig. 4.1.

It is interesting to analyse the value of $\mu_{\gamma Z}$ in the allowed space of parameters. Using Eqs. (C.6) and (D.31), the CP-even amplitude for $h \to \gamma Z$ is given by

$$\mathcal{A}^{\gamma Z}_{f1,f2} = \frac{Q}{c_w^2} F\left(\theta_L, \theta_R, \varphi\right)\left(g^V_{11} + g^V_{22}\right) A_{1/2}\left(\tau_\psi, \lambda_\psi\right) , \qquad g^V_{11} + g^V_{22} = -\frac{1}{2} - 2Qs_w^2 . \tag{4.3.37}$$

Note that the loops involving both f_1 and f_2 vanish as they are proportional to the Higgs coupling y_{12}, or to the form factor $B_{1/2}$ defined in Eq. (D.39), and they both vanish for $m_1 = m_2$. As the SM amplitude is negative, the new contribution interferes constructively as long as $Q(1+4s_w^2 Q) > 0$. The CP-odd amplitude $\tilde{\mathcal{A}}^{\gamma Z}_{f_1,f_2}$ is also non zero, because $g^V_{11} \neq g^V_{22}$, and it can be sizeable for large values of $\sin\varphi$. Let us distinguish the two regions of parameters allowed by $\mu_{\gamma\gamma}$:

(i) In the SM-like region at small Q, varying $(\theta_L - \theta_R)$ we find $-0.01 \lesssim \delta\mu_{\gamma Z} \lesssim +0.08$.

(ii) In the fine-tuned region at large Q we find $2.5 \lesssim \mu_{\gamma Z} \lesssim 3.2$ for $\varphi = 0$. This range slightly depends on the sign of Q, see Fig. 4.1. It is actually possible to obtain an even larger $\mu_{\gamma Z}$, while keeping $\mu_{\gamma\gamma}$ close to one. For example, taking for simplicity $s_R = 0$, the CP-odd amplitude reads

$$\tilde{\mathcal{A}}^{\gamma Z}_{f_1,f_2} = -4Q^2 c_L s_L \tan^2\theta_w \sin\varphi\, \tilde{A}_{1/2}\left(\tau_\psi, \lambda_\psi\right) . \tag{4.3.38}$$

For $\sin\varphi$ of order one, this contribution becomes important and one can reach $\mu_{\gamma Z} \simeq 7$.

When one allows for the two mass eigenstates $f_{1,2}$ to be non-degenerate, $m_1 < m_2$, the amplitudes for the diphoton channel become

$$\begin{aligned} \mathcal{A}^{\gamma\gamma}_{f_1,f_2} &\simeq 2Q^2\left[s_L^2 c_R^2 + c_L^2 s_R^2 - \left(\frac{m_1}{m_2} + \frac{m_2}{m_1}\right) c_L s_L c_R s_R \cos\varphi\right] A_{1/2}\left(\tau_1\right) , \\ \tilde{\mathcal{A}}^{\gamma\gamma}_{f_1,f_2} &\simeq 2Q^2\left(\frac{m_2}{m_1} - \frac{m_1}{m_2}\right) c_L s_L c_R s_R \sin\varphi\ \tilde{A}_{1/2}\left(\tau_1\right) . \end{aligned} \tag{4.3.39}$$

where we made the approximation $A_{1/2}(\tau_1) \simeq A_{1/2}(\tau_2)$, that is accurate for $4m^2_{1,2} \gg m_h^2$. For sufficiently large mass splitting the interference of $\mathcal{A}^{\gamma\gamma}_{f_1,f_2}$ with the SM can be constructive. In the γZ channel the analytic form of the amplitude becomes more involved, in particular the loops involving both f_1 and f_2 are non-zero, and the interference with the SM strongly depends on the ratio m_1/m_2. One can tune the parameters to cancel the corrections to $\mu_{\gamma\gamma}$ in Eq. (4.3.39), e.g. taking $\varphi = 0$ and $m_1/m_2 = (t_L/t_R)^{\pm 1}$. For the same set of parameters large contributions to the γZ channel are possible. For example one can reach $\mu_{\gamma Z} \simeq 2$ for $\theta_L \simeq \pi/6$, $\theta_R \simeq \pi/10$, $m_1/m_2 \simeq 1.8$, $m_2 \simeq 800$ GeV and $Q \simeq 9$. This region is compatible with S, T and all other constraints.

A similar analysis can be performed when $R_w = 2$ or larger in Eq. (4.3.30). In this case there are N_w pairs of mixing states, with $Q = -(N_w-1)/2+Y, \ldots, (N_w-1)/2+Y$. For each such sector, the mass matrix is

$$\mathcal{M}_Q = \begin{pmatrix} M_1 & \kappa_Q m_{12} \\ \kappa_Q m_{21} & M_2 \end{pmatrix} , \tag{4.3.40}$$

where κ_{Q_α} is the Clebsch-Gordan coefficient coming from the $SU(2)_w$ contraction, determined by Eq. (D.4), therefore each sector is controlled by the same physical parameters. In other words, the two mass eigenvalues, the two mixing angles and the CP-violating phase of a given sector determine univocally the other sectors too. The corrections to $\mu_{\gamma\gamma}$ and $\mu_{\gamma Z}$ are obtained summing over the contributions of N_w sectors, each being qualitatively analog to the case $R_w = 1$ analysed above. Note that, however, one cannot take $Q \to 0$ to recover the SM limit, because there are at least two sectors with different values of Q. Of course, the SM is still recovered for small values of the mixing angles. The two fine-tuned regions with $\mu_{\gamma\gamma} \simeq 1$ and large $\mu_{\gamma Z}$ are still possible. On the one hand, the different sectors can add up to realise $\mathcal{A}^{\gamma\gamma}_{new} \simeq -2\mathcal{A}^{\gamma\gamma}_{SM}$. On the other hand, for $R_w = 2$ we found a choice of mixing parameters such that $\mathcal{A}^{\gamma\gamma}_{f_1,f_2}$ vanishes in both the sectors with $Q = Y \pm 1/2$.

• ***Two VLLs coupled to each other, mixing with the SM fermions.*** Finally, let us discuss the possible interactions between $\psi_{1,2}$ in Eq. (4.3.30) and the SM leptons. A non-zero mixing occurs if and only if ψ_1 and/or ψ_2 are identified with the states E, L, Λ or Δ listed in Table 4.1. There are six such cases,

$$\begin{array}{lllll} R_w = 1: & E + L\ (Y=-1), & E + \Lambda\ (Y=1), & & \\ R_w = 2: & L + \Delta\ (Y=1/2), & \Lambda + \Delta\ (Y=-3/2), & \Lambda + \Delta_G\ (Y=3/2), & \\ R_w = 3: & \Delta + \Omega\ (Y=-1), & \Delta + \Omega_G\ (Y=1). & & \end{array} \tag{4.3.41}$$

There are three cases with an additional weak multiplet: a triplet $\Delta_G = (E, F, G) \sim (1, 3, -2)$, and two quartets $\Omega = (E^c, N, E, F) \sim (1, 4, -1/2)$ and $\Omega_G = (N, E, F, G) \sim (1, 4, -3/2)$, with $Q(G) = -3$. They do not couple directly to the SM leptons. In these three cases the $Q = 2$ sector couples to the Higgs and therefore may contribute significantly to $h\gamma\gamma$ and $h\gamma Z$. We have shown in section 4.3.2 that the mixing angles between the SM leptons and E, L, Λ or Δ must be very small, due to the strong constraints coming from the $Z\tau\tau$ couplings. With two VLLs the mass matrices become larger, but we expect the phenomenology to be qualitatively the same, up to possible fine-tuned cancellations in some observable. A crucial effect of the mixing is to make the new leptons decay into SM leptons. The components with $Q = 2, 3$ decay more slowly, since their decay chains require a virtual exchange of other components of the multiplet. We already reviewed in section 4.3.2 the direct bounds on heavy leptons with charge $Q = 1, 2$, decaying promptly into SM leptons. We are not aware of any dedicated search for a $Q = 3$ heavy lepton.

A detailed analysis of the parameter space is worth only in the context of a specific, well-motivated model, and it goes beyond the scope of this chapter. The case $E + L$ is analyzed in Ref. [133]. The phenomenology of a fourth vector-like family of leptons, $L + E + N$, is studied in detail in Ref. [134]. Here we comment only on the interesting possibility to generate the τ mass entirely from the mixing with the VLLs, in the limit where the SM Yukawa coupling $\overline{l_{\tau L}} H \tau_R$ vanishes. There are various ways to induce such coupling through mixing, that are illustrated in Fig. 4.2:

(a) In the case of E only, one can proceed through a Yukawa coupling connecting $l_{\tau L}$ to E_R, followed by two singlet vector-like mass terms.

(b) Analogously, with L only, one employs two doublet vector-like mass terms and a Yukawa connecting L_L to τ_R.

(c) In the case of $E + L$, one can employ a vector-like mass term both for the singlets and the doublets, with a Yukawa coupling involving only the new fermions. This case is particularly interesting, since it corresponds to the scenario of partial compositeness [81] in the τ sector: the SM leptons are elementary fields that mix linearly with composite VLLs, which couple in turn

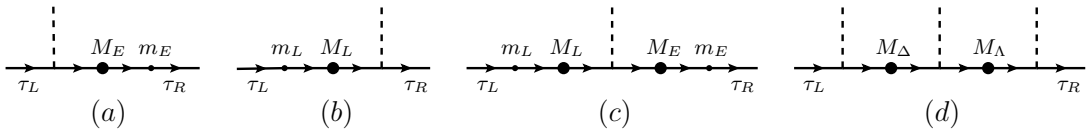

Figure 4.2: Different ways to generate the τ mass through mixing between the SM leptons and VLLs. The dashed lines stand for Higgs vev insertions, the small dots represent a mass mixing between a SM lepton and a VLL, and the big dots correspond to the mass of a VLL. The case (c) corresponds to the scenario of τ partial compositeness.

to a composite Higgs doublet. The SM leptons feel EWSB only through the mixing with heavy composite leptons. The $Q = 1$ mass matrix and its smallest eigenvalue take the form

$$\mathcal{M}_e = \begin{pmatrix} 0 & m_L & 0 \\ 0 & M_L & \frac{\lambda_{LE} v}{\sqrt{2}} \\ m_E & \frac{\lambda_{EL} v}{\sqrt{2}} & M_E \end{pmatrix} , \qquad m_\tau \simeq \frac{m_L}{M_L} \frac{m_E}{M_E} \frac{\lambda_{LE} v}{\sqrt{2}} . \tag{4.3.42}$$

The mixing with the heavy leptons also controls the deviations in the Z couplings,

$$\delta g^R_{\tau\tau} \simeq \frac{1}{2} \left(\frac{m_E}{M_E} \right)^2 , \qquad \delta g^L_{\tau\tau} \simeq \frac{1}{2} \left(\frac{m_L}{M_L} \right)^2 . \tag{4.3.43}$$

As these corrections are bounded by $R(Z \to \tau\tau)$, as shown in Eq. (C.27), we find that the physical value of m_τ can be generated for $\lambda_{EL} \gtrsim 2.5$, pointing indeed to a strong-coupling regime. The phenomenology of τ partial compositeness is studied e.g. in Ref. [135].

(d) Finally, in the case $(\psi_1, \psi_2) = (\Lambda, E)$, (L, Δ) or (Λ, Δ), the τ mass can be induced by three Yukawa couplings, connecting $l_{\tau L}$ to ψ_2, τ_R to ψ_1, and ψ_1 to ψ_2, respectively. Focusing on (Λ, Δ) for definiteness, one finds

$$m_\tau \simeq \frac{\lambda_\Delta v}{\sqrt{3} M_\Delta} \frac{\lambda_\Lambda v}{\sqrt{2} M_\Lambda} \frac{\lambda_{\Delta\Lambda} v}{\sqrt{6}} \simeq 2 \sqrt{\delta g^R_{\tau\tau} \delta g^L_{\tau\tau}} \frac{\lambda_{\Delta\Lambda} v}{\sqrt{6}} . \tag{4.3.44}$$

For $\lambda_{\Delta\Lambda} \gtrsim 4.5$ the physical value of m_τ can be generated.

4.3.4 Vector-like plus Majorana leptons (including higgsinos plus gauginos)

In this section we consider the interplay between Majorana leptons and VLLs, related by one or more Yukawa couplings. If there were no such couplings, the phenomenology would reduce to a trivial addition of the effects of Majorana leptons, see section 4.3.1, and of VLLs, see sections 4.3.2 and 4.3.3. For reference, the smallest sets of this kind are formed by three (four) chiral multiplets: (two copies of) N_R or Σ_R, plus a vector-like pair (E_L, E_R), (Λ_L, Λ_R) or (Δ_L, Δ_R).

• ***One VLL plus one Majorana lepton.*** The most general set formed by one Majorana lepton interacting with one VLL pair is

$$\chi_R \sim (1, R_w, 0) , \qquad \psi_L, \psi_R \sim (1, R_w \pm 1, -1/2) , \tag{4.3.45}$$

with $N_w \neq 2 + 4n$ to avoid the global $SU(2)_w$ anomaly. The corresponding Lagrangian is

$$-\mathcal{L}_{\chi\psi} = \tfrac{1}{2} M_\chi \overline{\chi^c_R} \chi_R + M_\psi \overline{\psi_L} \psi_R + \tilde{\lambda} \overline{\psi_L} \tilde{H} \chi_R + \lambda \overline{\chi^c_R} H \psi_R + h.c. . \tag{4.3.46}$$

The Majorana mass M_χ is absent in the case of even $SU(2)_w$ representations, $N_w = 4n$: in this case there is a conserved 'new lepton' number, and all multiplet components combine into Dirac fermions. There is a unique physical complex phase, that can be associated to M_χ, choosing M_ψ, $\tilde{\lambda}$ and λ real. Each component of the new leptons has a (demi-)integer charge Q, therefore it can decay to SM

leptons, either through renormalizable interactions or higher dimensional operators. For $R_w = 1$ or 3, couplings to the SM leptons can be added to the Lagrangian, as we will discuss later.

In the case $\psi \sim (R_w + 1)$, after EWSB one identifies: one pair of states with charges $Q = \pm(N_w+1)/2$, that combine in a VLL of mass M_ψ; three pairs of states with $Q = \pm(N_w-1)/2$, $\pm(N_w-3)/2$, ..., down to $Q = \pm 1$ ($\pm 1/2$) for N_w odd (even); when N_w is odd, three additional states with $Q = 0$. The 3×3 mass matrix in each sector takes the form

$$\mathcal{M}_Q = \begin{pmatrix} M_\chi & \kappa_Q \tilde{\lambda} v & \kappa_{-Q} \lambda v \\ \kappa_{-Q} \tilde{\lambda} v & 0 & M_\psi \\ \kappa_Q \lambda v & M_\psi & 0 \end{pmatrix} , \tag{4.3.47}$$

where we chose $Q \geq 0$ and a basis with the components of charge Q ($-Q$) on the left(right)-hand side of $\mathcal{M}_Q$. The $SU(2)_w$ Clebsch-Gordan coefficients $\kappa_{\pm Q}$ are defined by Eq. (D.4), and they also include for convenience the factor $1/\sqrt{2}$ from the Higgs doublet vev,

$$\kappa_{\pm Q} = \frac{1}{\sqrt{2}} \sqrt{\frac{N_w + 1 \pm 2Q}{N_w(N_w+1)}} . \tag{4.3.48}$$

In the case $\psi \sim (R_w - 1)$, there are three pairs of states with $Q = \pm(N_w - 3)/2, \pm(N_w - 5)/2, \ldots$, and three states with $Q = 0$ when N_w is odd. The 3×3 mass matrix in each of these sectors has the form of Eq. (4.3.47), but with Clebsch-Gordan coefficients given by

$$\kappa_{\pm Q} = \frac{1}{\sqrt{2}} \sqrt{\frac{N_w - 1 \mp 2Q}{N_w(N_w-1)}} . \tag{4.3.49}$$

There are also two pairs of states with $Q = \pm(N_w - 1)/2$ and mass matrix

$$\mathcal{M}_Q = \begin{pmatrix} M_\chi & \kappa_{-Q} \lambda v \\ \kappa_{-Q} \tilde{\lambda} v & M_\psi \end{pmatrix} . \tag{4.3.50}$$

This is the same structure of Eq. (4.3.32), that was extensively studied in section 4.3.3.

Note that each 3×3 or 2×2 sector depends on the same five parameters: two masses, two Yukawa couplings, and one physical phase. They determine all the mass eigenvalues and the mixing matrices. We do not attempt a scan of the parameter space here. The corrections to S, T, $\mu_{\gamma\gamma}$ and $\mu_{\gamma Z}$ from a sector with the mass matrix of Eq. (4.3.50) were analysed in section 4.3.3. We expect corrections of the same order from the other sectors. Coming to collider searches, for $N_w \neq 1, 3$ there is no mixing with the SM and the lightest mass eigenstate is stable, at least at the renormalizable level. When it is charged, one can apply the limits on stable leptons reported in Table 4.2. For N_w odd, the lightest state may be neutral, with the typical collider phenomenology of a dark matter candidate.

The phenomenology is radically different when N_w is even. In this case the Majorana mass is absent, $M_\chi = 0$, and the χ components are massless before EWSB, therefore one mass eigenvalue for each sector is of the order $\lambda\tilde{\lambda}v^2/M_\psi$. This implies that all masses are bound to the EW scale, whence the situation resembles the one of purely chiral sets of new fermions. In particular, one finds a correction to $h \to \gamma\gamma$ that depends only on Q: taking $M_\chi = 0$ in the mass matrix (4.3.47) or (4.3.50), and using the LET approximation of Eq. (D.24), we find a CP-even amplitude $\mathcal{A}^{\gamma\gamma}_{\chi\psi,Q} \simeq 8Q^2/3$ for a 3×3 sector, and the same for a 2×2 sector. For comparison, when N_w is odd the Majorana mass is allowed and one finds

$$\mathcal{A}^{\gamma\gamma,3\times3}_{\chi\psi,Q} \simeq -\frac{8}{3} \frac{\lambda v}{M_\chi} \frac{\tilde{\lambda} v}{M_\psi} Q^2 \left(\kappa^2_{-Q} + \kappa^2_Q\right) , \qquad \mathcal{A}^{\gamma\gamma,2\times2}_{\chi\psi,Q} \simeq -\frac{8}{3} \frac{\lambda v}{M_\chi} \frac{\tilde{\lambda} v}{M_\psi} Q^2 \kappa^2_{-Q} , \tag{4.3.51}$$

where we made the approximation $\lambda v, \tilde{\lambda} v \ll M_\chi, M_\psi$. The correction grows as the $\chi - \psi$ mixing parameters of the type $\lambda v/M$ increase, on the other hand S and T generally put a significant upper bound on these parameters. Obviously, in each model the total $\mathcal{A}^{\gamma\gamma}_{new}$ is the sum over all the sectors with different Q.

Let us say a few more words on the cases where χ and/or ψ mix with the SM leptons.

- $N + L$: for $R_w = 1$, the Majorana fermion is a sterile neutrino N, the vector-like fermion is a lepton doublet L, and the Lagrangian in Eq. (4.3.46) is extended to include $\lambda_N \overline{l_L} \tilde{H} N_R + \lambda_L \overline{L_L} H \tau_R + h.c.$. The full parameter space includes two real masses, four reals Yukawa couplings and two physical phases, that can be associated e.g. to λ and $\tilde{\lambda}$. The 2×2 mass matrix in the $Q = \pm 1$ sector is given by Eq. (4.3.13): the mixing with the SM is small due to the strong constraint from the $Z\tau\tau$ couplings, implying small deviations in $\mu_{\gamma\gamma}$ and $\mu_{\gamma Z}$. The 4×4 mass matrix in the $Q = 0$ sector is obtained by adding to Eq. (4.3.47) a first row and a first column of the form $(0, \lambda_N v/\sqrt{2}, 0, 0)$. There are some simple limiting cases. If $\lambda, \tilde{\lambda} \to 0$, the matrix reduces to two diagonal blocks, as N and L decouple from each other, and the phenomenology reduces to the one of the previous sections. If $M_{L,N}/v$ are much larger than the Yukawa couplings, all the mixing angles are small and the smallness of the light neutrino mass follows from the usual seesaw mechanism, $m_\nu \simeq \lambda_N^2 v^2/(2M_N)$. Still, m_ν can be small even in the presence of large Yukawa couplings. In particular, for $\lambda v, \tilde{\lambda} v \sim M_{N,L}$, large mixing angles are possible, and, correspondingly, such intricate neutral sector may induce significant corrections to the S and T parameters.

- For $R_w = 3$, the Majorana fermion is the triplet Σ and the vector-like fermion is the doublet L or the quartet Ω.

  $\Sigma + L$: the Lagrangian in Eq. (4.3.46) is extended to include $\lambda_\Sigma \overline{l_L} \tilde{H} \Sigma_R + \lambda_L \overline{L_L} H \tau_R + h.c.$. Up to different Clebsch-Gordan coefficients, the 4×4 neutral sector is the same as in the $N + L$ case. The mass matrix in the charged sector is

$$\mathcal{M}_1 = \begin{pmatrix} \sqrt{\frac{1}{2}}\lambda_\tau v & \sqrt{\frac{1}{3}}\lambda_\Sigma v & 0 \\ 0 & M_\Sigma & \sqrt{\frac{1}{3}}\lambda v \\ \sqrt{\frac{1}{2}}\lambda_L v & \sqrt{\frac{1}{3}}\tilde{\lambda} v & M_L \end{pmatrix} . \tag{4.3.52}$$

  The $Z\tau\tau$ couplings constrain both mixing parameters $\lambda_\Sigma v/M_\Sigma$ and $\lambda_L v/M_L$ to be small, as explained in sections 4.3.1 and 4.3.2, respectively. When the mixing with the SM is neglected, one is left with a special case of Eq. (4.3.50), which corresponds to the chargino mass matrix in supersymmetry. Note that, in the limit where λ_τ vanishes, there is still a contribution to the τ mass, $m_\tau \simeq (\lambda_\Sigma \lambda_L \lambda v^3)/(3\sqrt{2} M_\Sigma M_L)$, as illustrated in Fig. 4.2(d). Despite the constraint on the mixing from the $Z\tau\tau$ couplings, one can accommodate the correct size of m_τ for $\lambda \gtrsim 3$, see the discussion below Eqs. (4.3.42) and (4.3.44).

  $\Sigma + \Omega$: the Lagrangian in Eq. (4.3.46) is extended to include $\lambda_\Sigma \overline{l_L} \tilde{H} \Sigma_R + h.c.$, as the quartet does not mix with the SM. The 4×4 neutral sector has the same structure as in the $N + L$ and $\Sigma + L$ cases. The $Q = 1$ sector also has a 4×4 mass matrix, that is obtained from Eq. (4.3.47) by adding a first row $(\lambda_\tau v/\sqrt{2}, \lambda_\Sigma/\sqrt{3}, 0, 0)$, and a first column $(\lambda_\tau v/\sqrt{2}, 0, 0, 0)$. In addition, there is a $Q = 2$ state with mass M_Ω. There are no significant phenomenological novelties, as the effects of the SM mixing with Σ and of the Σ mixing with Ω mixing do not interfere significantly.

• ***One VLL plus two Majorana leptons.*** Let us come to sets of two Majorana leptons both interacting with one vector-like pair. One obvious possibility is to take two copies of the same Majorana lepton, that is, to replace χ_R in Eq. (4.3.45) with χ_{iR}, $i = 1, 2$, with the obvious doubling of each coupling involving χ in the Lagrangian. Note that N_w can be arbitrary and, for even N_w, the Majorana mass terms are forbidden but a Dirac mass term $M_\chi \overline{\chi^c_{1R}} \chi_{2R}$ is allowed. In all other respects, the mass matrix structures and the inherent phenomenology are a straightforward generalisation of those discussed above.

The second and last possibility to couple two Majorana leptons to one VLL is provided by the set

$$\chi_{1R} \sim (1, R_w, 0) , \qquad \psi_L, \psi_R \sim (1, R_w + 1, -1/2) , \qquad \chi_{2R} \sim (1, R_w + 2, 0) , \tag{4.3.53}$$

with N_w necessarily odd, and Lagrangian

$$-\mathcal{L}_{\chi\psi} = M_\psi \overline{\psi_L} \psi_R + \sum_{i=1}^{2} \left[\tfrac{1}{2} M_{\chi_i} \overline{\chi^c_{iR}} \chi_{iR} + \tilde{\lambda}_i \overline{\psi_L} \tilde{H} \chi_{Ri} + \lambda_i \overline{\chi^c_{Ri}} H \psi_R \right] + h.c. . \tag{4.3.54}$$

There are two pairs of states with $Q = \pm(N_w+1)/2$, with a mass matrix given by Eq. (4.3.50) with $M_\chi, \lambda, \tilde{\lambda} \to M_{\chi_2}, \lambda_2, \tilde{\lambda}_2$. In addition, there are four pairs of states with $Q = \pm(N_w-1)/2, \pm(N_w-3)/2, \ldots, \pm 1$, and four states with $Q=0$. The 4×4 mass matrix in each such sector takes the form

$$\mathcal{M}_Q = \begin{pmatrix} M_{\chi_1} & 0 & \kappa_{1,Q}\tilde{\lambda}_1 v & \kappa_{1,-Q}\lambda_1 v \\ 0 & M_{\chi_2} & \kappa_{2,Q}\tilde{\lambda}_2 v & \kappa_{2,-Q}\lambda_2 v \\ \kappa_{1,-Q}\tilde{\lambda}_1 v & \kappa_{2,-Q}\tilde{\lambda}_2 v & 0 & M_\psi \\ \kappa_{1,Q}\lambda_1 v & \kappa_{2,Q}\lambda_2 v & M_\psi & 0 \end{pmatrix} , \tag{4.3.55}$$

with $\kappa_{1,\pm Q}$ given by Eq. (4.3.48), and $\kappa_{2,\pm Q}$ given by Eq. (4.3.49) with $N_w \to N_w+2$. As in Eq. (4.3.51), one can estimate the contribution of this mass matrix to the $h\gamma\gamma$ coupling, by taking the LET approximation,

$$\mathcal{A}^{\gamma\gamma,4\times 4}_{\chi_1\chi_2\psi,Q} \simeq -\frac{8}{3}\sum_{i=1,2}\frac{\lambda_i v}{M_{\chi_i}}\frac{\widetilde{\lambda}_i v}{M_\psi}Q^2\left(\kappa^2_{i,-Q}+\kappa^2_{i,Q}\right) . \tag{4.3.56}$$

Let us discuss the minimal cases $R_w = 1$ and $R_w = 3$, that admit a mixing with the SM leptons.

- $N + L + \Sigma$: for $R_w = 1$, the new fermions have the gauge quantum numbers of the bino, the higgsinos and the wino in supersymmetry. Thus, the mass matrices (4.3.50) and (4.3.55) are a generalisation of the chargino ($Q=\pm 1$) and neutralino ($Q=0$) mass matrices, respectively (for a review see Ref. [136]). Supersymmetry restricts the Yukawa couplings to $\tilde{\lambda}_{1,2}/\lambda_{1,2} = -\tan\beta$, $\lambda_1/\lambda_2 = \tilde{\lambda}_1/\tilde{\lambda}_2 = -\tan\theta_w/\sqrt{3}$, and $\lambda_1 = -\cos\beta g'$. The effect of charginos and neutralinos on the Higgs boson couplings is analysed e.g. in Refs. [137–140]. In particular, the chargino loop contributing to $h\gamma\gamma$ and $h\gamma Z$ is controlled by the weak coupling g, and it is typically subleading compared to the SM top quark loop. Without the supersymmetry constraints, the most general chargino mass matrix has the structure of Eq. (4.3.32), therefore one can apply the results of section 4.3.3 for the Higgs decay amplitudes into $\gamma\gamma$ and γZ.

  In the absence of (R-parity conserving) supersymmetry, not only the four Yukawa couplings $\lambda_{1,2}$ and $\tilde{\lambda}_{1,2}$ are unconstrained, but in addition a mixing with the SM leptons is allowed: one should add to the Lagrangian in Eq. (4.3.54) the terms $\lambda_N \overline{l_L}\tilde{H}N_R + \lambda_\Sigma \overline{l_L}\tilde{H}\Sigma_R + \lambda_L \overline{L_L}H\tau_R + h.c.$. The $Q=\pm 1$ mass matrix becomes the one in Eq. (4.3.52), and the $Q=0$ mass matrix becomes 5×5, and it is obtained from Eq. (4.3.55) by adding a first row and column of the form $(0, \lambda_N v/\sqrt{2}, \lambda_\Sigma v/\sqrt{6}, 0, 0)$. Therefore, one can observe the phenomenological effects of N, Σ and L individually, as analysed in sections 4.3.1 and 4.3.2, as well as their interplay, already described above for $(N+L)$ and $(\Sigma+L)$. As usual, the mixing with the SM leptons is typically constrained to be small by the smallness of m_ν and by the $Z\tau\tau$ couplings, thus the modifications to the $h\nu\nu$ and $h\tau\tau$ couplings are suppressed. However, even a very small mixing with the SM offers decay modes to the heavy fermions, such that none is stable. A dedicated analysis of the full parameter space would be interesting, to characterise quantitatively the correlations among the different observables, and especially the deviations from the supersymmetric limit.

- $\Sigma + \Omega + \Xi$: for $R_w = 3$, the new fermions are a Majorana triplet, a vector-like quartet, and a Majorana quintuplet Ξ. There is a 2×2 sector with $Q=\pm 2$ given by Eq. (4.3.50). As the triplet mixes with the SM through $\lambda_\Sigma \overline{l_L}\tilde{H}\Sigma_R + h.c.$, there is a 5×5 sector with $Q=\pm 1$, that is obtained by adding to the matrix in Eq. (4.3.55) a first row $(\lambda_\tau v/\sqrt{2}, \lambda_\Sigma v/\sqrt{3}, 0, 0, 0)$ and a first column $(\lambda_\tau v/\sqrt{2}, 0, 0, 0, 0)$. This large number of charged states with potentially large mixing can give a significant correction to $\mu_{\gamma\gamma}$ and $\mu_{\gamma Z}$. For concreteness, neglecting the mixing with the SM and using the LET approximation, we find

$$\mathcal{A}^{\gamma\gamma}_{\Sigma\psi\Xi} \simeq -\frac{8}{3}\left(\frac{1}{3}\frac{\lambda_1 v}{M_\Sigma}\frac{\widetilde{\lambda}_1 v}{M_\Omega} + \frac{\lambda_2 v}{M_\Xi}\frac{\widetilde{\lambda}_2 v}{M_\Omega}\right) , \tag{4.3.57}$$

  to be compared with the SM top contribution, $\mathcal{A}^{\gamma\gamma}_t \simeq 16/9$. One should take into account the constraints (in particular S and T) on the mixing parameters $\sim \lambda v/M$. The neutral sector has

also a 5×5 mass matrix, obtained by adding a first column and row $(0, \lambda_\Sigma v/\sqrt{6}, 0, 0, 0)$ to to the matrix in Eq. (4.3.55). As usual, the vanishing neutrino mass requires $\lambda_\Sigma v/M_\Sigma$ to be very small.

4.4 Phenomenology of non-chiral quarks

In this section we discuss new coloured fermions that either form vector-like pairs, or admit a Majorana mass term. We will dub them 'quarks' even when they are not in the fundamental representation of $SU(3)_c$.

4.4.1 One vector-like quark

There are seven possible VLQs that mix with the SM quarks, as listed in Table 4.1. They have been extensively studied under various respects in the literature (see e.g. Refs. [84, 141–146]). Here we describe in a compact, systematic way the leading order constraints coming from EW precisions tests, direct searches at colliders, and Higgs couplings. As usual we restrict ourselves to mixing with the third family. In the top (bottom) sector, a mixing appears whenever the VLQ contains a component T (B) with the same charge as t (b). The components of each multiplet are displayed in Eq. (4.1.6). In the case of weak singlets or triplets, the SM Lagrangian is extended by

$$-\mathcal{L}_\psi = \lambda_\psi \overline{q_L} \tilde{H}(H) \psi_R + M_\psi \overline{\psi_L} \psi_R + h.c. \ , \qquad \text{for } \psi = T, X_Q(B, Y_Q) \ , \tag{4.4.1}$$

and, in the case of weak doublets, by

$$-\mathcal{L}_\psi = \lambda^t_\psi \overline{\psi_L} \tilde{H}(H) t_R + \lambda^b_\psi \overline{\psi_L} H(\tilde{H}) b_R + M_\psi \overline{\psi_L} \psi_R + h.c. \ , \qquad \text{for } \psi = Q(X_T, Y_B) \ , \tag{4.4.2}$$

with the further restriction $\lambda^b_{X_T} = \lambda^t_{Y_B} = 0$. The structure of the top (bottom) sector mass matrix is very close to the charged lepton one in the case of one VLL, therefore we will frequently refer to section 4.3.2. In the top sector one has

$$\mathcal{M}_t = \begin{pmatrix} \lambda_t \frac{v}{\sqrt{2}} & \kappa^t_\psi \lambda_\psi \frac{v}{\sqrt{2}} \\ 0 & M_\psi \end{pmatrix} \ , \ \psi = T, X_Q, Y_Q \ , \quad \mathcal{M}_t = \begin{pmatrix} \lambda_t \frac{v}{\sqrt{2}} & 0 \\ \kappa^t_\psi \lambda^t_\psi \frac{v}{\sqrt{2}} & M_\psi \end{pmatrix} \ , \ \psi = Q, X_T \ , \tag{4.4.3}$$

with Clebsch-Gordan coefficients $\kappa^t_{T,Q,X_T} = 1$, $\kappa^t_{X_Q} = \sqrt{1/3}$ and $\kappa^t_{Y_Q} = \sqrt{2/3}$. The rotation to the mass basis is parametrized as $\mathcal{M}_t = U_L diag(m_t, m_{t'}) U_R^\dagger$, in analogy with Eq. (4.3.14). In the bottom sector one has

$$\mathcal{M}_b = \begin{pmatrix} \lambda_b \frac{v}{\sqrt{2}} & \kappa^b_\psi \lambda_\psi \frac{v}{\sqrt{2}} \\ 0 & M_\psi \end{pmatrix} \ , \ \psi = B, X_Q, Y_Q \ , \quad \mathcal{M}_b = \begin{pmatrix} \lambda_b \frac{v}{\sqrt{2}} & 0 \\ \kappa^b_\psi \lambda^b_\psi \frac{v}{\sqrt{2}} & M_\psi \end{pmatrix} \ , \ \psi = Q, Y_B \ , \tag{4.4.4}$$

with $\kappa^b_{B,Q,Y_B} = 1$, $\kappa^b_{X_Q} = \sqrt{2/3}$ and $\kappa^b_{Y_Q} = \sqrt{1/3}$, and one can write $\mathcal{M}_b = \widetilde{U}_L diag(m_b, m_{b'}) \widetilde{U}_R^\dagger$.

In all cases except Q, the vector-like mass M_ψ and the three independent Yukawa couplings can be taken to be real. In the case of Q, there are four Yukawa couplings and one complex phase ϕ is physical. In full generality, one can choose $\lambda_{t,b}$ and $\lambda^{t,b}_Q$ real, and add a matrix $P_\phi = diag(e^{i\phi}, 1)$ on the left of $\mathcal{M}_b$. Then, Eq. (C.4) and Eq. (D.5) show that ϕ appears in the W couplings to the fermion mass eigenstates, while the Z and h couplings are independent from ϕ. It is very difficult to observe such CP-violating effect in the charged current, since it vanishes for $\lambda_b \to 0$, that is, it is always suppressed by the small ratio m_b/v. Coming to the mixing angles, the left- and right-hand ones are related as in the case of VLLs, see Eq. (4.3.15): in the case of weak doublet VLQs one finds

$$\tan\theta_L = \frac{m_t}{m_{t'}} \tan\theta_R < \tan\theta_R \ , \qquad \tan\widetilde{\theta}_L = \frac{m_b}{m_{b'}} \tan\widetilde{\theta}_R \ll \tan\widetilde{\theta}_R \ , \tag{4.4.5}$$

while for singlet or triplet VLQs, the same relations hold with $L \leftrightarrow R$. In the following we will drop the subscripts L, R and denote θ_ψ ($\widetilde{\theta}_\psi$) the largest mixing angle in the top (bottom) sector, for any

given VLQ ψ. For the multiplets with both the T and B components, the mass eigenvalues and the mixing angles in the top and bottom sectors are strictly related,

$$\begin{cases} m_{t'}^2 - m_{b'}^2 = s_\psi^2 (m_{t'}^2 - m_t^2) - \tilde{s}_\psi^2 (m_{b'}^2 - m_b^2) \\ s_\psi c_\psi (m_{t'}^2 - m_t^2) r_\psi = \tilde{s}_\psi \tilde{c}_\psi (m_{b'}^2 - m_b^2) \end{cases} , \tag{4.4.6}$$

where $r_{X_Q} = \sqrt{2}$, $r_{Y_Q} = 1/\sqrt{2}$, and $r_Q \equiv \lambda_Q^b / \lambda_Q^t$. Therefore, one can determine the bottom sector parameters, $m_{b'}$ and $\widetilde{\theta}_\psi$, as a function of the top sector one, $m_{t'}$ and θ_ψ, or vice versa. In the case $\psi = Q$, there is the additional freedom of the choice of r_Q. Note that the custodial symmetry is preserved in the Q sector if $r_Q = 1$, see Eq. (4.4.2). The mass splitting among the heavy quarks is controlled (at tree level) by the mixing with the SM. The mass ordering is determined as

$$\begin{array}{llll} T: & M_T \leq m_{t'} \ , & B: & M_B \leq m_{b'} \ , \\ X_T: & m_X = M_{X_T} \leq m_{t'} \ , & Y_B: & m_Y = M_{Y_B} \leq m_{b'} \ , \\ X_Q: & m_X = M_{X_Q} \leq m_{t'} \leq m_{b'} \ , & Y_Q: & m_Y = M_{Y_Q} \leq m_{b'} \leq m_{t'} \ , \end{array} \tag{4.4.7}$$

where we took implicitly into account the experimental upper bounds on the mixing and on $m_t/m_{t'}$, when needed to establish the ordering. In the case of Q, for $r_Q = 1$ one finds $M_Q \leq m_{b'} \leq m_{t'}$, but the ordering between b' and t' can change for different values of r_Q.

Masses and mixing angles are constrained by the perturbativity of the Yukawa couplings,

$$\left|\lambda_\psi^t\right| \simeq \left| \frac{\sqrt{2}}{\kappa_\psi^t} s_\psi \frac{m_{t'}}{v} \right| \ll 4\pi \ , \qquad \left|\lambda_\psi^b\right| \simeq \left| \frac{\sqrt{2}}{\kappa_\psi^b} \tilde{s}_\psi \frac{m_{b'}}{v} \right| \ll 4\pi \ . \tag{4.4.8}$$

Note that we do not impose a stronger upper bound such as $4\pi/\sqrt{N_c}$, for reasons discussed in Appendix D.1. The perturbativity of the SM couplings λ_t and λ_b is guaranteed a fortiori. For definiteness, in Figures 4.3 - 4.6 we delimit with a black dotted line the region of parameters where at least one Yukawa coupling becomes larger than 2π. In the case of Q both inequalities must be satisfied at the same time, therefore a large departure from $r_Q = 1$ leads to a stronger constraint, as illustrated by the comparison of the left and right panels of Fig. 4.6.

Important constraints come from the Z couplings to quarks, that are affected by the mixing as shown in Eq. (C.6). The tree-level deviations with respect to the SM are given by

$$\delta g^L_{Z\bar{b}b} = \tilde{s}_L^2 \left(\frac{1}{2} + T_B^3 \right) \ , \quad \delta g^R_{Z\bar{b}b} = \tilde{s}_R^2 T_B^3 \ , \qquad \delta g^L_{Z\bar{t}t} = s_L^2 \left(-\frac{1}{2} + T_T^3 \right) \ , \quad \delta g^R_{Z\bar{t}t} = s_R^2 T_T^3 \ , \tag{4.4.9}$$

where T_B^3 (T_T^3) is the weak isospin of the B (T) component of the VLQ under investigation. The $Zb\bar{b}$ couplings are measured less precisely than their leptonic analog, the $Z\tau^+\tau^-$ couplings, but nonetheless they are strongly constrained, especially for b_L. The top couplings to the Z boson are poorly constrained directly, however they also contribute at one loop to $Zb\bar{b}$. These constraints are summarised in appendix C.3 and they exclude the blue-shaded region in Figures 4.3 - 4.6. Deviations in $Z\overline{b_L}b_L$ are present at tree level in the case of B, Y_B, Y_Q and X_Q. However, in the case of the doublet Y_B, the deviation is suppressed by $(m_b/m_b')^2$ and the most important correction is the one to $Z\overline{b_R}b_R$. In the case of T and X_T, there is no bottom partner and the deviation to $Z\overline{b_L}b_L$ is induced at one loop mostly through $\delta g^L_{Z\bar{t}t}$, leading to a relatively weak constraint. Finally, in the case of Q, $\delta g^R_{\bar{b}b}$ is generated at tree level and $\delta g^L_{\bar{b}b}$ at one loop, the strongest constraint coming from the right-handed coupling.

The VLQ couplings to the EW gauge bosons are also constrained by the EW precision parameters S and T, whose expressions are provided in appendix C.2. Note that, in contrast with the tau and bottom sectors, in the top sector contributions proportional to powers of m_t/m_Z are not suppressed. In Figs. 4.3 - 4.6 we display in (light) yellow the region corresponding to the (68%) 99% C.L. ellipse of Fig. 10. Since S and T are proportional to the mixing between the SM quarks and the VLQ, one typically observes an upper bound $s_\psi, \tilde{s}_\psi \lesssim 0.05 - 0.20$, depending on the VLQ under consideration. Note that this bound relaxes as the heavy quark mass decreases, because S and T eventually vanish in the limit $m_{t'} \to m_t$ or $m_{b'} \to m_b$. Note also that a cancellation is possible among relatively large

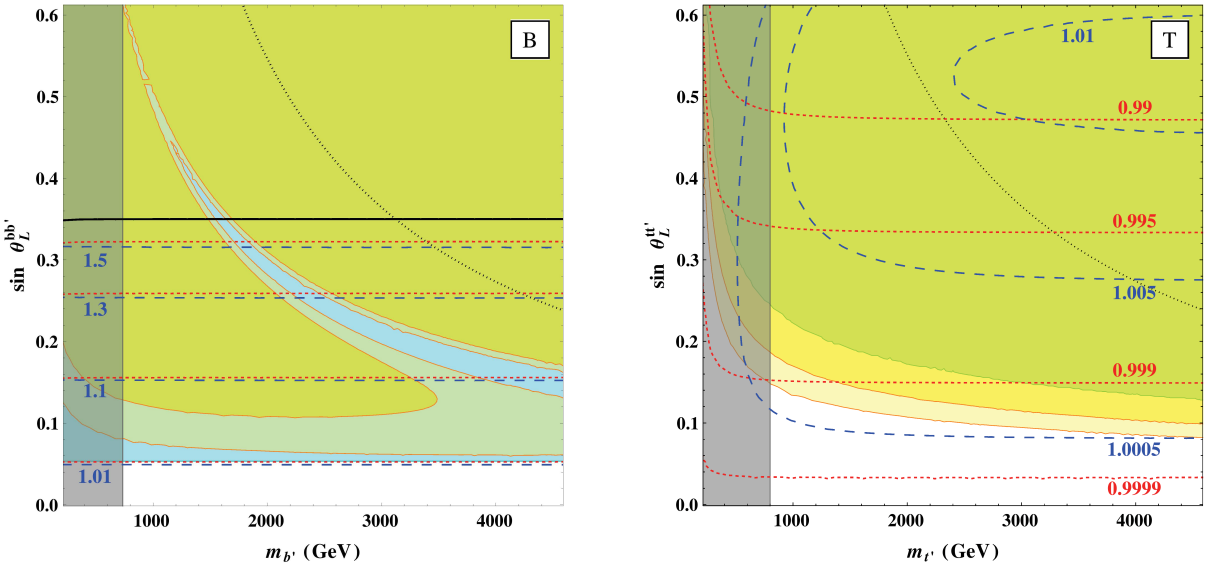

Figure 4.3: Constraints on the weak singlet VLQs B (left panel) and T (right panel), as a function of the mass of b' (t') and of the mixing angle between b_L and b'_L (t_L and t'_L). The region above the dotted black line is excluded by perturbativity. The blue-shaded region is excluded by the $Zb\bar{b}$ couplings. The (light) yellow-shaded region is excluded by the S and T parameters at (68%) 99% C.L.. The green-shaded region is just the intersection of the previous two. The grey-shaded region is excluded by the collider searches summarised in Table 4.3. The region above the solid black line is excluded by a rough global fit of the Higgs couplings at 99% C.L.. The dashed blue (dotted red) lines correspond to a few relevant values of the signal strength $\mu_{\gamma Z}$ ($\mu_{\gamma\gamma}$).

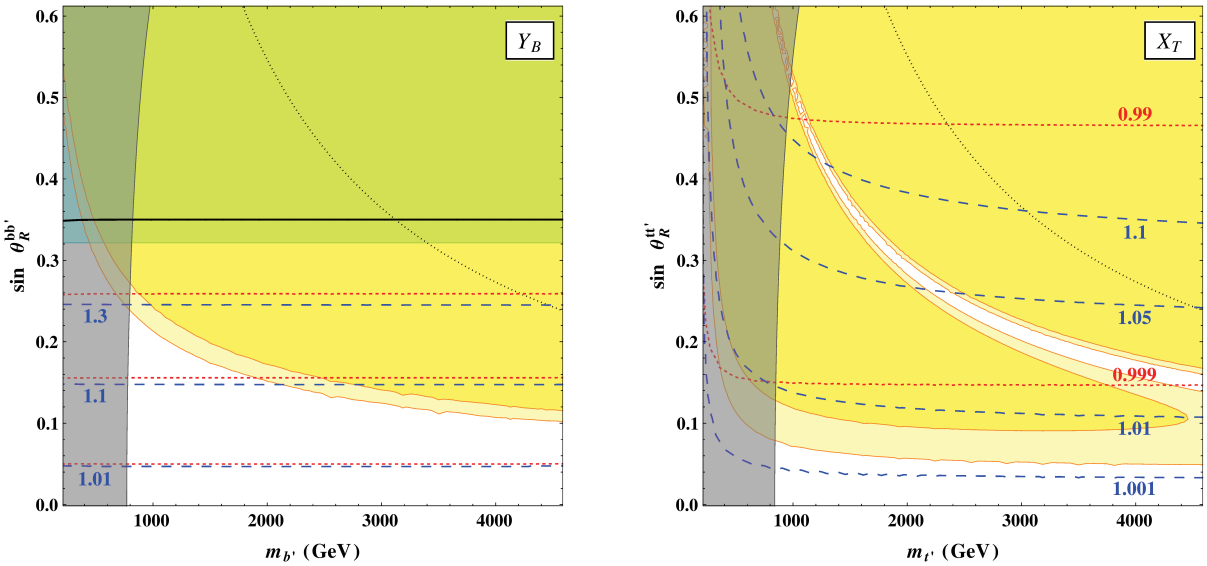

Figure 4.4: Constraints on the weak doublet VLQs Y_B ($Y = -5/6$, left panel) and X_T ($Y = +7/6$, right panel) as a function of the mass of b' (t') and of the mixing angle between b_R and b'_R (t_R and t'_R). The notation is the same as in Fig. 4.3.

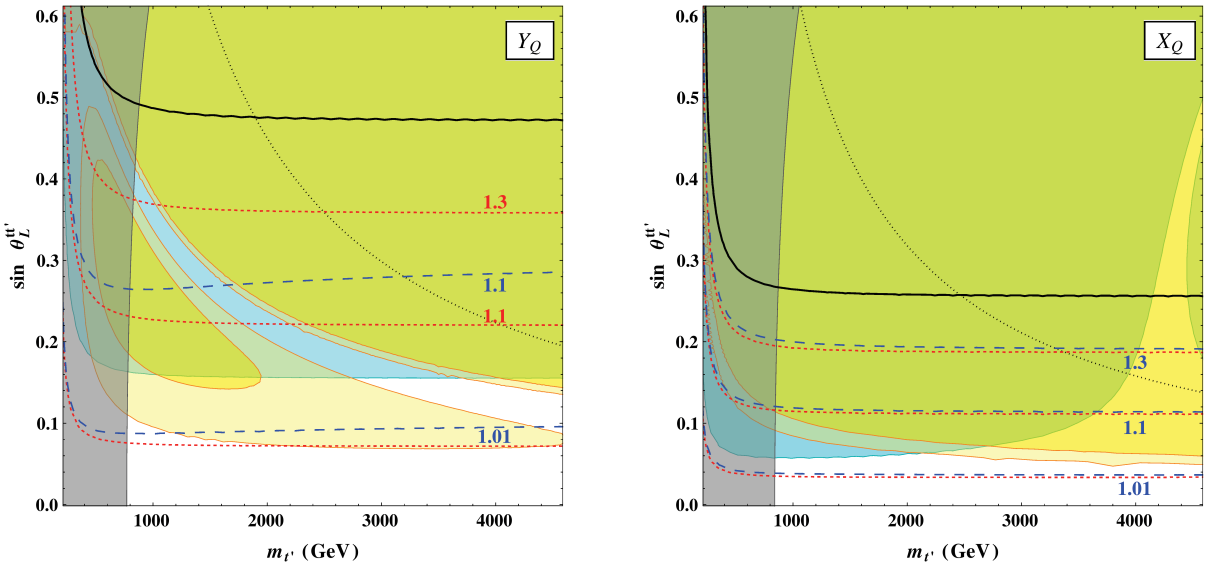

Figure 4.5: Constraints on the weak triplet VLQs Y_Q ($Y = -1/3$, left panel) and X_Q ($Y = +2/3$, right panel) as a function of the mass of t' and of the mixing angle between t_L and t'_L. The notation is the same as in Fig. 4.3.

contributions to S and T, such that large mixing angles may be allowed in a fine-tuned region of parameters. This is especially relevant in the case of X_T, because such region is not excluded by other constraints. Indeed, we find

$$T(X_T) \simeq \frac{3 s^2_{X_T}}{16\pi c_w^2 s_w^2} \frac{m_{t'}^2}{m_Z^2} \left[\frac{4}{3} s^2_{X_T} + \frac{m_t^2}{m_{t'}^2} \left(4 \ln \frac{m_t^2}{m_{t'}^2} + 6 \right) \right] , \quad S(X_T) \simeq \frac{s^2_{X_T}}{2\pi} \left(\frac{4}{3} \ln \frac{m_t^2}{m_{t'}^2} + 5 \right) , \tag{4.4.10}$$

where we dropped terms subleading in s_{X_T} and $m_t/m_{t'}$. As the logarithm is large and negative, a cancellation is possible in the T parameter even for large mixing: this explains the allowed strip in Fig. 4.4, that reaches $s_{X_T} \simeq 0.5$. A comment is in order for the case of Q: one would expect a milder constraint from T when the two Yukawa couplings $\lambda_Q^{t,b}$ respect the custodial symmetry, i.e. when $r_Q = 1$. However, even in this case there is an important deviation from the SM, because the residual custodial-breaking parameter, $(\lambda_t - \lambda_b)$, differs from the SM one, $\sqrt{2}(m_t - m_b)/v$, as soon as the mixing is non-zero.

Let us now turn to the direct searches of VLQs at colliders. As they are coloured, it is easier to produce them at the LHC, relatively to VLLs. Below ~ 1 TeV they are dominantly produced in pairs through strong interactions, while for higher masses single production by EW interactions can become dominant [142, 147]. The pair production mechanism, that dominates in the mass range probed at the 8 TeV LHC, is independent from the VLQ (all are colour triplets) and from the mixing parameters. The ATLAS and CMS searches focus on the following decay channels for the heavy quark mass eigenstates:

$$X \to tW^+ , \qquad t' \to tZ, th, bW^+ , \qquad b' \to bZ, bh, tW^- , \qquad Y \to bW^- . \tag{4.4.11}$$

Note that t' and b' can decay via neutral current at leading order, owing to their vector-like nature. Decays into another heavy quark coming from the same multiplet, such as $t' \to XW^-$, are kinematically suppressed; decays through loops may also be possible, but they are typically negligible [143]. Here we will disregard these sub-leading channels, and assume that the decay channels in Eq. (4.4.11) have unit branching ratio. In addition, the decays are assumed to be prompt, that is the case whenever the mixing angles are large enough to have an observable effect on the Higgs couplings.

The relative branching ratios of t' and b' in the three decay channels depend mostly on the weak isospin of the VLQ and on the mixing angles. Indeed, since the heavy quarks are already constrained to be heavier than a few hundred GeVs, in good approximation one can neglect the final state masses

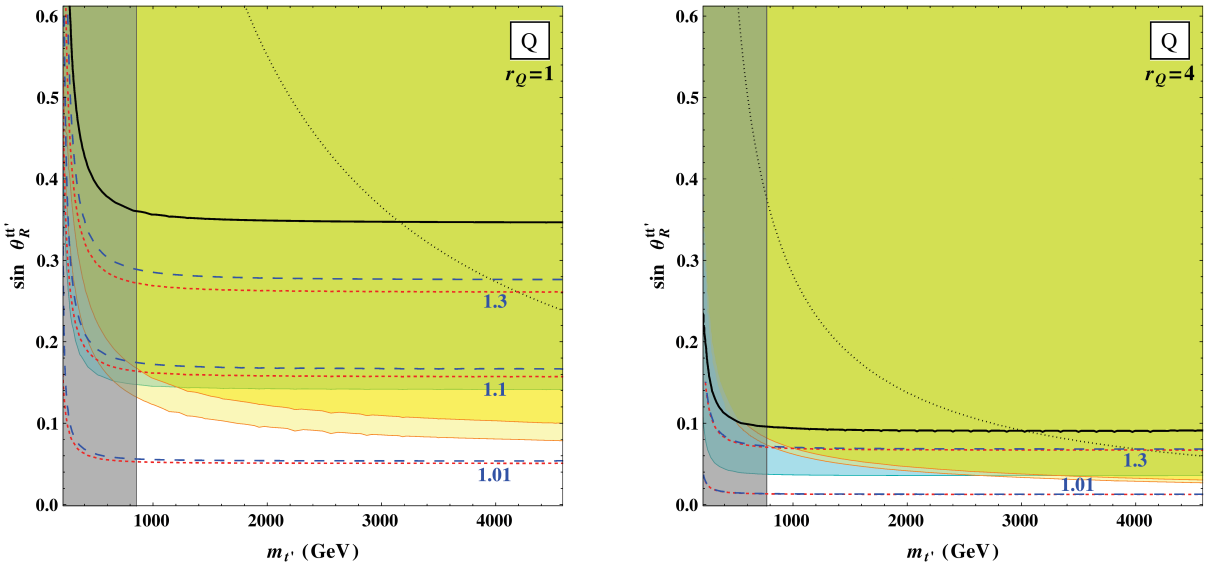

Figure 4.6: Constraints on the weak doublet VLQ Q as a function of the mass of t' and of the mixing angle between t_R and t'_R. The left panel corresponds to $\lambda_Q^t = \lambda_Q^b$ ($r_Q = 1$), and the right one to $4\lambda_Q^t = \lambda_Q^b$ ($r_Q = 4$). The notation is the same as in Fig. 4.3.

and find

$$\begin{aligned}
\Gamma(t' \to ht) &\simeq \frac{m_{t'}}{16\pi}\left(|y_{tt'}|^2 + |\tilde{y}_{tt'}|^2\right) \ , \\
\Gamma(t' \to Zt) &\simeq \frac{m_{t'}^3}{32\pi m_Z^2}\left(|(c_L^Z)_{tt'}|^2 + |(c_R^Z)_{tt'}|^2\right) \ , \\
\Gamma(t' \to Wb) &\simeq \frac{m_{t'}^3}{32\pi m_W^2}\left(|(c_L^W)_{bt'}|^2 + |(c_R^W)_{bt'}|^2\right) \ ,
\end{aligned} \tag{4.4.12}$$

and the same for $t' \leftrightarrow b'$ and $t \leftrightarrow b$. Here the Higgs couplings are defined by Eq. (D.5), and the Z and W couplings by Eq. (C.4). By a straightforward computation, one finds $Br\,(t' \to ht) \simeq Br\,(t' \to Zt)$ and

$$\begin{aligned}
T: \quad & Br\,(t' \to Zt) \simeq \frac{1}{2}\frac{1-s_T^2}{2-s_T^2} \ , && Br\,(t' \to Wb) \simeq \frac{1}{2-s_T^2} \ ; \\
X_T: \quad & Br\,(t' \to Zt) \simeq \frac{1}{2} \ , && Br\,(t' \to Wb) \simeq 0 \ ; \\
Q: \quad & Br\,(t' \to Zt) \simeq \frac{1}{2}\frac{1+s_Q^2(r_Q^2-1)}{r_Q^2+1+s_Q^2(r_Q^2-1)} \ , && Br\,(t' \to Wb) \simeq \frac{r_Q^2}{r_Q^2+1+s_Q^2(r_Q^2-1)} \ ; \\
X_Q: \quad & Br\,(t' \to Zt) \simeq \frac{1}{2}\frac{1+s_{X_Q}^2}{2+s_{X_Q}^2} \ , && Br\,(t' \to Wb) \simeq \frac{1}{2+s_{X_Q}^2} \ ; \\
Y_Q: \quad & Br\,(t' \to Zt) \simeq \frac{1}{2} \ , && Br\,(t' \to Wb) \simeq 0 \ .
\end{aligned} \tag{4.4.13}$$

As before, we neglected the SM masses and, therefore, the subdominant mixing angles in Eq. (4.4.5). Note however that some branching ratios are proportional to the SM masses at leading order, for example in the case of X_T one finds $Br\,(t' \to Wb) \simeq m_t^2/(c_{X_T}^4 m_{t'}^2)$. In the cases where both t' and b' are present, we used the relation $\tan\tilde{\theta}_\psi \simeq r_\psi \tan\theta_\psi$, that follows from Eq. (4.4.6) if one neglects m_b and m_t. The b' branching ratios are obtained from Eq. (4.4.13) by the replacements $T \to B$, $X_T \to Y_B$, $X_Q \leftrightarrow Y_Q$, $t' \to b'$, $t \leftrightarrow b$, $r_Q \to 1/r_Q$ and $s_\psi \to \tilde{s}_\psi$ for each ψ.

The experimental lower bounds on the mass of t' and b' are presented as a function of two independent branching ratios [148,149]. We choose, in the plane of branching ratios, their approximate values for the VLQ under consideration. To this purpose, we take the limit $s_\psi \to 0$ in Eq. (4.4.13) ($\tilde{s}_\psi \to 0$ in the case of b'), because the collider bound is relevant at small mixing angles, see Figs. 4.3 - 4.6). The only exception is X_T, where large mixing is possible, but in this case the strongest collider bound is the one on the component X. The lower bounds on each heavy quark mass are collected in Table

heavy quark	branching ratios	multiplets	mass bound
X $(Q=5/3)$	$Br_{Wt}=1$	X_T, X_Q	$m_X \geq 840$ GeV [150]
t' $(Q=2/3)$	$Br_{Wb}=\frac{1}{2},\ Br_{Zt}=Br_{ht}=\frac{1}{4}$	T, X_Q, $Q(r_Q=1)$	$m_{t'} \geq 800$ GeV [148]
	$Br_{Wb}=0,\ Br_{Zt}=Br_{ht}=\frac{1}{2}$	X_T, Y_Q, $Q(r_Q \ll 1)$	$m_{t'} \geq 855$ GeV [148]
	$Br_{Wb}=1,\ Br_{Zt}=Br_{ht}=0$	$Q(r_Q \gg 1)$, $Q+Y_B$	$m_{t'} \geq 920$ GeV [155]
	$Br_{Wb}=Br_{Zt}=0,\ Br_{ht}=1$	X_T+Q	$m_{t'} \geq 950$ GeV [148]
	$Br_{Wb}=Br_{ht}=0,\ Br_{Zt}=1$	X_T+Q	$m_{t'} \geq 800$ GeV [148]
	$Br_{Wb}+Br_{Zt}+Br_{ht}=1$	T, X_T, Q, Y_Q, X_Q	$m_{t'} \geq 720$ GeV [155]
b' $(Q=-1/3)$	$Br_{Wt}=\frac{1}{2},\ Br_{Zb}=Br_{hb}=\frac{1}{4}$	B, Y_Q, $Q(r_Q=1)$	$m_{b'} \geq 735$ GeV [148]
	$Br_{Wt}=0,\ Br_{Zb}=Br_{hb}=\frac{1}{2}$	Y_B, X_Q $Q(r_Q^2 \gg 1)$	$m_{b'} \geq 755$ GeV [151]
	$Br_{Wt}=1,\ Br_{Zb}=Br_{hb}=0$	$Q(r_Q^2 \ll 1)$, X_T+Q	$m_{b'} \geq 810$ GeV [150]
	$Br_{Wt}=Br_{Zb}=0,\ Br_{hb}=1$	$Q+Y_B$	$m_{b'} \geq 846$ GeV [153]
	$Br_{Wt}=Br_{hb}=0,\ Br_{Zb}=1$	$Q+Y_B$	$m_{b'} \geq 775$ GeV [148]
	$Br_{Wt}+Br_{Zb}+Br_{hb}=1$	B, Y_B, Q, Y_Q, X_Q	$m_{b'} \geq 582$ GeV [154]
Y $(Q=-4/3)$	$Br_{Wb}=1$	Y_B, Y_Q	$m_Y \geq 770$ GeV [148]

Table 4.3: Lower bounds at 95 % C.L. on the heavy quark masses $m_X, m_{t'}, m_{b'}$ and m_Y. The experimental searches assume pair production via strong interactions and prompt decays in the indicated channels. In the second column we specify the assumption on the heavy quark-decay branching ratios. Here Br_{Zt} stands for $Br\,(t' \to Zt)$, and so forth. In the third column we list the VLQ multiplets that correspond to those branching ratios, in the small mixing approximation. Here "X_T+Q" and "$Q+Y_B$" refer to pairs of VLQs with a custodial symmetry, that are discussed in section 4.4.2.

4.3, and vary between ~ 600 and 900 GeV [148,150–154]. The region excluded at 95 % C.L. is shaded in grey in Figs. 4.3 - 4.6. A detailed analysis of the lower bound on m_t' is presented in Ref. [85] for the case of the VLQ T, taking also into account indirect constraints from B-physics observables.

Let us now discuss the corrections induced by the VLQ on the Higgs boson couplings. The couplings of t, t', b and b' to the Higgs have the same form as those of τ and τ' in Eq. (4.3.19), with the obvious replacement of masses and mixing angles. The heavy quarks X and Y do not couple to the Higgs. The Higgs signal strengths at the LHC μ_α, defined in Eq. (D.40), are the product of three factors: Higgs production rate, partial decay rate and lifetime. While new leptons affect significantly the partial decay rate only, new quarks can modify substantially each factor. In particular, the Higgs production via gluon fusion is sensitive to a VLQ, and the mixing in the bottom sector can change significantly the total Higgs width Γ_h. Let us remind that, as discussed below Eq. (4.4.4), the Higgs couplings are CP-conserving for any VLQ.

When the VLQ contains a B component, the Higgs width into $b\bar{b}$ is modified, with respect to the SM, by a factor $R_{b\bar{b}} = (1-\tilde{s}_\psi^2)^2$ that, in the light of previously discussed constraints, can be as small as ~ 0.9. Since in the SM $h \to \bar{b}b$ is the dominant decay channel, this correction enhances μ_α for all other decay channels, through the factor Γ_h^{SM}/Γ_h. The Higgs production via gluon fusion is modified by a factor

$$R_{gg} = \frac{\left|\mathcal{A}_{SM}^{gg} + \frac{3}{4}s_\psi^2\left[A_{1/2}(\tau_{t'}) - A_{1/2}(\tau_t)\right] + \frac{3}{4}\tilde{s}_\psi^2\left[A_{1/2}(\tau_{b'}) - A_{1/2}(\tau_b)\right]\right|^2}{\left|\mathcal{A}_{SM}^{gg}\right|^2}\,, \tag{4.4.14}$$

where the form factors are defined in appendix D.2. The effect of the top sector is qualitatively different from the bottom one: given the collider lower bound on $m_{t',b'}$, their form factors are very close to the asymptotic value, $A_{1/2}(0) = 4/3$. While the t loop is also close to this value, the b has a

small mass and a suppressed form factor: $A_{1/2}(\tau_{t'})-A_{1/2}(\tau_t) \simeq -0.04$ and $A_{1/2}(\tau_{b'})-A_{1/2}(\tau_b) \simeq +1.41$ Therefore, when a b' is present (for $\psi = B, Y_B, Q, X_Q, Y_Q$), its effect dominates and the interference with the SM is constructive. An exception is possible for $\psi = Q$, where $\tilde{s}_Q/s_Q \ll 1$ for $r_Q \ll 1$, see Eq. (4.4.6). In the latter case, and when only a t' is present (for $\psi = T, X_T$), there is a slight destructive interference with the SM. The $t\bar{t}h$ production mode is also modified respect to the SM in the presence of $t - t'$ mixing, with a cross-section reduced by a factor c_ψ^4 .

In the diphoton channel

$$R_{\gamma\gamma} = \frac{\left|\mathcal{A}_{SM}^{\gamma\gamma} + \frac{4}{3}s_\psi^2\left[A_{1/2}(\tau_{t'}) - A_{1/2}(\tau_t)\right] + \frac{1}{3}\widetilde{s}_\psi^2\left[A_{1/2}(\tau_{b'}) - A_{1/2}(\tau_b)\right]\right|^2}{\left|\mathcal{A}_{SM}^{\gamma\gamma}\right|^2} \,. \tag{4.4.15}$$

Here the SM amplitude is negative, therefore the interference pattern is reversed with respect to R_{gg}. A few different values of the signal strength $\mu_{\gamma\gamma}$ are shown in Figs. 4.3 - 4.6 by dotted red lines. Once the other constraints are taken into account, one finds at most $\delta\mu_{\gamma\gamma} \sim 0.3$. Finally, for the Higgs decay into a photon and a Z, the new physics amplitude writes

$$\begin{aligned}\mathcal{A}_{SM+\psi}^{\gamma Z} - \mathcal{A}_{SM}^{\gamma Z} \;\simeq\; & \sum_{\alpha=t,b}\frac{3Q_\alpha}{c_w^2}\Big\{\delta g_{\alpha\alpha}^V A_{1/2}(\tau_\alpha,\lambda_\alpha) + s_{\psi,\alpha}^2\left[g_{\alpha'\alpha'}^V A_{1/2}(\tau_{\alpha'},\lambda_{\alpha'}) - g_{\alpha\alpha}^V A_{1/2}(\tau_\alpha,\lambda_\alpha)\right] \\ & + \; c_{\psi,\alpha}s_{\psi,\alpha}\frac{m_\alpha + m_{\alpha'}}{\sqrt{m_\alpha m_{\alpha'}}} g_{\alpha\alpha'}^V A_{1/2}(\tau_{\alpha'},\lambda_{\alpha'},\tau_\alpha,\lambda_\alpha)\Big\} \,,\end{aligned} \tag{4.4.16}$$

where $s_{\psi,t} \equiv s_\psi$, $s_{\psi,b} \equiv \widetilde{s}_\psi$, and we neglected the terms proportional to the form factor $B_{1/2}$, that are subdominant. Note also that there is no CP-violating amplitude, as both the h and Z couplings respect CP, see discussion below Eq. (4.4.4). The vector Z couplings are obtained from Eq. (C.6): one finds $\delta g_{\alpha\alpha}^V \equiv (g_{\alpha\alpha}^V - g_{\alpha\alpha}^{V,SM}) \sim s_{\psi,\alpha}^2$ and $g_{\alpha\alpha'}^V \sim s_{\psi,\alpha}$, so that the new physics amplitude of Eq. (4.4.16) is of the order of the mixing squared. The interference with the SM may be constructive or destructive depending on the sign of the Z couplings. A few different values of the signal strength $\mu_{\gamma Z}$ are shown in Figs. 4.3 - 4.6 by dashed blue lines. When a b' is present, both $\mu_{\gamma Z}$ and $\mu_{\gamma\gamma}$ receive a similar correction, dominated by the increase of R_{gg} and Γ_h^{SM}/Γ_h. A significant correction is possible for Y_B, with both $\delta\mu_{\gamma Z}$ and $\delta\mu_{\gamma\gamma}$ as large as ~ 0.3. On the other hand, in the case of T or X_T the corrections to the two channels are significantly different, because the small factor $A_{1/2}(\tau_{t'}) - A_{1/2}(\tau_t)$ in Eq. (4.4.15) suppresses the correction to $h\gamma\gamma$. In particular, for X_T one can have $\delta\mu_{\gamma Z} \sim 0.1$ with $\delta\mu_{\gamma\gamma} \sim 0.01$.

In our analysis we computed the relevant signal strengths μ_α for $\alpha = b\bar{b}$, $\gamma\gamma$, γZ, WW and ZZ, taking of course into account the corrections to R_{gg} and Γ_h. We compared these predictions with the allowed experimental ranges given in Table 4. By simply computing a χ^2 for these five channels, we determined the region of parameters disfavoured at 99% C.L., that is delimited by the solid black line in Figs. 4.3 - 4.6.

4.4.2 Two vector-like quarks (including b and t compositeness)

• ***Two VLQs not coupled to each other.*** Let us consider first a pair of VLQs (ψ, ψ') that do not couple to each other via a Yukawa coupling. In this case ψ and ψ' must be identified with one of the seven VLQs in table 4.1, and the phenomenological effects are, in most respects, a trivial addition of those of each VLQ separately, already discussed in section 4.4.1.

A noticeable exception occurs when the Yukawa couplings and the vector-like masses of ψ and ψ' respect an additional $SU(2)_R$ global symmetry, that provides custodial protection for the EW gauge boson couplings: when the parameters approach this custodial limit, the constraints from EW precision tests drastically relax with respect to the case of a unique VLQ. There are four pairs that may form a doublet under $SU(2)_R$: the weak singlets (T, B), the weak doublets (X_T, Q) or (Q, Y_B), and the weak triplets (X_Q, Y_Q). For illustration, we will concentrate on the case of doublets.

The two VLQs transform as bi-doublets under a custodial $SU(2)_L \times SU(2)_R$ symmetry, as long

as their Yukawa couplings to the SM fermions and their vector-like masses are equal,

$$\begin{aligned} -\mathcal{L}_{(X_T,Q)} &= \frac{\lambda_\psi}{\sqrt{2}}\overline{(X_T\ Q)_L}\begin{pmatrix} H \\ \tilde{H}\end{pmatrix} t_R + M_\psi \overline{(X_T\ Q)_L}\begin{pmatrix} X_T \\ Q\end{pmatrix}_R + h.c.\ , \\ -\mathcal{L}_{(Q,Y_B)} &= \frac{\lambda_\psi}{\sqrt{2}}\overline{(Q\ Y_B)_L}\begin{pmatrix} H \\ \tilde{H}\end{pmatrix} b_R + M_\psi \overline{(Q\ Y_B)_L}\begin{pmatrix} Q \\ Y_B\end{pmatrix}_R + h.c.\ . \end{aligned} \tag{4.4.17}$$

These are the smallest sets of top and bottom quark custodians, respectively [36,129,156]. Note that, in this custodial limit, the additional coupling $\overline{Q}_L H b_R$ ($\overline{Q}_L \widetilde{H} t_R$) must vanish in the top (bottom) case. Therefore, a mixing occurs only in the top (bottom) sector, and there are no deviations in the bottom (top) couplings, despite the presence of a b' (t') in the spectrum. The analysis is analogous to the case of τ custodians, discussed in section 4.3.3. For example, in the top case the linear combination $t'' \equiv (T^{(X_T)} - T^{(Q)})/\sqrt{2}$ does not couple to the Higgs and therefore it does not mix, while the orthogonal combination mixes with the SM top quark as in Eq. (4.4.3), to form the mass eigenstates t' and t. The mass spectrum is

$$\begin{aligned} m_{t''} = m_{b'} = m_X = M_\psi \leq m_{t'} \simeq \frac{M_\psi}{c_R} \qquad & (X_T, Q)\ , \\ m_{b''} = m_{t'} = m_Y = M_\psi \leq m_{b'} \simeq \frac{M_\psi}{\widetilde{c}_R} \qquad & (Q, Y_B)\ . \end{aligned} \tag{4.4.18}$$

Due to the custodial symmetry, the values of the heavy quark branching ratios into SM particles differ from the case of a single VLQ, discussed in section 4.4.1. We assume that the decays to another heavy quark are kinematically suppressed, because of the small mass splitting in Eq. (4.4.18), and once again we neglect the SM masses in the final state, as well as the $t - t'$ ($b - b'$) left-handed mixing angle, that is suppressed by $m_t/m_{t'}$ ($m_b/m_{b'}$). Consider for example the top case. The decays $t'/t'' \to Wb$ are suppressed as in Eq. (4.4.13) (here $r_Q = 0$). In addition $t' \to Zt$ vanishes because the $Q = 2/3$ components of X_T and Q have opposite weak isospin, and $t'' \to ht$ vanishes because t'' does not couple to the Higgs. Similar arguments hold in the bottom case. In summary one finds

$$\begin{aligned} BR(t'' \to Zt) \simeq Br(b' \to W^- t) \simeq Br(X \to W^+ t) \simeq Br(t' \to ht) \simeq 1 \qquad & (X_T, Q)\ , \\ BR(b'' \to Zb) \simeq Br(t' \to W^+ b) \simeq Br(Y \to W^- b) \simeq Br(b' \to hb) \simeq 1 \qquad & (Q, Y_B)\ . \end{aligned} \tag{4.4.19}$$

It is amusing that, in these two models, there is one heavy quark decaying exclusively in each of the possible decay channels listed in Eq. (4.4.11). The experimental lower bounds on these heavy quark masses can be read off Table 4.3.

The custodial symmetry protects the $Zb\bar{b}$ couplings: in the top case $\delta g^R_{t\bar{t}} = 0$ and the small $\delta g^L_{t\bar{t}} = (m_t/M_\psi)^2 s_R^2/2$ contributes to $Zb\bar{b}$ only at one loop; in the bottom case $\delta g^R_{b\bar{b}} = 0$ and $\delta g^L_{b\bar{b}} = (m_b/M_\psi)^2 \widetilde{s}_R^2/2$ is very suppressed by the bottom mass. Thus, in this custodial limit large mixing angles are not excluded, as shown in Fig. 4.7. Indeed, one can see that the constraint from the other EW precision parameters is significantly relaxed too, as T receives a small correction only, from the difference $(\lambda_t - \lambda_b)$, that is not SM-like because of the mixing, while S acquires a positive correction that remains in the ellipse unless the mixing is very large. Note that in the bottom sector the T parameter is almost independent from $m_{b'}$, since the smallness of m_b ensures $\lambda_b \simeq \lambda_b^{SM}$. On the other hand, when the mixing occurs in the top sector, the coupling λ_t and consequently the T parameter strongly depend on $m_{t'}$. The dominant constraints at small and large heavy quark masses come from the direct collider searches and from perturbativity, respectively. In the top case (right panel of Fig. 4.7), the mixing is not constrained by the fit of the Higgs coupling, as the bottom sector is SM-like. As a consequence, for 1.5 TeV $\lesssim m_{t'} \lesssim$ 2 TeV the mixing can be as large as $s_R \simeq 0.8$. The $\gamma\gamma$ Higgs decay channel can be suppressed at most by $\delta\mu_{\gamma\gamma} \simeq -0.03$, while the corrections to the γZ channel may be larger, up to $\delta\mu_{\gamma Z} \simeq +0.13$. In the bottom case (left panel of Fig. 4.7), the mixing in the bottom sector enhances all the other Higgs channels, as $R_{b\bar{b}} = (1 - \widetilde{s}_R^2)^2 < 1$. This leads to an upper bound $\widetilde{s}_R \lesssim 0.35$. Significant corrections as large as $\delta\mu_{\gamma\gamma} \simeq \delta\mu_{\gamma Z} \simeq 0.6$ are possible. Note that the Higgs signal strengths in Fig. 4.7 are similar to those with Y_B or X_T only, shown in Fig. 4.4. The difference is that the region allowed by EW precision tests largely inflated here, thanks to the

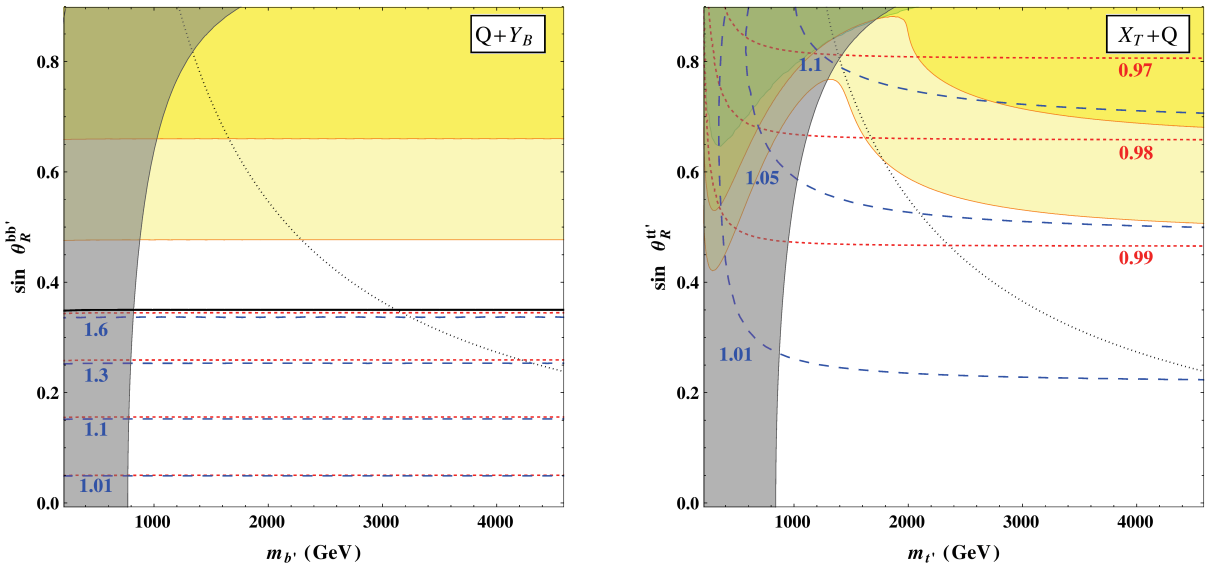

Figure 4.7: Constraints on the pairs of VLQs (Q, Y_B) (left panel) and (X_T, Q) (right panel), in the custodial limit (equal vector-like masses and Yukawa couplings), as a function of the mass of b' (t') and of the mixing angle between b_R and b'_R (t_R and t'_R). The notation is the same as in Fig. 4.3.

custodial symmetry.

• ***Two VLQs coupled to each other, not mixing with the SM fermions.*** Let us move to the case of two VLQs coupled to each other via Yukawa interactions. Their chiral components transform as

$$\psi_{1L}, \psi_{1R} \sim (R_c, R_w, Y) \ , \qquad \psi_{2L}, \psi_{2R} \sim (R_c, R_w + 1, Y + \frac{1}{2}) \ , \tag{4.4.20}$$

with $R_c \neq 1$. The corresponding Lagrangian is the same as in the case $R_c = 1$ (two VLLs), and it is given in Eq. (4.3.31). We bar the special case $R_c = \overline{R_c}$, $Y = 0$ and R_w odd ($Y + 1/2 = 0$ and R_w even), that allows for a Majorana mass terms for ψ_1 (ψ_2) and will be discussed in section 4.4.3. We also bar mixing with the SM quarks, that will be discussed at the end of the section. The effect of two VLQs on $\mu_{\gamma\gamma}$ was discussed in detail in Ref. [157].

The number of mass eigenstates with a given electric charge Q and the structure of their mass matrices are the same as in the case of two VLLs, see Eqs. (4.3.32) and (4.3.40). Therefore, there are five physical parameters: two masses $m_{1,2}$, two mixing angles $\theta_{L,R}$ and one phase φ, defined by Eq. (4.3.33). The analysis of the parameter space proceeds exactly as in section 4.3.3 and will not be repeated here, however the phenomenology is strongly modified as the colour representation R_c is non-trivial. The main differences are the following:

- The VLQs are pair-produced via strong interactions and, in the absence of mixing with the SM, the lightest state is stable and hadronises. The direct collider bounds on these particle masses are above one TeV, as we already described in some more detail in section 4.2.

- The contributions of the VLQs to the S and T parameters, as well as to the Higgs decay amplitudes into $\gamma\gamma$ and γZ, have the same form as in Eqs. (4.3.35) to (4.3.39), with an additional factor N_c. As in the case of VLLs, for $R_w = 1$ and large values of Q we find two regions of the mixing parameters where $\mu_{\gamma\gamma}$ remains SM-like, while $\mu_{\gamma Z}$ can strongly depart from one. (i) For two degenerate masses $m_1 = m_2$, the interference with the SM amplitude is destructive for $\gamma\gamma$ and constructive for γZ, as illustrated in Fig. 4.1. Therefore, there are values of the mixing parameters where accidentally $\mu_{\gamma\gamma}$ goes back to the allowed range, while at the same time one can even saturate the present upper bound $\mu_{\gamma Z} \lesssim 10$. Note that the gluon-gluon channel remains nearly SM-like, because its amplitude is not enhanced by the large factor Q^2. (ii) For $m_1 \neq m_2$, the amplitude $\mathcal{A}^{\gamma\gamma}_{f_1,f_2}$ in Eq. (4.3.37) can be tuned to zero, while at the same time one can have large contributions to $\mu_{\gamma Z}$ together with sufficiently small corrections to S and T. E.g. taking

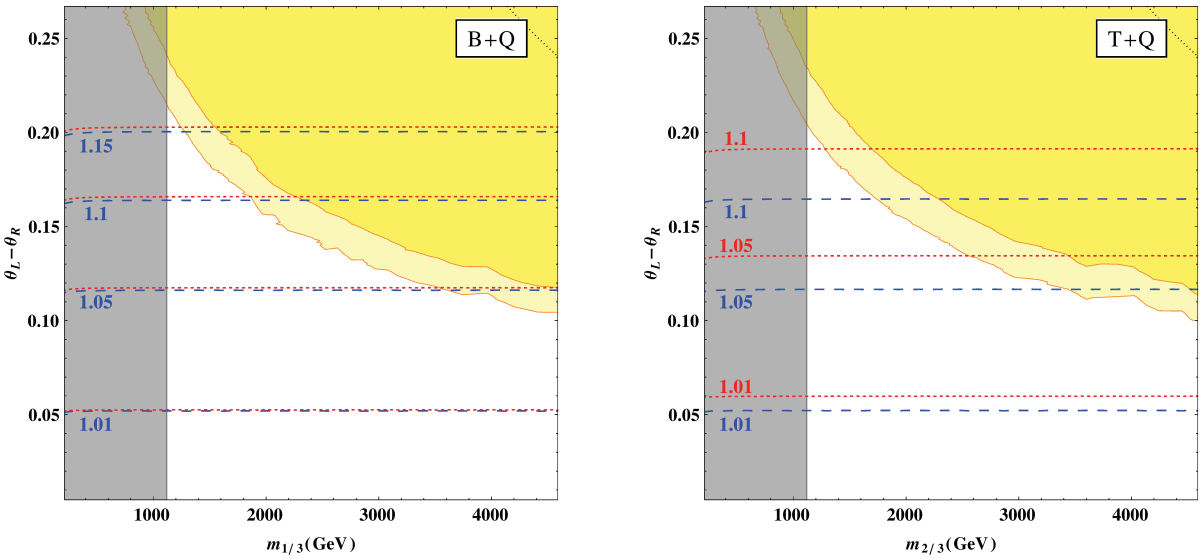

Figure 4.8: In the left (right) panel, we show the constraints on the pair of VLQs B and Q (T and Q), in the limit of vanishing mixing with the SM quarks, degenerate mass eigenvalues $m_{b'} = m_{b''} \equiv m_{1/3}$ ($m_{t'} = m_{t''} \equiv m_{2/3}$) and no CP violation, $\varphi = 0$. In this case the relevant mixing angle is $\theta_L - \theta_R$, see Eq. (4.3.35). The notation for the various constraints is the same as in Fig. 4.3.

$N_c = 3$, $Q \simeq 8$, mixing parameters $\varphi = 0$, $\theta_L \simeq \pi/8$, $\theta_R \simeq \pi/10$, $m_1/m_2 \simeq 1.3$ and $m_2 \simeq 1$ TeV, one obtains $\mu_{\gamma Z} \simeq 2$. For the cases $R_w > 1$, we refer to the discussion below Eq. (4.3.40).

- The VLQs also contribute to the Higgs production by gluon fusion, with an amplitude that can be easily obtained from the $\gamma\gamma$ one. For the pair of mass eigenstates f_1, f_2 of charge Q, one has $\mathcal{A}^{gg}_{f_1,f_2} = [3C(R_c)/2]/(N_c Q^2)\mathcal{A}^{\gamma\gamma}_{f_1,f_2}$, see appendix D.2. The interference with the SM is constructive in the gluon case, thus enhancing the Higgs production. Note that the gluon-gluon channel also receives a non-zero contribution from the $Q = 0$ sector.

For illustration, we display in Fig. 4.8 the parameter space for the case $R_c = 3$, $R_w = 1$ and $Y = -1/3$ ($Y = -2/3$), that corresponds to the pair of VLQs B and Q (T and Q), in the limit of no-mixing with the SM quarks. In Fig. 4.9 we illustrate how the constraints change for a larger colour representation, as we replaced $R_c = 3$ by $R_c = 8$. For definiteness, we assumed that there is no CP violation, $\varphi = 0$, and that the two mixing mass eigenstates $f_{1,2}$ of charge $Q = Y$ are degenerate in mass, $m_1 = m_2$. In the case of colour octets, larger deviations in the Higgs signal strengths are possible, but the various constraints are correspondingly stronger. One can reach $\mu_{\gamma Z} \simeq 1.4$ for the octets and $\mu_{\gamma Z} \simeq 1.2$ for the triplets. In the case $Y = -1/3$, $\mu_{\gamma\gamma}$ and $\mu_{\gamma Z}$ are very close to each other, because $\mathcal{A}^{\gamma Z}_{f_1,f_2}/\mathcal{A}^{\gamma\gamma}_{f_1,f_2} = (g^V_{11} + g^V_{22})/(Y c_w^2)$ is numerically close to one, see Eqs. (4.3.35) and (4.3.37), and $\mathcal{A}^{\gamma Z}_{SM}/\mathcal{A}^{\gamma\gamma}_{SM}$ is close to one as well. The strongest constraint on the mixing among the heavy states comes from the S and T parameters. In the octet case the fit of the main Higgs decay channels (see the end of section 4.4.1 for details) is also a relevant constraint. The mass scale $m_1 = m_2$ is constrained by the searches of stable coloured particles, discussed in section 4.2.

• ***Two VLQs coupled to each other, mixing with the SM fermions.*** Let us briefly discuss the possible interactions between the two VLQs $\psi_{1,2}$ in Eq. (4.4.20) and the SM quarks. This requires of course $R_c = 3$. A non-zero mixing with the bottom and/or top quark can occur if and only if at least one VLQ belongs to the set of seven VLQs in Table 4.1. The complete list is

$$\text{singlet} + \text{doublet} : \begin{cases} T + X_T\ (2t')\ , & T + Q\ (2t' + b')\ , \\ B + Q\ (t' + 2b')\ , & B + Y_B\ (2b')\ , \end{cases} \tag{4.4.21}$$

$$\text{doublet} + \text{triplet} : \begin{cases} X_T + Z_{X_T}\ (2t')\ , & X_T + X_Q\ (2t' + b')\ , \\ Q + X_Q\ (2t' + 2b')\ , & Q + Y_Q\ (2t' + 2b')\ , \\ Y_B + Y_Q\ (t' + 2b')\ , & Y_B + W_{Y_B}\ (2b')\ , \end{cases} \tag{4.4.22}$$

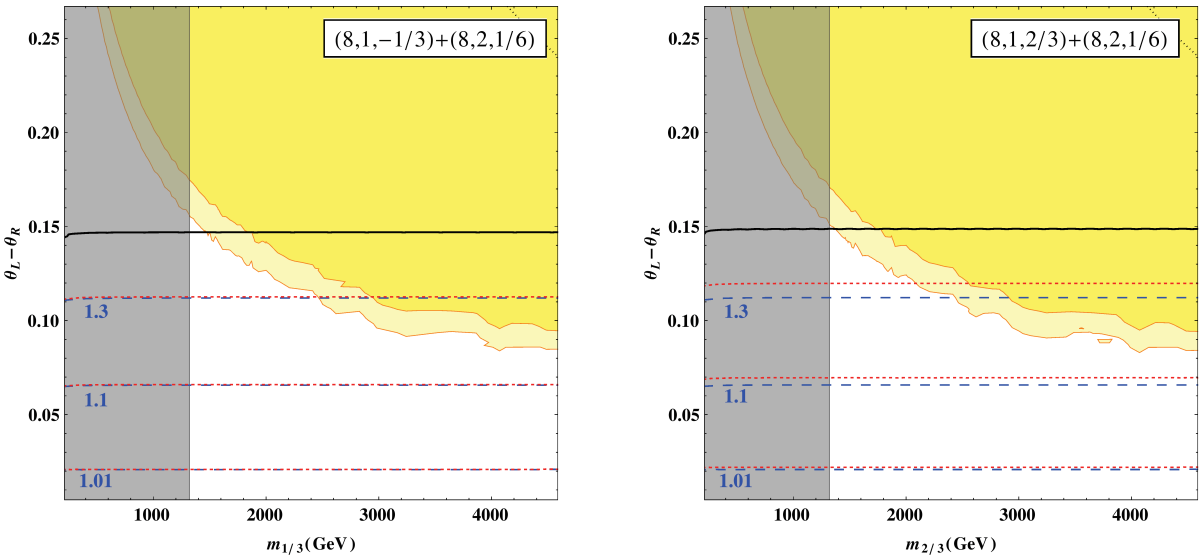

Figure 4.9: The same as in Fig. 4.8, but replacing colour triplets with colour octets.

$$\text{triplet} + \text{quartet} : \begin{cases} X_Q + \Omega_{X_T}\ (2t'+2b')\ , & X_Q + \Omega_Q\ (2t'+2b')\ , \\ Y_Q + \Omega_Q\ (2t'+2b')\ , & Y_Q + \Omega_{Y_B}\ (2t'+2b')\ , \end{cases} \tag{4.4.23}$$

where we indicated in brackets the number of new states mixing with the top and with the bottom quark. We also introduced a few new multiplets, with no Yukawa couplings to the SM fermions: $Z_{X_T} \sim (3,3,5/3)$, $W_{Y_B} \sim (3,3,-4/3)$, $\Omega_{X_T} \sim (3,4,7/6)$, $\Omega_Q \sim (3,4,1/6)$, and $\Omega_{Y_B} \sim (3,4,-5/6)$. They can be written in components as

$$Z_{X_T} = \begin{pmatrix} Z \\ X \\ T \end{pmatrix}\ , \quad W_{Y_B} = \begin{pmatrix} B \\ Y \\ W \end{pmatrix}\ , \quad \Omega_{X_T} = \begin{pmatrix} Z \\ X \\ T \\ B \end{pmatrix}\ , \quad \Omega_Q = \begin{pmatrix} X \\ T \\ B \\ Y \end{pmatrix}\ , \quad \Omega_{Y_B} = \begin{pmatrix} T \\ B \\ Y \\ W \end{pmatrix}\ , \tag{4.4.24}$$

where the two new exotic states Z and W have charges $Q(Z) = 8/3$ and $Q(W) = -7/3$. Recasting LHC searches, Ref. [158] puts a lower bound of 940 GeV on the mass of the $Q = 8/3$ state.

When there is only one t' (b') state, the mixing in the top (bottom) sector has the same pattern as in section 4.4.1. On the other hand, when there are two t' states, the top sector mass matrix takes the form

$$\mathcal{M}_t = \begin{pmatrix} \lambda_t \frac{v}{\sqrt{2}} & \lambda_1 \frac{v}{\sqrt{2}} & m_2 \\ m_1 & M_1 & \lambda_{12} \frac{v}{\sqrt{2}} \\ \lambda_2 \frac{v}{\sqrt{2}} & \lambda_{21} \frac{v}{\sqrt{2}} & M_2 \end{pmatrix}\ , \tag{4.4.25}$$

where we dropped possible Clebsch-Gordan coefficients. Here ψ_1 (ψ_2) is a weak singlet or triplet (doublet or quartet), m_1 (m_2) vanishes unless $\psi_1 = T$ ($\psi_2 = Q$), and $\lambda_{1,2}$ vanishes if $\psi_{1,2}$ is one of the multiplets in Eq. (4.4.24). The bottom sector mass matrix in presence of two b' states has an analog structure. The mixing with the SM is controlled by ratios of the type $\lambda v/M$ or m/M. They are mostly constrained by the $Zb\bar{b}$ couplings and by S and T. One typically expects $|\lambda v/M|, |m/M| \lesssim 0.1 - 0.2$, in analogy with Figs. 4.3 - 4.6. Possible cancellations among the various contributions could relax these constraints. A detailed analysis of the whole parameter space of these models is beyond the scope of this chapter. Some recent study can be found in Ref. [159], that discusses the phenomenology of the $2t'$ and $2t' + b'$ cases.

Let us focus on the possibility to generate the top mass (and analogously the bottom one) through the mixing with the VLQs, in the limit where the SM Yukawa coupling λ_t (λ_b) vanishes. This is possible whenever the determinant of $\mathcal{M}_t$ in Eq. (4.4.25) is non-zero for $\lambda_t = 0$, that is, if and only if the two VLQs both couple directly to the SM. The resulting top mass is of order $m_t \sim \lambda v(\lambda v/M)^2$, $\lambda v(m/M)$ or $\lambda v(m/M)^2$. The latter possibility is motivated by partial compositeness.

In this scenario, the SM fermions do not couple directly to the composite Higgs, therefore $\lambda_t = \lambda_1 = \lambda_2 = 0$ in Eq. (4.4.25). Rather, they couple linearly to a composite vector-like fermion with the same quantum numbers. This corresponds to the VLQs T and Q for the case of the top quark, leading to $m_t \simeq (m_T/M_T)(m_Q/M_Q)\lambda_{QT}v/\sqrt{2}$, and analogously B and Q for the case of the bottom. The phenomenology of top and bottom partners in composite models, and the associated constraints, are analysed e.g. in Refs. [156, 160, 161] (see also Ref. [147] for warped extra dimensional models).

4.4.3 Vector-like plus Majorana quarks

We define a Majorana quark to be a $Y = 0$ fermion multiplet in a non-trivial, real colour representation, $R_c = \overline{R_c} \neq 1$. Such object may couple to the Higgs only in the presence of a VLQ in the same colour representation. As a consequence, these new fermions do not mix with the SM ones and the lightest mass eigenstate is stable. For the smallest possible representation, $R_c = 8$, the searches for a stable gluino lead to a lower bound $\simeq 1.3$ TeV [94]. For bigger representations, $N_c \geq 27$, one expects an even more stringent limit, given the larger production cross-section and a similar hadronisation behaviour.

• ***One VLQ plus one Majorana quark.*** The most general set formed by a Majorana quark coupled to a VLQ can be written as

$$\chi_R \sim (R_c, R_w, 0)\ , \quad \psi_L, \psi_R \sim (R_c, R_w \pm 1, -1/2)\ , \qquad R_c = \overline{R_c} \neq 1\ . \tag{4.4.26}$$

If R_c is odd, one needs $N_w \neq 2 + 4n$ to avoid the global $SU(2)_w$ anomaly. The Lagrangian and the structure of the mass matrices are identical to the analogue leptonic case $R_c = 1$, see Eqs. (4.3.46) to (4.3.52). Here we discuss only the phenomenological differences due to the effect of colour. The new states contribute with an additional factor N_c to the one-loop diagrams for the S and T parameters, as well as for the Higgs signal strengths $\mu_{\gamma\gamma}$ and $\mu_{\gamma Z}$. In addition, they also contribute to the Higgs production via gluon fusion, with an amplitude related to the photon-photon one. For each sector of charge Q that couples to the Higgs, one has $\mathcal{A}^{\gamma\gamma}_{\chi\psi,Q} = (N_c Q^2)/[3C(R_c)/2]\mathcal{A}^{gg}_{\chi\psi,Q}$. The gluon-gluon channel receives a non-zero contribution even from the $Q = 0$ sector, that is present when N_w is odd.

Since the new quarks are necessarily heavy, their loop contributions can be estimated with good accuracy using the LET approximation, as described in Appendix D.2 and in section 4.3.4. In particular, $\mathcal{A}^{\gamma\gamma}_{\chi\psi,Q}$ is obtained from the amplitude in Eq. (4.3.51), times a factor N_c. For the gluon-gluon channel, summing over the different sectors one finds

$$\mathcal{A}^{gg}_{\chi\psi} \simeq K_{N_w} C(R_c) \frac{\lambda v}{M_\chi} \frac{\widetilde{\lambda} v}{M_\psi}\ , \tag{4.4.27}$$

where $K_1 = -4$, $K_2 = -2$, $K_3 = -8/3$, $K_4 = -2$, and so on. As the top quark amplitude is approximately equal to one, $\mathcal{A}^{\chi\psi}_{gg}$ gives roughly the ratio between the contribution of new fermions and the SM one. Note that either constructive or destructive interference with the SM amplitude is possible. The mixing parameters, of the generic form $\lambda v/M$, must satisfy the constraints from R_{gg} and $R_{\gamma\gamma}$, whose allowed ranges are given in Appendix D.3. In the minimal case with $R_c = 8$ and $R_w = 1$, only R_{gg} receives a correction, leading to the upper bound $|\lambda v/M| \lesssim 0.17$. One expects similar or even stronger bounds from S and T, in analogy with the cases of Figs. 4.8 and 4.9. Up to possible cancellations, a larger R_c leads to stronger constraints on the model, and to larger deviations in the Higgs couplings.

• ***One VLQ plus two Majorana quarks.*** Coming to sets formed by two Majorana quarks plus one VLQ, the first obvious possibility is to add a second copy of χ_R to the previous case. The additional Majorana multiplet automatically cancels the global $SU(2)$ anomaly, therefore N_w is arbitrary. The phenomenology is the generalisation of the one discussed above.

The second and last possibility is provided by the set

$$\chi_{1R} \sim (R_c, R_w, 0), \quad \psi_L, \psi_R \sim (R_c, R_w + 1, -1/2), \quad \chi_{2R} \sim (R_c, R_w + 2, 0), \quad R_c = \overline{R_c} \neq 1\ , \tag{4.4.28}$$

with N_w necessarily odd if R_c is odd. The Lagrangian is the same as in Eq. (4.3.54), and the structure of the mass matrices is also the same as in section 4.3.4. Let us just present the amplitude for Higgs production into gluon-gluon fusion, that is obtained by generalising Eq. (4.4.27),

$$\mathcal{A}^{gg}_{\chi_1\chi_2\psi}(R_w) \simeq C(R_c)\left(K_{N_w}\frac{\lambda_1 v}{M_{\chi_1}}\frac{\widetilde{\lambda}_1 v}{M_\psi} + K_{N_w+2}\frac{\lambda_2 v}{M_{\chi_2}}\frac{\widetilde{\lambda}_2 v}{M_\psi}\right) . \tag{4.4.29}$$

In the minimal case where $R_c = 8$ and $R_w = 1$, the allowed range for R_{gg} leads to a bound on the mixing parameters $|\lambda v/M| \lesssim 0.13$, where we assumed there is no hierarchy nor cancellations among the various mixing parameters. The $R_{\gamma\gamma}$ constraint is less restrictive.

4.5 Conclusions

We undertook a systematic analysis of new fermions interacting with the Higgs boson. Their properties (gauge charges, masses, Yukawa couplings) are significantly more constrained after the measurement of the Higgs mass and couplings at the first run of the LHC. It is intriguing to identify the few extensions of the SM that outlived this test. We especially aimed at those scenarios that may depart from the decoupling limit, in which the new fermions become very heavy and/or their mixing with the SM becomes very small.

In section 4.1 we presented the complete classification of sets of n chiral fermions interacting with the Higgs, for $n \leq 4$. While the minimal possibilities are well-known, already for $n = 3$ and 4 we singled out several exotic sets of fermions with a peculiar phenomenology. They emerge from a non-trivial interplay of several self-consistency conditions: cancellation of gauge anomalies, absence of charged massless components, non-zero Yukawa coupling to the SM Higgs doublet. In our classification we recovered as a special case the fermion content of well-motivated theories beyond the SM, such as the seesaw, supersymmetry, or partial compositeness. These cases are situated in a more general context, by considering the most general Lagrangian for the new fermions, not restricted by additional theoretical considerations. Would the evidence of a new particle emerge from data, one should indeed explore the full parameter space, before endorsing a specific model. We also argue that larger sets of new fermions, with $n \geq 5$, do not allow for qualitatively different phenomena, as all the possible building blocks of a fermion mass matrix already appeared in our classification.

In order to examine the phenomenology of the new fermions, in the appendices C and D we derived the general expression of the fermion couplings to the EW gauge bosons and to the Higgs boson, for fermions in arbitrary SM representations (R_c, R_w, Y). We also provided the formalism to define the gauge and Higgs boson couplings to the fermion mass eigenstates, after EWSB. Besides these tree-level results, we presented the general one-loop amplitudes for the gauge boson vacuum polarisation, $\Pi_{VV'}$, that allows to define the EW oblique parameters S and T, and for the Higgs coupling to gauge bosons, hVV', that allows to compute the rate for $h \to gg, \gamma\gamma, \gamma Z$.

Let us summarise the main results of our phenomenological survey of sections 4.2 to 4.4:

- Several exotic families of chiral fermions, that receive a mass from EWSB only, are still marginally compatible with EW precision tests and direct collider bounds. However, the coloured ones are neatly excluded, as they would greatly enhance the hgg coupling. On the other hand, a colourless family formed by two weak doublets and four singlets is still compatible with the measured $h\gamma\gamma$ coupling.

- The mixing of two or more sterile neutrinos with the SM leptons can have observable effects, despite the smallness of the neutrino masses. If the sterile neutrinos are lighter than the EW scale, they may modify significantly the Higgs invisible width; if heavier, they can appreciably contribute to the S and T parameters.

- In general, a heavy charged lepton τ' cannot mix significantly with the τ because of the $Z\tau\tau$-coupling constraint. Nonetheless, in a few special regions of parameters interesting phenomena are possible: (i) If $m_{\tau'} < m_h$, the decay rate for $h \to \tau'\tau$ can be significant despite the small mixing. (ii) When both τ_L and τ_R mix with heavy leptons, it is possible to generate m_τ entirely

through the small mixing permitted by the Z couplings, as long as the two heavy leptons are connected by a Yukawa coupling $\lambda \gtrsim 3$. (iii) If the new lepton sector is arranged to have an approximate custodial symmetry, the Z couplings are protected. In this case a large $\tau - \tau'$ mixing is allowed, and it may strongly suppress $h \to \tau\tau$.

- There are two extended classes of new fermions that can couple to the Higgs doublet without involving the SM fermions: either a pair of vector-like fermions, whose components can have an arbitrary charge Q, or a pair formed by a vector-like and a Majorana fermion, whose components have (demi-)integer Q. These fermion pairs were not studied in full generality in the previous literature, and they can produce large observable effects, even when the mixing with the SM fermions is zero. By varying their mass matrix parameters, one can typically scan over the full allowed range for the signal strength $\mu_{\gamma\gamma}$, while remaining in agreement with direct collider searches and EW precision tests. In most cases $\mu_{\gamma Z}$ receives a correction comparable to $\mu_{\gamma\gamma}$, but when the latter is accidentally close to one, it is possible to have $\delta\mu_{\gamma Z} \gg \delta\mu_{\gamma\gamma}$. We will discuss this point in detail below.

- The mixing θ of a heavy quark t' or b' with its SM partner is constrained by the EW precision tests. Nonetheless, the $b - b'$ mixing may significantly suppress the $hb\bar{b}$ coupling, leading to corrections as large as $\delta\mu_{\gamma\gamma} \simeq \delta\mu_{\gamma Z} \simeq 0.6$. We also notice two remarkable circumstances that allow for a large mixing: (i) The corrections to $Zb\bar{b}$ from $t - t'$ mixing are loop-suppressed and may be also suppressed by $(m_t/m_{t'})^2$. The T parameter receives opposite sign corrections that cancel each other for a specific value of $\sin\theta \times m_{t'}$. Both conditions can be realised in the case of the VLQ doublet (X, T), allowing for a large $\sin\theta \lesssim 0.5$. (ii) The Lagrangian of the new quarks can preserve a custodial symmetry, that suppresses the corrections to T as well as to the $Zb\bar{b}$ couplings. In this custodial subspace of parameters, the upper bound on the mixing relaxes, the exact value depending on the model: for the VLQ doublet Q coupled to t_R and b_R we find $\sin\theta \lesssim 0.15$, while for the two doublets $Q + Y_B$ coupled to b_R ($X_T + Q$ coupled to t_R) one can reach $\sin\theta \lesssim 0.45$ ($\sin\theta \lesssim 0.8$).

In the course of our analysis, we paid special attention to the relative contribution of the new fermions to $h \to \gamma\gamma$ and $h \to \gamma Z$, as the former rate is already constrained to be close to the SM prediction, while the latter could still depart strongly from its SM value. It is commonly believed that new physics cannot provide a large correction to the γZ channel without affecting $\gamma\gamma$ as well. Indeed, let us consider the effective Lagrangian before EWSB, that corresponds to the limit where the new fermions are heavier than the EW scale. There are several dimension-six operators involving the Higgs doublet H and the field-strengths $B_{\mu\nu}$, $W^a_{\mu\nu}$, listed e.g. in Ref. [162]. The operators contributing to $h\gamma Z$ can be generated, at one loop, only by two fermion multiplets coupled to H. At least one of these fermions has non-zero hypercharge, thus it necessarily induces the operator $H^\dagger H B_{\mu\nu} B^{\mu\nu}$ as well, that contributes to $h\gamma\gamma$. One can rephrase the same argument in terms of the effective Lagrangian for the hVV' couplings after EWSB, that is displayed in Eq. (D.8). The coefficients of the dimension-five operators, generated at one loop by the fermion mass eigenstate f_i, are given in Eq. (D.22) for $h\gamma\gamma$ and in Eq. (D.34) for $h\gamma Z$. The fermion f_i cannot contribute to the γZ channel only, simply because one needs a charge $Q_i \neq 0$ and a non-zero coupling y_i (or $\tilde{y}_i$) to the Higgs, therefore the $\gamma\gamma$ channel receives a contribution too. This argument, however, has some loopholes: first, the sum over all fermion mass eigenstates can lead to a cancellation in the signal strength $\mu_{\gamma\gamma}$ and not in $\mu_{\gamma Z}$, as the summands in the two channels differ by a factor $\sim g_i^V/Q_i$; second, $h\gamma Z$ receives an additional contribution from loops involving two fermion mass eigenstates, with off-diagonal couplings to both h and Z, see Eqs. (D.31) and (D.32).

As a matter of fact, in our survey of fermionic extensions of the SM, we encountered a few scenarios where $\delta\mu_{\gamma Z} \gg \delta\mu_{\gamma\gamma}$:

(i) One can exploit the order one differences between the Z and γ couplings and loop functions. For example, in the case of $t-t'$ mixing, $\delta\mu_{\gamma\gamma}$ is proportional to $A_{1/2}(\tau_{t'}) - A_{1/2}(\tau_t)$, that is very small as both form factors are close to the asymptotic value $A_{1/2}(0)$. On the contrary, the correction to $\mu_{\gamma Z}$ is controlled by $g^V_{t't'} A_{1/2}(\tau_{t'}, \lambda_{t'}) - g^V_{tt} A_{1/2}(\tau_t, \lambda_\tau)$, that is in general of order one. Also,

off-diagonal loops provide an additional contribution of the same order. Unfortunately, the absolute size of the correction is too small to be observed, as the mixing between the SM and new fermions is subject to the EW precision constraints. We find at best $\delta\mu_{\gamma\gamma} \ll \delta\mu_{\gamma Z} \simeq 0.2$, hardly visible even with 3000 fb^{-1} at 14 TeV, see Table 5.

(ii) A much larger $\delta\mu_{\gamma Z}$ is possible when new fermions couple to each other through the Higgs. Each sector of heavy states with given charges N_c and Q gives a contribution to the $h\gamma\gamma$ amplitude proportional to $\sum_i y_i v/m_i$. We found that the structure of the fermion mass matrix allows this sum to vanish, see the discussion below Eq. (4.3.39). At the same time, the γZ amplitude is proportional to $\sum_i g_i^V y_i v/m_i$. One can obtain e.g. $\mu_{\gamma Z} \simeq 2$, by means of a pair of states with $N_c Q s_\psi^2 \simeq 3$, where s_ψ is the relevant mixing parameter. Alternatively, the same effect is produced by several states with smaller charges. The required set of parameters can be in agreement with S and T as well. This opens a discovery opportunity for the second run of the LHC.

(iii) There is a second possibility to achieve a large $\mu_{\gamma Z}$. The signal strength $\mu_{\gamma\gamma}$ may be accidentally close to the SM, because the amplitude generated by two new fermion multiplets coupled to the Higgs has sign opposite to the SM one, and for $\mathcal{A}_f^{\gamma\gamma} \simeq -2\mathcal{A}_{SM}^{\gamma\gamma}$ one recovers $\mu_{\gamma\gamma} \simeq 1$. One needs either small weak multiplets with large charges, $N_c Q^2 s_\psi^2 \simeq 5$, or larger multiplets with smaller charges. In this region of parameters the S and T constraint can be satisfied and, moreover, one generically expects $\mu_{\gamma Z}$ much larger than one, because for large values of Q the amplitude $\mathcal{A}_f^{\gamma Z}$ interferes constructively with the SM. We find that one can almost saturate the present experimental bound $\mu_{\gamma Z} \lesssim 10$, therefore coming LHC data will be able to quickly probe this scenario.

In the cases listed above, a mild tuning of the parameters is sufficient to comply with the presently allowed range for $\mu_{\gamma\gamma}$, shown in Table 4. In the future, the room for a large $\mu_{\gamma Z}$ will progressively shrink.

The second run of the LHC, that recently started data taking at 13 TeV, will close in on most of the scenarios we have been considering. The allowed regions of parameters at low masses will be covered by direct searches for new fermionic resonances. The islands that survive at large mixing between the SM and new fermions will be probed by the increasing precision in the Higgs coupling measurements, even though there are models where one needs to wait for a high accuracy. In the absence of a signal, we shall be virtually cornered to the region of very heavy masses and/or very small mixing. Even when the new fermions are too heavy to be directly produced and mix negligibly with the SM, their Yukawa couplings to the Higgs can be effectively constrained by the radiative Higgs couplings.

C Electroweak precision tests in presence of new fermions

In this appendix we provide general formulas for the EW gauge boson couplings to fermions, as well as for their vacuum polarisation amplitudes. This allows to define and compute the oblique parameters S and T [163–166]. We discuss the experimental constraints on these parameters, as well as on the Z couplings to light SM fermions, such as $Zb\bar{b}$.

C.1 Electroweak gauge boson couplings

The couplings of the EW gauge bosons to a chiral fermion multiplet in a given representation (R_w, Y) of the EW gauge group are determined by the covariant derivative

$$D_\mu = \partial_\mu - igT^a W^a_\mu - ig'YB_\mu = \partial_\mu - i\frac{g}{\sqrt{2}}(T^+W^+_\mu + T^-W^-_\mu) - igT^3W^3_\mu - ig'YB_\mu \ , \tag{C.1}$$

where T^a are the $SU(2)_w$ generators for R_w, $T^\pm = T^1 \pm iT^2$ and $W^\pm_\mu = (W^1_\mu \mp iW^2_\mu)/\sqrt{2}$. In full generality, the resulting non-vanishing couplings are

$$\begin{aligned} &c^{W^\pm}(\overline{f_{m'}}, f_m) = \tfrac{g}{\sqrt{2}}(T^\pm)_{m'm} = \tfrac{g}{\sqrt{2}}\sqrt{j(j+1) - T^3_m(T^3_m \pm 1)}\,\delta_{m',m\pm1} \ , \\ &c^{W^3}(\overline{f_{m'}}, f_m) = gT^3_m\delta_{m'm} \ , \qquad c^B(\overline{f_{m'}}, f_m) = g'Y\delta_{m'm} \ , \end{aligned} \tag{C.2}$$

where $j = (N_w - 1)/2$ is the weak isospin, and the N_w components of R_w are labelled by $m, m' = -j, -j+1, \ldots, j-1, j$, and have electric charge $Q_m = T^3_m + Y$. It is straightforward to derive from Eq. (C.2) the couplings of $Z_\mu = c_w W^3_\mu - s_w B_\mu$ and $A_\mu = s_w W^3_\mu + c_w B_\mu$,

$$c^Z(\overline{f_{m'}}, f_m) = \frac{g}{c_w}(T^3_m - s^2_w Q_m)\delta_{m'm} \ , \qquad c^A(\overline{f_{m'}}, f_m) = eQ_m\delta_{m'm} \ . \tag{C.3}$$

After EWSB, for each value of the charge Q, the fermion mass term can be written as $\overline{f_{L\alpha}}(\mathcal{M}_Q)_{\alpha\beta}f_{R\beta}$, where $\alpha, \beta = 1, \ldots, n_Q$ run over the n_Q fermions of charge Q (in a given colour representation). In general the mass matrix is not diagonal and the mixing can be described by $f_{L\alpha} = (U^L_Q)_{\alpha i}f_{Li}$ and $f_{R\alpha} = (U^R_Q)_{\alpha i}f_{Ri}$, where f_i are the mass eigenstates. Therefore, the couplings of the gauge bosons to the mass eigenstates are

$$(c^V_{L,R})_{ij} = (c^V_{L,R})_{\alpha\beta}(U^{L,R}_Q)^*_{\alpha i}(U^{L,R}_{Q'})_{\beta j} \ , \quad V = W^\pm, W^3, B \ , \tag{C.4}$$

where the $(c^V_{L,R})_{\alpha\beta}$ are given in Eq. (C.2), and $Q = Q' \pm 1$ for $V = W^\pm$, $Q = Q'$ for $V = W^3, B$.

The mixing cancels out in the photon couplings, because $U(1)_{em}$ is unbroken, and one finds immediately $(c^A_{L,R})_{ij} = eQ\delta_{ij}$. The Z-boson couplings to the mass eigenstates, instead, do depend on the mixing. Using the parametrisation

$$\mathcal{L}_{\bar{f}fZ} = \frac{g}{c_w}Z_\mu \sum_{i,j}\overline{f}_i\gamma^\mu\left(g^L_{ij}P_L + g^R_{ij}P_R\right)f_j \equiv \frac{g}{c_w}Z_\mu \sum_{i,j}\overline{f}_i\gamma^\mu\left(g^V_{ij} - g^A_{ij}\gamma_5\right)f_j \ , \tag{C.5}$$

one finds

$$g^{L,R}_{ij} = T^3_\alpha\delta_{\alpha\beta}(U^{L,R}_Q)^*_{\alpha i}(U^{L,R}_Q)_{\beta j} - s^2_w Q\delta_{ij} \ , \qquad g^{V,A} \equiv \frac{g^L \pm g^R}{2} \ . \tag{C.6}$$

The matrices $g^{L,R}$ ($g^{V,A}$) are hermitian, with possibly non-vanishing off-diagonal entries. Note that the mixing of fermions with equal EW charges does not affect the couplings to the neutral gauge bosons: if T^3_α (or, equivalently, Y_α) is the same for all α, then one can use $(U^{L,R}_Q)^*_{\alpha i}(U^{L,R}_Q)_{\alpha j} = \delta_{ij}$, and the couplings to Z (as well as to W^3 and B) reduce to their unmixed values. Thus, the neutral-current couplings of SM fermions receive a correction, only when they mix with new fermions with a different value of T^3 (of Y). For example, the mixing of two left-handed fermions f_{La} and f_{Lb} of charge Q amounts to

$$U^L_Q = \begin{pmatrix} c & s \\ -s & c \end{pmatrix} \ , \qquad g^L = \begin{pmatrix} T^3_a - s^2_w Q & 0 \\ 0 & T^3_b - s^2_w Q \end{pmatrix} + (T^3_a - T^3_b)\begin{pmatrix} -s^2 & sc \\ sc & s^2 \end{pmatrix} \ .$$

In this chapter we assume that new fermions mix with the third SM family only. Indeed, flavour-changing neutral currents among the different SM families are strongly constrained experimentally.

C.2 Constraints from S and T

The vacuum polarisation amplitudes for the EW gauge bosons, defined by the effective momentum space Lagrangian

$$\mathcal{L}_\Pi = -W^+_\mu \Pi^{\mu\nu}_{WW}(p) W^-_\nu - \frac{1}{2} B_\mu \Pi^{\mu\nu}_{00}(p) B_\nu - W^3_\mu \Pi^{\mu\nu}_{30}(p) B_\nu - \frac{1}{2} W^3_\mu \Pi^{\mu\nu}_{33}(p) W^3_\nu \ , \tag{C.7}$$

can be decomposed into transverse and longitudinal parts,

$$\Pi^{\mu\nu}_{VV'}(p) = \Pi^T_{VV'}(p)(p^2 g^{\mu\nu} - p^\mu p^\nu) + \Pi^L_{VV'}(p) p^\mu p^\nu = \Pi_{VV'}(p^2) g^{\mu\nu} + (p^\mu p^\nu - \text{ terms}) \ . \tag{C.8}$$

As in the experiments the mass of the external fermions is much smaller than the EW scale, $m_f^2 \ll m_Z^2$, one can drop the $p^\mu p^\nu$-terms and expand in p^2,

$$\Pi_{VV'}(p^2) = \Pi_{VV'}(0) + p^2 \Pi'_{VV'}(0) + \mathcal{O}(p^4) \ . \tag{C.9}$$

The lowest terms in this expansion are sufficient to describe accurately the effect of heavy new physics: when new particles at scale m_F contribute to the vacuum polarisation amplitudes, the higher order corrections are suppressed by powers of m_Z^2/m_F^2. Taking into account that three coefficients can be traded for the experimental values of α, s_w and m_Z, and two others are determined by the Ward identities for the photon, one finds that two parameters are sufficient to characterise the effect of new physics at leading order in m_Z^2/m_F^2 [165,166]. The combination that describes the custodial symmetry breaking at leading order is given by

$$T \equiv \frac{1}{\alpha c_w^2 m_Z^2} \left[(\Pi_{33}(0) - \Pi^{SM}_{33}(0)) - (\Pi_{WW}(0) - \Pi^{SM}_{WW}(0)) \right] \ . \tag{C.10}$$

The combination that breaks the weak isospin at leading order, but respects the custodial symmetry, is given by

$$S \equiv \frac{4 s_w c_w}{\alpha m_Z^2} \left[(\Pi_{30}(m_Z^2) - (\Pi_{30}(0)) - (\Pi^{SM}_{30}(m_Z^2) - \Pi^{SM}_{30}(0)) \right] \simeq \frac{4 s_w c_w}{\alpha} [\Pi'_{30}(0) - \Pi'^{SM}_{30}(0)] \ . \tag{C.11}$$

The approximation in terms of amplitude derivatives evaluated at $p^2 = 0$ is appropriate only for new physics much heavier than m_Z that does not mix with light SM particles; in the general case one should keep the definition of S in terms of amplitude differences, to avoid unphysical singularities that may appear in the derivative. The subtracted SM contribution is evaluated at a reference point for the SM parameters. Following Ref. [1], if one takes $m_{t,ref} = 173$ GeV and $m_{h,ref} = 125$ GeV, the present experimental allowed ranges are given by

$$S = 0.05 \pm 0.11 \ , \qquad T = 0.09 \pm 0.13 \ , \tag{C.12}$$

with a correlation coefficient $\simeq 0.9$. In Fig. 10 we display the allowed region in the $S - T$ plane, that we adopt in the rest of the chapter to constrain the parameter space of each model.

In order to estimate the contributions to S and T, in any theory where the new physics is weakly coupled, one should just compute the one-loop diagram contributing to the EW gauge boson vacuum polarisation amplitudes, shown in Fig. 11. The most general couplings of the EW gauge bosons to the fermion mass eigenstates are defined in Eq. (C.4). The functions $\Pi_{VV'}(p^2)$ defined in Eq. (C.8) will receive different contributions from the left- and right-handed couplings,

$$\Pi_{VV'} = c_L^V c_L^{V'} \Pi_{LL} + c_R^V c_R^{V'} \Pi_{RR} + c_L^V c_R^{V'} \Pi_{LR} + c_R^V c_L^{V'} \Pi_{RL} \ . \tag{C.13}$$

Performing the computation with dimensional regularisation, one finds the following general result:

$$\begin{aligned} \Pi_{LL,RR}(p^2) \ = \ & \frac{N_c}{(4\pi)^2} \left[\frac{(m_1^2 - m_2^2)^3}{6p^4} \ln \frac{m_1^2}{m_2^2} - \frac{(m_1^2 - m_2^2)^2}{3p^2} - (m_1^2 + m_2^2) \left(\frac{1}{\bar{\epsilon}} + \ln \frac{4\pi^2 \mu^2}{m_1 m_2} + \frac{1}{6} \right) \right. \\ & + \left. \frac{2}{3} p^2 \left(\frac{1}{\bar{\epsilon}} + \ln \frac{4\pi^2 \mu^2}{m_1 m_2} + \frac{7}{6} \right) + \left(\frac{(m_1^2 - m_2^2)^2}{3p^2} + \frac{m_1^2 + m_2^2}{3} - \frac{2}{3} p^2 \right) R(p^2) \right] , \end{aligned} \tag{C.14}$$

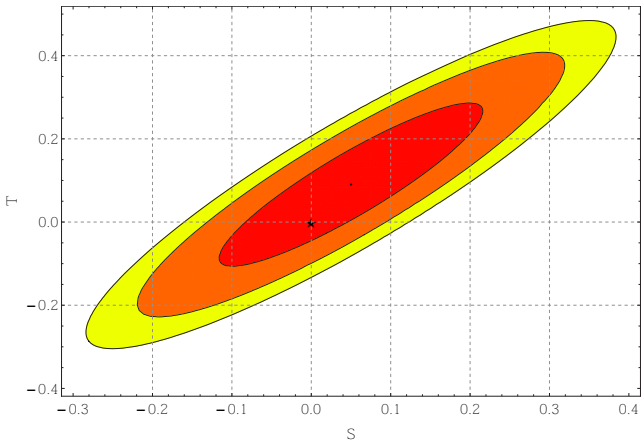

Figure 10: The 68 % (red), 95 % (orange) and 99 % (yellow) C.L. ellipses in the $S-T$ plane, from the fit of Ref. [1], with the other EW parameter U left free. The black dot indicates the best fit, while the star at $S=T=0$ is the SM point, with $m_{t,ref}=173$ GeV and $m_{h,ref}=125$ GeV.

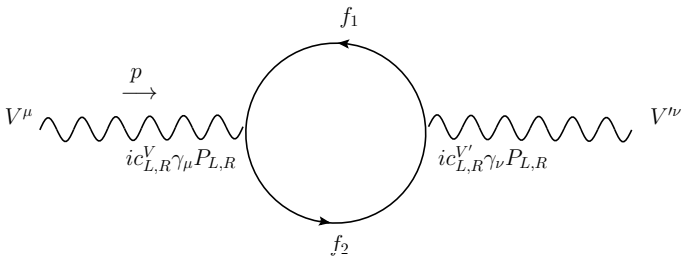

Figure 11: Contribution of two fermion mass eigenstates f_1 and f_2 to the vacuum polarisation amplitude for the gauge bosons V^μ and V'^ν. The relevant couplings are defined by $\mathcal{L}_{\bar{f}fV} = V_\mu \overline{f}_i \gamma^\mu [(c_L^V)_{ij} P_L + (c_R^V)_{ij} P_R] f_j$.

$$\Pi_{LR,RL}(p^2) = \frac{2N_c m_1 m_2}{(4\pi)^2}\left[-\frac{m_1^2-m_2^2}{2p^2}\ln\frac{m_1^2}{m_2^2}+\frac{1}{\bar{\epsilon}}+\ln\frac{4\pi^2\mu^2}{m_1 m_2}+\frac{3}{2}-R(p^2)\right], \tag{C.15}$$

where N_c is the dimension of the $SU(3)_c$ representation of the fermions $f_{1,2}$, $m_{1,2}$ are the masses of $f_{1,2}$, $\bar{\epsilon}$ and μ are defined by $\mathrm{d}^4k \equiv \mu^{4-n}\mathrm{d}^n k$ and $1/\bar{\epsilon} \equiv 2/(4-n) - \gamma - \ln\pi$ with $\gamma \simeq 0.5772$, and finally

$$R(p^2) \equiv \frac{\sqrt{\lambda}}{p^2}\log\frac{m_1^2+m_2^2-\sqrt{\lambda}-(p^2+i\epsilon)}{2m_1 m_2}\ , \qquad \lambda \equiv (m_1^2-m_2^2)^2 - 2p^2(m_1^2+m_2^2)+p^4\ . \tag{C.16}$$

Note that $R(p^2)$ is invariant for $\sqrt{\lambda} \to -\sqrt{\lambda}$ and it has a non-vanishing imaginary part for $p^2 > (m_1+m_2)^2$. When evaluating S in Eq. (C.11), one must include only the real part of $R(m_Z^2)$, while the imaginary part contributes to the decay width of the EW gauge bosons, that may be also modified with respect to its SM value. Note also that, when $f_{1,2}$ are Majorana fermions, one must include in the amplitude an additional symmetry factor 1/2.

Let us provide for convenience the form of $\Pi_{VV'}(p^2)$ in some relevant limits. For $m_1 = m_2 = 0$ one has

$$\Pi_{LL,RR}(p^2) = \frac{2N_c}{3(4\pi)^2}p^2\left(\frac{1}{\bar{\epsilon}}+\log\frac{4\pi^2\mu^2}{-(p^2+i\epsilon)}+\frac{7}{6}\right)\ , \qquad \Pi_{LR,RL}(p^2) = 0\ . \tag{C.17}$$

This limit is relevant for loops involving the light SM fermions (all but the top quark), whose mass can be neglected. In order to compute T and S (in the derivative approximation), it is sufficient to

compute the first and second term in the p^2-expansion of $\Pi_{VV'}(p^2)$, respectively:

$$\begin{aligned}
\Pi_{LL,RR}(0) &= -\frac{N_c}{(4\pi)^2}\left[(m_1^2+m_2^2)\left(\frac{1}{\bar\epsilon}+\ln\frac{4\pi^2\mu^2}{m_1 m_2}\right)+\frac{m_1^4+m_2^4}{m_1^2-m_2^2}\ln\frac{m_2}{m_1}\right], \\
\Pi_{LR,RL}(0) &= \frac{2N_c m_1 m_2}{(4\pi)^2}\left[\frac{1}{\bar\epsilon}+\ln\frac{4\pi^2\mu^2}{m_1 m_2}+\frac{1}{2}+\frac{m_1^2+m_2^2}{m_1^2-m_2^2}\ln\frac{m_2}{m_1}\right], \qquad \text{(C.18)} \\
\Pi'_{LL,RR}(0) &= \frac{2N_c}{3(4\pi)^2}\left[\frac{1}{\bar\epsilon}+\ln\frac{4\pi^2\mu^2}{m_1 m_2}-\frac{1}{6}-\frac{2m_1^2m_2^2}{(m_1^2-m_2^2)^2}+\frac{m_1^6+m_2^6-3m_1^4m_2^2-3m_1^2m_2^4}{(m_1^2-m_2^2)^3}\ln\frac{m_2}{m_1}\right], \\
\Pi'_{LR,RL}(0) &= \frac{N_c}{(4\pi)^2}\frac{m_1 m_2}{(m_1^2-m_2^2)^3}\left(m_1^4-m_2^4+4m_1^2m_2^2\ln\frac{m_2}{m_1}\right). \qquad \text{(C.19)}
\end{aligned}$$

For $m_1=0$ and $m_2=m$ (relevant e.g. for the bottom-top quark loop) one obtains

$$\Pi_{LL,RR}(0) = -\frac{N_c m^2}{(4\pi)^2}\left(\frac{1}{\bar\epsilon}+\ln\frac{4\pi^2\mu^2}{m^2}\right), \qquad \Pi'_{LL,RR}(0) = \frac{2N_c}{3(4\pi)^2}\left(\frac{1}{\bar\epsilon}+\ln\frac{4\pi^2\mu^2}{m^2}-\frac{1}{6}\right), \qquad \text{(C.20)}$$

and $\Pi_{LR,RL}(0)=\Pi'_{LR,RL}(0)=0$. For $m_1=m_2=m\neq 0$ (loops involving a unique fermion mass eigenstate) one reduces to

$$\Pi_{LL,RR}(0) = -\Pi_{LR,RL}(0) = -\frac{2N_c m^2}{(4\pi)^2}\left(\frac{1}{\bar\epsilon}+\ln\frac{4\pi^2\mu^2}{m^2}-\frac{1}{2}\right), \qquad \text{(C.21)}$$

$$\Pi'_{LL,RR}(0) = \frac{2N_c}{3(4\pi)^2}\left(\frac{1}{\bar\epsilon}+\ln\frac{4\pi^2\mu^2}{m^2}-1\right), \qquad \Pi'_{LR,RL}(0) = \frac{N_c}{3(4\pi)^2}. \qquad \text{(C.22)}$$

As an illustrative example, consider the case of a fermion "family" with no mixing with the SM fermions, formed by one weak doublet $Q_L=(T_L,B_L)\sim(R_c,2,Y)$ and two singlets $T_R\sim(R_c,1,Y+1/2)$ and $B_R\sim(R_c,1,Y-1/2)$, with $\dim(R_c)=N_c$. After EWSB they combine into two mass eigenstates T and B with masses m_T and m_B; their non-zero couplings to EW gauge bosons are obtained from Eq. (C.2),

$$\begin{aligned}
&c_L^{W^\pm}(T,B)=\frac{g}{\sqrt{2}}, \quad c_L^{W^3}(T)=\frac{g}{2}, \quad c_L^{W^3}(B)=-\frac{g}{2}, \\
&c_L^B(T)=c_L^B(B)=g'Y, \quad c_R^B(T)=g'\left(Y+\frac{1}{2}\right), \quad c_R^B(B)=g'\left(Y-\frac{1}{2}\right).
\end{aligned} \qquad \text{(C.23)}$$

To compute the correction to S, one should evaluate Eqs. (C.14-C.15) for $p^2=m_Z^2$ and $m_1=m_2=m_{T,B}$, while for $p^2=0$ one can use directly Eq. (C.21) with $m=m_{T,B}$. Adding the various contributions to Π_{30} as shown in Eq. (C.13), and replacing into Eq. (C.11), the result is

$$S_{T,B} = \frac{N_c}{6\pi}\left[\left(1-2Y\ln\frac{m_T^2}{m_B^2}\right)+\frac{m_Z^2}{m_T^2}\left(\frac{1}{2}+\frac{4Y}{3}\right)+\frac{m_Z^2}{m_B^2}\left(\frac{1}{2}-\frac{4Y}{3}\right)+\mathcal{O}\left(\frac{m_Z^4}{m_{T,B}^4}\right)\right]. \qquad \text{(C.24)}$$

If one adopted the approximate expression for S in terms of derivatives, given by the right-hand side of Eq. (C.11), then using Eq. (C.22) one finds only the first term in the squared bracket of Eq. (C.24), which is accurate for $m_{T,B}\gg m_Z$. To compute the correction to T, one should use Eq. (C.21) for the T and B loops that contribute to Π_{33}, and Eq. (C.18) for the T/B loop that contributes to Π_{WW}. Replacing into Eq. (C.10) one obtains

$$T_{T,B} = \frac{N_c}{16\pi c_w^2 s_w^2 m_Z^2}\left(m_T^2+m_B^2-2\frac{m_T^2m_B^2}{m_T^2-m_B^2}\ln\frac{m_T^2}{m_B^2}\right). \qquad \text{(C.25)}$$

Particularising these results to the case of the SM top and bottom quarks ($N_c=3$, $Y=1/6$), and neglecting the uncertainty on m_b as well as (m_b^2/m_t^2)-corrections, we can immediately extract the well-known dependence of S and T on the value of the top quark mass,

$$S_{top} = -\frac{1}{6\pi}\ln\frac{m_t^2}{m_{t,ref}^2}, \qquad T_{top} = \frac{3}{16\pi c_w^2 s_w^2}\frac{m_t^2-m_{t,ref}^2}{m_Z^2}. \qquad \text{(C.26)}$$

C.3 Constraints from $Zf\bar{f}$

The Z-boson couplings to the SM fermions are precisely measured. We discuss only those with the third family, since in this chapter we assume that the mixing of the new fermions with the light families is negligible. The deviations with respect to the SM can be expressed in terms of the Z partial decay width into any given final state $f\bar{f}$,

$$R(Z \to f\bar{f}) \equiv \frac{\Gamma(Z \to f\bar{f})}{\Gamma_{SM}(Z \to f\bar{f})} \equiv 1 + \delta R(Z \to f\bar{f}) \ , \quad f = \nu_\tau, \tau, b \ . \tag{C.27}$$

For each fermion f there are two independent couplings $g^{L,R}_{f\bar{f}}$ as shown in Eq. (C.6), that can be separately constrained if the angular distribution of the fermions is measured.

Beginning from leptons, the Z invisible width and its width into taus are determined at the per mil level [69], $\Gamma(Z \to inv) = 499.0 \pm 1.5$ MeV and $\Gamma(Z \to \tau^+\tau^-) = 84.08 \pm 0.22$ MeV. Given this precision and the relatively good agreement between the central values and the SM predictions, we constrain the mixing with the new leptons by imposing a rough 3σ upper bound,

$$|\delta R(Z \to inv)| \leq 9 \cdot 10^{-3} \ , \qquad \left|\delta R(Z \to \tau^+\tau^-)\right| \leq 8 \cdot 10^{-3} \ . \tag{C.28}$$

Coming to the Z coupling to bottom quarks, a more detailed discussion is worth, to fairly gauge the resulting constraint on the new fermions. The $Zb\bar{b}$ Lagrangian can be written as

$$\mathcal{L}_{Zb\bar{b}} = \frac{g}{c_w} Z_\mu \bar{b}\, \gamma^\mu \left[\left(g^L_{b\bar{b},SM} + \delta g^L_{b\bar{b}} \right) P_L + \left(g^R_{b\bar{b},SM} + \delta g^R_{b\bar{b}} \right) P_R \right] b \ , \tag{C.29}$$

where the SM couplings at tree-level are given by $g^L_{b\bar{b},SM} = -1/2 + s_w^2/3$ and $g^R_{b\bar{b},SM} = s_w^2/3$. Deviations at tree-level occur when the bottom quark mixes with a new fermion with a different value of T^3 (and Y). The present experimentally allowed range is given by [2]

$$\delta g^L_{b\bar{b}} = 0.0016 \pm 0.0015 \ , \qquad \delta g^R_{b\bar{b}} = 0.019 \pm 0.007 \ , \tag{C.30}$$

with a correlation coefficient $\simeq 0.8$. In Fig. 12 we display the allowed region in the $\delta g^R_{b\bar{b}} - \delta g^L_{b\bar{b}}$ plane. Note that the left- and right-handed couplings are determined with per mil and per cent precision, respectively, and the best fit region is incompatible with the SM at about 99% C.L.. In some analyses, a slightly better agreement is obtained, at about 95%, due to different details in the global electroweak fit, see e.g. Ref. [167]. The discrepancy with the SM comes mostly from the measurement of the forward-backward asymmetry A^b_{FB}, that may be just an upward statistical fluctuation, an unidentified systematic error, or alternatively an indication for a significant new-physics contribution. In this chapter, in order to constrain the new fermions that modify the $Zb\bar{b}$-couplings, we will conservatively enlarge the 99% C.L. region, by allowing it to shift towards the SM point, till the latter touches the 68% ellipse, as illustrated in Fig. 12. Such a shift roughly corresponds to introduce a systematic error in the measurement of A^b_{FB}.

The mixing with new fermions can be such that no tree-level deviations occur in the $Zb\bar{b}$-couplings, but they do occur in the $Wt\bar{b}$ coupling and/or in the $Zt\bar{t}$ couplings. These deviations may affect significantly $g^{L,R}_{b\bar{b}}$, because the contribution of one-loop diagrams involving the top quark and the W-boson is larger than the experimental uncertainty. Also new fermions may correct significantly $Zb\bar{b}$ at the one-loop level, if they are not much heavier than the top. The detailed structure of the one-loop corrections to $Zb\bar{b}$ can be found e.g. in Ref. [64], that we employ for our analysis of models with modified top couplings. For example, the correction to the left-handed coupling, from the top loops only, can be written as

$$\delta g^L_{b\bar{b}} = \delta g^L_{t\bar{t}} f_L(m_W/m_t) + \delta g^R_{t\bar{t}} f_R(m_W/m_t) + \delta g^L_{t\bar{b}} f_W(m_W/m_t) \ , \tag{C.31}$$

where $\delta g^{L,R}_{t\bar{t}}$ are defined in analogy to Eq. (C.29) with $t \leftrightarrow b$, the $Wt_L\overline{b_L}$ coupling is given by $(g/\sqrt{2})(1+\delta g^L_{t\bar{b}})$, and the functions $f_{L,R,W}$ can be extracted from Ref. [64].

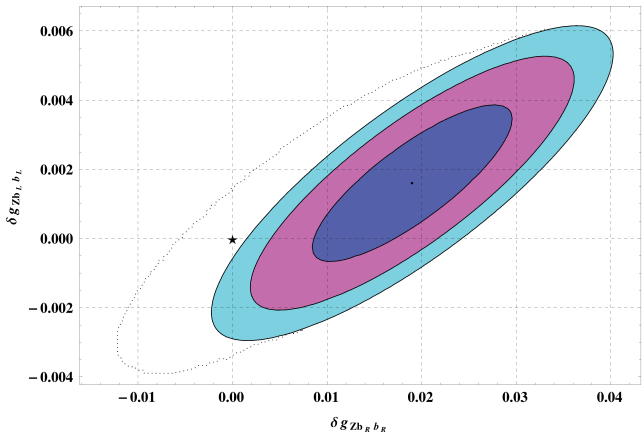

Figure 12: The 68 % (blue), 95 % (magenta) and 99 % (cyan) C.L. ellipses in the $\delta g^R_{b\bar{b}} - \delta g^L_{b\bar{b}}$ plane, extracted from Ref. [2]. The black dot indicates the best fit, while the star at the origin represents the SM. In our analysis, we allow for a larger parameter space, delimited by the dotted line, that is obtained by shifting the 99% ellipse towards the origin, till the SM point enters the 68% region.

D Higgs boson couplings in presence of new fermions

In this appendix we present a general parametrisation for the Yukawa couplings among the SM Higgs doublet and two arbitrary fermion multiplets. We then analyse the resulting modifications in the Higgs couplings to the SM particles, at leading order: corrections at tree-level to the Higgs-fermions couplings, and one-loop corrections to the Higgs-gauge bosons couplings. Finally, we briefly review the present experimental constraints on these couplings.

D.1 Tree-level Higgs couplings

The SM Yukawa couplings are given by

$$-\mathcal{L}_Y^{SM} = y_u \overline{q_L} u_R \tilde{H} + y_d \overline{q_L} d_R H + y_e \overline{l_L} e_R H + h.c. \ , \tag{D.1}$$

where $q_L = (u_L \, d_L)^T$, $H = (H^+ \, H^0)^T$ and $\tilde{H} \equiv i\sigma_2 H^*$ are $SU(2)_w$ doublets, while u_R, d_R and e_R are singlets, and flavour indexes are understood.

In full generality, the Higgs doublet may have a non-zero Yukawa interaction with any pair of chiral fermions that transform under $SU(3)_c \times SU(2)_w \times U(1)_Y$ as $\psi_L \sim (R_c, R_w, Y)$ and $\psi_R^{u,d} \sim (R_c, R_w - 1, Y \pm \frac{1}{2})$:

$$-\mathcal{L}_Y = \sum_{\psi_L} \left[\sum_{\psi_R^u} y_{\psi_L \psi_R^u} \left(\overline{\psi_L} \psi_R^u \tilde{H} \right) + \sum_{\psi_R^d} y_{\psi_L \psi_R^d} \left(\overline{\psi_L} \psi_R^d H \right) \right] + h.c. \ . \tag{D.2}$$

Here the parentheses stand for the appropriate contraction of the $SU(2)_w$ indexes. Let us denote the components of ψ_L by the index $m = j, j-1, \ldots, -j+1, -j$, where $j = (N_w - 1)/2$. Then, the multiplet $\overline{\psi_L}$ with components $(\overline{\psi_L})_m \equiv \overline{(\psi_L)_m}$ transforms in the conjugate representation R_w^*. It is possible to define a multiplet $\overline{\psi_L}'$ that properly transforms in the representation R_w, by using the $SU(2)_w$ conjugation matrix R, $(\overline{\psi_L}')_m = R_{mn} (\overline{\psi_L})_n \equiv (-1)^{j-m} \overline{(\psi_L)_{-m}}$. The $2j$ components of ψ_R^u pair with the upper (lower) $2j$ components of $\overline{\psi_L}'$ to form the upper (lower) component of a weak doublet D. The corresponding Clebsch-Gordan coefficients are given by

$$\left\langle j, j - \frac{1}{2}; m, -m \pm \frac{1}{2} \middle| \frac{1}{2}, \pm\frac{1}{2} \right\rangle = \pm(-1)^{j-m} \sqrt{\frac{j \pm m}{j(2j+1)}} \ . \tag{D.3}$$

Contracting D with $\tilde{H}$ into a weak singlet, $D_a(i\sigma_2)_{ab}\tilde{H}_b$, one finds

$$\left(\overline{\psi_L}\psi^u_R\tilde{H}\right) \equiv \sum_{m=-j+1}^{j}\sqrt{\frac{j+m}{j(2j+1)}}\left[\overline{(\psi_L)_m}(\psi^u_R)_{m-\frac{1}{2}}\tilde{H}_{\frac{1}{2}} + \overline{(\psi_L)_{-m}}(\psi^u_R)_{-m+\frac{1}{2}}\tilde{H}_{-\frac{1}{2}}\right]. \tag{D.4}$$

The same expression holds for $\psi^u_R \leftrightarrow \psi^d_R$ and $\tilde{H} \leftrightarrow H$ as well. Of course, all the results above also apply when one makes everywhere the replacement $L \leftrightarrow R$.

The relative size of the Clebsch-Gordan coefficients has important phenomenological consequences, e.g. the different components of the fermion multiplets acquire a different mass after EWSB. The overall normalisation of the $SU(2)_w$ contraction is also important, to establish the perturbative range for a Yukawa coupling y: for instance, the contribution of y to the Higgs wavefunction renormalisation at one-loop goes as $y^2/(16\pi^2)$ times the sum of the Clebsch-Gordan coefficients squared, taken over all possible isospin components in the loop. Adopting the above conventions, such a sum is normalised to one, and we can easily define the region where perturbation theory can be trusted, by requiring $y/(4\pi) \ll 1$. However, we keep the conventional normalisation for the doublet-doublet contraction into a singlet, with no overall factor $1/\sqrt{2}$, that strictly-speaking should be included: the issue of $SU(2)_w$ normalisation is more relevant for large weak multiplets.

We note that the perturbative upper bound on a Yukawa coupling y depends on the process under consideration. Schematically, the next-to-leading order amplitude is given by the leading order one times a factor $y^n g^m F_c/(16\pi^2)$, where g stands for other couplings such as gauge couplings, and F_c is the colour factor, with typical values $F_c = 1, N_c, C(R_c)$. In the example of the Higgs wavefunction normalisation adopted above, one has $n = 2$, $m = 0$ and $F_c = N_c$, therefore we could have taken into account the $SU(3)_c$ contraction by adding a factor $1/\sqrt{N_c}$ on the right-hand side of Eq. (D.4), or alternatively requiring $y\sqrt{N_c}/(4\pi) \ll 1$. However, the one-loop amplitudes relevant in our analysis (EW precision tests, Higgs couplings to fermions and gauge bosons, etc.) behave differently from each other, and the perturbativity criterion varies correspondingly. In some cases the colour enhancement is absent, or compensated by small gauge couplings, or by a small mixing between new and SM fermions. Therefore, we find more conservative to stick to the bound $y \ll 4\pi$.

At EWSB, H^0 can be replaced by $(v+h)/\sqrt{2}$, to obtain the couplings of the physical Higgs boson h to the fermions in the interaction basis. All fermions with equal charge and in the same colour representation may mix, and their mass matrix $\mathcal{M} = U_L diag(m_1, \ldots, m_n) U_R^\dagger$ may include both v-independent vector-like mass terms, and the EWSB contributions $\sim yv$. Thus, one can derive the h-couplings to the fermion mass eigenstates as follows:

$$\begin{aligned} -\mathcal{L} \;&\supset\; \overline{f_{L\alpha}}[\mathcal{M}(v)]_{\alpha\beta} f_{R\beta} + \overline{f_{L\alpha}}\frac{\partial}{\partial v}\left[\mathcal{M}(v)\right]_{\alpha\beta} f_{R\beta}\, h + h.c. \\ &= \sum_i m_i \overline{f_{Li}} f_{Ri} + \overline{f_{Lj}}\left[U_L^\dagger \frac{\partial \mathcal{M}(v)}{\partial v} U_R\right]_{jk} f_{Rk}\, h + h.c. \\ &= \sum_i m_i \overline{f_i} f_i + \overline{f_j}\,(y_{jk} + i\gamma_5 \tilde{y}_{jk})\, f_k\, h\ . \end{aligned} \tag{D.5}$$

where y and $\tilde{y}$ are hermitian matrices defined by

$$y = \frac{\lambda + \lambda^\dagger}{2}\ , \qquad \tilde{y} = \frac{\lambda - \lambda^\dagger}{2i}\ , \qquad \lambda \equiv U_L^\dagger \frac{\partial \mathcal{M}(v)}{\partial v} U_R\ . \tag{D.6}$$

In the CP-conserving case λ is real, therefore $y = y^T$ is real and $\tilde{y} = -\tilde{y}^T$ is imaginary. In the case of purely chiral masses (e.g. in the SM), one has $\mathcal{M}(v) \propto v$, therefore $\partial\mathcal{M}(v)/\partial v = \mathcal{M}/v$, $y = \lambda = diag(m_1, \ldots, m_n)/v$ and $\tilde{y} = 0$. On the other hand, in presence of both chiral and vector-like masses, the Higgs boson can have both scalar and pseudo-scalar, CP-even and CP-odd, diagonal and off-diagonal couplings to the fermions mass eigenstates, and its couplings are not proportional to the fermion masses. A simplification occurs in those SM extensions such that $(\partial\mathcal{M}/\partial v)_{\alpha\beta} = \mathcal{M}_{\alpha\beta} c_\beta$, that is, each row of the mass matrix has the same dependence on v. In this case $U_L^\dagger$ and U_L cancel out in λ and one finds $\lambda_{jk} = m_j \sum_\beta c_\beta (U_R^*)_{\beta j}(U_R)_{\beta k}$. Similarly, when $(\partial\mathcal{M}/\partial v)_{\alpha\beta} = c_\alpha \mathcal{M}_{\alpha\beta}$, one finds $\lambda_{jk} = m_k \sum_\alpha c_\alpha (U_L^*)_{\alpha j}(U_L)_{\alpha k}$.

The mixing with new fermions modifies the Higgs boson decay width into SM fermions at the tree-level. In addition, there may be new Higgs decay channels, with one or more new fermions in the final state, as long as they are lighter than h. In full generality, the Higgs decay width into two fermions at leading order is given by

$$\Gamma_{tree}(h \to \overline{f_j} f_k) = \frac{N_c \Delta_{jk}}{8\pi} m_h \left[|y_{jk}|^2 (\beta^+_{jk})^3 \beta^-_{jk} + |\tilde{y}_{jk}|^2 \beta^+_{jk} (\beta^-_{jk})^3 \right] \theta(m_h - m_j - m_k) \ , \tag{D.7}$$

where $\beta^\pm_{jk} \equiv [1 - (m_j \pm m_k)^2/m_h^2]^{1/2}$, $\Delta_{jk} = 2$ if the final state particles are identical Majorana fermions ($j = k$ and $f_j = f_j^c$), and $\Delta_{jk} = 1$ otherwise.

Besides the Yukawa couplings to fermions, the Higgs boson has tree-level couplings to WW, ZZ and to itself. In the presence of new fermions, all the tree-level couplings may receive corrections at the one-loop level. Even though these corrections may become relevant in view of precision measurements of the Higgs couplings, they represent in general a sub-leading effect and we will not discuss them further. In the following subsection we will focus instead on a more sensitive probe of new physics: those Higgs couplings that are absent at tree-level in the SM.

D.2 Loop-induced Higgs couplings

At one-loop new couplings are induced between the Higgs boson and the SM particles, that are absent at tree-level. In particular, $U(1)_{em}$ and $SU(3)_c$ gauge invariance prevents renormalizable couplings to photons and gluons, therefore the tree-level amplitudes for $h \to gg$, $h \to \gamma\gamma$ and $h \to Z\gamma$ are zero, and in addition the one-loop amplitudes for these processes are free from divergences. The effective Higgs boson couplings generated at one-loop can be described in full generality by two dimension-five operators,

$$\mathcal{L}_{hVV'} = \left(c_{hVV'} V_{\mu\nu} V'^{\mu\nu} + \frac{1}{2} \tilde{c}_{hVV'} V_{\mu\nu} V'_{\rho\sigma} \epsilon^{\mu\nu\rho\sigma} \right) h \ , \tag{D.8}$$

where $VV' = gg, \gamma\gamma, \gamma Z$ and $V_{\mu\nu} = G^a_{\mu\nu}, F_{\mu\nu}, Z_{\mu\nu}$ are the field strength tensors for the gluon, the photon and the Z, respectively. The CP-even (odd) coefficients $c_{hVV'}$ ($\tilde{c}_{hVV'}$) have mass dimension minus one, and may receive contributions from loops of both SM and new particles. One should be careful to avoid double-counting: if one considers $\mathcal{L}_{hVV'}$ as part of the effective Lagrangian valid below the EWSB scale v, $c_{hVV'}$ and $\tilde{c}_{hVV'}$ should include only the contributions of particles heavier than v.

In momentum space, the hVV' couplings are given by

$$\mathcal{L}_{hVV'}(p, p') = 2 \left[c_{hVV'} (p'^\mu p^\nu - p \cdot p' g^{\mu\nu}) + \tilde{c}_{hVV'} \epsilon^{\mu\nu\rho\sigma} p_\rho p'_\sigma \right] h(p + p') V_\mu(p) V'_\nu(p') \ . \tag{D.9}$$

The decay width of the Higgs boson into two vector bosons is then given by

$$\Gamma(h \to VV') = \frac{N_c \Delta_{VV'}}{8\pi} m_h^3 \, \beta^+_{VV'} \beta^-_{VV'} \left[c^2_{hVV'} \left(\beta^{+2}_{VV'} \beta^{-2}_{VV'} + \frac{6 m_V^2 m_{V'}^2}{m_h^4} \right) + \tilde{c}^2_{hVV'} \beta^{+2}_{VV'} \beta^{-2}_{VV'} \right] , \tag{D.10}$$

where $N_c = 8\,(1)$ for gluons (for γ and Z), $\Delta_{VV'} = 2$ for $V = V'$ and $\Delta_{VV'} = 1$ for $V \neq V'$, and finally $\beta^\pm_{VV'} \equiv [1 - (m_V \pm m_{V'})^2/m_h^2]^{1/2}$. In the following, we will match the explicit loop computation with the effective coefficients $c_{hVV'}$ and $\tilde{c}_{hVV'}$.

Higgs coupling to two gluons

The Higgs-gluon-gluon coupling c_{hgg} ($\tilde{c}_{hgg}$) receives a one-loop contribution from each coloured fermion with a non-zero CP-conserving (CP-violating) Yukawa coupling to the Higgs boson. The gluon coupling to fermions is determined by $SU(3)_c$ gauge invariance,

$$\mathcal{L}_{g\bar{f}f} = g_s \sum_i \overline{f_{ib}} \gamma^\mu A^a_\mu (T^a_i)_{bc} f_{ic} \ , \tag{D.11}$$

where T^a_i are the $SU(3)_c$ generators in the representation R_{ci} of the fermion f_i. As the $SU(3)_c$ symmetry is unbroken, there are no 'off-diagonal' gluon couplings to two different mass eigenstates.

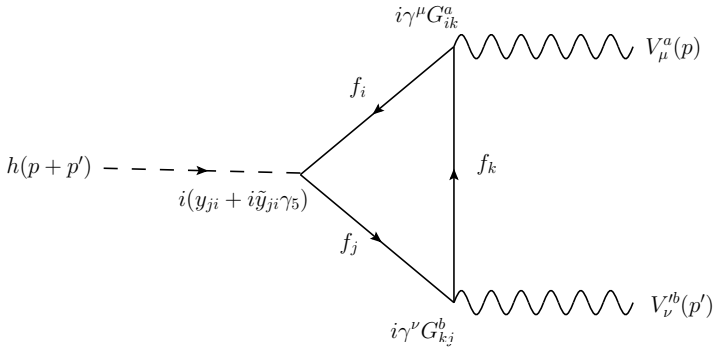

Figure 13: Fermionic triangle loop contributing to the coupling of the Higgs boson to two gauge bosons. A crossed diagram with the two gauge boson insertions interchanged has to be added too, and one must sum over all possible sets (f_i, f_j, f_k) of fermion mass eigenstates. For the gluons one has $G^a_{ik} = g_s\delta_{ik}T^a_i$, for the photon $G^\gamma_{ik} = e\delta_{ik}Q_i$, and for the Z boson $G^Z_{ik} = g(g^V_{ik} - \gamma_5 g^A_{ik})/c_w$.

Recall that the Higgs is mostly produced via gluon fusion, with a partonic cross-section that can be expressed as a function of the partial decay width,

$$\sigma(gg \to h; \hat{s}) = \frac{\pi^2}{8m_h}\delta(\hat{s} - m_h^2)\Gamma(h \to gg) \ . \tag{D.12}$$

In the SM, the contribution of the quarks triangle loop to $h \to gg$ reads

$$\Gamma_{SM}(h \to gg) = \frac{\alpha_s^2 m_h^3}{72\pi^3 v^2}\left|\frac{3}{4}\sum_q A_{1/2}(\tau_q)\right|^2 \ , \tag{D.13}$$

where $\tau_q \equiv m_h^2/(4m_q^2)$ and the form factor is given by

$$A_{1/2}(\tau) = \frac{2[\tau + (\tau-1)f(\tau)]}{\tau^2} \ , \quad f(\tau) = \begin{cases} \arcsin^2\sqrt{\tau} & \text{for } \tau \leqslant 1 \ , \\ -\frac{1}{4}\left(\log\frac{1+\sqrt{1-\tau^{-1}}}{1-\sqrt{1-\tau^{-1}}} - i\pi\right)^2 & \text{for } \tau > 1 \ . \end{cases} \tag{D.14}$$

As illustrated in Fig. 14, the top quark gives the dominant contribution, because $\tau_t \ll 1$ and $\tau_{b,c,\ldots} \gg 1$. In a generic extension of the SM, the fermions will couple to the Higgs as in Eq. (D.5), but only the diagonal, real couplings $y_i \equiv y_{ii}$ and $\tilde{y}_i \equiv \tilde{y}_{ii}$ are relevant for $h \to gg$. One obtains

$$\Gamma(h \to gg) = \frac{\alpha_s^2 m_h^3}{72\pi^3 v^2}\left(|\ \mathcal{A}_f^{gg}\ |^2 + |\ \tilde{\mathcal{A}}_f^{gg}\ |^2\right) \ , \tag{D.15}$$

where the CP-even and CP-odd amplitudes are

$$\mathcal{A}_f^{gg} = \frac{3}{2}\sum_i C(R_{ci})\frac{y_i v}{m_i}A_{1/2}(\tau_i) \ , \qquad \tilde{\mathcal{A}}_f^{gg} = \frac{3}{2}\sum_i C(R_{ci})\frac{\tilde{y}_i v}{m_i}\tilde{A}_{1/2}(\tau_i) \ , \qquad \tilde{A}_{1/2}(\tau) = 2\frac{f(\tau)}{\tau} \ , \tag{D.16}$$

with the Dynkin index $C(R_{ci})$ defined below Eq. (4.1.1).

By matching with Eq. (D.10), one finds that the contribution of a fermion loop to the effective hgg-couplings is

$$c^i_{hgg} = \frac{\alpha_s}{8\pi v}C(R_{ci})\frac{y_i v}{m_i}A_{1/2}(\tau_i) \ , \qquad \tilde{c}^i_{hgg} = \frac{\alpha_s}{8\pi v}C(R_{ci})\frac{\tilde{y}_i v}{m_i}\tilde{A}_{1/2}(\tau_i) \ , \tag{D.17}$$

where $c_{hgg} \equiv |\sum_i c^i_{hgg}|$ and $\tilde{c}_{hgg} \equiv |\sum_i \tilde{c}^i_{hgg}|$. In the heavy fermion limit, $2m_i \gg m_h$, one can use $A_{1/2}(0) = 4/3$ and $\tilde{A}_{1/2}(0) = 2$. We note that, in the literature, a factor $1/2$ is sometimes missing in the expression for $\tilde{c}^t_{hgg}$.

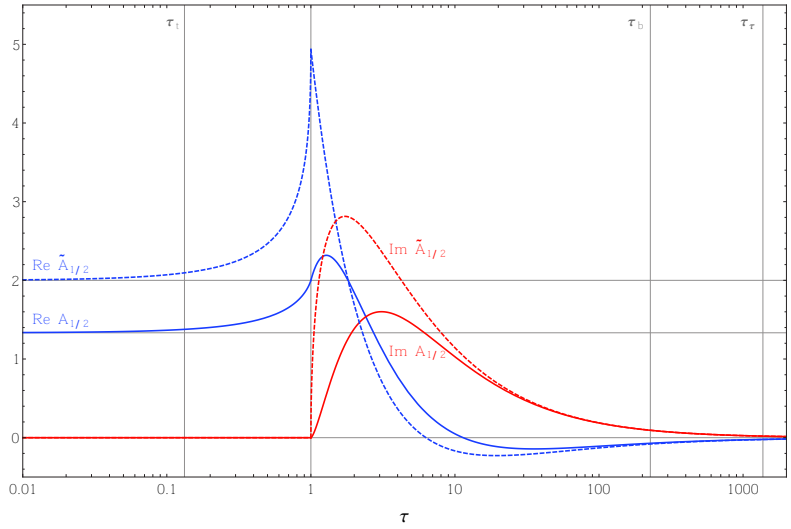

Figure 14: Real (blue lines) and imaginary (red lines) parts of the form factors $A_{1/2}(\tau)$ (solid lines) and $\tilde{A}_{1/2}(\tau)$ (dashed lines). The horizontal lines correspond to the asymptotic values 2, 4/3 and 0. The vertical lines correspond to the reference values $\tau_t \simeq 0.13$, $\tau = 1$, $\tau_b \simeq 230$ and $\tau_\tau \simeq 1300$.

One can use the Low Energy Theorem (LET) [168,169] (see also [170–172]) to evaluate the effective hVV' couplings induced by states much heavier than the EW scale. For a given sector of mixing states in the representation (R_c, Q) of $SU(3)_c \times U(1)_{em}$, the low energy result is a function of their mass matrix $\mathcal{M}$ only. For the CP-conserving and CP-violating [173] gluon-gluon case one finds, respectively,

$$c_{hgg}^{LET} = \frac{\alpha_s}{12\pi} C(R_c) \frac{\partial}{\partial v} \ln\left[\det\left(\mathcal{M}\mathcal{M}^\dagger\right)\right] , \qquad \tilde{c}_{hgg}^{LET} = \frac{\alpha_s}{4\pi} C(R_c) \frac{\partial}{\partial v} \arg\left[\det\left(\mathcal{M}\right)\right] . \tag{D.18}$$

This is very useful in the case of a large, complicated mass matrix $\mathcal{M}$, because this expression is much easier to evaluate, with respect to an explicit computation of the mass eigenvalues m_i and of the mass eigenstate couplings y_i and $\tilde{y}_i$. Note, however, that this approximation requires all the mass eigenstates in a given sector to be heavy, $2m_i \gg m_h$. It is easy to check the consistency of Eq. (D.17) and Eq. (D.18) for one heavy chiral fermion (e.g. the SM top quark), as $\mathcal{M}_i = m_i = y_i v$ and $A_{1/2}(\tau_i) \simeq 4/3$.

Higgs coupling to two photons

The fermions charged under $U(1)_{em}$ contribute to the Higgs-photon-photon couplings $c_{h\gamma\gamma}$ and $\tilde{c}_{h\gamma\gamma}$ at one loop. In the SM, there is also the contribution from W-boson loops, that we include using the SM tree-level couplings of the W to the Higgs and to the photon. The SM decay width is given by [168,169,174]

$$\Gamma_{SM}(h \to \gamma\gamma) = \frac{\alpha^2 m_h^3}{256\pi^3 v^2} \left| A_1(\tau_W) + \sum_{f_i \in SM} N_{ci} Q_i^2 A_{1/2}(\tau_i) \right|^2 , \tag{D.19}$$

where $\tau_W \equiv m_h^2/(4m_W^2)$, $\tau_i \equiv m_h^2/(4m_i^2)$, and the form factor for the W-loops reads

$$A_1(\tau) = -\frac{2\tau^2 + 3\tau + 3(2\tau - 1) f(\tau)}{\tau^2} . \tag{D.20}$$

The W contribution is dominant, $A_1(\tau_W) \simeq -8.36$, and it interferes destructively with the top-quark loop, $N_{ct} Q_t^2 A_{1/2}(\tau_t) \simeq 1.83$.

In presence of extra fermions, there are new contributions to $h \to \gamma\gamma$ that depend, as in the case of $h \to gg$, on the Yukawa couplings y_i and $\tilde{y}_i$,

$$\Gamma(h \to \gamma\gamma) = \frac{\alpha^2 m_h^3}{256\pi^3 v^2} \left[\mid A_1(\tau_W) + \mathcal{A}_f^{\gamma\gamma} \mid^2 + \mid \tilde{\mathcal{A}}_f^{\gamma\gamma} \mid^2 \right] , \tag{D.21}$$

where

$$\mathcal{A}_f^{\gamma\gamma} = \sum_i \frac{y_i v}{m_i} N_{ci} Q_i^2 A_{1/2}(\tau_i) , \qquad \tilde{\mathcal{A}}_f^{\gamma\gamma} = \sum_i \frac{\tilde{y}_i v}{m_i} N_{ci} Q_i^2 \tilde{A}_{1/2}(\tau_i) . \tag{D.22}$$

In terms of the coefficients of the effective Lagrangian Eq. (D.8), the contribution of each fermion is given by

$$c_{h\gamma\gamma}^i = \frac{\alpha}{8\pi v} \frac{y_i v}{m_i} N_{ci} Q_i^2 A_{1/2}(\tau_i) , \qquad \tilde{c}_{h\gamma\gamma}^i = \frac{\alpha}{8\pi v} \frac{\tilde{y}_i v}{m_i} N_{ci} Q_i^2 \tilde{A}_{1/2}(\tau_i) . \tag{D.23}$$

The LET approximation, for a set of heavy fermions in the representation (R_c, Q) with a mass matrix $\mathcal{M}$, is given by

$$c_{h\gamma\gamma}^{LET} = \frac{\alpha}{12\pi} Q^2 N_c \frac{\partial}{\partial v} \ln \left[\det \left(\mathcal{M}\mathcal{M}^\dagger \right) \right] , \qquad \tilde{c}_{h\gamma\gamma}^{LET} = \frac{\alpha}{4\pi} Q^2 N_c \frac{\partial}{\partial v} \arg \left[\det \left(\mathcal{M} \right) \right] , \tag{D.24}$$

in analogy with Eq. (D.18).

Higgs coupling to a Z boson and a photon

The last loop-induced coupling to be considered is $hZ\gamma$. It is generated by W-boson loops, that we take to be SM-like, as well as by fermionic triangle loops. The Z-boson couplings to fermion mass eigenstates are defined in Eq. (C.6).

The Higgs decay width into a photon and a Z in the SM is given by [175, 176]

$$\Gamma_{SM}(h \to \gamma Z) = \frac{\alpha g^2 c_w^2 m_h^3}{512\pi^4 v^2} \left(1 - \frac{m_Z^2}{m_h^2} \right)^3 \left| A_1(\tau_W, \lambda_W) + \sum_{f_i \in SM} \frac{N_{ci} Q_i g_i^V}{c_w^2} A_{1/2}(\tau_i, \lambda_i) \right|^2 , \tag{D.25}$$

where $\lambda_W \equiv m_Z^2/(4m_W^2) = (m_Z/m_h)^2 \tau_W \simeq 0.52\tau_W$, and analogously $\lambda_i \equiv m_Z^2/(4m_i^2) \simeq 0.52\tau_i$. Note that only the $Zf_i\bar{f}_i$ vector coupling contributes, $g_i^V = T_3(f_{Li})/2 - Q_i s_w^2$. The form factors are given by

$$A_1(\tau, \lambda) = 2\left[3 + 2\tau - 2\lambda(1 + 2\tau)\right] I_1(\tau, \lambda) - 16(1 - \lambda) I_2(\tau, \lambda) , \tag{D.26}$$

$$A_{1/2}(\tau, \lambda) = 4\left[I_2(\tau, \lambda) - I_1(\tau, \lambda) \right] , \tag{D.27}$$

where

$$I_1(\tau, \lambda) = -\frac{1}{2(\tau - \lambda)} + \frac{f(\tau) - f(\lambda)}{2(\tau - \lambda)^2} + \frac{\lambda[g(\tau) - g(\lambda)]}{(\tau - \lambda)^2} , \qquad I_2(\tau, \lambda) = \frac{f(\tau) - f(\lambda)}{2(\tau - \lambda)} , \tag{D.28}$$

$$g(\tau) = \begin{cases} \sqrt{\tau^{-1} - 1} \arcsin \sqrt{\tau} & \text{for} \quad \tau \leqslant 1 , \\ \dfrac{\sqrt{1 - \tau^{-1}}}{2} \left(\log \dfrac{1 + \sqrt{1 - \tau^{-1}}}{1 - \sqrt{1 - \tau^{-1}}} - i\pi \right) & \text{for} \quad \tau > 1 . \end{cases} \tag{D.29}$$

The normalisation is chosen to match with the $\gamma\gamma$ form factors: $A_1(\tau, 0) = A_1(\tau)$ and $A_{1/2}(\tau, 0) = A_{1/2}(\tau)$. The behaviour of $A_{1/2}(\tau, \lambda)$ is displayed in Fig. 15, for the relevant case $\lambda = (m_Z/m_h)^2\tau$. The W-boson and t-quark summands in Eq. (D.25) take the value $A_1(\tau_W, \lambda_W) \simeq -6.64$ and $N_{ct} Q_t g_t^V A_{1/2}(\tau_t, \lambda_t)/c_w^2 \simeq 0.37$, with the lighter SM fermions adding a very small contribution.

In a generic fermionic extension of the SM, we find a decay width

$$\Gamma(h \to \gamma Z) = \frac{\alpha g^2 c_w^2 m_h^3}{512\pi^4 v^2} \left(1 - \frac{m_Z^2}{m_h^2} \right)^3 \left[\mid A_1(\tau_W, \lambda_W) + \mathcal{A}_f^{Z\gamma} \mid^2 + \mid \tilde{\mathcal{A}}_f^{Z\gamma} \mid^2 \right] , \tag{D.30}$$

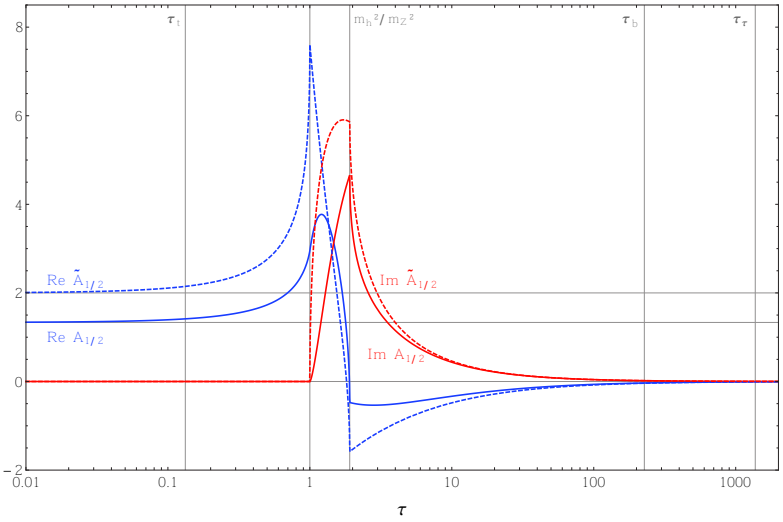

Figure 15: Real (blue lines) and imaginary (red lines) parts of the form factors $A_{1/2}(\tau,\lambda)$ (solid lines) and $\tilde{A}_{1/2}(\tau,\lambda)$ (dashed lines), for $\lambda = (m_Z/m_h)^2\tau \simeq 0.52\tau$. The horizontal lines correspond to the asymptotic values 2, 4/3 and 0. The vertical lines correspond to $\tau_t \simeq 0.13$, $\tau = 1$, $\tau \simeq 1.9$ ($\lambda = 1$), $\tau_b \simeq 230$ and $\tau_\tau \simeq 1300$.

with the CP-even and odd fermionic amplitudes given by

$$\mathcal{A}_f^{Z\gamma} = \sum_{j,k} \frac{N_{ck} Q_k v}{c_w^2 \sqrt{m_j m_k}} \left[\mathrm{Re}(g_{kj}^V y_{jk}) a_{1/2}(m_j, m_k, m_k) + i \mathrm{Im}(g_{kj}^A \tilde{y}_{jk}) b_{1/2}(m_j, m_k, m_k) \right] , \tag{D.31}$$

$$\tilde{\mathcal{A}}_f^{Z\gamma} = \sum_{j,k} \frac{N_{ck} Q_k v}{c_w^2 \sqrt{m_j m_k}} \left[\mathrm{Re}(g_{kj}^V \tilde{y}_{jk}) \tilde{a}_{1/2}(m_j, m_k, m_k) + i \mathrm{Im}(g_{kj}^A y_{jk}) \tilde{b}_{1/2}(m_j, m_k, m_k) \right] . \tag{D.32}$$

The explicit expression of the four independent form factors will be given below. As far as we know, this expression for $\Gamma(h \to \gamma Z)$, corresponding to a generic set of fermions, was not available in the literature. Here the sum runs over all pairs of fermion mass eigenstates: the triangular fermion loop is formed by one f_j propagator from the h vertex to the Z vertex, and two f_k propagators from Z to γ, and from γ to h. As both h and Z can have off-diagonal couplings, j and k can be different. Note that only those combination of couplings that are even under the charge conjugation C contribute, because the transition $h \to Z\gamma$ is even: under C, one has $Q \to -Q$, $g_{ij}^V \to -g_{ij}^{V*}$ and $x_{ij} \to x_{ji} = x_{ij}^*$, for $x = g^A, y, \tilde{y}$. The P and CP-even (odd) amplitude corresponds to an even (odd) number of axial-vector and pseudo-scalar couplings g^A and $\tilde{y}$.

Let us discuss first the loops involving one fermion mass eigenstate only ($j = k$). The diagonal couplings $g_i^{V,A}$, y_i and $\tilde{y}_i$ are all real, therefore the form factors $b_{1/2}$ and $\tilde{b}_{1/2}$ are irrelevant, while the others reduce to

$$a_{1/2}(m,m,m) = A_{1/2}(\tau,\lambda) , \qquad \tilde{a}_{1/2}(m,m,m) = \tilde{A}_{1/2}(\tau,\lambda) \equiv 4I_2(\tau,\lambda) . \tag{D.33}$$

These two form factors are displayed in Fig. 15 as a function of τ. As usual the normalisation matches with the $\gamma\gamma$ form factors, in particular $\tilde{A}_{1/2}(\tau,0) = \tilde{A}_{1/2}(\tau)$. Comparing with Eq. (D.10), one finds that the contributions of such fermion 'diagonal' loop to the effective $h\gamma Z$ couplings are

$$c_{h\gamma Z}^i = \frac{\alpha}{4\pi s_w c_w v} \frac{y_i v}{m_i} N_{c_i} Q_i g_i^V A_{1/2}(\tau_i,\lambda_i) , \qquad \tilde{c}_{h\gamma Z}^i = \frac{\alpha}{4\pi s_w c_w v} \frac{\tilde{y}_i v}{m_i} N_{cf} Q_i g_i^V \tilde{A}_{1/2}(\tau_i,\lambda_i) . \tag{D.34}$$

Let us now discuss the loops involving two fermion mass eigenstates ($j \neq k$). The form factors are

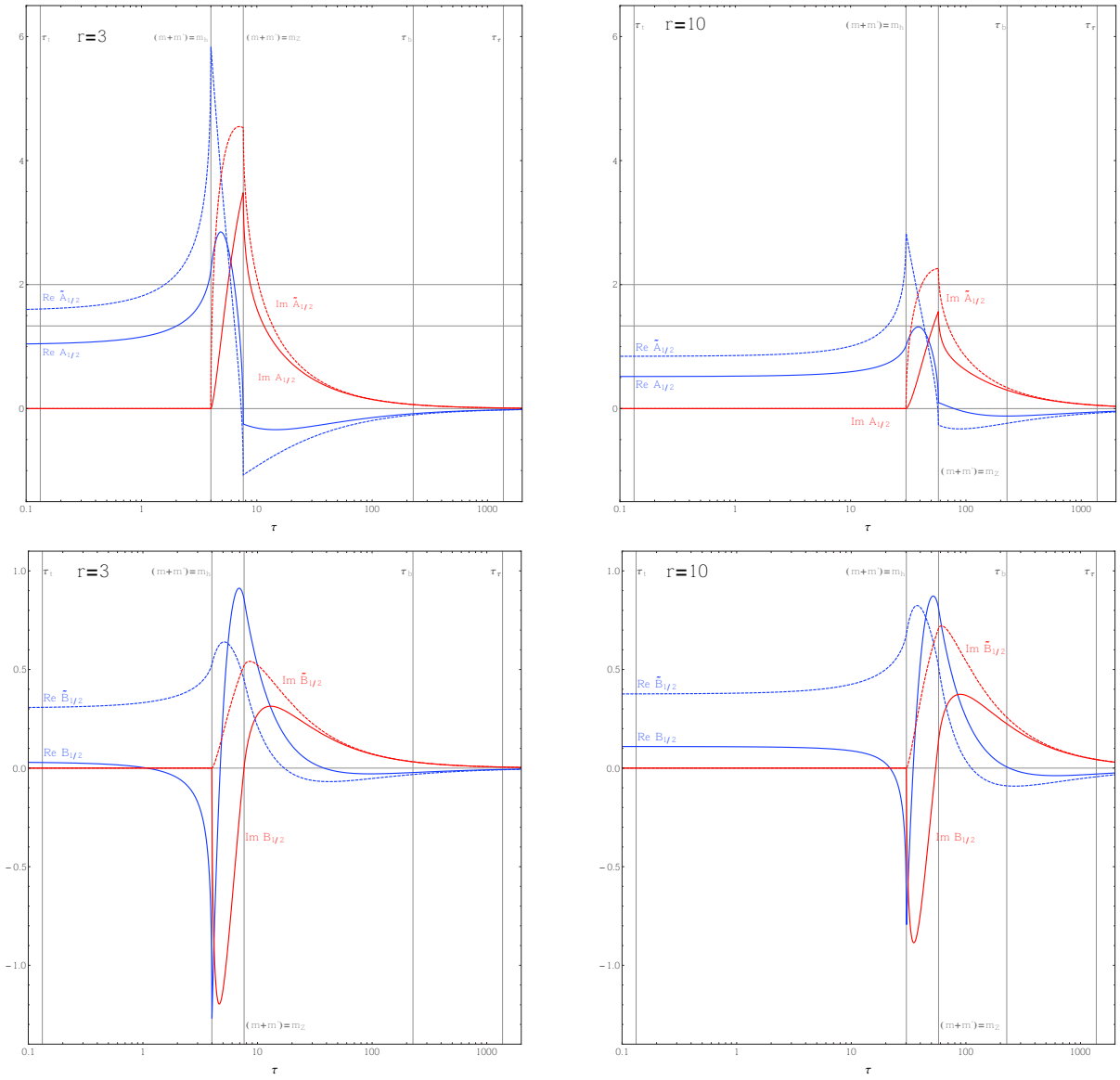

Figure 16: Form factors for the triangle loops involving two fermions of mass m and $m' = r\,m$, for $r = 3$ and $r = 10$, in the left and right-hand panels, respectively. We show the real (in blue) and imaginary (in red) parts of $A_{1/2}(\tau, \lambda, \tau/r^2, \lambda/r^2)$ (solid lines, upper panels), $\tilde{A}_{1/2}(\tau, \lambda, \tau/r^2, \lambda/r^2)$ (dashed, upper), $B_{1/2}(\tau, \lambda, \tau/r^2, \lambda/r^2)$ (solid, lower) and $\tilde{B}_{1/2}(\tau, \lambda, \tau/r^2, \lambda/r^2)$ (dashed, lower), as a function of $\tau \equiv 4m_h^2/m^2$, for a fixed value of $\lambda \equiv (m_Z/m_h)^2\tau \simeq 0.52\ \tau$. The horizontal lines correspond to the asymptotic values for the case $r = 1$ (see Fig. 15). The vertical lines correspond to the third family masses, $\tau_t \simeq 0.13$, $\tau_b \simeq 230$ and $\tau_\tau \simeq 1300$, and to the threshold values, $m + m' = m_h$ $[\tau = (1 + r)^2/4]$, and $m + m' = m_Z$ $[\tau = (m_h/m_Z)^2(1 + r)^2/4]$.

given by

$$\frac{a_{1/2}(m_j,m_k,m_k)}{\sqrt{m_j m_k}} = -\frac{4}{m_Z^2-m_h^2}\Bigg\{\left[\frac{A_0(m_j)-A_0(m_k)}{m_h^2}+1\right](m_j+m_k)$$
$$+\frac{B_0(m_h^2;m_j,m_k)}{m_Z^2-m_h^2}\left[(m_j+m_k)\left(2m_j^2-2m_k^2-m_h^2+\frac{m_Z^2}{m_h^2}(m_k^2-m_j^2)\right)+2m_k(m_h^2-m_Z^2)\right]$$
$$+\frac{B_0(m_Z^2;m_j,m_k)}{m_Z^2-m_h^2}\left[(m_j+m_k)(m_k^2-m_j^2)+m_k(2m_Z^2-m_h^2)+m_j m_h^2\right]$$
$$+C_0(m_Z^2,0,m_h^2;m_j,m_k,m_k)\left[2m_k^2(m_j+m_k)+m_k(m_Z^2-m_h^2)\right]\Bigg\}\,, \tag{D.35}$$

$$\frac{\tilde{a}_{1/2}(m_j,m_k,m_k)}{\sqrt{m_j m_k}} = -4\left[\frac{B_0(m_h^2;m_j,m_k)-B_0(m_Z^2;m_j,m_k)}{m_Z^2-m_h^2}(m_j-m_k)\right.$$
$$\left.+C_0(m_Z^2,0,m_h^2;m_j,m_k,m_k)m_k\right]\,, \tag{D.36}$$

$$\frac{b_{1/2}(m_j,m_k,m_k)}{\sqrt{m_j m_k}} = \frac{a_{1/2}(-m_j,m_k,m_k)}{\sqrt{m_j m_k}}\,,\qquad \frac{\tilde{b}_{1/2}(m_j,m_k,m_k)}{\sqrt{m_j m_k}} = \frac{\tilde{a}_{1/2}(-m_j,m_k,m_k)}{\sqrt{m_j m_k}}\,, \tag{D.37}$$

where A_0, B_0 and C_0 are the standard Passarino-Veltman scalar functions [177,178], in the convention of Ref. [179]. In the literature, these 'off-diagonal' loops are often neglected but, in models with significant h and Z off-diagonal couplings, they may provide a contribution to the decay width of the same order as the 'diagonal' loops. For example, the form factors in Eqs. (D.35)-(D.37) have been already employed in supersymmetric models to compute the charginos loops [180–182].

It is useful to combine all the loops involving two given fermions f_j and f_k. As $\mathrm{Re}(g^V_{kj}y_{jk}) = \mathrm{Re}(g^V_{jk}y_{kj})$ and $\mathrm{Im}(g^A_{kj}\tilde{y}_{jk}) = -\mathrm{Im}(g^A_{jk}\tilde{y}_{kj})$, the combinations that appear in the total amplitude are

$$A_{1/2}(\tau_j,\lambda_j,\tau_k,\lambda_k) \equiv \frac{1}{2}\left[a_{1/2}(m_j,m_k,m_k)+a_{1/2}(m_k,m_j,m_j)\right]\,, \tag{D.38}$$

$$B_{1/2}(\tau_j,\lambda_j,\tau_k,\lambda_k) \equiv \frac{1}{2}\left[b_{1/2}(m_j,m_k,m_k)-b_{1/2}(m_k,m_j,m_j)\right]\,, \tag{D.39}$$

and analog definitions for the CP-odd counterparts $\tilde{A}_{1/2}$ and $\tilde{B}_{1/2}$. In Fig. 16 we illustrate the behaviour of these four form factors as a function of $\tau = m_h^2/(4m^2)$, where m is the mass of the lightest fermion, for a fixed value of the ratio $r = m'/m$, where m' is the mass of the heaviest fermion. In the limit $r = 1$ one recovers the diagonal form factors, shown in Fig. 15. Since m' is the mass of a new charged fermion, it should be sufficiently large to comply with experimental lower bounds; requiring for example $m' > m_h$, one finds that only the region $\tau < r^2/4$ is relevant for phenomenology. Note that the behaviour of the form factors as $\tau \to 0$ is sensitive to the mass ratio: as r increases from 1 to infinity, the asymptotic regime settles at larger values of τ, and the asymptotic value of the form factors $A_{1/2}$ and $\tilde{A}_{1/2}$ tends to zero as $1/\sqrt{r}$. The form factors $B_{1/2}$ and $\tilde{B}_{1/2}$ are zero for $r = 1$, then become of order one as r grows, then tend to zero in the large-r limit.

D.3 Experimental constraints on the Higgs couplings

Here we collect the constraints on the Higgs couplings that we use in our analysis. For a given Higgs-decay final state α, the LHC measures the signal strength μ_α defined as

$$\mu_\alpha \equiv \frac{\sigma(pp\to h)}{\sigma^{SM}(pp\to h)}\frac{Br(h\to\alpha)}{Br^{SM}(h\to\alpha)} = \frac{\sigma(pp\to h)}{\sigma^{SM}(pp\to h)}\frac{\Gamma(h\to\alpha)}{\Gamma^{SM}(h\to\alpha)}\frac{\Gamma_h^{SM}}{\Gamma_h}\,, \tag{D.40}$$

where Γ_h is the total Higgs width. In Table 4 we report the present determination of μ_α for $\alpha = \gamma\gamma, ZZ^*, WW^*, b\bar{b}, \tau\tau, \gamma Z, \mu\mu$ as well as on the invisible width, by the ATLAS and CMS collaborations.

	ATLAS	CMS	ATLAS+CMS
$\sqrt{s}$	7+8 TeV	7+8 TeV	7+8 TeV
$\mathcal{L}$	$4.7 + 20.3\ fb^{-1}$	$5.1 + 19.7\ fb^{-1}$	
m_h	125.36 ± 0.41 GeV [79]	$125.02^{+0.29}_{-0.31}$ GeV [77]	125.09 ± 0.24 GeV [78]
$\mu_{\gamma\gamma}$	$1.17^{+0.28}_{-0.26}$ [79]	1.12 ± 0.24 [77]	$1.13^{+0.24}_{-0.21}$ [96]
$\mu_{ZZ^* \to 4l}$	$1.46^{+0.40}_{-0.34}$ [79]	1.00 ± 0.29 [77]	$1.29^{+0.29}_{-0.25}$ [96]
μ_{WW^*}	$1.18^{+0.24}_{-0.21}$ [79]	0.83 ± 0.21 [77]	$1.08^{+0.22}_{-0.19}$ [96]
$\mu_{\tau\tau}$	$1.44^{+0.42}_{-0.37}$ [79]	0.91 ± 0.28 [77]	$1.07^{+0.35}_{-0.28}$ [96]
$\mu_{b\bar{b}}$	$0.63^{+0.39}_{-0.37}$ [79]	0.84 ± 0.44 [77]	$0.65^{+0.37}_{-0.28}$ [96]
μ_{global}	$1.18^{+0.15}_{-0.14}$ [79]	1.00 ± 0.14 [77]	$1.09^{+0.11}_{-0.10}$ [96]
$\mu_{\gamma Z}$	< 11.0 [184]	< 9.5 [185]	
$\Gamma_{invisible}/\Gamma_h$	< 0.29 [186]	< 0.58 [187]	

Table 4: Higgs signal strengths measured by the ATLAS and CMS collaborations at $\sqrt{s} = 7$ and 8 TeV and their combination. The error bars and upper limits correspond respectively to $\pm 1\sigma$ and 95% C.L.. In this chapter we adopt the value of the Higgs mass and of the signal strengths from the combined fit of the ATLAS and CMS data, reported in the last column.

The expected precision for a luminosity of $300 - 3000$ fb^{-1} at 14 TeV [9, 183] is reported for these same channels in Table 5.

From a global fit of the Higgs data, one can also extract information on the Higgs coupling to gluons. Taking a rough extrapolation from the fit in Fig. 16 of Ref. [96], we find $0.5 \lesssim R_{gg} \lesssim 1.8$ at 99% C.L., where R_{gg} is defined in Eq. (4.2.4). In the same way we extract the analogue quantity for the diphoton channel, $0.5 \lesssim R_{\gamma\gamma} \lesssim 1.9$ at 99% C.L., that we employ throughout this chapter.

The new fermions may or may not affect each of the three factors on the right-hand side of Eq. (D.40). Let us discuss first the Higgs production cross section. The dominant gluon fusion channel can be modified at leading order only by coloured fermions. The weak-vector-boson fusion and associated production can be modified, at tree level, only by fermions mixing with the initial state quarks: as we limit our analysis to mixing with the third family, we neglect these modifications. Finally, the $t\bar{t}$ associated production can be corrected by those fermions mixing with the top quark. Concerning the total Higgs decay width Γ_h, the dominant branching ratio into $b\bar{b}$ is affected by fermions mixing with the bottom quark, and the second dominant decay channel into WW^* is not modified by new fermions at leading order. Finally, Γ_h may be modified significantly by new invisible decays, that are possible in the presence of sterile neutrinos. When both $\sigma(pp \to h)$ and Γ_h are close to their SM value, the signal strength in Eq. (D.40) reduces to $\mu_\alpha \simeq R_\alpha$, where

$$R_\alpha \equiv \frac{\Gamma(h \to \alpha)}{\Gamma^{SM}(h \to \alpha)} = \frac{|\mathcal{A}^\alpha_{SM} + \mathcal{A}^\alpha_{new}|^2 + |\widetilde{\mathcal{A}}^\alpha_{new}|^2}{|\mathcal{A}^\alpha_{SM}|^2} \,. \tag{D.41}$$

Here $\mathcal{A}^\alpha_{new}$ and $\widetilde{\mathcal{A}}^\alpha_{new}$ are the parity-even and odd new physics amplitudes, respectively. The approximation $\mu_\alpha \simeq R_\alpha$ holds for all colourless new fermions, with the possible exception of light sterile neutrinos.

Several groups performed global fits of the Higgs couplings to the SM particles, allowing for deviations in both the fermionic and bosonic decay channels, see e.g. Refs. [188–195]. The fit of Ref. [196] analyzed deviations in the Higgs couplings in the presence of new fermions only.

	ATLAS	[183]	CMS	[9]
$\Delta\mu_\alpha/\mu_\alpha$	300 fb^{-1}	3000 fb^{-1}	300 fb^{-1}	3000 fb^{-1}
$\gamma\gamma$	0.13	0.09	[0.06,0.12]	[0.04,0.08]
ZZ	0.11	0.09	[0.07,0.11]	[0.04,0.07]
WW	0.13	0.11	[0.06,0.11]	[0.04,0.07]
$\tau\tau$	0.21	0.19	[0.08,0.14]	[0.05,0.08]
$b\bar{b}$	0.26	0.14	[0.11,0.14]	[0.05,0.07]
γZ	0.46	0.30	[0.62,0.62]	[0.20,0.24]
$\mu\mu$	0.39	0.16	[0.40,0.42]	[0.20,0.24]
$\Gamma_{invisible}/\Gamma_h$	< 0.22	< 0.14	$< [0.17, 0.28]$	$< [0.06, 0.17]$

Table 5: Expected relative uncertainty at 1σ on the signal strengths μ_α for ATLAS and CMS. The expected precisions correspond to $\sqrt{s} = 14$ TeV and $\mathcal{L} = 300$ and 3000 fb^{-1}. We also display the expected limit at 95% C.L. on $\Gamma_{invisible}/\Gamma_h$ for the same luminosities. For CMS the two numbers correspond to two different estimations of the future uncertainties [9].

Chapter 5

Two Higgs doublet extended by new fermions

In this chapter, we turn to another kind of low energy extensions of the SM that is, a Higgs sector extended with a second Higgs doublet. In addition, we also introduce new fermions with couplings to the two scalar doublets. This chapter can be viewed as an enlargement of the precedent framework where the effects of new fermions are now studied in a more general context.

We do not classify all of the possible extensions as we did in chapter 4. Indeed, the consistent fermionic extensions that we have isolated in the case of one doublet remain the same with a second doublet. Note that it is particular to this extended Higgs sector as for instance, with a new scalar singlet that gets a vev after EWSB, the classification of the possible cases should be different. For simplicity, we focus only on VL fermions coupling to the two Higgs doublets. As before, we study the constraints coming from the couplings measurements of the 125 GeV Higgs boson and the ones coming from the EWPT.

The first idea of this chapter was to reproduce the diphoton excess at 750 GeV and at the same time the excess in the LFV decay $h \to \tau\mu$. The former excess has now disappeared with the recent LHC data. However, the results of this chapter are still interesting and can easily be generalised. Indeed, in order to control the light Higgs coupling to two photons such that the latter remains SM-like, we use the mechanisms presented in chapter 4. In general, these mechanisms lead to a large $h\gamma Z$ coupling. This is already an interesting signal of new physics. Furthermore, if the same mechanisms are realised in a 2HDM framework, one can reasonably expect that the couplings of the heavy Higgses to two photons receive in general large contributions. This is in fact possible and in this way we were able to address the diphoton excess by reproducing the large cross sections $\sigma(pp \to H, A \to \gamma\gamma)$ where H and A are respectively the CP-even and CP-odd heavy Higgses. As the 750 GeV diphoton excess is now gone, our framework and our mechanisms to control $h \to \gamma\gamma$ can be generalised to resonances with a larger mass than 750 GeV. Indeed, if there is an extended Higgs sector containing a doublet, the decays of the scalar and pseudo-scalar resonances in two photons remain an interesting channel. As the cross sections $\sigma(pp \to H, A \to \gamma\gamma)$ was really important for the 750 GeV excess, our framework can easily serves as a benchmark. As it was possible to reproduce such very large cross section, one can easily transpose our model to smaller cross section at a larger invariant mass.

In addition, the second excess associated to the decay $h \to \tau\mu$ is still there and our model can be modify to only explain this excess. Indeed, it is enough to remove the VL fermions from the model or equivalently, to decoupled them from the low energy theory by sending the VL masses to higher scales. With all of the above arguments, let us now assume for the exercise that the diphoton excess at 750 GeV is not a statistical fluctuation.

The ATLAS and CMS collaborations have presented few months ago the indications for a diphoton excess at at an invariant mass of 750 GeV [3,4]. As mentioned above, this excess has now disappeared but we will consider for the exercise that the excess is still there. Aside the diphoton excess, some hints of anomalies persist in the LHC run-I data. Notably there is a 2.4σ excess at CMS in the $h \to \tau^{\pm}\mu^{\mp}$ decay of the 125 GeV Standard Model-like Higgs boson h [126], corresponding to a best-fit

branching ratio $\mathrm{BR}(h \to \tau^\pm\mu^\mp) = 0.84^{+0.39}_{-0.37}\,\%$. This is compatible with the ATLAS analysis which finds $\mathrm{BR}(h \to \tau^\pm\mu^\mp) = 0.77 \pm 0.62\,\%$ [125].

One of the simplest renormalisable models allowing for a $h \to \tau^\pm\mu^\mp$ branching ratio of the order of a percent is the two-Higgs-doublet model (2HDM) [197–200] with lepton flavour violating Yukawa couplings. This model has been studied before [201–207], and, with renewed interest, after the CMS excess was announced [208–214]. The aim of the present chapter is to study whether a simple 2HDM could explain both the diphoton excess and the LFV Higgs decay. The LHC excess has been studied in the 2HDM in [215–223], and several authors have combined it with other observables, such as the dark matter abundance [224–233], or B-physics anomalies [234–236]. In the 2HDM, candidates for the 750 GeV resonance are the heavier scalar Higgs h_2 and the pseudoscalar A. They can reproduce the observed cross-section times branching ratio into photons if they couple to heavy vector-like charged fermions, as has been discussed by several authors, e.g. [215–217, 237–239]. The data [3, 4] suggest a broad resonance, which could be due to the exchange of nearly degenerate h_2 and A [238, 240].

We consider a CP-conserving 2HDM of type I in the decoupling limit [241], where the second doublet has a mass ~ 750 GeV. We work in the "Higgs basis", where $H_1 = [0, (v + h_1)/\sqrt{2}]$ denotes the doublet which gets a vacuum expectation value $v \simeq 246$ GeV, and which has Standard Model Yukawa couplings. The second doublet $H_2 = [H^+, (h_2 + iA)/\sqrt{2}]$ does not couple to Standard Model fermions, except for a LFV Yukawa to $\tau^\pm\mu^\mp$. The physical Higgs bosons are the CP-even h and H, the pseudoscalar A and the charged Higgses $H^\pm$. In the decoupling limit, the light h is almost aligned on the vev, making it the Standard-Model-like Higgs of 125 GeV.

In section 5.1 we show how to enhance the H and A couplings to gluons and photons, by introducing new vector-like charged fermions, while respecting the bounds from electroweak precision tests and h signal strengths. We neglect the charged Higgs H^+ because it contributes little to $H, A \to \gamma\gamma$. A small mixing with h_2 allows the LFV decay $h \to \tau^\pm\mu^\mp$, as discussed in section 5.2. In section 5.3, we demonstrate that one can accommodate the 750 GeV excess from the decays of H and A, in agreement with the LFV excess. Finally, we give some final comments in section 5.4.

5.1 Two Higgs doublets coupling to extra matter

In this section we neglect the misalignment between the CP-even mass basis, and the "Higgs" basis, and focus on the Higgs couplings to new fermions. That is, we consider the limit where the Standard Model Higgs boson h is identified with h_1, and the second Higgs doublet H_2 does not couple to the Standard Model, except for its gauge interactions. Therefore, $H = h_2$ and A cannot decay to Standard Model particles at tree-level. We include the misalignment in the following section, in order to obtain $h \to \tau^\pm\mu^\mp$.

In order for H and/or A to play the role of the 750 GeV resonance, we need to introduce a large effective coupling to $\gamma\gamma$, as well as to gg, in the hypothesis that the resonance is produced via gluon fusion. If the production is dominated by quarks, that have a smaller parton density function, one needs an even larger coupling to $\gamma\gamma$. We will discuss quantitatively these two possibilities in section 5.3 .

To provide an explicit realization for such effective couplings, we introduce two vector-like fermions, that transform under $SU(3)_c \times SU(2)_w \times U(1)_Y$ as $D \sim (R_c, 2, Q + 1/2)$ and $S \sim (R_c, 1, Q)$, with interactions

$$-\mathcal{L} = M_D \overline{D_L} D_R + M_S \overline{S_L} S_R + \lambda_i^D \overline{D_L} H_i S_R + \lambda_i^S \overline{S_L} H_i^\dagger D_R + h.c. \,. \tag{5.1.1}$$

The state of electric charge $Q + 1$ has mass M_D and no Yukawa couplings. The two states of charge Q couple to the Higgs doublets, and their mass matrix is non-diagonal because of the vev of H_1. We will denote the mass eigenvalues by $M_1 \leq M_2$. Note that, in order to induce the couplings $H\gamma\gamma$ and $A\gamma\gamma$ (and analogously for gluons), one needs either $\lambda_1^S \lambda_2^D \neq 0$ or $\lambda_1^D \lambda_2^S \neq 0$. This is illustrated diagrammatically in Fig. 5.1, and it amounts to generate the effective operator $H_2^\dagger H_1 F_{\mu\nu} F^{\mu\nu}$ via a fermion loop.

The couplings $\lambda_1^{D,S}$ are constrained as they contribute to the h-decays into $\gamma\gamma$ and gg, as well as by the precision electroweak parameters S and T. Indeed, vector-like charged fermions were employed in

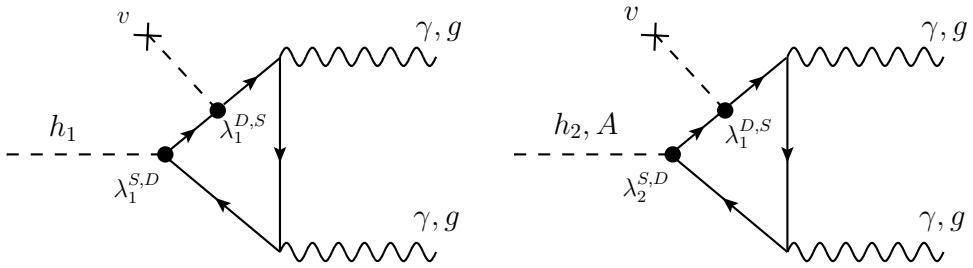

Figure 5.1: The contributions of two vector-like fermions, a doublet D and a singlet S, to the effective couplings between the Higgs doublets and two photons or gluons. As we work in the basis where the vev resides in H_1, one finds that the h_1 couplings (left-hand side) are proportional to $\lambda_1^D\lambda_1^S$, while the h_2 and A couplings (right-hand side) are proportional to either $\lambda_1^S\lambda_2^D$ or $\lambda_1^D\lambda_2^S$.

the past to explain the transient excess in the $h \to \gamma\gamma$ channel, see e.g. [189, 242]. A detailed analysis of the allowed parameter space is provided in Ref. [11]. Here we describe two illustrative cases:

(1) Degenerate fermion masses, $M_1 = M_2$. This is the case for $M_D = M_S$ and $\lambda_1^S = -\lambda_1^D$. Choosing $M_{1,2} = 1$ TeV, $R_c = 3$ and $|Q| \leq 2$, one finds an upper bound $(\lambda_1^S v)/(\sqrt{2}M_1) \lesssim 0.25$. This bound is determined essentially by the T parameter, that is proportional to $N_c \equiv \dim(R_c)$ and independent from Q. When $|Q| > 2$ a stronger bound comes from the Higgs signal strengths. For $R_c = 8$ and $|Q| \leq 3$, one needs $(\lambda_1^S v)/(\sqrt{2}M_1) \lesssim 0.12$. In this case the bound comes from the hgg coupling.

(2) One vanishing Yukawa coupling, e.g. $\lambda_1^D = 0$. This pattern strongly suppresses the correction to the couplings $h\gamma\gamma$ and hgg, because, in the limit of heavy fermions, they are proportional to $\lambda_1^D\lambda_1^S$. However, an upper bound on λ_1^S still exists, coming from the T parameter, $(\lambda_1^S v)/(\sqrt{2}M_1) \lesssim 0.35$ (0.25) for $R_c = 3$ (8) and $M_1 = 1$ TeV. Note that T does not depend on the hypercharge, therefore it turns out that one can take it very large, say $Q \sim 10$, without violating the constraints.

Let us now turn to the heavy Higgs doublet H_2. Its couplings to the fermion mass eigenstates are easily derived [11] in terms of the parameters in the Lagrangian of Eq. (5.1.1). Then, one can compute the decay width into two photons for the scalar H and the pseudoscalar A. The result is particularly compact in the limit $M_H \ll 2M_{1,2}$, since in this case the loop form factor $A_{1/2}[M_H^2/(4M_i^2)]$ is the same for both fermions in very good approximation, $A_{1/2}(0) = 4/3$. Similarly, for A we use the loop form factor $\tilde{A}_{1/2}(0) = 2$. Then, one obtains

$$\frac{\Gamma(H \to \gamma\gamma)}{M_H} = \frac{\alpha^2}{256\pi^3}\left|\frac{2vM_H}{3M_1M_2}N_cQ^2(\lambda_2^D\lambda_1^S + \lambda_2^S\lambda_1^D)\right|^2 , \tag{5.1.2}$$

$$\frac{\Gamma(A \to \gamma\gamma)}{M_A} = \frac{\alpha^2}{256\pi^3}\left|\frac{vM_A}{M_1M_2}N_cQ^2(\lambda_2^D\lambda_1^S - \lambda_2^S\lambda_1^D)\right|^2 , \tag{5.1.3}$$

In the same approximation, the widths into two gluons read

$$\frac{\Gamma(H \to gg)}{M_H} = \frac{\alpha_s^2}{32\pi^3}\left|\frac{2vM_H}{3M_1M_2}C(R_c)(\lambda_2^D\lambda_1^S + \lambda_2^S\lambda_1^D)\right|^2 , \tag{5.1.4}$$

$$\frac{\Gamma(A \to gg)}{M_A} = \frac{\alpha_s^2}{32\pi^3}\left|\frac{vM_A}{M_1M_2}C(R_c)(\lambda_2^D\lambda_1^S - \lambda_2^S\lambda_1^D)\right|^2 , \tag{5.1.5}$$

where $C(R_c)$ is the index of the color representation. Note that the ratio of H-rates over A-rates is given by a factor $(2|\lambda_2^D\lambda_1^S + \lambda_2^S\lambda_1^D|)^2/(3|\lambda_2^D\lambda_1^S - \lambda_2^S\lambda_1^D|)^2$.

For definiteness, consider the case (2) described above, $\lambda_1^D = 0$, and take $M_H \simeq M_A \simeq 750$ GeV. Then, one obtains

$$\frac{\Gamma_{A\gamma\gamma}}{M_A} \simeq \frac{9}{4}\frac{\Gamma_{H\gamma\gamma}}{M_H} \simeq 1.4 \cdot 10^{-6} \left(\frac{1\ \text{TeV}}{M_2}\right)^2 \left(\frac{N_c}{3}\right)^2 \left(\frac{Q}{2}\right)^4 \left(\frac{\lambda_2^D}{3}\right)^2 , \tag{5.1.6}$$

$$\frac{\Gamma_{Agg}}{M_A} \simeq \frac{9}{4}\frac{\Gamma_{Hgg}}{M_H} \simeq 4.4 \cdot 10^{-6} \left(\frac{1\ \text{TeV}}{M_2}\right)^2 \left(\frac{C(R_c)}{1/2}\right)^2 \left(\frac{\lambda_2^D}{3}\right)^2 , \tag{5.1.7}$$

where we chose $(\lambda_1^S v)/(\sqrt{2}M_1) \simeq 0.35$, that is the largest value allowed by the T parameter for $R_c = 3$. In the case of a colour octet, $N_c = 8$ and $C(R_c) = 3$, there is a slightly stronger upper bound, $(\lambda_1^S v)/(\sqrt{2}M_1) \simeq 0.25$: therefore, one gains a factor ~ 3 in $\gamma\gamma$ and a factor ~ 20 in gg.

Note that one can reproduce the same rates with smaller Yukawa couplings: taking N pairs of vector-like fermions, all with equal charges and coupling λ_2^D, the rates scale as $(N\lambda_2^D)^2$. From a theoretical point of view, it may be more justified to introduce several vector-like fermions, but with charges related to the Standard Model ones, such as one or more vector-like families, composed of t, b and τ partners. Adding over their contributions one could obtain a qualitative similar effect.

One should also remark that the heavy fermion loops also induce decays of H and A to $Z\gamma$, ZZ and WW, with width of the same order as (or slightly smaller than) for $\gamma\gamma$. However, the upper bounds from the 8 TeV LHC are weaker than the one on $\gamma\gamma$, as discussed e.g. in Ref. [243]. Therefore, they are presently unconstraining. At run 2, the better perspective appears to be the observation of the $Z\gamma$ channel.

5.2 The $\tau^\pm\mu^\mp$ decay of the 125 GeV Higgs boson

Flavour-changing Higgs couplings are generic in the 2HDM, but their effects are not seen in low energy precision experiments searching for lepton or quark flavour change. So a discrete symmetry, which forbids flavour-changing Yukawa couplings, is usually imposed on the 2HDM. To allow for LFV h decays, without generating undesirable flavour-changing processes, we suppose that our 2HDM almost has a discrete symmetry: all the Standard Model fermions have the usual Yukawa couplings to H_1 ("type I" model), and the only two couplings of H_2 to Standard Model fermions are the $\mu\tau$ LFV ones,

$$\mathcal{L} = -\rho_{\tau\mu}\overline{L_\tau}H_2\mu_R - \rho_{\mu\tau}\overline{L_\mu}H_2\tau_R + \text{h.c.} \tag{5.2.1}$$

(see Refs. [202, 244] for a more formal analysis). Recall that the diagonalisation of the fermion mass matrices diagonalises the Yukawa couplings of H_1, which carries the vev. Therefore, the LFV couplings are attributed, by definition, to the doublet H_2 with zero vev. Note that Eq. (5.2.1) amounts to assume that μ and τ numbers are not conserved, while electron number remains a good symmetry at the renormalizable level. Such symmetry has to be slightly broken to allow for viable neutrino masses. In general, this breaking will propagate radiatively to the H_2 Yukawa couplings, however the size of this effect can be sufficiently small, as it strongly depends on the specific neutrino mass model. In section 5.3 we will also consider a scenario where H_2 is produced from an additional Yukawa coupling to b quarks, that can be added without phenomenological problems.

The CP-even mass eigenstates h and H are misaligned with respect to the vev by an angle that is commonly parametrized as $\beta - \alpha$:

$$\begin{aligned} h &= \sin(\beta-\alpha)h_1 + \cos(\beta-\alpha)h_2 , \\ H &= \cos(\beta-\alpha)h_1 - \sin(\beta-\alpha)h_2 . \end{aligned} \tag{5.2.2}$$

In the decoupling limit [241, 244], $\sin(\beta-\alpha) \simeq 1$ and

$$\cos(\beta-\alpha) = -\frac{\Lambda_6 v^2}{M_H^2} , \tag{5.2.3}$$

where the Higgs potential contains a term $\Lambda_6 H_2^\dagger H_1 H_1^\dagger H_1 + h.c.$, in the basis where H_1 has no vev. The coupling of h to $\tau^\pm\mu^\mp$ is therefore proportional to $\cos(\beta-\alpha)\rho$, and one obtains

$$BR(h\to\tau^\pm\mu^\mp) \simeq \frac{m_h}{16\pi\Gamma_h}\cos^2(\beta-\alpha)\Big(|\rho_{\tau\mu}|^2+|\rho_{\mu\tau}|^2\Big)\ . \tag{5.2.4}$$

The CMS best-fit is $BR(h\to\tau^\pm\mu^\mp)=0.0084$ [126], which gives

$$\cos(\beta-\alpha)(|\rho_{\tau\mu}|^2+|\rho_{\mu\tau}|^2)^{1/2} \simeq 0.0037\ , \tag{5.2.5}$$

where the width was taken at its Standard Model value, $\Gamma_h \simeq 4.1$ MeV.

In the 2HDM, the CMS excess in $h\to\tau^\pm\mu^\mp$ is consistent with the current upper bound $BR(\tau\to\mu\gamma)\leq 2.6\times10^{-7}BR(\tau\to\mu\nu\bar{\nu})$ [245,246]. However, the extra fermions which enhance $H,A\to\gamma\gamma$ as in Eqs. (5.1.2)-(5.1.3), will also enhance the rate for $\tau\to\mu\gamma$ [201]: if a neutral Higgs is exchanged between its $\gamma\gamma$ and $\bar{\tau}\mu$ vertices, and one of the photons connects to the lepton line, a diagram for $\tau\to\mu\gamma$ is obtained. Such diagrams with a top loop were calculated in the 2HDM in [247]. From their results, the combined contribution of H and A can be estimated, for $M_1\simeq M_2$ and $\lambda_1^D=0$, as

$$\frac{m_\tau}{v^2}A_L \simeq \frac{e\alpha}{128\pi^3}\frac{v}{\sqrt{2}M_1^2}N_c Q^2\lambda_2^D\lambda_1^S\rho^*_{\tau\mu}\ , \tag{5.2.6}$$

where the experimental bound is $384\pi^2(A_L^2+A_R^2)\leq 2.6\times10^{-7}$. With the definition of Yukawa couplings given in Eq. (5.1.1), it turns out that choosing a large λ_2^D (λ_2^S) leads to a destructive (constructive) interference among the H and A amplitudes. This was taken into account in Eq. (5.2.6), where the difference in loop integral functions was chosen $\simeq 1/2$, as given in [247] for $M_1^2/M_H^2\simeq 2$. A similar estimate can be made for A_R. We neglect the h contribution to $\tau\to\mu\gamma$, because its coupling to $\gamma\gamma$ is not enhanced, see scenario (2) in section 5.1. So the Babar-Belle bound on $\tau\to\mu\gamma$ could be satisfied for

$$\frac{N_c}{3}\left(\frac{Q}{2}\right)^2\frac{\lambda_2^D}{3}\lambda_1^S\rho_{\tau\mu}\lesssim 0.07\ , \tag{5.2.7}$$

which sets a lower bound on $\cos(\beta-\alpha)$ when combined with Eq. (5.2.5):

$$\cos^2(\beta-\alpha)\gtrsim 0.003\left(\frac{N_c}{3}\right)^2\left(\frac{Q}{2}\right)^4\left(\frac{\lambda_2^D}{3}\right)^2\left(\lambda_1^S\right)^2\ . \tag{5.2.8}$$

If the masses and couplings were purposefully tuned, it might be possible to suppress the $\tau\to\mu\gamma$ amplitude even further, so we will consider Eq. (5.2.8) to be a preference but not an exclusion.

5.3 Reproducing the 750 GeV excess

Let us discuss the decay widths of H and A as a function of the Higgs mixing $\cos(\beta-\alpha)$ and of the LFV couplings $\rho_{\mu\tau,\tau\mu}$.

The mixing does not affect the couplings of the pseudoscalar A, for which the discussion of section 5.1 applies. On the other hand, the misalignment parametrised in Eq. (5.2.2) implies that the Yukawa couplings to h and H become

$$\lambda_h^{D,S}=\sin(\beta-\alpha)\lambda_1^{D,S}+\cos(\beta-\alpha)\lambda_2^{D,S}\ ,\qquad \lambda_H^{D,S}=\cos(\beta-\alpha)\lambda_1^{D,S}-\sin(\beta-\alpha)\lambda_2^{D,S}\ . \tag{5.3.1}$$

The H decay widths into photons and gluons are obtained by replacing $\lambda_2^{D,S}$ with $\lambda_H^{D,S}$ in Eqs. (5.1.2) and (5.1.4). Similarly, for the corrections to $h\to\gamma\gamma$ and $h\to gg$ due to the heavy fermions, one has to replace $\lambda_1^{D,S}$ with $\lambda_h^{D,S}$. In addition, all the h couplings to the Standard Model particles n's are modified, $g_{hn\bar{n}}=\sin(\beta-\alpha)g^{SM}_{hn\bar{n}}$. Since several Higgs signal strengths have been tested at LHC-8 TeV with 10% precision, the Higgs mixing is bounded from above

$$\cos^2(\beta-\alpha)\lesssim 0.1\ . \tag{5.3.2}$$

This is consistent with Eq. (5.2.8). As discussed in section 5.1, the corrections to $h \to \gamma\gamma$ and $h \to gg$ may lead to a slightly stronger upper bound on $\cos(\beta-\alpha)$, if the couplings $\lambda_2^{D,S}$ are very large. However, such bound drops for $\lambda_1^S \cdot \lambda_1^D \to 0$, see case (2) in section 5.1. Finally, the contributions to S and T from scalar loops are small in the 2HDM close to the decoupling limit [202, 248], as we explicitly checked for our choice of the parameters.

The mixing has an important effect on the total width of H, since the latter can decay to Standard Model particles n's, with coupling $g_{Hn\bar{n}} = \cos(\beta-\alpha) g^{SM}_{hn\bar{n}}$. The dominant contributions read, at the tree level,

$$\begin{aligned} \frac{\Gamma(H \to t\bar{t}, W^+W^-, ZZ)}{M_H} &\simeq \frac{\cos^2(\beta-\alpha)}{8\pi\, v^2}\left[3m_t^2 + \frac{M_H^2}{2} + \frac{M_H^2}{4}\right] \\ &\simeq 0.33\cos^2(\beta-\alpha)\ , \end{aligned} \tag{5.3.3}$$

where, for the latter numerical estimate, we used the accurate values of the widths for $M_H \simeq 750$ GeV, as given in Ref. [249]. Here we neglected the channel $H \to hh$, because the corresponding trilinear scalar coupling may be suppressed, by conveniently choosing the scalar potential parameters. Recall that the cross-section for $pp \to H \to \gamma\gamma$ is proportional to $\Gamma(H \to gg)/\Gamma_H^{tot}$, where the numerator corresponds to the assumed dominant H production mode, and the denominator is the total width of H. Therefore, the contribution of H to the excess degrades as soon as $\Gamma(H \to gg)/M_H \lesssim 0.33\cos^2(\beta-\alpha)$.

The LFV couplings $\rho_{\mu\tau,\tau\mu}$ also open an additional decay channel for both H and A, with a width

$$\frac{\Gamma(H \to \tau^\pm\mu^\mp)}{M_H} \simeq \frac{\Gamma(A \to \tau^\pm\mu^\mp)}{M_A} \simeq \frac{1}{16\pi}\left(|\rho_{\tau\mu}|^2 + |\rho_{\mu\tau}|^2\right) \simeq \frac{3\cdot 10^{-7}}{\cos^2(\beta-\alpha)}\ , \tag{5.3.4}$$

where the last equality comes from Eq. (5.2.5).

One should also mention that the presently preferred width of the excess, $\Gamma \sim 45$ GeV, could be mimicked by two narrow resonances close in mass. Indeed, the mass split between H and A is given, in the decoupling limit, by $M_H^2 - M_A^2 \simeq \Lambda_5 v^2$, where the term $\frac{1}{2}\Lambda_5 (H_1^\dagger H_2)^2 + h.c.$ appears in the Higgs potential. This is naturally of the correct order of magnitude for $\Lambda_5 \simeq 1$. Note, however, that the H-mediated cross-section tends to be suppressed relatively to the A-mediated one by two factors: the additional Higgs width in Eq. (5.3.3), and the factor 4/9 from the loop form factors, see Eqs. (5.1.6)-(5.1.7).

Let us put all the constraints together to identify the possible windows of parameters that allow to reproduce the 750 GeV excess in agreement with the preferred $h \to \tau^\pm\mu^\mp$ rate. The resonant LHC total cross-section, in the crude zero-width approximation, reads

$$\sigma(pp \to H(A) \to \gamma\gamma) = \sum_i P_i \frac{\Gamma(H(A) \to i)\Gamma(H(A) \to \gamma\gamma)}{s\,\Gamma_{tot} M_{H(A)}}\ , \tag{5.3.5}$$

where $s = (13\text{ TeV})^2$, $M_{H(A)} \simeq 750$ GeV, and the P_i coefficients are the integrals for convoluting over parton densities, that define the parton luminosities for each species i:

$$\begin{aligned} P_{gg} &\equiv \frac{\pi^2}{8}\int_{\frac{M^2}{s}}^1 \frac{d\,x}{x} g(x) g(\frac{M^2}{x\,s}), \\ P_{\bar{q}q} &\equiv \frac{4\pi^2}{9}\int_{\frac{M^2}{s}}^1 \frac{d\,x}{x}\left[q(x)\,\bar{q}(\frac{M^2}{x\,s}) + \bar{q}(x)\,q(\frac{M^2}{x\,s})\right]. \end{aligned} \tag{5.3.6}$$

Consistency with the absence of resonances at 8 TeV favours i to be either gluons or bs, for which the luminosity is $P_{\bar{b}b} \simeq 14$ and $P_{gg} \simeq 2000$ (we used for Eq. (5.3.6) the latest pdfs from Ref. [250]).

We focus first on gluon-gluon fusion as the dominant production mechanism. This channel enjoys the largest parton density functions, so it is sufficient to have $\Gamma(H, A \to \gamma\gamma)/M_{H,A} \simeq 10^{-6}$ [237], as long as $\Gamma_{tot}^{H,A} \simeq \Gamma(H, A \to gg)$. However, the latter is loop-suppressed as shown in Eq. (5.1.7). The total cross-section for some choices of the parameters is shown in Fig. 5.2 as a function of $\cos(\beta-\alpha)$.

Note that for completeness and cross-check, we have also compared with the more elaborated invariant mass distribution $d\sigma/dM(gg \to H(A) \to \gamma\gamma)$ where $M \equiv \sqrt{\hat{s}}$ is the $\gamma\gamma$ invariant mass, that we have calculated taking into account the exact width dependence, and integrating this expression over an appropriate large range for M around the resonance. The numerical differences with the narrow-width approximation expression in Eq. (5.3.5) is at most 2-3 % for all the relevant parameter choices discussed below, as could be intuitively expected since the total width of either A or H remains in all cases sufficiently moderate with respect to the resonance mass, such that the narrow width approximation is justified a posteriori. We can envisage two scenarios:

(A) For both H and A to contribute significantly to the excess, both the tree-level widths in Eq. (5.3.3) and Eq. (5.3.4) should be small compared with $\Gamma(H, A \to gg)$. So the optimal value for the Higgs mixing is $\cos^2(\beta-\alpha) \simeq 10^{-3}$, that minimizes the sum of the tree-level widths. Then, to reach a cross-section of a few fbs one needs $\Gamma(H, A \to gg)\Gamma(H, A \to \gamma\gamma)/M_{H,A}^2 \gtrsim 5 \cdot 10^{-10}$. To reach this value for both H and A requires some stretch in the parameters, e.g. in Eqs. (5.1.2)-(5.1.5) one should take $R_c = 8$, $Q = 3$, $\lambda_2^S = -1$, $\lambda_2^D = 5$, $M_1 = M_2$ and $\lambda_1^S = -\lambda_1^D$ with the corresponding constraint $(\lambda_1^S v)/(\sqrt{2}M_1) \lesssim 0.12$. In addition, the amplitude for $\tau \to \mu\gamma$ in this scenario exceeds the indicative bound of Eq. (5.2.7) by about an order of magnitude.

(B) If one neglects the putative large width of the excess, the H contribution to the signal is no longer necessary. In the case of the pseudoscalar A, only the tree-level width in Eq. (5.3.4) competes with gluon fusion, therefore the signal can be maximized by taking the Higgs mixing as large as allowed by Standard Model constraints, $\cos^2(\beta-\alpha) \simeq 0.1$ (see Eq. (5.3.2)). Then, one can reach a cross-section of a few fb's as long as $\Gamma(A \to gg)\Gamma(A \to \gamma\gamma)/M_A^2 \gtrsim 3 \cdot 10^{-12}$, as realized with the reference values in Eqs. (5.1.6)-(5.1.7). The bound (5.2.8) from $\tau \to \mu\gamma$ is satisfied for these parameters.

Let us compare with the alternative possibility that the production of H and A is not dominated by gluon fusion, rather by $b\bar{b} \to H, A$. The parton density functions give a suppression of order 100 with respect to gluons, so that the excess requires $\Gamma(H, A \to \gamma\gamma)/M_{H,A} \gtrsim 2 \cdot 10^{-4}$ [237]. The advantage is that a Yukawa coupling $(\rho_b/\sqrt{2})\bar{b}(h_2 + i\gamma_5 A)b$ can easily overcome the other tree-level widths in Eq. (5.3.3) and Eq. (5.3.4),

$$\frac{\Gamma(H \to b\bar{b})}{\sin^2(\beta-\alpha)M_H} \simeq \frac{\Gamma(A \to b\bar{b})}{M_A} \simeq \frac{3\rho_b^2}{16\pi} \simeq 0.06\rho_b^2 \ . \tag{5.3.7}$$

Indeed, one can reproduce the preferred value $\Gamma \simeq 45$ GeV for $\rho_b \simeq 1$. Moreover, there is no constraint from dijet searches at 8 TeV, as the b-quark parton density function is very small. Therefore, one identifies the following scenario:

(C) When $\Gamma_{tot}^{H,A} \simeq \Gamma(H, A \to b\bar{b})$, both H and A contribute to the excess, as long as $\Gamma(H, A \to \gamma\gamma) \simeq 2 \cdot 10^{-4}$. Confronting with Eq. (5.1.6), one needs a pair of vector-like fermions with $R_c = 3$ and $Q = 7$, or $R_c = 8$ and $Q = 5$. Note that is difficult to avoid such large exotic charges by augmenting the number of multiplets in the loop, as the signal scales with Q^4. As discussed in section 5.1, such large Q can be compatible with Higgs decays and the S and T parameters, however the bound of Eq. (5.2.8) from $\tau \to \mu\gamma$ is exceeded by a factor of few.

The total cross-sections, combining both the gluon fusion and $b\bar{b}$ production channels, are shown in Fig. 5.3 as a function of $\cos(\beta-\alpha)$, for $Q = 5$ and other parameters as in Fig. 5.2. Here the cross-sections are calculated with the exact width dependence and integrating $d\sigma/dM(gg, b\bar{b} \to H(A) \to \gamma\gamma)$. In fact due to the dominant contribution of the $b\bar{b}$ decay to the total width Γ_{tot} in this case, the $b\bar{b}$ production channel largely dominates (for instance the gluon fusion process contributes to the total cross-section by about $\sim 10\%$ only for $R_c = 8$, and much less for $R_c = 3$). Note that in this case the discrepancy with the cross-sections in the narrow width approximation of Eq. (5.3.5) amounts to 7-8 %, for the parameter choices discussed above, that is roughly of order $\Gamma_{tot}^{H,A}/M_{H,A}$.

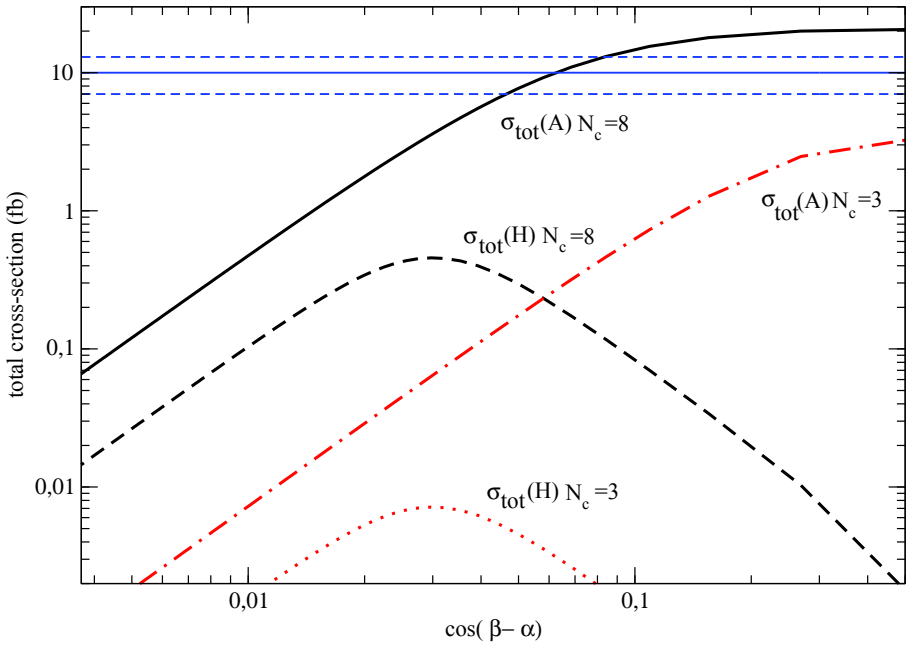

Figure 5.2: The total cross-section $\sigma(pp \to H(A) \to \gamma\gamma)$ in fb, assuming the gluon fusion production channel, as a function of $\cos(\beta - \alpha)$, for a pair of vector-like fermions in the color representation $R_c = 3$ or $R_c = 8$, as indicated. We fixed their charge, $Q = 2$, and their Yukawa couplings to H and A, $\lambda_2^D = 3$ and $\lambda_2^S = 0$. The horizontal band is the preferred cross-section at 1σ for the ATLAS excess [3, 4].

5.4 Final comments

Assuming that the diphoton excess at an invariant mass of 750 GeV was a physical signal and not a statistical fluctuation, we entertained for the exercise the possibilities that both the latter $\gamma\gamma$ excess and the $h \to \tau^\pm\mu^\mp$ excess are due to new physics. A minimal way to introduce (renormalisable) flavour violation and extra bosons to the Standard Model is to add a second Higgs doublet. Its $\tau \leftrightarrow \mu$ coupling may be connected to large $2-3$ mixing in the neutrino sector, in scenarios where the Yukawa couplings of charged leptons and neutrinos are related.

The neutral scalars H and A can play the role of the 750 GeV resonance, even though the strength of the excess in the early 13 TeV data is significantly larger than the one expected in the 2HDM alone. We take this as a hint that additional states close to the TeV are present in the underlying theory, with large Yukawa couplings to the second Higgs doublet. We have shown that a pair of vector-like fermions is sufficient to reproduce the right cross-section, and respect all other constraints. However, such fermions must have gauge charges larger than the Standard Model fermions: indicatively, for a Yukawa $\simeq 3$ and $R_c \leq 8$, one needs $|Q| \geq 2$ in scenarios (A) and (B), and $|Q| \geq 5$ in scenario (C), see section 5.3 . Alternatively, several pairs of fermions have to be introduced. These are important indications to constrain those well-motivated extensions of the Standard Model that predict vector-like fermions, such as top partners.

Were the heavy Higgses to have no couplings to Standard Model fermions, then $gg \to H, A \to \gamma\gamma$ is a natural discovery channel. However, to explain $h \to \tau^\pm\mu^\mp$, the heavy Higgses must interact with $\tau^\pm\mu^\mp$, and mixing is required between h and H. Both requirements gives Standard Model decay channels to H and A, which reduces $BR(H, A \to gg, \gamma\gamma)$; nonetheless we find three scenarios that fit both excesses. In addition, the mixing must respect both a lower bound to reproduce the LFV excess,

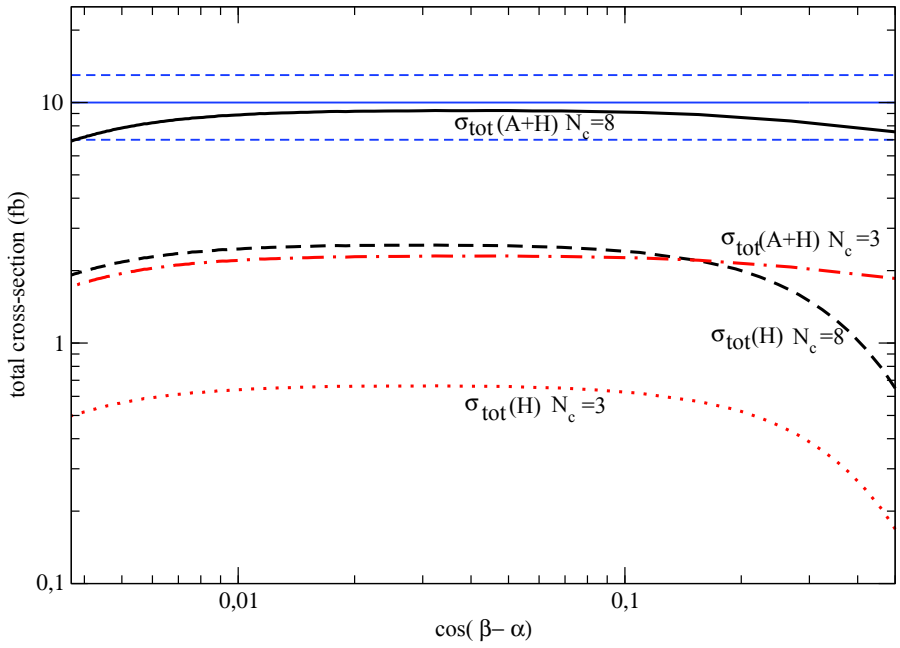

Figure 5.3: The same as in Fig. 5.2, but adding a $b\bar{b}$ production channel with $\rho_b = 1$, see Eq. (5.3.7), and increasing the vector-like fermion charge, $Q = 5$. Here we displayed the cross-section for H only, as well as the cross-section for H plus A.

and an upper bound to protect the 125 GeV Higgs couplings: $10^{-3} \lesssim \cos(\beta - \alpha) \lesssim 0.3$.

The decay $\tau \to \mu\gamma$ is a particular challenge for this model, because the heavy Higgses couple to $\tau^{\pm}\mu^{\mp}$ and have an enhanced coupling to $\gamma\gamma$. In combination, these interactions give a "Barr-Zee" contribution to $\tau \to \mu\gamma$ which is dangerously large. By choosing the Yukawas to obtain destructive interference between A and H, we find that at least two of the scenarios are compatible with the current experimental limit on $\tau \to \mu\gamma$.

Of course, the $\gamma\gamma$ excess at 750 GeV has now disappeared but we assumed for the exercise that it was not the case. Indeed, the framework that we have presented is general enough to be applied in a more general context. For instance, it can be generalised to a diphoton resonance with a larger mass than 750 GeV and with a smaller cross section. The latter point would relax a lot of constraints such that our model appears as a benchmark and it proves that it is possible to induce a large $\gamma\gamma$ cross section. If another diphoton excess appear in the future, our model could be an interesting possibility. Also, one should not forget that it explains the $h \to \tau\mu$ decay even if there is no diphoton excess.

Finally, let us make some comments on possible outlooks for this work. Our model could also be extended by considering VL families that respect the T parameter. Indeed in the above construction, we have considered one VL singlet and one VL doublet mixing through their Yukawa couplings to the first Higgs doublet H_1. This minimal field content was inspired from chapter 4 as it contains only four multiplets. An interesting possibility, would be to consider a less minimal field content but with a greater theoretical motivation. For instance, one can consider one VL doublet $D \sim (R_c, 2Q + 1/2)$ and two VL singlets $S_1 \sim (R_c, 1, Q + 1)$ and $S_2 \sim (R_c, 1, Q)$ that is six multiplets. In this way, there is a custodial limit where the Yukawa couplings to H_1 do not vanish. Then, with this field content, the constraints coming from the EWPT are relaxed and it is easier to reproduce an excess. Note that the above VL family could also be relevant in the context of a SM-like Higgs sector.

In general, it is interesting to try to explain different experimental anomalies at the same time.

Clearly, this is a different phenomenological approach to new physics than the one of chapter 4 where we rather consider the consequences of extending the SM with new states.

Part III

Composite Higgs models and their ultra-violet completions

In the precedent part of the manuscript, we have focussed on minimal extensions of the SM. The latter are valid at low energy that is at the EW scale, and by minimal we intend extensions where only few light states are added to the SM. By hypothesis, these states are the low energy manifestation of a more complete UV theory where the other heavy states are decoupled from the EW scale. Then, in order to remain as model independent as possible, we did not specify the UV completion of these minimal extensions. However, such a UV completion is not just theoretically relevant at high energy. Indeed, the symmetries of the UV completion manifest at low energy and constrain the effective theory such that the parameter space of the latter may be reduced when interpreted in a UV framework.

In this third part, we rather follow a different approach to new physics and study more complete UV theories. This second approach is less model independent but more justified from a theoretical point of view. Our focus will be on composite Higgs models that bring a solution to the hierarchy problem as discussed in section 1.6. These models allow to stabilise the EW scale by invoking the presence of a new strong sector that condensates at low energy and generate a composite pNGB Higgs. In this picture, the mass of the Higgs boson is protected from large radiative corrections by the shift symmetry associated with the Goldstone nature of the Higgs.

We first remind the basic ideas behind a composite Higgs in chapter 6. In particular, we discuss how a composite Higgs can solve the naturalness problem of the EW scale. To that end, we introduce an effective description of CHMs which is based only on the global symmetries of the model. This effective description has some limitations and in chapter 7, we introduce four dimensional UV completions of CHMs. The latter are based on a hypercolour gauge symmetry that becomes strongly coupled at low energy and condensates to form a composite Higgs. We classify the different minimal possibilities and outline the most relevant one. In the sequel, in chapters 8 and 9 we present in great details respectively the EW and the coloured sector of the most minimal UV completion of composite Higgs models. We compute among other things, the masses of the lightest mesonic resonances present in the spectrum using the non-perturbative techniques of the NJL model. Finally, we present some prospects for the UV completions of composite Higgs models in chapter 10. We discuss in particular the possible estimation of the baryonic masses in the NJL framework.

Chapter 6

Effective models of composite Higgs

This chapter is an introduction to composite Higgs models. All of the discussion focuses on effective realisations of composite Higgs models which are based on considerations about the global symmetries of the models and not on a possible underlying gauge symmetry. This is analogous to the chiral Lagrangian of QCD which is a simplified and effective description of QCD at low energy and is based only on the chiral symmetry but not on the gauge $SU(3)_c$ symmetry. As the effective approach to CHMs is not the aim of this manuscript, we present only the most relevant features in this chapter (see e.g. Refs. [251, 252] for details).

We first present in section 6.1 the mains ideas behind this kind of models and show how the naturalness problem of the EW scale can be solved within this framework. Then, in section 6.2 we discuss more deeply the possibility of a composite Higgs and in particular its pNGB nature. We present the minimal composite Higgs model (MCHM) based on the pattern of symmetry breaking $SO(5)/SO(4)$ and derive the deviations that appear in the Higgs couplings to the SM gauge bosons. In section 6.3, we present the mechanism of partial compositeness which allows to generate a mass for the SM fermion and derive the deviations appearing in the Higgs couplings to SM fermions. Next, in section 6.4, we present the breaking of the EW symmetry in the composite Higgs context, that is, we compute the Higgs potential generated from the linear couplings between the top quark and its partners. Finally, we give some concluding remarks in section 6.5.

6.1 Naturalness of the electroweak scale in composite Higgs models

The Higgs is a scalar boson and all of the other known particles of this kind are QCD bound states. Thus, it is quite legitimate to ask if the same could be true for the Higgs. Clearly, QCD can not be responsible of the formation of the Higgs as the mass of the QCD resonances are close to the confinement scale, that is, close to $\Lambda_{QCD} \sim 1$ GeV $\ll m_h \simeq 125$ GeV. Then, if we want to realise this possibility, one should invoke the presence of a new strong dynamics that condensates and forms a Higgs boson as a bound state. The above argument gives a strong motivation in favour of composite Higgs models. However, this is not the main one which rather comes from the hierarchy (naturalness) problem of the EW scale and has been discussed on general grounds in section 1.6.

Indeed, suppose that the Higgs is a composite object, a bound state resulting from the condensation of a new strong dynamics. Then rather than being a point-like particle as in the SM, it has a finite geometric size l_H. The resulting confinement scale $m_* = 1/l_H$ is of the TeV order. In that case, the Higgs receives only low energy radiative contributions to its mass, that is, the Higgs is not sensitive to contributions above the compositeness scale m_* as in this energy range, the dynamical degrees of freedom are not the composite resonances but rather the elementary fields charged under the strong dynamics. For the above mechanism to work, it is essential that the Higgs size or equivalently the scale of confinement is itself natural that is, there should be no naturalness problem to put m_* at the TeV scale.

In addition, the composite Higgs can be naturally lighter than the other strong resonances if it emerges as a pNGB. This is similar to the pions in QCD which have a mass $m_\pi \sim 100$ MeV $\ll m_\rho \simeq 0.8$ GeV. The pNGB Higgs is associated with a global symmetry G spontaneously broken by

the condensation of the strong sector down to a subgroup H. This breaking occurs at a scale f which is the equivalent of the pion decay constant F_π. The pattern of global symmetry breaking $G \to H$ leads to $n = dim(G) - dim(H)$ NGBs. Suppose now that we gauge a subgroup $H_0 \subset G$ such that $H_1 = H \cap H_0$ is the unbroken gauge group. Then among the n NGBs, $n_0 = dim(H_0) - dim(H_1)$ are eaten to give a mass to the gauge bosons associated to H_0. The remaining $n - n_0$ are pNGBs.

In the above picture, both SM gauge bosons and fermions are elementary in opposition with the composite nature of the Higgs and the other strong resonances. In particular, the SM gauge fields are associated to H_0. For simplicity we consider only the EW part of the SM gauge group that is $H_0 = G_{SM} = SU(2)_L \times U(1)_Y$. In order to have a composite pNGB Higgs, one requires two basic conditions: (i) the SM gauge group can be embedded in the unbroken subgroup H ($G_{SM} \subset H$) and (ii) the coset G/H contains at least one $SU(2)_L$ doublet that can be identified with the Higgs doublet.

If the above two conditions are realised, G_{SM} is unbroken at least at tree-level and the Higgs doublet is one of the pNGBs living in the coset G/H. Its potential vanishes at tree-level as a consequence of the Goldstone symmetry. As G is in fact explicitly broken by the couplings between the SM gauge fields and the strong sector, loops of SM gauge bosons will generate a Higgs potential. In addition, coupling the SM fermions to the strong sector generate another contribution to the Higs potential. This loop-induced potential can in principle break the EW symmetry (see section 6.4) and generates a non-zero Higgs mass.

In this way, the EW scale v is determined dynamically from the details of the Higgs potential and can be smaller than the scale of spontaneous breaking f. This is different from technicolour theories [253, 254] where there is no gap between v and f, as in that cases G_{SM} is partly embedded in H such that the spontaneous breaking of the global symmetry at the scale f also breaks the EW symmetry [1]. In composite Higgs models, there is a gap between between the scale of the composite NGBs f and the EWSB scale v. More precisely, there is a misalignment angle θ which parametrises the difference between the alignment of the strong condensate breaking G toward H and the alignment of the Higgs vev breaking the EW symmetry. This misalignment is constrained to be small ie $\langle\theta\rangle \ll 1$ which leads to the condition

$$\xi \equiv \frac{v^2}{f^2} = \sin^2\langle\theta\rangle \ll 1 \ , \tag{6.1.1}$$

where the ratio $\xi = (v/f)^2$ is determined by the orientation of G_{SM} inside G with respect to H. This is the mechanism of misalignment and the degree of misalignment as we will see sets the size of the corrections to all precision observables.

In the above composite Higgs framework, as a consequence of the Goldstone symmetry, the Higgs is lighter than the other strong resonances. By naive dimensional analysis, the mass scale of the strong resonances is $m_* \sim g_* f$ where $1 \lesssim g_* \lesssim 4\pi$ is a generic coupling that belongs to the strong sector. The Higgs gets instead a much lighter mass $m_h \sim g_{SM} f$ where $g_{SM} \lesssim 1$ is a generic SM coupling that explicitly breaks the global symmetry G. In the limit where $f \to \infty$ ($\xi \to 0$) with fixed v, the Higgs stays light at the EW scale while the other strong resonances becomes infinitely heavy. In this decoupling limit, the corrections to all precision observables and the deviations in the Higgs couplings due to the pNGB nature of the Higgs also disappear. Then, the pNGB Higgs may behave like an elementary one and all of the strong resonances can be decoupled from the EW scale. However, in this decoupling limit, the higgs mass should be fine-tuned and the hierarchy problem is not anymore solved. Then, one should accommodate between a small f where there is a small fine-tuning and a large f where all of the Higgs couplings and precision measurements are SM-like.

6.2 The minimal composite Higgs model

In this section, we present some aspects that follow from the NGB nature of the Higgs. We study in particular one effective realisation of the composite Higgs paradigm based on the coset $SO(5)/SO(4)$. This is the minimal composite Higgs model (MCHM) [255] from the effective point of view. The aim is to become more familiar with the predictions of CHMs as we will later consider in details a UV completion of the next-to minimal CHM [256] in chapters 8, 9 and 10.

[1] In technicolour theories, the Higgs is not a pNGB but potentially one of the lightest scalar resonances.

Let us now consider the minimal possible composite Higgs model for which the strongly interacting sector has a global symmetry $G = SO(5) \times U(1)_x$ spontaneously broken down to $H = SO(4) \times U(1)_x$. As discussed in section 6.1, in CHMs the SM gauge group is embedded in the unbroken global symmetry H. The embedding is simple as $SO(4)$ is isomorphic to $SU(2)_L \times SU(2)_R$ (see section 1.3 and 6.5) which leads to the relation $Y = T^3_R + x$. Note that the custodial symmetry is also embedded in a trivial way into H. The coset $G/H = SO(5)/SO(4)$ implies four NGBs transforming in the fundamental of $SO(4)$ or equivalently as a complex doublet H of $SU(2)_L$. Under a $SU(2)_R$ transformation, the Higgs doublet H mixes with its conjugate $\tilde{H}$ and $\Phi = \left(\tilde{H} \quad H\right)/\sqrt{2}$ transforms as a bidoublet of $SU(2)_L \times SU(2)_R$.

We now derive the effective action that encodes the interactions between the NGBs and the SM elementary fields. More precisely, we derive the interactions between the composite Higgs boson and the SM gauge fields. We postpone to section 6.3 the case of the SM fermion couplings to the composite Higgs. The four NGB leaving in the coset $SO(5)/SO(4)$ can be parametrised as

$$\Sigma(x) = \Sigma_0 e^{\Pi(x)/f} \ , \qquad \Pi(x) = -iT^{\hat{A}} h^{\hat{A}}(x)/\sqrt{2} \ , \qquad \Sigma_0 = (0,0,0,0,1) \ , \tag{6.2.1}$$

where $T^{\hat{A}}$ are the broken generators associated to the coset space and Σ_0 is the vacuum. An explicit basis for the $SO(5)$ generators can be found in Ref. [251]. Using this explicit form of the generators, the field Σ can be written as

$$\Sigma = \frac{\sin(h/f)}{h}\left(h_1, h_2, h_3, h_4, h\cot(h/f)\right) \ , \qquad h \equiv \sqrt{(h^{\hat{A}})^2} \ , \tag{6.2.2}$$

Let us assume for the moment that the full global symmetry G is gauged. At the quadratic level, in momentum space, the most general $SO(5) \times U(1)_x$-invariant Lagrangian is

$$\mathcal{L} = \frac{1}{2} T^{\mu\nu}\left[\Pi_0^X(q^2) X_\mu X_\nu + \Pi_0(q^2) Tr[A_\mu A_\nu] + \Pi_1(q^2)\Sigma A_\mu A_\nu \Sigma^T\right] \ , \tag{6.2.3}$$

where X_μ and $A_\mu = A^A_\mu T^A + A^{\hat{A}}_\mu T^{\hat{A}}$ are the $U(1)_x$ and $SO(5)$ gauge bosons [T^A are the unbroken generators associated to $SO(4)$]. As $SO(5)$ is by definition only spontaneously broken and not explicitly, the Lorentz structure of the above equation is transverse ($T^{\mu\nu} = \eta^{\mu\nu} - q^\mu q^\nu/q^2$), reflecting the conservation of the $SO(5)$ current. Our goal is to derive the Higgs couplings to the SM gauge boson. We are not interested in the derivative Higgs interactions and consequently, the field Σ has been treated as a classical background field with vanishing momentum. Note that the strong dynamics has been integrated out in Eq. (6.2.3) and parametrised by the form factors Π_0^X and $\Pi_{0,1}$. Note also that we restrict to the quadratic order in the SM gauge fields as we want to make a comparison with the SM prediction that is with the couplings c^{SM}_{hVV} and c^{SM}_{hhVV} of Eq. (1.2.5).

Expanding at first order around the vacuum ($\Sigma = \Sigma_0 + \cdots$), we obtain

$$\mathcal{L} = \frac{1}{2} T^{\mu\nu}\left[\Pi_0^X(q^2) X_\mu X_\nu + \Pi_A(q^2) A^A_\mu A^A_\nu + \Pi_{\hat{A}}(q^2) A^{\hat{A}}_\mu A^{\hat{A}}_\nu\right] \ , \tag{6.2.4}$$

where the form factors factors associated to the unbroken and broken generators are respectively given by $\Pi_A = \Pi_0$ and $\Pi_{\hat{A}} = \Pi_0 + \Pi_1/2$. Assuming that we are in the large N limit (large number of hypercolours), the two point functions can be written as an infinite sum of narrow resonances (see section 2.4) as follows

$$\langle J^A_\mu J^B_\nu \rangle = T^{\mu\nu}\delta^{AB}\Pi_A(q^2) = (q^2\eta_{\mu\nu} - q_\mu q_\nu)\delta^{AB}\sum_n \frac{f^2_{\rho_n} M^2_{\rho_n}}{q^2 - M^2_{\rho_n}} \ , \tag{6.2.5}$$

$$\langle J^{\hat{A}}_\mu J^{\hat{B}}_\nu \rangle = T^{\mu\nu}\delta^{\hat{A}\hat{B}}\Pi_{\hat{A}}(q^2) = (q^2\eta_{\mu\nu} - q_\mu q_\nu)\delta^{\hat{A}\hat{B}}\left[\sum_n \frac{f^2_{A_n} M^2_{A_n}}{q^2 - M^2_{A_n}} + \frac{1}{q^2}\frac{f^2}{2}\right] \ , \tag{6.2.6}$$

Note that in the case of $\Pi_{\hat{A}}$,that is, the axial correlator, in addition to the axial resonances there is also a contribution from the NGBs which have the right quantum numbers to couple with the current $J^{\hat{A}}_\mu$. We deduce that, at zero momentum, $\Pi_0(0)$ vanishes and similarly for $\Pi^X_0(0)$ while $\Pi_1(0) = f^2$.

We now turn back to the original Lagrangian in Eq. (6.2.3) and switch-off the unphysical gauge fields, keeping only the SM ones. From Eq. (6.2.2), we obtain

$$\begin{aligned}\mathcal{L} = \frac{1}{2}T^{\mu\nu}\Bigg[&\left(\Pi_0^X(q^2)+\Pi_0(q^2)+\frac{\sin^2(h/f)}{4}\Pi_1(q^2)\right)B_\mu B_\nu \\ &+\left(\Pi_0(q^2)+\frac{\sin^2(h/f)}{4}\Pi_1(q^2)\right)A_\mu^{AL}A_\nu^{AL} \\ &+2\sin^2(h/f)\Pi_1(q^2)\hat{H}^\dagger T^{AL}Y\hat{H}A_\mu^{AL}B_\nu\Bigg]\ ,\end{aligned} \tag{6.2.7}$$

where B_μ and A_μ^{AL} are respectively the hypercharge and $SU(2)_L$ gauge fields associated to the generators Y and T_L^A. We have also defined

$$\hat{H} = \frac{1}{h}\begin{pmatrix} h^1 - ih^2 \\ h^3 - ih^4\end{pmatrix}\ . \tag{6.2.8}$$

We expand the form factors at small momenta compare to the mass scale of the resonances of the strong sector ($q^2 \ll M_\rho^2$). One can always perform an $SO(4)$ rotation to align the Higgs vev along the h^3 direction: $(h^1,h^2,h^3,h^4)=(0,0,1,0)$ and $H^T=(0,1)$ such that

$$\begin{aligned}\mathcal{L} \;=\; T^{\mu\nu}\Bigg[&\frac{1}{2}\left(\frac{f^2\sin^2(\langle h\rangle/f}{4}\right)(B_\mu B_\nu + W_\mu^3 W_\nu^3 - 2W_\mu^3 B_\nu) + \left(\frac{f^2\sin^2(\langle h\rangle/f}{4}\right)W_\mu^+ W_\nu^- \\ &+\frac{q^2}{2}\left[\Pi_0'(0)W_\mu^{AL}W_\nu^{AL} + (\Pi_0'(0)+\Pi_0^{X\prime}(0))B_\mu B_\nu\right]+\cdots\Bigg]\ ,\end{aligned} \tag{6.2.9}$$

where the expansion of the form factors is the following $\Pi_i(q^2)=\Pi_i(0)+q^2\Pi_i'(0)+\cdots$ and we make the identifications

$$\frac{1}{g^2} = -\Pi_0'(0)\ , \qquad \frac{1}{g'^2} = -(\Pi_0'(0)+\Pi_0^{X\prime}(0))\ , \qquad \xi = \frac{v^2}{f^2} = \sin^2\frac{\langle h\rangle}{f}\ . \tag{6.2.10}$$

Expanding around the vev, that is , $h^{\hat{A}} = \begin{pmatrix}0 & 0 & \langle H\rangle + h & 0\end{pmatrix}^T$, we obtain

$$\begin{aligned} f^2\sin^2\frac{h}{f} \;&=\; f^2\left[\sin^2\frac{\langle h\rangle}{f} + 2\sin\frac{\langle h\rangle}{f}\cos\frac{\langle h\rangle}{f}\left(\frac{h}{f}\right) + (1-2\sin^2\frac{\langle h\rangle}{f})\left(\frac{h}{f}\right)^2+\cdots\right] \\ &=\; v^2 + 2v\sqrt{1-\xi}h + (1-2\xi)h^2+\cdots\end{aligned} \tag{6.2.11}$$

Replacing the above result and the ones in Eq. (6.2.10) in the Lagrangian of Eq. (6.2.7), we finally obtain for the SM gauge boson couplings to the Higgs

$$c_{hVV} = c_{hVV}^{SM}\sqrt{1-\xi}\ , \qquad c_{hhVV} = c_{hhVV}^{SM}(1-2\xi)\ , \tag{6.2.12}$$

In the limit $\xi \to 0$ or equivalently when the scale of the NGBs $f\to\infty$ (v fixed), one recovers the SM Higgs couplings. Physically, the resonances of the strong sector become infinitely heavy and decouple. In the opposite limit where $\xi=1$ ($v=f$), there is no gap between the EW scale and the scale of the NGBs (no vacuum misalignment). In that case, the strong dynamics behaves quite similarly to a minimal technicolour model. Let us note that we can obtain the same results staring from the kinetic term of the Σ field in the chiral Lagrangian that is from $(D_\mu\Sigma)^\dagger(D^\mu\Sigma)$. This is done in appendix E for the the next-to-minimal CHM based on the coset $SO(6)/SO(5)$.

Finally, let us make some comments on the EWPT. Due to the embedding of the SM gauge group in the global symmetry of the strong sector, the latter couples with the SM gauge bosons and then contributes to the EWPT. Following Ref. [251], one obtains for the contribution of the strong sector to the S parameter

$$S = 2\pi\xi\Pi_1'(0) = 4\pi\xi\sum_n\left(f_{\rho_n}^2 - f_{A_n}^2\right)\ , \tag{6.2.13}$$

where only the third term of Eq. (6.2.3) contributes to S as contrary to the other ones, it may involve two different SM gauge bosons (W^3_μ and B_μ). Note that the derivative $\Pi_1'(0)$ is a consequence of the heavy (compare to the EW scale) composite resonances [see Eq. (C.11)]. The second equality is valid in the large N limit where the form factor can be saturated by an infinite sum of narrow resonances. The above contribution to S is then interpreted as the tree-level exchange of spin one resonances coupling to the SM gauge bosons. In addition, there is also the contributions coming from the modifications of the SM couplings which modify the diagrams involving SM particles. Note that all the contributions to S vanish in the decoupling limit where $\xi \to 0$. In the same way, one can estimate the contributions to the T parameter. In that case, there is no contributions coming from the tree-level exchange of spin one resonances because the $SO(4)$ coset contains the custodial symmetry as a subgroup. This feature is crucial for any viable CHM otherwise the contributions to the T parameter would be too large to respect the experimental constraints. For instance, a more minimal coset of the form $SU(3)/SU(2) \times U(1)$ is not a good candidate for CHMs as the unbroken symmetry does not contain the custodial symmetry. Then in general, non-zero contributions to T comes from loops of heavy fermions and vectors as well as from the deviations in the SM couplings. In any case, the contributions to the T parameter are loop suppressed in CHMs, contrary to the S parameter where there are tree-level contributions.

The above deviations in the Higgs couplings as well as the contributions to the S and T parameters put strong constraints on the parameters of the CHM. In particular, the degree of misalignment ξ should be roughly smaller than 0.1, that is, the scale of the chiral Lagrangian f should be larger than around 1 TeV [257]. This lower bound on f is important as it fixes the scale of the strong sector that is, the scale of the composite resonances (see chapter 8).

6.3 Partial compositeness

We now turn to the SM fermions. The latter have to couple with the Higgs in order to get a mass after EWSB. Then one needs to generate Yukawa couplings from the strong sector as the latter contains the Higgs boson. There are two main ways to do that.

In the first one, the breaking of the EW symmetry is transmitted to the fermionic sector of the SM through the following operator:

$$\Delta\mathcal{L} = \sum_\Psi \lambda_\Psi \overline{\Psi}_{SM}\Psi_{SM}\mathcal{O} \ , \qquad \mathcal{O} = \overline{\Psi}_{HC}\Psi_{HC} \ . \tag{6.3.1}$$

At some high scale Λ_{UV}, the exchange of massive states generates the above four-fermion operators between two SM fermions and two hypercolour fermions. Below the scale of condensation $\Lambda \simeq 4\pi f$, the composite operator $\mathcal{O}$ interpolates the Higgs field: $\lambda_\Psi \mathcal{O} \simeq g_\rho(\Lambda/\Lambda_{UV})^{[\mathcal{O}]-1}H$. Then, the operator in Eq. (6.3.1) becomes a Yukawa coupling between the Higgs H and the SM fermions. This is illustrated in figure 6.1 and the corresponding mass is of the order [2]

$$m_\Psi \simeq v g_\rho \left(\frac{\Lambda}{\Lambda_{UV}}\right)^{[\mathcal{O}]-1} \simeq v\frac{4\pi}{\sqrt{N}}\left(\frac{\Lambda}{\Lambda_{UV}}\right)^{[\mathcal{O}]-1} \ . \tag{6.3.2}$$

This mechanism is the same than in technicolour theories. The resulting mass depends on the dimension of the operator $\mathcal{O}$ that can significantly differ from its classical value of three. One can show that for consistency [251], the dimension of $\mathcal{O}$ can not be smaller than two implying at least a suppression factor (Λ/Λ_{UV}) in the masses of the SM fermions. Note that if the operator of Eq. (6.3.1) is generated, operators with four SM fermions should also be generated. They are suppressed by a factor $1/\Lambda^2_{UV}$ (from the exchange of a massive state with mass of the order of Λ_{UV}) and are expected to violate flavour and CP, then strongly constraining Λ_{UV}. In technicolour theories, the suppression factor $(\Lambda/\Lambda_{UV}) \simeq (4\pi f/\Lambda_{UV})$ with $f = v$, implies too small masses while in CHMs one can still obtain large enough mass as $\Lambda \simeq 4\pi f \gg v$. However, the price to pay is a fine-tuning of the vacuum

[2] The canonical dimension of the operator in Eq. (6.3.1) is 6 such that the anomalous dimension $\gamma = [\mathcal{O}] - 1$ is equal to 2 if $\mathcal{O}$ takes its canonical value of 3.

misalignment which should be very small, that is, $\xi = v^2/f^2 \ll 1$. The problem of FCNC is solved in the same way. Then, with the above mechanism realised in CHMs, one can generate the masses of the SM fermions and avoid large FCNC but the model is quite similar to the SM as a large fine-tuning is necessary. In addition, there is no simple explanation of the mass hierarchy of the SM fermions.

Figure 6.1: Mechanisms that generate a mass for the SM fermions from couplings to the strong dynamics. The diagram on the left corresponds to a four-fermion operator of the form $\overline{\Psi}_L^{SM}\Psi_R^{SM}\mathcal{O}$ where $\mathcal{O} = \overline{\Psi}_{HC}\Psi_{HC}$. The diagram on the right corresponds to the mechanism of partial compositeness and is generated from linear couplings between the SM fermions and the strong sector of the form $\overline{\Psi}_{L,R}^{SM}\mathcal{O}$ where $\mathcal{O} = \overline{\Psi}_{HC}\Psi_{HC}\Psi_{HC}$.

The second way to generate the masses of the SM fermions suppose that, at the scale Λ_{UV}, linear couplings between one SM fermion and a composite operator are generated. The breaking of the EW symmetry is then transmitted to the SM fermions via

$$\Delta\mathcal{L} = \lambda_\Psi \overline{\Psi}_{SM}\mathcal{O} + h.c.\ , \qquad \mathcal{O} = \{\overline{\Psi}_{HC}\Psi_{HC}\Psi_{HC}, \cdots\}\ . \tag{6.3.3}$$

In that case, the operator $\mathcal{O}$ is a fermionic operator and not a scalar one as before. The simple way to realise such operator is with three technifermions, that is, to couple SM fermions linearly with composite trilinear baryons. The latter should have the same quantum numbers than the SM fermions multiplet under consideration. Thus, there is at least one composite operator for each SM fermionic multiplets. At low energy, the Higgs field is interpolated by two of these fermionic operators that is by $\mathcal{O}_L\mathcal{O}_R$ where $\mathcal{O}_L$ and $\mathcal{O}_R$ are respectively associated with a left-handed and a right-handed SM fermion. The naive estimate of the SM fermion mass is

$$m_\Psi = v g_\rho \lambda_L(\Lambda)\lambda_R(\Lambda)\ , \tag{6.3.4}$$

where $\lambda_{L,R}$ stand for the couplings of Eq. (6.3.3) and are associated respectively to $\mathcal{O}_{L,R}$. The values of $\lambda_{L,R}$ at low energy, that is, at the scale Λ, are determined by the dimension of the corresponding operator of the strong sector. More precisely the anomalous dimensions $\gamma_{L,R}$ coming from the running of $\lambda_{L,R}$ from Λ_{UV} down to Λ imply

$$\lambda_{L,R}(\Lambda) = \lambda_{L,R}(\Lambda_{UV})\left(\frac{\Lambda}{\Lambda_{UV}}\right)^{\gamma_{L,R}}\ , \tag{6.3.5}$$

where the anomalous dimensions are defined according to $\gamma_{L,R} = [\mathcal{O}_{L,R}] - 5/2$. [3] The estimate of the SM fermions masses crucially depends on the values of the anomalous dimensions. For instance, if $\gamma_{L,R} > 0$, one has

$$m_\Psi \simeq v g_\rho \left(\frac{\Lambda}{\Lambda_{UV}}\right)^{\gamma_L+\gamma_R} \simeq v\frac{4\pi}{\sqrt{N}}\left(\frac{\Lambda}{\Lambda_{UV}}\right)^{\gamma_L+\gamma_R}\ . \tag{6.3.6}$$

This expression looks really similar to the one of Eq. (6.3.2). However, $\gamma_L + \gamma_R$ can be close or even equal to zero in that case while it was not the case before because $[\mathcal{O}] - 1 > 1$. Then, if the sum of the anomalous dimensions is close to zero, the scale Λ_{UV} can be very large without suppressing the

[3] If the operator of Eq. (6.3.3) is realised with trilinear baryons, its canonical dimension is 6 such that the anomalous dimension $\gamma_{L,R} = [\mathcal{O}_{L,R}] - 5/2$ is equal to 2 if $\mathcal{O}_{L,R}$ take their canonical value of 9/2.

SM masses. Also, a large value of Λ_{UV} suppresses any flavour and CP violating operators with four-fermion generated at that scale. Within this picture and provided that small anomalous dimensions $\gamma_{L,R}$ exist (the dimension of the operator in Eq. (6.3.3) should strongly differ from its canonical value), the problems appearing in the first mechanism are solved without any fine-tuning on f.

In addition, when $(\Lambda/\Lambda_{UV}) \ll 1$, differences of $\mathcal{O}(1)$ in the anomalous dimension can generate hierarchies in the masses of the SM fermions which may give a natural explanation of the flavour puzzle.

6.3.1 The basic idea of partial compositeness

As we have seen, the linear couplings between the SM fermions and the strong sector represent an appealing way to communicate the breaking of the EW symmetry to the fermionic sector of the SM and to generate the SM fermion masses. An interesting feature of these linear couplings is that they becomes mass mixing terms at low energy. Indeed, below the condensation scale Λ, the composite operator $\mathcal{O}$ can excite heavy fermionic resonances. Then the linear coupling of Eq. (6.3.3) become mass mixing terms between the elementary fermions Ψ^{SM} and a composite fermions Ψ^{HC}_n associated to the excitations of the operator $\mathcal{O}$. We assume that the composite fermions are heavy, that is, they receive a mass from the strong dynamics (not from the Higgs vev) and are then VL with respect to the SM gauge group. The mixing terms takes the following form

$$-\mathcal{L}^f_{mix} = \sum_n \lambda^n_\Psi (\overline{\Psi}_{SM} \Psi^n_r + h.c.) \ , \tag{6.3.7}$$

where $\lambda^n_\Psi = \langle 0|\mathcal{O}|\Psi^n_r\rangle$ and the sum runs over all of the fermionic composite resonances Ψ^n_r. Similarly, the currents associated to the global symmetry G have the right quantum numbers to excite a tower of spin one resonances ρ_n. The latter mix with the elementary gauge fields V_μ through

$$\mathcal{L}^{gauge}_{mix} = \sum_n M_{\rho_n} f_{\rho_n} A_\mu \rho^\mu_n \ , \tag{6.3.8}$$

where $\langle 0|J_\mu|\rho_n(\epsilon_r)\rangle = \epsilon^r_\mu M_{\rho_n} f_{\rho_n}$. This is in complete analogy with the $\rho-$photon mixing in QCD. As a consequence of the above relations, the physical fermions and vector boson will be an admixture of elementary and composite states. This is the so-called partial compositeness mechanism [81].

As a first example of this mechanism, let us consider a simplified case where only the first resonance of each tower mixes with its corresponding elementary state. For simplicity, we consider only the top quark sector. Indeed, the latter is the heaviest SM state and as we will see it mixes more with the composite resonances. The effective Lagrangian describing the mixing between the elementary top multiplets q_L and t_R with the corresponding composite resonances $Q_{L,R} = \begin{pmatrix} \mathcal{T}_{L,R} & \mathcal{B}_{L,R} \end{pmatrix}^T$ and $T_{L,R}$ is

$$-\mathcal{L} = M_Q \overline{Q} Q + M_T \overline{T} T + \left[\Delta_{t_R} \overline{T}_L t_R + \Delta_{q_L} \overline{q}_L Q_R + \lambda_{QT} \overline{Q}_L \tilde{H} T_R + \lambda_{TQ} \overline{T}_L \tilde{H}^\dagger Q_R + h.c. \right] \ , \tag{6.3.9}$$

where we have omitted for simplicity the kinetic terms. The above Lagrangian can be rewritten as follows

$$-\mathcal{L} = \overline{T}_L \left(\lambda_{t_R} t_R + M_T T_R \right) + \left(\lambda_{q_L} \overline{q}_L + M_Q \overline{Q}_L \right) Q_R + \lambda_{QT} \overline{Q}_L \tilde{H} T_R + \lambda_{TQ} \overline{T}_L \tilde{H}^\dagger Q_R + h.c. \tag{6.3.10}$$

Before EWSB, the heavy and light mass eigenstates are defined by

$$\left\{ \begin{array}{rcl} t'_R &=& \frac{1}{M_R} \left(\Delta_{t_R} t_R + M_T T_R \right) \ , \\ t''_L &=& \frac{1}{M_L} \left(\Delta_{q_L} t_L + M_Q \mathcal{T}_L \right) \ , \end{array} \right. \qquad \left\{ \begin{array}{rcl} t^{SM}_R &=& \frac{1}{M_R} \left(\lambda_{t_R} t_R - M_T T_R \right) , \\ t^{SM}_L &=& \frac{1}{M_L} \left(\lambda_{q_L} t_L - M_Q \mathcal{T}_L \right) \ , \end{array} \right. \tag{6.3.11}$$

where $M_R = \sqrt{\lambda^2_{t_R} + M^2_T}$ and $M_L = \sqrt{\lambda^2_{q_L} + M^2_Q}$ are respectively the masses of the heavy partners t'_R and t''_L. The remaining VL multiplet does not mix such that $t'_L = T_L$ and $t''_R = \mathcal{T}_R$. The SM fermions

$t^{SM}_{L,R}$ are massless before EWSB but one can see that they acquire a composite part. More precisely, one can define the following mixing angles

$$\cos\theta_R = \frac{M_T}{M_R}\,, \qquad \sin\theta_R = \frac{\lambda_{t_R}}{M_R}\,, \qquad \cos\theta_L = \frac{M_Q}{M_L}\,, \qquad \sin\theta_L = \frac{\lambda_{q_L}}{M_L}\,. \tag{6.3.12}$$

The linear couplings λ_{t_R,q_L} can be naturally much smaller than the mass scale $M_{Q,T} \sim m_*$ of the composite fermions as they do not belong to the strong sector. Then, the SM fermions are mainly elementary and the latter part is given by $\cos\theta_{L,R}$. However, they also contain a small composite part given by $\sin\theta_{L,R}$. These composite parts are crucial as they couple to the Higgs doublet. Then, after EWSB, the SM top quark t^{SM} gets a non-zero mass from the Higgs vev. From the complete mass matrix after EWSB

$$\begin{pmatrix} \bar{t}_R & \overline{\mathcal{T}}_R & \overline{T}_R \end{pmatrix} \begin{pmatrix} 0 & 0 & \lambda_{t_R} \\ 0 & M_Q & \lambda_{TQ} v/\sqrt{2} \\ \lambda_{q_L} & \lambda_{QT} v/\sqrt{2} & M_T \end{pmatrix} \begin{pmatrix} t_L \\ \mathcal{T}_L \\ T_L \end{pmatrix} + h.c. \tag{6.3.13}$$

one sees that a non-zero mass for the top quark is generated only if the two linear couplings λ_{t_R} and λ_{q_L} are non-zero and the Yukawa coupling λ_{QT} (which has a SM-like structure) is also non-zero. This picture is displayed in figure 6.2. Note that the heavy masses $M_{L,R}$ receive only small corrections from the EWSB as $v \ll m_*$. The effective Yukawa coupling of the top quark is

$$\lambda_t = \lambda_{QT} \sin\theta_L \sin\theta_R\,. \tag{6.3.14}$$

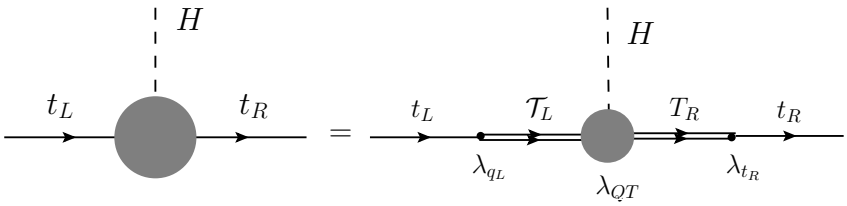

Figure 6.2: Explicit realisation of the partial compositeness mechanism in the top sector. The first resonance of each tower mixes with its corresponding elementary state, that is, t_L and t_R mix respectively with $\mathcal{T}_L$ and T_R. These mixing are controlled by the linear couplings λ_{q_L} and λ_{t_R} while the relevant coupling of the strong resonances to the composite Higgs is λ_{QT}.

Note that the same mechanism can be present for all of the other SM fermions but in that case, the linear couplings should be smaller as the other SM fermions are lighter than the top quark. From Eq. (6.3.14), one sees that the degree of compositeness $\sin\theta_{L,R}$, controls the mass of the SM fermions. The top quark has the largest degree of compositeness and is then the SM fermion that couples the most with the strong sector due to its large mass. Consequently, it plays a particular role in CHMs as we will see in section 6.4.

6.3.2 Higgs couplings to fermions

Let us now explore in deeper details the partial compositeness mechanism. We assume that the elementary fermionic content of the SM couples linearly to composite operators of the strong sector. The operators of the strong sectors belong to complete representations of the global symmetry G while in general, the elementary fermions not. As a consequence, the linear couplings break the global symmetry G and then the loops of elementary fermions induce a potential for the Higgs boson. The dominant contributions come from the top and bottom quarks since they have the larger masses, their couplings to the strong sector is also larger (see subsection 6.3.1). For simplicity we then restrict

to the elementary top and bottom quarks. The linear couplings between the SM fermions and the composite sector are given by

$$\mathcal{L}_{int}^{fermions} = \sum_{\psi} \lambda_\psi \overline{\psi} \mathcal{O}_\psi + h.c. = \lambda_q \overline{q}_L \mathcal{O}_q + \lambda_u \overline{u}_R \mathcal{O}_u + \lambda_d \overline{d}_R \mathcal{O}_d + h.c. \tag{6.3.15}$$

Similarly to the gauge bosons couplings, one can derive the effective Lagrangian for the elementary quarks in the Higgs background. To do that, one needs to specify the representation in which the composite operators $\mathcal{O}_\psi$ belong. Again, we consider the minimal $SO(5)/SO(4)$ model but the results can easily be transposed to other non-minimal models. For instance, we can assume that the strong operators transform in the spinorial representation of $SO(5)$. We then construct complete spinorial representation of $SO(5)$ in which the SM quarks are embedded. One has

$$\Psi_q = \begin{pmatrix} q_L \\ Q_L \end{pmatrix} , \qquad \Psi_u = \begin{pmatrix} q_R^u \\ \begin{pmatrix} u_R \\ d'_R \end{pmatrix} \end{pmatrix} , \qquad \Psi_d = \begin{pmatrix} q_R^d \\ \begin{pmatrix} u'_R \\ d_R \end{pmatrix} \end{pmatrix} \tag{6.3.16}$$

where $Q_L, q_R^{u,d}, u'_R$ and d'_R are non-dynamical spurions. More precisely, one can rewrite the Lagrangian of Eq. (6.3.15) in a $SO(5)$-invariant form using the above multiplets. In this way, the linear couplings λ_π are promoted to spurions and their vev lead to the Lagrangian of Eq. (6.3.15). The spinorial representation of $SO(5)$ decomposes under $SU(2)_L \times SU(2)_R$ as follows: $4_{SO(5)} = (2,1) + (1,2)$ such that each fields $\Psi_{q,u,d}$ contains one $SU(2)_L$ doublet and one $SU(2)_R$ triplet. The effective Lagrangian invariant under $SO(5) \times U(1)_x$ for the elementary quarks is then

$$\mathcal{L} = \sum_{\psi=q,u,d} \overline{\Psi}_\psi \not{p} \left[\Pi_0^\psi(p) + \Pi_1^\psi(p) \Gamma_i \Sigma_i \right] \Psi_\psi + \sum_{\psi=u,d} \overline{\Psi}_q \left[M_0^\psi(p) + M_1^\psi(p) \Gamma_i \Sigma_i \right] \Psi_\psi \ , \tag{6.3.17}$$

where as before, the field Σ has been treated as a constant background and we restricted to the quadratic order in momentum space. Note that the spurions are not physical fields, they just allow to write the above effective Lagrangian into an invariant form. The form factors $\Pi_{0,1}^\psi$ and $M_{0,1}^\psi$ ($\psi = q, u, d$) are the equivalent of Π_0^X and $\Pi_{0,1}$ in the effective Lagrangian involving the SM gauge bosons. They encode the effect of the strong dynamics and their poles give the masses of the fermionic resonances of the composite sector. The explicit expression of the gamma matrices (see Ref. [251]), that is, of the $SO(5)$ generators in the spinorial representation leads to

$$\Gamma^i \Sigma_i = \begin{pmatrix} \mathbb{1} \cos(h/f) & \hat{\sigma} \sin(h/f) \\ \hat{\sigma}^\dagger \sin(h/f) & -\mathbb{1} \cos(h/f) \end{pmatrix} , \qquad \hat{\sigma} \equiv \sigma^{\hat{a}} h^{\hat{a}}/h \ , \qquad \sigma^{\hat{a}} = \{\vec{\sigma}, -i\mathbb{1}\} \ . \tag{6.3.18}$$

Keeping only the top quark multiplets $q_L = (t_L, b_L)$ and t_R as physical dynamical fields we obtain the effective Lagrangian associated to these fields

$$\begin{aligned} \mathcal{L} \ = \ & \overline{q}_L \not{p} \left[\Pi_0^q(p) + \Pi_1^q(p) \cos(h/f) \right] q_L + \overline{t}_R \not{p} \left[\Pi_0^u(p) - \Pi_1^u(p) \cos(h/f) \right] t_R \\ & + \sin(h/f) M_1^u(p) \overline{q}_L \hat{H}^c t_R + h.c. \end{aligned} \tag{6.3.19}$$

where $\hat{H}^c = i\sigma^2 \hat{H}$. Note that we have neglected the effect of the other elementary fermions as their contributions are negligible compare to the one of the top quark. This is due to their small couplings to the strong sector.

One can extract the top quark mass from the above effective Lagrangian. More precisely, from the Yukawa term between t_L and $_R$ we get in the low energy limit ($p \simeq 0$)

$$m_t \simeq \frac{v}{f} \frac{M_1^u(0)}{\sqrt{[\Pi_0^q(0) + \Pi_1^q(0)][\Pi_0^u(0) - \Pi_1^u(0)]}} \ . \tag{6.3.20}$$

With this identification, the second term of the expansion of $\sin(h/f)$ around the Higgs vev gives the Higgs coupling to the top quark

$$\underline{\text{MCHM}_4} : \qquad c_{h\overline{f}f} = c_{h\overline{f}f}^{SM} \sqrt{1-\xi} \ , \tag{6.3.21}$$

Note that the above deviation compare to the SM prediction is valid for every SM fermions embedded in the spinorial representation of $SO(5)$. This embedding is commonly denoted by MCHM_4.

There exist other possibilities for the embedding of the SM fermions inside multiplets of $SO(5)$. For instance, SM fermions can be embedded in the fundamental representation [36] ($MCHM_5$) which leads to

$$\underline{\text{MCHM}_5}: \qquad c_{h\bar{f}f} = c_{h\bar{f}f}^{SM}\frac{(1-2\xi)}{\sqrt{1-\xi}} \ . \tag{6.3.22}$$

Let us mention that, other possibilities for the embedding of the elementary fermions are the 10 (MCHM_10) and 14 (MCHM_14) representations of $SO(5)$ which have also been investigated in the literature. Then, elementary fermions can be embedded in the same representation of $SO(5)$ like the $4, 5, 10$ or 14 or even, depending of the elementary fermion, in different representations.

Let us comment on possible UV completions. In any of the above cases, one needs to form the composite baryons with an odd number of fermions. Restricting to trilinear ones, it is not guarantee that the composite baryons can transform in the 4, 5, 10 or 14 of $SO(5)$. Only some of these representations may be accessible in a particular UV completion. However, from the effective point of view, we do not know the available representations. This model-dependence motivates the construction of UV completions of CHMs.

6.4 The composite Higgs potential

Up to now, we have assumed that the Higgs potential at its minimum can correctly break the EW symmetry. Under this hypothesis, we have derived the deviations that appear in the Higgs couplings to the SM fermions and gauge bosons compared to the SM predictions. In this section, we discuss the EWSB in CHMs, and show that it is mainly due to the linear couplings of the SM top quark.

Before turnig on the interactions between the elementary sector and the strongly coupled sector, the global symmetry G is only spontaneously broken, such that the potential of the NGBs is flat. This is a consequence of the Goldstone shift symmetry. When we couple the two sectors however, the global symmetry is explicitly broken and a potential is generated. This potential shall break the EW symmetry and generate a mass for the Higgs.

In general, there are two distinct sources that contribute to the Higgs potential, namely the gauge contribution and the top contribution

$$V(h) = V(h)_{top} + V(h)_{gauge} \ . \tag{6.4.1}$$

Indeed, only a part of the global symmetry G corresponds to the SM group that is, the SM gauge bosons couple only to few currents of $SO(5)$. Then gauging this part explicitly breaks the global symmetry. In the same way, the composite fermions belong to complete representations of $SO(5)$ but not the SM ones. Then linear couplings between composite and elementary fermions break the global symmetry G.

The gauge contribution can be obtained by resuming the series of 1-loop diagrams of figure 6.3. This leads to the following potential [251]

$$V(h)_{gauge} = \frac{9}{2}\int\frac{d^4Q}{(2\pi)^4}\ln\left[1+\frac{\Pi_1(Q^2)}{4\Pi_0(Q^2)}\sin^2(h/f)\right] \ . \tag{6.4.2}$$

The gauge contribution alone is always positive such that it is not possible to destabilise the Higgs potential in this way and not possible to trigger EWSB (see discussions in subsections 2.5.1 and 8.1.5). Then one needs another source of explicit breaking in order to break the EW symmetry.

This other source of explicit breaking comes from the top quark. Indeed, the 1-loop top and bottom quarks contribution is [251]

$$\begin{aligned} V(h) \ = \ & -2N_c\int\frac{d^4p}{(2\pi)^4}\left[2\ln\left(1+\frac{\Pi_1^q}{\Pi_0^q}\cos\frac{h}{f}\right)+\ln\left(1-\frac{\Pi_1^u}{\Pi_0^u}\cos\frac{h}{f}\right)\right. \\ & \left.+\ln\left(1-\frac{[M_1^u\sin(h/f)]^2}{p^2[\Pi_0^q+\Pi_1^q\cos(h/f)][\Pi_0^u-\pi_1^u\cos(h/f)]}\right)\right] \ , \end{aligned} \tag{6.4.3}$$

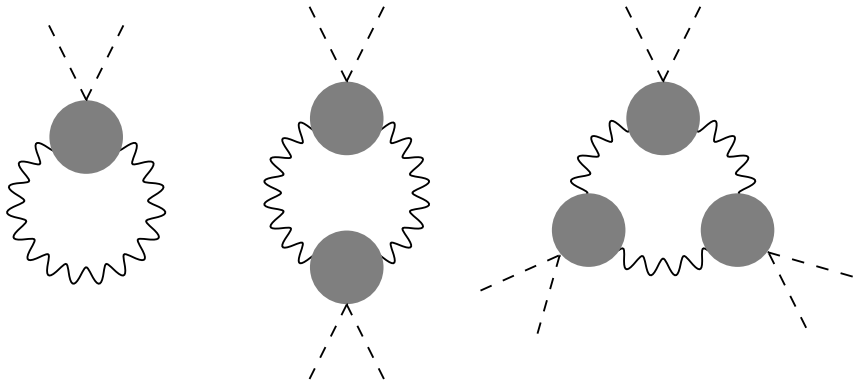

Figure 6.3: 1-loop contribution of the SM gauge fields to the Higgs potential. The grey blobs encode the strong dynamics and correspond to the form factor Π_1

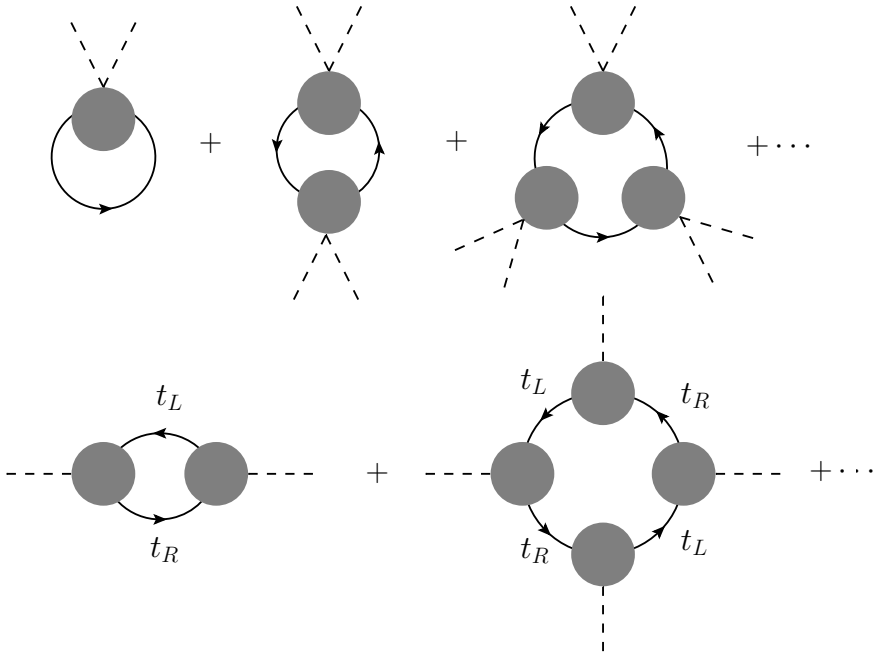

Figure 6.4: 1-loop contribution of the SM top and bottom quarks to the Higgs potential. Upper row: diagrams where the same elementary field either $q_L = (t_L\ b_L)$ or t_R, circulates in the loop. These diagrams are associated with the form factors $\Pi^q_{0,1}$ and $\Pi^u_{0,1}$ [see Eq. (6.3.19)]. Lower row: diagrams where the form factors are M^u_1 and both t_L and t_R circulate in the loop.

The above potential comes from the resummation of the one-loop diagrams of figure 6.4. Assuming that all of the form factors converge fast enough at large Euclidian momenta, the potential can be approximate by expanding the logarithms at first order. One has

$$V(h) \simeq \alpha \cos\frac{h}{f} - \beta \sin^2\frac{h}{f}\ , \tag{6.4.4}$$

where

$$\begin{aligned} \alpha &= 2N_c \int \frac{d^4q}{(2_p i)^4}\left(\frac{\Pi^u_1}{\Pi^u_0} - 2\frac{\Pi^q_1}{\Pi^q_0}\right)\ , \\ \beta &= \int \frac{d^4q}{(2_p i)^4}\left[2N_c \frac{(M^u_1)^2}{-q^2(\Pi^q_0+\Pi^q_1)(\Pi^u_0-\Pi^u_1)} - \frac{9}{8}\frac{\Pi_1}{\Pi_0}\right]\ . \end{aligned} \tag{6.4.5}$$

Then, even if the gauge contribution is positive, EWSB can be triggered by the top contribution if $\alpha \leqslant 2\beta$. In that case, the minimum of the potential is at

$$\xi = \sin^2 \frac{\langle h \rangle}{f} = 1 - \left(\frac{\alpha}{2\beta} \right)^2 \ . \tag{6.4.6}$$

Then, small values of ξ require a tuning between α and β. This is a general feature of CHMs, the misalignment of the vacuum comes from the interplay of different terms in the potential. Thus, one expects from the potential of Eq. (6.4.4) an order one value for the misalignment ($\xi \sim 1$) or no breaking at all ($\xi = 0$) while a small value for the misalignment is less likely and should arise only through a fine-tuned cancellation among the different terms in the potential. Then, the value of ξ gives a rough estimate of the tuning of the theory. As the Higgs coupling measurements and the EWPT restrict $\xi \lesssim 0.1$, the tuning should be at least of the order of 10%. Note that in other composite Higgs models, based on other cosets, the form of the Higgs potential may change compared to Eq. (6.4.4) but, qualitatively, the features presented here remain valid.

Taking the second derivative of the potential, we extract the Higgs mass

$$m_h^2 = 2\beta \frac{\xi}{f^2} \simeq 2N_c \frac{y_t^2}{8\pi^2} m_*^2 \xi \ , \tag{6.4.7}$$

where the second equality comes from the evaluation of β neglecting the gauge contributions and identifying the top mass [see Eq. (6.3.20)]. From the above expression, one sees that the Higgs mass is one-loop induced by the linear couplings of the top quarks [factor $y_t^2/(8\pi^2)$] that explicitly break the global $SO(5)$ symmetry. A further suppression compare to the scale of the composite resonances m_* comes from the factor ξ. Note that one also recovers that in the decoupling limit, the Higgs mass remains at the EW scale as $m_h^2 \sim m_*^2 v^2/f^2 \sim v^2$ in the limit where the strong sector is decoupled.

Finally, with a UV completion of CHMs, with only the linear couplings as free parameters [4], one should be able to compute explicitly all of the form factors of the theory instead of making rough estimates of them. In this way, one could compute for instance the parameters α and β to see if the breaking of the EW symmetry is possible or not. This is briefly discussed in chapter 10.

6.5 Concluding remarks

In this chapter, we have presented an effective approach to CHMs. The latter is based only on the global symmetry of the strong sector and more precisely on the pattern of spontaneous symmetry breaking G/H. We have considered as an example the minimal composite Higgs model which is based on the coset $SO(5)/SO(4)$.

Let us summarise the main features of CHMs that we have learnt from this minimal model

- The composite Higgs emerges as a pNGB after the condensation of a new strong sector. This condensation breaks at low energy the global symmetry G of the strong sector down its subgroup H. Then, the coset G/H should contain at least a Higgs doublet with the same quantum numbers than in the SM.

- The SM gauge symmetry should be embedded into the global symmetry G as the Higgs is charged under G_{SM}. More precisely, in CHMs G_{SM} is not broken by the condensation of the strong dynamics such that it is embedded inside the unbroken global symmetry H ($G_{SM} \subset H$).

- In order to avoid tree-level contribution to the T parameter, also the custodial symmetry $G_{cus} = SU(2)_L \times SU(2)_R$ should be embedded into H. This leads to the minimal coset $SO(5)/SO(5)$ and to the next-to-minimal one $SO(6)/SO(5)$.

[4] The top and the Higgs mass may fix some free parameters of the UV completion.

- The Goldstone nature of the Higgs boson induces deviations with respect to the SM predictions. The latter appear in the Higgs couplings to the SM gauge bosons and fermions. These deviations are parametrised by the degree of misalignment $\xi = v^2/f^2$, that is, the angle between the orientation of the subgroup H and the one of G_{SM} inside the global symmetry G. There exist a decoupling limit where $\xi \to 0$ or equivalently $f \to \infty$ with fixed v. In this limit, only the Higgs remains at the EW scale while all of the other resonances of the strong sector are decoupled. Also, in this regime all of the deviations vanish and the Higgs boson behaves like the SM one. The contributions from the strong dynamics to the S and T parameters also vanish in the decoupling limit. However, one recover the hierarchy problem as the misalignment ξ require a large tuning to be small.

- In order to respect the EWPT and the Higgs couplings measurements, $\xi = v^2/f^2 \lesssim 0.1$, which transposes to $f \gtrsim 1$ TeV. Then, the scale f should be small in order to respect the experimental constraints but not too small otherwise the tuning is important and the hierarchy problem is not solved.

- Due to the Goldstone symmetry, the tree-level Higgs potential is flat. Gauging the SM explicitly breaks the global symmetry G which induces a potential at one-loop for the Higgs. However, as $G_{SM} \subset H$, this breaking does not destabilise the Higgs potential.

- The Higgs potential is destabilised by linear couplings between the elementary fermions and the composite resonances because these couplings also break explicitly G. The dominant contributions comes from the heavy SM fermions and, consequently, the top quark drives the EWSB.

- The two explicit breaking sources, the gauging of the SM group and the linear couplings, induce a mixing between the elementary particles and the composite resonances such that the SM fermions and gauge bosons contain a composite part. The top quark which is the heaviest SM particle interacts the most with the strong sector and has then the most important degree of compositeness. The top partners that mix with the top are expected to be the lightest baryonic resonances [36].

As we have seen, the effective approach to composite Higgs models is relevant as it allows to derive informations about the low energy regime of CHMs. However, only the lightest resonances can be taken into account in the effective Lagrangian. The latter is also parametrised in term of form factors, which encode the unknown strong dynamics. These form factors can not be computed, only the zero momentum part is fixed. They are then a priori independent and can not be related to the fundamental parameters of the theory (for instance the number of hypercolours). The limited informations about the UV dynamics that is about the underlying gauge symmetry is then problematic. As another example, one assumes the representation of G in which the composite resonances belong. This choice leads to particular deviations in the Higgs couplings to the SM fermions. However, one is not sure that such representation can be realised in practise in an UV complete model. For instance, the gauge contraction could forbid some global representations.

Then, the necessity to go beyond the effective approach and to construct UV completions appears. It is also theoretically appealing to realise the composite Higgs paradigm explicitly. In a UV completion, we should be able to compute explicitly, in term of more fundamental parameters, the form factors that appear in the chiral Lagrangian. One can also compute the masses of the composite resonances as well as some strong quantities like f in term of the fundamental parameters of the theory. In addition, the quantum numbers of all resonances are known such that there are no ambiguities for the representations of the composite baryons. We will present the classification of the minimal UV completions in the next chapter and study in details the most minimal one of in chapters 8, 9 and 10.

Chapter 7

Introduction and classification of the minimal ultra-violet completions of composite Higgs models

In the precedent chapter we have introduced an effective approach to composite Higgs models. The latter encodes only the low energy physics of CHMs and is based on the global symmetries of the theory. Indeed, only the pNGBs bosons (including the Higgs bosons) and possibly few other light resonances present in the spectrum appear in the chiral Lagrangian of CHMs. Thus, this is mostly a phenomenological approach which is justified by the non-perturbative behaviour of the theory in the IR. However, the informations about the underlying strong dynamics are limited in that case. For instance, the parameters of the chiral Lagrangian like the form factors are a priori independent and can not be predicted in term of fundamental parameters of the theory. Also, the strong sector can have a more complex structure than in the effective approach. For instance, aside the EW sector from which the Higgs emerges, a coloured sector containing the top partners is generally required. This sector can also contain light coloured resonances which are not included in the effective approach. Furthermore, in the effective approach, one embeds the elementary fermions in representations of the global symmetry but it is a strong assumption as due to the underlying hypercolour gauge symmetry, some representations could be forbidden. Finally, it is theoretically appealing to find an explicit realisation of the effective approach otherwise if one demonstrates that it is not possible, the effective model is no longer interesting. Then the necessity to go beyond the chiral approach and to construct UV completions appears [1]. The latter have a purely fermionic content in order to not transpose at a higher scale the hierarchy problem. The new fermions are charged under an hypercolour gauge symmetry G_{HC} and when this gauge symmetry becomes strongly coupled in the IR, a fermionic condensate forms and breaks the global symmetry leading to the emergence of a pNGB Higgs.

In this chapter, we present a classification of the minimal UV completions of CHMs. The material is mainly based on the work done in Ref. [10]. The classification is at the group theoretical level and then the conditions imposed to construct the UV completions are necessary for their viability but not sufficient by themselves. The interest is to isolate the most "minimal" UV completion that will be studied in the next chapters and to highlight its main features.

We first present in section 7.1 the necessary requirements to obtain a viable UV completion. We show how to realise the desire patter of spontaneous symmetry breaking with a purely femionic content in the theory in section 7.2 while we present the result of the classification in section 7.3. Finally in sections 7.4 and 7.5 we outline the quantum numbers of the composite resonances expected for each cosets and we make a critical discussion of the problems not addressed during the classification. We conclude by isolate the most minimal UV completion that will be studied in chapters 8, 9 and 10.

[1] Note that the UV completions of CHMs are not UV complete in the sense that they require additional physics at a higher energy scale $\Lambda_{UV} \gg \Lambda \simeq 4\pi f$. For instance, the linear couplings between the elementary top quark and its partners is generated at Λ_{UV} from a four-fermion interaction (see section 6.3)

7.1 Basic requirements

Let us first begin by the basic requirements that an UV completion should respect. As a first step, we restrict to four-dimensional models [2] with a purely fermionic matter content. The latter point insures that we do not introduce a new hierarchy problem at a higher scale. These new fermions are charged under the hypercolour gauge symmetry G_{HC} and a condensate of fermions forms when the theory becomes strongly coupled at low energy. In this way, the global symmetry G_F is spontaneously broken down to its subgroup H_F and the coset G_F/H_F contains a pNGB Higgs doublet.

Then, we look for a theory with n_i fermions in a representation R_i of G_{HC} where the index i stands for the different hypercolour irreducible representations. For $i = 1, \cdots, p$, the resulting anomaly-free global symmetry is $G_F = SU(n_1) \times \cdots SU(n_p) \times U(1)^{p-1}$. An important point is the presence of $U(1)$ symmetries whose only one among the p possibilities is anomalous. These symmetries are in general (but not always) spontaneously broken after condensation possibly leading to additionally light pNGBs. As a well know example, in QCD, the axial $U(1)_A$ symmetry is anomalous while the $U(1)_V$ is not spontaneously broken.

The SM fermions are of course neutral under G_{HC} but the hypercolour fermions should have appropriate quantum numbers under the SM gauge group in order to give rise to a composite Higgs and to top partners as bound states. In general the flavour group G_F is a semi-simple ($p > 1$) Lie group: one part corresponds to the EW sector from which the Higgs emerges as a pNGB and another part corresponds to the coloured sector containing the top partners such that $G_F = G_F^{EW} \times G_F^c$. A priori, several condensates may or not form in each sector changing the pattern of symmetry breaking G_F/H_F. The important point is that G_F^{EW} must be broken in order for G_F^{EW}/H_F^{EW} to contain the pNGB Higgs. However, for the coloured sector there is no such restriction and $G_F^c = H_F^c$ is a viable possibility. In the next, we assume for simplicity that the coloured sector is spontaneously broken.

We also restrict to theories which are asymptotically free because in general a strongly coupled theory in the IR is asymptotically free. The one-loop beta function is given by

$$\beta_0 = \frac{22}{3} C(\mathbf{Ad}) - \frac{4}{3} \sum_i C(R_i) n_i \ , \tag{7.1.1}$$

where $C(\mathbf{Ad}, R_i)$ are the Dynkin indices of the adjoint representation $\mathbf{Ad}$ and of the fermionic representations R_i of G_{HC} while n_i are the number of fermions in the representation R_i. To preserve asymptotic freedom, one needs $\beta > 0$. One can easily check that QCD with $C(\mathbf{Ad}) = 8$, $C(R = F) = C(\overline{R} = \overline{F}) = 1/2$ and $n_F = n_{\overline{F}} = 6$ is asymptotically free in the UV.

To summarise, we look at four-dimensional theories containing only fermions which are charged under a new gauge symmetry called hypercolour and these theories are asymptotically free in the UV. The list of the basic requirements [10] needed for the UV completions of a composite Higgs model is the following

- The hypercolour gauge symmetry G_{HC} should be free from anomalies (see section 1.4). Note that this is always the case for $SO(N)$ or $Sp(2N)$ but not for $SU(N)$.
- The theory should be free from Witten (global) anomalies [86]. This is the case for $G_{HC} = SU(N)$ with $N > 2$ and $SO(N)$ but not for $Sp(2N)$ [remember that $SU(2) \cong Sp(2)$].
- The following symmetry breaking pattern $G_F \to H_F$ should be possible and $H_F \supset G_{cus} \supset G_{SM}$ where $G_{cus} = SU(3)_c \times SU(2)_L \times SU(2)_R \times U(1)_x$. In this way, the SM gauge symmetry is not spontaneously broken by the condensation and the extra $SU(2)_R$ symmetry avoid large corrections to the T parameter. In addition, the $U(1)_x$ symmetry allows to get realistic hypercharges for the fermions of the coloured sector (and consequently for the top partners) as $Y = T_R^3 + x$.
- The SM group G_{SM} contained in H_F should be free from global anomalies as it will be gauged when the hypercolour fermions are coupled to the SM.

[2] UV completions in higher dimensional models have been considered in the literature (see Ref. [251] for an introduction and other references).

- The coset G_F/H_F should contain at least a Higgs doublet transforming as $(1,2,2)_0$ of G_{cus}. In general other pNGBs are expected and their masses should of course be larger than the experimental limits.

- After condensation the theory should produce top partners as the latter have to couple linearly with the top quark in order to generate a potential for the Higgs. Then the spectrum of resonances should contain spin 1/2 bound states which are singlets of G_{HC} and have the opposite quantum numbers of SM top quark multiplets q_L and t^c_R that is $(\overline{3},2)_{-1/6}$ and $(3,1)_{2/3}$ under $SU(3)_c \times SU(2)_L \times U(1)_Y$. For simplicity we restrict to trilinear bound states but in principle states with a higher number of fundamental fermions are a possibility. Note that partners for each standard model fermions is not a necessary requirement.

The above constraints are imposed to classify the possible UV competions of CHMs in section 7.3.

7.2 Construction of the patterns of global symmetry breaking

Before turning to the classification, let us briefly comment on the way that we can realise the desire patterns of spontaneous symmetry breaking G_F/H_F with only a fermionic content in the theory. By hypothesis, all of the global symmetries are spontaneously broken [3]. In other words, the condensates in the EW and in the coloured sectors are non zero and one should then be able to form gauge invariant operators with an even number of fermions. The condensates are gauge invariant as we assume that G_{HC} remains unbroken. For simplicity, we assume that among the non-zero condensates some of them are fermionic bilinears. This assumption is crucial in the NJL framework (see chapter 3) and is quite reasonable because it is the case in QCD which is the only known strongly coupled theory in nature. However in principle, the two-fermions condensates can be zero and other order parameters can be responsible of the spontaneous symmetry breaking. Following the hypothesis of two-fermion condensates, one should be able to construct gauge invariant bilinears for the hypercolour fermions. This is equivalent to say that the fundamental fermions acquire a dynamical mass after the condensation. The fermionic content of the theory should be such that all fermions can be rendered massive in a gauge invariant way.

There are three possibilities which depend on the nature of the gauge representation. If the fermions are in a complex representation of G_{HC}, one needs an equal number of fermions ψ and ψ' respectively in the complex representation R and in its conjugate representation $\overline{R}$. In that case, the invariant mass term is

$$\mathcal{L}_m = -M(\psi\psi' + h.c.) \ , \tag{7.2.1}$$

where the flavour and hypercolour contractions are underlying for the moment. In the above equation, all fermions have a common mass M but in principle, M can be a matrix in the flavour space. However in that case the global vector symmetries (associated to H_F) are explicitly broken. We do not consider this possibility here because it is too subtle without an observed spectrum. We refer to subsection 2.2.2 where this feature is realised in the QCD context. The two other possibilities correspond to a fermion ψ in a real or a pseudo-real representation R of G_{HC}. In those cases, one can form a gauge invariant mass term of the following form

$$\mathcal{L}_m = -\frac{1}{2}M(\psi\psi + h.c.) \ , \tag{7.2.2}$$

where the factor 1/2 is present to take into account the two identical fermions [4]. The important point is that in the complex case, one needs two fermions ψ and ψ' while in the real or pseudo-real cases one needs only one fermion ψ. As we will see in the next, this leads to two different kind of global symmetries.

[3] Except possibly some $U(1)$ symmetries which are not important for our present purpose.

[4] Note that a very particular case is when two fermions are in two different real or pseudo-real representations of G_{HC} with the same dimension. In that case, it may be possible to form a gauge invariant mass term as the one in Eq. (7.2.1). For instance it is the case for $G_{HC} = SO(N)$ with $\psi \sim \mathbf{Spin}$ and $\psi' \sim \mathbf{Spin}'$ (see subsection 7.3.2).

For the moment, we have not considered the flavour symmetry but in all of the above cases (complex, real or pseudo-real), one can take several fermions transforming in the same gauge representation such that ψ^a (ψ'^a) are in fact flavour multiplets. Then taking N replicas of these fermions ($a = 1, \cdots, N$), one obtains a global symmetry $G_F = SU(N)$ in the real and pseudo-real cases while in the complex case one obtains $G_F = SU(N) \times SU(N)'$. There are also additional $U(1)$ symmetries which are unimportant for our present discussion. From Eqs. (7.2.1) and (7.2.2), we obtain the following two-fermions condensates: $\langle \psi\psi' \rangle$ in the complex case and $\langle \psi\psi \rangle$ in the real and pseudo-real cases.

As $\langle \psi\psi' \rangle$ or $\langle \psi\psi \rangle$ are different from zero by hypothesis, the pattern of spontaneous symmetry breaking is entirely dictated by the symmetry properties of these condensate [258]. In the complex case, it is easy to show that the mass term of Eq. (7.2.1) breaks $G_F = SU(N) \times SU(N)'$ down to its diagonal subgroup $H_F = SU(N)_D$. Indeed, the fermions ψ and ψ' transform in a an opposite way under $SU(N)_D$: ψ transforms in the fundamental representation of $SU(N)_D$ while ψ' in its conjugate representation such that $\psi\psi'$ is invariant under H_F. The real and pseudo-real cases are simplest. In the real case, $R = \overline{R}$ and the gauge contraction in Eq. (7.2.2) or equivalently in the condensate is symmetric such that the flavour contraction has to be symmetric (the Lorentz contraction is symmetric). Then the condensate $\langle \psi\psi \rangle$ transforms in the symmetric representation of $SU(N)$ and the antisymmetric part of this global symmetry remains unbroken. The latter corresponds to $SO(N)$ and the resulting pattern of symmetry breaking is $G_F/H_F = SU(N)/SO(N)$. In the pseudo-real case, $R^* = \overline{R}$ and the gauge contraction is antisymmetric. Consequently, the flavour contraction is also antisymmetric and the symmetric part of $SU(N)$ remains unbroken. This leads to the pattern of symmetry breaking $G_F/H_F = SU(N)/Sp(N)$. Note that in the latter case, one imperatively needs an even number of hypercolour fermions as $Sp(N)$ exists only for N even.

More complex schemes of global symmetry breaking G_F/H_F, like those relevant for the UV completions of composite Higgs models, are built from several sets of fermions and each set obey to one of the above scenario (real, pseudo-real or complex case). In general we have for the global symmetry $G_F = SU(n_1) \times \cdots SU(n_p) \times U(1)^{p-1}$. As already mentioned, in the context of composite Higgs models one needs two sectors: an EW sector where the pNGB Higgs belongs and a coloured sector where the top partners emerges as baryonic bound states. The presence of two sectors restrict the possibilities to $p = 2$ and $p = 3$. The $p = 3$ case corresponds in general to a coloured sector built from two fermions in a complex representation of G_{HC} while in the EW sector there are only real or pseudo-real fermions. Note that the minimal effective CHM, discussed in chapter 6, is based on the coset $SO(5)/SO(4)$. As the $SO(5)$ global symmetry is not an exchange symmetry of the $SU(N)$ type, it is not trivial to realise an $SO(5)$ global symmetry from the above arguments. This point is discussed in Ref. [259]. This problem is not present for the next-to minimal effective CHM which is based on $SO(6)/SO(5) \cong SU(4)/Sp(4)$ and is one of the possibilities that we will encounter in section 7.3 and present in details in chapters 8, 9 and 10.

We now consider a more restrictive but interesting class of theories which are vector-like gauge theories. So far, we have assumed that the spontaneous symmetry breaking occurs through the formation of two-fermions condensates which breaks G_F down to the desired subgroup H_F. This is an important hypothesis as in principle, a non-zero condensate breaking for instance G_{HC} could form. In vector-like theories, no assumptions on the form of the condensate are required. Indeed if the theory condensates and the global symmetry is broken, the pattern of symmetry breaking is completely determined. According to the Vafa-Witten theorem (see section 2.2.5), in vector-like theories, $G_F = SU(N_f) \times SU(N_f)'$ and $H_F = SU(N_f)_V$; $G_F = SU(2N_f)$ and $H_F = SO(2N_f)$ (real case) or $H_F = Sp(2N_f)$ (pseudo-real case). These patterns of symmetry breaking are the same than the ones we have presented for any theory, not necessarily vector-like. However, in VL theories there is no assumptions about the form of the condensate, one just needs to know if the spontaneous breaking occurs or not. Then vector-like theories are more appealing from a theoretical point of view.

Finally, let us mention that in some cases one can explicitly demonstrate that the symmetry breaking happens using the so-called 't Hooft anomaly matching (see subsection 2.3 for the case of QCD). This is discussed in subsection 9.1.1 in the context of the minimal UV complete CHM. For

VL theories one can demonstrate that the spontaneous symmetry breaking occurs with the 't Hooft anomaly matching and we know the unbroken subgroup H_F. In non-VL theories we can use the same procedure and proof that the breaking occurs. However in that case we do not know what is the unbroken global symmetry.

7.3 Results of the classification

We now present the results of the classification with the requirements of section 7.1. We restrict to the cases where $p = 2$ and 3 [10] where the global non-anomalous symmetry is $G_F = SU(n_1) \times \cdots SU(n_p) \times U(1)^{p-1}$. Composite models with $p > 3$ are less minimal and bring no additional features.

Fixing the hypercolour gauge group G_{HC} and the set of irreducible representations R_i satisfying the constraints, there is generically several allowed values for the integers n_i. However, we restrict to the smallest possibility in each cases in order to remain as minimal as possible. Larger values of n_i leads to non-minimal models with a larger number of fermions and bigger cosets.

Note that in the $p = 1$ case where $G_F = SU(n)$, there is two cases that respect the requirements of section 7.1. However, these models are not very promising because of the difficulties with proton stability [10]. Indeed, among the large number of pNGBs, some of them mediate proton decay as the multiplets of $SU(n)$ contained in general mesonic resonances charged both under $SU(2)_L$ and $SU(3)_c$. Then we will not consider these theories as minimal UV completions and turn directly to the $p = 2$ and $p = 3$ cases. In the sequel, we follow the procedure of Ref. [10] to derive the allowed UV completions.

7.3.1 Case of two fermions (p=2)

Let us consider the case of two fermions in different irreducible representations of G_{HC}. In that case, for the EW sector we have m fermions ψ in the representation R_1 of G_{HC} and for the coloured sector we have n fermions X in the representation R_2. The corresponding non-anomalous global symmetry is $G_F = SU(m) \times SU(n) \times U(1)$. First, we want that the unbroken subgroup of $SU(m)$ that is $SO(m)$ or $Sp(m)$ contains $G_{cus}^{EW} = SU(2)_L \times SU(2)_R$ which is the part of the custodial group in the EW sector. In addition, we want that the coset $SU(m)/SO(m)$ or $SU(m)/Sp(m)$ contains the Higgs doublet in the appropriate representation of G_{cus}. This two requirements lead to $m \geq 4$ if R_1 is pseudo-real and $m \geq 5$ if R_1 is real. Then, for the EW sectors the two minimal cosets are $SU(4)/Sp(4)$ and $SU(5)/SO(5)$. The first possibility corresponds in fact to the next-to minimal effective composite Higgs model as $SU(4)/Sp(4) \cong SO(6)/SO(5)$ [256].

The other $SU(n)$ group is associated with the coloured sector and should contain the other part of the custodial symmetry that is $G_{cus}^c = SU(3)_c \times U(1)_x$ in an anomaly free way (as $SU(3)_c$ will be gauged). This requires $n \geq 6$ and leads to the following two minimal cosets: $SU(6)/SO(6)$ and $SU(6)/Sp(6)$. Note that, the coloured sector sector gives rise to additional pNGB which may eventually be light. However, they have to respect the present allowed bounds [260]. It can be the case by introducing a mass explicitly breaking $SU(6)$ but invariant under $SU(3)_c \times U(1)_x$. Moreover, in some cases QCD gauges contributions are enough to lifted the pNGBs masses up to the present allowed bounds. These two possibilities are discussed in section 9.2.4 in the context of the minimal UV completion.

Now we have the minimal patterns of symmetry breaking for the $p = 2$ case, one can determine the allowed gauge groups and representations satisfying the requirement of section 7.1. We can immediately eliminate the possibility $G_{HC} = SU(N)$. Indeed, in that case the one-loop beta function of Eq. (7.1.1) is

$$\beta_0 = \frac{22}{3}N - \frac{4}{3}mC(R_1) - 8C(R_2) \ , \qquad m = 4, 5 \ , \tag{7.3.1}$$

where we have used $C(\mathbf{Ad}) = N$ for $SU(N)$, $m = 4, 5$ depending if R_1 is real or pseudo-real and we have replaced $n = 6$ for R_2. As R_1 is real or pseudo-real, it does not contribute to the gauge anomalies and thus R_2 must also be real or pseudo-real since its anomaly contribution can not be

compensate against anything. In all cases where the representations are not complex, the asymptotic freedom is lost and the possibility $G_{HC} = SU(N)$ is excluded. In the same way, exceptional groups are eliminated [10]. The Dynkin indices, relevant to check the loss of asymptotic freedom, of the lowest dimensional representations of $SU(N)$, $SO(N)$ and $Sp(2N)$ are reported in table 7.1.

G_{HC}	R	dim(R)	$C(R) \equiv \ell(R)/2$	C/R/PR
$Sp(2N)$	$\square \equiv \mathbf{F}$	$(2N)$	$1/2$	PR
	$\begin{smallmatrix}\square\\\square\end{smallmatrix} \equiv \mathbf{A}_2$	$(2N+1)(N-1)$	$(N-1)$	R
	$\square\square \equiv \mathbf{S}_2 = \mathbf{Ad}$	$N(2N+1)$	$(N+1)$	R
$SO(N)$	$\square \equiv \mathbf{F}$	N	$1/2$	R
	Spin, Spin$'$	$2^{\lfloor (N+1)/2 \rfloor}/2$		R/PR/C
	$\begin{smallmatrix}\square\\\square\end{smallmatrix} \equiv \mathbf{A}_2 = \mathbf{Ad}$	$\frac{N(N-1)}{2}$	$\frac{N-2}{2}$	R
	$\square\square \equiv \mathbf{S}_2$	$\frac{(N-1)(N+2)}{2}$	$\frac{N+2}{2}$	R
$SU(N)$	$\square \equiv \mathbf{F}$	N	$1/2$	C
	$\mathbf{Ad}$	N^2-1	N	R
	$\begin{smallmatrix}\square\\\square\end{smallmatrix} \equiv \mathbf{A}_2$	$\frac{N(N-1)}{2}$	$\frac{N-2}{2}$	C
	$\square\square \equiv \mathbf{S}_2$	$\frac{N(N+1)}{2}$	$\frac{N+2}{2}$	C

Table 7.1: The dimensions $d(R)$, Dynkin index $C(R)$ and nature (real, pseudo-real or complex) of the lowest dimensional representations R of the $Sp(2N)$, $SO(N)$ and $SU(N)$ groups in which the fermions ψ and $X(\tilde{X})$ transform. The coefficient $C(R)$ is defined in subsection A and for the case of $SU(N)$ it respects $C(\overline{R}) = C(R)$. The Casimir coefficient $C_2(R)$ can easily be extracted from the relation $d(R)C_2(R) = d(\mathbf{Ad})C(R)$. Note that the spinorial representations of $SO(N)$ can be real, pseudo-real or complex depending on N (see table 7.2). Note also that depending on the value of N, some representations are not allowed. For e.g. this is the case in $SU(2) \cong Sp(2)$ for which $\mathbf{A}_2$ is not present. Finally, the symbol $\lfloor x \rfloor$ denotes the integer part of x and the Dynkin index of the *Spin* representation of $SO(N)$ is equal to $1/2$ for $N < 7$ and to $C(\mathbf{Spin}) = 2^{\lfloor (N+1)/2 \rfloor}/2^5$ otherwise.

We now consider the possibility $G_{HC} = Sp(2N)$ with $N \geq 2$ as $SU(2) \cong Sp(2)$. In that case, we have $C(\mathbf{F}) < C(\mathbf{A}_2) < C(\mathbf{S}_2 = \mathbf{Ad}) < \cdots$ as it can be seen from table 7.1. The only exception is for $Sp(6)$ where $C(\mathbf{A}_3) = 5/2$ is between $C(\mathbf{A}_2) = 2$ and $C(\mathbf{Ad}) = 4$. Note that the two representations $\mathbf{A}_2$ and $\mathbf{Ad}$ are real for $Sp(2N)$ while $\mathbf{F}$ and $\mathbf{A}_3$ are pseudo-real. We have restricted to lowest dimensional representations as they may respect the constraint of asymptotic freedom and in addition, they lead to minimal models. We will start by considering the representation with the largest Dynkin indices as the asymptotic freedom requirement is more difficult to respect in these cases. From Eq. (7.1.1) and the results above, the beta function is given by

$$\beta_0 = \frac{22}{3}(N+1) - \frac{4}{3}mC(R_1) - 8C(R_2) \ , \qquad m = 4, 5 \ . \tag{7.3.2}$$

The only case where $\mathbf{A}_3$ is allowed is for $Sp(6)$ with four $R_1 = \mathbf{A}_3$ and six $R_2 = \mathbf{F}$. However, in that case R_1 and R_2 are both pseudo-real and no baryons (odd number of fermions) are allowed. Now we consider the adjoint representation $\mathbf{Ad}$. If $R_2 = \mathbf{Ad}$, asymptotic freedom is lost. Then the only case where asymptotic freedom is preserved is for five $R_1 = \mathbf{Ad}$ and six $R_2 = \mathbf{F}$ with $2N \geq 12$ [5]. Note that

[5] Four fermions in the representation $R_1 = \mathbf{Ad}$ lead to a coset $SU(4)/SO(4)$ which is not relevant for a composite Higgs model.

it is possible to form top partners with the right quantum numbers in that case which appears as a viable UV complete CHM. It is listed in table 7.3 with the other models respecting the constraints of section 7.1. Moreover, due to the pseudo-reality of R_2, the baryons are constructed from an even (odd) number of fermions X (ψ). Then the $U(1)_x$ charge is fixed to $-1/3$ for the coloured fermions in order to have top partners with the correct hypercharges (see section 7.4.3). Similarly, the representation $R_1 = \mathbf{Ad}$ can be replaced by $R_1 = \mathbf{A}_2$ which have a smallest Dynkin index and is still real. One can see from Eq. (7.3.2) that there is no constraint from asymptotic freedom in this case [just $N \geq 2$ to forbid the case $Sp(2) \cong SU(2)$]. The last possible case with $Sp(2N)$ is four $R_1 = \mathbf{F}$ and six $R_2 = \mathbf{A}_2$. The asymptotic freedom leads to $2N \leq 36$ and as R_1 is pseudo-real, the baryons are made of an even (odd) number of fermions ψ (X) leading to a $U(1)_x$ charge for the coloured fermions equal to $2/3$.

The last possibility for the $p = 2$ case corresponds to $G_{HC} = SO(N)$ with $N \geq 7$ as the groups $SO(N < 7)$ are isomorphic to other SU or Sp groups. For $SO(N)$, the adjoint representation corresponds to the two-index antisymmetric representation ie $\mathbf{Ad} = \mathbf{A}_2$ which is real. Then the one-loop beta function is

$$\beta_0 = \frac{11}{3}(N-2) - \frac{4}{3}mC(R_1) - 8C(R_2) \ , \qquad m = 4, 5 \ . \tag{7.3.3}$$

Following the same procedure than for $Sp(2N)$ we find a viable case with five $R_1 = \mathbf{S}_2$ and six $R_2 = \mathbf{F}$ where asymptotic freedom requires $N \geq 55$. In the same way, five $R_1 = \mathbf{Ad}$ and six $R_2 = \mathbf{F}$ with $N \geq 15$ is possible. Note that, in the first case, the number of hypercolours is too large to be interesting for phenomenology.

Compare to $Sp(2N)$, there are also spinorial irreducible representations in $SO(N)$. The representations R_1 and R_2 can not be both spinorial otherwise, one could not construct baryons (one can not contract the three spinor indices) and one of the two must be a vector representation. Then we obtain two cases where $R_1 = \mathbf{F}$ and $R_2 = \mathbf{Spin}$ or $R_1 = \mathbf{Spin}$ and $R_2 = \mathbf{F}$ [6]. In both cases, asymptotic freedom leads to the constraint $N \leq 14$ (remember that $N \geqslant 7$). Furthermore, $N = 10$ and $N = 14$ are excluded as in this case the **Spin** representation is complex. The top partners requirements, leads to further restrictions and exclude the cases $N = 8, 12$ [10]. The $U(1)_x$ charge of the fermions X depends on the fermion which transforms in the **Spin** representation. Indeed, to contract the spinorial indices one needs two fermions in the **Spin** representation for each trilinear baryons. Then when $R_1 = \mathbf{F}$ and $R_2 = \mathbf{Spin}$ top partners are of the type ψXX and the $U(1)_x$ charges of the fermions X is $-1/3$. On the contrary, for $R_1 = \mathbf{Spin}$ and $R_2 = \mathbf{F}$ the top partners are of the type $\psi\psi X$ and then the $U(1)_x$ charge is rather $2/3$. Note that when the **Spin** representation is real, the top partners can a priori be of both type ($\psi\psi X$ or ψXX) and one can choose the charge to be equal to $-1/3$ or $2/3$. The reality of the **Spin** representation of any $SO(N)$ group can be extracted from table 7.2.

$SO(N)$	R/PR/C	$SO(N)$	R/PR/C
$SO(2+8k)$	C	$SO(7+8k)$	R
$SO(3+8k)$	PR	$SO(8+8k)$	R
$SO(4+8k)$	PR	$SO(9+8k)$	R
$SO(5+8k)$	PR	$SO(10+8k)$	C
$SO(6+8k)$	C		

Table 7.2: Nature of the *Spin* representation of $SO(N)$ for arbitrary N ($k = 0, 1, \cdots$). The abbreviations R, PR and C respectively refer to real, pseudo-real and complex representations.

[6] We do not specify the chirality of the **Spin** representation as one can choose one or the other.

7.3.2 Case of three fermions (p=3)

Let us now consider the case of three irreducible representations of G_{HC}. For the EW sector, we still stick to the minimal cases of subsection 7.3.1 where the coset is $SU(4)/Sp(4)$ or $SU(5)/SO(5)$. The difference compare to the $p = 2$ case appears then in the coloured sector where the $SU(3)_c$ symmetry is not embedded inside a subgroup of $SU(6)$ but rather in the diagonal part of the semi-simple group $SU(3) \times SU(3)'$. Then the global symmetry is $G_F = SU(m) \times SU(3) \times SU(3)' \times U(1) \times U(1)'$ where the $SU(3)$ and $SU(3)'$ global symmetries are generated respectively by the coloured fermions X and $\tilde{X}$ of table 7.8 and $m = 4$ or 5.

To allow a symmetric embedding of $SU(3)_c$ and then avoid $SU(3)_c$ anomalies, a further restriction is that $d(R_2) = d(R_3)$ and $C(R_2) = C(R_3)$ with $R_2 \neq R_3$. This restriction ruled out all symplectic and exceptional groups. Note that if $R_2 = R_3$, we come back to the case with an $SU(6)$ global symmetry in the coloured sector. In order to reproduce top partners with right quantum numbers, the $U(1)_x$ charge is fixed and is equal to $-1/3$ for fermion X and to $+1/3$ for the fermions $\tilde{X}$. This is because top partners are always made of two coloured fermions (see subsection 7.4.3).

We first consider the case of $G_{HC} = SU(N)$. Due to the symmetric embedding, the one-loop beta

G_{HC}	R_1 (fermions ψ)	R_2 (fermions X)	R_3 (fermions $\tilde{X}$)	Restrictions
$SU(4) \times SU(6)/Sp(4) \times SO(6)$				
$Sp(2N)$	$4 \times \mathbf{F}$	$6 \times \mathbf{A_2}$		$2 \leq N \leq 18$
$SO(N)$	$4 \times \mathbf{Spin}$	$6 \times \mathbf{F}$		$N = 11, 13$
$SU(5) \times SU(3) \times SU(3)/SO(5) \times SU(3)$				
$SU(N)$	$5 \times \mathbf{A_2}$	$3 \times \mathbf{F}$	$3 \times \overline{\mathbf{F}}$	$N = 4$
$SO(N)$	$5 \times \mathbf{F}$	$3 \times \mathbf{Spin}$	$3 \times \mathbf{Spin}'$	$N = 8, 10, 12, 14$
$SU(5) \times SU(6)/SO(5) \times Sp(6)$				
$Sp(2N)$	$5 \times \mathbf{A_2}$	$6 \times \mathbf{F}$		$N \geq 2$
$Sp(2N)$	$5 \times \mathbf{Ad}$	$6 \times \mathbf{F}$		$N \geq 6$
$SO(N)$	$5 \times \mathbf{F}$	$6 \times \mathbf{Spin}$		$N = 11, 13$
$SU(5) \times SU(6)/SO(5) \times SO(6)$				
$SO(N)$	$5 \times \mathbf{S_2}$	$6 \times \mathbf{F}$		$N \geq 55$
$SO(N)$	$5 \times \mathbf{Ad}$	$6 \times \mathbf{F}$		$N \geq 15$
$SO(N)$	$5 \times \mathbf{Spin}$	$6 \times \mathbf{F}$		$N = 7, 9$
$SO(N)$	$5 \times \mathbf{F}$	$6 \times \mathbf{Spin}$		$N = 7, 9$

Table 7.3: The minimal UV completions of composite Higgs model [10] based on the hypercolour gauge groups $G_{HC} = SU(N)$, $SO(N)$ or $Sp(2N)$. The UV completions are classify according to the pattern of global symmetries breaking which determines the number of pNGBs in the EW and coloured sector. The restriction on the number of hypercolours mainly comes from the requirement of asymptotic freedom but also from the presence of baryons and in particular of top partners in the spectrum.

function is the same than in Eq. (7.3.1). Then, imposing asymptotic freedom leads to the case where $R_1 = \mathbf{Ad}$, $R_2 = \mathbf{F}$ and $R_3 = \overline{\mathbf{F}}$ which corresponds to the EW coset $SU(5)/SO(5)$ as the adjoint representation is real. There is also three particular cases with a fixed number of hypercolours: i) $G_{HC} = SU(4)$ with $R_1 = \mathbf{A}_2$, $R_2 = \mathbf{F}$ and $R_3 = \overline{\mathbf{F}}$ [EW coset $SU(5)/SO(5)$], ii) $G_{HC} = SU(6)$ with $R_1 = \mathbf{A}_3$, $R_2 = \mathbf{F}$ and $R_3 = \overline{\mathbf{F}}$ [EW coset $SU(4)/Sp(4)$] and iii) $G_{HC} = SU(6)$ with $R_1 = \mathbf{A}_3$, $R_2 = \mathbf{A}_2$ and $R_3 = \overline{\mathbf{A}}_2$ [EW coset $SU(4)/Sp(4)$]. However, among these four cases, only the first of the three particular ones is viable after imposing the requirements coming from the top partners. Indeed, for the general $SU(N)$ case with $R_1 = \mathbf{Ad}$, $R_2 = \mathbf{F}$ and $R_3 = \overline{\mathbf{F}}$, there is top partners (no $SU(3)_c$ triplets) as the gauge invariant trilinears containing EW and coloured fermions are $(\psi X \tilde{X}) = \psi^i_j X_k \tilde{X}^l \delta^k_i \delta^j_l$, $(\psi^\dagger X X^\dagger)$ and $(\psi^\dagger \tilde{X} \tilde{X}^\dagger)$. For $SU(6)$ with $R_1 = \mathbf{A}_3$, $R_2 = \mathbf{F}$ and $R_3 = \overline{\mathbf{F}}$, all of the trilinear baryons contains an odd number of hypercolour indices and then, can not be contracted with the invariant tensors δ^j_i, ϵ_{ijklmn} and ϵ^{ijklmn}. Finally, for $SU(6)$ with $R_1 = \mathbf{A}_3$, $R_2 = \mathbf{A}_2$ and $R_3 = \overline{\mathbf{A}}_2$, the only allowed trilinear baryons are (XXX) and $(\tilde{X}\tilde{X}\tilde{X})$ which are $SU(2)_L$ singlets and can not serve as top partners.

Let us finally consider the case of $SO(N)$. As we need two different representations R_2 and R_3 realising a symmetric embedding of $SU(3)_c$ inside G_{SM} one can take $R_2 = \mathbf{Spin}$ and $R_3 = \mathbf{Spin}'$. The $\mathbf{Spin}'$ representation has opposite chirality than the $\mathbf{Spin}$ and is consequently different. Note that, the number of hypercolour N should be even [10] and with $R_1 = \mathbf{F}$, asymptotic freedom allows $N = 8, 10, 12, 14$. Top partners can be constructed for all of these cases.

7.4 Quantum numbers of the composite resonances

The above classification (see table 7.3) has been done according to the number of irreducible representations of the hypercolour gauge group G_{HC}. However, from a more phenomenological point of view, it is more relevant to consider the pattern of global symmetry breaking G_F/H_F as a distinction between the different models. Indeed, a particular coset fixes the quantum numbers of the resonances under the SM gauge group as well as their production from the SM gauge interactions. This information being crucial for the direct searches at collider [260], we list here the quantum numbers under the SM gauge group $SU(3)_c \times SU(2)_L \times U(1)_Y$ of the different resonances associated to the different cosets. In other words, we embed the SM gauge group inside the unbroken global symmetries and we decompose the representations of H_F into its subgroup G_{SM}. The decomposition of the representations can be found e.g. in Ref. [261] and a good review on Weyl fermions in Ref. [262]. This decomposition may seem tedious but we think that it can be useful to differentiate the different UV completions.

We first begin in subsection 7.4.1 by the mesons of the EW sector where the coset is $SU(4)/Sp(4)$ or $SU(5)/SO(5)$. Then we present the mesons of the coloured sector in subsection 7.4.2 with corresponding cosets $SU(6)/SO(6)$, $SU(6)/Sp(6)$ or $SU(3) \times SU(3)'/SU(3)_D$ [7] . Finally, we present the quantum numbers of the (trilinar) baryonic resonances in subsection 7.4.3.

7.4.1 Electroweak sectors

Let us start with the EW sector associated with the fundamental fermions ψ. As we have seen, there is two minimal cosets: $G_F^{EW}/H_F^{EW} = SU(4)/Sp(4)$ and $SU(5)/SO(5)$, which contain a Higgs doublet and also respect the custodial symmetry. The fundamental fermion ψ^a_i is a left-handed fermion in the representation R_1 of the hypercolour gauge symmetry [index $i = 1, \cdots, \dim(\mathrm{R}_1)$] and in the fundamental representation of the favour symmetry, that is, $SU(4)$ or $SU(5)$ (index $a = 1, \cdots, 4$ or 5). The $SU(2)_L \times SU(2)_R$ part of G_{cus} is embedded inside the unbroken global symmetry as well as the $SU(2)_L \times U(1)_Y$ part of G_{SM}. Then, the fundamental fermions as well as the resonances of the EW sector decompose into these two subgroups.

[7] Note that it is not possible to form a gauge bilinear invariant with one EW fermion and one coloured fermion as it can be seen from table 7.3.

- $SU(4)/Sp(4)$ **coset**

In the case where $G_F^{EW} = SU(4)$, the flavour symmetry $SU(4)$ is spontaneously broken to $H_F^{EW} = Sp(4)$ as the fundamental fermions ψ transform in a pseudo-real representation of the hypercolour gauge group G_{HC}. The latter decompose as [261]

$$\psi \sim 4_{SU(4)} = 4_{Sp(4)} = (2,1) + (1,2) = 2_0 + 1_{\pm 1/2} \ , \tag{7.4.1}$$

respectively under, $SU(4)$, $Sp(4)$, $SU(2)_L \times SU(2)_R \subset G_{cus}$ and $SU(2)_L \times U(1)_Y \subset G_{SM}$. Note that ψ is obviously not charged under $G_{cus}^c = SU(3)_c \times U(1)_x$. Then as $Y = T_R^3 + x$, the hypercharge of the EW fermions only originates from $SU(2)_R$ while the hypercharge of the coloured fermions originates from $U(1)_x$.

Let us consider the product of two (anti-)fundamental representations of $SU(4)$

$$4 \times 4 = 6_a + 10_s \ , \qquad 4 \times \overline{4} = 1 + 15_{Ad} \ , \tag{7.4.2}$$

where the subscripts a, s and Ad refer respectively to a symmetric, antisymetric contractions and to the adjoint representation. We are interested by the symmetry properties of the fermionic bilinears as the latter have the same quantum numbers than the physical resonances. The hypercolour contraction of the scalar bilinear $(\psi\psi)$ being antisymmetric due to the pseudo-reality of the gauge representation, the flavour contraction has to be antisymmetric as well. Note that, the Lorentz contraction is symmetric as $\psi_i^a \psi_j^b = \psi_j^b \psi_i^a$. As a consequence $(\psi\psi)$ transforms in the 6_a of $SU(4)$ and not in the 10_s. This sextet of $SU(4)$ decomposes into a singlet and a quintuplet under $Sp(4)$. For the vector bilinear $(\psi\sigma^\mu\psi^\dagger)$, there is no such properties of symmetry or antisymmetry as ψ is different from $\psi^\dagger$. Then $(\psi\sigma^\mu\psi^\dagger) \sim (1+15)_{SU(4)}$ where the adjoint representation decomposes under $Sp(4)$ as a 5 and a 10. Finally, for the tensor bilinear $(\psi\sigma^{\mu\nu}\psi)$, the hypercolour contraction is antisymmetric like for the scalar bilinear but the Lorentz contraction is antisymmetric leading to $(\psi\sigma^{\mu\nu}\psi) \sim 10_s$ of $SU(4)$. To summarise, we have

$$(\psi\psi) \sim 6_{SU(4)} = (1+5)_{Sp(4)} \ , \qquad (\psi\sigma^{\mu\nu}\psi) \sim 10_{SU(4)} = 10_{Sp(4)} \ , \tag{7.4.3}$$

$$(\psi\sigma^{\mu}\psi^\dagger) \sim (1+15)_{SU(4)} = (1+5+10)_{Sp(4)} \ . \tag{7.4.4}$$

The scalar bilinear leads to spin zero resonances which are scalar or pseudo-scalar with respect to the coset space. In the same way, the vector and tensor bilinears lead to spin one resonances which are vector or axial-vector. More precisely, the scalar and pseudo-scalar resonances are associated to the broken symmetry and leave in the coset $SU(4)/Sp(4)$. Then they transform as a $(1+5)$ of $Sp(4)$. For the spin one resonances, the vectors are associated to the unbroken symmetry $Sp(4)$ and then transform as a 10 while the axial-vectors are associated to the broken symmetry and transform as a $(1+5)$. The decompositions of the representations in Eqs. (7.4.3) and (7.4.4) under the custodial and SM subgroups of $Sp(4)$ proceed as follow

$$5_{Sp(4)} = (2,2) + (1,1) = 2_{\pm 1/2} + 1_0 \ , \tag{7.4.5}$$

$$10_{Sp(4)} = (3,1) + (2,2) + (1,3) = 3_0 + 2_{\pm 1/2} + 1_{\pm 1} + 1_0 \ . \tag{7.4.6}$$

Of course, the $Sp(4)$ singlets decompose into singlets with zero hypercharge. To determine the hypercharge of the resonances, we use $Y = T_R^3 + x = T_R^3$ where the last equality is only valid in the EW sector. All of these results are summarised in table 7.4.

- $SU(5)/SO(5)$ **coset**

We now follow exactly the same procedure for the second EW coset $G_F^{EW}/H_F^{EW} = SU(5)/SO(5)$where $SU(5)$ is spontaneously broken to $SO(5)$ as the fundamental fermion ψ transforms in a real representation of the hypercolour gauge group G_{HC}. The latter decompose as follow

$$\psi \sim 5_{SU(5)} = 5_{SO(5)} = (2,2) + (1,1) = 2_{\pm 1/2} + 1_0 \ , \tag{7.4.7}$$

	$SU(4)$	$Sp(4)$	$SU(2)_L \times SU(2)_R$	$SU(2)_L \times U(1)_Y$
ψ^a	4	4	$(2,1)+(1,2)$	$2_0 + 1_{\pm 1/2}$
$(\psi^a \psi^b)$	6	$1+5$	$(2,2)+2(1,1)$	$2_{\pm 1/2} + 1_0 + 1_0$
$(\psi^a \sigma^\mu \psi_b^\dagger)$	$1+15$	$1+5$	$(2,2)+2(1,1)$	$2_{\pm 1/2} + 1_0 + 1_0$
		$+10$	$(3,1)+(2,2)+(1,3)$	$3_0 + 2_{\pm 1/2} + 1_{\pm 1} + 1_0$
$(\psi^a \sigma^{\mu\nu} \psi^b)$	10	10	$(3,1)+(2,2)+(1,3)$	$3_0 + 2_{\pm 1/2} + 1_{\pm 1} + 1_0$

Table 7.4: Quantum numbers of the EW resonances when the coset is $G_H^{EW}/H_F^{EW} = SU(4)/Sp(4)$. The representations are decomposed according to the subgroups $H_F^{EW} = Sp(4)$, $G_{cus}^{EW} = SU(2)_L \times SU(2)_R$ and $SU(2)_L \times U(1)_Y$.

respectively under, $SU(5)$, $SO(5)$, $SU(2)_L \times SU(2)_R \subset G_{cus}$ and $SU(2)_L \times U(1)_Y \subset G_{SM}$. The product of two (anti-)fundamental representations of $SU(5)$ is the following

$$5 \times 5 = 10_a + 15_s \ , \qquad 5 \times \overline{5} = 1 + 24_{Ad} \ . \tag{7.4.8}$$

The hypercolour contraction of the scalar bilinear $(\psi\psi)$ being symmetric as the gauge representation is real, the flavour contraction have to be symmetric as well. As a consequence $(\psi\psi)$ transform in the 15_s of $SU(5)$. For the vector bilinear $(\psi\sigma^\mu\psi^\dagger)$ there is no symmetry properties and $(\psi\sigma^\mu\psi^\dagger) \sim (1{+}24)_{SU(5)}$ of $SU(5)$. Finally, the tensor bilinear $(\psi\sigma^{\mu\nu}\psi)$ is symmetric in the hypercolour space and then the flavour contraction has to be antisymmetric leading to $(\psi\sigma^{\mu\nu}\psi) \sim 10_a$ of $SU(5)$. To summarise, we have

$$(\psi\psi) \sim 15_{SU(5)} = (1+14)_{SO(5)} \ , \qquad (\psi\sigma^{\mu\nu}\psi) \sim 10_{SU(5)} = 10_{SO(5)} \ , \tag{7.4.9}$$

$$(\psi\sigma^{\mu}\psi^\dagger) \sim (1+24)_{SU(5)} = (1+10+14)_{SO(5)} \ . \tag{7.4.10}$$

The decompositions of the resonances in Eqs. (7.4.9) and (7.4.10) under the custodial and SM subgroups of $SO(5)$ is the following

$$14_{SO(5)} = (3,3)+(2,2)+(1,1) = 3_{\pm 1} + 3_0 + 2_{\pm 1/2} + 1_0 \ , \tag{7.4.11}$$

$$10_{SO(5)} = (3,1)+(2,2)+(1,3) = 3_0 + 2_{\pm 1/2} + 1_{\pm 1} + 1_0 \ . \tag{7.4.12}$$

An interesting point is that the 10 of $Sp(4)$ is the same than the 10 of $SO(5)$. Consequently, we expect the same vectors multiplets in the two cases. If uncoloured vectors resonances with quantum numbers other than those of Eq. (7.4.12) are discovered at collider, it will greatly compromise all the models listed in table 7.3. The results on the quantum numbers of the mesonic resonances of the $SU(5)/SO(5)$ sector are summarised in table 7.5.

7.4.2 Coloured sectors

We now turn to the coloured sector. The latter contains the fundamental fermions X in the case of $G_F^c = SU(6)$ and the fermions X and $\tilde{X}$ in the case of $G_F^c = SU(3) \times SU(3)'$. The three minimal cosets are: $G_F^c/H_F^c = SU(6)/SO(6)$, $SU(6)/Sp(6)$ and $SU(3) \times SU(3)'/SU(3)_D$. In the $SU(6)$ case, the fundamental fermion X_i^f is a left-handed fermion in the representation R_2 of the hypercolour gauge symmetry [index $i = 1, \cdots, \dim(\mathrm{R}_2)$] and in the fundamental representation of the favour symmetry that is $SU(6)$ (index $f = 1, \cdots, 6$). In the case of $SU(3) \times SU(3)'$, we have two left-handed fermions X_i^f and $\tilde{X}_{i'}^{f'}$ respectively in the representations R_2 and R_3 of the hypercolour gauge symmetry and in the fundamental representations of $SU(3)$ and $SU(3)'$. Note that the gauge indices

	$SU(5)$	$SO(5)$	$SU(2)_L \times SU(2)_R$	$SU(2)_L \times U(1)_Y$
ψ^a	5	5	$(2,2)+(1,1)$	$2_{\pm 1/2}+1_0$
$(\psi^a\psi^b)$	15	$1+14$	$(3,3)+(2,2)+2(1,1)$	$3_{\pm1}+3_0+2_{\pm1/2}+1_0+1_0$
$(\psi^a\sigma^\mu\psi^\dagger_b)$	$1+24$	$1+14$	$(3,3)+(2,2)+2(1,1)$	$3_{\pm1}+3_0+2_{\pm1/2}+1_0+1_0$
		$+10$	$(3,1)+(2,2)+(1,3)$	$3_0+2_{\pm1/2}+1_{\pm1}+1_0$
$(\psi^a\sigma^{\mu\nu}\psi^b)$	10	10	$(3,1)+(2,2)+(1,3)$	$3_0+2_{\pm1/2}+1_{\pm1}+1_0$

Table 7.5: Quantum numbers of the EW resonances when the coset is $G_H^{EW}/H_F^{EW} = SU(5)/SO(5)$. The representations are decomposed according to the subgroups $H_F^{EW} = SO(5)$, $G_{cus}^{EW} = SU(2)_L \times SU(2)_R$ and $SU(2)_L \times U(1)_Y$.

i and i' are different as they belong respectively to two different representations R_2 and R_3. However, the dimension of the two representations are the same and $i, i' = 1, \cdots, \dim(\mathrm{R}_2)$ (see table 7.3). In the same way, the flavour indices $f, f' = 1, \cdots, 8$ as they both belong to an $SU(3)$ group. As we have seen, the $SU(3)_c \times U(1)_x$ part of G_{cus} is embedded inside the unbroken global symmetry [8] as well as the $SU(3)_c \times U(1)_Y$ part of G_{SM}. Then, the fundamental fermions as well as the resonances of the coloured sector decompose into these two subgroups. The coloured fermions are not charged under $G_{cus}^{EW} = SU(2)_L \times SU(2)_R$ which is contained in the EW sector. Then the hypercharge of the coloured fermions only originates from $U(1)_x$ and is given by $Y = x$.

Now we have seen how the decomposition works for cosets of the type $SU(N)/SO(N)$ and $SU(N)/Sp(N)$, we briefly present in subsections 7.4.2 and 7.4.2 the result of the decomposition for the first two cosets with global symmetry $SU(6)$. Then we present in more details the last coset in subsection 7.4.2.

- $SU(6)/SO(6)$ **coset**

We begin the coloured sector by the coset $G_F^c/H_F^c = SU(6)/SO(6)$. The fundamental fermion X decomposes as follow

$$X \sim 6_{SU(6)} = 6_{SO(6)} = 3_x + \overline{3}_{-x} = \begin{pmatrix} \chi_x \\ \tilde{\chi}_{-x} \end{pmatrix} , \tag{7.4.13}$$

respectively under, $SU(6)$, $SO(6)$ and $SU(3)_c \times U(1)_Y \subset G_{SM}$. Note that we do not specify the transformation under $U(1)_x$ as for the coloured fermions we have $x = Y$. Note also that the hypercharge is not fixed as the top partners can contain one or two coloured fermion (see subsection 7.4.3). The product of two (anti-)fundamental representations of $SU(6)$ is given by

$$6 \times 6 = 15_a + 21_s , \qquad 6 \times \overline{6} = 1 + 35_{Ad} . \tag{7.4.14}$$

The hypercolour contraction of the scalar bilinear (XX) being symmetric as the gauge representation is real, the flavour contraction have to be symmetric as well. As a consequence (XX) transform in the 21_s of $SU(6)$. The vector bilinear $(X\sigma^\mu X^\dagger)$ transforms as $(1+35)_{SU(6)}$ of $SU(6)$ while the tensor bilinear $(X\sigma^{\mu\nu}X)$ is symmetric in the hypercolour space and then the flavour contraction has to be antisymmetric leading to $(X\sigma^{\mu\nu}X) \sim 15_a$ of $SU(6)$. To summarise, we have

$$(XX) \sim 21_{SU(6)} = (1+20')_{SO(6)} , \qquad (X\sigma^{\mu\nu}X) \sim 15_{SU(6)} = 15_{SO(6)} , \tag{7.4.15}$$

$$(X\sigma^\mu X^\dagger) \sim (1+35)_{SU(6)} = (1+20'+15)_{SO(6)} . \tag{7.4.16}$$

[8] More precisely in the $SU(6)$ cases, $U(1)_x$ is embedded inside the $SO(6)$ or $Sp(6)$ while in the $SU(3)\times SU(3)'\times U(1)_D$ case it corresponds to the diagonal $U(1)_D$ symmetry (the equivalent of $U(1)_V$ in QCD).

Note that in $SU(6)$ there is three inequivalent representations of dimension 20: the representations 20, 20′ and 20″. then we should be careful for the decomposition into the SM group that the 21 of $SU(6)$ decomposes into a singlet and a 20′. The decomposition of the resonances in Eqs. (7.4.15) and (7.4.16) under the SM subgroups of $SO(6)$ is the following

$$15_{SO(6)} = 8_0 + 3_{-2x} + \overline{3}_{2x} + 1_0 \ , \qquad 20'_{SO(6)} = 8_0 + 6_{2x} + \overline{6}_{-2x} \ . \tag{7.4.17}$$

Note that the $U(1)_Y$ charges are easily determined from Eq. (7.4.13) as the fermion X decomposes into a triplet χ and an anti-triplet $\tilde{\chi}$ with respective hypercharge x and $-x$. Then the coloured octets and singlets can only come from the products $\chi\tilde{\chi}, \chi\chi^\dagger, \cdots$ which have zero hypercharge. In the same way, sextets and anti-triplets come from the products $\chi\chi, \tilde{\chi}\tilde{\chi}$ and have then an hypercharge equal to $2x$. The results on the quantum numbers of the mesonic resonances of the $SU(6)/SO(6)$ sector are summarised in table 7.6.

	$SU(6)$	$SO(6)$	$SU(3)_c \times U(1)_Y$
X^f	6	6	$3_x + \overline{3}_{-x}$
$(X^f X^g)$	21	$1 + 20'$	$8_0 + 6_{2x} + \overline{6}_{-2x} + 1_0$
$(X^f \sigma^\mu X^\dagger_g)$	$1 + 35$	$1 + 20'$	$8_0 + 6_{2x} + \overline{6}_{-2x} + 1_0$
		$+15$	$8_0 + 3_{-2x} + \overline{3}_{2x} + 1_0$
$(X^f \sigma^{\mu\nu} X^g)$	15	15	$8_0 + 3_{-2x} + \overline{3}_{2x} + 1_0$

Table 7.6: Quantum numbers of the coloured resonances when the coset is $G^c_H/H^c_F = SU(6)/SO(6)$. The representations are decomposed according to the subgroups $H^c_F = SO(6)$and $SU(3)_c \times U(1)_Y$. Note that the hypercharge is not fixed and can be equal to $x = 2/3$ and $x = -1/3$.

- $SU(6)/Sp(6)$ **coset**

We now consider the coset $G^c_F/H^c_F = SU(6)/SO(6)$. In that case, the fundamental fermion X decomposes as follow

$$X \sim 6_{SU(6)} = 6_{Sp(6)} = 3_{-1/3} + \overline{3}_{1/3} = \begin{pmatrix} \chi_{-1/3} \\ \tilde{\chi}_{1/3} \end{pmatrix} \ , \tag{7.4.18}$$

respectively under, $SU(6)$, $Sp(6)$ and $SU(3)_c \times U(1)_Y \subset G_{SM}$. The decomposition under the SM group is the same than for the $SO(6)$ case however, the hypercharge is now equal to $-1/3$ as the top partners contains two coloured fermions (see subsection 7.4.3).

The hypercolour contraction of the scalar bilinear (XX) being antisymmetric as the gauge representation is pseudo-real, the flavour contraction have to be antisymmetric as well. As a consequence (XX) transform in the 15_a of $SU(6)$. The vector bilinear $(X\sigma^\mu X^\dagger)$ still transforms as $(1+35)_{SU(6)}$ of $SU(6)$ while the tensor bilinear $(X\sigma^{\mu\nu}X)$ is antisymmetric in the hypercolour space and then the flavour contraction has to be symmetric leading to $(X\sigma^{\mu\nu}X) \sim 21_s$ of $SU(6)$. To summarise, we have

$$(XX) \sim 15_{SU(6)} = (1+14)_{Sp(6)} \ , \qquad (X\sigma^{\mu\nu}X) \sim 21_{SU(6)} = 21_{Sp(6)} \ , \tag{7.4.19}$$

$$(X\sigma^\mu X^\dagger) \sim (1+35)_{SU(6)} = (1+14+21)_{Sp(6)} \ . \tag{7.4.20}$$

The decompositions of the resonances in Eqs. (7.4.19) and (7.4.20) under the SM subgroups of $Sp(6)$ is the following

$$14_{Sp(6)} = 8_0 + 3_{2/3} + \overline{3}_{-2/3} \ , \qquad 21_{Sp(6)} = 8_0 + 6_{-2/3} + \overline{6}_{2/3} + 1_0 \ . \tag{7.4.21}$$

The results on the quantum numbers of the mesonic resonances of the $SU(6)/Sp(6)$ sector are summarised in table 7.7.

	$SU(6)$	$Sp(6)$	$SU(3)_c \times U(1)_Y$
X^f	6	6	$3_x + \overline{3}_{-x}$
$(X^f X^g)$	15	$1 + 14$	$8_0 + 3_{2/3} + \overline{3}_{-2/3} + 1_0$
$(X^f \sigma^\mu X_g^\dagger)$	$1 + 35$	$1 + 14$	$8_0 + 3_{2/3} + \overline{3}_{-2/3} + 1_0$
		$+15$	$8_0 + 6_{-2/3} + \overline{6}_{2/3} + 1_0$
$(X^f \sigma^{\mu\nu} X^g)$	21	21	$8_0 + 6_{-2/3} + \overline{6}_{2/3} + 1_0$

Table 7.7: Quantum numbers of the coloured resonances when the coset is $G_H^c/H_F^c = SU(6)/Sp(6)$. The representations are decomposed according to the subgroups $H_F^c = Sp(6)$and $SU(3)_c \times U(1)_Y$.

- $SU(3) \times SU(3)'/SU(3)_V$ **coset**

Finally, let us consider the last coset of the coloured sector that is $G_F^c/H_F^c = SU(3) \times SU(3)'/SU(3)_D$. In that case, the fundamental fermion X and $\tilde{X}$ decomposes as follow

$$X \sim (3,1) = 3_{-1/3} \ , \qquad \tilde{X} \sim (1,3) = \overline{3}_{1/3} \ , \tag{7.4.22}$$

respectively under, $SU(3) \times SU(3)'$, $SU(3)_D \times U(1)_x \subset G_{cus}$. Note that $SU(3)_D \equiv SU(3)_c$ and in the coloured sector we have $x = Y$ such that $SU(3)_D \times U(1)_x$ is equivalent to $SU(3)_c \times U(1)_Y$. As we have seen in subsection 7.3.2, the gauge representation of the coloured fermions can be complex, real or pseudo-real depending on the UV completion. Then there is two distinct cases. Let us begin by the complex case where the scalar bilinear is $(X\tilde{X})$ and transforms in the $(3,3)$ of $SU(3) \times SU(3)'$. The tensor bilinear is $(X\sigma^{\mu\nu}\tilde{X})$ transforms as the scalar bilinear while there is two vector bilinears which are $(X\sigma^\mu X^\dagger)$ and $(\tilde{X}\sigma^\mu \tilde{X}^\dagger)$ and transform respectively as $(1,1) + (8,1)$ and $(1,1) + (1,8)$. To summarise, we have

$$(X\tilde{X}) \sim (3,3) = (1+8)_0 \ , \qquad (X\sigma^{\mu\nu}\tilde{X}) \sim (3,3) = (1+8)_0 \ , \tag{7.4.23}$$

$$(X\sigma^\mu X^\dagger) \sim (1,1) + (8,1) = (1+8)_0 \ , \qquad (\tilde{X}\sigma^\mu \tilde{X}^\dagger) \sim (1,1) + (1,8) = (1+8)_0 \ , \tag{7.4.24}$$

under $SU(3) \times SU(3)'$ and $SU(3)_c \times U(1)_Y$ respectively. This is the usual decomposition which occurs in the QCD case. We can see it more easily by introducing the Dirac fermion

$$\mathcal{X} = \begin{pmatrix} X \\ \tilde{X}^\dagger \end{pmatrix} \ , \qquad \overline{\mathcal{X}} = \begin{pmatrix} \tilde{X} & X^\dagger \end{pmatrix} \tag{7.4.25}$$

Then the scalar and vector bilinears are

$$(\overline{\mathcal{X}}\mathcal{X}) = (\tilde{X}X + X^\dagger \tilde{X}^\dagger) \ , \qquad (\overline{\mathcal{X}}\gamma^\mu \mathcal{X}) = (X^\dagger \overline{\sigma}^\mu X + \tilde{X}\sigma^\mu \tilde{X}^\dagger) \ , \tag{7.4.26}$$

and similarly for the pseudo-scalar, axial and tensor bilinears.

Let us now consider the cases where the gauge representations of the coloured fermions are not complex but rather real or pseudo-real. In that cases, we have new possibilities to form a bilinear gauge invariant compare to the complex case. For the scalars bilinears, we also have (XX) and $(\tilde{X}\tilde{X})$ and the same for the tensor bilinears while for the vector we now have $(X\sigma^\mu \tilde{X}^\dagger)$. In addition of course to the bilinears in Eqs. (7.4.23) and (7.4.24). The new allowed bilinears transform as follow

$$(XX) \sim (\overline{3}_a, 1) + (6_s, 1) = \overline{3}_a + 6_s \ , \qquad (\tilde{X}\tilde{X}) = (1, \overline{3}_a) + (1, 6_s) = 3_a + \overline{6}_s \ , \tag{7.4.27}$$

$$(X\sigma^{\mu\nu}X) \sim (\overline{3}_a, 1) + (6_s, 1) = \overline{3}_a + 6_s \ , \qquad (\tilde{X}\sigma^{\mu\nu}\tilde{X}) = (1, \overline{3}_a) + (1, 6_s) = 3_a + \overline{6}_s \ , \tag{7.4.28}$$

$$(X\sigma^\mu \tilde{X}^\dagger) \sim (3,\overline{3}) = \overline{3}_a + 6_s \ . \tag{7.4.29}$$

In Dirac notation, these bilinears come the conjugate Dirac multiplet

$$\mathcal{X}^c = \begin{pmatrix} \tilde{X} \\ X^\dagger \end{pmatrix} \ , \qquad \overline{\mathcal{X}^c} = \begin{pmatrix} X & \tilde{X}^\dagger \end{pmatrix} \tag{7.4.30}$$

which leads to

$$(\overline{\mathcal{X}^c}\mathcal{X}) = (XX + \tilde{X}^\dagger \tilde{X}^\dagger) \ , \qquad (\overline{\mathcal{X}^c}\gamma^\mu \mathcal{X}) = (\tilde{X}^\dagger \overline{\sigma}^\mu X + X\sigma^\mu \tilde{X}^\dagger) \ , \tag{7.4.31}$$

and similarly for the pseudo-scalar, axial and tensor modes. These bilinears do not correspond to mesonic resonances in QCD or in QCD-like theories (with two complex gauge representations) as they are not gauge invariant in that cases. However, it does not remain true for fermions in real or pseudo-real gauge representations. As in the precedent subsections, in the real and pseudo-real cases the flavour representations are restricted by the symmetry properties of the gauge and Lorentz contractions. In the real case, the gauge contraction is symmetric and only the symmetric (antisymmetric) contraction is present for the scalar (tensor) bilinears. For instance (XX) transform as a $\overline{3}_{-2/3}$ of $SU(3)_c \times U(1)_Y$ while $(X\sigma^{\mu\nu}X)$ transforms as a $6_{-2/3}$. For the vector bilinears there is no such restriction and they transform as in Eq (7.4.29). As mentioned above, one can identify the vector and axial-vector contained in $(X\sigma^\mu \tilde{X}^\dagger)$. Indeed, the vectors transform in the same representation than the ones contains in the tensor bilinear while the axial-vectors transform in the same representation than the scalar bilinear. In the pseudo-real case, this is the opposite, only the antisymmetric (symmetric) contraction is present for the scalar (tensor) bilinears and again there is no such restriction for the vector bilinears. The above results on the quantum numbers of the mesonic resonances of the $SU(3) \times SU(3)'/SU(3)_D$ sector are summarised in table 7.8.

	$SU(3) \times SU(3)'$		$SU(3)_c \times U(1)_Y$	
X^f	$(3,1)$		$3_{-1/3}$	
$\tilde{X}_f$	$(1,3)$		$\overline{3}_{1/3}$	
$(X^f \tilde{X}_g)$, $(X^f \sigma^{\mu\nu} \tilde{X}_g)$	$(3,3)$		$(1+8)_0$	
$(X^f \sigma^\mu X^\dagger_g)$	$(1,1)+(8,1)$		$(1+8)_0$	
$(\tilde{X}_f \sigma^\mu \tilde{X}^{\dagger g})$	$(1,1)+(1,8)$		$(1+8)_0$	
	R	PR	R	PR
$(X^f X^g)$	$(6,1)$	$(\overline{3},1)$	$6_{-2/3}$	$\overline{3}_{-2/3}$
$(\tilde{X}_f \tilde{X}_g)$	$(1,6)$	$(1,\overline{3})$	$\overline{6}_{2/3}$	$3_{2/3}$
$(X^f \sigma^\mu \tilde{X}^{\dagger g})$	$(3,\overline{3})$		$(\overline{3}+6)_{-2/3}$	
$(X^f \sigma^{\mu\nu} X^g)$	$(\overline{3},1)$	$(6,1)$	$\overline{3}_{-2/3}$	$6_{-2/3}$
$(\tilde{X}_f \sigma^{\mu\nu} \tilde{X}_g)$	$(1,\overline{3})$	$(1,6)$	$3_{2/3}$	$\overline{6}_{2/3}$

Table 7.8: Quantum numbers of the coloured resonances when the coset is $G^c_H/H^c_F = SU(3) \times SU(3)'/SU(3)_D$. The representations are decomposed according to the subgroup $SU(3)_c \times U(1)_Y$. Note that as explained in the text, in the real (R) and pseudo-real cases (PR) there is additional allowed resonances.

7.4.3 Baryonic sectors

In the two precedent subsections, we have presented the quantum numbers of the EW and coloured resonances. We now consider the baryonic sector of the UV completions. For simplicity, we restrict to trilinears bound states. Note that similarly, for the mesons we implicitly restricted to bilinear bound states. The different possible baryons depend on the particular model of table 7.3 under consideration. Indeed, if the global symmetries change, the representation of the baryons change as well. Then we will consider each kind of coset separately and study the allowed baryons and their quantum numbers as we did for the mesons in the next subsections. In particular, we will focus on the top partners as they are an indispensable ingredient to realise the partial compositeness paradigm present in composite Higgs models (see chapter 6). The top partners have the opposite quantum numbers of the top multiplets q_L and t_R^c that is $Q_L \sim (\overline{3}, 2, -1/6)$ and $T_R^c \sim (3, 1, 2/3)$. In addition, as the top partners couple by definition linearly to the top, they should have the same chirality that we choose to be left-handed (with the above quantum numbers) by convention.

- $SU(4) \times SU(6)/Sp(4) \times SO(6)$ **coset**

Let us begin by the coset $G_F/H_F = SU(4) \times SU(6)/Sp(4) \times SO(6)$. In that case, the EW fermions ψ are in a pseudo-real representation of G_{HC} while the coloured fermions X are in a real representation. Then in all generality, the baryons should contain an even number of ψ leading for the trilinear baryons to the five following possibilities

$$\Psi^{abf} = (\psi^a \psi^b X^f) \ , \qquad \Psi^a_{bf} = (\psi^a \psi^\dagger_b X^\dagger_f) \ , \qquad \Psi^f_{ab} = (\psi^\dagger_a \psi^\dagger_b X^f) \ , \tag{7.4.32}$$

$$\Psi^{fgh} = (X^f X^g X^h) \ , \qquad \Psi^f_{gh} = (X^f X^\dagger_g X^\dagger_h) \ , \tag{7.4.33}$$

plus their conjugates. Note that the brackets stand for hypercolour contraction (multiple and independent contractions are possible). We also assume spin-1/2 baryons but in principle other Lorentz representations are allowed. For example, $\Psi^{abf} \sim (1/2, 0) + (3/2, 0)$ and $\Psi^a_{bf} \sim (1/2, 0) + (1/2, 1)$ under the Lorentz group. Top partners are left or right-handed spin 1/2 fermions and consequently we will restrict to the representations $(1/2, 0)$ and $(0, 1/2)$ in the next. Note that in Eqs. (7.4.32) and (7.4.33), the baryons contain either three left-handed fermions either one left-handed and two right-handed fermions. This is just a convention (as the conjugate fermions have the opposite chirality) but in this way, all of the baryons that we will consider are left-handed that is they transform as $(1/2, 0)$ exactly like Q_L and T_R^c.

We now focus only on the top partners that is on the baryons in Eq. (7.4.32). One can easily check that some of these baryons are top partners. For example, let us consider the baryon $\Psi^{abf} \sim (6, 6) + (10, 6)$ under $SU(4) \times SU(6)$. Using the results of subsections 7.4.1 and 7.4.2 we find that the $SU(4) \times SU(6)$ representations decompose as follow under $SU(3)_c \times SU(2)_L \times U(1)_Y$

$$(6, 6) = (3, 2)_{7/6} + (\overline{3}, 2)_{-1/6} + 2(3, 1)_{2/3} + h.c. \tag{7.4.34}$$

$$\begin{aligned}(10, 6) = (3, 2)_{7/6} + (\overline{3}, 2)_{-1/6} + (3, 1)_{2/3} + (3, 1)_{5/3} \\ + (3, 1)_{-1/3} + (3, 3)_{2/3} + h.c.\end{aligned} \tag{7.4.35}$$

Then in addition to other baryons we have the desired top partners $Q_L \sim (\overline{3}, 2, -1/6)$ and $T_R^c \sim (3, 1, 2/3)$. All of the other decompositions are reported in table 7.9.

Note that the x charge of the fermions X is equal to 2/3 in order to have top partners Q_L and T_R^c but the doublet Q_L can also serve as a bottom partner. In addition, as it can be seen in table 7.9, we have bottom partners $B_R^c \sim (3, 1, -1/3)$ in some cases. However the bottom partner B_R^c is not always present as it is the case for T_R^c. If we rather choose $x = -1/3$, the situation is reversed that is each baryons decompose in bottom partners B_R^c but not always in top partners T_R^c.

Note also that the UV completions are VL compare to the SM group such that the decomposition of (r_4, r_6) under the SM group is the same than the ones of $(\overline{r_4}, r_6), (r_4, \overline{r_6})$ and $(\overline{r_4}, \overline{r_6})$, where r_4

Baryon	$SU(4)\times SU(6)$	$SU(3)_c\times SU(2)_L\times U(1)_Y$
Ψ^{abf}	$(6,6)$	$(3,2)_{7/6}+(\overline{3},2)_{-1/6}+2(3,1)_{2/3}+h.c.$
	$(10,6)$	$(3,3)_{2/3}+(3,2)_{7/6}+(\overline{3},2)_{-1/6}$ $+(3,1)_{5/3}+(3,1)_{2/3}+(3,1)_{-1/3}+h.c.$
Ψ^a_{bf}	$(1,\overline{6})$	$(3,1)_{2/3}+h.c.$
	$(15,\overline{6})$	$(3,3)_{2/3}+2(3,2)_{7/6}+2(\overline{3},2)_{-1/6}$ $+(3,1)_{5/3}+2(3,1)_{2/3}+(3,1)_{-1/3}+h.c.$

Table 7.9: Quantum numbers of the baryonic resonances containing the top partners in the case where the coset is $G_F/H_F = SU(4)\times SU(6)/Sp(4)\times SO(6)$. As explained in the text, $\Psi^{ab}_f\sim(6,\overline{6})+(10,\overline{6})$ under $SU(4)\times SU(6)$, decomposes in the same way than Ψ^{abf} under the SM group. The top partners $Q_L\sim(\overline{3},2)_{-1/6}$ and $T^c_R\sim(3,1)_{2/3}$ are written in blue.

and r_6 are representations of $SU(4)$ and $SU(6)$ respectively. Then $\Psi^{abf}\sim(6,6)+(10,6)$ and $\Psi^{ab}_f\sim(6,\overline{6})+(10,\overline{6})$ decompose in the same way under G_{SM}.

Finally, depending on the gauge contraction, some flavour representations can be absent. For instance, in the case of Ψ^{abf}, the flavour contraction between the two fermions ψ leads to a 6 antisymmetric and a 10 symmetric of $SU(4)$. Depending on the symmetry property of the gauge contraction (and also on the Lorentz contraction), one of the two representations can be absent. For all of the baryons in Eq. (7.4.32), the gauge indices can be contracted in the proper way to form a gauge invariant in the two cases of table 7.3. For example let us consider again Ψ^{abf}. In the case $G_{HC}=Sp(2N)$, the fermion ψ transforms in the fundamental representation of $Sp(2N)$ while the fermion X in the representation $\mathbf{A}_2$. Then Ψ^{abf} is made of $\psi^{a\alpha}_i\psi^{b\beta}_j X^{f\gamma}_{kl}$ where $i,j,\cdots$ are hypercolour indices, $a,b,\cdots$ flavour indices and $\alpha,\beta,\cdots$ Lorentz indices. To obtain a baryon, we should contract the gauge and Lorentz indices. We obtain two inequivalent contractions depending on the uncontracted Lorentz index

$$\psi^{a\alpha}_i\psi^{b\beta}_j X^{f\gamma}_{kl}\Omega_{ik}\Omega_{lj}(\epsilon_{\alpha\beta}+\epsilon_{\alpha\gamma})\ , \tag{7.4.36}$$

where $\Omega_{ij}=-\Omega_{ji}$ is the invariant tensor of $Sp(2N)$ and the contraction $\Omega_{il}\Omega_{kj}$ is equivalent as $X_{ij}=-X_{ji}$. Also, $\Omega_{ij}\Omega_{lk}$ is not possible as the representation $\mathbf{A}_2$ is traceless ie $X_{ij}\Omega_{ji}=0$ (see chapter 8). Then the exchange of the flavour indices a and b with the Lorentz contraction $\epsilon_{\alpha\beta}$ is antisymmetric and the non-zero flavour contraction is the $6_{SU(4)}$. For the contraction $\epsilon_{\alpha\gamma}$, there is no properties of symmetry and the two flavour representations are present. Doing the same thing in the case of $G_{HC}=SO(N)$ one finds that the baryons in Eqs. (7.4.32) and (7.4.33) can be contracted in a gauge invariant way.

Note that for baryons like Ψ^a_{bf}, there is no restriction of symmetry as the three fermions are different. In the next, we will not determine the allowed flavour representations. As we have seen, in general all of them are allowed if one consider all of the gauge and Lorentz contractions. However, we will check that it is possible to form a gauge invariant.

- $SU(5)\times SU(6)/SO(5)\times Sp(6)$ **coset**

We now follow exactly the same procedure for the coset $G_F/H_F=SU(5)\times SU(6)/SO(5)\times Sp(6)$. As the EW fermions ψ are in a real representation of G_{HC} and the coloured fermions X in a pseudo-real representation, the baryons are made of an even number of X fermions. Then the trilinears baryons are the following

$$\Psi^{afg}=(\psi^a X^f X^g)\ ,\quad \Psi^a_{fg}=(\psi^a X^\dagger_f X^\dagger_g)\ ,\quad \Psi^f_{ag}=(\psi^\dagger_a X^f X^\dagger_g)\ , \tag{7.4.37}$$

$$\Psi^{abc} = (\psi^a \psi^b \psi^c) \ , \quad \Psi^a_{bc} = (\psi^a \psi^\dagger_b \psi^\dagger_c) \ , \tag{7.4.38}$$

plus their conjugate. Compare to the precedent coset, the top partners in Eq. (7.4.37) contain two fermions X instead of one and their $U(1)_x$ charge is equal to $-1/3$. The decompositions of the trilinears baryons containing the top partners are reported in table 7.10. Let us just note that due to the VL embedding of the SM group inside G_F, $\Psi^a_{fg} \sim (5, \overline{15}) + (5, \overline{21})$ under $SU(5) \times SU(6)$, decomposes in the same way than Ψ^{afg} under the SM group.

Baryon	$SU(5) \times SU(6)$	$SU(3)_c \times SU(2)_L \times U(1)_Y$
Ψ^{afg}	$(5, 15)$	$[(8,2)_{1/2} + (1,2)_{1/2} + (3,2)_{7/6} + (\overline{3},2)_{-1/6}$ $+(3,1)_{2/3} + h.c.] + (8,1)_0 + (1,1)_0$
	$(5, 21)$	$[(8,2)_{1/2} + (1,2)_{1/2} + (\overline{6},2)_{7/6} + (\overline{6},2)_{1/6}$ $+(\overline{6},1)_{2/3} + h.c.] + (8,1)_0 + (1,1)_0$
Ψ^f_{ag}	$(\overline{5}, 1)$	$(1,2)_{\pm 1/2} + (1,1)_0$
	$(\overline{5}, 35)$	$[2(8,2)_{1/2} + (1,2)_{1/2} + (3,2)_{7/6} + (\overline{3},2)_{-1/6}$ $+(3,1)_{2/3} + (\overline{6},2)_{7/6} + (\overline{6},2)_{1/6} + (\overline{6},1)_{2/3} + h.c.]$ $+2(8,1)_0 + (1,1)_0$

Table 7.10: Quantum numbers of the baryonic resonances containing the top partners in the case where the coset is $G_F/H_F = SU(5) \times SU(6)/SO(5) \times Sp(6)$. As explained in the text, $\Psi^a_{fg} \sim (5, \overline{15}) + (5, \overline{21})$ under $SU(5) \times SU(6)$, decomposes in the same way than Ψ^{afg} under the SM group. The top partners $Q_L \sim (\overline{3}, 2)_{-1/6}$ and $T^c_R \sim (3, 1)_{2/3}$ are written in blue.

Finally, all of the baryons in Eqs. (7.4.37) and (7.4.38) can be contracted in gauge singlets for $G_{HC} = Sp(2N)$ with $R_1 = \mathbf{A}_2, \mathbf{Ad}$ and $R_2 = \mathbf{F}$. Similarly for $G_{HC} = SO(N)$ with $R_1 = \mathbf{F}$ and $R_2 = \mathbf{Spin}$, the baryons in Eq. (7.4.37) can form gauge singlets but not the ones in Eq. (7.4.38).

- $SU(5) \times SU(6)/SO(5) \times SO(6)$ **coset**

The next coset that we investigate is $G_F/H_F = SU(5) \times SU(6)/SO(5) \times SO(6)$. Now, the EW fermions ψ and the coloured fermions X are both in a real representation of G_{HC}. Then, there is no restriction on the number of fermions ψ or X in the baryons (the total number of fermions has only to be odd to form a baryon). As a consequence, the trilinears baryons are those of Eqs. (7.4.32), (7.4.33), (7.4.37) and (7.4.38). Of course, the decomposition of these baryons under the SM is not the same than before as the coset is different. As the number of X fermions is not fixed in the baryons, one can choose for the $U(1)_x$ charge $x = 2/3$ or $x = -1/3$. The decomposition of the baryons containing the top partners is reported in table 7.11 for $x = 2/3$ and in table 7.12 for $x = -1/3$. In the case of $x = 2/3$, one see that the top partners are only present for the baryons of Eqs. (7.4.32) and (7.4.33). On the contrary, for $x = -1/3$ all of the baryons in table 7.12 contain top partners. Then from this point of view, the case $x = -1/3$ seems to be more promising.

As before, due to the VL embedding of the SM group inside the global symmetriesΨ^f_{ab} decomposes as Ψ^{abf} under the SM group as well as Ψ^a_{fg} decomposes as Ψ^{afg}.

We now comment on the possibility to form $SO(N)$ gauge invariants depending on the details of the gauge contractions. First in the cases where $R_1 = \mathbf{S}_2$ or $R_1 = \mathbf{Ad}$ and $R_2 = \mathbf{F}$, the baryons in Eqs. (7.4.32) and (7.4.33) are all excluded as in these cases there is five gauge indices which can not be all contracted with the invariant tensor δ_{ij}. However, the baryons in Eqs. (7.4.37) and (7.4.38) can be contracted in a gauge invariant way. In the same way, for $R_1 = \mathbf{F}$ and $R_2 = \mathbf{Spin}$, the baryons in

Baryon	$SU(5) \times SU(6)$	$SU(3)_c \times SU(2)_L \times U(1)_Y$
Ψ^{abf}	$(10,6)$	$(3,3)_{2/3} + (3,2)_{7/6} + (\overline{3},2)_{-1/6} + (3,1)_{5/3}$ $+(3,1)_{-1/3} + (3,1)_{2/3} + h.c.$
	$(15,6)$	$(3,3)_{5/3} + (3,3)_{-1/3} + (3,3)_{2/3} + (3,2)_{7/6}$ $+(\overline{3},2)_{-1/6} + 2(3,1)_{2/3} + h.c.$
Ψ^a_{bf}	$(1,\overline{6})$	$(3,1)_{2/3} + h.c.$
	$(24,\overline{6})$	$(3,3)_{5/3} + (3,3)_{-1/3} + 2(3,3)_{2/3} + 2(3,2)_{7/6}$ $+2(\overline{3},2)_{-1/6} + (3,1)_{5/3} + (3,1)_{-1/3} + 2(3,1)_{2/3} + h.c.$
Ψ^{afg}	$(5,15)$	$[(8,2)_{1/2} + (3,2)_{-5/6} + (3,2)_{-11/6} + (3,1)_{-4/3}$ $+(1,2)_{1/2} + h.c.] + (8,1)_0 + (1,1)_0$
	$(5,21)$	$[(8,2)_{1/2} + (6,2)_{11/6} + (6,2)_{5/6} + (6,1)_{4/3}$ $+(1,2)_{1/2} + h.c.] + (8,1)_0 + (1,1)_0$
Ψ^f_{ag}	$(\overline{5},1)$	$(1,2)_{\pm 1/2} + (1,1)_0$
	$(\overline{5},35)$	$[2(8,2)_{1/2} + (6,2)_{11/6} + (6,2)_{5/6} + (6,1)_{4/3}$ $+(3,2)_{-5/6} + (3,2)_{-11/6} + (3,1)_{-4/3} + (1,2)_{1/2} + h.c.]$ $+2(8,1)_0 + (1,1)_0$

Table 7.11: Quantum numbers of the baryonic resonances containing the top partners in the case where the coset is $G_F/H_F = SU(5) \times SU(6)/SO(5) \times SO(6)$ and the $U(1)_x$ charge of the fermions X is $x = 2/3$. As before, Ψ^f_{ab} decomposes as Ψ^{abf} under the SM group as well as Ψ^a_{fg} decomposes as Ψ^{afg}. The top partners $Q_L \sim (\overline{3},2)_{-1/6}$ and $T^c_R \sim (3,1)_{2/3}$ are written in blue. In the cases where $R_1 = \mathbf{S}_2, \mathbf{Ad}$ and $R_2 = \mathbf{F}$ and the case where $R_1 = \mathbf{F}$ and $R_2 = \mathbf{Spin}$, the baryons Ψ^{abf} and Ψ^a_{bf} are excluded while in the case where $R_1 = \mathbf{Spin}$ and $R_2 = \mathbf{F}$, the baryons Ψ^{afg} and Ψ^f_{ag} are excluded as explained in the text.

Eqs. (7.4.32) and (7.4.33) are excluded as one can not contract the spinorial index of the fermion X. Finally, for $R_1 = \mathbf{Spin}$ and $R_2 = \mathbf{F}$, the baryons in Eqs. (7.4.37) are excluded as the spinorial index of ψ is not contracted.

- $SU(5) \times SU(3) \times SU(3)'/SO(5) \times SU(3)_D$ **coset**

Finally, the last coset is $G_F/H_F = SU(5) \times SU(3) \times SU(3)'/SO(5) \times SU(3)_D$. In that case, the fermions ψ are in a real representation of hypercolour while the fermions X and $\tilde{X}$ can be in a real, pseudo-real or complex representation depending on the value of N (see tables 7.3 and 7.2). The trilinear baryons are the following

$$\Psi^{af}_g = (\psi^a X^f \tilde{X}_g) \ , \quad \Psi^{ag}_f = (\psi^a X^\dagger_f \tilde{X}^{\dagger g}) \ , \quad \Psi^{fg}_a = (\psi^\dagger_a X^f \tilde{X}^{\dagger g}) \ , \tag{7.4.39}$$

$$\Psi_{afg} = (\psi^\dagger_a X^\dagger_f \tilde{X}_g) \ , \quad \Psi^a_{fg} = (\psi^a \tilde{X}_f \tilde{X}_g) \ , \quad \Psi^{afg} = (\psi^a X^f X^g) \ , \tag{7.4.40}$$

$$\Psi'^{afg} = (\psi^a \tilde{X}^{\dagger f} \tilde{X}^{\dagger g}) \ , \quad \Psi'^a_{fg} = (\psi^a X^\dagger_f X^\dagger_g) \ , \tag{7.4.41}$$

Baryon	$SU(5) \times SU(6)$	$SU(3)_c \times SU(2)_L \times U(1)_Y$
Ψ^{abf}	$(10, 6)$	$(3,3)_{-1/3} + (\overline{3},2)_{-1/6} + (3,2)_{-5/6} + (3,1)_{2/3}$ $+(3,1)_{-4/3} + (3,1)_{-1/3} + h.c.$
	$(15, 6)$	$(3,3)_{2/3} + (3,3)_{-4/3} + (3,3)_{-1/3} + (\overline{3},2)_{-1/6}$ $+(3,2)_{-5/6} + 2(3,1)_{-1/3} + h.c.$
Ψ^{af}_b	$(1, \overline{6})$	$(3,1)_{-1/3} + h.c.$
	$(24, \overline{6})$	$(3,3)_{2/3} + (3,3)_{-4/3} + 2(3,3)_{-1/3} + 2(\overline{3},2)_{-1/6}$ $+2(3,2)_{-5/6} + (3,1)_{2/3} + (3,1)_{-4/3} + 2(3,1)_{-1/3} + h.c.$
Ψ^{afg}	$(5, 15)$	$[(8,2)_{1/2} + (3,2)_{7/6} + (\overline{3},2)_{-1/6} + (3,1)_{2/3}$ $+(1,2)_{1/2} + h.c.] + (8,1)_0 + (1,1)_0$
	$(5, 21)$	$[(8,2)_{1/2} + (6,2)_{-7/6} + (6,2)_{-1/6} + (6,1)_{-2/3}$ $+(1,2)_{1/2} + h.c.] + (8,1)_0 + (1,1)_0$
Ψ^{af}_g	$(\overline{5}, 1)$	$(1,2)_{\pm 1/2} + (1,1)_0$
	$(\overline{5}, 35)$	$[2(8,2)_{1/2} + (6,2)_{-7/6} + (6,2)_{-1/6} + (6,1)_{-2/3}$ $+(3,2)_{7/6} + (\overline{3},2)_{-1/6} + (3,1)_{2/3} + (1,2)_{1/2} + h.c.]$ $+2(8,1)_0 + (1,1)_0$

Table 7.12: Quantum numbers of the baryonic resonances containing the top partners in the case where the coset is $G_F/H_F = SU(5) \times SU(6)/SO(5) \times SO(6)$ and the $U(1)_x$ charge of the fermions X is $x = -1/3$. As before, Ψ^f_{ab} decomposes as Ψ^{abf} under the SM group as well as Ψ^a_{fg} decomposes as Ψ^{afg}. The top partners $Q_L \sim (\overline{3},2)_{-1/6}$ and $T^c_R \sim (3,1)_{2/3}$ are written in blue. In the cases where $R_1 = \mathbf{S}_2, \mathbf{Ad}$ and $R_2 = \mathbf{F}$ and the case where $R_1 = \mathbf{F}$ and $R_2 = \mathbf{Spin}$, the baryons Ψ^{abf} and Ψ^a_{bf} are excluded while in the case where $R_1 = \mathbf{Spin}$ and $R_2 = \mathbf{F}$, the baryons Ψ^{afg} and Ψ^f_{ag} are excluded as explained in the text.

plus their conjugate and for simplicity, we used the index of $SU(3)_c$ instead of $SU(3) \times SU(3)'$. For example $\tilde{X}^{f'} = \tilde{X}_f$ that is $\tilde{X}$ is a triplet of $SU(3)'$ and decomposes as an antitriplet of $SU(3)_c$. Note that we restricted to top partners with two coloured fermions and one ψ. There is only two inequivalent decompositions as the above baryons contain only one ψ or $\psi^\dagger$ and there is no distinction between them as the SM group is embedded in a VL way inside $SU(5)$. Moreover, the $SU(3)_c$ product can only leads to 3×3 or $\overline{3} \times 3$.

The first possibility is $\Psi^{af}_g \sim (5,3,3) = (5,1) + (5,8)$ for which the decomposition is equivalent to the one for $\Psi^{ag}_f \sim (5,\overline{3},\overline{3}) = (\overline{5},1) + (\overline{5},8)$ under $SU(5) \times SU(3) \times SU(3)'$ and $SU(5) \times SU(3)_c$ respectively. In the same way, $\Psi^{fg}_a \sim (\overline{5},3,\overline{3}) = (\overline{5},\overline{3}) + (\overline{5},6)$ is equivalent to $\Psi^{afg} = (5,\overline{3},1) + (5,6,1) = (5,\overline{3}) + (5,6)$ and similarly for Ψ'^{afg}. The remaining baryons decompose in the conjugate coloured representations of Ψ^{fg}_a. For example $\Psi_{afg} \sim (\overline{5},\overline{3},3) = (\overline{5},3) + (\overline{5},6)$ which is equivalent to the decomposition of Ψ^a_{fg} and Ψ'^a_{fg}. The results of the decomposition of the $SU(5) \times SU(3)_c$ representations into the SM group is displayed in table 7.13.

Note that the case where the gauge symmetry is $SU(4)$ (see table 7.3) is particular. Indeed, in this case the invariant tensors which allow to form gauge invariants are δ^i_j, ϵ^{ijkl} and ϵ_{ijkl}. Then the two first baryons of Eq. (7.4.39) can not be contracted in a gauge invariant way as there is three indices of the fundamental and one of the anti-fundamental (for instance $\psi^{aij} X^{fk} \tilde{X}_{gl}$). This case is the only

one with an SU gauge symmetry.

Baryon	$SU(5) \times SU(3) \times SU(3)'$	$SU(3)_c \times SU(2)_L \times U(1)_Y$
Ψ_g^{af}	$(5,3,3)$	$(8,2)_{\pm 1/2} + (1,2)_{\pm 1/2} + (8,1)_0 + (1,1)_0$
Ψ_a^{fg}	$(\overline{5},3,\overline{3})$	$(\overline{3},2)_{-7/6} + (\overline{3},2)_{-1/6} + (\overline{3},1)_{-2/3}$ $+(6,2)_{-7/6} + (6,2)_{-1/6} + (6,1)_{-2/3}$
Ψ_{afg}	$(\overline{5},\overline{3},3)$	$(3,2)_{7/6} + (3,2)_{1/6} + (3,1)_{2/3}$ $+(\overline{6},2)_{7/6} + (\overline{6},2)_{1/6} + (\overline{6},1)_{2/3}$

Table 7.13: Quantum numbers of the baryonic resonances containing the top partners in the case where the coset is $G_F/H_F = SU(5) \times SU(3) \times SU(3)'/SO(5) \times SU(3)_D$. As explained in the text, we only display the inequivalent decompositions: Ψ_g^{af} and Ψ_f^{ag} transform in the same way under G_{SM} as well as Ψ_a^{fg} which transforms as Ψ^{afg} and Ψ'^{afg} and finally Ψ_{afg} which transforms as Ψ^a_{fg} and Ψ'^a_{fg}. Note that the triplet of $SU(3)'$ decomposes in an antitriplet of $SU(3)_c$ while the triplet of $SU(3)$ remains a triplet of $SU(3)_c$. The top partners $Q_L \sim (\overline{3},2)_{-1/6}$ and $T_R^c \sim (3,1)_{2/3}$ are written in blue.

7.5 Discussion

Finally, let us conclude this chapter by discussing few interesting points which have not been addressed during the classification.

First, there is no proof that the desire spontaneous symmetry breaking occurs and we simply assume that it is the case. We impose asymptotic freedom in the UV and expect that the correct condensate forms in the IR. In some cases the 't Hooft anomaly matching conditions can proof that the symmetry breaking occurs but the demonstration is not always fruitful and depends on the details of the model. For example one can demonstrate (see chapter 9) that in the model with $Sp(2N)$ gauge symmetry and global symmetry $SU(4) \times SU(6)/Sp(4) \times SO(6)$, the $SU(4)$ symmetry must be broken. However, the $SU(6)$ symmetry can be broken or remain unbroken.

Another important point related to the first one, is the implicit hypothesis that G_{HC} and $SU(3)_c$ are not broken at low energy by the condensation of the strong sector. Indeed, the bilinear that condensates should be invariant under the latter symmetries. In some cases, this feature is not obvious as it is discussed in Ref. [10].

Next, we require the presence of top partners but it is not possible to have partners for all the SM fermions. In particular, a bottom partner B_R^c is available in some cases but not always. This point is not too problematic as due to its large mass, the top can be treated separately than the other SM fermions.

Finally, some models contains a very large number of hypercoulour which leads to Landau pole too close to the EW scale. The most minimal cases from this point of view are the first, third and fifth models of table 7.3.

Let us now discuss the minimality of the UV completions of table 7.4.12 completions. As a criterion of minimality, one can choose first the number of pNGBs present in the electroweak sector and then the ones in the coloured sector. This criterion can be justified by the fact that the pNGBs of the EW sector are necessarily close to the EW scale due to the presence of the Higgs. At the contrary, the coloured pNGBs can be heavier and be decoupled from the EW scale more easily. Then, to respect the experimental bounds, it is easier to have the smallest possible EW coset. Consequently, theories based on the coset $SU(4) \times SU(6)/Sp(4) \times SO(6)$ are the less minimal ones with respectively five and twenty pNGBs in the EW and coloured sectors. The other coset are listed in table 7.3 by order of minimality.

Moreover, some models are VL theories which is a nice feature as a lot of non-perturbative results are available in this case. There is only two such possibilities corresponding to the two first entries of table 7.3. Only one extension respects the above argument of minimality. This minimal model is based on a $Sp(2N)$ hypercolour gauge symmetry ($2 \leq N \leq 18$) with a coset $SU(4) \times SU(6)/Sp(4) \times SO(6)$. We will focus on this model in the sequel and study it in great details in chapters 8, 9 and 10.

Chapter 8

The EW sector of the minimal UV completion

Following the results of chapter 7, we study in this chapter the most "minimal" UV completion of a composite Higgs model. The latter is based on the EW coset $SU(4)/Sp(4)$, the coloured coset $SU(6)/SO(6)$ and the underlying gauge symmetry $Sp(2N)$. It is one of the minimal possible UV complete CHM and it was first introduced in this context in Ref. [259]. We focus here on the phenomenology of the EW sector and postpone the study of the coloured sector to chapter 9.

The $SU(4)$ global symmetry is realised by four fermions ψ in the fundamental representation of the $Sp(2N)$ gauge symmetry. As the fundamental fermions ψ transform in a pseudo-real gauge representation, at low energy a non-zero condensate $\langle\psi^a\psi^b\rangle$ spontaneously breaks the global $SU(4)$ symmetry down to $Sp(4)$. This breaking leads to the emergence of five NGBs. Four of them have the quantum numbers of the complex Higgs doublet while the other one is a SM gauge singlet. In CHMs, a potential for the NGBs is generated from linear couplings between the top quark and its composite partners (see section 6.4). These couplings explicitly break the $SU(4)$ global symmetry such that the NGBs become pNGBs. In particular, the Higgs gets a mass and a non-zero vev which spontaneously breaks the EW symmetry. The other source of explicit breaking contributing to the Higgs potential comes from the gauging of the SM gauge group. More precisely, as the Higgs emerges from the EW sector, the $SU(2)_L \times U(1)_Y$ part of the SM gauge group is embedded inside the global $SU(4)$ symmetry. These two sources of explicit breaking are crucial in CHMs as they connect the strong sector to the SM. However, in this chapter we assume that the EWSB occurs and we do not introduce explicitly the linear couplings of the top quark. This is a reasonable first approximation as our analysis mainly focus on the strong dynamics and the EWSB effects are subleading in that case. On the contrary, it is simple to gauge the SM group and we explore some of the resulting consequences.

The underlying idea of this chapter and of the next one is to transpose the concepts and computations developed for QCD to the composite Higgs case. Then, the analysis decomposes in two main axes: (i) a theoretical point of view of the theory using the non-perturbative results of chapter 2 and (ii) a more phenomenological approach where the model is expressed in term of four-fermions interactions and the computations are done within the NJL framework. The latter being introduced in chapter 3.

Let us make some critical comments about our analysis. First, most of the non-perturbative computations are done within the NJL approximation. However, the latter is only valid in a restricted domain which depends on the values of the four-fermions couplings. For instance, the NJL model does not account for the confinement of hypercolour such that large unphysical imaginary parts may develop in the calculations. This feature appear close to the critical coupling of the NJL and it may leads to a lower bound on the four-fermion couplings. Also, the NJL approximation is valid as long as the dynamical mass M_ψ is lower than the cut-off Λ which gives an upper limit on the four-fermion couplings. We then identify the domain of validity of the NJL approximation but one should not forget that the theory could lie in a regime where this approximation breaks down.

Secondly, as already mentioned, we do not parametrise the EWSB such that the Higgs is massless in first crude approximation. Of course, the physical Higgs boson has a non-zero mass and our analysis should be viewed as a preliminary step toward a more complete model. Indeed, our predictions for the other (non Goldstone) resonances are reasonable as the corrections due to the EWSB are in general small compare to the effects of the strong dynamics.

The chapter is organised as follow. We first begin in section 8.1 by a presentation of some general (number of flavours N_f is free) properties of flavour (global) symmetries in vector-like gauge theories. We present the Vaffa-Witten theorem in subsection 8.1.1 and outline its consequences for VL theories that is, the restriction of the allowed symmetry breaking patterns. In particular, the $SU(2N_f)$ global symmetry present in the EW sector (see chapter 7) can only be spontaneously broken to $Sp(2N_f)$ (fermions in a pseudo-real representation) or to $SO(2N_f)$ (fermions in a real representation). We then introduce in all generality the broken ($\mathcal{J}_\mu^{\hat{A}}$) and unbroken ($\mathcal{J}_\mu^{A}$) global currents in these two cases as well as the properties of the corresponding generators ($T^{\hat{A}}$ and T^{A}) with respect to the vacuum of the theory. Note that these general considerations are also valid for the coloured sector as it corresponds to the real case with $N_f = 3$.

Next, in subsection 8.1.2 we present the 't Hooft anomaly matching (see section 2.3 for the QCD case) and outline in particular that a theory containing only fermions in pseudo-real representation can not form baryons at all. Then, in the case of the EW sector in isolation, the $SU(4)$ global symmetry must be spontaneously broken as the matching can not be done with composite baryons. This feature is of course altered when the coloured sector which contains other fundamental fermions is introduced as it is discussed in chapter 9. We then introduce in subsection 8.1.4 the sum rules resulting of the breaking patterns $SU(2N)/Sp(2N)$ and $SU(2N)/SO(2N)$ (see section 2.4 for the QCD case). Some interesting relations between the correlators and other strongly coupled quantities are also derived. Finally in subsection 8.1.5, the couplings to external gauge fields are considered that is, the coupling of the strong sector to the SM gauge group. In this way, general formulas for the radiative corrections to the masses of the pNGBs are derived as well as the anomalous couplings of the pNGBs to the external SM gauge fields (see section 2.5 for the equivalent in QCD).

In section 8.2, we particularise the above results to the EW sector and study in details this sector using the non-perturbative techniques of the NJL model. The analysis focus on the mesonic resonances of the theory that is, on the spectrum of the lightest spin zero and spin one states. We first introduce the four-fermion interactions of the scalar sector in subsection 8.2.1 where we outline the presence of the 't Hooft term that parametrises the explicit breaking of the $U(1)_\psi$ anomaly. Note that in the case of $SU(4)/Sp(4)$, this 't Hooft term is accidentally a four-fermion interaction. We use the Schwinger-Dyson equation to derive the dynamical mass M_ψ acquired by the fundamental fermions ψ after the condensation of the strong dynamics and then compute in subsection 8.2.2 the scalar and pseudo-scalar masses from the Bethe Salpether equation. We outline in particular the presence of the NGBs $G^{\hat{A}}$ and of the pseudo-scalar η associated to the $U(1)\psi$ anomaly. We also discuss the domain of validity of the NJL approximation.

Next, we introduce the vector four-fermion interactions and compute the vector and axial-vector masses respectively in subsections 8.2.3 and 8.2.4. Due to the vector interactions, an axial-pseudo-scalar mixing is present. We take into account this mixing to compute the Goldstone decay constant $F_G = \sqrt{2}f$ in subsection 8.2.5 where we also compute other strong quantities like the scalar and pseudo-scalar constants G_i ($i = \sigma, \eta, S^{\hat{A}}, S^{\hat{A}}$). The phenomenological analysis of the spectrum of mesonic resonances is presented in subsection 8.2.6. For this purpose, we assume that the four-fermion interactions originate from an $Sp(2N)$ current-current operator (see section 3.2.3 for the QCD case). In this hypothesis, there are only three free-parameters in the theory: the coupling of the current-current operator (κ_A), the coupling of the 't Hooft term (κ_B) and the number of hypercolour N. In addition, the mass spectrum is studied in unit of $f \gtrsim 1$ TeV, which fixes the scale Λ of the NJL model. The numerical analysis leads to spin zero and spin one resonance masses in the multi TeV range for $f = 1$ TeV but the latter can easily be decoupled for larger values of f. Note in particular that depending on the anomaly, the pseudo-scalar η can be light as its mass is directly proportional to

κ_B. Also, the vectors V_μ^A can be one of the lightest states, for instance lighter than the scalar singlet σ ($M_V \lesssim M_\sigma = 2M_\psi$), if the four-fermions couplings κ_A and κ_B are sufficiently large.

Finally, using all of the above results, we study in subsection 8.2.7 the realisation of the Weinberg-like and scalar sum rules present in the model. We compare two approaches: the realisation of the sum rules directly from the correlators as computed within the NJL framework and the saturation of the sum rules with the first light resonances.

In appendix E, from the $SU(4)/Sp(4)$ chiral Lagrangian, we make the link between the UV theory and its effects at low energy: we identify the Goldstone decay constant f that parametrises all of the low energy deviations compare to the SM predictions ($\xi = v^2/f^2$ see chapter 6).

8.1 General properties of flavour symmetries in vector-like gauge theories

The composite-Higgs model that we will study belongs to the class of vector-like gauge theories, namely an asymptotically free and confining gauge theory, with a set of N_f Dirac fermions transforming under a (possibly reducible) self-contragredient (i.e. unitarily equivalent to its complex conjugate) representation of the gauge group, in such a way that it is possible to make all fermions massive in a gauge invariant way[1]. Exact results concerning non-perturbative dynamical aspects in these theories are scarce, and in this section we briefly review some of those that are actually available. They concern issues related to the spontaneous breaking of the global flavour symmetries and the spectrum of low-lying bound states.

8.1.1 Restrictions on the pattern of spontaneous symmetry breaking

An important result for the spontaneous breaking of the global flavour symmetry group G for fermions with vector-like couplings to gauge fields has been obtained by Vafa and Witten [38]. The theorem they have proven makes the following statement: *in any vector-like gauge theory with massless fermions and vanishing vacuum angles, the subgroup H_m of the flavour group G that corresponds to the remaining global symmetry when all fermion flavours are given identical gauge invariant masses, cannot be spontaneously broken.* In other words, if G undergoes spontaneous breaking towards some subgroup H, then $H_m \subseteq H$ (in the absence of any vacuum angle). This theorem is particularly powerful when H_m corresponds to a maximal subgroup of G, since it then allows only two alternatives: either G is not spontaneously broken at all, or G is spontaneously broken towards H_m. This is actually what happens in the three cases that we can encounter in vector-like theories [258, 264]: $G = SU(N_f)_L \times SU(N_f)_R$ and $H_m = SU(N_f)_V$[2]; $G = SU(2N_f)$ and $H_m = SO(2N_f)$; $G = SU(2N_f)$ and $H_m = Sp(2N_f)$.

Of particular interest for the discussion that follows are the Nœther currents $\mathcal{J}_\mu^A$, corresponding to the generators T^A of the unbroken subgroup H_m, and $\mathcal{J}_\mu^{\hat{A}}$, corresponding to the generators $T^{\hat{A}}$ in the coset G/H_m. Since the latter is a symmetric space for the three cases that have just been listed, we will usually refer to the currents $\mathcal{J}_\mu^A$ ($\mathcal{J}_\mu^{\hat{A}}$) as vector (axial) currents. When the fermions transform under an irreducible but real ($\epsilon = +1$ below) or pseudo-real ($\epsilon = -1$) representation of the gauge group, $G = SU(2N_f)$, and $H_m = SO(2N_f)$ or $H_m = Sp(2N_f)$, respectively. In these two cases, it is convenient to write the fermion fields in terms of left-handed Weyl spinors ψ_α. The currents are then defined as follow [$\overline{\psi}_i \equiv \psi_j^\dagger \left(\Omega_\varepsilon\right)_{ji}$, where i and j denote gauge indices, while spinor and flavour indices are omitted]:

$$\mathcal{J}_\mu^A = \frac{1}{2}\left(\Omega_\varepsilon\right)_{ij}\left[\varepsilon\overline{\psi}_i\overline{\sigma}_\mu T^A\psi_j - \psi_i\sigma_\mu\left(T^A\right)^T\overline{\psi}_j\right] , \qquad \mathcal{J}_\mu^{\hat{A}} = \frac{1}{2}\left(\Omega_\varepsilon\right)_{ij}\left[\varepsilon\overline{\psi}_i\overline{\sigma}_\mu T^{\hat{A}}\psi_j - \psi_i\sigma_\mu\left(T^{\hat{A}}\right)^T\overline{\psi}_j\right] . \tag{8.1.1}$$

[1] It is also possible to give all fermions gauge invariant masses in the case of an odd number of Weyl fermions in the same *real* representation of the gauge group. Such theories do not have a conserved fermion number, and are not vector-like. Although it can provide interesting composite-Higgs models, as discussed, for instance, in Ref. [263], this class of theories will not be addressed here.

[2] The issue of the $U(1)_V$ symmetry is somewhat subtle, but we will not need to discuss it here.

The gauge contraction Ω_ε is an invariant tensor under the action of the gauge group, which is symmetric for $\varepsilon = +1$ and antisymmetric for $\varepsilon = -1$, with $\left(\Omega_\varepsilon^2\right)_{ij} = \varepsilon\delta_{ij}$. The generators T^A and $T^{\hat{A}}$ are characterised by the properties

$$T^A\Sigma_\varepsilon + \Sigma_\varepsilon\left(T^A\right)^T = 0 \ , \qquad T^{\hat{A}}\Sigma_\varepsilon - \Sigma_\varepsilon\left(T^{\hat{A}}\right)^T = 0 \ , \tag{8.1.2}$$

and are normalised as

$$\mathrm{Tr}(T^AT^B) = \frac{1}{2}\delta^{AB} \ , \qquad \mathrm{Tr}(T^{\hat{A}}T^{\hat{B}}) = \frac{1}{2}\delta^{\hat{A}\hat{B}} \ , \qquad \mathrm{Tr}(T^AT^{\hat{B}}) = 0 \ . \tag{8.1.3}$$

The $2N_f \times 2N_f$ matrix Σ_ε is an invariant tensor of the subgroup H_m of the flavour group. It plays for this subgroup a role analogous to the role played by Ω_ε for the gauge group. In particular, it can be chosen real, it is symmetric for $\varepsilon = +1$ and antisymmetric for $\varepsilon = -1$, and satisfies $\Sigma_\varepsilon^2 = \varepsilon\mathbb{1}$, where $\mathbb{1}$ denotes the $2N_f \times 2N_f$ unit matrix in flavour space.

8.1.2 't Hooft's anomaly matching condition

Whereas the theorem of Vafa and Witten restricts the pattern of spontaneous breaking of the global flavour symmetry group G, it does not by itself provide information on which alternative will eventually be realized. Additional information is required to that effect. The anomaly matching condition proposed by 't Hooft [39] can prove helpful in this respect. This condition uses the fact that the Ward identities satisfied by the three-point functions of the Nœther currents corresponding to the symmetry group G receive anomalous contributions from the massless elementary fermions [40–42]

$$i(q_1+q_2)^\rho \int d^4x_1 \int d^4x_2\, e^{iq_1\cdot x_1 + iq_2\cdot x_2}\langle \mathrm{vac}|T\{\mathcal{J}_\mu^A(x_1)\mathcal{J}_\nu^B(x_2)\mathcal{J}_\rho^{\hat{C}}(0)\}|\mathrm{vac}\rangle = -\frac{d_{HC}}{8\pi^2}\,\epsilon_{\mu\nu\alpha\beta}q_1^\alpha q_2^\beta d^{AB\hat{C}} \ , \tag{8.1.4}$$

with $d^{AB\hat{C}} = 2\mathrm{tr}(\{T^A, T^B\}T^{\hat{C}})$, where the trace is over the flavour group only, and d_{HC} denotes the dimension of the representation of the gauge group under which the fermions transform. These anomalous contributions imply that the corresponding three-point functions have very specific physical singularities at vanishing momentum transfer [39, 43, 44]. Moreover, this type of singularities can only be produced by physical intermediate states of spin zero or of spin one-half. If the symmetries of G are not spontaneously broken, the first option is excluded. If the theory confines, this then implies that it has to produce massless spin one-half bound states (baryons). These fermionic bound states will occur in multiplets of G, and their multiplicities must be chosen such as to exactly reproduce the coefficient of the singularities in the current three-point functions. If it is not possible to saturate this anomaly coefficients with the exchange of massless fermionic bound states only, then massless spin-zero bound states coupled to the currents of G are required, and hence G is spontaneously broken. If this anomaly matching condition can be satisfied with massless spin one-half bound states only, the spontaneous breaking of G towards H_m is not a necessity, but it cannot be excluded either.

In particular, the global symmetry is necessarily spontaneously broken if, after confinement, the theory cannot produce fermionic bound states at all. If we restrict ourselves to constituent fermions in the fundamental representation of the gauge group, this happens when the gauge group is $SU(2N)$, $SO(2N)$, or $Sp(2N)$. In these cases, the flavour group G therefore necessarily suffers spontaneous breaking towards H_m. On the contrary, fermionic baryons can be formed in the case of $SU(N)$ or $SO(N)$ gauge groups with N odd. Novel fermionic bound states may be possible if one admits elementary fermions transforming in other representations than the fundamental under the gauge group. We will discuss one such scenario below in section IV.

8.1.3 Mass inequalities

Various inequalities [265–269] involving the masses of the gauge-singlet bound states in vector-like gauge theories provide additional insight into the fate of flavour symmetries of vector-like confining gauge theories, complementary to the constraints arising from the Vafa-Witten theorem and 't Hooft's anomaly matching condition. The most rigorous versions of these inequalities hold under the same

positivity constraint on the path-integral measure in euclidian space as required for the proof of the Vafa-Witten theorem, namely the absence of any vacuum angle. A review on these inequalities is provided by Ref. [270]. Of particular interest in the present context is the inequality of the type [265, 267–269]

$$M_{1/2} \geq C(N, N_f) M_0 \ , \tag{8.1.5}$$

involving, on the one hand, the mass $M_{1/2}$ of any baryon state and, on the other hand, the mass M_0 of the lightest quark-antiquark spin 0 states having the flavour quantum numbers of the G/H_m currents. The precise value of the (positive) constant $C(N, N_f)$ and its dependence on the number of hypercolours N and/or number of flavours N_f is not so important here, the main point being that such an inequality again provides a strong indication that the flavour symmetry G is necessarily spontaneously broken towards G/H_m.

8.1.4 Super-convergent spectral sum rules

Assuming that G is spontaneously broken towards H_m, correlation functions that are at the same time order parameters become of particular interest, since they enjoy a smooth behaviour at short distances. These improved high-energy properties allow in turn to write super-convergent sum rules for the corresponding spectral densities. The paradigmatic example is provided by the Weinberg sum rules [47], once interpreted [271] and justified in the framework of QCD and of the operator-product expansion [272], including non-perturbative power corrections [273].

Here we will consider two-point functions of certain fermion-bilinear operators, when the fermions transform under an irreducible but real or pseudo-real representation of the gauge group. Specifically, these operators comprise the Nœther currents defined in Eq. (8.1.1), to which we add the scalar and pseudoscalar densities defined as

$$\mathcal{S}^{\hat{A}} = \frac{1}{2} (\Omega_\varepsilon)_{ij} \left[\overline{\psi}_i T^{\hat{A}} \Sigma_\varepsilon \overline{\psi}_j + \psi_i \Sigma_\varepsilon T^{\hat{A}} \psi_j \right] \ , \qquad \mathcal{S}^0 = \frac{1}{2} (\Omega_\varepsilon)_{ij} \left[\overline{\psi}_i T^0 \Sigma_\varepsilon \overline{\psi}_j + \psi_i \Sigma_\varepsilon T^0 \psi_j \right] \ ,$$
$$\mathcal{P}^{\hat{A}} = \frac{1}{2i} (\Omega_\varepsilon)_{ij} \left[\overline{\psi}_i T^{\hat{A}} \Sigma_\varepsilon \overline{\psi}_j - \psi_i \Sigma_\varepsilon T^{\hat{A}} \psi_j \right] \ , \qquad \mathcal{P}^0 = \frac{1}{2i} (\Omega_\varepsilon)_{ij} \left[\overline{\psi}_i T^0 \Sigma_\varepsilon \overline{\psi}_j - \psi_i \Sigma_\varepsilon T^0 \psi_j \right] \ . \tag{8.1.6}$$

The singlet densities are normalised consistently with the other densities by taking $T^0 = \mathbb{1}/(2\sqrt{N_f})$. The two-point correlation functions of interest are then defined as

$$\begin{aligned} \Pi_V(q^2) \delta^{AB} (q_\mu q_\nu - \eta_{\mu\nu} q^2) &= i \int d^4x \, e^{iq\cdot x} \langle \mathrm{vac} | T\{ \mathcal{J}_\mu^A(x) \mathcal{J}_\nu^B(0) \} | \mathrm{vac} \rangle \ , \\ \Pi_A(q^2) \delta^{\hat{A}\hat{B}} (q_\mu q_\nu - \eta_{\mu\nu} q^2) &= i \int d^4x \, e^{iq\cdot x} \langle \mathrm{vac} | T\{ \mathcal{J}_\mu^{\hat{A}}(x) \mathcal{J}_\nu^{\hat{B}}(0) \} | \mathrm{vac} \rangle \ , \end{aligned} \tag{8.1.7}$$

$$\begin{aligned} \Pi_S(q^2) \delta^{\hat{A}\hat{B}} &= i \int d^4x \, e^{iq\cdot x} \langle \mathrm{vac} | T\{ \mathcal{S}^{\hat{A}}(x) \mathcal{S}^{\hat{B}}(0) \} | \mathrm{vac} \rangle \ , \\ \Pi_P(q^2) \delta^{\hat{A}\hat{B}} &= i \int d^4x \, e^{iq\cdot x} \langle \mathrm{vac} | T\{ \mathcal{P}^{\hat{A}}(x) \mathcal{P}^{\hat{B}}(0) \} | \mathrm{vac} \rangle \ , \end{aligned} \tag{8.1.8}$$

where $\hat{A} \neq 0$, $\hat{B} \neq 0$, and

$$\begin{aligned} \Pi_{S^0}(q^2) &= i \int d^4x \, e^{iq\cdot x} \langle \mathrm{vac} | T\{ \mathcal{S}^0(x) \mathcal{S}^0(0) \} | \mathrm{vac} \rangle \ , \\ \Pi_{P^0}(q^2) &= i \int d^4x \, e^{iq\cdot x} \langle \mathrm{vac} | T\{ \mathcal{P}^0(x) \mathcal{P}^0(0) \} | \mathrm{vac} \rangle \ . \end{aligned} \tag{8.1.9}$$

The combinations

$$\Pi_{V\text{-}A}(q^2) \equiv \Pi_V(q^2) - \Pi_A(q^2) \ , \tag{8.1.10}$$

$$\Pi_{S\text{-}P}(q^2) \equiv \Pi_S(q^2) - \Pi_P(q^2) \ , \qquad \Pi_{S\text{-}P^0}(q^2) \equiv \Pi_S(q^2) - \Pi_{P^0}(q^2) \ , \qquad \Pi_{S^0\text{-}P}(q^2) \equiv \Pi_{S^0}(q^2) - \Pi_P(q^2) \ , \tag{8.1.11}$$

are order parameters[3] for the spontaneous breaking of $SU(2N_f)$ towards H_m for all values of q^2. As a consequence, these two-point functions behave smoothly at short distances ($Q^2 \equiv -q^2 > 0$):

$$\lim_{Q^2\to+\infty} \left(Q^2\right)^2 \times \Pi_{V\text{-}A}(-Q^2) = 0 \,, \qquad \lim_{Q^2\to+\infty} Q^2 \times \{\Pi_{S\text{-}P}(-Q^2)\,;\, \Pi_{S^0\text{-}P}(-Q^2)\,;\, \Pi_{S\text{-}P^0}(-Q^2)\} = \{0\,;\,0\,;\,0\} \,. \tag{8.1.12}$$

From these short-distance properties, one then derives the following super-convergent spectral sum rules

$$\int_0^\infty dt\, \mathrm{Im}\Pi_{V\text{-}A}(t) = 0 \,, \qquad \int_0^\infty dt\, t\, \mathrm{Im}\Pi_{V\text{-}A}(t) = 0 \,, \tag{8.1.13}$$

$$\int_0^\infty dt\, \mathrm{Im}\Pi_{S\text{-}P}(t) = 0 \,, \qquad \int_0^\infty dt\, \mathrm{Im}\Pi_{S^0\text{-}P}(t) = 0 \,, \qquad \int_0^\infty dt\, \mathrm{Im}\Pi_{S\text{-}P^0}(t) = 0 \,. \tag{8.1.14}$$

We will examine in the following to which extent these Weinberg-type sum rules, whose validity is quite general in view of the short-distance properties of asymptotically free vector-like gauge theories, are actually satisfied in the specific NJL four-fermion interaction approximation. For the sake of completeness, let us mention that the two-point function

$$\Pi_{AP}(q^2)\delta^{\hat{A}\hat{B}} q_\mu = \int d^4x\, e^{iq\cdot x} \langle \mathrm{vac}|T\{\mathcal{J}_\mu^{\hat{A}}(x)\mathcal{P}^{\hat{B}}(0)\}|\mathrm{vac}\rangle \,, \tag{8.1.15}$$

also defines an order-parameter. However, there is no associated sum rule, since, as a consequence of the Ward identities, this correlator is entirely saturated by the Goldstone-boson pole ($\langle \mathcal{S}^0\rangle$ denotes the vacuum expectation value of $\mathcal{S}^0$)

$$\Pi_{AP}(q^2) = \frac{1}{q^2}\, \frac{\langle \mathcal{S}^0\rangle}{\sqrt{N_f}} \,. \tag{8.1.16}$$

It may be useful to stress, at this stage, that the sum rules displayed above are only valid in the absence of any explicit symmetry breaking effects. Introducing, for instance, masses for the fermions would modify the short-distance properties of these correlators, and thus spoil the convergence of the integrals of the corresponding spectral functions. Let us briefly illustrate the changes that occur by giving the fermions a common mass m, so that the currents belonging to the subgroup H_m remain conserved. For the remaining currents, one now has

$$\partial^\mu \mathcal{J}_\mu^{\hat{A}} = 2m\mathcal{P}^{\hat{A}} \,. \tag{8.1.17}$$

As far as the current-current correlators are concerned, while the two-point function of the vector currents remains transverse, the correlator of two axial currents receives a longitudinal part,

$$i\int d^4x\, e^{iq\cdot x} \langle \mathrm{vac}|T\{\mathcal{J}_\mu^{\hat{A}}(x)\mathcal{J}_\nu^{\hat{B}}(0)\}|\mathrm{vac}\rangle = \delta^{\hat{A}\hat{B}} \left[\Pi_A(q^2)(q_\mu q_\nu - \eta_{\mu\nu}q^2) + \Pi_A^L(q^2) q_\mu q_\nu\right] \,. \tag{8.1.18}$$

If one considers only corrections that are at most linear in m, then one can still write a convergent sum rule,

$$\int_0^\infty dt \left[\mathrm{Im}\Pi_V(t) - \mathrm{Im}\Pi_A(t) - \mathrm{Im}\Pi_A^L(t)\right] = \mathcal{O}(m^2) \,. \tag{8.1.19}$$

Notice that the Ward identities relate this longitudinal piece to the two-point function of the pseudoscalar densities and to the scalar condensate,

$$(q^2)^2 \Pi_A^L(q^2) = 4m^2 \Pi_P(q^2) + 2m \frac{\langle \mathcal{S}^0\rangle}{\sqrt{N_f}} \,. \tag{8.1.20}$$

[3] Concerning $\Pi_{S\text{-}P}(q^2)$, this statement and the ensuing sum rule hold only to the extent that the tensor $d^{\hat{A}\hat{B}\hat{C}} \equiv 2\mathrm{tr}(\{T^{\hat{A}}, T^{\hat{B}}\}T^{\hat{C}})$ does not vanish identically, which is not the case, for instance, when $G = SU(2)_L \times SU(2)_R$ and $H_m = SU(2)_V$, but also, more interestingly for our purposes, when $G = SU(4)$ and $H_m = Sp(4)$.

The presence of a fermion mass m also shifts the masses of the Goldstone bosons away from zero, by an amount $\Delta_m M_G^2$ whose expression, at first order in m, actually follows from this identity and reads

$$F_G^2 \Delta_m M_G^2 = -2m \frac{\langle \mathcal{S}^0 \rangle}{\sqrt{N_f}} + \mathcal{O}(m^2 \ln m) \ . \tag{8.1.21}$$

This formula involves the Goldstone-boson decay constant F_G in the limit where m vanishes, defined as

$$\langle \, \mathrm{vac} \, | \, \mathcal{J}_\mu^{\hat{A}}(0) \, | G^{\hat{B}}(p) \rangle = i p_\mu F_G \delta^{\hat{A}\hat{B}} \ , \qquad p^2 = 0 \ . \tag{8.1.22}$$

Defining the coupling of the Goldstone bosons to the pseudoscalar densities,

$$\langle \, \mathrm{vac} \, | \, \mathcal{P}^{\hat{A}}(0) \, | G^{\hat{B}}(p) \rangle = G_G \delta^{\hat{A}\hat{B}} \ , \qquad p^2 = 0 \ , \tag{8.1.23}$$

the identity obtained in Eq. (8.1.16) implies

$$F_G G_G = - \frac{\langle \mathcal{S}^0 \rangle}{\sqrt{N_f}} \ , \tag{8.1.24}$$

in the massless limit.

In contrast to the symmetry currents and to quantities derived from them, like F_G or $\Pi_{V/A}(q^2)$ for instance, the (pseudo)scalar densities and their matrix elements, whether $\Pi_{S/P}(q^2)$ or G_G, need to be multiplicatively renormalised, and are therefore not invariant under the action of the renormalisation group. This dependence on the short-distance renormalisation scale does not impinge on the validity or usefulness of the sum rules in Eqs. (8.1.14) or (8.1.19), which hold at every scale. Likewise, this scale dependence is exactly balanced out between the right- and left-hand sides of relations like (8.1.16) or (8.1.24).

8.1.5 Coupling to external gauge fields

Eventually, some currents of the global symmetry group G become weakly coupled to the standard model gauge fields. If, in the absence of these weakly coupled gauge fields, the global symmetry group G is spontaneously broken towards H_m, turning on the gauge interactions will produce two effects. First, the Goldstone bosons will acquire radiatively generated masses. Second, transitions of a single Goldstone boson into a pair of gauge bosons are induced and, at lowest order in the couplings to the external gauge fields, the amplitude describing the transition towards a pair zero-virtuality gauge bosons is fixed by the anomalous Ward identities in Eq. (8.1.4). Let us briefly discuss these two aspects in general terms.

Let $|G^{\hat{A}}(p)\rangle$ denote the massless Goldstone-boson states corresponding to the generators $T^{\hat{A}}$ spanning the (symmetric) coset space G/H_m. In the presence of a perturbation that explicitly breaks the global symmetry, these Goldstone bosons become pseudo-Goldstone bosons, and their masses are shifted away from zero. At lowest order in the external perturbation, these mass shifts are given by

$$\Delta M^2_{G_{\hat{A}}} = -\langle G^{\hat{A}}(p) | \Delta\mathcal{L}(0) | G^{\hat{A}}(p) \rangle \ , \qquad p^2 = 0 \ , \tag{8.1.25}$$

with $\Delta\mathcal{L}(x)$ the symmetry-breaking interaction term in the Lagrangian. We are interested in particular in an interaction due to the presence of massless gauge fields that is considered weak (in particular non confining) at the scale under consideration, so that its effect can be considered as a perturbation. These external gauge fields couple to some linear combinations of the currents of the global symmetry group G. For a single gauge field $\mathcal{W}^\mu$, this interaction reads

$$\mathcal{L}_{\rm int} = -i g_{\mathcal{W}} \mathcal{W}^\mu \mathcal{J}_\mu^{\mathcal{W}} \ , \qquad \mathcal{J}_\mu^{\mathcal{W}} = \frac{1}{2} (\Omega_\varepsilon)_{ij} \left[\varepsilon \overline{\psi}_i \overline{\sigma}_\mu T^{\mathcal{W}} \psi_j - \psi_i \sigma_\mu \big(T^{\mathcal{W}}\big)^T \overline{\psi}_j \right] \ , \tag{8.1.26}$$

where $T^{\mathcal{W}}$ is an element of the algebra of G. At first non trivial order in the corresponding coupling $g_{\mathcal{W}}$, one has

$$\Delta\mathcal{L}(x) = \frac{g_{\mathcal{W}}^2}{2} \int \frac{d^4q}{(2\pi)^4} \frac{\eta^{\mu\nu}}{q^2} \int d^4y \, e^{iq\cdot y} T\{\mathcal{J}_\mu^{\mathcal{W}}(x+y) \mathcal{J}_\nu^{\mathcal{W}}(x)\} \ . \tag{8.1.27}$$

Decomposing $T^{\mathcal{W}}$ as $T^{\mathcal{W}} = T^W + T^{\hat{W}}$, where T^W ($T^{\hat{W}}$) is a linear combination of the generators T^A ($T^{\hat{A}}$) of H_m (of G/H_m), and taking further the soft-Goldstone-boson limit in Eq. (8.1.25), then results in the following expressions for the mass shifts [258, 274]

$$\Delta M^2_{G_{\hat{A}}} = -\frac{3}{4\pi} \times \frac{1}{F_G^2} \times \frac{g^2_{\mathcal{W}}}{4\pi} \times \int_0^\infty dQ^2\, Q^2\, \Pi_{V\text{-}A}(-Q^2) \times \left[\sum_{\hat{B}} \left(f^{\hat{A}W\hat{B}} \right)^2 - \sum_{B} \left(f^{\hat{A}\hat{W}B} \right)^2 \right] \,. \tag{8.1.28}$$

Again, F_G refers to the Goldstone-boson decay constant in the limit where any explicit symmetry-breaking effects vanish, see Eq. (8.1.22), and we have used the short-hand notation

$$\mathrm{Tr}\left(T^W [T^{\hat{A}}, T^{\hat{B}}] \right) \equiv \frac{1}{2i}\, f^{\hat{A}W\hat{B}} \,, \qquad \mathrm{Tr}\left(T^{\hat{W}} [T^{\hat{A}}, T^{B}] \right) \equiv \frac{1}{2i}\, f^{\hat{A}\hat{W}B} \,, \tag{8.1.29}$$

with the generators normalised as in Eq. (8.1.3). Since, according to the Witten inequality [266], $-Q^2\, \Pi_{V\text{-}A}(Q^2)$ is positive, the sign of $\Delta M^2_{G_{\hat{A}}}$, and hence the misalignment of the vacuum, hinges on the sign of the last factor on the right-hand side of Eq. (8.1.28). If it is positive, $\Delta M^2_{G_{\hat{A}}}$ is positive, and the vacuum is stable under this perturbation by a weak gauge field. If it is negative, then $\Delta M^2_{G_{\hat{A}}}$ is negative, which signals the instability of the unperturbed vacuum under this perturbation. In particular, if the gauge field couples only to the currents $\mathcal{J}^A_\mu$ corresponding to the unbroken generators (i.e. $T^{\hat{W}} = 0$), then $\Delta M^2_{G_{\hat{A}}} \geq 0$. This is the case, for instance, of the electromagnetic field in QCD, which gives the charged pions a positive mass [48] (see also the discussion in Ref. [275]),

$$\Delta M^2_{\pi^\pm} = -\frac{3}{4} \times \frac{1}{F_\pi^2} \frac{\alpha}{\pi} \times \int_0^\infty dQ^2\, Q^2\, \Pi^{QCD}_{V\text{-}A}(-Q^2) \,, \tag{8.1.30}$$

while the neutral pion remains massless. If several gauge fields are present, the total mass shift is given by a sum of contributions of the type (8.1.28), one for each gauge field, and the stability of the vacuum may then also depend on the relative strengths of the various gauge couplings. For instance, if a subgroup H_W of H_m is gauged, and if the Goldstone bosons transform as an irreducible representation R_W under H_W, the (positive) induced mass shift can be expressed [274] in terms of the quadratic Casimir invariant of H_W for the representation R_W,

$$\Delta M^2_{G_{\hat{A}}} = -\frac{3}{4\pi} \times \frac{1}{F_G^2} \times \frac{g^2_{\mathcal{W}}}{4\pi} \times \int_0^\infty dQ^2\, Q^2\, \Pi_{V\text{-}A}(-Q^2) \times C_2^{(H_W)}(R_W) \,. \tag{8.1.31}$$

The expression (8.1.28) can also be rewritten as a contribution to the effective potential induced by a gauge-field loop. In terms of the Goldstone field

$$U(x) = e^{iG(x)/F_G} \Sigma_\varepsilon \,, \qquad G(x) = 2 \sum_{\hat{A}} G^{\hat{A}}(x) T^{\hat{A}} \,, \tag{8.1.32}$$

the relevant terms of the effective low-energy Lagrangian read [276]

$$\mathcal{L}_{\text{eff}} = \frac{F_G^2}{4} \langle \partial_\mu U^\dagger \partial^\mu U \rangle - C_{\mathcal{W}} \langle T^{\mathcal{W}} U \left(T^{\mathcal{W}} \right)^T U^\dagger \rangle + \cdots \,, \tag{8.1.33}$$

with $\langle \cdots \rangle$ denoting the flavour trace, and

$$C_{\mathcal{W}} = -\frac{3}{8\pi} \times \frac{g^2_{\mathcal{W}}}{4\pi} \times \int_0^\infty dQ^2\, Q^2\, \Pi_{V\text{-}A}(-Q^2) \,. \tag{8.1.34}$$

As a side remark, let us notice that the procedure used here in order to determine the induced mass shifts of the Goldstone bosons can also be applied in the case where $\Delta\mathcal{L}$ in Eq. (8.1.25) stands for a mass term for the fermions, e.g.

$$\Delta_m \mathcal{L} = -2\sqrt{N_f}\, m\, \mathcal{S}^0 \,. \tag{8.1.35}$$

Going successively through the same steps, one then reproduces the expression given in Eq. (8.1.21).

We now turn to the second issue, namely the matrix element for the transition of a Goldstone bosons into a pair of external gauge bosons with zero virtualities. At lowest order in the gauge couplings, and for $q^2 = (p-q)^2 = 0$, this matrix element reads

$$g_{\mathcal{W}}^2 \times i \int d^4x\, e^{iq\cdot x} \langle \text{vac}|T\{\mathcal{J}_\mu^{\mathcal{W}}(x)\mathcal{J}_\nu^{\mathcal{W}}(0)\}|G^{\hat{A}}(p)\rangle = -\frac{g_{\mathcal{W}}^2 d_{HC}}{8\pi^2 F_G}\epsilon_{\mu\nu\rho\sigma}q^\rho p^\sigma d^{WW\hat{A}}\left[1+\mathcal{O}(m)\right] \ , \quad (8.1.36)$$

with $d^{WW\hat{A}} \equiv 2\text{Tr}(\{T^W, T^W\}T^{\hat{A}})$, and d_{HC} denotes the dimension of the representation of the hypercolour gauge group to which the fermions making up the current $\mathcal{J}_\mu^{\mathcal{W}}(x)$ belong. Here we are assuming (this will be the case of interest in the context of the composite Higgs models discussed below) that only generators of H_m are weakly coupled to the external gauge fields (i.e. $T^{\hat{W}} = 0$). The expression on the right-hand side is then obtained by saturating the Ward identity in Eq. (8.1.4) with the Goldstone poles. Again, if the fermions are given masses, there are corrections, indicated as $\mathcal{O}(m)$. At the level of the low-energy theory, this coupling is reproduced by the Wess-Zumino-Witten effective action [49–51]. Writing only the relevant term, one has

$$\mathcal{L}_{\text{eff}}^{\text{WZW}} = -\frac{g_{\mathcal{W}}^2 d_{HC}}{64\pi^2 F_G}\epsilon_{\mu\nu\rho\sigma}\mathcal{W}^{\mu\nu}(x)\mathcal{W}^{\rho\sigma}(x)\sum_{\hat{A}} d^{WW\hat{A}}G^{\hat{A}}(x) + \cdots \ . \quad (8.1.37)$$

8.2 The electroweak sector

In this section we analyse a composite model for the Higgs sector of the SM. We consider a flavour symmetry group $G = SU(4) \simeq SO(6)$, spontaneously broken towards a subgroup $Sp(4) \simeq SO(5)$. The five Goldstone bosons transform as $(1_L, 1_R) + (2_L, 2_R)$ under the custodial symmetry $SU(2)_L \times SU(2)_R \subset Sp(4)$, corresponding to a real scalar singlet plus the complex Higgs doublet. Composite Higgs models based on this coset has been studied in Refs. [256, 277, 278], as effective theories with a non-specified strongly-coupled dynamics. A simple UV completion is provided by a gauge theory with four Weyl fermions ψ^a in a pseudoreal representation of the gauge group, that form a condensate $\langle\psi^a\psi^b\rangle \neq 0$. Such a theory was considered in Refs. [10, 279–281], as a minimal hypercolour model. The first analysis of the low energy dynamics of this theory in terms of four-fermion interactions (à la NJL) was provided in Ref. [259]. We extend this former study by deriving additional phenomenological predictions. We will particularise the general results of section 8.1 to this specific case, and in addition we will compute the masses of the spin-zero and spin-one bound states, as well as their decay constants, by using NJL techniques.

8.2.1 Scalar interactions of fermion bilinears and the mass gap

Let us consider a $Sp(2N)$ hypercolour gauge theory and introduce four Weyl spinors ψ^a, in the fundamental representation of $Sp(2N)$, which is pseudoreal. The transformation properties of these elementary fermions are summarised in Table 8.1. The dynamics of the $SU(4)/Sp(4)$ spontaneous symmetry breaking can be studied in terms of four-fermion interactions, constructed out of hypercolour-invariant, spin-zero fermion bilinears, in a gauge NJL-like manner [52, 53, 56, 60, 282]. The Lagrangian reads [259]

$$\mathcal{L}_{scal}^{\psi} = \frac{\kappa_A}{2N}(\psi^a\psi^b)(\overline{\psi}_a\,\overline{\psi}_b) - \frac{\kappa_B}{8N}\left[\epsilon_{abcd}(\psi^a\psi^b)(\psi^c\psi^d) + h.c.\right], \quad (8.2.1)$$

where $a, b, \cdots = 1, 2, 3, 4$ are $SU(4)$ indices, ϵ_{abcd} is the Levi-Civita symbol and $\kappa_{A,B}$ are real, dimensionful couplings. The phase of κ_B can be absorbed by the phase of ψ, so that we may take κ_B real and positive without loss of generality.[4] Each fermion bilinear between brackets is contracted into a Lorentz and $Sp(2N)$ invariant. The hypercolour-invariant contraction is defined as

$$(\psi^a\psi^b) \equiv \psi_i^a\Omega_{ij}\psi_j^b = -(\psi^b\psi^a), \quad (8.2.2)$$

[4] In comparison to Ref. [259], we choose an opposite sign for κ_B, and a different but equivalent vacuum alignment defined by Eq. (8.2.6). Combining these two different conventions, the mass gap defined by Eq. (8.2.17) has the same expression as in Ref. [259]. This is because the two vacua are related by a $U(4)$ transformation with determinant minus one, that changes the sign of ϵ_{abcd}.

where Ω is the antisymmetric $2N \times 2N$ matrix

$$\Omega = \begin{pmatrix} 0 & \mathbb{1}_N \\ -\mathbb{1}_N & 0 \end{pmatrix}. \tag{8.2.3}$$

The antisymmetry of the hypercolour contraction implies antisymmetry in the flavour $SU(4)$ indices. Other four-fermion interactions, involving spin-one fermion bilinears, are irrelevant for the discussion of spontaneous symmetry breaking. We will introduce them later, in section 8.2.3, when we discuss spin-one resonances.

	Lorentz	$Sp(2N)$	$SU(4)$	$Sp(4)$
ψ_i^a	$(1/2, 0)$	$\square_i$	4^a	4
$\overline{\psi}_{ai} \equiv \psi_{aj}^\dagger \Omega_{ji}$	$(0, 1/2)$	$\square_i$	$\overline{4}_a$	4^*
$M^{ab} \sim (\psi^a \psi^b)$	$(0, 0)$	1	6^{ab}	$5+1$
$\overline{M}_{ab} \sim (\overline{\psi}_a \overline{\psi}_b)$	$(0, 0)$	1	$\overline{6}_{ab}$	$5+1$
$a^\mu \sim (\overline{\psi}_a \overline{\sigma}^\mu \psi^a)$	$(1/2, 1/2)$	1	1	1
$(V^\mu, A^\mu)_a^b \sim (\overline{\psi}_a \overline{\sigma}^\mu \psi^b)$	$(1/2, 1/2)$	1	15_b^a	$10+5$

Table 8.1: The transformation properties of the elementary fermions, and of the spin-0 and spin-1 fermion bilinears, in the electroweak sector of the model. Spinor indexes are understood, and brackets stand for a hypercolour-invariant contraction of the $Sp(2N)$ indexes.

Note that for $\kappa_B = 0$ there is an additional global $U(1)_\psi$ symmetry, which reflects a classical invariance of the $Sp(2N)$ gauge theory, the associated Nœther current being

$$\mathcal{J}^0_{\psi\mu} = -\frac{1}{2}\Omega_{ij}\left[\overline{\psi}_i \overline{\sigma}_\mu \psi_j + \psi_i \sigma_\mu \overline{\psi}_j\right], \tag{8.2.4}$$

as follows from Eq. (8.1.1) upon taking $\varepsilon = -1$ and a singlet generator normalised to $\mathbb{1}_4$. At the quantum level, this current has a hypercolour gauge anomaly,

$$\partial^\mu \mathcal{J}^0_{\psi\mu} = \frac{N_f^\psi g_{HC}^2}{32\pi^2} \sum_{I=1}^{N(2N+1)} \epsilon_{\mu\nu\rho\sigma} G_{HC}^{I,\mu\nu} G_{HC}^{I,\rho\sigma}, \tag{8.2.5}$$

and it is explicitly broken by instantons [283, 284]. Here $N_f^\psi = 2$ is the number of Dirac flavours. The effect of the instantons can be represented by an effective vertex [60, 283–285] that breaks the $U(1)_\psi$ invariance. The important observation here is that for $2N_f^\psi = 4$ Weyl fermions in the fundamental representation of the $Sp(2N)$ gauge group, this effective vertex is precisely given by the term proportional to κ_B. It is both quartic in the fermion fields, which provides the amount of $U(1)_\psi$ breaking required, for $N_f^\psi = 2$, by the index theorem and the instanton solution with unit winding number, and invariant under the $SU(4)$ global symmetry [286]. It plays the same role as the analogous six-fermion 't Hooft determinant effective Lagrangian [60, 283–285] for QCD with three flavours, that parametrises the instanton-induced anomaly interactions, explaining an η' mass much greater than the masses of the other Goldstone boson states. Similarly, in the present case, $\kappa_B \neq 0$ is therefore crucial to evade the additional $U(1)_\psi$ Goldstone boson.

While this picture is essentially correct when considering the electroweak $SU(4)$ sector in isolation, we stress that it will be significantly modified when a coloured sector is introduced, in order to provide composite partners for the top quark, as we will discuss in section 9.1. This sector also has an anomalous extra $U(1)_X$ symmetry, but one linear combination of the two $U(1)$ currents remains anomaly free, which implies that the effective 't Hooft determinant term is no longer given by the

κ_B operator. This will have some important consequences on the spectrum of resonances, but at a first stage we prefer to neglect the mixing with the coloured sector, as the results are much more transparent and it will be easy to generalise them.

We assume that the $SU(4)$ global symmetry is exact, that is, we work in the chiral limit where ψ^a has no elementary mass term. The $SU(4)$ Nœther currents are given by Eq. (8.1.1), with $\Omega_\epsilon = \Omega$ defined in Eq. (8.2.3). The $SU(4)$ generators decompose into five broken ones, $T^{\hat{A}}$, living in the $SU(4)/Sp(4)$ coset, and ten unbroken ones, T^A, whose explicit expressions are given in appendix F. They satisfy the conditions spelled out in Eq. (8.1.2), where Σ_ϵ stands for

$$\Sigma_0 \equiv \begin{pmatrix} 0 & 0 & 1 & 0 \\ 0 & 0 & 0 & 1 \\ -1 & 0 & 0 & 0 \\ 0 & -1 & 0 & 0 \end{pmatrix} . \tag{8.2.6}$$

By introducing in a standard manner [56, 259, 282] an auxiliary (antisymmetric) scalar field M, transforming as a gauge singlet and a flavour $SU(4)$ sextet, the Lagrangian (8.2.1) can be rewritten equivalently as

$$\begin{aligned} \mathcal{L}^{\psi}_{scal} \;=\; & -\frac{1}{\kappa_A+\kappa_B}\left[\left(\kappa_A M^*_{ab} - \frac{\kappa_B}{2}\epsilon_{abcd}M^{cd}\right)(\psi^a\psi^b) + h.c.\right] \\ & -\frac{2N\kappa_A}{(\kappa_A+\kappa_B)^2}M^{ab}M^*_{ab} + \frac{1}{2}\frac{N\kappa_B}{(\kappa_A+\kappa_B)^2}(\epsilon_{abcd}M^{ab}M^{cd} + h.c.) \;, \end{aligned} \tag{8.2.7}$$

where the equation of motion for M gives

$$M^{ab} = -\frac{\kappa_A+\kappa_B}{2N}\left(\psi^a\psi^b\right) . \tag{8.2.8}$$

The matrix field M, being complex and antisymmetric, can always be rotated by an $SU(4)$ transformation into the form

$$M = \begin{pmatrix} 0 & 0 & m_1 & 0 \\ 0 & 0 & 0 & m_2 \\ -m_1 & 0 & 0 & 0 \\ 0 & -m_2 & 0 & 0 \end{pmatrix} . \tag{8.2.9}$$

Once $(\psi^a\psi^b)$ condenses, M acquires a vacuum expectation value (vev) and the Yukawa couplings induce dynamical fermion masses. One can derive from Eq. (8.2.7) the one-loop Coleman-Weinberg effective potential [287], by integrating over fermions, and study the occurrence of spontaneous symmetry breaking by looking for a non-trivial minimum with $\langle m_{1,2}\rangle \neq 0$ [259]. One finds that spontaneous symmetry breaking is only possible for $2\langle m_1\rangle = 2\langle m_2\rangle \equiv M_\psi$, in agreement with the Vafa-Witten theorem. Below we provide an alternative derivation of the same result, which will also be useful for studying the spectrum of scalar resonances.

It is convenient to introduce the combination

$$\overline{M}_{ab} = \frac{1}{\kappa_A+\kappa_B}\left(\kappa_A M^*_{ab} - \frac{\kappa_B}{2}\epsilon_{abcd}M^{cd}\right), \tag{8.2.10}$$

that can be expanded around the vacuum as

$$\overline{M} = \frac{1}{2}M_\psi\Sigma_0 + \left(\sigma + i\eta'\right)\Sigma_0 T^0_\psi + \left(S^{\hat{A}} + iG^{\hat{A}}\right)\Sigma_0 T^{\hat{A}} . \tag{8.2.11}$$

The matrix $\overline{M}$ decomposes, according to $6_{SU(4)} = (1+5)_{Sp(4)}$, into a scalar singlet σ, a pseudoscalar singlet η', a scalar quintuplet $S^{\hat{A}}$, and a pseudoscalar quintuplet $G^{\hat{A}}$, which will be identified with the physical meson resonances. Using the identity $\epsilon_{abcd} = -(\Sigma_0)_{ab}(\Sigma_0)_{cd} + (\Sigma_0)_{ac}(\Sigma_0)_{bd} - (\Sigma_0)_{ad}(\Sigma_0)_{bc}$, and since, as already noted, κ_B can be taken real and positive without loss of generality, the Lagrangian (8.2.7) can be rewritten as

$$\mathcal{L}^{\psi}_{scal} = -(\psi\overline{M}\psi + h.c.) - N\left[P_-(\sigma^2 + G^2_{\hat{A}}) + P_+(\eta'^2 + S^2_{\hat{A}})\right] , \tag{8.2.12}$$

where

$$P_\pm = \frac{\kappa_A}{\kappa_A^2 - \kappa_B^2} \pm \frac{\kappa_B}{\left|\kappa_A^2 - \kappa_B^2\right|} = \frac{1}{\kappa_A \mp \kappa_B} \ . \tag{8.2.13}$$

The sign in the last equality corresponds to the case $\kappa_A^2 > \kappa_B^2$, that will turn out to be the relevant region of parameter space. Eqs. (8.2.11) and (8.2.12) define the Feynman rules for the fermion Yukawa couplings to the mesons: the four-fermion interactions mediated by σ and $G^{\hat{A}}$ are proportional to P_-^{-1}, while the interactions mediated by η' and $S^{\hat{A}}$ are proportional to P_+^{-1}.

Indeed, the Lagrangian in Eq. (8.2.1) can be directly written in terms of the fermion bilinears coupled to the mesons, upon using Fierz identities for $SU(4)$ and $Sp(4)$, derived in Appendix I. The replacements $\delta_a^c\delta_b^d - \delta_a^d\delta_b^c = 4(\Sigma_0 T^0_\psi)_{ab}(T^0_\psi\Sigma_0)^{cd} + 4(\Sigma_0 T^{\hat{A}})_{ab}(T^{\hat{A}}\Sigma_0)^{cd}$ and $\epsilon_{abcd} = -4(\Sigma_0 T^0_\psi)_{ab}(\Sigma_0 T^0_\psi)_{cd} + 4(\Sigma_0 T^{\hat{A}})_{ab}(\Sigma_0 T^{\hat{A}})_{cd}$ in Eq. (8.2.1), lead to

$$\begin{aligned}\mathcal{L}^\psi_{scal} &= 2\frac{\kappa_A}{(2N)}\left[\left(\psi\Sigma_0 T^0_\psi\psi\right)\left(\overline{\psi}T^0_\psi\Sigma_0\overline{\psi}\right) + \left(\psi\Sigma_0 T^{\hat{A}}\psi\right)\left(\overline{\psi}T^{\hat{A}}\Sigma_0\overline{\psi}\right)\right] \\ &+ \frac{\kappa_B}{(2N)}\left[\left(\psi\Sigma_0 T^0_\psi\psi\right)\left(\psi\Sigma_0 T^0_\psi\psi\right) - \left(\psi\Sigma_0 T^{\hat{A}}\psi\right)\left(\psi\Sigma_0 T^{\hat{A}}\psi\right) + h.c.\right] \ . \end{aligned} \tag{8.2.14}$$

Most of the resonance spectrum calculations could be performed directly from the four-fermion interactions in Eq. (8.2.14). Nonetheless, the introduction of auxiliary fields is convenient, because Eq. (8.2.11) identifies the relevant scalar degrees of freedom, which will become dynamical resonances upon $1/N$ resummation of the interactions in their respective channels, as we will examine below.

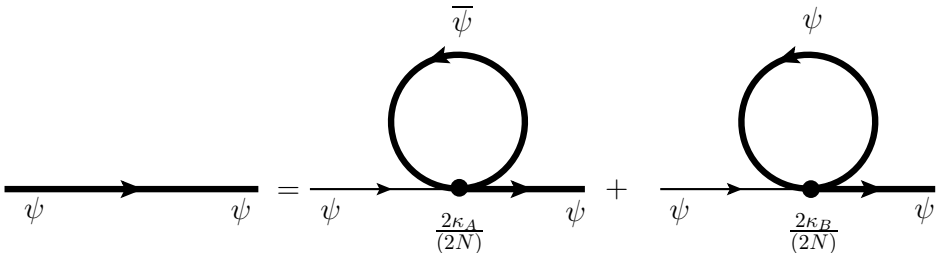

Figure 8.1: Graphical illustration of the mass gap equation, in the leading $1/N$-approximation. Thick and thin lines represent dressed and bare fermion propagators, respectively.

The first important step for the dynamical calculations of the resonance spectrum is to determine the mass gap, namely whether a non-trivial dynamical fermion mass, signalling the spontaneous breaking of $SU(4)$ to $Sp(4)$, develops within the NJL approximation. Let us consider the self-consistent mass gap equation [52, 56, 282], obtained from the one-loop tadpole graph, as illustrated in Fig. 8.1. It is well-known that this is equivalent to computing the minimum of the one-loop effective potential. Note that, just like for the standard NJL model, only the σ-exchange does contribute, namely only the spin-zero, parity-even, $Sp(4)$-singlet fermion bilinear can take a vev. Therefore the mass-gap equation involves solely the inverse coupling P_-. The computation of the diagrams in Fig. 8.1 leads to a self-consistent condition on the dynamical fermion mass M_ψ,

$$-iM_\psi = 2\left(i\frac{2P_-^{-1}}{8(2N)}\right)(-2)Tr[\Omega^2]Tr[\Sigma_0^2]\int^\Lambda \frac{d^4k}{(2\pi)^4}\frac{iM_\psi}{k^2 - M_\psi^2 + i\varepsilon} \ , \tag{8.2.15}$$

where the first factor 2 accounts for the normalisation $M_\psi \equiv 2\langle m_{1,2}\rangle$, (-2) is the trace over Weyl spinor indices in the loop, $Tr[\Omega^2] = -2N$ is the trace over hypercolour, and $Tr[\Sigma_0^2] = -4$ the one over flavour. Note that the factors $2N$ cancel, thanks to the appropriate large-N normalisation of the original couplings $\kappa_{A,B}$ in Eq. (8.2.14). Thus, one obtains

$$1 - 4P_-^{-1}\tilde{A}_0(M_\psi^2) = 0 \ , \tag{8.2.16}$$

where the basic one-loop scalar integral $\tilde{A}_0$ is defined in appendix G. In order to regularise the otherwise divergent integral, we introduce a (covariant 4-dimensional) cut-off Λ, which parametrises the scale at which the effective four-fermion interaction ceases to be valid and all degrees of freedom of the underlying gauge theory become relevant. Computing the integral, the gap equation takes the explicit form

$$1 - \frac{M_\psi^2}{\Lambda^2} \ln\left(\frac{\Lambda^2 + M_\psi^2}{M_\psi^2}\right) = \frac{4\pi^2}{\Lambda^2} P_- \equiv \frac{1}{\xi} \,, \tag{8.2.17}$$

in full agreement with the minimisation of the one-loop effective potential in Ref. [259].

Eq. (8.2.17) has a non-trivial solution, $M_\psi \neq 0$, as long as $\xi > 1$, which implies $\kappa_A^2 > \kappa_B^2$ and $P_-^{-1} = \kappa_A + \kappa_B > 4\pi^2/\Lambda^2$. The existence of a minimal, critical coupling to realize spontaneous symmetry breaking is a characteristic property of the NJL model. On the other hand, the consistency requirement $M_\psi/\Lambda \lesssim 1$ implies an upper bound on the coupling, $\xi \equiv \Lambda^2(\kappa_A + \kappa_B)/(4\pi^2) \lesssim (1 - \ln 2)^{-1} \simeq 3.25$, see also Fig. 8.3 below. Note that, if the underlying $Sp(2N)$ gauge theory confines, it necessarily breaks $SU(4)$ into $Sp(4)$ as a consequence of the anomaly matching discussed in section 8.1.2, because the fermions ψ cannot form baryons. This means that the true strong dynamics has to correspond to a super-critical value of $\kappa_A + \kappa_B$. Note that this conclusion holds for the ψ-sector in isolation, but it may not be the case when a coloured X-sector will be added in section 9.1, and baryons become possible, see the discussion in section 9.1.1. Note also that, in the NJL large-N approximation, the mass gap M_ψ and the fermion condensate,

$$\frac{1}{2}\langle(\psi^a\psi^b) + (\overline{\psi}^a\overline{\psi}^b)\rangle \equiv \langle\Psi\Psi\rangle\Sigma_0^{ab}, \qquad \langle\Psi\Psi\rangle = \frac{1}{\sqrt{N_f^\psi}}\langle S_0^\psi\rangle, \tag{8.2.18}$$

corresponding to the tadpole in Fig. 8.1, are trivially related:

$$\langle\Psi\Psi\rangle \equiv -2(2N) M_\psi \tilde{A}_0(M_\psi^2) = -\frac{N}{\kappa_A + \kappa_B} M_\psi. \tag{8.2.19}$$

We have also indicated the direct relation between the quark condensate and the vacuum expectation value $\langle S_0^\psi\rangle$ of the singlet scalar density, at this level of NJL approximation, with S_0^ψ defined in Eq. (8.1.6).

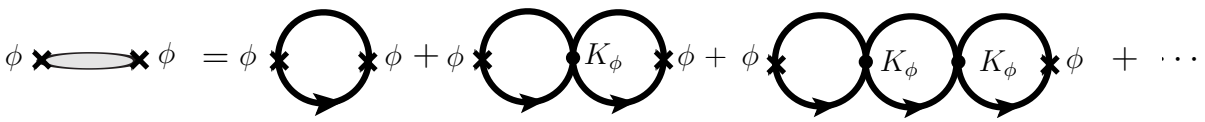

Figure 8.2: Resummation of leading $1/N$ graphs for a mesonic two-point correlator, corresponding to a composite meson exchange.

8.2.2 Masses of scalar resonances

The masses and the couplings of the composite mesonic resonances can be computed, at first order in $1/N$, by performing the resummation of the dominant large-N graphs contributing to the two-point functions with the appropriate quantum numbers, according to a well-known procedure [52, 56, 60, 282, 288]. The resummation takes the form of a geometric series, as illustrated in Fig. 8.2. For the two-point functions defined in Eqs. (8.1.8) and (8.1.9), the outcome of this procedure translates into the generic formula

$$\overline{\Pi}_\phi(q^2) \equiv \frac{\tilde{\Pi}_\phi(q^2)}{1 - 2K_\phi\tilde{\Pi}_\phi(q^2)} \,, \tag{8.2.20}$$

where K_ϕ are combinations of the four-fermion couplings in Eq. (8.2.14). The expressions of K_ϕ and of the one-loop correlators $\tilde{\Pi}_\phi(q^2)$ have been collected in Table 8.2. In this section, we will discuss the scalar and pseudoscalar channels, while the spin-one channels will be discussed in section 8.2.4.

Before starting this discussion, we would like to make a few remarks on the resummed correlators, some of which being also relevant for the spin-one channels.

- Expression (8.2.20) is not applicable in this simple form in the pseudoscalar channel, $\phi = G^{\hat{A}}$, η', due to the fact that, at one loop, the axial two-point function also receives a longitudinal part, which will then mix with the pseudoscalar two-point function when the resummation in Fig. 8.2 is performed. For the time being, we can ignore these aspects, which will be treated in detail in Section 8.2.5, and, in the meantime, we proceed with the general discussion of masses and couplings on the basis of Eq. (8.2.20).

- The corresponding resonance masses M_ϕ are determined by the poles of the resummed propagators,
$$1 - 2K_\phi \tilde{\Pi}_\phi(q^2 = M_\phi^2) = 0 \ . \tag{8.2.21}$$
In order to discuss some general features of this type of equation, let us point out that the functions $\tilde{\Pi}_\phi(q^2)$ can be defined in the cut complex q^2-plane, where the cut lies on the real positive axis and starts at $q^2 = 4M_\psi^2$. The cut results from a logarithmic branch point, so that the functions $\tilde{\Pi}_\phi(q^2)$ become multi-valued through analytic continuation across the cut. These properties simply reflect those of the function $\tilde{B}_0(q^2, M_\psi^2)$ itself. In general, Eq. (8.2.21) has solutions for complex values of q^2, lying on the second Riemann sheet, which are interpreted as resonances, generated dynamically through the resummation procedure.

- Other solutions to Eq. (8.2.21) than poles on the second sheet are possible. For instance, there can exist a critical value $K_\phi^{\rm crit}$, such that if the coupling K_ϕ satisfies $K_\phi \geq K_\phi^{\rm crit} > 0$, then Eq. (8.2.21) possesses (in addition) a real solution $0 \leq M_\phi \leq 2M_\psi$ [289], corresponding to a two-fermion bound state. As we will see below, this situation arises in the singlet pseudoscalar channel (and also in the vector channel, but this time for $K_\phi \leq K_\phi^{\rm crit} < 0$). As K_ϕ moves towards $K_\phi^{\rm crit}$ from above, the bound-state mass moves from zero towards the value $2M_\psi$. When $K_\phi < K_\phi^{\rm crit}$, this solution of Eq. (8.2.21) moves back towards the origin, but now on the real axis of the second Riemann sheet, and thus becomes a "virtual-state" solution [289].

- Another aspect concerning the solutions of Eq. (8.2.21) is intimately connected to the fact that, in order to make this equation meaningful, it has been necessary to introduce a regularisation for the function $\tilde{B}_0(q^2, M_\psi^2)$. As a consequence, there are solutions corresponding to real, but negative, values of q^2, $q^2 = -M_{\text{gh-}\phi}^2 \gtrsim -3\Lambda^2$. These "ghost" singularities[5] of the functions $\overline{\Pi}_\phi(q^2)$ occur quite far from the physical region, and have only a small influence on, for instance, the values of the resonance masses. When determining the latter, we thus systematically discard them. But they have to be taken into account when considering more global properties of the functions $\overline{\Pi}_\phi(q^2)$, like the spectral sum rules of Section 8.1.4. These will be discussed within the framework of the NJL approximation below, in Section 8.2.7.

- From a practical point of view, resonance solutions to Eq. (8.2.21) will not be determined by looking for poles on the second sheet, rather by solving a real equation as follows. We rewrite the denominator of Eq. (8.2.20) as $1 - 2K_\phi \tilde{\Pi}_\phi(q^2) = c_0^\phi(q^2) + c_1^\phi(q^2) q^2$, where the q^2-dependence of the coefficients $c_{0,1}^\phi(q^2)$ comes from the loop function $\tilde{B}_0(q^2, M_\psi^2)$ only, see table 8.2. The meson mass is then defined implicitly by
$$M_\phi^2 = \text{Re}[g_\phi(M_\phi^2)] \ , \qquad g_\phi(q^2) \equiv -\frac{c_0^\phi(q^2)}{c_1^\phi(q^2)} \ . \tag{8.2.22}$$
The value M_ϕ obtained this way remains a good approximation to the mass given by the real part of the resonance pole, as long as the imaginary part of $g_\phi(M_\phi^2)$ remains small,
$$\left| \frac{\text{Im}[g_\phi(M_\phi^2)]}{\text{Re}[g_\phi(M_\phi^2)]} \right| < 1 \ . \tag{8.2.23}$$

[5] These pathologies are absent if the Pauli-Villars regularisation is adopted [290], but they reappear in another guise.

Indeed, the solution of Eq. (8.2.22) may be larger than the threshold, $M_\phi^2 > 4M_\psi^2$, so that the loop function $\tilde{B}_0(M_\phi^2, M_\psi^2)$ develops an imaginary part. This may happen in the case of the $Sp(4)$-singlet pseudoscalar state, see Eq. (8.2.26), and it always happens in the case of the non-singlet scalar state, see Eq. (8.2.28). This imaginary part corresponds to the unphysical decay of a meson into two constituent fermions, and reflects the well known fact that the NJL model does not account for confinement. In what follows, it will be understood that resonance masses are defined as the solutions of Eq. (8.2.22) and, in order to define a consistency condition for the NJL approximation to be trustable, we will require that Eq. (8.2.23) holds. Note also that, when extracting the expressions of the pole masses, it will be often convenient to take advantage of the gap equation (8.2.16), in order to obtain a simpler form of the solutions.

ϕ	K_ϕ	$\tilde{\Pi}_\phi(q^2)$
$G^{\hat{A}}$	$2(\kappa_A+\kappa_B)/(2N)$	$\tilde{\Pi}_P(q^2) = (2N)\big[\tilde{A}_0(M_\psi^2) - \frac{q^2}{2}\tilde{B}_0(q^2, M_\psi^2)\big]$
η'	$2(\kappa_A-\kappa_B)/(2N)$	
$S^{\hat{A}}$	$2(\kappa_A-\kappa_B)/(2N)$	$\tilde{\Pi}_S(q^2) = (2N)\big[\tilde{A}_0(M_\psi^2) - \frac{1}{2}(q^2-4M_\psi^2)\tilde{B}_0(q^2, M_\psi^2)\big]$
σ	$2(\kappa_A+\kappa_B)/(2N)$	
V_μ^A	$-2\kappa_D/(2N)$	$\tilde{\Pi}_V(q^2) = \frac{1}{3}(2N)\big[-2M_\psi^2\tilde{B}_0(0, M_\psi^2) + (q^2+2M_\psi^2)\tilde{B}_0(q^2, M_\psi^2)\big]$
$A_\mu^{\hat{A}}$	$-2\kappa_D/(2N)$	$\tilde{\Pi}_A(q^2) = \frac{1}{3}(2N)\big[-2M_\psi^2\tilde{B}_0(0, M_\psi^2) + (q^2-4M_\psi^2)\tilde{B}_0(q^2, M_\psi^2)\big]$
a_μ	$-2\kappa_C/(2N)$	$\tilde{\Pi}_A^L(q^2) = -2(2N)M_\psi^2\tilde{B}_0(q^2, M_\psi^2)$
$A_\mu^{\hat{A}} - G^{\hat{A}}$		$\tilde{\Pi}_{AP}(q^2) = -(2N)M_\psi\tilde{B}_0(q^2, M_\psi^2)$
$a_\mu - \eta'$		

Table 8.2: The couplings K_ϕ and the expressions of the one-loop spin-0 and spin-1 two-point functions. We also give the expression of the mixed (one-loop) pseudoscalar-longitudinal axial correlator, that enters in the analysis of both the quintuplet and singlet sectors. The explicit calculation of the correlators $\tilde{\Pi}_\phi(q^2)$ is detailed in appendix H.

After these general considerations, we now turn to the analysis of the scalar and pseudoscalar channels of the model. The functions $\tilde{\Pi}_{S/P}(q^2)$ correspond to the one-loop estimates of the two-point functions $\Pi_{S/P}(q^2)$ defined in Eq. (8.1.8). Notice that one needs $K_\phi \propto 1/N$, in order for the $1/N$-expansion to be well-defined. Indeed, according to section 8.2.1 (see also Table 8.2), we have $K_{\sigma,G} = 2(\kappa_A+\kappa_B)/(2N)$ and $K_{S,\eta'} = 2(\kappa_A-\kappa_B)/(2N)$.

Let us consider first the pseudoscalar channels, ignoring, for the time being, the issue of mixing with the longitudinal part of the axial correlator. After taking the traces and evaluating the momentum integral, the pseudoscalar two-point correlator in the $SU(4)$ sector takes the form

$$\tilde{\Pi}_P(q^2) = (2N)\left[\tilde{A}_0(M_\psi^2) - \frac{q^2}{2}\tilde{B}_0(q^2, M_\psi^2)\right], \tag{8.2.24}$$

where the loop function $\tilde{B}_0(q^2, M^2)$ is given in appendix G. In the case of the Goldstone states $G^{\hat{A}}$, Eq. (8.2.21) becomes

$$1-4\frac{(\kappa_A+\kappa_B)}{2N}\tilde{\Pi}_P(M_G^2) = 1-4(\kappa_A+\kappa_B)\left[\tilde{A}_0(M_\psi^2) - \frac{M_G^2}{2}\tilde{B}_0(M_G^2, M_\psi^2)\right] = 2M_G^2(\kappa_A+\kappa_B)\tilde{B}_0(M_G^2, M_\psi^2) = 0\,, \tag{8.2.25}$$

and the term proportional to $\tilde{A}_0$ cancels out upon using the mass-gap equation, Eq. (8.2.16), a well-known feature of the standard NJL model [52, 56]. As a consequence, one is left with an exactly massless inverse propagator, $M_G = 0$, as it should be for the Goldstone boson state.

A similar computation for the $Sp(4)$-singlet pseudoscalar η', using the information provided by Table 8.2, leads to

$$M^2_{\eta'} = g_{\eta'}(M^2_{\eta'}) = \frac{2\tilde{A}_0(M^2_\psi)}{\tilde{B}_0(M^2_{\eta'}, M^2_\psi)} \left(1 - \frac{P_+}{P_-}\right) = -\frac{\kappa_B}{\kappa_A^2 - \kappa_B^2} \frac{1}{\tilde{B}_0(M^2_{\eta'}, M^2_\psi)} \,, \tag{8.2.26}$$

where we have again used Eq. (8.2.16). In the above equation and in the following expressions of the resonance masses, it is implicitly assumed that only the real part of $g_\phi(M^2_\phi)$ is taken into account, according to Eq. (8.2.22). Note that the constraint $\kappa_A^2 > \kappa_B^2$, needed for the existence of a non-trivial solution of the gap equation, also ensures that $M^2_{\eta'}$ is positive. As it will be discussed in subsection 9.2.5, a similar but stronger constraint holds when the coloured sector is introduced. To roughly estimate the expected range for $M_{\eta'}$, one may notice that $\tilde{B}_0(q^2, M^2_\psi)$ is real and has a rather moderate q^2 dependence for $q^2 \ll 4M^2_\psi$, so that if $M^2_{\eta'}$ lies in this range, one can use the approximate expression

$$M^2_{\eta'} \simeq -\frac{\kappa_B}{\kappa_A^2 - \kappa_B^2} \frac{1}{\tilde{B}_0(0, M^2_\psi)} \simeq \frac{4}{\xi} \frac{\kappa_B/\kappa_A}{1 - \kappa_B/\kappa_A} \frac{\Lambda^2}{\ln(\Lambda^2/M^2_\psi) - 1} \,, \tag{8.2.27}$$

where the expression for $\tilde{B}_0(0, M^2_\psi)$ is given in Eq. (G.3). Thus $M_{\eta'}$ may become arbitrarily small for $\kappa_B/\kappa_A \to 0$, as the extra $U(1)_\psi$ symmetry is restored when $\kappa_B = 0$, and η' turns into the associated Goldstone boson. However, $M_{\eta'}$ rapidly increases with κ_B/κ_A to become of order Λ. Note that, in the large-N limit, one expects $M^2_{\eta'} \sim 1/N$, as for the η' mass in QCD [291]. This indicates that the four-fermion couplings, normalised as in Eq. (8.2.1), should scale as $\kappa_B/\kappa_A \sim 1/N$. Large-$N$ arguments indicate that κ_A is N-independent, as the associated four-fermion operator is generated from the hypercolour current-current interaction (for details see appendix I.1). Therefore, the correct scaling is reproduced for $\kappa_B = \overline{\kappa}_B/(2N)$, with an N-independent $\overline{\kappa}_B$, and the associated four-fermion operator, induced by the hypercolour anomaly, scales as $1/N^2$. This will be consistent with the effect of the anomaly in the complete model that includes the coloured sector, see section 9.1.3.

For the scalar channels, the two-point function is to be found in Table 8.2, and the corresponding scalar resonance masses are

$$M^2_\sigma = 4M^2_\psi \,, \qquad M^2_S = 4M^2_\psi + M^2_{\eta'} \frac{\tilde{B}_0(M^2_{\eta'}, M^2_\psi)}{\tilde{B}_0(M^2_S, M^2_\psi)} \simeq M^2_\sigma + M^2_{\eta'} \,, \tag{8.2.28}$$

where one recognises the same relation $M_\sigma = 2M_\psi$, as in the standard NJL model for QCD with two flavours. The relation $M^2_S \simeq M^2_{\eta'} + M^2_\sigma$ holds again if one can neglect the difference between the function $\tilde{B}_0(p^2, M^2_\psi)$ evaluated at $p^2 = M^2_{\eta'}$ and at $p^2 = M^2_S$.

We stress that all previous expressions for the spectrum of spin-zero resonances hold in the pure chiral limit, where the $SU(4)/Sp(4)$ Goldstone bosons $G^{\hat{A}}$, including the Higgs, are massless. Eventually, they will receive a non-zero effective potential, radiatively induced by the SM gauge and Yukawa couplings, which break explicitly the $SU(4)$ symmetry. In particular, the top quark Yukawa coupling is generically expected to destabilise the vacuum, and to trigger EWSB, see Refs. [252, 292] for reviews. This implies that the masses of some resonances, obtained in the NJL large-N approximation, may receive corrections of order $\mathcal{O}(m^2_{top}/\Lambda^2)$. These represent typically mild corrections for the non-Goldstone resonances, whose masses $\sim \Lambda$ are significantly larger than the electroweak scale. Thus, the qualitative features of the spectrum of meson resonances are not expected to depart from those exhibited here, once the effect of the explicit symmetry-breaking couplings is added to the picture. One should also remember that, in any case, the NJL large-N approximation already constitutes a limitation to the precision that can be achieved. The radiative contribution to the pseudo-Goldstone Higgs mass, induced from the external electroweak gauge fields, is given in Eq. (F.7) (see also the general discussion in section 8.1.5). However, this contribution plays a secondary role in EWSB: since

it is positive, it cannot destabilise the $Sp(4)$-invariant vacuum, and it should be overcome by the one from the top Yukawa coupling [252, 292].

In the traditional NJL literature [52, 56, 60, 282], the resonance masses are determined from the resummed scattering amplitudes for $\psi\psi \to \psi\psi$ in the various channels. These amplitudes involve the same couplings K_ϕ and functions $\tilde{\Pi}_\phi(p^2)$ as in Eq. (8.2.20). Moreover, they also allow to define couplings between the elementary fermions and the resonances. The interested reader will find a brief discussion of these issues, not directly related to our main purposes, in App. H.

8.2.3 Vector interactions of fermion bilinears

Let us now consider vector bilinears, in order to study spin-one resonances. There are two independent four-fermion vector-vector operators, that can be written as

$$\mathcal{L}^{\psi}_{vect} = \frac{\kappa'_C}{2N}\left(\overline{\psi}_a\overline{\sigma}^\mu\psi^a\right)\left(\overline{\psi}_b\overline{\sigma}_\mu\psi^b\right) + \frac{\kappa'_D}{2N}\left(\overline{\psi}_a\overline{\sigma}^\mu\psi^b\right)\left(\overline{\psi}_b\overline{\sigma}_\mu\psi^a\right) \ , \tag{8.2.29}$$

where the coupling constants κ'_C and κ'_D are real. With the overall minus sign convention, it turns out that consistent (non-tachyonic) spin-one resonance masses are obtained for $\kappa'_{C,D} > 0$, in the same way as for the NJL vector interaction in QCD. Applying the $SU(4)$ Fierz identity given by Eq. (I.22), the Lagrangian can be rewritten in the 'physical' channels, corresponding to definite $Sp(4)$ representations,

$$\mathcal{L}^{\psi}_{vect} = \frac{\kappa_C}{2N}\left(\overline{\psi}\,T^0_\psi\,\overline{\sigma}^\mu\psi\right)^2 + \frac{\kappa_D}{2N}\left(\overline{\psi}T^A\overline{\sigma}^\mu\psi\right)^2 + \frac{\kappa_D}{2N}\left(\overline{\psi}\,T^{\hat{A}}\,\overline{\sigma}^\mu\psi\right)^2 \ , \tag{8.2.30}$$

where $\kappa_D = 2\kappa'_D$, $\kappa_C = 8\kappa'_C + 2\kappa'_D$, and contracted flavour indexes are understood, as well as summations over generator labels A and $\hat{A}$. Introducing auxiliary vector fields, the vector sector Lagrangian takes the form

$$\mathcal{L}^{\psi}_{vect} = -a_\mu(\overline{\psi}\,T^0_\psi\,\overline{\sigma}^\mu\psi) - V^A_\mu(\overline{\psi}\,T^A\,\overline{\sigma}^\mu\psi) - A^{\hat{A}}_\mu(\overline{\psi}\,T^{\hat{A}}\,\overline{\sigma}^\mu\psi) - \frac{N}{2\kappa_C}a^\mu a_\mu - \frac{N}{2\kappa_D}\left(V^A_\mu V^{A\mu} + A^{\hat{A}}_\mu A^{\hat{A}\mu}\right), \tag{8.2.31}$$

with vectors $V^A_\mu \sim 10_{Sp(4)}$, and axial vectors $(a_\mu, A^{\hat{A}}_\mu) \sim (1+5)_{Sp(4)}$. Their transformation properties are summarised in Table 8.1. This Lagrangian defines the strength of the four-fermion interactions in the three physical channels mediated by a_μ, V^A_μ and $A^{\hat{A}}_\mu$.

We remark that additional spin-one resonances can be associated to the fermion bilinear $(\psi^a\sigma^{\mu\nu}\psi^b) \sim 10_{Sp(4)}$, or to its conjugate. However, one can check that the corresponding four-fermion interactions vanish because of Lorentz and/or $SU(4)$ invariance. Therefore, to describe these resonances one should consider higher-dimensional operators. Although such an exercise is feasible with analogous NJL techniques, it goes beyond the scope of this analysis.

In general, the couplings κ_C and κ_D are additional free parameters with respect to those in the spin-zero sector, and in the following we will provide expressions for the vector masses and couplings as functions of these couplings. However, κ_C and κ_D may be related to the scalar sector coupling κ_A, if one assumes that the low-energy effective interactions, between two hypercolour-singlet fermion bilinears, originate from a one-hypergluon exchange current-current interaction, as determined by the underlying hypercolour gauge interaction. This may be justified in the large-N approximation (or equivalently 'ladder' approximation for the current-current interaction) and it proves to be a reasonably good approximation in the NJL-QCD case [60, 293]. Under such an assumption, one can apply Fierz identities for Weyl, as well as for $SU(4)$ and $Sp(2N)$, indices, as detailed in appendix I, in order to relate the coefficients of the various four-fermion operators. We obtain that the vector couplings of Eq. (8.2.30) are simply related to the scalar coupling of Eq. (8.2.14) by

$$\kappa_A = \kappa_C = \kappa_D \ . \tag{8.2.32}$$

An analogous relation holds in the NJL-QCD case [60], where the couplings of the scalar-scalar and vector-vector interactions are identical. We will use Eq. (8.2.32) as a benchmark for numerical illustration, however one should keep in mind that the true dynamics may appreciably depart from this naive relation.

8.2.4 Masses of vector resonances

The vector meson masses can be computed, at leading order in the $1/N$ expansion, similarly to the scalar meson channels, from the resummed two-point functions, and the geometric series illustrated in Fig. 8.2 now leads, in this approximation, to the following expressions for the vector or axial two-point correlators $\Pi_{V,A}(p^2)$ defined in Eq. (8.1.7),

$$\overline{\Pi}_{V/A}(q^2) \equiv -\frac{\tilde{\Pi}_{V/A}(q^2)}{q^2[1-2K_{V/A}\tilde{\Pi}_{V/A}(q^2)]}, \tag{8.2.33}$$

We have introduced one-loop correlators $\tilde{\Pi}_{V/A}(q^2)$ with a normalisation that is more convenient for our purposes, so that $\tilde{\Pi}_{V/A}(q^2) \equiv -q^2\Pi_{V/A}(q^2)|_{1-loop}$. Similarly, for the one-loop axial longitudinal part we have $\tilde{\Pi}_A^L(q^2) \equiv q^2\Pi_A^L(q^2)|_{1-loop}$, where $\Pi_A^L(q^2)$ is defined in Eq. (8.1.18). More precisely, upon taking the traces over spinor indices, flavour and hypercolour, the one-loop two-point vector and axial correlators take the form,

$$\tilde{\Pi}_V^{\mu\nu,AB}(q) = \tilde{\Pi}_V(q^2)T^{\mu\nu}\delta^{AB}, \qquad \tilde{\Pi}_A^{\mu\nu,\hat{A}\hat{B}}(q) = \left[\tilde{\Pi}_A(q^2)T^{\mu\nu} + \tilde{\Pi}_A^L(q^2)L^{\mu\nu}\right]\delta^{\hat{A}\hat{B}}, \tag{8.2.34}$$

where the transverse and longitudinal projectors are defined as

$$T^{\mu\nu} = \eta^{\mu\nu} - \frac{q^\mu q^\nu}{q^2}\ , \qquad L^{\mu\nu} = \frac{q^\mu q^\nu}{q^2}, \tag{8.2.35}$$

and where the expressions of the functions $\tilde{\Pi}_{V/A}(q^2)$ and $\tilde{\Pi}_A^L(q^2)$ are given in Table 8.2. One should be cautious to adopt a regularisation that preserves $SU(4)$ current conservation for the one-loop correlators, which is not the case with the standard NJL cutoff regularisation. There are various ways to deal with this well-known problem [56], the simplest being to use dimensional regularisation for the intermediate stages of the calculation. In this way the one-loop vector correlator is automatically transverse. In the final expression for the correlators, the formally divergent loop function $\tilde{B}_0$ can be written as a function of the $D = 4$ cutoff Λ, see Eq. (G.4). The latter is then interpreted as the physical cutoff of the NJL model.

As compared to the two-point axial correlator in the massless limit, defined by Eq. (8.1.7), and as already mentioned in Section 8.2.2, the one-loop expression (8.2.34) also exhibits a longitudinal part. This is a specific trait of the NJL model, where the dynamically generated mass M_ψ acts here like an explicit symmetry-breaking term. We will come back later on the manner this longitudinal piece is taken care of. For the time being, one may notice that the transverse part of the two-point axial correlator reproduces the expected physical features. Indeed, the resummed function $\overline{\Pi}_A(q^2)$ exhibits the massless pole[6] due to the contribution of the Goldstone bosons, but it also has a pole from the axial-vector state $A_\mu^{\hat{A}}$. This second pole mass is extracted from Eq. (8.2.21), by injecting the coupling $K_A = -2\kappa_D/(2N)$ [7] and the transverse part of the correlator, $\tilde{\Pi}_A(q^2)$. One obtains

$$M_A^2 = -\frac{3}{4\kappa_D\tilde{B}_0(M_A^2, M_\psi^2)} + 2M_\psi^2\frac{\tilde{B}_0(0, M_\psi^2)}{\tilde{B}_0(M_A^2, M_\psi^2)} + 4M_\psi^2\ . \tag{8.2.36}$$

The pole mass equation for the axial vector singlet a_μ is obtained with the replacements $\kappa_D \to \kappa_C$ and $M_A \to M_a$.

The V_μ^A pole mass can likewise be extracted from Eq. (8.2.21), with the replacements $K_\phi \to K_V = -2\kappa_D/(2N)$ and $\tilde{\Pi}_\phi(p^2) \to \tilde{\Pi}_V(p^2)$. This leads to

$$M_V^2 = -\frac{3}{4\kappa_D\tilde{B}_0(M_V^2, M_\psi^2)} + 2M_\psi^2\frac{\tilde{B}_0(0, M_\psi^2)}{\tilde{B}_0(M_V^2, M_\psi^2)} - 2M_\psi^2\ . \tag{8.2.37}$$

[6] As expected, such a massless pole does not occur in $\overline{\Pi}_V(q^2)$, defined in Eq. (8.2.33), since, as can be inferred from Table 8.2, $\tilde{\Pi}_V(q^2)$ vanishes for $q^2 = 0$.

[7] Note the relative minus sign between the four-fermion couplings in the Lagrangian of Eq. (8.2.30), and the couplings $K_{V,A}$ that enter in the denominator of the resummed correlators in Eq. (8.2.33). This follows from the proper definition of the argument of the associated geometric series.

In estimating the sizes of the spin-one resonance masses, note that $\tilde{B}_0(p^2, M_\psi^2)$ is real for $0 \leq p^2 \leq 4M_\psi^2$, and negative in the physically relevant range of $0 < M_\psi^2 < \Lambda^2$, with $|\tilde{B}_0(p^2, M_\psi^2)| \geq |\tilde{B}_0(0, M_\psi^2)|$. The term proportional to $1/\kappa_D$ on the right-hand side of Eqs. (8.2.37) and (8.2.36) is positive for $\kappa_D > 0$, and gives the dominant contribution to $M_{V,A}$ for, roughly, $\kappa_D M_\psi^2 \lesssim 4\pi^2$, that is $(M_\psi/\Lambda)^2 \lesssim 1/\xi$ when one takes $\kappa_D \simeq \kappa_A \gg \kappa_B$. By neglecting the difference between $\tilde{B}_0(M_V^2, M_\psi^2)$ and $\tilde{B}_0(M_A^2, M_\psi^2)$, we obtain the usual NJL relation between the axial and vector masses,

$$M_A^2 \simeq M_V^2 + 6M_\psi^2 \ . \tag{8.2.38}$$

When one adopts the exact self-consistent pole mass definitions, M_A is somewhat below the prediction of Eq. (8.2.38), by typically $5 - 10\%$. Also, the singlet mass M_a is equal to M_A when $\kappa_D = \kappa_C$ as in Eq. (8.2.32). As already mentioned in the general considerations at the beginning of Section 8.2.2, depending on the values of the couplings, one may have resonance masses satisfying $M_\phi^2 > 4M_\psi^2$, in which case $\tilde{B}_0(M_\phi^2, M_\psi^2)$ develops an imaginary part. Indeed, this is always the case for M_A, as one reads off Eq. (8.2.38). In such cases, the resonance mass is obtained upon solving Eq. (8.2.22), and we consider that the NJL predictions remain sensible as long as the width Γ_ϕ of the resonance, defined in Eq. (8.2.23), does not exceed its mass.

8.2.5 Goldstone decay constant and pseudoscalar-axial mixing

A key parameter of the composite sector is the Goldstone boson decay constant F_G, the analogous of F_π in QCD. We recall that, when the Higgs is a composite pseudo-Goldstone boson, the electroweak precision parameters, such as S, T, and the Higgs couplings receive corrections of order $(v/f)^2$ with respect to their SM value, where $v \simeq 246$ GeV and $f \equiv \sqrt{2}F_G$. Here f is the Goldstone decay constant in the normalisation that is generally adopted in the composite Higgs literature.[8] Thus, f is the physical scale most directly constrained by precision measurements, $f \gtrsim (0.5 - 1)$ TeV, the exact bound depending on the spontaneous symmetry breaking pattern, as well as on the flavour representations of the spin-one and spin-one-half composite resonances coupled to the SM fields. Therefore, it will be convenient to express all the resonance masses in units of f, and in the following we will adopt the more conservative bound $f \gtrsim 1$ TeV.

The decay constant F_G, as defined by Eq. (8.1.22), can most directly be extracted from the two-point axial transverse correlator, introduced in Eq. (8.1.7), through the residue of the Goldstone boson pole. Identifying this correlator in the NJL approximation with the resummed correlator defined by Eq. (8.2.33) and using the explicit expression in Table 8.2, one obtains

$$F_G^2 = \lim_{q^2 \to 0} \left[-q^2 \overline{\Pi}_A(q^2) \right] = \frac{\tilde{\Pi}_A(0)}{1 - 2K_A \tilde{\Pi}_A(0)} = \frac{\tilde{F}_G^2}{1 - 2K_A \tilde{F}_G^2} = g_A(0) \tilde{F}_G^2 \ , \tag{8.2.39}$$

where we have defined the axial coupling form factor

$$g_A(q^2) \equiv [1 - 2K_A \tilde{\Pi}_A^L(q^2)]^{-1} = \left[1 + \frac{4\kappa_D}{2N} \tilde{\Pi}_A^L(q^2) \right]^{-1} \tag{8.2.40}$$

and the one-loop decay constant

$$\tilde{F}_G^2 \equiv \tilde{\Pi}_A(0) = -2\,(2N)\, M_\psi^2 \tilde{B}_0(0, M_\psi^2) = \tilde{\Pi}_A^L(0). \tag{8.2.41}$$

At this point, one should remark that $\tilde{F}_G$ would be the complete NJL result for the Goldstone decay constant only if one would consider the scalar sector in isolation, i.e. by switching off the axial vector coupling κ_D. However, since by definition the Goldstone boson couples to the axial current, a non-zero κ_D implies a non-trivial mixing of the pseudoscalar and axial vector channels, that affects the

[8] The relation $f \equiv \sqrt{2}F_G$ follows from our definitions of F_G, see Eq. (8.1.22), and of the Goldstone matrix U, see Eq. (8.1.32). After the gauging of the SM group, the covariant derivative acting on the Goldstone bosons reads $D_\mu U = \partial_\mu U - i\mathcal{V}_\mu U - iU\mathcal{V}_\mu^T$, where the external source $\mathcal{V}_\mu$ is defined by Eq. (F.6). This determines the non-linear corrections to the electroweak precision parameters in terms of v/f.

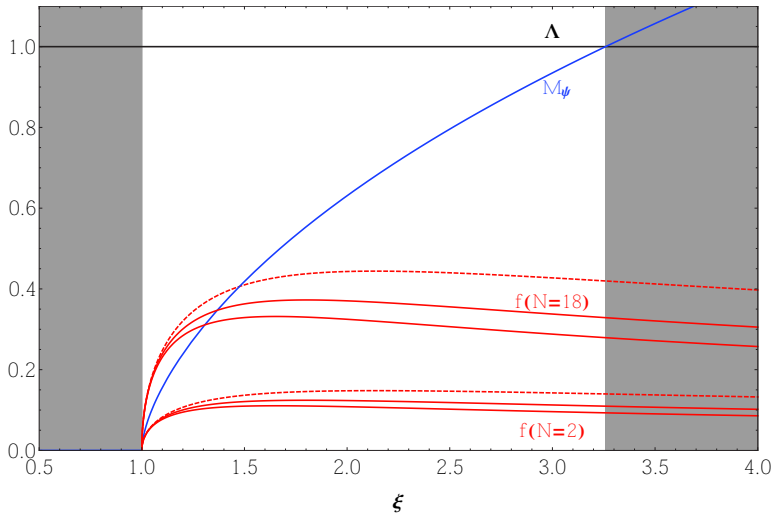

Figure 8.3: The mass gap M_ψ and the Goldstone decay constant $f = \sqrt{2}F_G$, in units of the cutoff Λ, as a function of the dimensionless coupling $\xi \equiv (\kappa_A + \kappa_B)\Lambda^2/(4\pi^2)$. For $\xi \leq 1$ there is no spontaneous symmetry breaking, $M_\psi = 0$, while for $\xi \gtrsim 3.25$ one has $M_\psi \gtrsim \Lambda$ and the NJL description is no longer reliable. The decay constant f is proportional to $\sqrt{N}$, where $Sp(2N)$ is the hypercolour gauge group. In the complete model including a coloured sector (see section 9.1), one finds that $N \geq 2$ is required to allow for fermion-trilinear top partners, and $N \leq 18$ is needed to preserve hypercolour asymptotic freedom [259]. One further needs $N \leq 6$ to avoid Landau poles in the SM gauge couplings below 100 TeV (see section 8.2.6). The red dashed line indicates the non-resummed decay constant $\tilde{f} = \sqrt{2}\tilde{F}_G$, while the upper (lower) red solid line corresponds to the resummed f, for $\kappa_D = \kappa_A$ and $\kappa_B = 0$ ($\kappa_B = \kappa_A$).

expression of the decay constant. In order to take into account this effect and to define consistently F_G, one needs to consider the resummed transverse axial-vector correlator $\overline{\Pi}_A(q^2)$ of Eq. (8.2.33), as shown in (8.2.39) above. This equation gives the complete NJL approximation for F_G, which should be matched with its experimental value, once it becomes available, as is the case of F_π in the NJL approximation of QCD [56, 60].

The behaviour of F_G is illustrated in Fig. 8.3, as a function of the dimensionless coupling ξ. Combining the definition of ξ in Eq. (8.2.17) with the explicit form of $\tilde{B}_0(0, M_\psi^2)$ given in Eq. (G.3), one obtains

$$\tilde{F}_G^2 = \frac{N}{4\pi^2}\Lambda^2 \left(\frac{\xi - 1}{\xi} - \frac{M_\psi^2}{\Lambda^2 + M_\psi^2} \right) . \tag{8.2.42}$$

Closely above the critical coupling, $\xi = 1$, the mass gap is much smaller than the cutoff, $M_\psi \ll \Lambda$, and $\tilde{F}_G$ grows rapidly with ξ. As $\xi - 1$ becomes of order one, the mass gap approaches the cutoff, $M_\psi \lesssim \Lambda$, while $\tilde{F}_G$ stops growing and remains below the cutoff by a factor of a few, $\tilde{f} \equiv \sqrt{2}\tilde{F}_G \simeq \sqrt{N}\Lambda/10$. The resummed F_G, see Eq. (8.2.39), is smaller, as K_A is negative. In Fig. 8.3 we assumed Eq. (8.2.32) to hold, so that $K_A = -4\pi^2\xi/[N\Lambda^2(1 + \kappa_B/\kappa_A)]$, which leads to $f \simeq (0.6 - 0.8)\tilde{f}$.

As already mentioned at several places in this section, a non-vanishing axial-vector coupling $\kappa_D \neq 0$ implies a nontrivial mixing between the pseudoscalar and the axial longitudinal channel. Therefore, the definition of the resummed pseudoscalar correlator $\overline{\Pi}_P(q^2)$ in Eq. (8.2.20) should be appropriately generalised in order to account for this mixing. In the process, we will also define a resummed axial longitudinal correlator $\overline{\Pi}_A^L(q^2)$, we will recover consistency relations among the Goldstone decay constants, and determine more precisely the properties of the non-Goldstone pseudoscalar η'. We discuss first the quintuplet $G - A^\mu$ mixing, while the similar analysis of the singlet $\eta' - a^\mu$ mixing is presented at the end of this section.

The mixing phenomenon is best described using a matrix formalism, so that we are led to consider

$$\mathbf{K}_G = \begin{pmatrix} K_G & 0 \\ 0 & K_A \end{pmatrix} , \qquad \mathbf{\Pi}(q^2) = \begin{pmatrix} \tilde{\Pi}_P(q^2) & \sqrt{q^2}\,\tilde{\Pi}_{AP}(q^2) \\ \sqrt{q^2}\,\tilde{\Pi}_{AP}(q^2) & \tilde{\Pi}_A^L(q^2) \end{pmatrix} . \tag{8.2.43}$$

Explicit expressions for all the entries of these matrices can be found in Table 8.2. Notice the appearance of $\tilde{\Pi}_{AP}(q^2)$, the one-loop expression of the mixed correlator $\Pi_{AP}(q^2)$ introduced in Eq. (8.1.15), and of the one-loop longitudinal axial correlator $\tilde{\Pi}_A^L(q^2)$ defined in Eq. (8.2.34). Note that, consistently with the normalisation of $\tilde{\Pi}_A^L(q^2)$ in Eq. (8.2.34), the matrix $\mathbf{\Pi}(q^2)$ has been defined so that all its entries have the same dimensions, whence the factor of $\sqrt{q^2}$ in front of $\tilde{\Pi}_{AP}(q^2)$. The resummed large-N two-point matrix correlator $\overline{\mathbf{\Pi}}_G$ in this basis is then given by

$$\overline{\mathbf{\Pi}}_G \equiv \mathbf{\Pi} + \mathbf{\Pi}\,(2\mathbf{K}_G)\,\mathbf{\Pi} + \cdots = (\mathbb{1} - 2\mathbf{\Pi}\mathbf{K}_G)^{-1}\mathbf{\Pi} , \tag{8.2.44}$$

which is the analog of Eqs. (8.2.20) and (8.2.33). From Eqs (8.2.43), (8.2.44) one then obtains

$$\begin{aligned} \overline{\mathbf{\Pi}}_G(q^2) &\equiv \begin{pmatrix} \overline{\Pi}_G(q^2) & \sqrt{q^2}\,\overline{\Pi}_{AG}(q^2) \\ \sqrt{q^2}\,\overline{\Pi}_{AG}(q^2) & q^2\,\overline{\Pi}_A^L(q^2) \end{pmatrix} \\ &= \frac{1}{D_G(q^2)} \begin{pmatrix} \tilde{\Pi}_P(q^2)[1 - 2K_A\tilde{\Pi}_A^L(q^2)] + 2K_A q^2\tilde{\Pi}_{AP}^2(q^2) & \sqrt{q^2}\,\tilde{\Pi}_{AP}(q^2) \\ \sqrt{q^2}\,\tilde{\Pi}_{AP}(q^2) & \tilde{\Pi}_A^L(q^2)[1 - 2K_G\tilde{\Pi}_P(q^2)] + 2K_G q^2\tilde{\Pi}_{AP}^2(q^2) \end{pmatrix} , \end{aligned} \tag{8.2.45}$$

with

$$D_G \equiv \det(\mathbb{1} - 2\mathbf{\Pi}\mathbf{K}_G) = (1 - 2K_G\tilde{\Pi}_P)(1 - 2K_A\tilde{\Pi}_A^L) - 4K_G K_A q^2\tilde{\Pi}_{AP}^2 = 2(\kappa_A + \kappa_B)q^2\,\tilde{B}_0(q^2, M_\psi^2). \tag{8.2.46}$$

The last expression in this equation is obtained after using the gap-equation (8.2.16) and the relation $\tilde{\Pi}_{AP}^2(q^2) = -(1/2)(2N)\tilde{B}_0(q^2, M_\psi^2)\tilde{\Pi}_A^L(q^2)$. Using the relevant expressions in Table 8.2, gives explicitly

$$\overline{\Pi}_G(q^2) = \frac{1}{2}(2N)\frac{2\tilde{A}_0(M_\psi^2)g_A^{-1}(q^2) - q^2\tilde{B}_0(q^2, M_\psi^2)}{D_G(q^2)}, \qquad \overline{\Pi}_{AG}(q^2) = \frac{\tilde{\Pi}_{AP}(q^2)}{D_G(q^2)}, \qquad \overline{\Pi}_A^L(q^2) = 0. \tag{8.2.47}$$

Note in particular that the *resummed* longitudinal axial correlator $\overline{\Pi}_A^L(q^2)$ vanishes identically, thus consistently recovering the conservation of the axial current in the exact chiral limit, in spite of the nonzero mass gap, that induces a non-vanishing longitudinal axial correlator at the one-loop level, $\tilde{\Pi}_A^L \propto M_\psi^2$. Also the resummed mixed correlator $\overline{\Pi}_{AG}(q^2)$ satisfies the relation (8.1.16), which shows that it is entirely saturated by the Goldstone-boson pole.

Now one can extract the NJL prediction for the Goldstone constants F_G and G_G, defined by Eqs. (8.1.22) and (8.1.23) respectively. The residue of $\overline{\Pi}_G(p^2)$ with respect to the Goldstone boson pole gives the pseudoscalar decay constant,

$$G_G^2 = -\lim_{q^2\to 0} q^2\overline{\Pi}_G(q^2) = -\frac{(2N)}{8(\kappa_A + \kappa_B)^2\tilde{B}_0(0, M_\psi^2)}g_A^{-1}(0) . \tag{8.2.48}$$

Next, the residue of $\overline{\Pi}_{AG}(q^2)$ determines $F_G G_G$,

$$F_G G_G = -\lim_{q^2\to 0} q^2\overline{\Pi}_{AG}(q^2) = \frac{(2N)}{2}\frac{M_\psi}{(\kappa_A + \kappa_B)} = 2(2N)M_\psi\,\tilde{A}_0(M_\psi^2) , \tag{8.2.49}$$

that satisfies Eq. (8.1.24), by taking the expression for $\langle S_0^\psi\rangle$ derived from Eq. (8.2.19). Combining Eqs. (8.2.48) and (8.2.49), and using the gap equation, one consistently recovers the very same expression of F_G in Eq. (8.2.39), as obtained from the resummed axial transverse correlator. Note that, if one had computed G_G in the limit of vanishing axial-vector coupling, $\kappa_D = 0$, by taking the residue of $\overline{\Pi}_P$ in Eq. (8.2.20), one would have missed the (inverse) axial form factor $g_A(0)$, see Eq. (8.2.48). Such correction is important e.g. when analysing the possible saturation of the scalar spectral sum rules, that will be discussed in section 8.2.7.

Obviously, a similar pseudoscalar-axial mixing mechanism also affects the singlet sector of the model, as soon as the axial singlet coupling κ_C is non-vanishing. The resummed correlator matrix for the singlet sector, $\overline{\mathbf{\Pi}}_{\eta'}$, is defined in complete analogy with Eq. (8.2.44), by taking the same one-loop correlator matrix $\mathbf{\Pi}$, but replacing the couplings, $K_G \to K_{\eta'}$ and $K_A \to K_a$ (i.e. $\kappa_D \to \kappa_C$), respectively for the pseudoscalar and axial-vector channels, according to Table 8.2. One main consequence of the mixing is that the pseudoscalar singlet mass $M_{\eta'}$ is corrected with respect to Eq. (8.2.26), that holds for the pseudoscalar sector "in isolation". The η' mass rather corresponds to the pole of the determinant

$$D_{\eta'} \equiv \det(\mathbb{1}-2\mathbf{\Pi}\mathbf{K}_{\eta'}) = (1-2K_{\eta'}\tilde{\Pi}_P)g_a^{-1}-4K_{\eta'}K_a q^2\tilde{\Pi}^2_{AP} = 8\kappa_B\tilde{A}_0(M_\psi^2)g_a^{-1}+2(\kappa_A-\kappa_B)q^2\tilde{B}_0(q^2,M_\psi^2)\,, \tag{8.2.50}$$

where we defined an axial singlet form factor,

$$g_a(q^2) = \left[1+\frac{4\kappa_C}{2N}\tilde{\Pi}^L_A(q^2)\right]^{-1}\,, \tag{8.2.51}$$

in complete analogy with Eq. (8.2.40) for the non-singlet sector. Therefore Eq. (8.2.26) gets modified ("renormalised") by the (inverse) axial singlet form factor,

$$M^2_{\eta'} = -\frac{\kappa_B}{\kappa_A^2-\kappa_B^2}\,\frac{1}{\tilde{B}_0(M^2_{\eta'},M^2_\psi)}\,g_a^{-1}(M^2_{\eta'})\,, \tag{8.2.52}$$

which is the final expression that we will use in numerical illustrations of the mass spectrum in the next subsection.

8.2.6 The mass spectrum of the resonances

The resonance masses have to be proportional to the unique independent energy scale of the theory, that is convenient to choose as $f \equiv \sqrt{2}F_G$, defined in Eq. (8.2.39), as explained above. To fix ideas, one can take f just above the lower bound imposed by electroweak precision tests, that is conservatively given by $f = 1$ TeV. Since the resonance masses are N-independent and $f \sim \sqrt{N}$, in principle the resonances become lighter and lighter in the large-N limit. However, if the model is augmented with coloured fermions to provide top partners, as we will do in section 9.1, the $Sp(2N)$ asymptotic freedom is lost (at one loop) for $N \geq 19$ [259]. Moreover, these coloured fermions are also charged under $U(1)_Y$, resulting in Landau poles in the SM gauge couplings (α_1 and α_3) possibly too close to the condensation scale of the strong sector. A naive one-loop estimation of the running of the SM gauge couplings in presence of the hypercolour fermions leads to the appearance of Landau poles around 100 (500) TeV for $N = 6$ (5) while for $N = 4$, the Landau poles appear above $4 \cdot 10^3$ TeV. Then, a more reasonable interval for the number of hypercolours is $2 \leq N \leq 6$ and for the numerical illustration, we take the conservative value $N = 4$.

The resonance masses are a function of the couplings $\kappa_{A,B,C,D}$ of the four-fermion operators. For the numerical illustration, we will assume Eq. (8.2.32) to hold, $\kappa_C = \kappa_D = \kappa_A$, and we will trade the two remaining, independent couplings for the dimensionless parameters $\xi \equiv (\kappa_A + \kappa_B)\Lambda^2/(4\pi^2)$ and κ_B/κ_A.

Let us describe the main feature of the mass spectrum. Since we work in the chiral limit approximation, the resonances are complete multiplets of the unbroken $Sp(4)$ symmetry, and the Goldstone bosons $G_{\hat{A}}$ are massless. In the spin-zero sector, there are three independent massive states: the singlet scalar σ and the five-plet scalar $S_{\hat{A}}$, see Eq. (8.2.28), as well as the singlet pseudoscalar η', see Eq. (8.2.26). The latter is the would-be Goldstone boson of the anomalous $U(1)_\psi$, therefore $M_{\eta'}$ vanishes when this symmetry is restored, that is when $\kappa_B/\kappa_A \to 0$. In the spin-one sector, there are two independent masses: the singlet axial vector a^μ and the five-plet axial vector $A^\mu_{\hat{A}}$ are mass-degenerate as we assume $\kappa_C = \kappa_D$, with mass given by Eq. (8.2.36), while the ten-plet vector V^μ_A has a different mass, see Eq. (8.2.37). Even though we neglect the mass splitting among the different electroweak components, in view of collider searches it is important to keep in mind the electroweak

charges of the resonances, that are fixed by the decomposition of the $Sp(4)$ representation under the $SU(2)_w \times U(1)_Y$ gauged subgroup:

$$1_{Sp(4)} = 1_0 \,, \qquad 5_{Sp(4)} = (2_{1/2} + h.c.) + 1_0 \,, \qquad 10_{Sp(4)} = 3_0 + (2_{1/2} + h.c.) + (1_1 + h.c.) + 1_0 \,. \tag{8.2.53}$$

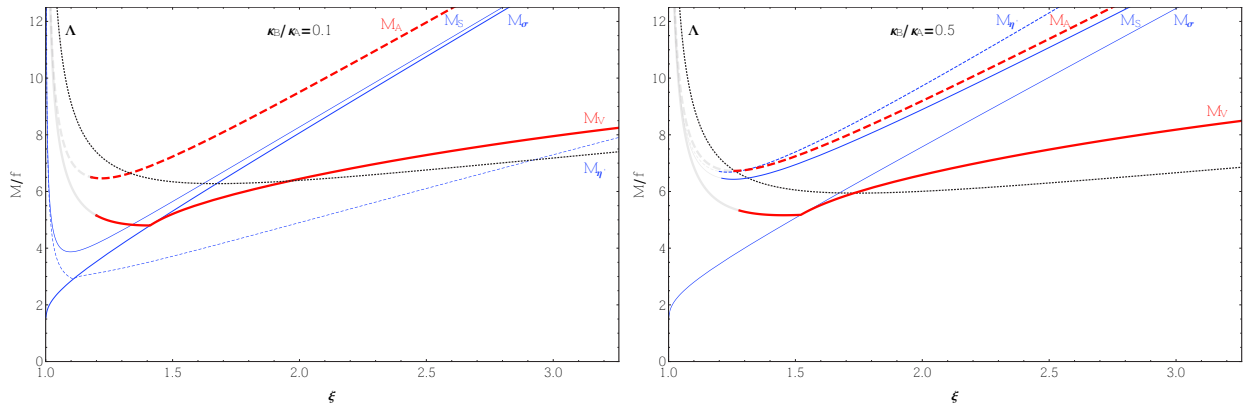

Figure 8.4: The masses of the electroweak resonances in units of the Goldstone decay constant f, for $N = 4$ (the masses scale with $1/\sqrt{N}$), as a function of the coupling ξ, for $\kappa_B/\kappa_A = 0.1$ (left-hand panel) and $\kappa_B/\kappa_A = 0.5$ (right-hand panel). We displayed the full physical range for ξ, according to Fig. 8.3. Each curve is shaded when the corresponding pole mass equation develops a large, unphysical imaginary part, $|\mathrm{Im}[g_\phi(M_\phi^2)]/\mathrm{Re}[g_\phi(M_\phi^2)]| > 1$. The dotted line is the cutoff of the constituent fermion loops.

In Fig. 8.4 we display the five independent resonance masses, $M_{\sigma,\eta',S,V,A}$, as a function of ξ, for two representative values of κ_B/κ_A. While $M_\sigma = 2M_\psi$ grows over the entire range for ξ, the other four masses follow a different pattern: they appear to be several times larger than f when ξ is very close to one (see the discussion in the next paragraph), then they steeply decrease to reach a minimum $\sim (2-3)f$ for an intermediate value of ξ, and finally they grow roughly linearly for $\xi \gtrsim 1.5$. We recall the two approximate mass relations, $M_S \simeq (M_\sigma^2 + M_{\eta'}^2)^{1/2}$ and $M_A \simeq (M_V^2 + 3M_\sigma^2/2)^{1/2}$, that hold neglecting pole mass differences in the loop form factor. As a consequence, one has always $M_A > M_S > M_\sigma$, with a similar asymptotic value at large ξ. On the contrary, M_V decreases until it becomes degenerate with M_σ, then it grows with a weaker slope. Finally, $M_{\eta'}$ may also become smaller than M_σ at large values of ξ, but only for a sufficiently small value of κ_B/κ_A. For example, taking $f = 1$ TeV, $N = 4$ and $\kappa_B/\kappa_A = 0.1$, the resonance masses for two representative values of ξ are

$$\begin{aligned} \xi = 1.3 \quad &: \quad M_A \simeq 6.6 \text{ TeV}, \quad M_V \simeq 4.9 \text{ TeV}, \quad M_S \simeq 4.6 \text{ TeV}, \quad M_\sigma \simeq 4.1 \text{ TeV}, \\ &\quad\; M_{\eta'} \simeq 3.3 \text{ TeV} \,, \\ \xi = 2.0 \quad &: \quad M_A \simeq 9.5 \text{ TeV}, \quad M_V \simeq 6.4 \text{ TeV}, \quad M_S \simeq 8.3 \text{ TeV}, \quad M_\sigma \simeq 8.1 \text{ TeV}, \\ &\quad\; M_{\eta'} \simeq 4.9 \text{ TeV} \,. \end{aligned} \tag{8.2.54}$$

In general, electroweak resonances lighter than $\simeq 4f \simeq 4$ TeV are possible in two cases: the scalar σ becomes light when one approaches the critical coupling $\xi = 1$, where the mass gap vanishes; the pseudoscalar η' becomes light as κ_B/κ_A tends to zero, where the anomalous $U(1)_\psi$ symmetry is restored. These two singlet states, together with the SM singlet Goldstone boson $\hat{G^3}$, may be observed as the lightest scalar resonances at the LHC, beside the 125 GeV Higgs boson. In section 9.2.5 we will discuss the mixing of σ and η' with the analogous singlet states of the colour sector, that will induce corrections to their masses.

A comment is in order on the region close to the critical coupling. In the limit $\xi \to 1$, one finds that $M_\sigma/f \sim [-\log(\xi-1)]^{-1/2}$ vanishes, while the other resonance masses diverge relatively to f, $M_{V,A,S,\eta'}/f \sim (\xi-1)^{-1/2}$. The lightness of σ may be interpreted as the signal that scale invariance is

recovered below $\xi = 1$, while all other resonances decouple in this limit. However, we should remark that, for some of these heavy resonances, the NJL computation of their mass cannot be trusted close to the critical coupling, because the pole of the resummed propagator develops a large, unphysical imaginary part. Recall, from the general discussion at the beginning of section 8.2.2, that the curves in Fig. 8.4 are the solution of Eq. (8.2.22),[9] where the imaginary part of $g_\phi(M_\phi^2)$ has been neglected. The curves in Fig. 8.4 are shaded when $|\mathrm{Im}[g_\phi(M_\phi^2)]/\mathrm{Re}[g_\phi(M_\phi^2)]| > 1$, where we consider that the corresponding result cannot be trusted anymore. This happens when $\xi \lesssim (1.2 - 1.3)$, for the vector and axial-vector resonances, with mass $M_{V/A}$ close to the cutoff of the NJL model.

Let us also comment on the complementary limit where ξ is so large that M_ψ/Λ becomes of order one, as illustrated in Fig. 8.3. In this case Fig. 8.4 shows that the resonances become heavier than Λ (except for η', if κ_B/κ_A is small enough). This is not necessarily problematic: while the mass M_ψ of constituent fermions in the loops need to be smaller than the loop cutoff Λ, external mesons heavier than Λ do not harm the consistency of the NJL approximation. Indeed, in QCD the NJL model predicts rather accurately resonance masses twice as large as the cutoff. Nonetheless, we notice that, for $M_i \sim \Lambda$, the value of the two-point function $\tilde{B}_0(M_i^2, M_\psi^2)$ becomes sensitive to the chosen regularisation, defined in appendix G, as the cutoff-dependent finite terms become sizeable. As a consequence, we observe that the mass values in this region may vary up to a few 10% in different regularisation schemes. This is an intrinsic theoretical uncertainty of the NJL approximation.

The resonance masses in units of $f \equiv \sqrt{2}F_G$ may be compared with recent lattice results for the same model [294,295] which provide scalar and (axial) vector mass results in the same units.[10] Actually we can only compare with the latter available lattice simulations performed to date for this model only for an underlying $SU(2)$ gauge theory, thus equivalent to the $Sp(2N)$, $N = 1$ case of our more general study. Given that the vector and scalar masses scale as $1/\sqrt{N}$ (this scaling originates solely from F_G), the rescaled mass values illustrated for $N = 4$ in Fig. 8.4 get enhanced by a factor 2 for $N = 1$, which can be directly compared with the lattice results [294], in the chiral limit: $M_V/f = 13.1 \pm 2.2$, $M_A/f = 14.5 \pm 3.6$. The latter results, although affected with relatively large uncertainties, indicate a more moderate $V - A$ mass splitting than is generally expected from the NJL model, see Eq. (8.2.38), unless M_ψ is rather small, which corresponds in the NJL framework to rather small values of ξ. More precisely, typically the previous central lattice values can be (approximately) matched for $\xi \simeq 1.1$, therefore not far above the critical NJL coupling value, where on the other hand the NJL calculation becomes less reliable, as already explained above, since entering the ξ range where the V and A width both become relatively large. But accounting for the lattice uncertainties, the above values are also easily matched alternatively for rather large ξ values, where the NJL prediction is also more reliable: for example for $N = 1$ and $\xi = 1.6$ [$\xi = 1.9$], $M_V/f|_{NJL} \simeq 11$[12.5], $M_A/f|_{NJL} \simeq 15.3$[18]. [NB recall that the V, A masses are mildly dependent on k_B, which enters only indirectly from the mass gap. One should also keep in mind that the Fierz-induced relation (8.2.32) is assumed for the axial and vector coupling κ_D in Fig. 8.4, and since the dominant contribution to the V, A masses scales as $1/\kappa_D$, a somewhat smaller (larger) κ_D would induce somewhat larger (smaller) V, A masses, for a fixed ξ value]. At least one may tentatively conclude from this comparison that intermediate ξ values, say $1.2 \lesssim \xi \lesssim 1.6$ approximately, as well as very large $\xi > 2$, appear more disfavoured.

Concerning the lightest scalar masses, Ref. [295] provides the very recent lattice estimates $M_\sigma/f = 19.2(10.8)$, $M_{\eta'}/f = 12.8(4.7)$, and $M_S/f = 16.7(4.9)$, in the chiral limit (where the scalar non-singlet S is called a_0 in Ref. [295]). Compared with Fig. 8.4 (rescaled for $N = 1$) and combined with the V, A-mass results, ξ values very close to 1 appear disfavoured by the σ mass, even when taking its lowest lattice value above, because in this region the NJL prediction for M_σ is much smaller than M_V, as it is clear from $M_\sigma = 2M_\psi$ (see also Fig. 8.4). The NJL (approximate) relation $M_S^2 \simeq M_\sigma^2 + M_{\eta'}^2$ (see Eq. (8.2.28)), can be fulfilled within the large lattice uncertainties, although the rather high

[9] The function $\mathrm{Re}\,\tilde{B}_0(q^2, M_\psi^2)$ develops a cusp at $q^2 = 4M_\psi^2$. Through the definition of the masses M_ϕ adopted here, this cusp naturally shows up in Fig. 8.4 (and in Fig. 8.7 below) as soon as the value of a resonance mass goes through $2M_\psi$. In practice, this only occurs for M_V and $M_{\eta'}$, at the cross-over from a bound state to a genuine resonance.

[10] Our normalisation of f, see footnote 8, appears consistent with what is called F_{PS} in the notations of Ref. [294] thus we compare our NJL predictions in units of f directly with their numbers, assuming that the same normalisation has been used in those lattice calculations.

lattice central value of M_σ is in tension with this relation. So putting all together it may indicate that relatively large values of $\xi \simeq 1.6-2$, well above the NJL critical coupling, are more favoured by lattice results. Concerning the η' singlet mass, at this stage it may be compared with the NJL η' mass, which we recall is most sensitive to κ_B/κ_A values. Modulo the large lattice uncertainties, the comparison with lattice results appears thus to indicate not too small, rather intermediate $\kappa_B/\kappa_A \simeq 0.2-0.4$ values, such that $M_{\eta'}$ is not small, rather slightly below (or comparable to) M_V.

In conclusion the comparison of NJL and lattice results appears roughly consistent, at least the lattice results may be matched for some definite values of the NJL parameters ξ and κ_B/κ_A, with no strong tensions. But it appears still an essentially qualitative comparison at the present stage, given both the intrinsic NJL uncertainties amply discussed previously, as well as the still relatively large lattice systematic uncertainties, specially for the scalar resonances: so unfortunately it cannot be taken yet as giving tight constraints on the effective NJL model parameters. Note also that other recent lattice simulations of composite Higgs model resonances are available in the literature (see e.g. [296, 297]), but are based on different gauge symmetries and/or global symmetry breaking pattern, thus not directly comparable with our results.

8.2.7 Comparison with spectral sum rules

Several authors [288, 290, 298] have addressed the issue of spectral sum rules, discussed in general terms in Section 8.1.4, in the context of the NJL approximation applied to QCD. In this Section, we will study them in the context of the NJL approximation to the underlying $Sp(2N)$ gauge dynamics of the present composite Higgs framework. The aim will be to check whether these sum rules provide additional constraints on the parameters of the model, namely ξ and κ_B/κ_A.

It seems only natural to identify the spectral densities appearing in the sum rules displayed in Eqs. (8.1.13) and (8.1.14) with the discontinuities of the resummed NJL two-point correlators [11] discussed in the preceding subsections, i.e.

$$\mathrm{Im}\,\Pi_{V/A}(t) = \lim_{\epsilon\to 0^+} \frac{\overline{\Pi}_{V/A}(t+i\epsilon) - \overline{\Pi}_{V/A}(t-i\epsilon)}{2i}, \tag{8.2.55}$$

or, in the singlet scalar and pseudoscalar channels,

$$\mathrm{Im}\,\Pi_{S^0/P^0}(t) = \lim_{\epsilon\to 0^+} \frac{\overline{\Pi}_{\sigma/\eta'}(t+i\epsilon) - \overline{\Pi}_{\sigma/\eta'}(t-i\epsilon)}{2i}, \tag{8.2.56}$$

and analogous relations between $\mathrm{Im}\,\Pi_{S/P}(t)$ and $\overline{\Pi}_{S/G}(t)$. Before discussing the sum rules of Section 8.1.4 under these identifications, let us recall that the sum rules themselves follow from the short-distance properties, which reflect the properties of the underlying $Sp(2N)$ gauge dynamics, of the two-point functions under consideration, and from general properties of quantum field theories, here essentially invariance under the Poincaré group and the spectral property. The latter allow to extend the definitions of the functions $\Pi_\phi(t)$ to functions in the complex t-plane, with all singularities (poles and branch points) confined to the positive real axis. The former then allow to write down unsubtracted dispersion relations for the appropriate combinations of two-point correlators, from which the sum rules follow. The necessity to introduce a regularisation (here the cut-off Λ), in order to render the one-loop correlators $\tilde{\Pi}_\phi(t)$ finite, and to perform the resummation shown in Fig. 8.2, leads to functions $\overline{\Pi}_\phi(t)$ that will in general not respect all the required properties. For instance, with the choice of regularisation adopted in the present study, ghost poles at $q^2 = -M^2_{\text{gh-}\phi}$, i.e. on the *negative* real q^2-axis, will appear, as discussed at the beginning of Section 8.2.2. This situation is well known in the context of the NJL approximation applied to QCD, where it has been examined quite extensively by the authors of Ref. [290], and we refer the reader to this article for additional details.

[11] At the level of one-loop two-point correlators, the spectral sum rule (8.1.19) is trivially satisfied, provided one identifies m with M_ψ, due to the identity $\tilde{\Pi}_V(q^2) - \tilde{\Pi}_A(q^2) = -\tilde{\Pi}^L_A(q^2)$. The identities

$$\tilde{\Pi}_S(q^2) - \tilde{\Pi}_P(q^2) = \tilde{\Pi}_S(q^2) - \tilde{\Pi}_{\eta'}(q^2) = \tilde{\Pi}_\sigma(q^2) - \tilde{\Pi}_G(q^2) = 2(2N)M^2_\psi \tilde{B}_0(q^2, M^2_\psi)$$

allow only for the difference of the two last sum rules in Eq. (8.1.14), involving $\tilde{\Pi}_{S\text{-}\eta'} - \tilde{\Pi}_{\sigma\text{-}G}$, to be satisfied at one-loop.

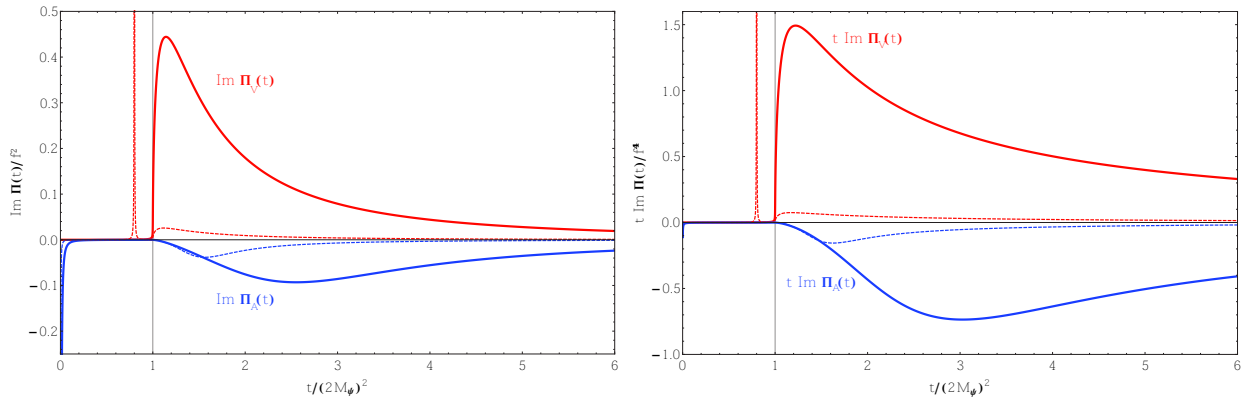

Figure 8.5: The figure on the left shows the spectral functions $\mathrm{Im}\,\Pi_V(t)$ (upper curves, in red) and $-\mathrm{Im}\,\Pi_A(t)$ (lower curves, in blue), as a function of $t/(2M_\psi)^2$ and in units of f^2, such that the plotted quantities are dimensionless and N-independent. The solid and dashed lines correspond to $\xi = 1.3$ and $\xi = 2$, respectively. The value of the parameter κ_B/κ_A has been taken equal to 0.1 in all cases. The narrow vector bound state below the continuum starting at $t = (2M_\psi)^2$ (materialised on the figures by the vertical line) is present in $\mathrm{Im}\,\Pi_V(t)$ when $\xi = 2$, but disappears for smaller values of ξ. The pion pole appears clearly in $\mathrm{Im}\,\Pi_A(t)$, but the axial-vector resonance has a mass that is always greater that $4M_\psi^2$, and therefore a narrow sub-threshold peak never occurs. The figure on the right likewise shows the functions $t\,\mathrm{Im}\,\Pi_V(t)$ and $t\,\mathrm{Im}\,\Pi_A(t)$. The latter are in units of f^4 and consequently scale like $1/N$.

The spectral densities resulting from the identifications in Eqs. (8.2.55) and (8.2.56) are shown in Figs. 8.5 and 8.6 (in order to make the figure more readable, we have kept ϵ in the definitions (8.2.55) and (8.2.56) very small, but finite). It is most instructive to analyse them in conjunction with the spectrum of the mesonic resonances, as given in Fig. 8.4, and with the general discussion at the beginning of Section 8.2.2. Figure 8.5 shows the vector and axial spectral functions for two different values of the parameter ξ. In the axial case, one recognises the contribution from the pion pole at $t = 0$, and no other narrow bound state. Only a rather broad resonance peak appears above the $t = 4M_\psi^2$ threshold, where the continuum starts. This is in agreement with Fig. 8.4, which shows that M_A is always greater than $M_\sigma = 2M_\psi$. In the vector channel, a narrow bound state appears below the $2M_\psi$ threshold for $\xi = 2$, but is absent (it has moved to the real axis on the second Riemann sheet) for $\xi = 1.3$, and is replaced by a resonance peak. Again, this agrees with Fig. 8.4, where one sees that M_V becomes greater than $2M_\psi$ when ξ takes values below ~ 1.4.

For the non-singlet scalar spectral density, shown on the left panel of Fig. 8.6, there is no narrow bound state lying below the threshold of the continuum, whatever the value of ξ. However, the larger the value of ξ, the more the resonance peak moves closer to the threshold. The shape of $\mathrm{Im}\,\Pi_S(t)$ is also sensitive to κ_B/κ_A. In the pseudoscalar non-singlet channel, only the massless pion pole shows up, and $\mathrm{Im}\,\Pi_P(t)$ is not sensitive to the value of κ_B/κ_A. The singlet scalar spectral density, shown on the right panel of Fig. 8.6, presents a narrow peak at the threshold, for any value of ξ and κ_B/κ_A. In the pseudoscalar singlet channel, the features of the spectral function become also sensitive to this second parameter, as can already be inferred upon comparing the two panels of Fig. 8.4. In particular, a narrow sub-threshold bound state is only present for smaller values of κ_B/κ_A.

An illustration of the two Weinberg-type sum rules of Eq. (8.1.13), as well as the sum rules of Eq. (8.1.14), is provided by Fig. 8.7. The integrals compared there, as functions of the coupling ξ and for two values of κ_B/κ_A, run over the whole positive t-axis, which means that, for the sake of illustration, the NJL description has been kept even beyond its expected range of validity. Of course, it is certainly difficult to ascribe any physical meaning to the spectral densities for values of, say, $t/\Lambda^2 \gtrsim 2$ [note that, for ξ close to the critical coupling, one has $2M_\psi \ll \Lambda$, therefore the NJL description holds up

The sum rule involving $\Pi_{S\text{-}P}$ is not expected to hold, since this correlator does not constitute an order parameter for $SU(4)/Sp(4)$, see footnote 3.

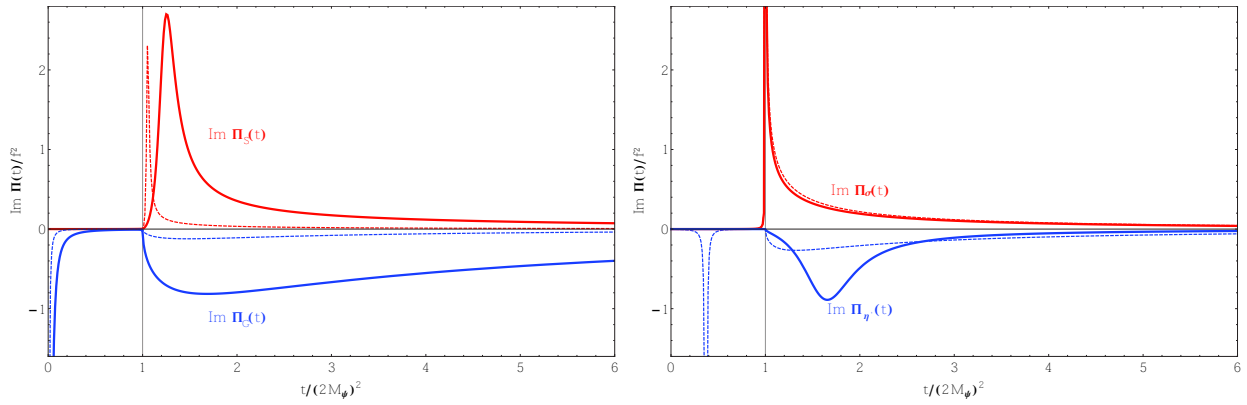

Figure 8.6: The left-hand panel shows the non-singlet spectral functions $\mathrm{Im}\,\Pi_S(t)/10$ (upper curves, in red) and $-\mathrm{Im}\,\Pi_G(t)$ (lower curves, in blue), as functions of $t/(2M_\psi)^2$, for $\kappa_B/\kappa_A = 0.1$, and for $\xi = 1.3$ (solid lines) and $\xi = 2$ (dashed lines). In the right-hand panel we fix $\xi = 2$ and show the singlet spectral functions $\mathrm{Im}\,\Pi_\sigma(t)$ (dashed red) and $-\mathrm{Im}\,\Pi_{\eta'}(t)$ (dashed blue) for $\kappa_B/\kappa_A = 0.1$, as well as $\mathrm{Im}\,\Pi_\sigma(t)$ (solid red) and $-\mathrm{Im}\,\Pi_{\eta'}(t)/20$ (solid blue) for $\kappa_B/\kappa_A = 0.5$. The narrow η' bound state is present only for the smallest value of κ_B/κ_A. A narrow σ pole appears in all cases right at the threshold $t = 4M_\psi^2$. Note that the spectral functions are all expressed in units of f^2, such that they are dimensionless and have no N-dependence.

to a large value of $t/(2M_\psi)^2$]. Beyond this value of t, the NJL description ceases to be appropriate, and we have to assume that the underlying $Sp(2N)$ gauge dynamics takes over. However, from the experience with QCD [299], it is expected that the matching between the two regimes is not very smooth. Keeping this proviso in mind, we show, on the left-hand panel of Fig. 8.7, the ratio of the integrals $\int dt\ \mathrm{Im}\,\Pi_V(t)$ and $\int dt\ \mathrm{Im}\,\Pi_A(t)$, as well as the ratio of the integrals $\int dt\ t\ \mathrm{Im}\,\Pi_V(t)$ and $\int dt\ t\ \mathrm{Im}\,\Pi_A(t)$. Similarly, the right-hand panel shows the ratios of the integrals $\int dt\ \mathrm{Im}\,\Pi_{\eta'}(t)$ and $\int dt\ \mathrm{Im}\,\Pi_S(t)$, and of the integrals $\int dt\ \mathrm{Im}\,\Pi_G(t)$ and $\int dt\ \mathrm{Im}\,\Pi_\sigma(t)$. If the sum rules were satisfied exactly for all values of ξ, all these curves would be a constant equal to one. This is obviously not the case. The general trend is that the departure from the sum rules is more important for larger values of ξ. This is in line with Fig. 8.4, from which we infer that the continuum, corresponding to $\sqrt{t} > 2M_\psi$, starts close to the cut-off Λ when $\xi \gtrsim 1.5$, therefore the NJL description becomes questionable soon after the threshold. On the right-hand panel of Fig. 8.7 we also show the ratio of the integrals $\int dt\ \mathrm{Im}\,\Pi_G$ and $\int dt\ \mathrm{Im}\,\Pi_S$. Since $\Pi_{S\text{-}P}$ is not an order parameter of the $SU(4)$ spontaneous breaking (see footnote 3), there is no corresponding sum rule, and indeed this ratio deviates significantly from unity, already for lower values of ξ.

In view of the difficulties to interpret the meaning of the sum rules, expressed in terms of the spectral densities provided by the NJL description through Eqs. (8.2.55) and (8.2.56), one may consider an alternative approach, at least when $\mathrm{Im}\,\tilde{\Pi}_\phi(M_\phi^2)$ vanishes or is sufficiently small so that it can be neglected. This happens, for instance, for the Goldstone state, or for $\tilde{\Pi}_V(M_V^2)$ when there is a sub-threshold vector bound state. In that case each correlator exhibits a single real pole, or narrow resonance [except for both the Goldstone pole and the axial-meson resonance in $\overline{\Pi}_A(q^2)$, the latter not being very narrow, though], and one can saturate the sum rules with these narrow states. Introducing, similarly to F_G and to G_G in Eqs. (8.1.22) and (8.1.23), respectively, decay constants defined as

$$\langle 0|\mathcal{J}_\mu^A(0)|V^B(p;\lambda)\rangle \equiv f_V M_V\, \epsilon_\mu^{(\lambda)}(p)\delta^{AB}\ , \qquad \langle 0|\mathcal{J}_\mu^{\hat{A}}(0)|A^{\hat{B}}(p;\lambda)\rangle \equiv f_A M_A\, \epsilon_\mu^{(\lambda)}(p)\delta^{\hat{A}\hat{B}}\ , \quad (8.2.57)$$

where $\epsilon_\mu^{(\lambda)}(p)$ is the polarisation vector associated to V or A, with $\sum_\lambda \epsilon_\mu^{(\lambda)}(p)\epsilon_\nu^{(\lambda)*}(p) = -(\eta_{\mu\nu} - p_\mu p_\nu/M_{V,A}^2)$, as well as

$$\langle 0|\mathcal{S}^{\hat{A}}|S^{\hat{B}}(p)\rangle = G_S\delta^{\hat{A}\hat{B}}, \qquad \langle 0|\mathcal{S}^0|\sigma(p)\rangle = G_\sigma, \qquad \langle 0|\mathcal{P}^0|\eta'(p)\rangle = G_{\eta'}, \quad (8.2.58)$$

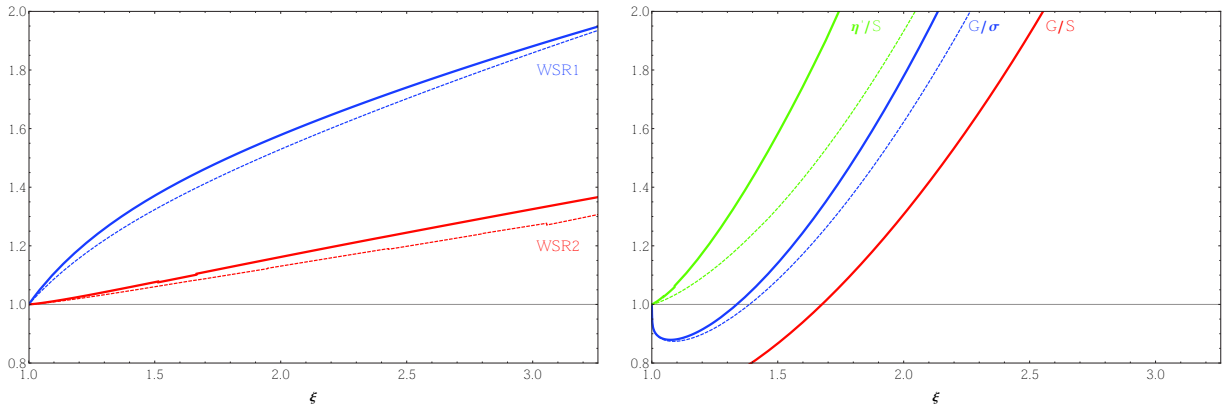

Figure 8.7: Left panel: the ratio of the integrals, taken over the whole positive t-axis, $\int dt\ \mathrm{Im}\,\Pi_V(t)/\int dt\ \mathrm{Im}\,\Pi_A(t)$ (blue, upper curves) and $\int dt\ t\ \mathrm{Im}\,\Pi_V(t)/\int dt\ t\ \mathrm{Im}\,\Pi_A(t)$ (red, lower curves), as a function of the parameter ξ, and for $\kappa_B/\kappa_A = 0.1$ (solid lines) and $\kappa_B/\kappa_A = 0.5$ (dashed lines). Right panel: the ratio of the integrals, taken over the whole positive t-axis, $\int dt\ \mathrm{Im}\,\Pi_{\eta'}(t)/\int dt\ \mathrm{Im}\,\Pi_S(t)$ (green, upper curves), $\int dt\ \mathrm{Im}\,\Pi_G(t)/\int dt\ \mathrm{Im}\,\Pi_\sigma(t)$ (blue, middle curves) and $\int dt\ \mathrm{Im}\,\Pi_G(t)/\int dt\ \mathrm{Im}\,\Pi_S(t)$ (red, lower curve), as a function of the parameter ξ, for $\kappa_B/\kappa_A = 0.1$ (solid lines) and $\kappa_B/\kappa_A = 0.5$ (dashed lines, not shown in the G/S case). Note that the above ratios are independent from N.

the sum rules become, in this narrow-width, single-resonance approximation,

$$f_V^2 M_V^2 - f_A^2 M_A^2 - F_G^2 = 0, \qquad f_V^2 M_V^4 - f_A^2 M_A^4 = 0, \tag{8.2.59}$$

and

$$G_\sigma^2 - G_G^2 = 0, \qquad G_S^2 - G_{\eta'}^2 = 0. \tag{8.2.60}$$

Now, taking the various expressions of the meson masses, decay constants, as obtained from the NJL large-N approximation above, one can check to which extent these Weinberg-type and scalar sum rules are actually saturated by the first resonance from each of the available spectra. To proceed, one may first rewrite the *resummed* two-point correlators of Eq. (8.2.33) in the pole-dominance form: from Eqs. (8.2.33) and (8.2.57), the residues of the vector and axial-vector channels are defined by

$$f_{V/A}^2 M_{V/A}^2 = \lim_{q^2 \to M_{V,A}^2} (q^2 - M_{V/A}^2)\ \overline{\Pi}_{V/A}(q^2) = \frac{-1}{(2K_{V/A})^2} \left[M_{V/A}^2\, \frac{\mathrm{d}\tilde{\Pi}_{V/A}(q^2)}{\mathrm{d}q^2}\bigg|_{q^2=M_{V/A}^2} \right]^{-1}, \tag{8.2.61}$$

where in the second equality, we have expanded the denominator of $\overline{\Pi}_{V/A}(q^2)$ around the complex pole $M_{V/A}^2$ and used Eq. (8.2.21). Similarly to the definition of the resonance masses in Eq. (8.2.22), one should however adopt a prescription to deal with the unphysical imaginary parts, NJL artefacts of the lack of confinement properties. We adopt the following prescription: (i) the residues are evaluated at the real pole masses $M_{V,A}^2 = \mathrm{Re}[g_{V,A}(M_{V,A}^2)]$ defined by Eq. (8.2.22), and (ii) we similarly define $f_{V,A}^2$ by the real parts of their right-hand-side expressions in Eq. (8.2.61). Of course, in the range of parameter space where the left-over imaginary contributions in Eqs. (8.2.61) become large, it puts a definite limit of reliability of the NJL calculation, as will be specified below. According to this prescription, we obtain explicitly for the vector decay constant,

$$f_V^2 = -\frac{3(2N)}{16\kappa_D^2 M_V^4}\, Re\left[\frac{1}{\tilde{B}_0(M_V^2, M_\psi^2) + (M_V^2 + 2M_\psi^2)\tilde{B}_0'(M_V^2, M_\psi^2)} \right]. \tag{8.2.62}$$

The axial decay constant f_A^2 is obtained in a similar way by making the following replacements $M_V \to M_A$ and $(M_V^2 + 2M_\psi^2) \to (M_A^2 - 4M_\psi^2)$ in the previous equation.

Similarly, for the spin zero channels, the residues are defined by

$$G_\phi^2 \equiv -\lim_{q^2\to M_\phi^2}(q^2-M_\phi^2)\overline{\Pi}_\phi(q^2) = \frac{1}{(2K_\phi)^2}\left[\frac{\mathrm{d}\tilde{\Pi}_\phi(q^2)}{\mathrm{d}q^2}\Big|_{q^2=M_\phi^2}\right]^{-1} . \tag{8.2.63}$$

From Eqs. (8.2.20) and (8.2.58), the scalar decay constants are explicitly given by

$$G_{\sigma,S}^2 = -\frac{1}{2(2N)K_{\sigma,S}^2}\ Re\left[\frac{1}{\tilde{B}_0(M_{\sigma,S}^2,M_\psi^2)+(M_{\sigma,S}^2-4M_\psi^2)\tilde{B}_0'(M_{\sigma,S}^2,M_\psi^2)}\right] , \tag{8.2.64}$$

while for the pseudo-scalar decay constants we obtain

$$G_{G,\eta'}^2 = -\frac{1}{2(2N)K_{G,\eta'}^2}\ Re\left[\frac{g_{A,a}^{-1}(M_{G,\eta'}^2)}{\tilde{B}_0(M_{G,\eta'}^2,M_\psi^2)+M_{G,\eta'}^2\tilde{B}_0'(M_{G,\eta'}^2,M_\psi^2)}\right] , \tag{8.2.65}$$

where the axial vector-pseudoscalar mixing (see section 8.2.5) brings the factor $g_{A,a}^{-1}(M_{G,\eta'}^2)$ for G and η' respectively.

Generally, we cannot expect the sum rules in the narrow width approximation to be very well satisfied, both because of the already discussed inherent approximations of the NJL framework, and also since the narrow width approximation itself is not justified in a substantial part of the parameter range, as we will examine more precisely below. To be more specific, we will use the standard definition of the width,

$$M_\phi\Gamma_\phi = \frac{\mathrm{Im}\,\tilde{\Pi}_\phi(M_\phi^2)}{\mathrm{Re}\,\tilde{\Pi}_\phi'(M_\phi^2)} , \tag{8.2.66}$$

with $\tilde{\Pi}_\phi'(q^2)$ denoting the derivative of $\tilde{\Pi}_\phi(q^2)$ with respect to q^2. By evaluating explicitly Eq. (8.2.66) for the relevant resonances one may control the validity range of the narrow width approximation.

Before a precise illustration of the deviations from the sum rules relations in Eqs. (8.2.59) and (8.2.60) in the parameter space of the model, it is instructive to examine more closely the NJL expressions of the involved quantities, Eqs. (8.2.62), (8.2.37) and (8.2.36). Namely, let us assume momentarily that we could crudely neglect the q^2 dependence of $\tilde{B}_0$, i.e. taking $\tilde{B}_0(M_V^2,M_\psi^2)\simeq\tilde{B}_0(M_A^2,M_\psi^2)\equiv\tilde{B}_0$ (therefore taking also its derivative to vanish, $\tilde{B}_0'(q^2)\simeq 0$). Within this approximation, the second sum rule in Eq. (8.2.59) is immediately satisfied, see Eq. (8.2.62), while for the first sum rule, one can write after simple algebra:

$$f_V^2M_V^2 - f_A^2M_A^2 \simeq f_V^2(6M_\psi^2)\left[1+\mathcal{O}\left(\frac{M_\psi^2}{M_V^2}\right)\right] \simeq -F_G^2\left[1+\mathcal{O}\left(\frac{M_\psi^2}{M_V^2}\right)\right] , \tag{8.2.67}$$

where in the first equality we used the fact that the relation in Eq. (8.2.38) becomes exact in this approximation, and in the last equality we used Eqs. (8.2.62) and (8.2.37) in the same approximation, and identified F_G^2 from its expression in Eq. (8.2.41). This simple exercise shows explicitly and rather intuitively where the bulk of deviations from WSR comes from: one infers that the sum rules in Eq. (8.2.59) will, in general, not be satisfied, since the quantities they involve are the pole masses, $M_V^2 = Re[M_V^2(M_V^2)]$ and $M_A^2 = Re[M_A^2(M_A^2)]$, the Goldstone decay constant $F_G^2 = F_G^2(0)$, and the vector decay constants $f_{V,A}^2$ in Eq. (8.2.62), actually evaluated at the different V,A pole masses and involving also the non-vanishing derivative $\tilde{B}_0'(M_{V/A}^2)$. Accordingly since the relevant expressions like Eq. (8.2.62) are to be evaluated at *different* values of q^2, this implies not quite negligible differences in $\tilde{B}_0(q^2)$, and in its derivative. Only to the extent that they display a rather mild q^2-dependence will the narrow-width version (8.2.59) of the sum rules approximatively hold [12]. Moreover, the crudely neglected terms $\mathcal{O}(M_\psi^2/M_V^2)$ in Eq. (8.2.67) are actually not so negligible, the less when ξ increases, just as M_A^2/M_V^2 also increases with ξ. Thus, we generally expect stronger deviations from Eq. (8.2.59) for larger ξ values.

[12] We note that those finding and observations are qualitatively similar to the WSR results for the NJL model applied to low energy QCD in ref. [299], although those authors used somewhat different approximations than ours.

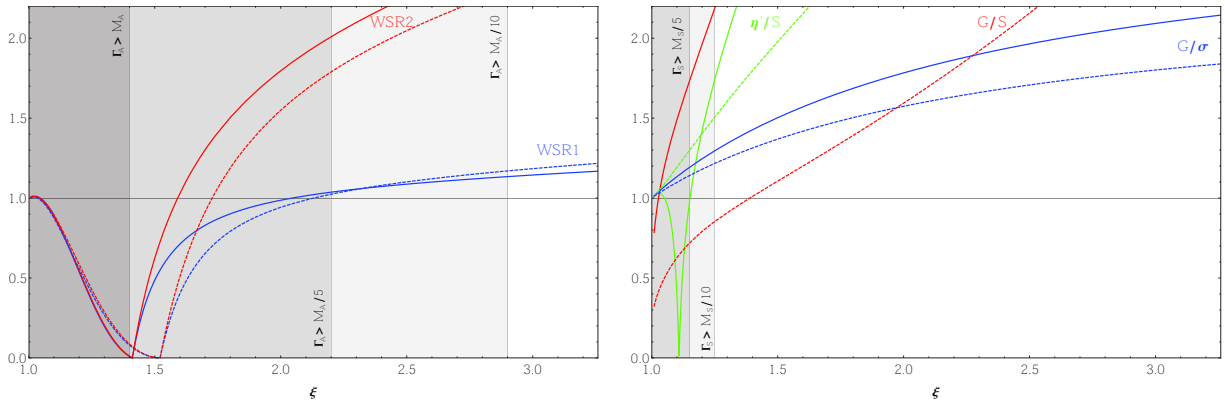

Figure 8.8: Left panel: the two ratios $(f_V^2 M_V^2)/(F_G^2 + f_A^2 M_A^2)$ (WSR1, blue lines) and $(f_V^2 M_V^4)/(f_A^2 M_A^4)$ (WSR2, red lines) as functions of the coupling ξ, for $\kappa_B/\kappa_A = 0.1$ (solid lines) and $\kappa_B/\kappa_A = 0.5$ (dashed lines). Right panel: the analog for scalar sum rules. Also indicated are the values of the most relevant resonance widths, calculated from Eq. (8.2.66) for $\kappa_B/\kappa_A = 0.1$.

In order to illustrate more precisely the deviations from the Weinberg-like sum rules of Eq. (8.2.59), taking now the "exact" expressions of $f_{V/A}$, $M_{V/A}$ according to our NJL calculations and prescriptions above, we consider the two ratios

$$\mathrm{WSR}_1 \equiv \frac{f_V^2 M_V^2}{F_G^2 + f_A^2 M_A^2} \ , \qquad \mathrm{WSR}_2 \equiv \frac{f_V^2 M_V^4}{f_A^2 M_A^4} \ , \tag{8.2.68}$$

which would both equal unity if the sum rules were satisfied in their narrow-width versions. Similarly, for the scalar sum rules we consider the two ratios G_G^2/G_σ^2 and $G_{\eta'}^2/G_S^2$. The behaviour of these ratios with respect to ξ and κ_B/κ_A are illustrated in the left and right panels of Fig. 8.8 for the Weinberg and scalar sum rules respectively. We also indicate some specific values of the relevant resonance widths, calculated from Eq. (8.2.66) for the reference value $\kappa_B/\kappa_A = 0.1$. The corresponding shaded regions thus indicate approximately the range where the narrow width approximation can be trusted or not. (NB the V, A widths are very weakly sensitive to κ_B/κ_A values, so that the indicated ranges are also approximately valid for $\kappa_B/\kappa_A = 0.5$. In contrast the η' and S widths grow rapidly with κ_B, such that the indicated boarder $\Gamma_S/M_S = 1/5(1/10)$ are pushed for $\kappa_B/\kappa_A = 0.5$ to larger ξ, $\xi \simeq 1.7(2)$ respectively).

The two sum rules of Eq. (8.2.59) are actually reasonably satisfied in some specific ξ ranges, respectively either for intermediate values $1.6 \lesssim \xi \lesssim 2$, or for ξ very close to 1. Conversely the deviations appear maximal in the range $\xi \simeq 1.2 - 1.6$ and again for very large ξ. Most of these features can be understood more intuitively with the help of the above analysis. The intermediate range where the deviations are the smallest corresponds to a range where at the same time, the narrow width approximation is well justified, and the relevant pole mass differences are still moderate such that the relevant q^2 arguments of $\tilde{B}_0(q^2)$ are not widely different. Then for very large ξ values, while the A width is becoming smaller, one enters the regime of increasingly large differences in the relevant $\tilde{B}_0(M_{A/V}^2)$, thus increasing the deviations, although the first WSR remains relatively good. The second WSR sum rule shows more rapidly increasing and important deviations for larger ξ, as intuitively expected since the fourth power of the masses enhances the increasing M_A/M_V ratio. The WSR values are not very sensitive to the ratio κ_B/κ_A, but depend mostly on ξ: a larger κ_B value essentially shifts the values of the sum rules in Fig. 8.8, as it implies larger values of $\kappa_A + \kappa_B$. Conversely for decreasing ξ, the narrow width approximation becomes totally unreliable, say for $\xi \lesssim 1.6$ in the case of Γ_A, where correspondingly the deviations are seen to be maximal. Moreover, when approaching (from below) the threshold $M_V^2 = 4M_\psi^2$, Γ_V is vanishing, but $Re[\tilde{B}_0'(M_V^2, M_\psi^2)]$ tends toward infinity, such that $f_V^2 \to 0$, see Eq. (8.2.62). This happens around $\xi \simeq 1.4$ (1.5) for $\kappa_B/\kappa_A = 0.1$ (0.5). This peculiar feature can be understood as follow. When moving towards the threshold from below, the residue of the vector resonance, $f_V^2 M_V^2$, tends to zero, because its contribution to the spectral

function is progressively transferred from the sub-threshold to the continuum part of the spectral function. Since in the pole dominance approximation one only considers the lightest resonances, just below the threshold the continuum contribution is not included within Eq. (8.2.62), therefore the crossing of the threshold appears problematic in our NJL approximation. Of course, this pathological behaviour is not present in Fig. 8.7, where we consider the complete two-point functions, that include also the continuum contributions. Finally, very close to the critical coupling $\xi \simeq 1$, although both $\Gamma_{V,A}$ are large, the mass gap in this region is relatively very small, $M_\psi \ll \Lambda$, such that $M_A - M_V$ is minimal, and $F_G \simeq M_\psi$ is also relatively small. Thus taking the real contributions prescriptions according to Eq. (8.2.62), one is again very close to the ideal approximation above discussed, leading to Eq. (8.2.67).

From those results, if considering that the best possible matching of the Weinberg-type sum rules, established on more general dynamical grounds, may be more important than the possible limitations of the NJL model approximation (somewhat in the spirit of Ref. [299]), one could be tempted to infer some preferred ξ range, where both deviations are minimal (although as clear from the figure it is not possible to satisfy the two WSR exactly for the same ξ value). However, given the limitations of the NJL dynamical approximation, partly responsible for the non-perfectly matched Weinberg-type sum rules, we consider this only as an indicative trend rather than a genuine dynamical constraint on the couplings.

Concerning next the scalar sum rules, note that the above relations in Eqs. (8.2.64) and (8.2.65) do not lead to $G_G^2(q^2) - G_\sigma^2(q^2) = 0$ and $G_{\eta'}^2(q^2) - G_S^2(q^2) = 0$, which would be valid if evaluating all expressions at the same q^2 value. This is due to the pseudo-scalar axial mixing, i.e. a term proportional to $g_{A,a}(q^2)$ does not vanish in the difference. In addition, for $G_G^2(q^2) - G_S^2(q^2)$, there is a term proportional to κ_B, that indicates that this difference is not a sum rule, consequently the discrepancy increases with κ_B. Indeed, as can be seen on Fig. 8.8, some of the scalar sum rules are approximately satisfied very close to $\xi = 1$, but are rapidly and badly invalidated for larger ξ, even though the narrow width approximation is justified in this region. This is mainly due to very large differences in the argument of the relevant $\tilde{B}_0(p^2)$, and also, as above discussed, due to the non-vanishing κ_B. Note that, similarly to what is discussed above for the WSRs, the scalar sum rule associated to the η' may exhibit a pathological behaviour, when the lightest resonances do not incorporate the dominant contributions. Indeed, η' crosses the threshold for $\kappa_B/\kappa_A = 0.1$ and the associated ratio $G_{\eta'}^2/G_S^2$ tends to zero in this regime, that lies around $\xi = 1.1$.

In summary, the mismatch between the NJL predictions and the spectral sum rules resides in the gap between the contribution of the low-lying resonances and the full spectral functions. Given these limitations in the comparison of our results with the spectral sum rules, and since our interest is mostly the phenomenology of the lightest composite states, in the following we will keep studying the full range for the parameters ξ and κ_B/κ_A.

E $SU(4)/Sp(4)$ chiral Lagrangian

The aim of this appendix is to make the link between the EW sector presented in section 8.2 and the effective approach described in chapter 6. More precisely, we relate the Goldstone decay constant F_G to the scale of the chiral Lagrangian usually denoted by f. This relation is crucial as all of the low energy deviations compare to the SM predictions are parametrised by $\xi = v^2/f^2$ and then f is experimentally constrained by the EWPT and the Higgs coupling measurements to be $\gtrsim 1$ TeV. Let us start with the following chiral Lagrangian

$$\mathcal{L} = \frac{F_G^2}{4}\langle (D_\mu U)^\dagger (D^\mu U)\rangle + \cdots \tag{E.1}$$

where we restrict to the lowest order in the chiral expansion. For the moment, the derivation remains completely general and can be applied to the coset $SU(4)/Sp(4)$ as well as to other non-minimal EW cosets. The Goldstone matrix $U(x)$ contains the pNGB fields $G(x)$

$$U(x) = e^{iG(x)/F_G}\Sigma_\epsilon \ , \qquad G(x) = 2\sum_{\hat{A}} G^{\hat{A}}(x) T^{\hat{A}} \ , \tag{E.2}$$

and the vacuum Σ_ϵ is conveniently chosen to respect

$$\Sigma_\epsilon^\dagger = \Sigma_\epsilon^T = \epsilon\Sigma_\epsilon \ , \qquad \Sigma_\epsilon^2 = \epsilon \mathbb{1} \ . \tag{E.3}$$

The covariant derivative $D_\mu U$ explicitly writes

$$D_\mu U = \partial_\mu U - i(v_\mu + a_\mu)U - iU(v_\mu + a_\mu)^T \ , \tag{E.4}$$

where v_μ and a_μ are the external sources coupling respectively to the vector (unbroken) and axial (broken) currents $\mathcal{J}_\mu^A$ and $\mathcal{J}_\mu^{\hat{A}}$ defined in subsection 8.1.1. The external sources are defined by

$$v_\mu = \sum_A v_\mu^A \ T^A \ , \qquad a_\mu = \sum_{\hat{A}} a_\mu^{\hat{A}} \ T^{\hat{A}} \tag{E.5}$$

where the broken ($T^{\hat{A}}$) and unbroken (T^A) generators of $SU(2N_f)$ respect the relations in Eq. (8.1.2). In the real case where $\epsilon = +1$, the unbroken generators T^A correspond to the generators of $SO(2N_f)$ while the broken generators $T^{\hat{A}}$ span the coset $SU(2N_f)/SO(2N_f)$. In the pseudo-real case where $\epsilon = -1$, the unbroken and broken generators are respectively associated to the subgroup $Sp(2N_f)$ and to the coset $SU(2N_f)/Sp(2N_f)$. In our case of interest that is for $SU(4)/Sp(4)$, we are of course in the pseudo-real case with $N_f = 2$. The covariant derivative of Eq. (E.4) can be rewritten as follow

$$D_\mu U = \partial_\mu U - i\epsilon \ [v_\mu, U\Sigma_\epsilon]\Sigma_\epsilon - i\epsilon \ \{a_\mu, U\Sigma_\epsilon\}\Sigma_\epsilon \ , \tag{E.6}$$

where we have used the following relations

$$v_\mu U + U v_\mu^T = \epsilon \ [v_\mu, U\Sigma_\epsilon]\Sigma_\epsilon \ , \qquad a_\mu U + U a_\mu^T = \epsilon \ \{a_\mu, U\Sigma_\epsilon\}\Sigma_\epsilon \ . \tag{E.7}$$

Kinetic term and Goldstone decay constant

First, we need to check the normalisation of the Goldstone bosons kinetic term in Eq. (E.1). We expand the Goldstone matrix around the vacuum Σ_ϵ ie $U \simeq \Sigma_\epsilon + iG(x)/F_G\Sigma_\epsilon + \cdots$. The covariant derivative of Eq. (E.6) becomes

$$D_\mu U = \frac{i}{F_G}(\partial_\mu G)\Sigma_\epsilon - 2ia_\mu\Sigma_\epsilon + \frac{1}{F_G}[v_\mu, G(x)]\Sigma_\epsilon + \frac{1}{F_G}\{a_\mu, G(x)\}\Sigma_\epsilon + \cdots \tag{E.8}$$

Taking only the derivative part of the above relation we obtain

$$\begin{aligned}\frac{F_G^2}{4}\langle(D_\mu U)^\dagger(D^\mu U)\rangle &= \frac{1}{4}\langle(\partial_\mu G)(\partial^\mu G)\rangle + \cdots \\ &= \sum_{\hat{A},\hat{B}}\langle T^{\hat{A}}T^{\hat{B}}\rangle(\partial_\mu G^{\hat{A}})(\partial^\mu G^{\hat{B}}) + \cdots \\ &= \frac{1}{2}\sum_{\hat{A}}(\partial_\mu G^{\hat{A}})(\partial^\mu G^{\hat{A}}) + \cdots \end{aligned} \tag{E.9}$$

such that the pNGB $G^{\hat{A}}$ are well canonically normalised.

Now we derive the definition of the decay constant F_G. From Eq. (E.8), we consider the derivative part and the leading term containing an axial source a_μ that is $-2ia_\mu\Sigma_\epsilon$. We have

$$\begin{aligned}\frac{F_G^2}{4}\langle(D_\mu U)^\dagger(D^\mu U)\rangle &= -F_G\langle(\partial_\mu G)a^\mu\rangle + \cdots \\ &= -2F_G\sum_{\hat{A},\hat{B}}\langle T^{\hat{A}}T^{\hat{B}}\rangle(\partial_\mu G^{\hat{A}})a^{\mu\hat{B}} + \cdots \\ &= -F_G\sum_{\hat{A}}(\partial_\mu G^{\hat{A}})a^{\mu\hat{A}} + \cdots \end{aligned} \tag{E.10}$$

such that in momentum space, the Goldstone decay constant F_G is defined by the following matrix element

$$\langle 0|\mathcal{J}_\mu^{\hat{A}}(0)|G^{\hat{B}}(p)\rangle = iF_G\ p_\mu\delta^{\hat{A}\hat{B}}\ , \tag{E.11}$$

that is, the same definition compare to Eq. (8.1.22). As expected, the Goldstone bosons $G^{\hat{A}}$ couple only to the axial current $\mathcal{J}_\mu^{\hat{A}}$ and the coupling is derivative. There is no such coupling involving the vector currents as there is no term involving only the vector sources v_μ in the covariant derivative: the term $[v_\mu, U\Sigma_\epsilon] \simeq [v_\mu, \Sigma_\epsilon^2] + \cdots$ cancel at first order in the expansion around the vacuum.

GB couplings to SM gauge bosons

Let us now consider the couplings of the pNGB to the SM gauge fields. We consider a composite Higgs model such that the SM gauge group is embedded in the unbroken symmetry group H (not in the coset space G/H). As a consequence, to introduce the SM gauge fields we only need to consider the vector sources v_μ and then the following term of the chiral Lagrangian

$$\begin{aligned}\frac{F_G^2}{4}\langle(D_\mu U)^\dagger(D^\mu U)\rangle &= \frac{F_G^2}{4}\langle([v_\mu, U\Sigma_\epsilon]\Sigma_\epsilon)^\dagger\ [v_\mu, U\Sigma_\epsilon]\Sigma_\epsilon\rangle + \cdots \\ &= \frac{F_G^2}{2}\langle v_\mu v^\mu - e^{-iG(x)/F_G}\ v_\mu\ e^{iG(x)/F_G}\ v^\mu\rangle + \cdots \end{aligned} \tag{E.12}$$

The embedding of the SM gauge group inside H obviously depends on G/H itself such that we now restrict to the $SU(4)/Sp(4)$ case. The extension to other pattern of symmetry breaking G/H is straightforward. Using the explicit form of the broken $SU(4)$ generators derived in appendix F, one obtains for the Goldstone matrix

$$G(x) = \frac{1}{\sqrt{2}}\begin{pmatrix} G^{\hat{3}} & G^{\hat{1}} - iG^{\hat{2}} & 0 & -iG^{\hat{4}} + G^{\hat{5}} \\ G^{\hat{1}} + iG^{\hat{2}} & -G^{\hat{3}} & iG^{\hat{4}} - G^{\hat{5}} & 0 \\ 0 & -iG^{\hat{4}} - G^{\hat{5}} & G^{\hat{3}} & G^{\hat{1}} + iG^{\hat{2}} \\ iG^{\hat{4}} + G^{\hat{5}} & 0 & G^{\hat{1}} - iG^{\hat{2}} & -G^{\hat{3}} \end{pmatrix}\ , \tag{E.13}$$

from which we derive

$$G^2(x) = \frac{1}{2}\vec{G}^2(x)\ \mathbb{1}_4\ , \qquad \vec{G}^2(x) \equiv \sum_{\hat{A}} G^{\hat{A}}(x)G^{\hat{A}}(x)\ . \tag{E.14}$$

From the above relations, we obtain

$$
\begin{aligned}
e^{iG(x)/F_G} &= \left[1-\frac{1}{2!}\left(\frac{|\vec{G}(x)|}{\sqrt{2}F_G}\right)^2+\frac{1}{4!}\left(\frac{|\vec{G}(x)|}{\sqrt{2}F_G}\right)^4+\cdots\right]\mathbb{1}_4 \\
&\quad +i\frac{G(x)}{F_G}\frac{1}{\frac{|\vec{G}(x)|}{\sqrt{2}F_G}}\left[\left(\frac{|\vec{G}(x)|}{\sqrt{2}F_G}\right)-\frac{1}{3!}\left(\frac{|\vec{G}(x)|}{\sqrt{2}F_G}\right)^3+\frac{1}{5!}\left(\frac{|\vec{G}(x)|}{\sqrt{2}F_G}\right)^5+\cdots\right] \\
&= \cos\left(\frac{|\vec{G}(x)|}{\sqrt{2}F_G}\right)\mathbb{1}_4+i\sqrt{2}\frac{G(x)}{|\vec{G}(x)|}\sin\left(\frac{|\vec{G}(x)|}{\sqrt{2}F_G}\right)\,, \qquad \text{(E.15)}
\end{aligned}
$$

where $|\vec{G}|\equiv\sqrt{\vec{G}^2}$. Inserting the above relation in Eq.(E.12) we get

$$
\begin{aligned}
\frac{F_G^2}{4}\langle(D_\mu U)^\dagger(D^\mu U)\rangle &= \frac{F_G^2}{2}\sin^2\left(\frac{|\vec{G}(x)|}{\sqrt{2}F_G}\right)\langle v^\mu v_\mu\rangle \qquad \text{(E.16)}\\
&\quad -\frac{F_G^2}{|\vec{G}(x)|^2}\sin^2\left(\frac{|\vec{G}(x)|}{\sqrt{2}F_G}\right)\langle G(x)v_\mu G(x)v^\mu\rangle+\cdots
\end{aligned}
$$

We now restrict $G(x)$ to the pNGB $G^{\hat{1}}\equiv h(x)$ and $G^{\hat{3}}\equiv\eta(x)$. The other NGBs $G^{\hat{2},\hat{4},\hat{5}}$ being the would be Goldstone boson eaten by the W and Z bosons after EWSB. Then the Goldstone matrix reads

$$
G(x)=\frac{1}{\sqrt{2}}\begin{pmatrix}\eta(x) & h(x) & 0 & 0\\ h(x) & -\eta(x) & 0 & 0\\ 0 & 0 & \eta(x) & h(x)\\ 0 & 0 & h(x) & -\eta(x)\end{pmatrix}\,. \qquad \text{(E.17)}
$$

For the external vector sources v_μ, we restrict to the gauged part ie to the SM gauge fields

$$
\begin{aligned}
v_\mu &= g(W_\mu^1T_L^1+W_\mu^2T_L^2+W_\mu^3T_L^3)+g'B_\mu T_R^3 \\
&= \frac{g}{2}\begin{pmatrix}g'/gB_\mu & 0 & 0 & 0\\ 0 & W_\mu^3 & 0 & iW_\mu^1+W_\mu^2\\ 0 & 0 & -g'/gB_\mu & 0\\ 0 & -iW_\mu^1+W_\mu^2 & 0 & -W_\mu^3\end{pmatrix}\,, \qquad \text{(E.18)}
\end{aligned}
$$

Inserting Eqs. (E.17) and (E.18) in Eq. (E.16) we get

$$
\frac{F_G^2}{4}\langle(D_\mu U)^\dagger(D^\mu U)\rangle = g^2\frac{F_G^2}{2}\frac{h^2}{h^2+\eta^2}\sin^2\left(\frac{\sqrt{h^2+\eta^2}}{\sqrt{2}F_G}\right)[W_\mu^+W^{\mu-}+\frac{1}{2c_w^2}Z_\mu Z^\mu]+\cdots \qquad \text{(E.19)}
$$

where we have used Eqs. (1.2.9) and (1.2.11) of chapter 1. Keeping now only the Higgs field ie taking $\eta(x)=0$ and introducing a vev for the Higgs: $h(x)\to h(x)+\langle h\rangle$ we get

$$
\begin{aligned}
\frac{F_G^2}{4}\langle(D_\mu U)^\dagger(D^\mu U)\rangle &= g^2\frac{F_G^2}{2}\left[\sin^2\left(\frac{\langle h\rangle}{\sqrt{2}F_G}\right)+\sqrt{2}\,\frac{h(x)}{F_G}\sin\left(\frac{\langle h\rangle}{\sqrt{2}F_G}\right)\right. \qquad \text{(E.20)}\\
&\quad \left.+\frac{h^2(x)}{2F_G^2}(1-2\sin^2\left(\frac{\langle h\rangle}{\sqrt{2}F_G}\right))+\mathcal{O}(h^3)\right][W_\mu^+W^{\mu-}+\frac{1}{2c_w^2}Z_\mu Z^\mu]+\cdots
\end{aligned}
$$

To obtain the above equation, we have expanded around the vacuum $\langle h\rangle$ using

$$
\sin\left(\frac{h(x)+\langle h\rangle}{\sqrt{2}F_G}\right)=\sin\left(\frac{\langle h\rangle}{\sqrt{2}F_G}\right)+\frac{h(x)}{\sqrt{2}F_G}\cos\left(\frac{\langle h\rangle}{\sqrt{2}F_G}\right)-\frac{1}{2}\left(\frac{h(x)}{\sqrt{2}F_G}\right)^2\sin\left(\frac{\langle h\rangle}{\sqrt{2}F_G}\right)+\mathcal{O}(h^3) \qquad \text{(E.21)}
$$

From Eq. (E.20), we identify the masses of the SM gauge bosons: $M_W=gv/2$ and $M_Z=M_W/(\sqrt{2}c_w)$ and then the EW vev $v\simeq 246$ GeV. The latter takes the following form

$$
v=\sqrt{2}F_G\sin\left(\frac{\langle h\rangle}{\sqrt{2}F_G}\right)\,, \qquad \xi\equiv\sin^2\left(\frac{\langle h\rangle}{\sqrt{2}F_G}\right)=\frac{v^2}{2F_G^2}\,. \qquad \text{(E.22)}
$$

Then we finally have

$$\frac{F_G^2}{4}\langle (D_\mu U)^\dagger (D^\mu U)\rangle = \left(M_W^2 + gM_W\sqrt{1-\xi}\; h(x) + \frac{g^2}{4}(1-2\xi)\; h^2(x)\right) [W_\mu^+ W^{\mu-} + \frac{1}{2c_w^2} Z_\mu Z^\mu] + \cdots \tag{E.23}$$

and the deviations to the SM Higgs couplings parametrised by ξ are

$$\frac{c_{hVV}}{c_{hVV}^{SM}} = \sqrt{1-\xi}\;, \qquad \frac{c_{hhVV}}{c_{hhVV}^{SM}} = (1-2\xi)\;. \tag{E.24}$$

The link between the usual scale of the chiral Lagrangian f and the Goldstone decay constant F_G defined by Eq. (E.11) is $f = \sqrt{2}F_G$.

Chapter 9

The coloured sector of the minimal UV completion

In the precedent chapter, we have presented the EW sector of the minimal UV complete CHM. This sector contains the composite Higgs boson that emerges as a pNGB of the spontaneous breaking of the $SU(4)$ global symmetry. Beside the EW sector, CHMs also contain a coloured sector (see chapter 7) from which top partners are supposed to emerge as bound states. The top partners are a crucial ingredient of CHMs as they are supposed to drive the breaking of the EW symmetry. Indeed, they couple linearly with the top quark and these couplings explicitly breaks the global symmetries, generating in this way a potential for the NGBs and finally a mass for the Higgs boson.

In our case, the minimal coloured sector consistent with the $SU(4)/Sp(4)$ breaking pattern of the EW sector is based on $SU(6)/SO(6)$. The $SU(6)$ symmetry is the minimal way to embed the $SU(3)_c$ gauge symmetry in a VL way that is, without introducing gauge anomalies. This global symmetry is realised by six fermions X transforming under the strong dynamics in a different representation compare to the fermions ψ. The requirement to form baryons as well as the preservation of asymptotic freedom in the UV lead to only one possibility for the gauge representation of the fermions X that is the two index antisymmetric representation of $Sp(2N)$. This representation is real such that a non-zero condensate $\langle X^f X^g \rangle$ breaks the $SU(6)$ symmetry down to $SO(6)$. In addition, baryons with an even number of ψ (of pseudo-real fermions) are allowed in general. Restricting to trilinear baryons, the two possibilities are $(\psi^a \psi^b X^f)$ and $(X^f X^g X^h)$ where the first one contains top partners charged both under QCD and under the EW symmetry. Note that the spontaneous breaking of the $SU(6)$ symmetry is not a necessity in the coloured sector contrary to the EW sector where the $SU(4)$ symmetry must be broken in order for the Higgs to emerge as a pNGB.

The chapter is organised as follow. We first introduce the coloured fundamental fermions X^f. Similarly to the $SU(4)$ sector, the coloured sector has an anomalous $U(1)_X$ symmetry. However, one combination of the two anomalous $U(1)_\psi$ and $U(1)_X$ symmetries, respectively associated with the EW and the coloured sector, is in non-anomalous. This feature is slightly different in QCD [1] where there are two $U(1)$ symmetry but only one sector such that the non-anoamlous $U(1)_V$ symmetry is not spontaneously broken. In the present case, the non-anomalous $U(1)$ symmetry is spontaneously broken after condensation which leads to another, possibly light pNGB. Another interesting point is that the anomalous combination remains explicitly broken even in the large N limit due to the large dimension of gauge representation in which the fermions X belong. This is not the case in QCD where the quarks belong to the fundamental representation such that the $U(1)_A$ anomaly disappears in the large N_c limit (see subsection U(1) axial anoamly). In subsection 9.1.1, we study in details the patterns of symmetry breaking. We use the 't Hooft anomaly matching and show that the global symmetry of the EW sector must be broken. However, for the coloured sector, the matching with composite

[1] More precisely, in QCD there are two sectors: one associated with the left-handed quarks q_L transforming as triplets of $SU(3)_c$ and one associated with the right-handed quarks q_R^c transforming as anti-triplet. The two sectors lead to only one condensate $[\langle \overline{q} q \rangle = \langle \overline{q}_L q_R + \overline{q}_R q_L \rangle]$ after the spontaneous breaking of the chiral symmetry such that there is only one anomalous $U(1)$ symmetry, the axial $U(1)_A$. However, the second non-anomalous symmetry $U(1)_V$ is not spontaneously broken by the QCD condensate and then differs from the present case.

baryonic states is possible such that the global symmetry could be broken or remains unbroken. This is a very important result because we have proof [2] that the CHM under study generate a pNGB Higgs. This is not a trivial result and it could be interesting to do the same exercise with all of the other possible CHMs of table 7.3. We consider in subsection 9.1.2 the sum rules of the coloured sector. Most of them have the same form than the EW sector in isolation that is Π^X_{V-A}, Π^X_{S-P}, $\Pi^X_{S^0-P}$ and $\Pi^X_{S-P^0}$ are order parameters of the $SU(6)/SO(6)$ spontaneous breaking. However, in addition to the other order parameters, there is also $\Pi^{\psi X}_{S^0}$ and $\Pi^{\psi X}_{P^0}$ from which we derived two additional sum rules. The latter are associated with the non-anomalous $U(1)$ symmetry as the corresponding charge is spontaneously broken after condensation . Then we expect in general additional features when the two sectors are not in isolation.

The link between the EW and the coloured sectors is encoded by the 't Hooft term which parametrises the breaking of the anomalous symmetry. This operator is presented in subsection 9.1.3, it is made of the two species of fermions, ψ and X. As usual with a 't Hooft term, we isolate the relevant part which contribute in the NJL approximation.

In section 9.2 we study the coloured sector with the NJL techniques. We first derive in subsection 9.2.1 the effective four-fermion interactions relevant for the NJL computations. We also derive the two mass gap equations giving the dynamical masses M_ψ and M_X. The latter form a coupled system due to the 't Hooft term that link the two sectors. This feature can be compared with the three flavours case in QCD (see subsection 3.2.4) where there are two coupled mass gap: one for $\langle\overline{u}u\rangle = \langle\overline{d}d\rangle$ and one for $\langle\overline{s}s\rangle$. However, the origin of the coupling between the two mass gap is not the same. In QCD, it is mainly due to the flavour structure of the current mass matrix while in our case, it is due to the effective four-fermion interaction $(\psi\psi)(XX)$ coming from the 't Hooft term. Next, in subsections 9.2.2 and 9.2.3, we derive the masses of the scalar and vector coloured resonances. We restrict to the non-singlet resonances as there is no mixing with the EW resonances. The phenomenological analysis of the non-singlet masses is given in subsection 9.2.4. One finds that the coloured pNGB can be sufficiently heavy that is above the collider bounds due to the radiation QCD corrections coming from the gauging of the SM group. However, the price is to have a scale f a bit larger from its lower bound of around 1 TeV. Another way to respect the experimental bounds is to introduce an explicit breaking mass term $m_X X^f X^f$ which is the equivalent of the current masses in QCD. In that case, fixing f at 1 TeV one easily respect the experimental bounds with a sufficiently large value of m_X. However, the explicit breaking mass contributes to all of the other channels and the coloured pNGBs tend to be of the same order than the coloured vector masses. Note that, for the numerical analysis, we again use simple phenomenological relations between the couplings of the four-fermion interactions that come from the current-current hypothesis. The relations in each sectors are well-defined (between scalar and vector couplings) but we note that it is not the case between the EW and the coloured sector. For simplicity and for phenomenological reasons we assume that the strength of the four-fermions interactions in the EW and in the coloured sectors are the same.

Finally, we present the singlet sector in subsection 9.2.5. We introduce the mixing formalism used in the NJL to estimate the masses and other decay constants. Indeed, the four-fermion interaction involving the two species of fundamental fermions induces a mixing between the EW and coloured (pseudo)scalar singlets.

We also collect some additional material related to both the EW and the coloured sectors in the appendices. In appendix F, we construct explicitly the $SU(4)$ and $SU(6)$ generators and identify the embedding of the SM gauge group. We also give the radiative corrections of the coloured pNGs coming from the gauging of the SM group. In appendix G and H, we respectively give the explicit form of the one-loop functions $\tilde{A}_0$ and $\tilde{B}_0$ and we present the computation of the one-loop two points functions $\tilde{\Pi}_i$ $(i = S, P, V, A, AP)$ used in the NJL computations. The latter have already been considered in section 3.2 in the context of Dirac fermions and we generalise these result to the case of Weyl fermions. Finally, in appendix I, we start from the $Sp(2N)$ current-current operators and we make the link between the coefficients of the four-fermions interactions. We also take the time to collect general results on Fierz transformations such that the procedure can easily be applied to other UV

[2] Note that for the matching, we make the reasonable hypothesis to restrict to trilinear baryons. This can be justified in the maximal attractive channel framework (see subsection 10.2.1).

completions.

9.1 Adding the coloured sector

An appealing way to couple the SM fermions to the composite Higgs is to introduce a linear coupling between each SM fermion and a composite fermion resonance with the same quantum numbers. Such an approach, known as fermion partial compositeness [81, 82], is especially attractive in the case of the top quark: relatively light composite top partners allow to induce the required, large top Yukawa coupling. In order for the composite sector to contain partners for the top (and possibly the other SM quarks), one needs to introduce constituent fermions X^f that are charged under the colour group $SU(3)_c$. It is not possible to constitute a 'baryon' (a hypercolour invariant spin-1/2 bound state) if X^f transforms under the fundamental, pseudo-real representation of $Sp(2N)$. Following [259], we rather assume that X^f transforms under the two-index, real representation of $Sp(2N)$ that is antisymmetric, $X^f_{ij} = -X^f_{ji}$, and traceless, $X^f_{ij}\Omega_{ji} = 0$. This irreducible representation has dimension $(2N+1)(N-1)$. In order to embed a $SU(3)_c$ triplet-antitriplet pair, one has to introduce six such fermions, $f = 1, \ldots, 6$. Then, the theory acquires a flavour symmetry $SU(6) \supset SU(3)_c$, with $X^f \sim 6_{SU(6)} = (3 + \bar{3})_{SU(3)_c}$. The addition of such an X-sector modifies several results that we have derived for the ψ-sector in isolation, because the underlying $Sp(2N)$ dynamics connects the two sectors in a highly non-trivial way, as we now describe.

	Lorentz	$Sp(2N)$	$SU(6)$	$SO(6)$
X^f_{ij}	$(1/2, 0)$	$\square_{ij}$	6^f	6
$\overline{X}_{fij} \equiv \Omega_{ik} X^\dagger_{fkl} \Omega_{lj}$	$(0, 1/2)$	$\square_{ij}$	$\overline{6}_f$	6
$M_c^{fg} \sim (X^f X^g)$	$(0, 0)$	1	21^{fg}	$20' + 1$
$\overline{M}_{cfg} \sim (\overline{X}_f \overline{X}_g)$	$(0, 0)$	1	$\overline{21}_{fg}$	$20' + 1$
$a^\mu_X \sim (\overline{X}^f \overline{\sigma}^\mu X_f)$	$(1/2, 1/2)$	1	1	1
$(V^\mu_c, A^\mu_c)^g_f \sim (\overline{X}_f \overline{\sigma}^\mu X^g)$	$(1/2, 1/2)$	1	35^f_g	$15 + 20'$

Table 9.1: The transformation properties of the elementary fermions, the spin-0 and spin-1 fermion bilinears, in the colour sector of the model. Spinor indexes are understood, and brackets stand for a hypercolour-invariant contraction of the $Sp(2N)$ indexes.

Once both types of fermions ψ^a and X^f are in presence, the flavour symmetry group becomes $G = SU(4) \times SU(6) \times U(1)$, where $U(1)$ is the non-anomalous linear combination of the two axial symmetries $U(1)_\psi$ and $U(1)_X$, which separately are both anomalous with respect to $Sp(2N)$. The current corresponding to the $U(1)_\psi$ transformations and its divergence were already given in Eqs. (8.2.4) and (8.2.5), respectively. In the case of the $U(1)_X$ transformations, the corresponding expressions read [a sum over the flavour indices is understood, gauge and spinor indices are omitted]

$$\mathcal{J}^0_{X\mu} = \frac{1}{2}\left[\left(\overline{X}\overline{\sigma}_\mu X\right) - \left(X\sigma_\mu \overline{X}\right)\right] \ , \tag{9.1.1}$$

$$\partial^\mu \mathcal{J}^0_{X\mu} = 4\sqrt{3}\, m_X \mathcal{P}^0_X + 2(N-1)\, \frac{N^X_f g^2_{HC}}{32\pi^2} \sum_{I=1}^{N(2N+1)} \epsilon_{\mu\nu\rho\sigma} G^{I,\mu\nu}_{HC} G^{I,\rho\sigma}_{HC} \ , \tag{9.1.2}$$

where the factor $N^X_f = 3$ accounts for the number of flavours in the X-sector. In the above, $\overline{X}$, as defined in Table 9.1 below, transforms under the $Sp(2N)$ gauge group in the same way as X, and the gauge-invariant bilinear fermion contractions between X and X are defined as

$$(X^f X^g) \equiv X^f_{ij} \Omega_{jk} X^g_{kl} \Omega_{li} = \mathrm{tr}(X^f \Omega X^g \Omega) \ . \tag{9.1.3}$$

Contractions like $(\overline{X}_f\overline{X}_g)$ and $(\overline{X}_f X^g)$ are defined in the same way. For later use we have also introduced a flavour independent mass term for the X fermions,

$$\mathcal{L}_m^X = -2\sqrt{3}\, m_X \mathcal{S}_X^0 \ , \tag{9.1.4}$$

with

$$\mathcal{S}_X^0 = \frac{1}{2}\left[(\overline{X}T_X^0\Sigma_0^c\overline{X}) + (X\Sigma_0^c T_X^0 X)\right] \ , \qquad \mathcal{P}_X^0 = \frac{1}{2i}\left[(\overline{X}T_X^0\Sigma_0^c\overline{X}) - (X\Sigma_0^c T_X^0 X)\right] \ , \tag{9.1.5}$$

in agreement with the general definitions given in Eq. (8.1.6) and the normalisation adopted there for the singlet scalar and pseudoscalar densities, that is $T_X^0 = \mathbb{1}/(2\sqrt{3})$. Note that the singlet contraction of two fermions in the (anti-)fundamental of $SU(6)$ is realized through the matrix

$$\Sigma_0^c = \begin{pmatrix} 0 & \mathbb{1}_3 \\ \mathbb{1}_3 & 0 \end{pmatrix} \ , \tag{9.1.6}$$

that determines the $SU(6)/SO(6)$ vacuum direction. The two conditions in Eq. (8.1.2) are satisfied with $\Sigma_\epsilon = \Sigma_0^c$ and the $SU(6)$ generators T^F and $T^{\hat{F}}$ defined in appendix F.2.

Examining the respective $U(1)_\psi$ and $U(1)_X$ anomaly coefficients, it is easily seen that the combination of the two axial singlet currents given by

$$\mathcal{J}_\mu^0 = \ell(\square)\mathcal{J}_{X\mu}^0 - \frac{3}{2}\ell(\begin{smallmatrix}\square\\\square\end{smallmatrix})\mathcal{J}_{\psi\mu}^0 = \frac{3}{2}\ell(\begin{smallmatrix}\square\\\square\end{smallmatrix})\left(\psi^a\sigma_\mu\overline{\psi}_a\right) - \ell(\square)\left(X^f\sigma_\mu\overline{X}_f\right) \ , \tag{9.1.7}$$

is free from the gauge anomaly,

$$\partial^\mu\mathcal{J}_\mu^0 = 4\sqrt{3}\, m_X \mathcal{P}_X^0 \ , \tag{9.1.8}$$

where the Dynkin index $\ell(r)$ of the representation r of the gauge group $Sp(2N)$ gives the normalisation of the $Sp(2N)$ generators $T^I(r)$ in this representation,

$$\mathrm{tr}[T^I(r)T^J(r)] = \frac{1}{2}\ell(r)\delta^{IJ} \ , \qquad \ell(\square) = 1 \ , \qquad \ell(\begin{smallmatrix}\square\\\square\end{smallmatrix}) = 2(N-1) \ . \tag{9.1.9}$$

Consequently, the axial singlet transformation of *both* the ψ and X fermions, with charges satisfying

$$q_\psi = -3(N-1)q_X \ , \tag{9.1.10}$$

is a true symmetry of the theory, even at the quantum level, in the limit where m_X vanishes.

The introduction of fermions in the two-index antisymmetric representation of the $Sp(2N)$ gauge group has another consequence. The first coefficient of the β-function of the gauge coupling g_{HC} now reads

$$b_0 = \frac{11}{3}C_2(\mathrm{adj}) - \frac{4}{3}\sum_{i=\psi,X} N_f^i\ell(r_i) = \frac{2}{3}(11 - 4N_f^X)\left[N + 1 - 2\frac{4N_f^X - N_f^\psi}{4N_f^X - 11}\right] . \tag{9.1.11}$$

Therefore, as soon as $N_f^X \geq 3$, b_0 stays positive and asymptotic freedom is preserved (at one loop) only if the number of colours N is bounded from above,

$$N < 2\frac{4N_f^X - N_f^\psi}{4N_f^X - 11} - 1 \qquad [N_f^X \geq 3], \tag{9.1.12}$$

which, in the case at hand ($N_f^\psi = 2$ and $N_f^X = 3$), means $N \leq 18$. This upper bound prevents us from considering the limit $N \to \infty$ at the level of the fundamental hypercolour theory once the sector of X fermions has been introduced. Notice, however, that independently from the existence of this upper bound on N, the anomalous contribution on the left-hand side of Eq. (9.1.2) would not vanish in the 't Hooft limit $N \to \infty$, with Ng_{HC}^2 staying constant. Despite the absence of a well-defined large-N limit at the level of the fundamental theory, it remains useful to keep the naive counting in powers of $1/N$ at the level of the NJL description of the dynamics, since it allows, for instance, to identify contributions which will be numerically suppressed even for already moderate values of N. Therefore, when, in the sequel, we mention or use the $1/N$ expansion, it will thus always be understood that it refers to the NJL context.

9.1.1 The pattern of flavour symmetry breaking

Concerning the pattern of spontaneous symmetry breaking, there are now two possible fermion bilinears that may form a condensate. A non-zero $\langle \psi^a \psi^b \rangle$ would break $SU(4) \times U(1)$ to $Sp(4)$, with NGBs transforming as $(5+1)_{Sp(4)}$. A non-zero $\langle X^f X^g \rangle$ would break $SU(6) \times U(1)$ to $SO(6)$, with NGBs in the representation $(20'+1)_{SO(6)} = (8+6+\bar{6}+1)_{SU(3)_c}$. Light coloured scalars are phenomenologically problematic because of the strong bounds from collider searches. An important contribution to their mass is induced by gluon loops, as discussed in section 8.1.5, in appendix F.2, and section 9.2.2. Another possibility to lift the coloured NGBs from the low energy spectrum is to introduce the mass term (9.1.4), that breaks explicitly $SU(6) \times U(1)$ to $SO(6)$. Alternatively, if $SU(6)$ does not undergo spontaneous breaking, coloured NGBs would be absent. However, we will show below that the matching of anomalies would then require massless, coloured fermions, that again call for a large radiative mass or $m_X \neq 0$.

Since we have adopted the same fermion content as in [259], let us stress some differences with respect to the discussion of flavour symmetries in that analysis. First, the non-anomalous axial $U(1)$ symmetry was not discussed: we will show that it has several phenomenological consequences. Second, the colour triplet and antitriplet components of X^f were treated separately, and the global symmetry was identified with $SU(3) \times SU(3) \times U(1)_V$, broken by a mass term to $SU(3)_c \times U(1)_V$. However, these are just maximal subgroups of the complete global symmetry $SU(6)$, and of the complete unbroken subgroup $SO(6)$, respectively. The pattern is different from QCD, because there quarks and antiquarks transform under different representations of the gauge group, while here the six copies of X^f transform in the same way under $Sp(2N)$. Note that $U(1)_V$ was introduced in [259] in order to provide top partners with the appropriate SM hypercharge, but remarkably such a symmetry is automatically present, as one of the unbroken generators within $SO(6)$.

Once both the elementary fermions ψ^a and X^f are introduced, one can form several baryons. As a consequence, the anomaly matching condition provides non-trivial constraints on the spontaneous symmetry breaking, as discussed in section 8.1.2. If one denotes by V the conserved currents associated to the H_m generators, and by A the conserved currents associated to the generators of the coset G/H_m (see section 8.1.1), one needs only consider the anomaly matching constraints that arise from the $\langle VVA \rangle$ correlators. Then, to each fermion transforming in the representation r of G is associated an anomaly coefficient $A(r)$, which is defined by

$$2\mathrm{tr}(T^{\hat{A}}(r)\{T^B(r), T^C(r)\}) = A(r) d^{\hat{A}BC} \ , \tag{9.1.13}$$

where $T^A(r)$ and $T^{\hat{A}}(r)$ are the generators of H_m and of G/H_m, respectively, in the representation r, and $d^{\hat{A}BC}$ is an invariant tensor that depends on G. The generators of the fundamental representation r_0 are normalised as in Eq. (9.1.9), and its anomaly coefficient is fixed to $A(r_0) = 1$. The anomaly matching condition can be written as

$$\sum_i n_i A(r_i) = \sum_i n'_i A(r_i) \ , \tag{9.1.14}$$

where the left-hand (right-hand) sum runs over the representations of the constituent (composite) fermions, and n_i (n'_i) are their multiplicities. If this equality cannot be satisfied, then G necessarily undergoes spontaneous symmetry breaking.

In the model under investigation, the possible trilinear baryons consist of

$$\Psi^{abf} = (\psi^a \psi^b X^f) \ , \ \ \Psi^{ab}_f = (\psi^a \psi^b \overline{X}_f) \ , \ \ \Psi^{af}_b = (\psi^a \overline{\psi}_b X^f) \ , \ \ \Psi^{fgh} = (X^f X^g X^h) \ , \ \ \Psi^{fg}_h = (X^f X^g \overline{X}_h) \ , \tag{9.1.15}$$

plus their conjugates, where the brackets stand for a spin-1/2, hypercolour-singlet contraction (multiple, independent contractions of this kind may be possible). Each Ψ decomposes in several irreducible representations (r_4, r_6) of $SU(4) \times SU(6)$, each corresponding to an independent baryon state: for example $\Psi^{abf} \sim [(6,6) + (10,6)]$. In addition, exotic baryons are also possible, formed by a larger, odd number of constituent fermions.

Let us begin with the $SU(4)^3$ anomaly. As ψ lies in the fundamental representation of $SU(4)$, its anomaly coefficient is $A_4(4) = 1$. The $SU(4)$ representations contained in $\psi^a \psi^b$ or $\psi^a \overline{\psi}_b$ have

coefficients $A_4(1) = A_4(6) = A_4(15) = 0$ and $A_4(10) = 8$. Therefore, the anomaly matching between ψ and the trilinear baryons Ψ reads

$$2N \cdot A_4(4) = 2N = \sum_{(r_4,r_6)} n_{(r_4,r_6)} A_4(r_4) \cdot \dim(r_6) = n_{(10,6)} 6 \cdot 8 \ , \tag{9.1.16}$$

where the sum runs over the various massless baryon states, and $n_{(r_4,r_6)}$ is their multiplicity. One can generalise the result to include exotic baryons: in full generality, hypercolour invariance requires the total number of ψ and $\overline{\psi}$ fermions to be even, then, to obtain a fermion, one needs that the total number of X and $\overline{X}$ is odd. One can check [261] that (i) the anomaly coefficient of any $SU(4)$ representation, contained in $4 \times \cdots \times 4$ an even number of times, is a multiple of 8, and (ii) the dimension of any $SU(6)$ representation, contained in $6 \times \cdots \times 6$ an odd number of time, is a multiple of 2. As a consequence, the right-hand side of Eq. (9.1.16) generalises to a multiple of $2 \cdot 8$, and the matching is possible only for $N = 8n$, with n integer. An example with $N = 8$ is provided by one exotic baryon $(\psi\psi XXX) \sim (10, 20)$ plus three copies of $(\overline{\psi\psi}X) \sim (\overline{10}, 6)$. In summary, for $N \neq 8n$ $SU(4)$ necessarily spontaneously breaks to $Sp(4)$ and the corresponding NGB decay constant F_G is non-zero. Strictly speaking, the other order parameters, such as the condensate $\langle\psi\psi\rangle$, may still vanish, for instance if a discrete symmetry subgroup leaves the vacuum invariant but not the $(\psi\psi)$ operator [300]. This is, however, a rather unlikely situation to happen [301], and we will assume that the spontaneous symmetry breaking of the $SU(4)$ flavour group (towards its $Sp(4)$ subgroup) is due to the formation of a non-vanishing $\langle\psi\psi\rangle$ condensate. This corresponds actually to the dynamical situation described by the NJL framework, where $SU(4)$ order parameters like the condensate are proportional to F_G.

Next, let us consider the $SU(6)^3$ anomaly. The crucial observation is that there are baryons, contained either in $(\psi\overline{\psi}X)$ or $(XX\overline{X})$, that transform under the representation $(1, 6)$. These states have evidently the same anomaly coefficient $A_6(6) = 1$ as the constituent fermion X, therefore the matching is trivially possible for any value of N:

$$(2N + 1)(N - 1) \cdot A_6(6) = \sum_{(r_4,r_6)} n_{(r_4,r_6)} \dim(r_4) \cdot A_6(r_6) = n_{(1,6)} 1 \cdot A_6(6) + \dots \ , \tag{9.1.17}$$

where the ellipsis stands for the contribution of larger representations, that are not relevant in the present context. As a consequence, the spontaneous breaking of $SU(6)$ is not a necessity, and in particular one may have $\langle XX\rangle = 0$.

Note that the massless baryons required by anomaly matching carry colour and are phenomenologically excluded. Once these baryons are made heavy by explicit symmetry breaking, there are no exact NGBs either, and again one cannot tell whether the dynamics breaks spontaneously $SU(6)$ or not. Indeed, in either case an explicit symmetry breaking mass term $m_X XX$ is required for specular reasons: in the unbroken phase, one needs it to give a sufficiently large mass to the coloured baryons; in the broken phase, the mass term is necessary to make the coloured NGBs sufficiently heavy. Ref. [302] argues that the mass of the top partners can be controlled by the parameter m_X, if one assumes to be in the unbroken phase.

Finally, one should consider the anomalies involving the non-anomalous $U(1)$. The anomaly for $U(1)SU(6)^2$ is easily matched for any N, by the same set of baryons that matches the $SU(6)^3$ anomaly. We also proved that the other anomalies involving $U(1)$, that is $U(1)SU(4)^2$ and $U(1)^3$, can be matched for any N as well, but using a different set of baryons in each case. It is highly non-trivial to match all $U(1)$ anomalies at the same time, and thus preserve this symmetry from spontaneous breaking. As we have already argued though, it is quite unlikely that the spontaneous breaking of the $SU(4)$ flavour symmetry happens without, at the same time, also triggering the spontaneous breaking of the $U(1)$ symmetry.

In the following sections, we will apply the NJL techniques to the complete model including the electroweak and the colour sector. In particular, we will study the mass gap equations that determine $\langle\psi\psi\rangle$ and $\langle XX\rangle$ in terms of the coefficients of the four-fermion operators. For $N \neq 8n$, only the phase $\langle\psi\psi\rangle \neq 0$ of the NJL model should be considered as a good approximation of the full dynamics, while $\langle XX\rangle$ is not constrained by the matching of anomalies. For $N = 8n$, both condensates may or may not vanish.

9.1.2 Sum rules and pseudoscalar decay constants in the flavour-singlet sector

As a last point to be discussed in this section, let us recall that in section 8.1.4 we introduced the spectral sum rules for a simple group G that undergoes spontaneous breaking. That discussion applies to the ψ-sector alone, with coset $SU(4)/Sp(4)$, as well as to the X-sector in isolation, with coset $SU(6)/SO(6)$. In the complete model, one can also construct correlation functions involving simultaneously the two sectors and that are order parameters for the whole symmetry group $SU(4) \times SU(6) \times U(1)$, i.e. involving also the non-anomalous axial singlet transformations. This leads to additional sum rules that may constrain the resonance spectrum. At the level of two-point functions, the relevant order parameters involving the two sectors are:

$$\begin{aligned} \Pi^{\psi X}_{S^0}(q^2) &= i\int d^4x\, e^{iq\cdot x}\langle \mathrm{vac}|T\{\mathcal{S}^0_\psi(x)\mathcal{S}^0_X(0)\}|\mathrm{vac}\rangle \ , \\ \Pi^{\psi X}_{P^0}(q^2) &= i\int d^4x\, e^{iq\cdot x}\langle \mathrm{vac}|T\{\mathcal{P}^0_\psi(x)\mathcal{P}^0_X(0)\}|\mathrm{vac}\rangle \ . \end{aligned} \tag{9.1.18}$$

From them we derive two additional spectral sum rules, valid in the limit where m_X vanishes:

$$\int_0^\infty dt\ \mathrm{Im}\Pi^{\psi X}_{S_0}(t) = 0 \ , \qquad \int_0^\infty dt\ \mathrm{Im}\Pi^{\psi X}_{P_0}(t) = 0 \ , \tag{9.1.19}$$

which respectively constrain the spectrum of scalar and pseudo-scalar singlets resonances.

One could examine the realization of these sum rules in the NJL framework, similarly to what we did for the electroweak sector in section 8.2.7, for instance investigating whether the first low-lying resonances in each channel saturate them. Here we rather describe some of the expected features in general terms, independently from the NJL approximation. In the singlet pseudoscalar channel, we expect two states. The first one is the Goldstone boson η_0 produced by the spontaneous breaking of the non-anomalous axial $U(1)$ symmetry. The second one is a massive pseudoscalar state η', which corresponds to the second Goldstone boson that would be present in the absence of the gauge anomaly in the divergences of the $U(1)_\psi$ and $U(1)_X$ currents. These states both couple to the (partially) conserved $U(1)$ current, defined in Eq. (9.1.7) above,

$$\langle \mathrm{vac}|\mathcal{J}^0_\mu(0)|\eta_0(p)\rangle = iF_{\eta_0}p_\mu \ , \qquad \langle \mathrm{vac}|\mathcal{J}^0_\mu(0)|\eta'(p)\rangle = iF_{\eta'}p_\mu \ . \tag{9.1.20}$$

In the limit where m_X vanishes, F_{η_0} remains nonzero and $F_{\eta'} \sim \mathcal{O}(m_X)$, whereas for the masses $M^2_{\eta_0} \sim \mathcal{O}(m_X)$ while $M^2_{\eta'}$ does not vanish. Of course, there are also couplings to the individual, non conserved, $U(1)_\psi$ and $U(1)_X$ currents, defined in Eqs. (8.2.4) and (9.1.1), respectively

$$\begin{aligned} \langle \mathrm{vac}|\mathcal{J}^0_{\psi\mu}(0)|\eta_0(p)\rangle &= iF^\psi_{\eta_0}p_\mu \ , & \langle \mathrm{vac}|\mathcal{J}^0_{\psi\mu}(0)|\eta'(p)\rangle &= iF^\psi_{\eta'}p_\mu \ , \\ \langle \mathrm{vac}|\mathcal{J}^0_{X\mu}(0)|\eta_0(p)\rangle &= iF^X_{\eta_0}p_\mu \ , & \langle \mathrm{vac}|\mathcal{J}^0_{X\mu}(0)|\eta'(p)\rangle &= iF^X_{\eta'}p_\mu \ . \end{aligned} \tag{9.1.21}$$

According to the expressions given in Eqs. (8.2.4), (9.1.1), and (9.1.7), these four decay constants are related to the ones in the preceding equation through $F_{\eta_0,\eta'} = F^X_{\eta_0,\eta'} - 3(N-1)F^\psi_{\eta_0,\eta'}$. Both η_0 and η' states also couple to the singlet pseudoscalar densities,

$$\begin{aligned} \langle \mathrm{vac}|\mathcal{P}^0_\psi(0)|\eta_0(p)\rangle &= G^\psi_{\eta_0} \ , & \langle \mathrm{vac}|\mathcal{P}^0_\psi(0)|\eta'(p)\rangle &= G^\psi_{\eta'} \ , \\ \langle \mathrm{vac}|\mathcal{P}^0_X(0)|\eta_0(p)\rangle &= G^X_{\eta_0} \ , & \langle \mathrm{vac}|\mathcal{P}^0_X(0)|\eta'(p)\rangle &= G^X_{\eta'} \ , \end{aligned} \tag{9.1.22}$$

and through Eq. (9.1.8) the two following relations hold:

$$F_{\eta_0}M^2_{\eta_0} = 4\sqrt{3}\, m_X G^X_{\eta_0} \ , \qquad F_{\eta'}M^2_{\eta'} = 4\sqrt{3}\, m_X G^X_{\eta'} \ . \tag{9.1.23}$$

Although they do not lead to sum rules, it is both interesting and useful to consider two-point correlators involving the axial singlet current and the singlet pseudoscalar densities, defined in analogy to Eq. (8.1.15) for the non-singlet case,

$$\begin{aligned} \Pi^\psi_{A^0P^0}(q^2)q_\mu &= \int d^4x\, e^{iq\cdot x}\langle \mathrm{vac}|T\{\mathcal{J}^0_\mu(x)\mathcal{P}^0_\psi(0)\}|\mathrm{vac}\rangle \ , \\ \Pi^X_{A^0P^0}(q^2)q_\mu &= \int d^4x\, e^{iq\cdot x}\langle \mathrm{vac}|T\{\mathcal{J}^0_\mu(x)\mathcal{P}^0_X(0)\}|\mathrm{vac}\rangle \ . \end{aligned} \tag{9.1.24}$$

$\Pi^{\psi}_{A^0P^0}(q^2)$ are order parameters for $SU(4)\times U(1)$ and for $SU(6)\times U(1)$, respectively, and in the limit where the current $\mathcal{J}^0_\mu(x)$ is conserved they are both saturated by the massless η_0 pole, as in Eq. (8.1.16). In the presence of the mass m_X, this is no longer true, and the Ward identities give

$$q^2\Pi^{\psi}_{A^0P^0}(q^2) = 4\sqrt{3}m_X\Pi^{\psi X}_{P^0}(q^2) - 6(N-1)\langle\mathcal{S}^0_\psi\rangle\ , \quad q^2\Pi^{X}_{A^0P^0}(q^2) = 4\sqrt{3}m_X\Pi^{X}_{P^0}(q^2) + 2\langle\mathcal{S}^0_X\rangle\ . \tag{9.1.25}$$

These lead, in particular, to the constraints

$$4\sqrt{3}m_X\Pi^{\psi X}_{P^0}(0) = 6(N-1)\langle\mathcal{S}^0_\psi\rangle\ , \qquad 4\sqrt{3}m_X\Pi^{X}_{P^0}(0) = -2\langle\mathcal{S}^0_X\rangle\ , \tag{9.1.26}$$

as well as

$$F_{\eta_0}G^{\psi}_{\eta_0} = 6(N-1)\langle\mathcal{S}^0_\psi\rangle + \mathcal{O}(m_X)\ , \qquad F_{\eta_0}G^{X}_{\eta_0} = -2\langle\mathcal{S}^0_X\rangle + \mathcal{O}(m_X)\ , \tag{9.1.27}$$

which provide useful cross-checks for the NJL calculation.

9.1.3 Effective couplings induced by the hypercolour gauge anomaly

As we have just discussed, apart from the $SU(6)$ symmetry, there is also an additional, not required, $U(1)_X$ (classical) symmetry. In order to study the description of the $Sp(2N)$ hypercolour gauge anomaly at the level of the NJL framework, let us first discuss the X-sector in isolation. The sector of gauge configurations with unit winding number now induces $2(N-1)$ fermionic zero modes per flavour (in the present case, $N^X_f = 3$) for the Dirac operator corresponding to the X and $\overline{X}$ fermions (the uninteresting case $N = 1$ is, of course, discarded). Through the index theorem, these zero modes induce a violation of the $U(1)_X$ charge by $12(N-1)$ units, which, as already discussed in Section 8.2.1 for the colourless sector, has to be reproduced by the effective 't Hooft vertex. In the case of an $Sp(4)$ gauge group ($N = 2$), it is straightforward to construct an operator $\mathcal{O}_X$ that induces this violation of the invariance under $U(1)_X$, while at the same time preserving the invariance under the $SU(6)$ flavour group:

$$\mathcal{O}_X = -\frac{1}{6!}\epsilon_{f_1\cdots f_6}\epsilon_{g_1\cdots g_6}(X^{f_1}X^{g_1})\cdots(X^{f_6}X^{g_6}) = -\det(X^fX^g)\ , \tag{9.1.28}$$

where the determinant is taken in the six-dimensional flavour space. For $N > 2$ and only 6 Weyl fermions at our disposal, one obvious extension of the above operator satisfying the required properties would consist in taking $\mathcal{O}_X^{N-1}$. One should, however, be aware that, on the one hand, this simple procedure might not comply with the properties of the 't Hooft vertex as arising from the Grassmann integration over the fermionic collective coordinates[3], and, on the other hand, that the 't Hooft vertex could also involve derivatives of the fermion fields. An example where this second feature is known to happen is provided by the case of an $SU(2) \simeq Sp(2)$ gauge group with fermions in the adjoint representation [306]. Delving more deeply into these issues would, however, take us too far astray. Moreover, dealing with a term involving derivatives of the fermion fields is beyond the NJL framework as it is usually understood. From the point of view of the latter, the term $\mathcal{O}_X^{N-1}$, possessing all the required symmetry properties, is quite appropriate, and henceforth we will assume that at the level of the NJL approach, it provides the required description of the explicit breaking of the $U(1)_X$ symmetry by instantons.

The preceding discussion considered the $SU(6)$ sector in isolation and, apart from some subtle aspects due to the representation of the gauge group under which the X fermions transform, has essentially paralleled the related discussion for the $SU(4)$ sector in Section 8.2.1. We will now bring the two sectors together and, as was already the case for the discussion of the anomaly matching conditions in the preceding subsection, we will find that when acting together the two sectors unravel new features. Indeed, the structure of anomaly-driven effective terms is actually different, as one should take into account that a combination of $U(1)_X$ and $U(1)_\psi$ transformations, as given in Eq. (9.1.10), remains non-anomalous. This drastically changes the form of appropriate effective interactions generalising the 't Hooft terms usually being given by a (flavour) determinant, since ψ and X are not in the same

[3] Useful introductions to instantons are provided by Refs. [303–305]

representation. Combining this information with the discussion above and in Section 8.2.1, the lowest dimensional operator that breaks both $U(1)_\psi$ and $U(1)_X$ axial singlet symmetries, while preserving the $U(1)$ symmetry generated by the combination (9.1.7), reads

$$\mathcal{L}_{\psi X} = A_{\psi X} \frac{\mathcal{O}_\psi}{(2N)^2} \left[\frac{\mathcal{O}_X}{[(2N+1)(N-1)]^6} \right]^{(N-1)} + h.c. \ , \tag{9.1.29}$$

with $\mathcal{O}_X$ defined above and $\mathcal{O}_\psi$ the antisymmetric four-fermion second term in Eq. (8.2.1):

$$\mathcal{O}_\psi = -\frac{1}{4}\epsilon_{abcd}(\psi^a\psi^b)(\psi^c\psi^d) \ . \tag{9.1.30}$$

The constant $A_{\psi X}$ can be taken real and positive by adjusting the phase of ψ. Its normalisation in Eq. (9.1.29) has been conveniently chosen in order to compensate the different powers of N contained in the condensates, see Eqs. (8.2.19) and (9.2.4). This normalisation, with an N-independent coefficient $A_{\psi X}$, would reproduce the correct behaviour of the $U(1)_{\psi,X}$ anomaly in the large-N limit, would the latter exist, see the discussion around Eqs. (9.1.11) and (9.1.12). Indeed, Eq. (9.1.2) shows that the effect of the anomaly would not vanish in this limit, as $(N-1)g_{HC}^2 \sim (N-1)/N \sim 1$. As we will see in Section 9.2.5, a trace of this feature appears in the mass of the η', which is proportional to $A_{\psi X}$, $M_{\eta'}^2 \sim A_{\psi X}[1+\mathcal{O}(1/N)]$.

After formation of the two condensates $\langle\psi\psi\rangle$ and $\langle XX\rangle$, the interaction (9.1.29) will generate effective four-fermion interaction for ψ, and X, as well as a mixed $\psi\psi XX$ term, upon replacing appropriate number of fermion bilinears by their respective condensate (i.e. closing the loops). To identify these four-fermion interactions, relevant for the computation of the meson spectrum, let us first consider for simplicity the $SU(6) \to SO(6)$ sector. The fermion bilinear can be decomposed as

$$(X^f X^g) \equiv 2(T_X^0\Sigma_0^c)^{gf}\left(X\Sigma_0^c T_X^0 X\right) + 2(T^{\hat{F}}\Sigma_0^c)^{gf}\left(X\Sigma_0^c T^{\hat{F}} X\right) \ , \tag{9.1.31}$$

in terms of the $SO(6)$ singlet and the two-index symmetric traceless components. Then, taking into account combinatorial factors, the operator of Eq. (9.1.28) can be decomposed as [4]

$$\mathcal{O}_X = \frac{1}{27}\left[(X\Sigma_0^c T_X^0 X)^6 - 3(X\Sigma_0^c T_X^0 X)^4 (X\Sigma_0^c T^{\hat{F}} X)(X\Sigma_0^c T^{\hat{F}} X) + \cdots\right] \ , \tag{9.1.32}$$

where a sum over the $SU(6)$ generators $T^{\hat{F}}$ belonging to the $SU(6)/SO(6)$ coset is understood. For the $SU(4) \to Sp(4)$ sector, the similar appropriate decomposition into $Sp(4)$ invariant bilinears reads

$$\mathcal{O}_\psi = \left(\psi\Sigma_0 T_\psi^0\psi\right)\left(\psi\Sigma_0 T_\psi^0\psi\right) - \left(\psi\Sigma_0 T^{\hat{A}}\psi\right)\left(\psi\Sigma_0 T^{\hat{A}}\psi\right) \ . \tag{9.1.33}$$

Next we insert the results (9.1.32) and (9.1.33) into the full effective Lagrangian Eq. (9.1.29), and obtain

$$\begin{aligned}\mathcal{L}_{\psi X} =& \frac{A_{\psi X}}{(27)^{N-1}}\Bigg[\left(\frac{\psi\Sigma_0 T_\psi^0\psi}{(2N)}\right)^2\left(\frac{X\Sigma_0^c T_X^0 X}{(2N+1)(N-1)}\right)^{6(N-1)} - \left(\frac{\psi\Sigma_0 T^{\hat{A}}\psi}{(2N)}\right)^2\left(\frac{X\Sigma_0^c T_X^0 X}{(2N+1)(N-1)}\right)^{6(N-1)} \\ & -3(N-1)\left(\frac{\psi\Sigma_0 T_\psi^0\psi}{(2N)}\right)^2\left(\frac{X\Sigma_0^c T_X^0 X}{(2N+1)(N-1)}\right)^{6(N-1)-2}\left(\frac{X\Sigma_0^c T^{\hat{F}} X}{(2N+1)(N-1)}\right)^2\Bigg] + \cdots \ ,\end{aligned} \tag{9.1.34}$$

where the ellipsis denotes other interaction terms, of no relevance for our purposes. The overall constant $A_{\psi X}$ in (9.1.34) remains arbitrary for the moment, but the ratios of the coefficients of the three effective $XXXX$, $\psi\psi\psi\psi$, and $\psi\psi XX$ terms that will matter are fixed. All effective couplings in the singlet and non-singlet sectors are thus related to the unique coupling $A_{\psi X}$ in Eq. (9.1.29), times appropriate powers of the two condensates and combinatoric factors (see section 9.2.1 below).

[4] The coefficient of $\left(X\Sigma_0^c T_X^0 X\right)^6$ in $\det(X^f X^g)$ is $2^6\det(\Sigma_0^c T_X^0) = -1/27$, and the coefficient of $\left(X\Sigma_0^c T_X^0 X\right)^4\left(X\Sigma_0^c T^{\hat{F}} X\right)\left(X\Sigma_0^c T^{\hat{G}} X\right)$ is $2^6\det(\Sigma_0^c T_X^0)(2\sqrt{3})^2\frac{1}{2}\left[\mathrm{tr}(T^{\hat{F}})\mathrm{tr}(T^{\hat{G}}) - \mathrm{tr}(T^{\hat{F}}T^{\hat{G}})\right] = \frac{1}{9}\delta^{\hat{F}\hat{G}}$.

9.2 Spectrum of meson resonances in presence of the coloured sector

In this section we will compute the condensates and the masses of mesons, once the coloured sector is added to the electroweak sector, including their mixing through Eq. (9.1.34). The two sectors share the same $Sp(2N)$ hypercolour gauge interaction, therefore one can, in principle, relate the sizes of the effective four-fermion operators in the two sectors. One may assume, in particular, that the effective interactions between hypercolour-singlet fermion bilinears originate from $Sp(2N)$ current-current operators (see appendix I). In this approximation one can link, to some extent, the couplings of the coloured operators to the electroweak ones. In this way the mass gap and the spectrum in the $SU(6)$ sector are connected to the ones in the $SU(4)$ sector.

9.2.1 The mass gap in a theory with two sectors

Let us begin by the coloured scalar operators, that are relevant for the mass gap and for the spin-zero mesons. Besides the anomalous operator (9.1.34), there is one more independent four-fermion operator that describes the dynamics in analogy with the electroweak sector Lagrangian in Eq. (8.2.1),

$$\mathcal{L}^X_{scal} = \frac{\kappa_{A6}}{(2N+1)(N-1)}(X^f X^g)(\overline{X}_f \overline{X}_g) - \frac{1}{2} m_X \left[(X\Sigma_0^c X) + (\overline{X}\Sigma_0^c \overline{X})\right] \ , \tag{9.2.1}$$

where the coupling constant κ_{A6} is real and its normalisation by an inverse factor $(2N+1)(N-1)$ has been conveniently chosen to compensate the trace over hypercolour in the X-fermion one-loop two-point functions (see appendix H). In contrast with the electroweak sector, we also include in Eq. (9.2.1) an explicit symmetry-breaking mass m_X, already introduced in Eq. (9.1.4), which can be chosen real and positive by tuning the phase of X. Note that also $A_{\psi X}$ in Eq. (9.1.34) can be chosen real and positive, by tuning the phase of ψ. Such a mass term may be phenomenologically necessary to raise the masses of the coloured pNGBs, in order to comply with direct collider detection limits [260]. More generally, a non-zero m_X leads to several qualitative effects that are worth to be explored. As the contraction over $Sp(2N)$ indices in Eq. (9.1.3) is symmetric in hypercolour space, the scalar bilinear $(X^f X^g)$ must be symmetric in flavour space, that is, it transforms as the 21_s representation of $SU(6)$, to be compared with $(\psi^a \psi^b)$, which transforms as the 6_a of $SU(4)$. Since $21_{SU(6)} = (1+20)_{SO(6)}$, one can rewrite the Lagrangian (9.2.1) in the physical basis, as

$$\begin{aligned} \mathcal{L}^X_{scal} \ &= \ \frac{2\kappa_{A6}}{(2N+1)(N-1)} \left[(X\Sigma_0^c T^0_X X)(\overline{X} T^0_X \Sigma_0^c \overline{X}) + (X\Sigma_0^c T^{\hat{F}} X)(\overline{X} T^{\hat{F}} \Sigma_0^c \overline{X})\right] \\ &\quad -\frac{1}{2} m_X \left[(X\Sigma_0^c X) + (\overline{X}\Sigma_0^c \overline{X})\right], \end{aligned} \tag{9.2.2}$$

where $T^{\hat{F}}$ are the 20 broken generators spanning the $SU(6)/SO(6)$ coset.

Combining the effect of the operators in Eqs. (8.2.14), (9.1.34) and (9.2.2), one can derive a system of two coupled gap equations for the $SU(4)$ and $SU(6)$ sectors,

$$\begin{cases} 1 - 4(\kappa_A + \kappa_B)\tilde{A}_0(M_\psi^2) = 0 \ , \\ 1 - 4(\kappa_{A6} + \kappa_{B6})\tilde{A}_0(M_X^2) - \dfrac{m_X}{M_X} = 0, \end{cases} \tag{9.2.3}$$

which determine the dynamical masses M_ψ and M_X as functions of the four couplings $\kappa_{A,B,A6,B6}$ and of the mass m_X. More precisely, when $m_X \neq 0$ the scale M_X is not entirely generated by the dynamics, see Fig. 9.3. Just like in the electroweak sector M_ψ can be traded for $\langle \Psi\Psi \rangle$, see Eq. (8.2.19), the NJL dynamical mass M_X is also related to the condensate $\langle XX \rangle$ in the coloured sector,

$$\langle XX \rangle \equiv \frac{1}{\sqrt{N_f^X}} \langle S_0^X \rangle = -2(2N+1)(N-1) M_X \tilde{A}_0(M_X^2), \tag{9.2.4}$$

where the factor $(2N+1)(N-1)$ comes from the trace over hypercolour. The two mass gap equations are coupled because the first operator in Eq. (9.1.34) induces both the κ_B and κ_{B6} terms in Eq. (9.2.3).

These contributions are obtained by closing all but one fermion bilinears into a tadpole loop, as illustrated in Fig. 9.1 for the case of the ψ-sector. This amounts to replacing each bilinear by the associated condensate, and to add a combinatorial factor 2 in κ_B, as one ψ-bilinear out of 2 is not closed, and $6(N-1)$ in κ_{B6}, as one X-bilinear out of $6(N-1)$ is not closed. Therefore, the anomalous terms in the gap equations are related to the original anomaly coefficient $A_{\psi X}$ by

$$\kappa_B \equiv \frac{A_{\psi X}}{2\cdot 27^{N-1}}\left[\frac{4N_f^X\langle XX\rangle^2}{(2N+1)^2(N-1)^2}\right]^{3(N-1)}\frac{2}{2N} = [4M_X\tilde{A}_0(M_X^2)]^{6(N-1)}\,\frac{A_{\psi X}}{2N}\,, \tag{9.2.5}$$

$$\begin{aligned}\kappa_{B6} &\equiv \frac{A_{\psi X}}{2\cdot 27^{N-1}}\left[\frac{4N_f^\psi\langle\psi\psi\rangle^2}{(2N)^2}\right]\left[\frac{4N_f^X\langle XX\rangle^2}{(2N+1)^2(N-1)^2}\right]^{3(N-1)-1}\frac{6(N-1)}{(2N+1)(N-1)}\\ &= \frac{4N}{2N+1}\frac{M_\psi^2}{M_X^2}\frac{\tilde{A}_0^2(M_\psi^2)}{\tilde{A}_0^2(M_X^2)}\,\kappa_B\,.\end{aligned} \tag{9.2.6}$$

The combinatorial factors will be essential, among other things, to recover the singlet Goldstone boson, see section 9.2.5. The effective couplings $\kappa_{B,B6}$ are normalised such as to contribute to the gap equations (9.2.3) as for a single sector in isolation. However, since they are functions of both dynamical masses, $\kappa_{B,B6} = \kappa_{B,B6}(M_\psi^2, M_X^2)$, the two gap equations are actually coupled in a non trivial way.

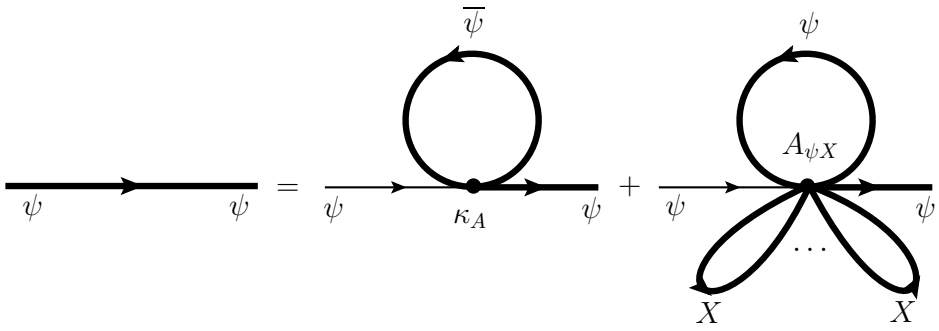

Figure 9.1: Graphical illustration of the mass-gap equation in the ψ sector. The convention for the propagator lines are the same as in Fig. 8.1. The first term, proportional to κ_A, remains the same as in the electroweak sector in isolation. The second term, proportional to $A_{\psi X}$, is obtained by closing one loop of ψ-fermions and $6(N-1)$ loops of X-fermions in Eq. (9.1.34). The mass-gap equation in the X-sector is obtained in an analogous way, with an additional term proportional to the explicit fermion mass m_X.

Let us analyse in some detail the system (9.2.3) of two coupled gap equations, because it is qualitatively different from the canonical NJL gap equation of QCD, and, to the best of our knowledge, it was not studied in the previous literature. It is convenient to take the effective coupling κ_B as the free parameter characterising the effect of the hypercolour anomaly, that is, to express κ_{B6} as a function of κ_B according to Eq. (9.2.6). This choice makes it easier to compare with the electroweak sector in isolation, and it also simplifies the algebraic form of the solutions of Eq. (9.2.3). As we have seen in section 8.2.1, the $SU(4)$ sector forms a condensate and a non-zero dynamical mass M_ψ is generated when $\xi \equiv (\kappa_A+\kappa_B)\Lambda^2/(4\pi^2)$ is above the critical value $\xi = 1$. Similarly, in the chiral limit $m_X = 0$, a non-zero dynamical mass M_X is generated when $\xi_c \equiv (\kappa_{A6}+\kappa_{B6})\Lambda^2/(4\pi^2) > 1$. Beyond that, the general resolution of the set of equations (9.2.3) coupled through Eq. (9.2.6) is very involved, especially for $m_X \neq 0$, and they can only be solved numerically. Still, it is instructive to consider a few special cases.

Case $m_X = 0$, $\kappa_B = 0$

When $\kappa_B = 0$, i.e. $A_{\psi X} = 0$, the two gap equations decouple. It is convenient to introduce dimensionless variables and functions in order to rewrite them in the form

$$\begin{cases} 1 - \xi_A \bar{A}(x_\psi) = 0 \ , \\ 1 - \xi_{A6} \bar{A}(x_X) = 0 \ , \end{cases} \tag{9.2.7}$$

where $x_{\psi,X} \equiv M^2_{\psi,X}/\Lambda^2$, $\xi_{A,A6} \equiv (\Lambda^2/4\pi^2)\kappa_{A,A6}$, and $\bar{A}(x) \equiv 1 - x\ln(1+1/x)$. The solutions of the two equations in (9.2.7) are simply related as

$$x_\psi(\xi_A) = x_X\,(\xi_{A6}) \ . \tag{9.2.8}$$

The result is to restrict the range of the allowed values of $\xi|_{\kappa_B=0} = \xi_A$, as compared to the case of one sector in isolation. Indeed, imposing that both conditions $0 \leq x_\psi(\xi_A) \leq 1$ and $0 \leq x_X(\xi_{A6}) \leq 1$ be satisfied simultaneously requires

$$\max\left(1, \frac{\kappa_A}{\kappa_{A6}}\right) \leq \xi \leq \min\left(1, \frac{\kappa_A}{\kappa_{A6}}\right) \frac{1}{1-\ln 2} \qquad (\kappa_B = 0) \ . \tag{9.2.9}$$

Hence, for $\kappa_A/\kappa_{A6} > 1$ the minimal value of ξ is larger than unity, whereas for $\kappa_A/\kappa_{A6} < 1$, the highest value allowed for ξ is reduced, see Fig. 9.3. These considerations do not depend explicitly on the value of N, although the actual values of κ_A and of κ_{A6}, being determined by the hypercolour dynamics, will depend on N.

Thus, although the two gap equations are decoupled, the presence of the second one impinges on the possible values allowed for the coupling of the second one, and vice-versa. This simply illustrates the fact that while the two gap equations may be decoupled, they nevertheless share the same effective-theory cutoff Λ.

Case $m_X = 0$, $\kappa_B \neq 0$

By treating κ_B as an extra free parameter, the first equation in the system (9.2.3) is formally identical to the gap equation for the electroweak sector in isolation, Eq. (8.2.17), with solution $x_\psi = x_\psi(\xi)$. Then, rewriting κ_{B6} as a function of κ_B according to Eq. (9.2.6), the second gap equation becomes a self-consistent relation for x_X, that depends on N, ξ, ξ_{A6}, and $\xi_B \equiv (\Lambda^2/4\pi^2)\kappa_B$:

$$\begin{cases} 1 - \xi \bar{A}(x_\psi) = 0 \ , \\ \mathcal{G}(x_X, \xi_{A6}) \equiv x_X \bar{A}(x_X)\left[1 - \xi_{A6}\bar{A}(x_X)\right] = \dfrac{4N}{2N+1}\xi_B \dfrac{x_\psi(\xi)}{\xi^2} \ . \end{cases} \tag{9.2.10}$$

Note that the second equality assumes a consistent solution of the first equation, $x_\psi(\xi)$, which requires $1 < \xi < 1/(1-\ln 2)$. In practice we solve numerically the first equation for $x_\psi(\xi)$, then we use it as an input to solve numerically the second one for $x_X(\xi)$.

In Fig. 9.2 we plot $\mathcal{G}(x, \xi_{A6})$ as a function of x, for a few representative values of ξ_{A6}, as well as the right-hand side of the second equation in (9.2.10), for two values of N and ξ_B, assuming for simplicity two equal mass gaps, $x_\psi = x_X = x$. The intersection between the dashed and solid curves determines the solution $x_X = x_X(N, \xi, \xi_{A6}, \xi_B)$. The function $\mathcal{G}(x, \xi_{A6})$ vanishes at $x = 0$ and, for any fixed value $0 < x < 1$, it decreases with ξ_{A6}. For $\xi_{A6} \leq 1$, $\mathcal{G}(x, \xi_{A6})$ increases in the whole interval $0 \leq x \leq 1$, while for $\xi_{A6} > 1$ it decreases to negative values for small x, then increases as x moves towards unity, becoming positive before $x = 1$, as long as $\xi_{A6} < 1/(1-\ln 2)$. On the other hand, the function $x_\psi(\xi)/\xi^2$ satisfies $0 \leq x_\psi(\xi)/\xi^2 \lesssim 1/10$ for $0 \leq x \leq 1$. Since $\xi_B \geq 0$, there is therefore no solution to the second equation in (9.2.10) in the interval $0 \leq x_X \leq 1$ when $\xi_{A6} \geq 1/(1-\ln 2)$. In contrast, for values $1 < \xi_{A6} < 1/(1-\ln 2)$ there is always a non-trivial solution with $x_X < 1$, as long as the right-hand side of the second equation in (9.2.10) is sufficiently small. Finally, for $0 < \xi_{A6} < 1$ the occurrence of a solution happens only for a sufficiently large ξ_B, also depending on N. The latter properties actually reflect the critical value $\xi_{A6} + \xi_{B6} > 1$, necessary in order to obtain a non-trivial

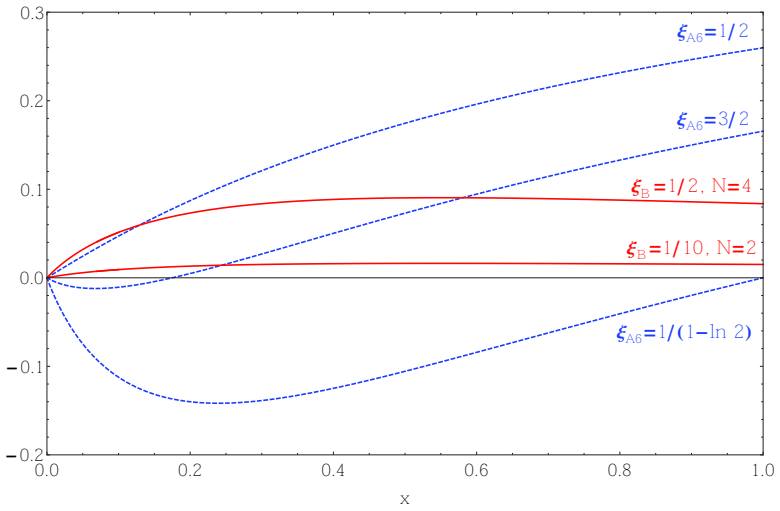

Figure 9.2: Dotted curves: the function $\mathcal{G}(x, \xi_{A6})$ for three representative values of ξ_{A6} as indicated. Thick curves: right-hand side of the second equation in (9.2.10) for two values of N and ξ_B as indicated, and taking $x_\psi = x$.

mass-gap, here somewhat disguised by the change of variables. Note that for fixed values of N, ξ and ξ_B, the value of x_X increases with ξ_{A6}.

One can make one more step in the analytical study of the two coupled gap equations. Moving the term proportional to ξ_B in the first equation of (9.2.10) to its right-hand side, one may now eliminate ξ_B between the two equations, and obtain

$$\mathcal{G}(x_\psi, \xi_A) = \left(\frac{1}{2} + \frac{1}{4N}\right) \mathcal{G}(x_X, \xi_{A6}) \ . \tag{9.2.11}$$

A few simple remarks follow from this relation. First, if one of the masses, say M_X, has been determined as a function of ξ_A, ξ_{A6} and ξ_B, then the relation of M_ψ to M_X involves only ξ_A, ξ_{A6} and N, and not ξ_B. Second, this relation becomes rapidly independent of N as N increases. Third, the relatively simple Eq. (9.2.11) precisely gives the exact dependence of the ratio of the two mass gaps, M_X/M_ψ, as functions of the basic input parameters (although it is an implicit relation, due to the non-linearity in the masses M_X, M_ψ), as illustrated for a few representative case in Fig. 9.3. More precisely, Eq. (9.2.11) may be trivially expressed as

$$\frac{M_\psi^2}{M_X^2} = \left(\frac{1}{2} + \frac{1}{4N}\right) \frac{\bar{A}^2(x_X)[1 - \xi_{A6}\bar{A}(x_X)]}{\bar{A}^2(x_\psi)[1 - \xi_A \bar{A}(x_\psi)]} \ . \tag{9.2.12}$$

This indeed shows that, as long as $M_\psi^2, M_X^2 \ll \Lambda^2$ [which implies $\bar{A}(x_X) \simeq \bar{A}(x_\psi)$ since $\bar{A}(x) \equiv 1 - x\ln(1+1/x) \simeq 1 + M^2/\Lambda^2 \ln(\Lambda^2/M^2)$], one obtains $M_\psi < M_X$, at least for $\xi_A \simeq \xi_{A6}$. Indeed, the peculiar case of equal mass gaps, $x_\psi = x_X$, that is the one illustrated in Fig. 9.2, can only be obtained for significantly different values of ξ_A and ξ_{A6} (for instance when $N = 4$, $\xi_{A6} = 1/2$ and $\xi_B = 1/2$, one has $x_\psi = x_X \simeq 0.13$, that corresponds to $\xi_A \simeq 0.9$).

In the above considerations we have kept κ_A and κ_{A6} (equivalently, ξ_A and ξ_{A6}) arbitrary. Let us now examine more precisely a few typical situations concerning those parameters. When κ_{A6} is larger than κ_A, the $SU(6)$ sector first forms a condensate for $\xi < 1$ (see Fig. 9.3), and then $M_X > M_\psi$. In the opposite case where κ_{A6} is smaller than κ_A, the $SU(6)$ sector forms a condensate for a value $\xi > 1$, and $M_X < M_\psi$. If $\xi_{A6} \gg \xi_A$, the mass gap grows rather fast, so that one eventually obtains a very large $M_X \sim \Lambda$, and conversely a very large M_ψ if $\xi_{A6} \ll \xi_A$. Thus to obtain predictive calculations in both sectors from the NJL model, it requires that $\xi_A \sim \xi_{A6}$ are roughly of the same magnitude. In this way, there is a non-zero interval for the values of ξ where the NJL predictions can be trusted ($\xi, \xi_c > 1$ and $M_{\psi,X} < \Lambda$) in both sectors. Note that apart from these NJL consistency considerations,

in principle no value of the ratio ξ_A/ξ_{A6} is theoretically excluded, but the case $M_\psi = 0$ and $M_X \neq 0$ evidently does not describe a composite Higgs model since then the spectrum of resonances does not contain a pNGB Higgs doublet. For $\xi_A = \xi_{A6}$, i.e. $\kappa_A = \kappa_{A6}$, and still for $m_X = 0$, the ratio M_X/M_ψ thus depends only of the value of κ_B and N, as given precisely by the relation in Eq. (9.2.12). When ξ_B is close to zero, one gets $M_\psi \simeq M_X$, since the two gap equations are almost decoupled. Next, when ξ_B increases, there is a complicated balance between the N, M_ψ and M_X dependence in Eq. (9.2.6), to determine κ_{B6}/κ_B, but the ratio M_X/M_ψ is consistently determined from the relatively simple relation in Eq. (9.2.12). This implies $\kappa_{B6} > \kappa_B$ and M_X slightly above M_ψ, with a M_X/M_ψ ratio that increases rather slowly with ξ_B, and is also a slowly increasing function of N. For instance for $N = 2$, $M_X/M_\psi \simeq 1.14 - 1.21$ for $\kappa_B/\kappa_A = 0.01 - 0.5$.

Finally, let us briefly discuss the most general case $m_X \neq 0$. The above considerations give of course only approximate relations, which however remains relatively good as long as m_X remains moderate, $m_X \ll M_X$. For $m_X \neq 0$ there is no critical coupling ξ_c in the $SU(6)$ sector, as the minimal value of M_X is obviously non-zero, being equal to m_X. A non-zero m_X evidently leads to $M_X > M_\psi$ for equivalent coupling values in the two sectors, see Fig. 9.3.

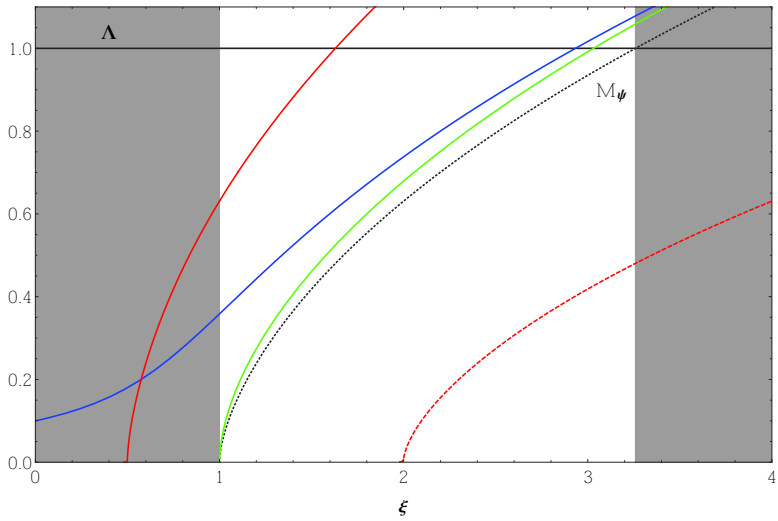

Figure 9.3: Comparison between the mass gap M_ψ of the EW sector (black dotted line) and the mass gap M_X of the coloured sector for few representatives cases. When $\kappa_{A6} = \kappa_A$, $m_X = 0$ and $\kappa_B/\kappa_A = 0$, the two dynamical masses are equal, $M_\psi = M_X$. To illustrate the behaviour of M_X with respect to the free parameters of the theory (ξ, κ_B/κ_A, κ_{A6}/κ_A, m_X and N) we illustrate small departures from this particular case. The solid (dashed) red line corresponds to $\kappa_{A6} = 2(1/2)\kappa_A$ with $\kappa_B/\kappa_A = 0$, $m_X = 0$ and $N = 4$. In these cases, the critical coupling of the coloured sector ($\xi_c = 1$) is respectively smaller or larger than the one in the EW sector ($\xi = 1$). Next, the solid blue (green) line corresponds to $\kappa_{A6} = \kappa_A$, $N = 4$ with $\kappa_B/\kappa_A = 0$ ($\kappa_B/\kappa_A = 0.1$) and $m_X = \Lambda/10$ ($m_X = 0$). In the case where there is an explicit breaking mass m_X, there is no critical coupling in the coloured sector as the lowest value of M_X is simply m_X. Finally note that M_X is almost independent of the number of hypercolour N.

A couple of remarks are in order. In section 9.2.5 we will see that the scalar singlet sector is consistent only for a very small value of κ_B/κ_A, see Eqs. (9.2.31) and (9.2.40). This is due to the requirement of vacuum stability, that is not apparent in the mass-gap equations (9.2.3). For example, this upper bound implies that a value $\xi_B = 1/2$, as illustrated in Fig. 9.2, is actually not possible. This in turns sets a lower bound on ξ_{A6}, in order to stay above the critical value, $\xi_{A6} + \xi_{B6} > 1$, and to obtain a non-zero value of M_X. Let us now comment on the dynamical relation between κ_B and the original anomalous parameter $A_{\psi X}$, given in Eq. (9.2.5), that involves M_X and N. In the whole allowed range $1 < \xi < (1 - \ln 2)^{-1} \simeq 3.25$, even when $M_X \simeq \Lambda$ for large ξ, the factor in square brackets in Eq. (9.2.5) is small in Λ^3 units, essentially because of the loop-suppression, $4M_X \tilde{A}_0(M_X^2) \simeq (4-8)\cdot 10^{-3}\Lambda^3$ (with moderate dependence on κ_B/κ_A and N). This implies a strong

suppression of the effective coupling ξ_B due to the large power $6(N-1)$ in Eq. (9.2.5), even for the minimal value $N=2$. Unfortunately, the original Lagrangian parameter $A_{\psi X}$ originates from non-perturbative dynamics that is not under control at the present stage, therefore its size is essentially arbitrary, see also the discussion in subsection 9.1.3 after Eq. (9.1.28). Therefore, we can just remark that, whatever the actual size of $A_{\psi X}$, the corresponding value of κ_B is strongly suppressed by the dynamics. This may help to comply with the upper bound from vacuum stability on κ_B/κ_A, that behaves as $1/N$ for sufficiently large N, as we shall discuss in section 9.2.5, because the effective coupling κ_B in Eq. (9.2.5) contains a power-N suppression factor.

9.2.2 Masses of coloured scalar resonances

The scalar and pseudoscalar resonances associated to X-fermion bilinears transform under the flavour symmetry as $21_{SU(6)} = (1+20)_{SO(6)}$. In analogy with the ψ-fermion sector, we can define a matrix $\overline{M}_c$ in flavour space,

$$\overline{M}_c = \frac{1}{2} M_X \Sigma_0^c + (\sigma_X + i\eta_X)\, \Sigma_0^c T_X^0 + \left(S_c^{\hat{F}} + i G_c^{\hat{F}}\right) \Sigma_0^c T^{\hat{F}} \ , \tag{9.2.13}$$

where the components σ_X (η_X) and $S_c^{\hat{F}}$ ($G_c^{\hat{F}}$) are respectively the $SO(6)$-singlet and twenty-plet (pseudo)scalars. The relevant operators for the computation of the spin-zero meson masses are those given in Eq. (9.2.2), plus the effective four-fermions operators ψ^4, X^4 and $\psi^2 X^2$, that are induced by the anomalous Lagrangian of Eq. (9.1.34), after spontaneous symmetry breaking,

$$\begin{aligned}
\mathcal{L}_{\psi X}^{eff} &= \frac{\kappa_B}{2N}\left[\left(\psi\Sigma_0 T_\psi^0 \psi\right)\left(\psi\Sigma_0 T_\psi^0 \psi\right) - \left(\psi\Sigma_0 T^{\hat{A}}\psi\right)\left(\psi\Sigma_0 T^{\hat{A}}\psi\right) + h.c.\right] \\
&+ \frac{\kappa_{B6}}{(2N+1)(N-1)}\left[(6N-7)\left(X\Sigma_0^c T_X^0 X\right)\left(X\Sigma_0^c T_X^0 X\right) - \left(X\Sigma_0^c T^{\hat{F}} X\right)\left(X\Sigma_0^c T^{\hat{F}} X\right) + h.c.\right] \\
&+ \frac{\kappa_{\psi X}}{2N}\left[\left(\psi\Sigma_0 T_\psi^0\psi\right)\left(X\Sigma_0^c T_X^0 X\right) + h.c.\right] \ ,
\end{aligned} \tag{9.2.14}$$

where κ_B and κ_{B6}, defined in Eq. (9.2.5) and (9.2.6) respectively, are the same couplings that appear in the gap equations. Note the factor $(6N-7)$ that multiples κ_{B6}, because here two X-fermion bilinears out of $6(N-1)$ are not closed into a loop, which implies a combinatorial factor $6(N-1)[6(N-1)-1]/2$. The additional coupling $\kappa_{\psi X}$ is defined by

$$\begin{aligned}
\kappa_{\psi X} &\equiv \frac{A_{\psi X}}{27^{N-1}}\left[\frac{4N_f^\psi \langle\psi\psi\rangle^2}{(2N)^2}\right]^{\frac{1}{2}}\left[\frac{4N_f^X\langle XX\rangle^2}{(2N+1)^2(N-1)^2}\right]^{3(N-1)-\frac{1}{2}}\frac{2\cdot 6(N-1)}{(2N+1)(N-1)} \\
&= \frac{8\sqrt{6}N}{2N+1}\frac{M_\psi}{M_X}\frac{\tilde{A}_0(M_\psi^2)}{\tilde{A}_0(M_X^2)}\,\kappa_B \ ,
\end{aligned} \tag{9.2.15}$$

and it controls the mixing between the $Sp(4)$ and $SO(6)$ (pseudo)scalar singlets σ_ψ (η_ψ) and σ_X (η_X), which will be treated separately in section 9.2.5. Note that all three effective couplings vanish if $\langle XX\rangle = 0$. When $\langle XX\rangle \neq 0$ both κ_{B6} and $\kappa_{\psi X}$ are fully determined as a function of M_ψ, M_X and κ_B. From Eqs. (9.2.2) and (9.2.14) one can derive the four-fermion couplings for each physical channel,

$$K_{\sigma_X(\eta_X)} = 2\frac{[\kappa_{A6} \pm (6N-7)\,\kappa_{B6}]}{(2N+1)(N-1)} \ , \qquad K_{S_c(G_c)} = 2\frac{[\kappa_{A6} \mp \kappa_{B6}]}{(2N+1)(N-1)} \ , \tag{9.2.16}$$

For convenience, all the relevant four-fermion couplings for the X-sector spin-zero and spin-one mesons are collected in Table 9.2, together with the associated one-loop two-point functions.

We now calculate the masses of the scalar and pseudo-scalar non-singlet resonances $S_c^{\hat{F}}$ and $G_c^{\hat{F}}$. As already mentioned above, for the scalar and pseudo-scalar singlet σ_X and η_X, there is a mixing with the corresponding resonances σ_ψ and η_ψ of the electroweak sector, so that the whole singlet sector will be treated separately in section 9.2.5.

Concerning the non-singlet pNGB G_c, we should also consider more generally a non-trivial pseudoscalar-axial vector mixing for non-vanishing vectorial four-fermion couplings, as we anticipate will be introduced below in Section 9.2.3, in analogy with the electroweak sector discussed in Section 8.2.5. With the additional explicit breaking mass term m_X of Eq. (9.2.1), the pseudoscalar-axial mixing formalism of Section 8.2.5 can easily be generalised with explicitly m_X-dependent resummed matrix correlator $\overline{\mathbf{\Pi}}_{G_c}(m_X)$, the analog of Eq. (8.2.44), (8.2.47) for the coloured sector. Note that all of the one-loop two-point functions $\tilde{\Pi}(p^2, M_X^2) \equiv \tilde{\Pi}_i^X(p^2)$ of the $SU(6)$ sector can be obtained from those in table 8.2 with the following replacements: $M_\psi \to M_X$ and $(2N) \to (2N+1)(N-1)$ (see appendix H for details). Accordingly the pNGB obviously gets a nonzero mass, whose expression is obtained from the zero of the determinant, analogous to (8.2.46) for the $SU(4)$ sector, as

$$D_{G_c} = \frac{m_X}{M_X} g_{A_c}^{-1} + 2(\kappa_{A6} + \kappa_{B6})\tilde{B}_0(p^2, M_X^2)\, p^2 \equiv 2(\kappa_{A6} + \kappa_{B6})\tilde{B}_0(p^2, M_X^2)(p^2 - M_{G_c}^2). \qquad (9.2.17)$$

The calculation of the scalar $S_c^{\hat{F}}$ mass is simpler and follows the same derivation as for the scalar

ϕ	K_ϕ	$\tilde{\Pi}_\phi^X(q^2)$
$G_c^{\hat{F}}$	$\frac{2(\kappa_{A6}+\kappa_{B6})}{(2N+1)(N-1)}$	$\tilde{\Pi}_P^X(q^2) = (2N+1)(N-1)\big[\tilde{A}_0(M_X^2) - \frac{q^2}{2}\tilde{B}_0(q^2, M_X^2)\big]$
η_X	$\frac{2[\kappa_{A6}-(6N-7)\kappa_{B6}]}{(2N+1)(N-1)}$	
$\eta_\psi - \eta_X$	$\frac{-\kappa_{\psi X}}{(2N)}$	
$S_c^{\hat{F}}$	$\frac{2(\kappa_{A6}-\kappa_{B6})}{(2N+1)(N-1)}$	$\tilde{\Pi}_S^X(q^2) = (2N+1)(N-1)\big[\tilde{A}_0(M_X^2) - \frac{1}{2}(q^2 - 4M_X^2)\tilde{B}_0(q^2, M_X^2)\big]$
σ_X	$\frac{2[\kappa_{A6}+(6N-7)\kappa_{B6}]}{(2N+1)(N-1)}$	
$\sigma_\psi - \sigma_X$	$\frac{\kappa_{\psi X}}{(2N)}$	
$V_c^{\mu F}$	$\frac{-2\kappa_{D6}}{(2N+1)(N-1)}$	$\tilde{\Pi}_V^X(q^2) = \frac{1}{3}(2N+1)(N-1)\big[-2M_X^2\tilde{B}_0(0, M_X^2) + (q^2 + 2M_X^2)\tilde{B}_0(q^2, M_X^2)\big]$
$A_c^{\mu\hat{F}}$	$\frac{-2\kappa_{D6}}{(2N+1)(N-1)}$	$\tilde{\Pi}_A^X(q^2) = \frac{1}{3}(2N+1)(N-1)\big[-2M_X^2\tilde{B}_0(0, M_X^2) + (q^2 - 4M_X^2)\tilde{B}_0(q^2, M_X^2)\big]$
a_X^μ	$\frac{-2\kappa_{C6}}{(2N+1)(N-1)}$	$\tilde{\Pi}_A^{XL}(q^2) = -2(2N+1)(N-1)M_X^2\tilde{B}_0(q^2, M_X^2)$
$A_c^{\mu\hat{F}} - G_c^{\hat{F}}$		$\tilde{\Pi}_{AP}^X(q^2) = -(2N+1)(N-1)M_X\tilde{B}_0(q^2, M_X^2)$
$a_X^\mu - \eta_X$		

Table 9.2: The four-fermion couplings K_ϕ in the X-sector, and the associated one-loop two-point functions $\tilde{\Pi}_\phi^X(q^2)$. The latter are related to the two-point functions of the ψ-sector as follows: $\tilde{\Pi}_\phi^\psi(q^2) = \tilde{\Pi}_\phi(q^2, M_\psi^2, 2N)$ and $\tilde{\Pi}_\phi^X(q^2) = \tilde{\Pi}_\phi[q^2, M_X^2, (2N+1)(N-1)]$, where $\tilde{\Pi}_\phi(q^2, M_\psi^2, 2N)$ are defined in Table 8.2. We also give the expression of the mixed (one-loop) pseudoscalar-longitudinal axial correlator, as well as those of the couplings mixing the singlet scalars of the two sectors, σ_ψ and σ_X, and the singlet pseudoscalars η_ψ and η_X. The explicit calculation of the correlators $\tilde{\Pi}_\phi^X(q^2)$ is detailed in appendix H.

mass of the $SU(4)$ sector. Thus we obtain

$$M^2_{G_c} = -(\frac{m_X}{M_X})\frac{g^{-1}_{A_c}(M^2_{G_c})}{2(\kappa_{A6}+\kappa_{B6})\tilde{B}_0\left(M^2_{G_c},M^2_X\right)}\ , \qquad M^2_{S_c} = 4M^2_X - \frac{8\kappa_{B6}\tilde{A}_0(M^2_X)+\frac{m_X}{M_X}}{2(\kappa_{A6}-\kappa_{B6})\tilde{B}_0\left(M^2_{S_c},M^2_X\right)}\ . \tag{9.2.18}$$

where as before the pole masses are defined as $M^2_{G_c} = M^2_{G_c}(p^2 = M^2_{G_c})$. Accordingly, similarly to M^2_η in Eq. (8.2.52), when a non-vanishing coloured sector vector coupling κ_{D6} is considered (see Section 9.2.3), the pseudo-scalar Goldstone mass $M^2_{G_c}$ is renormalised by the (inverse) axial form factor $g^{-1}_{A_c}(p^2 \equiv M^2_{G_c}) \equiv 1 - 2K_{A_c}\tilde{\Pi}^{LX}_A(M^2_{G_c})$ where K_{A_c} is defined in Table 9.2.

Note that there is another source of explicit symmetry breaking which may a priori leads to sizeable contributions to the masses. Indeed when we switch on the SM gauge interactions, new contributions to the masses of the coloured states arise. In the following, we will only consider the gauge corrections to the masses of the pNGB, since the latter are the lightest resonances of the coloured sector, therefore those corrections are more relevant than e.g. for the other scalar states. The gauge contributions to the pNGB masses are given in general terms in section 8.1.5 and in appendix F.2 for the particular case of the $SU(6)$ sector. The pNGB $G^{\hat{F}}_c$ decompose as an octet $O_c \sim 8_0$ and two sextet $(S_c + \overline{S}_c) \sim (6_{4/3} + \overline{6}_{-4/3})$ under $SU(3)_c \times U(1)_D$. Consequently, there are two sources of gauge contributions which lead to a mass splitting between the octet and sextet components: one from the gauging of QCD and one from the gauging of the hypercharge. However, from Eq. (F.14) one can see that the QCD corrections are almost the same for the two components as $\Delta M^2_{O_c}/\Delta M^2_{S_c}|_{QCD} = 9/10$. For simplicity we will neglect this small difference. In addition, the contribution coming from the gauging of $U(1)_Y$ is sub-dominant compared to the one from QCD, and we will safely neglect it. This is due to the small value of the ratio g'/g_s at the energy scale of a few TeVs we are interested in. Then the gauge contributions mainly originate from QCD and to evaluate the latter, we need to compute the integral in Eq. (F.14) within the NJL framework. To do that, we simply cut the integral at $Q^2 = \Lambda^2$, where Λ stands for the cutoff of the NJL model, and F_{G_c} is given by the expression

$$F^2_{G_c} = -2(2N+1)(N-1)M^2_X\tilde{B}_0(M^2_{G_c},M^2_X)g_{A_c}(M^2_{G_c})\ , \tag{9.2.19}$$

which can easily be inferred adapting Eqs. (8.2.41) and (8.2.39) to the $SU(6)$ sector. Note that, for simplicity, the mass M_{G_c} in the right-hand side is taken without gauge corrections. The resulting radiative pNGB masses, obtained from Eq. (F.14), are illustrated in the left panel of Fig. 9.4, where by definition $M^2_{G_c} = \Delta M^2_{O_c}$, as $m_X = 0$. These numerical results will be discussed in more details in section 9.2.4. Let us just mention that this gauge-induced mass could be sufficient by itself to comply with the lower collider bounds [260].

9.2.3 Masses of coloured vector resonances

In order to calculate the masses of the vector and axial-vector resonances present in the coloured sector, we start from the following vector-vector four-fermion operators

$$\mathcal{L}^X_{vect} = \frac{\kappa_{C6}}{(2N+1)(N-1)}\left(\overline{X}\,T^0_X\,\overline{\sigma}^\mu X\right)^2 + \frac{\kappa_{D6}}{(2N+1)(N-1)}\left[\left(\overline{X}\,T^F\,\overline{\sigma}^\mu X\right)^2 + \left(\overline{X}\,T^{\hat{F}}\,\overline{\sigma}^\mu X\right)^2\right], \tag{9.2.20}$$

where as in the electroweak sector, due to the global $SU(6)$ symmetry, the four-fermions coupling κ_{D6} of the vector channel is the same as the axial non-singlet channel. From the above operators we obtain the vector and axial-vector four-fermions couplings K_{V_c}, K_{A_c} and K_{a_X} (see table 9.2) and we derive the masses of the vector V^F_c and axial $A^{\hat{F}}_c, a_X$ resonances

$$M^2_{V_c} = -\frac{3}{4\kappa_{D6}\tilde{B}_0(M^2_{V_c},M^2_X)} + 2M^2_X\frac{\tilde{B}_0(0,M^2_X)}{\tilde{B}_0(M^2_{V_c},M^2_X)} - 2M^2_X, \tag{9.2.21}$$

$$M^2_{A_c} = -\frac{3}{4\kappa_{D6}\tilde{B}_0(M^2_{A_c},M^2_X)} + 2M^2_X\frac{\tilde{B}_0(0,M^2_X)}{\tilde{B}_0(M^2_{A_c},M^2_X)} + 4M^2_X\ . \tag{9.2.22}$$

Just like in the electroweak sector, if one neglects the p^2 dependence of the $\tilde{B}_0$ function, one obtains the usual NJL relation between the axial and vector masses, that is $M_{A_c}^2 \simeq M_{V_c}^2 + 6M_X^2$. The mass of the axial singlet a_c^μ is obtained by making the replacements $A_c^\mu \to a_X^\mu$ and $\kappa_{D6} \to \kappa_{C6}$ in Eq. (9.2.22). Note that we have not considered the following operator

$$\mathcal{L}_{vect}^{\psi X} = \frac{\kappa_{\psi X}^V}{(2N)} \left(\overline{\psi}\, T_\psi^0\, \overline{\sigma}^\mu \psi\right) \left(\overline{X}\, T_X^0\, \overline{\sigma}_\mu X\right) \ , \tag{9.2.23}$$

which induces a mixing between the axial singlets of the two sectors, a_ψ^μ and a_X^μ. This mixing term respects all symmetries of the theory and should be present in general. However, we neglected it as it is not generated by applying a Fierz transformation to the $Sp(2N)$ current-current operators in Eq. (I.8).

Note also that in principle, the spin one masses receive SM gauge contributions as $V_c^\mu \sim 15_{SO(6)} = (1+8+3+\overline{3})_{SU(3)_c}$ and $A_c^\mu \sim 20_{SO(6)} = (8+6+\overline{6})_{SU(3)_c}$. However, following the discussion of section 9.2.2 for the scalar masses, we will not consider such contributions here.

9.2.4 The mass spectrum of the coloured resonances

In general the couplings of the four-fermion operators are free parameters. However κ_{A6} and $\kappa_{C6,D6}$ may be related if we assume that the dynamics is induced by $Sp(2N)$ current-current operators. In this case, as in the ψ-sector, we find that the scalar and vector four-fermion couplings are equal, see appendix I.4. However, we also find that the size of these couplings relatively to the ones in the electroweak sector is not fixed by the current-current approximation. The reason is that, contrary to the case of the ψ-sector, the X-sector current-current operator cannot be recast in terms of $Sp(2N)$ singlet-singlet operators only, see appendix I.4. Nonetheless in this section, for the sake of illustration, we will take equal couplings in the two sectors

$$\kappa_{A6} = \kappa_{C6} = \kappa_{D6} = \kappa_A \ . \tag{9.2.24}$$

With this choice, as shown in Fig. 9.3, the range of validity of the NJL approximation is approximatively the same in the two sectors.

The resonance masses of the coloured sector are illustrated in Fig. 9.4. To ease the comparison with the electroweak sector, the masses are in units of $f = \sqrt{2}F_G \gtrsim 1$ TeV, and are plotted as functions of the coupling ξ defined by Eq. (8.2.17). Note that in section 8.2.6, for the $SU(4)$ sector in isolation, the only constraint from vacuum stability was $\kappa_B/\kappa_A < 1$: here we anticipate a similar but stronger bound, see Eqs. (9.2.31) and (9.2.40) below. Consequently the value of κ_B/κ_A is fixed to 0.01 for illustration, which is safely below this upper bound in the case $N = 4$. Then, if one assumes that Eq. (9.2.24) holds, there is just one additional free parameter compared to the $SU(4)$ sector in isolation, namely the explicit symmetry-breaking mass term m_X. We illustrate two representative cases: one with no explicit breaking, $m_X = 0$, and another one with explicit symmetry breaking, for which we take as a representative value $m_X = 0.1f$.

In the case with no explicit breaking (left panel of Fig. 9.4), the behaviour of the masses is qualitatively similar to the $SU(4)$ sector, except for the pNGBs G_c. This is due to the relations between the couplings of the four-fermion interactions: $\kappa_A = \kappa_{A6}$ and $\kappa_B \sim \kappa_{B6} \ll \kappa_A$. The pNGB of the coloured sector receive a significant contribution to their masses from the gauging of the colour group, as discussed in section 9.2.2. As it can be seen from Fig. 9.4, this contribution satisfies $\Delta M_{G_c} \gtrsim 1.3f$, which is enough to comply with the present collider bounds, as long as $f \gtrsim 1$ TeV. Thus, we conclude that it is actually possible to introduce top quark partners without the need of an explicit mass term m_X for the coloured fermions. On the other hand, if we want to raise the mass of coloured pNGBs, keeping a low mass scale of the theory, $f = 1$ TeV, one needs to introduce a non-zero m_X, as illustrated in the right panel of Fig. 9.4 for $m_X = 0.1f$. As all the coloured masses receive a contribution from m_X, for sufficiently large values of m_X one could even decouple the coloured sector from the electroweak sector.

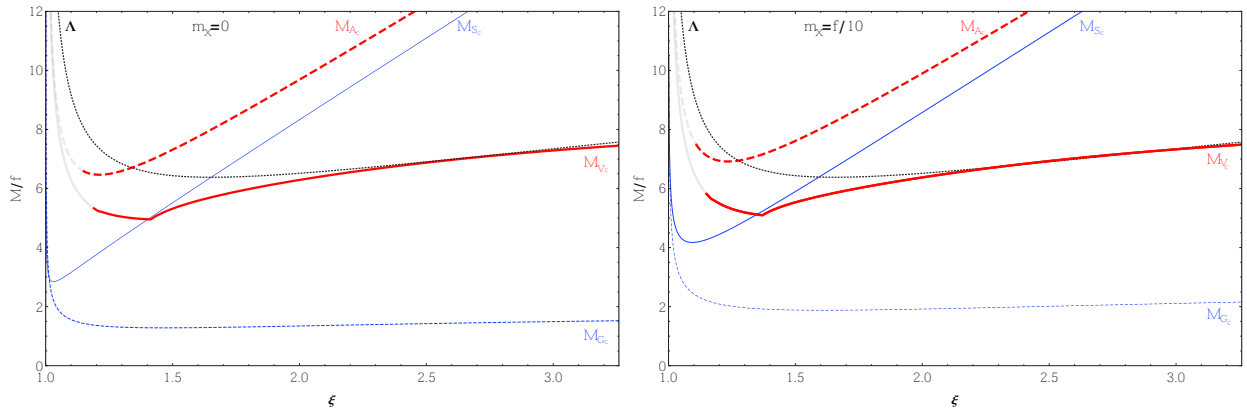

Figure 9.4: The masses of the coloured resonances in units of the Goldstone decay constant $f \equiv \sqrt{2} f_G$, for $N = 4$ (the masses scale as $1/\sqrt{N}$), as a function of the coupling ξ, for $\kappa_B/\kappa_A = 0.01$, $\kappa_{A6} = \kappa_A$, $m_X = 0$ (left-hand panel) and $m_X = f/10$ (right-hand panel). We displayed the full physical range for ξ, according to Fig. 8.3. Each curve is shaded when the corresponding pole mass develops a large, unphysical imaginary part, $|\mathrm{Im} g_\phi(M_\phi^2)/\mathrm{Re} g_\phi(M_\phi^2)| > 1$, as defined from Eq. (8.2.23). The dotted line is the cutoff of the constituent fermion loops. The Goldstone mass M_{G_c} include the radiative corrections as discussed in section 9.2.2.

Finally, we display here the masses of the colour resonances for the same parameters as in Eq. (8.2.54), $N = 4$, $\xi = 1.3$ and $\xi = 2$, fixing $\kappa_B/\kappa_A = 0.01$ and for the two representative values of m_X:

$$\begin{aligned}
&\xi = 1.3,\ m_X = 0 \quad : \quad && M_{A_c} \simeq 6.6 \text{ TeV}, \quad M_{V_c} \simeq 5.1 \text{ TeV}, \quad M_{S_c} \simeq 4.3 \text{ TeV}, \\
& && M_{G_c} \simeq \ 1.3\text{TeV} \ , \\
&\xi = 1.3,\ m_X = 0.1 \text{ TeV} \quad : \quad && M_{A_c} \simeq 7.0 \text{ TeV}, \quad M_{V_c} \simeq 5.2 \text{ TeV}, \quad M_{S_c} \simeq 4.9 \text{ TeV}, \\
& && M_{G_c} \simeq 2.0 \text{ TeV} \ . \qquad (9.2.25)
\end{aligned}$$

$$\begin{aligned}
&\xi = 2.0,\ m_X = 0 \quad : \quad && M_{A_c} \simeq 9.7 \text{ TeV}, \quad M_{V_c} \simeq 6.3 \text{ TeV}, \quad M_{S_c} \simeq 8.4 \text{ TeV}, \\
& && M_{G_c} \simeq \ 1.4\text{TeV} \ , \\
&\xi = 2.0,\ m_X = 0.1 \text{ TeV} \quad : \quad && M_{A_c} \simeq 9.9 \text{ TeV}, \quad M_{V_c} \simeq 6.4 \text{ TeV}, \quad M_{S_c} \simeq 8.5 \text{ TeV}, \\
& && M_{G_c} \simeq 1.8 \text{ TeV} \ . \qquad (9.2.26)
\end{aligned}$$

9.2.5 Flavour-singlet sector

The mixing in the (scalar and pseudoscalar) singlet sector, induced by the $U(1)$-breaking Lagrangian Eq. (9.1.34), is most conveniently treated in matrix formalism. Furthermore, since our model includes non-vanishing singlet axial vector couplings both in the $SU(4)$ and $SU(6)$ sectors, concerning the pseudoscalars we should take into account the additional nontrivial pseudoscalar-axial singlet mixing, similarly to the case of the $SU(4)$ sector in isolation treated in Section 8.2.5. Accordingly, we should consider 2×2 and 4×4 matrix equations, respectively, for the complete scalar and pseudoscalar sectors.

Scalar-singlet mixing

Let us start with the scalar sector and consider the diagonal one-loop scalar-correlator matrix $\mathbf{\Pi}_{\sigma_\psi \sigma_X}$ and the matrix of scalar-singlet couplings $\mathbf{K}_{\sigma_\psi \sigma_X}$,

$$\mathbf{\Pi}_{\sigma_\psi \sigma_X} = \begin{pmatrix} \tilde{\Pi}_S^\psi & 0 \\ 0 & \tilde{\Pi}_S^X \end{pmatrix} , \qquad \mathbf{K}_{\sigma_\psi \sigma_X} = \begin{pmatrix} K_{\sigma_\psi} & K_{\psi X} \\ K_{\psi X} & K_{\sigma_X}, \end{pmatrix} \qquad (9.2.27)$$

where K_{σ_ψ}, K_{σ_X} and $K_{\psi X} \equiv \kappa_{\psi X}/(2N)$ are collected in Tables 8.2 and 9.2. Note that when $K_{\psi X} = 0$ (equivalently $A_{\psi X} = 0$) there is no mixing between the singlets σ_ψ and σ_X. For simplicity, we have used the shorthand notations $\tilde{\Pi}_i^\psi \equiv \tilde{\Pi}_i(p^2, M_\psi^2)$ and $\tilde{\Pi}_i^X \equiv \tilde{\Pi}_i(p^2, M_X^2)$ for the one-loop correlators. From the above matrices, one can now define the resummed matrix scalar correlator $\overline{\mathbf{\Pi}}_{\sigma_\psi \sigma_X}$

$$\overline{\mathbf{\Pi}}_{\sigma_\psi\sigma_X} = \mathbf{\Pi}_{\sigma_\psi\sigma_X} + \mathbf{\Pi}_{\sigma_\psi\sigma_X}\,(2\mathbf{K}_{\sigma_\psi\sigma_X})\,\mathbf{\Pi}_{\sigma_\psi\sigma_X} + \cdots = (\mathbb{1} - 2\mathbf{\Pi}_{\sigma_\psi\sigma_X}\,\mathbf{K}_{\sigma_\psi\sigma_X})^{-1}\,\mathbf{\Pi}_{\sigma_\psi\sigma_X}\,, \tag{9.2.28}$$

and the resonance mass eigenvalues are obtained from the roots of the determinant $\det(\mathbb{1} - 2\mathbf{\Pi}_{\sigma_\psi\sigma_X}\,\mathbf{K}_{\sigma_\psi\sigma_X}) = 0$. Explicitly one obtains

$$\begin{aligned} \det(\mathbb{1} - 2\mathbf{\Pi}_{\sigma_\psi\sigma_X}\mathbf{K}_{\sigma_\psi\sigma_X}) &= 1 - 2K_{\sigma_\psi}\tilde{\Pi}_S^\psi - 2K_{\sigma_X}\tilde{\Pi}_S^X + 4\left(K_{\sigma_\psi}K_{\sigma_X} - K_{\psi X}^2\right)\tilde{\Pi}_S^\psi\tilde{\Pi}_S^X \\ &= c_0^S(p^2) + c_1^S(p^2)p^2 + c_2^S(p^2)(p^2)^2\,, \end{aligned} \tag{9.2.29}$$

where the coefficients $c_i^S(p^2)$ are functions of the couplings K_i, and of the loop functions $\tilde{A}_0(M_\psi^2)$, $\tilde{A}_0(M_X^2)$, $\tilde{B}_0(p^2, M_\psi^2)$, and $\tilde{B}_0(p^2, M_X^2)$. (The last form of the determinant, as a quadratic form in p^2, is an abusive but convenient oversimplification, given that the additional dependence in p^2 involved in $c_i^S(p^2)$ and originating from $\tilde{B}_0(p^2, M_{\psi,X}^2)$ does not induce additional pole structure: thus the pole mass eigenvalues are obtained from the roots of this quadratic equation, however evaluated at self-consistent p^2 values). In other words, the scalar-singlet masses are given by

$$M_{\sigma_0,\sigma'}^2 = \mathrm{Re}[g_{\sigma_0,\sigma'}(M_{\sigma_0,\sigma'}^2)]\,, \qquad g_{\sigma_0,\sigma'}(p^2) \equiv \frac{-c_1^S(p^2) \pm \sqrt{[c_1^S(p^2)]^2 - 4c_2^S(p^2)c_0^S(p^2)}}{2c_2^S(p^2)}\,. \tag{9.2.30}$$

The explicit expressions of the two scalar singlet masses $M_{\sigma_0}^2, M_{\sigma'}^2$ are straightforwardly derived from the above equations, but are not very simple or telling, even in the chiral limit $m_X = 0$, so that we refrain from giving them here. In the numerical illustrations below we use those exact expressions.

As we will examine quantitatively below, a nontrivial property of the lightest scalar mass M_{σ_0} is that it is a *decreasing* function of κ_B/κ_A [at least as long as m_X remains moderate, in its natural range $m_X \ll \Lambda$], in such a way that it even vanishes at a critical κ_B/κ_A value, and becomes formally tachyonic beyond. This critical κ_B^c value should therefore be considered as an intrinsic upper bound, since beyond this value the effective scalar potential is destabilised, in such a way that the minimisation in the NJL framework is totally unreliable. As mentioned above, the exact expression of M_{σ_0} from Eq. (9.2.30) is rather involved, but it is clear that $M_{\sigma_0}(\kappa_B)$ can only vanish if $c_0^S(\kappa_B) = 0$ in Eq. (9.2.29) (irrespectively of additional p^2-dependence from the $\tilde{B}_0$ function). Actually the most general exact value κ_B^c such that $M_{\sigma_0}(\kappa_B^c) = 0$ is not a very simple expression in terms of the relevant parameters $N, M_X, M_\psi, \cdots$, as it results from solving a quadratic equation in κ_B (after eliminating other relevant parameters $\kappa_A, \kappa_{A6}, \kappa_{B6}, \cdots$ upon using the gap-equations (9.2.3) and relations (9.2.6)). But since this upper bound on κ_B happens to be small for any N, a very reasonable approximation is obtained by expanding M_{σ_0} to first order in κ_B, in the chiral limit $m_X = 0$, which leads to

$$M_{\sigma_0}^2(m_X = 0, \kappa_B^c) = 0 \qquad \Rightarrow \qquad \kappa_B^c \simeq -\frac{1}{16}\frac{2N+1}{N(3N-4)}\frac{M_X^4 B_6}{M_\psi^2 A_4^2}\,. \tag{9.2.31}$$

The bound $\kappa_B < \kappa_B^c$ involves non-trivially the dynamical masses $M_{\psi,X}$. Except in the extreme case $M_X \gg M_\psi$, this bound implies in general $\kappa_B/\kappa_A \ll 1$ already for $N = 2$, and it becomes more stringent as $\sim 1/N$ for larger values of N. Typically, in the chiral limit $m_X = 0$, one finds $\kappa_B^c/\kappa_A \simeq 0.12$ for $N = 2$, and $\kappa_B^c/\kappa_A \simeq 0.04$ for $N = 4$. As we will see in section 9.2.5, there is another upper bound on κ_B, originating from the pseudoscalar-singlet mixing, also related to vacuum stability, which has a numerical value very close to the one in Eq. (9.2.31), although being analytically different. As we will examine in concrete illustrations below, these bounds put stringent restrictions on the singlet mass spectrum. As we will further explain below for the pseudoscalar case, this constraint should be viewed as an appropriate generalisation of the constraint $\kappa_B/\kappa_A < 1$, that applies to the $SU(4)$ sector in isolation.

Concerning the scalar decay constants, defined formally in Eqs. (8.2.58) with the obvious replacement $S \to S_0^\psi, S_0^X$, they can be derived by following a procedure quite similar to the one explained in Sec III.D. They are defined by the residues of the diagonal elements of $\overline{\mathbf{\Pi}}_{\sigma_\psi\sigma_X}$ at the respective σ_0, σ' pole masses

$$(G^\psi_{\sigma_i})^2 \equiv -\lim_{p^2\to M^2_{\sigma_i}}(p^2-M^2_{\sigma_i})\overline{\mathbf{\Pi}}_{\sigma_\psi\sigma_X,11}(p^2)\ , \qquad (G^X_{\sigma_i})^2 \equiv -\lim_{p^2\to M^2_{\sigma_i}}(p^2-M^2_{\sigma_i})\overline{\mathbf{\Pi}}_{\sigma_\psi\sigma_X,22}(p^2)\ . \tag{9.2.32}$$

These decay constants enter in the scalar sum rules in combination with the other (pseudo)scalar decay constants. We refrain here to give their explicit expressions which are not simple. Let us just note that the results obtained from Eq. (9.2.32) can be crosschecked with the off-diagonal elements of $\overline{\mathbf{\Pi}}_{\sigma_\psi\sigma_X}$ as $G^\psi_{\sigma_i}G^X_{\sigma_i} = -\lim_{p^2\to M^2_{\sigma_i}}(p^2-M^2_{\sigma_i})\overline{\mathbf{\Pi}}_{\sigma_\psi\sigma_X,12}(p^2)$.

Pseudoscalar-singlet mixing

Considering now the more involved pseudoscalar sector, we start from the complete 4×4 matrix coupling and correlator to account both for singlet mixing and pseudoscalar-axial singlet vectors a^μ_ψ, a^μ_X mixing,. The latter mixing is treated similarly to the pseudoscalar-axial mixing for the Goldstone boson sector as considered in section 8.2.5. Accordingly we have

$$\mathbf{K}_{\eta_\psi\eta_X} = \begin{pmatrix} K_{\eta_\psi} & -K_{\psi X} & 0 & 0 \\ -K_{\psi X} & K_{\eta_X} & 0 & 0 \\ 0 & 0 & K_a & 0 \\ 0 & 0 & 0 & K_{a_c} \end{pmatrix}\ , \qquad \mathbf{\Pi}_{\eta_\psi\eta_X} = \begin{pmatrix} \tilde\Pi^\psi_P & 0 & \sqrt{p^2}\tilde\Pi^\psi_{AP} & 0 \\ 0 & \tilde\Pi^X_P & 0 & \sqrt{p^2}\tilde\Pi^X_{AP} \\ \sqrt{p^2}\tilde\Pi^\psi_{AP} & 0 & \tilde\Pi^{L\psi}_A & 0 \\ 0 & \sqrt{p^2}\tilde\Pi^X_{AP} & 0 & \tilde\Pi^{LX}_A \end{pmatrix}\ , \tag{9.2.33}$$

where all the relevant pseudoscalar and axial-vector correlators and couplings for the $SU(4)$ and $SU(6)$ sectors are given respectively in Tables 8.2, and 9.2 (and we have used in Eq. (9.2.33) the same short-hand notation as in section 9.2.5). From the above matrices, we obtain the resummed two-point correlator defined as

$$\overline{\mathbf{\Pi}}_{\eta_\psi\eta_X} = (\mathbb{1} - 2\mathbf{\Pi}_{\eta_\psi\eta_X}\,\mathbf{K}_{\eta_\psi\eta_X})^{-1}\,\mathbf{\Pi}_{\eta_\psi\eta_X}\ . \tag{9.2.34}$$

According to the previous equation, the pseudoscalar mass eigenvalues are given by the zeros of the determinant of $\mathbb{1} - 2\mathbf{K}_{\eta_\psi\eta_\mathbf{X}}\mathbf{\Pi}_{\eta_\psi\eta_\mathbf{X}}$, which we give explicitly only in the chiral $m_X = 0$ limit for simplicity. Note that the latter determinant keeps the form of a quadratic equation, apart from further p^2-dependence from the $\tilde B_0$ function appearing in the coefficients. After using the relevant relations Eqs. (9.2.5), (9.2.6) and (9.2.15) and the mass gap Eqs. (9.2.3) to express all the effective four-fermion couplings κ_i in terms of κ_B alone, we obtain

$$\det[\mathbb{1} - 2\mathbf{K}_{\eta_\psi\eta_\mathbf{X}}\mathbf{\Pi}_{\eta_\psi\eta_\mathbf{X}}(p^2)] = p^2\left[c_1^P(p^2) + p^2 c_2^P(p^2)\right]\ , \tag{9.2.35}$$

where in notations similar to the scalar case, we define the relevant coefficients of the quadratic equation as

$$c_1^P(p^2) = 4\frac{\kappa_B A_4}{(2N+1)A_6M_X^2}\left[12N(N-1)B_4(p^2)M_\psi^2 g_{a_c}^{-1}(p^2) + (2N+1)B_6(p^2)M_X^2 g_a^{-1}(p^2)\right]\ , \tag{9.2.36}$$

$$c_2^P(p^2) = -\frac{B_4(p^2)B_6(p^2)}{(2N+1)A_6^2M_X^2}\left[24N(N-1)\kappa_B A_4 M_\psi^2 - (2N+1)(\kappa_A-\kappa_B)A_6M_X^2\right]\ , \tag{9.2.37}$$

with the shorthand notations $A_4 \equiv \tilde A_0(M_\psi^2)$, $A_6 \equiv \tilde A_0(M_X^2)$ and similarly for the B_4, B_6 functions. The appearance of the axial singlet form factors g_a, g_{a_c} is a result of the pseudoscalar-axial singlet mixing

$$g_a^{-1}(p^2) = 1 + \frac{4\kappa_C}{2N}\tilde\Pi_A^{L\psi}(p^2)\ , \qquad g_{a_c}^{-1}(p^2) = 1 + \frac{4\kappa_{C6}}{(2N+1)(N-1)}\tilde\Pi_A^{LX}(p^2)\ . \tag{9.2.38}$$

The pseudoscalar analog of the term $c_0^S(p^2)$ in the determinant of $\mathbb{1} - 2\mathbf{K}_{\eta_\psi\eta_\mathbf{X}}\mathbf{\Pi}_{\eta_\psi\eta_\mathbf{X}}$ vanishes in the chiral limit $m_X = 0$, as is explicit in Eq. (9.2.35), after non-trivial cancellations using the gap

equations (9.2.3), and Eqs.(9.2.5) and (9.2.6), which thus exhibits the remaining singlet Goldstone boson associated with the non-anomalous combination of $U(1)_\psi$ and $U(1)_X$. Obviously, the other pseudoscalar singlet has a non-vanishing mass even for $m_X = 0$, with a relatively compact expression,

$$M^2_{\eta'} = \mathrm{Re}[g_{\eta'}(M^2_{\eta'})] + \mathcal{O}(m_X) \ , \qquad g_{\eta'}(p^2) \equiv -\frac{c_1^P(p^2)}{c_2^P(p^2)} \ . \tag{9.2.39}$$

Note that for sufficiently large N (but keeping in mind $N \leq 18$), $M^2_{\eta'}$ is of order $\mathcal{O}(N^0)$, using that $\kappa_B \simeq 1/N$, while the not-shown $\mathcal{O}(m_X)$ term is of order $1/N$. This is naively compatible with the behaviour of the anomaly, which also goes like a constant for sufficiently large values of N, see Eq. (9.1.2) (considering that $g^2_{HC} \simeq 1/N$).

An important, interesting feature of the whole model emerges from the examination of Eq. (9.2.39): for any p^2, the function $g_{\eta'}(p^2)$ has a *pole* at a particular value of κ_B, as follows from Eq. (9.2.37),

$$\frac{\kappa_B/\kappa_A}{1-\kappa_B/\kappa_A} = \frac{1}{24}\frac{2N+1}{N(N-1)}\frac{A_6 M_X^2}{A_4 M_\psi^2} \ . \tag{9.2.40}$$

In other words, the η' mass grows rapidly and decouples when approaching from below the critical value of κ_B defined by Eq. (9.2.40). This is not unexpected, as it is simply a generalisation of a property already observed in the $SU(4)$ sector in isolation. In the latter case, recall that the mass-gap equation (8.2.16) has solutions only for $\kappa_B^2 < \kappa_A^2$, as discussed after Eq. (8.2.17): as also explained in Ref. [259], and apparent in Eqs. (8.2.12) and (8.2.13), for $\kappa_B > \kappa_A$ the effective potential is destabilised around the origin, already at tree level and, although one could expect a spontaneous symmetry breaking of some of the symmetries, one cannot perform a proper minimisation to determine the vacuum, within the NJL framework. This feature is reflected also directly in the resonance mass spectrum, where the η' mass (for the $SU(4)$ sector in isolation) of Eq. (8.2.26) clearly has a pole for $\kappa_B = \kappa_A$ and becomes tachyonic for large κ_B. Now the critical value in the full model, determined by Eq. (9.2.40), should be considered accordingly as an absolute upper bound on κ_B/κ_A. It takes a more involved dynamical form (depending also on the mass gaps M_ψ, M_X values) precisely because the mixing, as induced by the effective operators in Eq. (9.1.34), couples non-trivially the two sectors, mass gaps and couplings, and involves combinatorial factors with N dependence. Note that, upon using the relation (9.2.6), the critical coupling in (9.2.40) translates into a simpler upper limit on κ_{B6}, approximately:

$$\frac{\kappa_{B6}}{\kappa_A} < \frac{1}{6(N-1)}\frac{A_4}{A_6} \ , \tag{9.2.41}$$

(upon neglecting higher order terms in κ^2_{B6}), in which the combinatoric factor $6(N-1)$ can be understood upon comparing with Eq. (9.2.14), such that Eq. (9.2.41) is a more transparent analog of the limit $\kappa_B < \kappa_A$ in the $SU(4)$ sector in isolation (let aside the presence of the loop functions A_4/A_6, that reflects the non-trivial dynamical connection between the two sectors). The bottom line is that Eq. (9.2.40) gives a tight upper bound on κ_B/κ_A, due in particular to the small coefficient $1/24$. To get an idea, consider the chiral limit $m_X = 0$: as discussed in section 9.2.1, then M_X lies slightly above M_ψ, with e.g. $M_X/M_\psi \simeq 1.15$ for $N = 2$ and small κ_B/κ_A. Thus, neglecting for simplicity the relatively small differences in the $\tilde{A}_0$ loop functions, Eq. (9.2.40) gives typically $\kappa_B/\kappa_A < 5/48(M_X^2/M_\psi^2) \simeq 0.12$ for $N = 2$, and the latter ratio decreases quite rapidly for larger N due to the $\sim 1/N$ behaviour of Eq. (9.2.40), for instance $\kappa_B/\kappa_A < 1/32(M_X^2/M_\psi^2) \simeq 0.04$ for $N = 4$.

More precisely, the physical upper bound on κ_B/κ_A is even more stringent. As the "running" mass $g_{\eta'}(p^2)$ grows rapidly when approaching from below the limiting value of κ_B/κ_A defined by Eq. (9.2.40), the corresponding pole-mass self-consistent equation for $M^2_{\eta'}$, given in Eq. (9.2.39), ceases to have a solution for a slightly smaller value of κ_B/κ_A. Moreover a large width develops much below this bound, which turns out to rapidly exceed the pole mass. Accordingly, the NJL description of the η' mass loses its validity for even smaller values of κ_B/κ_A. For a not too small $m_X \neq 0$, as discussed above M_X can be substantially larger than M_ψ, therefore the bound in Eq. (9.2.40) is delayed to larger κ_B/κ_A. Still, it remains quite constraining as long as m_X remains moderate with respect to Λ. In summary, the detailed structure of the mixing turns out to put a tight constraint on κ_B/κ_A, with important consequences for the resonance mass spectrum, as we will illustrate below.

For $m_X \neq 0$, the exact expressions of the two pseudoscalar singlet masses $M_{\eta_0}, M_{\eta'}$ (used in our numerical analysis) become rather involved: Eq. (9.2.35) is modified to a "quadratic" polynomial equation in p^2 (i.e. upon formally neglecting the additional p^2-dependence coming from the loop functions, entering the polynomial coefficients). This is then more similar to the eigenvalue equation of the scalar case above, see Eqs. (9.2.29), (9.2.30), now with coefficients $c_i^P(p^2)$ which depends on m_X, where the coefficient of $(p^2)^0$ takes the form

$$c_0^P = 8A_4\kappa_B \frac{m_X}{M_X}\, g_a^{-1}\, g_{a_c}^{-1}\,. \tag{9.2.42}$$

Indeed, the pNGB η_0 mass is given to very good approximation by the first order expansion in c_0^P, namely

$$M_{\eta_0}^2 = -\frac{c_0^P(M_{\eta_0}^2)}{c_1^P(M_{\eta_0}^2)}\,, \tag{9.2.43}$$

which essentially captures its correct behaviour as long as κ_B/κ_A is moderate and $m_X \ll \Lambda$. For large values of N, $M_{\eta_0}^2$ is of order $1/N$.

Once having determined the η_0 and η' masses, one can proceed to extract all relevant pseudoscalar decay constants from the pole mass residues of the matrix elements $\overline{\mathbf{\Pi}}^{ij}_{\eta_\psi\eta_X}(q^2)$ $(i,j=1,\cdots,4)$ where the resummed two-point correlator $\overline{\mathbf{\Pi}}_{\eta_\psi\eta_X}(q^2)$ is defined in Eq. (9.2.34). The procedure is similar to the one explained in section 8.2.5 for the simpler non-singlet case. More precisely, from the definitions of the decay constants $F_{\eta_0}^{\psi(X)}$, $G_{\eta_0}^{\psi(X)}$ in Eqs. (9.1.21) and (9.1.22), one obtains in general for $m_X \neq 0$

$$\lim_{q^2\to M_{\eta_0}^2}(q^2-M_{\eta_0}^2)\overline{\mathbf{\Pi}}^{11(22)}_{\eta_\psi\eta_X}(q^2) \equiv -(G_{\eta_0}^{\psi(X)})^2\,, \qquad \lim_{q^2\to M_{\eta_0}^2}(q^2-M_{\eta_0}^2)\overline{\mathbf{\Pi}}^{12,21}_{\eta_\psi\eta_X}(q^2) \equiv -G_{\eta_0}^{\psi}G_{\eta_0}^{\psi}\,, \tag{9.2.44}$$

$$\begin{aligned}
&\lim_{q^2\to M_{\eta_0}^2}\frac{(q^2-M_{\eta_0}^2)}{\sqrt{p^2}}\overline{\mathbf{\Pi}}^{13,31}_{\eta_\psi\eta_X}(q^2) \equiv -\frac{G_{\eta_0}^{\psi}F_{\eta_0}^{\psi}}{2\sqrt{2}}\,, \qquad \lim_{q^2\to M_{\eta_0}^2}\frac{(q^2-M_{\eta_0}^2)}{\sqrt{p^2}}\overline{\mathbf{\Pi}}^{14,41}_{\eta_\psi\eta_X}(q^2) \equiv -\frac{G_{\eta_0}^{\psi}F_{\eta_0}^{X}}{2\sqrt{3}}\,,\\
&\lim_{q^2\to M_{\eta_0}^2}\frac{(q^2-M_{\eta_0}^2)}{\sqrt{p^2}}\overline{\mathbf{\Pi}}^{23,32}_{\eta_\psi\eta_X}(q^2) \equiv -\frac{G_{\eta_0}^{X}F_{\eta_0}^{\psi}}{2\sqrt{2}}\,, \qquad \lim_{q^2\to M_{\eta_0}^2}\frac{(q^2-M_{\eta_0}^2)}{\sqrt{p^2}}\overline{\mathbf{\Pi}}^{24}_{\eta_\psi\eta_X}(q^2) \equiv -\frac{G_{\eta_0}^{X}F_{\eta_0}^{X}}{2\sqrt{3}}\,,
\end{aligned} \tag{9.2.45}$$

as well as

$$\begin{aligned}
&\lim_{q^2\to M_{\eta_0}^2}\frac{(q^2-M_{\eta_0}^2)}{q^2}\overline{\mathbf{\Pi}}^{33}_{\eta_\psi\eta_X}(q^2) \equiv -\frac{(F_{\eta_0}^{\psi})^2}{8}\,, \qquad \lim_{q^2\to M_{\eta_0}^2}\frac{(q^2-M_{\eta_0}^2)}{q^2}\overline{\mathbf{\Pi}}^{44}_{\eta_\psi\eta_X}(q^2) \equiv -\frac{(F_{\eta_0}^{X})^2}{12}\,,\\
&\qquad\qquad \lim_{q^2\to M_{\eta_0}^2}\frac{(q^2-M_{\eta_0}^2)}{q^2}\overline{\mathbf{\Pi}}^{34,43}_{\eta_\psi\eta_X}(q^2) \equiv -\frac{F_{\eta_0}^{\psi}F_{\eta_0}^{X}}{4\sqrt{6}}\,,
\end{aligned} \tag{9.2.46}$$

where the factors $2\sqrt{2}$ and $2\sqrt{3}$ take into account the normalisation of the $U(1)_\psi$ and $U(1)_X$-currents respectively. Similar expressions hold for the η' with the obvious replacement $\eta_0 \to \eta'$. Notice that the information on both diagonal and non-diagonal terms allow to extract unambiguously the signs of $G_{\eta_0(\eta')}^{\psi(X)}$ and $F_{\eta_0(\eta')}^{\psi(X)}$. In the chiral limit, the pole of the η_0 migrates from the longitudinal to the transverse axial correlator. Consequently, in that case one can not extract the decay constants $F_{\eta_0}^{\psi(X)}$ from Eq. (9.2.46) but only from Eq. (9.2.45).

In the following for simplicity we present analytical results only for the chiral limit $m_X = 0$. Let us consider the resummed axial longitudinal correlators, given by $q^2\overline{\Pi}^L_{a_{\psi(X)}}(q^2) = 8(12)\overline{\mathbf{\Pi}}^{33(44)}_{\eta_\psi\eta_X}(q^2)$ and $q^2\overline{\Pi}^L_{a_\psi a_X}(q^2) = 4\sqrt{6}\ \overline{\mathbf{\Pi}}^{34,43}_{\eta_\psi\eta_X}(q^2)$, see Eq. (9.2.46). One can check that the linear combination corresponding to the conserved $U(1)$ current, vanishes for any q^2

$$\overline{\Pi}_0^L(q^2) = 9(N-1)^2\overline{\Pi}^L_{a_\psi}(q^2) - 6(N-1)\overline{\Pi}^L_{a_\psi a_X}(q^2) + \overline{\Pi}^L_{a_X}(q^2) = 0\,, \qquad \overline{\Pi}^L_{a_\psi a_X} = \sqrt{\overline{\Pi}^L_{a_\psi}\,\overline{\Pi}^L_{a_X}}\,. \tag{9.2.47}$$

This is an important check, since the $U(1)$-current is conserved, despite the nonzero mass gap spoiling the Ward identity at the naive one-loop level. Then, once fully resummed, there is no longitudinal part in the corresponding axial two-points function, generalising, for the more involved singlet sector, the results obtained in section 8.2.5 for the simpler $SU(4)$ sector in isolation with (Goldstone) pseudoscalar-axial mixing. Coming now to the decay constants defined from Eqs. (9.2.44) and (9.2.45), using the gap-equations (9.2.3) and the constraints among the effective couplings in Eqs. (9.2.5), (9.2.6) and (9.2.15), after some algebra one obtains (in the chiral limit)

$$\begin{aligned}(G^{\psi}_{\eta_0})^2 &= \frac{-12(2N)^2(N-1)A_4^2M_\psi^2 g_a^{-1}(0)g_{a_c}^{-1}(0)}{12N(N-1)B_4(0)M_\psi^2 g_{a_c}^{-1}(0)+(2N+1)B_6(0)M_X^2 g_a^{-1}(0)}\,,\\ (G^{X}_{\eta_0})^2 &= \frac{(2N+1)^2A_6^2M_X^2}{6(2N)^2A_4^2M_\psi^2}(G^{\psi}_{\eta_0})^2\,,\end{aligned} \tag{9.2.48}$$

$$\begin{aligned}(F^{\psi}_{\eta_0})^2 &= \frac{-96(2N)^2(N-1)B_4^2(0)M_\psi^4 g_a(0)g_{a_c}^{-1}(0)}{12N(N-1)B_4(0)M_\psi^2 g_{a_c}^{-1}(0)+(2N+1)B_6(0)M_X^2 g_a^{-1}(0)}\\ &= \tilde{\Pi}_A^{L\psi}(0)g_a(0)\left[1-4\kappa_B\frac{A_4B_6(0)g_a^{-1}(0)}{A_6\,c_1^P(0)}\right]\,,\end{aligned} \tag{9.2.49}$$

$$\begin{aligned}(F^{X}_{\eta_0})^2 &= \frac{-24(N-1)(2N+1)^2B_6^2(0)M_X^4 g_a(0)^{-1}g_{a_c}(0)}{12N(N-1)B_4(0)M_\psi^2 g_{a_c}^{-1}(0)+(2N+1)B_6(0)M_X^2 g_a^{-1}(0)}\\ &= \tilde{\Pi}_A^{LX}(0)g_{a_c}(0)\left[1-24\kappa_B\frac{(2N)(N-1)B_4(0)A_4M_\psi^2 g_{a_c}^{-1}(0)}{(2N+1)A_6M_X^2\,c_1^P(0)}\right]\,.\end{aligned} \tag{9.2.50}$$

Notice from the second expressions of Eqs. (9.2.49) and (9.2.50) that the naive expressions of these decay constants, namely when the two sectors are in isolation, are respectively recovered for $M_X\to 0$ ($M_\psi\to 0$) as intuitively expected. One can compute in a similar way the decay constants associated to the η'. We do not explicitly give them because the η' is not a pNGB and these expressions are rather involved. The $U(1)$-conserved current $\mathcal{J}_0^\mu$ of Eq. (9.1.7) implies

$$F_{\eta_0,\eta'}=F^X_{\eta_0,\eta'}-3(N-1)F^{\psi}_{\eta_0,\eta'}\,. \tag{9.2.51}$$

From Eqs. (9.2.49) and (9.2.50), we obtain the decay constant of the η_0 in the chiral limit

$$F^2_{\eta_0}=-24(N-1)\left[12N(N-1)B_4M_\psi^2g_a(0)+(2N+1)B_6M_X^2g_{a_c}(0)\right]+\mathcal{O}(m_X)\,,\quad F^2_{\eta'}(m_X)=\mathcal{O}(m_X)\,. \tag{9.2.52}$$

As expected on general grounds (see section 9.1.2), F_{η_0} is non-zero in the chiral limit while $F_{\eta'}$ vanishes. Furthermore, one can also check, after some algebra, that the generally expected relations in Eq. (9.1.23) are indeed well satisfied (at least up to terms of higher orders in m_X^2) by our expressions above, which is a very non-trivial crosscheck of the NJL calculations. Likewise the general relations given in Eq. (9.1.27) are also well satisfied, providing an additional non-trivial crosscheck.

Actually in the chiral limit the decay constants F_{η_0} for the true Goldstone can be more directly calculated from the resummed transverse axial correlator $\overline{\Pi}_{a_\psi}(q^2)$ and $\overline{\Pi}_{a_X}(q^2)$ evaluated at $q^2=0$, in direct analogy with the non-singlet calculation of F_G. From Eq. (8.2.39), one obtains

$$F^2_{\eta_0}\equiv\lim_{q^2\to 0}[-q^2\overline{\Pi}_0(q^2)]=-\lim_{q^2\to 0}q^2[9(N-1)^2\overline{\Pi}_{a_\psi}(q^2)+\overline{\Pi}_{a_X}(q^2)]\,, \tag{9.2.53}$$

where the second equality comes from Eq. (9.1.7), taking into account that there is no mixing for the transverse contributions, i.e. $\overline{\Pi}_{a_\psi a_X}(q^2)=0$. The transverse resummed correlators are simply given by expressions similar to the one in Eq. (8.2.39): $-q^2\overline{\Pi}_{a_\psi}(q^2)=8\tilde{\Pi}^{\psi}_A(q^2)g_A(q^2)$ and $-q^2\overline{\Pi}_{A_X}(q^2)=12\tilde{\Pi}^{X}_A(q^2)g_{A_c}(q^2)$. Thus using the expression of the one-loop functions $\tilde{\Pi}^{\psi(X)}_A(0)$ from Table 8.2 and Table 9.2 directly gives

$$F^2_{\eta_0}=9(N-1)^2\left[-16(2N)M_\psi^2\tilde{B}_0(0,M_\psi^2)g_a(0)\right]+\left[-24(2N+1)(N-1)M_X^2\tilde{B}_0(0,M_X^2)g_{a_c}(0)\right]\,, \tag{9.2.54}$$

which is consistent with Eq. (9.2.52).

The mass spectrum of the singlet resonances

We now study the mass spectrum of the scalar and pseudo-scalar singlet resonances. Before turning to the more involved case including the mixing between the resonances from the EW and the coloured sectors, let us consider the instructive no-mixing case, where $A_{\psi X} = 0$ and consequently $\kappa_B = \kappa_{B6} = \kappa_{\psi X} = 0$. From Eq. (9.2.29) we obtain for the scalar singlets masses

$$A_{\psi X} = 0 : \qquad M^2_{\sigma_0} = 4M^2_\psi = M^2_{\sigma_\psi} \ , \qquad M^2_{\sigma'} = 4M^2_X - \frac{m_X}{M_X}\frac{1}{2\kappa_{A6}B_6(M^2_{\sigma'})} = M^2_{\sigma_X} \ , \quad (9.2.55)$$

which of course reproduce the masses in isolation. As discussed above, in our benchmark case where $\kappa_{A6} = \kappa_A$ we have $M_\psi \leqslant M_X$, so that in the no-mixing case we have $M^2_{\sigma_0} \leqslant M^2_{\sigma'}$ where the equality is valid for $m_X = 0$. In the same way, from Eq. (9.2.35) we obtain for the pseudo-scalar masses

$$A_{\psi X} = 0 : \qquad M^2_{\eta_0} = 0 = M^2_{\eta_\psi} \ , \qquad M^2_{\eta'} = -\frac{m_X}{M_X}\frac{g_{a_c}^{-1}}{2\kappa_{A6}B_6} = M^2_{\eta_X} \ . \quad (9.2.56)$$

Again, the latter expressions reproduce those in isolation and $M^2_{\eta_0} \leqslant M^2_{\eta'}$ where the equality is valid for $m_X = 0$.

Once we switch on the mixing, important new features arise, as discussed above: in particular, the non trivial tight bound on κ_B from Eq. (9.2.40), and the corresponding rapid growth of $M_{\eta'}$ when approaching from below the critical value of κ_B. This is illustrated in Fig. 9.5 for $N = 2$ and $N = 4$. Consequently, the η' mass is very sensitive to κ_B: $M_{\eta'}$ may be of order f for $\kappa_B/\kappa_A \ll 0.01$, but once κ_B/κ_A grows to larger values, already well below the bound of Eq. (9.2.40), η' decouples rapidly.

Another interesting feature is implicit in the η_0 mass expression Eq.(9.2.43): namely, M_{η_0} rapidly reaches an asymptotic limit for moderate κ_B values, for fixed N, and this (approximate) maximum decreases as $1/N$ for large N, as also illustrated in Fig. 9.5. More precisely, in the approximation of neglecting the differences in momenta of the loop functions, one obtains for large N values

$$M^2_{\eta_0} \simeq -\frac{A_6}{B_6}\frac{1}{3N}\frac{m_X}{M_X}\frac{M^2_X}{M^2_\psi} + \mathcal{O}(1/N^2) \, . \quad (9.2.57)$$

Of course η_0 being a pNGB, $M^2_{\eta_0}$ vanishes linearly in m_X. This shows in addition that M_{η_0} is approximately κ_B-independent, once κ_B takes moderately large values, as shown in Fig. 9.5. Its mass can be well below f, for sufficiently large N and/or small m_X.

The two *scalar* singlet masses are defined implicitly by Eq. (9.2.30). The heaviest state σ' always lies in the multi-TeV range, as illustrated in Figs. 9.5 and 9.6. More interestingly, as already explained, the lightest scalar mass M_{σ_0} is a decreasing function of κ_B/κ_A and vanishes at a critical value approximately given by Eq. (9.2.31). Such value is not identical to the one defined by Eq. (9.2.40), but is numerically very close to the latter, more precisely it lies always (slightly) below, for any $N \geq 2$. This is illustrated in Fig. 9.5 for $N = 2$ and $N = 4$. Beyond the critical value of κ_B/κ_A, σ_0 becomes tachyonic and the effective scalar potential is destabilised, therefore M_{σ_0} can be very small just before reaching the critical value of κ_B/κ_A.

Finally we also illustrate in Fig. 9.6 the ξ-dependence of the scalar and pseudoscalar singlet masses, for representative values of N, and κ_B/κ_A fixed safely below the upper bound from Eq. (9.2.40). Notice that M_{σ_0} vanishes for a sufficiently low ξ value, where one saturates the condition of Eq. (9.2.31), because the right-hand side of this equation decreases with ξ. As a consequence, the whole meson mass spectrum should not be trusted for ξ smaller than this critical value, as the vacuum becomes unstable.

To conclude this section, let us briefly discuss the η_0 couplings to the SM gauge bosons. As discussed at the end of section 8.1.5, in the chiral limit the anomalous coupling of a pseudo-Goldstone boson to a pair of gauge bosons is fully determined by the Wess-Zumino-Witten effective action. While the $SU(4)/Sp(4)$ [$SU(6)/SO(6)$] pseudo-Goldstone bosons may couple only to the electroweak (colour) gauge bosons, the η_0 is specially interesting as it couples to both, because it couples to both the ψ and X-fermion number currents $\mathcal{J}^0_{\psi\mu}$ and $\mathcal{J}^0_{X\mu}$. The two currents have a $U(1)_Y$ anomaly, and

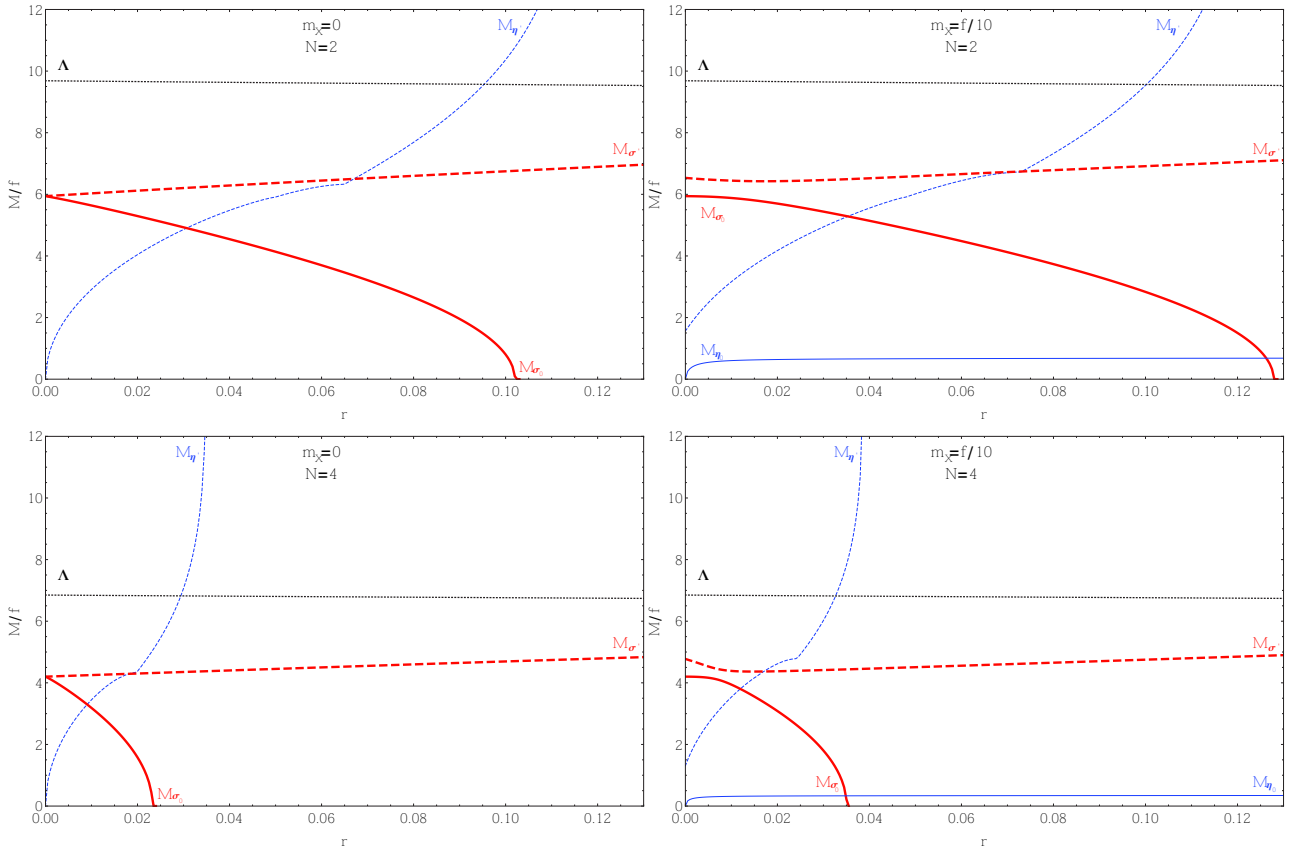

Figure 9.5: Singlet scalar and pseudoscalar meson masses in units of f, for a fixed value of the coupling $\xi = 1.3$, as a function of $r \equiv \kappa_B/\kappa_A$, for $N = 2$ (top) and $N = 4$ (bottom), and for $m_X = 0$ (left) and $m_X = f/10$ (right). The Goldstone boson η_0 is massless in the chiral limit.

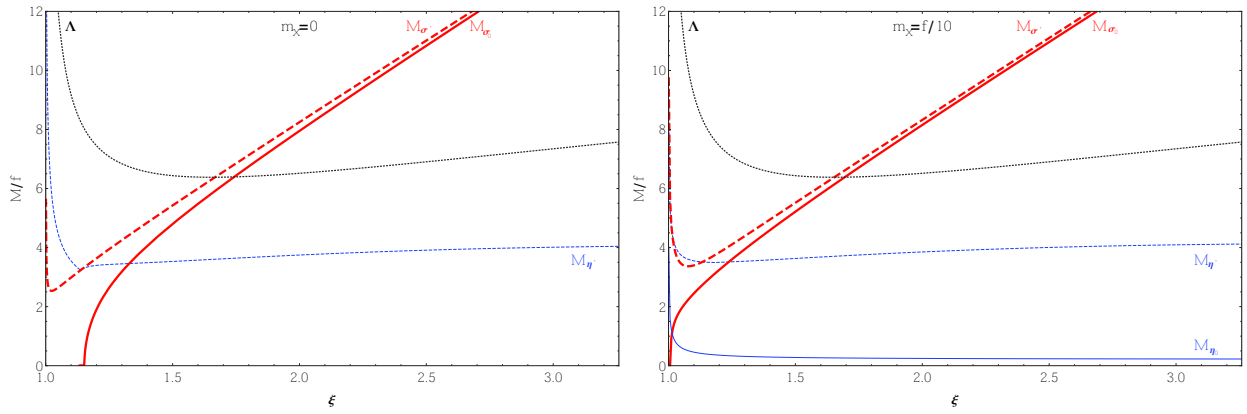

Figure 9.6: Singlet scalar and pseudoscalar meson masses in units of f, as a function of ξ for $N = 4$, $\kappa_B/\kappa_A = 0.01$, $m_X = 0$ (left panel) and $m_X = f/10$ (right panel). The Goldstone boson η_0 is massless in the chiral limit.

$\mathcal{J}^0_{\psi\mu}$ [$\mathcal{J}^0_{X\mu}$] has a $SU(2)_L$ [$SU(3)_c$] anomaly as well. Then, specialising Eq. (8.1.37) to our model, the η_0 couplings to the SM gauge bosons take the form

$$\begin{aligned}\mathcal{L}^{WZW}_{eff,\eta_0} &= -\frac{1}{16\pi^2}(2N)\left[-3(N-1)\right]\frac{\eta_0}{F_{\eta_0}}\left(g^2 W_{i\mu\nu}\tilde{W}_i^{\mu\nu} + g'^2 B_{\mu\nu}\tilde{B}^{\mu\nu}\right) \\ &\quad -\frac{1}{16\pi^2}(2N+1)(N-1)\frac{\eta_0}{F_{\eta_0}}\left(2g_s^2 G_{a\mu\nu}\tilde{G}_a^{\mu\nu} + \frac{16}{3}g'^2 B_{\mu\nu}\tilde{B}^{\mu\nu}\right) \\ &= \eta_0\left[k^0_{\gamma\gamma} e^2 A_{\mu\nu}\tilde{A}^{\mu\nu} + k^0_{gg} g_s^2 G_{a\mu\nu}\tilde{G}_a^{\mu\nu} + \dots\right] ,\end{aligned} \tag{9.2.58}$$

where the first (second) line is the contribution of the ψ (X) fermion loops, and the dots stand for couplings involving the Z or W field-strengths. Here $\tilde{F}_{\mu\nu} \equiv \epsilon_{\mu\nu\rho\sigma}F^{\rho\sigma}/2$ and the coefficients $k^0_{\gamma\gamma,gg}$ are straightforwardly computed using $B_{\mu\nu} \supset c_w A_{\mu\nu}$, $W_{3\mu\nu} \supset s_w A_{\mu\nu}$, and $e = g s_w = g' c_w$, and similarly for couplings involving the Z or W field-strengths. The decay widths into massless gauge bosons are

$$\Gamma(\eta_0 \to \gamma\gamma) = 4\pi\alpha_{em}^2 M_{\eta_0}^3 (k^0_{\gamma\gamma})^2 , \qquad \Gamma(\eta_0 \to gg) = 32\pi\alpha_s^2 M_{\eta_0}^3 (k^0_{gg})^2 . \tag{9.2.59}$$

Note that these rates are determined only by group theory factors, up to the decay constant F_{η_0}. The latter can be computed in the NJL approximation, and the result is given in Eq. (9.2.52). Thus, the golden channel for the discovery of η_0 at the LHC is production via gluon-gluon fusion and decay in two gauge bosons: di-jet, di-photon, γZ, ZZ and WW final states. We recall that the mass of η_0 is induced by the explicit breaking of the anomaly-free $U(1)$ symmetry: this is due either to an explicit mass term for the constituent fermions, $m_X \neq 0$, or to the proto-Yukawa couplings of the SM fermions to the composite sector, that we do not specify in this analysis. Our NJL result for M_{η_0} is given in Eqs. (9.2.43), (9.2.57). The corrections to Eq. (9.2.58), that strictly holds in the chiral limit, are expected to be subleading, as long as η_0 is significantly lighter than the non-Goldstone resonances. Note that the ratio $\Gamma(\eta_0 \to gg)/\Gamma(\eta_0 \to \gamma\gamma) = 18(2N+1)^2/(N-4)^2 \cdot \alpha_s^2/\alpha_{em}^2$ is independent from F_{η_0} and M_{η_0}, and it larger than $2 \cdot 10^4$ for any N. Thus a discovery appears more likely in the di-jet channel. Indeed, the alleged di-photon resonance at 750 GeV could not be fitted by η_0, because the gluons-to-photons ratio is too large [307].

F Generators of the flavour group and embedding of the SM group

In this appendix, we give explicit representations for the generators of the flavour groups $SU(4)$ and $SU(6)$ and describe how the SM gauge fields are coupled to the elementary fermion fields. There are general procedures to construct a basis of the Gell-Mann type for any $SU(n)$ group, starting from the well-known representations of the generators for the cases $n = 2$ and $n = 3$, see for instance [308]. The relations in Eq. (8.1.2) allow to distinguish the generators T^A for the unbroken subgroups, $Sp(4)$ and $SO(6)$, from the generators $T^{\hat{A}}$ in the corresponding coset spaces. For $n = 2N_f$ flavours, choosing the $2N_f \times 2N_f$ matrix Σ_ε in the form

$$\Sigma_\varepsilon = \begin{pmatrix} 0 & \mathbb{1} \\ \varepsilon\mathbb{1} & 0 \end{pmatrix}, \tag{F.1}$$

the general solution of Eq. (8.1.2) can be expressed as [258]

$$T^A = \begin{pmatrix} \mathcal{A}^A & \mathcal{B}^A \\ \mathcal{B}^{A\dagger} & -(\mathcal{A}^A)^T \end{pmatrix}, \qquad T^{\hat{A}} = \begin{pmatrix} \mathcal{C}^{\hat{A}} & \mathcal{D}^{\hat{A}} \\ \mathcal{D}^{\hat{A}\dagger} & +(\mathcal{C}^{\hat{A}})^T \end{pmatrix}, \tag{F.2}$$

where the $N_f \times N_f$ submatrices $\mathcal{A}^A$ and $\mathcal{C}^{\hat{A}}$ are hermitian, with $\mathcal{C}^{\hat{A}}$ traceless, whereas $(\mathcal{B}^A)^T = -\varepsilon\mathcal{B}^A$ and $(\mathcal{D}^{\hat{A}})^T = +\varepsilon\mathcal{D}^{\hat{A}}$.

F.1 The $SU(4)$ sector

According to the preceding discussion, the 15 $SU(4)$ generators can be chosen as follows. The 10 generators of the subgroup $Sp(4)$ read

$$T^{1,2,3,4} = \frac{1}{2\sqrt{2}} \begin{pmatrix} \sigma_{1,2,3,0} & 0 \\ 0 & -\sigma^T_{1,2,3,0} \end{pmatrix}, \quad T^{5,6,7} = \frac{1}{2\sqrt{2}} \begin{pmatrix} 0 & \sigma_{1,3,0} \\ \sigma_{1,3,0} & 0 \end{pmatrix}, \quad T^{8,9,10} = \frac{1}{2\sqrt{2}} \begin{pmatrix} 0 & i\sigma_{1,3,0} \\ -i\sigma_{1,3,0} & 0 \end{pmatrix}, \tag{F.3}$$

where σ_i, $i = 1, 2, 3$ denote the Pauli matrices while σ_0 stands for the 2×2 unit matrix. The corresponding coset $SU(4)/Sp(4)$ is then generated by the 5 matrices

$$T^{\hat{1},\hat{2},\hat{3}} = \frac{1}{2\sqrt{2}} \begin{pmatrix} \sigma_{1,2,3} & 0 \\ 0 & \sigma^T_{1,2,3} \end{pmatrix}, \qquad T^{\hat{4}} = \frac{1}{2\sqrt{2}} \begin{pmatrix} 0 & \sigma_2 \\ \sigma_2 & 0 \end{pmatrix}, \qquad T^{\hat{5}} = \frac{1}{2\sqrt{2}} \begin{pmatrix} 0 & i\sigma_2 \\ -i\sigma_2 & 0 \end{pmatrix}. \tag{F.4}$$

The set of generators

$$T^{1,2,3}_{L,R} = \frac{T^{10} \mp T^9}{\sqrt{2}}, \quad \frac{T^7 \mp T^6}{\sqrt{2}}, \quad \frac{T^4 \mp T^3}{\sqrt{2}} \tag{F.5}$$

constitute a $SU(2)_L \times SU(2)_R$ subalgebra of $Sp(4)$, and provide the generators for the electroweak interaction and the custodial symmetry. The generator $T^{\hat{3}}$ is associated with a NGB singlet under $SU(2)_L \times SU(2)_R$, whereas the remaining four generators of the $SU(4)/Sp(4)$ coset correspond to the Higgs bidoublet H, transforming as $(2_L, 2_R)$. Under the diagonal $SU(2)_V$ subgroup, generated by $T^a_L + T^a_R$, the generators $T^{\hat{2}}$, $T^{\hat{4}}$, $T^{\hat{5}}$ transform as a triplet, and $T^{\hat{1}}$ as a singlet.

The external electroweak gauge fields $W^{1,2,3}_\mu$ and B_μ will then couple to the ψ fermions through the combination

$$-i\mathcal{V}_\mu \equiv -ig\left(W^1_\mu T^1_L + W^2_\mu T^2_L + W^3_\mu T^3_L\right) - ig' B_\mu T^3_R \,. \tag{F.6}$$

According to Eq. (8.1.28), the masses of the NGBs that are radiatively induced by the gauging are given by

$$\Delta M^2_H = \Delta M^2_{\hat{1},\hat{2},\hat{4},\hat{5}} = -\frac{3}{4\pi} \times \frac{1}{F_G^2} \int_0^\infty dQ^2\, Q^2\, \Pi^\psi_{V\text{-}A}(-Q^2) \times \frac{1}{16\pi}(3g^2 + g'^2)\,, \qquad \Delta M^2_{\hat{3}} = 0\,. \tag{F.7}$$

Of course, this positive contribution to the Higgs doublet mass should be overcome by a negative one from the top quark couplings, in order to trigger EWSB.

One can estimate quantitatively ΔM_H^2 from the explicit form of the correlator $\Pi^{\psi}_{V-A}(-Q^2)$ as computed in the NJL approximation. If one assumes further that the lightest resonances saturate in good approximation the correlator (see section 8.2.7), the integrand takes the simplified form

$$-Q^2\overline{\Pi}^{\psi}_{V-A}(-Q^2) \simeq F_G^2 + f_A^2 M_A^2 \frac{Q^2}{Q^2+M_A^2} - f_V^2 M_V^2 \frac{Q^2}{Q^2+M_V^2} \ , \tag{F.8}$$

where the expressions of the resonance masses and decay constants are explicitly given sections 8.2.4, 8.2.5 and 8.2.7. Integrating Eq. (F.8) over Q^2 up to the NJL cutoff Λ^2, one obtains

$$-\int_0^{\Lambda^2} dQ^2 Q^2 \overline{\Pi}^{\psi}_{V-A}(-Q^2) \simeq \left(F_G^2 + f_A^2 M_A^2 - f_V^2 M_V^2\right)\Lambda^2 + f_V^2 M_V^4 \ln\frac{\Lambda^2+M_V^2}{M_V^2} - f_A^2 M_A^4 \ln\frac{\Lambda^2+M_A^2}{M_A^2} \ . \tag{F.9}$$

Assuming that the Weinberg sum rules (8.2.59) hold, the first term proportional to Λ^2 vanishes while the remaining terms simplify and lead to

$$\Delta M_H^2 \simeq \frac{3}{64\pi^2}\frac{1}{F_G^2}(3g^2+g'^2)\ f_V^2 M_V^4 \ln\frac{M_A^2}{M_V^2} \ . \tag{F.10}$$

This estimation of ΔM_H^2 is of course relevant only if the $V-A$ correlator is well saturated by the lightest resonances and the Weinberg sum rules hold.

F.2 The $SU(6)$ sector

We decompose the 35 $SU(6)$ generators according to the $SO(6)$ subgroup and the coset $SU(6)/SO(6)$. We denote by λ_a, $a=1,2,\dots 8$, the $SU(3)$ Gell-Mann matrices, and we also define $\lambda_0 = \sqrt{2/3}\, diag(1,1,1)$. A convenient basis for the 15 unbroken generators is given by

$$T^{1,\cdots,8,9} = \frac{1}{2\sqrt{2}}\begin{pmatrix}\lambda_{1,\cdots,8,0} & 0\\ 0 & -\lambda^T_{1,\cdots,8,0}\end{pmatrix}, \quad T^{10,11,12} = \frac{1}{2\sqrt{2}}\begin{pmatrix}0 & \lambda_{2,5,7}\\ \lambda_{2,5,7} & 0\end{pmatrix}, \quad T^{13,14,15} = \frac{1}{2\sqrt{2}}\begin{pmatrix}0 & i\lambda_{2,5,7}\\ -i\lambda_{2,5,7} & 0\end{pmatrix}. \tag{F.11}$$

The eight generators $T^{1,\cdots,8}$ together with T^9 form a $SU(3)_C\times U(1)_D$ maximal subalgebra, that can accommodate the strong interaction gauge group, as well as a part of the hypercharge gauge group $U(1)_Y$, with $Y = T^3_R + D$. The 20 broken generators read

$$\begin{aligned} T^{\hat{1},\cdots,\hat{8}} &= \frac{1}{2\sqrt{2}}\begin{pmatrix}\lambda_{1,\cdots,8} & 0\\ 0 & \lambda^T_{1,\cdots,8}\end{pmatrix}, \\ T^{\hat{9},\cdots,\hat{14}} = \frac{1}{2\sqrt{2}}\begin{pmatrix}0 & \lambda_{1,3,4,6,8,0}\\ \lambda_{1,3,4,6,8,0} & 0\end{pmatrix}, &\quad T^{\hat{15},\cdots,\hat{20}} = \frac{1}{2\sqrt{2}}\begin{pmatrix}0 & i\lambda_{1,3,4,6,8,0}\\ -i\lambda_{1,3,4,6,8,0} & 0\end{pmatrix}. \end{aligned} \tag{F.12}$$

The generators $T^{\hat{1},\cdots,\hat{8}}$ are associated to the NGBs multiplet $O_c \sim 8_0$ under $SU(3)_C\times U(1)_D$, while $T^{\hat{9},\cdots,\hat{20}}$ correspond to the NGBs $(S_c+\overline{S}_c)\sim(6_{4/3}+\overline{6}_{-4/3})$.

The constituent fermions X transform as $(3_{2/3}+\overline{3}_{-2/3})$ under $SU(3)_C\times U(1)_D$, where the normalization of the D-charge is chosen to reproduce the correct hypercharge of top quark partners. Therefore, the external colour gauge fields $G_\mu^{1,\cdots,8}$ and B_μ couple to the X fermions through the combination

$$-ig_c\sqrt{2}G^a_\mu T^a - ig'\frac{4}{\sqrt{3}}B_\mu T^9 \ . \tag{F.13}$$

According to Eq. (8.1.28), the masses of the NGBs that are radiatively induced by the gauging are given by

$$\begin{aligned} \Delta M^2_{O_c} &= \Delta M^2_{\hat{1},\cdots,\hat{8}} = -\frac{3}{4\pi}\times\frac{1}{F^2_{G_c}}\int_0^\infty dQ^2\, Q^2\,\Pi^X_{V\text{-}A}(-Q^2)\times\frac{3}{4\pi}g_s^2 \ , \\ \Delta M^2_{S_c} &= \Delta M^2_{\hat{9},\cdots,\hat{20}} = -\frac{3}{4\pi}\times\frac{1}{F^2_{G_c}}\int_0^\infty dQ^2\, Q^2\,\Pi^X_{V\text{-}A}(-Q^2)\times\frac{1}{4\pi}\left(\frac{10}{3}g_s^2+\frac{16}{9}g'^2\right) \ . \end{aligned} \tag{F.14}$$

The quantitative estimate of the integral of the $V-A$ two-point function is discussed in section 9.2.2.

G Loop functions

The one-loop integrals relevant for our purposes are the one- and two-point functions,

$$\tilde{A}_0(m^2) \equiv i \int \frac{d^4k}{(2\pi)^4} \frac{1}{k^2 - m^2 + i\epsilon} , \qquad \tilde{B}_0(p^2, m^2) \equiv i \int \frac{d^4k}{(2\pi)^4} \frac{1}{(k^2 - m^2)\left[(p+k)^2 - m^2\right]} . \quad \text{(G.1)}$$

[We adopted the notation $\tilde{A}_0$ and $\tilde{B}_0$ in order to avoid confusion with the standard one-loop functions A_0 and B_0 [177], which are defined in Euclidean metric and dimensional regularisation, and differ also by an overall factor $i(16\pi^2)$ in $D = 4$ dimensions.]

In the context of the NJL model, the one-point function is regularised by introducing a cut-off Λ on the Euclidean four-momentum,

$$\tilde{A}_0(m^2) = \frac{\Lambda^2}{16\pi^2}\left[1 - \frac{m^2}{\Lambda^2} \ln \frac{\Lambda^2 + m^2}{m^2}\right] . \quad \text{(G.2)}$$

The zero-momentum two-point function is given by

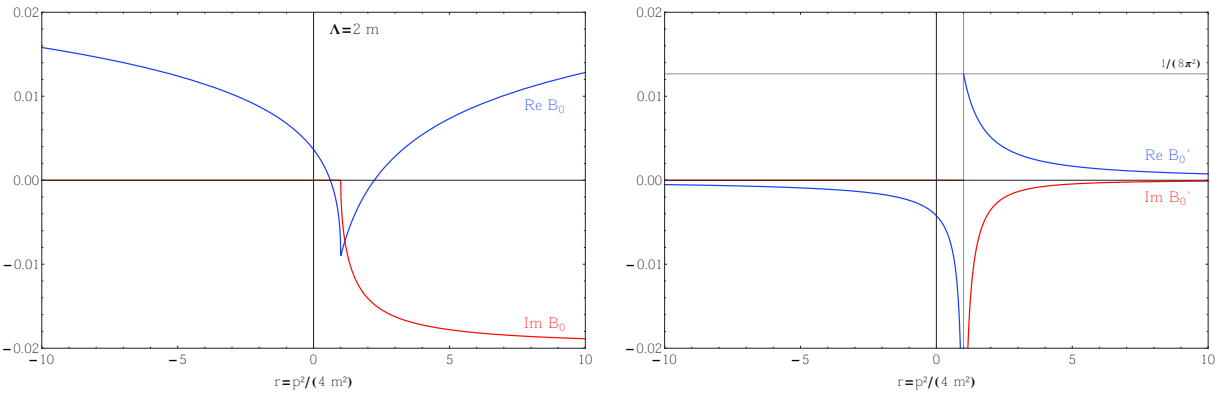

Figure 7: Left panel: Real (blue curve) and imaginary parts (red curve) of $\tilde{B}_0(p^2, m^2)$ [see Eq. (G.4)] as a function of $r = p^2/(4m^2)$. According to figure 8.3, a reasonable value for the second parameter of the $\tilde{B}_0(p^2, m^2)$ function is fixed by the relation $\Lambda = 2m$. The imaginary part becomes non-zero only above the threshold $r = 1$ or equivalently above $p^2 = 4m^2$. Right panel: Real (blue curve) and imaginary parts (red curve) of the derivative of $\tilde{B}_0(p^2, m^2)$ [see Eq. (G.6)] with respect to the parameter r. Due to the cusp in the real part of $\tilde{B}_0(p^2, m^2)$ at the threshold, the corresponding derivative is discontinue. Below $r = 1$, the real part of the derivative tends to $-\infty$ while above $r = 1$, it tends to $1/(8\pi^2)$ [$df(r)/dr$ tends to 4].

$$\tilde{B}_0(0, m^2) = \frac{d\tilde{A}_0(m^2)}{dm^2} = \frac{1}{16\pi^2}\left[\frac{\Lambda^2}{\Lambda^2 + m^2} - \ln\frac{\Lambda^2 + m^2}{m^2}\right] = \frac{1}{16\pi^2}\left[1 - \ln\frac{\Lambda^2}{m^2} + \mathcal{O}\left(\frac{m^2}{\Lambda^2}\right)\right] . \quad \text{(G.3)}$$

For the finite, p^2-dependent part of the two-point function, we adopt the simple regularisation

$$\tilde{B}_0(p^2, m^2) = \tilde{B}_0(0, m^2) + \frac{1}{32\pi^2} f\left(\frac{p^2}{4m^2}\right) , \quad \text{(G.4)}$$

where

$$f(r) = \begin{cases} 4\left(\dfrac{1-r}{r}\right)^{1/2} \arctan\left(\dfrac{r}{1-r}\right)^{1/2} - 4 & \text{(for } 0 < r < 1\text{)} \\ 4\left(\dfrac{r-1}{r}\right)^{1/2} \left[\ln(\sqrt{r} + \sqrt{r-1}) - i\,\dfrac{\pi}{2}\right] - 4 & \text{(for } 1 < r\text{)} \\ 4\left(\dfrac{r-1}{r}\right)^{1/2} \left[\ln(\sqrt{-r} + \sqrt{1-r})\right] - 4 & \text{(for } r < 0\text{) .} \end{cases} \quad \text{(G.5)}$$

We remark that the finite terms are regularisation-dependent, therefore our expression may differ from analogous ones in the NJL literature at order p^2/Λ^2. The first derivative of the two-point function is given by

$$\frac{d\tilde{B}_0(p^2,m^2)}{dp^2} = \frac{1}{4m^2}\frac{d\tilde{B}_0(p^2,m^2)}{dr} = \frac{1}{32\pi^2}\frac{1}{4m^2}\frac{df(r)}{dr} \ , \tag{G.6}$$

where

$$\frac{df(r)}{dr} = \begin{cases} \dfrac{2}{r^2}\left[r - \left(\dfrac{r}{1-r}\right)^{1/2} \arctan\left(\dfrac{r}{1-r}\right)^{1/2}\right] & (\text{for } 0<r<1) \\ \dfrac{2}{r^2}\left[r + \left(\dfrac{r}{r-1}\right)^{1/2} \left(\ln[\sqrt{r}+\sqrt{r-1}] - i\,\dfrac{\pi}{2}\right)\right] & (\text{for } 1<r) \\ \dfrac{2}{r^2}\left[r - \left(\dfrac{r}{r-1}\right)^{1/2} \left[\ln(\sqrt{-r}+\sqrt{1-r})\right]\right] & (\text{for } r<0) \ . \end{cases} \tag{G.7}$$

Note that, contrary to $\tilde{B}_0(p^2,m^2)$, its derivative depends only on one parameter that can be conveniently chosen to be $r = p^2/(4m^2)$. The $\tilde{B}_0(p^2,m^2)$ function and its derivative are displayed in figure 7.

H Two-point correlators of fermion bilinears at one loop

In this appendix we present the detailed computation of the five one-loop two-point functions $\tilde{\Pi}_\phi(q^2,M_f^2) = \tilde{\Pi}^f_\phi(q^2)$ where $\phi = \{S,P,V,A,AP\}$ and M_f is the dynamical mass of the hypercolour fermions $f = \psi, X$. These two-point functions are crucial quantities in the NJL model as they are involved in the estimation of the masses and decay constants of the EW and coloured composite resonances (see sections 8.2 and 9.2). For the two-component Weyl spinors, we follow the conventions of Ref. [262] (ψ and $\psi^\dagger$ propagate in the loops). The Feynman rules appearing in the vertices can be extracted from the currents and densities given respectively in Eqs. (8.1.1) and (8.1.6).

Let us first focus on the EW sector. In the scalar and pseudo-scalar non-singlet channels we get

$$\begin{aligned} i\tilde{\Pi}^{\psi}_{S(P)}(q^2)\delta^{\hat{A}\hat{B}} &= (-1)\int^\Lambda \frac{d^4k}{(2\pi)^4} Tr\left[i\Sigma_0 T^{\hat{A}}\Omega\Gamma_{S(P)}\,\frac{i\sigma\cdot k}{k^2-M_\psi^2}\,iT^{\hat{B}}\Sigma_0\Omega\Gamma^\dagger_{S(P)}\,\frac{i\overline{\sigma}\cdot(k+q)}{(k+q)^2-M_\psi^2}\right] \\ &+ (-1)\int^\Lambda \frac{d^4k}{(2\pi)^4} Tr\left[i\Sigma_0 T^{\hat{A}}\Omega\Gamma_{S(P)}\,\frac{iM_\psi\Sigma_0\Omega}{k^2-M_\psi^2}\,i\Sigma_0 T^{\hat{B}}\Omega\Gamma_{S(P)}\,\frac{iM_\psi\Sigma_0\Omega}{(k+q)^2-M_\psi^2}\right] \end{aligned} \tag{H.1}$$

where the first (second) integral corresponds to the loop involving the kinetic (massive) part of the propagators. The factors $\Gamma_{S(P)} = 1\ (i)$, which distinguish the scalar and pseudo-scalar channels, are a consequence of Eq. (8.1.6). These factors are the equivalent of the γ_5 matrix in Dirac notation and they give a relative sign between the two channels in the second term of Eq. (H.1) exactly like in QCD. Similarly for the vector and axial-vector two points functions one obtains

$$\begin{aligned} i\tilde{\Pi}^{\mu\nu,AB(\hat{A}\hat{B})}_{V(A)}(q^2,M_\psi^2) &= (-1)\int^\Lambda \frac{d^4k}{(2\pi)^4} Tr\left[iT^{A(\hat{A})}\overline{\sigma}^\mu\,\frac{i\sigma\cdot k}{k^2-M_\psi^2}\,iT^{B(\hat{B})}\overline{\sigma}^\nu\,\frac{i\sigma\cdot(k+q)}{(k+q)^2-M_\psi^2}\right] \\ &+ (-1)\int^\Lambda \frac{d^4k}{(2\pi)^4} Tr\left[iT^{A(\hat{A})}\overline{\sigma}^\mu\,\frac{iM_\psi\Sigma_0\Omega}{k^2-M_\psi^2}\,(-iT^{B(\hat{B})})^T\sigma^\nu\,\frac{iM_\psi\Sigma_0\Omega}{(k+q)^2-M_\psi^2}\right] \ , \end{aligned} \tag{H.2}$$

where the functions $\tilde{\Pi}^{\mu\nu,AB(\hat{A}\hat{B})}_{V(A)}(q^2)$ are defined in Eq. (8.2.34). The vector and axial-vector channels only distinguish from the flavour trace [see Eqs. (8.1.2) and (8.1.3)] which again gives a relative sign

between the two channels in the second integral. Finally, for the axial-pseudoscalar two point function one has

$$i\tilde{\Pi}^{\mu,\hat{A}\hat{B}}_{AP}(q^2,M_\psi^2) \equiv i\tilde{\Pi}^{\psi}_{AP}(q^2)p^\mu\delta^{\hat{A}\hat{B}} = (-1)\int^\Lambda \frac{d^4k}{(2\pi)^4}Tr\left[iT^{\hat{A}}\overline{\sigma}^\mu\ \frac{i\sigma\cdot k}{k^2-M_\psi^2}\ iT^{\hat{B}}\Sigma_0\Omega\Gamma_P\ \frac{iM_\psi\Sigma_0\Omega}{(k+q)^2-M_\psi^2}\right]$$
$$+ (-1)\int^\Lambda \frac{d^4k}{(2\pi)^4}Tr\left[iT^{\hat{A}}\cdot\overline{\sigma}^\mu\ \frac{iM_\psi\Sigma_0\Omega}{k^2-M_\psi^2}\ i\Sigma_0T^{\hat{B}}\Omega\Gamma^\dagger_P\ \frac{i\sigma\cdot(k+q)}{(k+q)^2-M_\psi^2}\right] , \tag{H.3}$$

where this time, the integrals contain both the kinetic and the massive parts of the propagators. Evaluating the Lorentz, flavour and hypercolour traces, one can check that the above equations are well consistent with the ones given in table 8.2. Note that the correlators in the singlet channels are obtained by replacing the generators $T^{\hat{A}}$ by the normalised identity matrix T^0_ψ which only changes the flavour tensor structure of the loops, leading to the same result for the two-point functions $\tilde{\Pi}^f_\phi(q^2)$.

Let us now turn to the correlators of the coloured $SU(6)$ sector. The latter can be derive in complete analogy with the ones in the EW sector. Aside the obvious replacements $M_\psi \to M_X$, $\Sigma_0 \to \Sigma_0^c$ and $T^0_\psi \to T^0_X$, the major modification originates from the hypercolour traces. Indeed, the fermions X are in the two-index antisymmetric and traceless representation of $Sp(2N)$. Consequently, the hypercolour traces give a factor $(2N+1)(N-1)$ [instead of $(2N)$ [5]] which of course corresponds to the dimension of the hypercolour $X-$representation. Note that this difference with respect to the EW sector can easily be infer by considering the vector form $X^{\hat{I}}$ $[\hat{I}=1,\cdots,(2N+1)(N-1)]$ define in Eq. (I.6). Then, the one-loop two-point functions $\tilde{\Pi}^X_\phi(q^2)$, summarised in table 9.2, are related to the ones in the EW sector as follow

$$\tilde{\Pi}^{\psi}_\phi(q^2) = \tilde{\Pi}_\phi(q^2,M_\psi^2,2N)\ , \qquad \tilde{\Pi}^{X}_\phi(q^2) = \tilde{\Pi}_\phi[q^2,M_X^2,(2N+1)(N-1)]\ . \tag{H.4}$$

As explained in section 8.2.2, the resummation of the above one-loop two-point functions, at leading order in $1/N$, gives the NJL resummed correlators, $\overline{\Pi}_\phi$, from which the masses and decay constants of the composite resonances are extracted. Usually, in the NJL literature, one considers the T-matrix element $\overline{T}_\phi(q^2)$, rather than $\overline{\Pi}_\phi(q^2)$. As illustrated in Fig. 8, the geometrical series that defines $\overline{T}_\phi$ starts with the four-fermion interaction K_ϕ, instead of the one-loop two-point function $\tilde{\Pi}^f_\phi(q^2)$, see Fig. 8.2. Consequently the T-matrix element is given by

$$\overline{T}_\phi(q^2) = \frac{K_\phi}{1-\,2K_\phi\,\tilde{\Pi}^f_\phi(q^2)}\ . \tag{H.5}$$

The poles of $\overline{T}_\phi(q^2)$ and $\overline{\Pi}_\phi(q^2)$ are of course the same and given by $1 = 2K_\phi\,\tilde{\Pi}^f_\phi(M_\phi^2)$. The only difference comparing Eqs. (8.2.20) and (H.5) comes from the numerators of the series which lead different residues. The residues of $\overline{\Pi}^f_\phi$ have been extensively studied in sections 8.2 and 9.2 while the residues of the T-matrix are the couplings $g_{\phi ff}$ of the physical resonance ϕ to the fundamental fermions f. In analogy with Eq. (8.2.63), these couplings are given by

$$g^2_{\phi ff} = -\lim_{q^2\to M^2_\phi}(q^2-M^2_\phi)\overline{T}_\phi(q^2) = \left[2\,\frac{d\tilde{\Pi}^f_\phi(q^2)}{dq^2}\bigg|_{q^2=M^2_\phi}\right]^{-1}\ . \tag{H.6}$$

They behave like $\simeq 1/\sqrt{N}$, as expected from general large-N considerations.

[5] More precisely, due to the antisymmetry of the hypercolour singlet contractions, the corresponding traces of the EW sector contribute to the one-loop functions with a factor $\pm(2N)$ where the sign corresponds to a particular (massive or kinetic) loop in a given channel. The minus sign is always compensate by the flavour trace which contains in that case $\Sigma_0^2 = -\mathbb{1}$. On the contrary, the hypercolour and flavour contractions in the coloured sectors are symmetric and always positive.

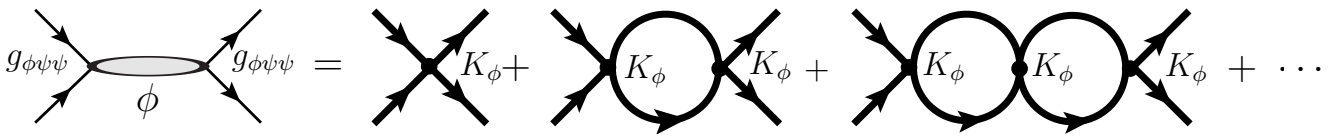

Figure 8: Resummation of leading $1/N$ graphs for a mesonic T-matrix element, $\overline{T}_\phi$, corresponding to a composite meson exchange.

I Relating four-fermion operators by Fierz identities

The couplings of the various four-fermions operators may be related under some assumption on the underlying dynamics (see Refs. [60, 309] for the case of QCD). In this way one can predict the relative strength of the various physical channels (spin-zero versus spin-one, electroweak sector versus colour sector, etc.). We will start from $Sp(2N)$ current-current operators, that encode the ultraviolet dynamics in the 'ladder' approximation, that holds when N is (moderately) large, and we will use Fierz transformations to generate the various $Sp(2N)$ singlet-singlet operators. We will also take the opportunity to summarise general results on Fierz transformations associated to the $SU(N)$ and $Sp(2N)$ groups.

I.1 Hypercolour current-current operators

Let us derive the $Sp(2N)$ current-current operators from the covariant derivatives of the fermions ψ and X. They belong to the fundamental representation, $\psi \sim \square$, and to the two-index, traceless ($X_{ij}\Omega_{ji} = 0$) and antisymmetric ($X_{ij} = -X_{ji}$) representation, $X \sim \begin{smallmatrix}\square\\\square\end{smallmatrix}$. The covariant derivatives read

$$(D^\mu\psi)_i = \left[\partial^\mu\delta_{ij} - ig_{HC}(T^I)_{ij}\mathcal{G}^\mu_I\right]\psi_j \ , \tag{I.1}$$

$$(D^\mu X)_{ij} = \partial^\mu X_{ij} - ig_{HC}\left[(T^I)_{ik}X_{kj} + (T^I)_{jk}X_{ik}\right]\mathcal{G}^\mu_I = \left[\partial^\mu\delta_{ik}\delta_{jl} - ig_{HC}(T^I_X)_{ijkl}\mathcal{G}^\mu_I\right]X_{kl} \ , \tag{I.2}$$

where $\mathcal{G}^\mu_I$ are the hypergluon fields, g_{HC} is the hypercolour gauge coupling. The hypercolour generators acting on ψ_j, $(T^I)_{ij}$, and on X_{kl}, $(T^I_X)_{ijkl} \equiv (T^I)_{ik}\delta_{jl} - \delta_{il}(T^I)_{jk}$, are normalised as

$$\mathrm{Tr}(T^IT^J) \equiv \frac{1}{2}\ell\left(\square\right)\delta^{IJ} = \frac{1}{2}\delta^{IJ} \ , \qquad \mathrm{Tr}(T^I_XT^J_X) \equiv (T^I_X)_{ijkl}(T^J_X)_{klij} \equiv \frac{1}{2}\ell\left(\begin{smallmatrix}\square\\\square\end{smallmatrix}\right)\delta^{IJ} = (N-1)\delta^{IJ} \ . \tag{I.3}$$

The non-derivative terms in Eqs. (I.1) and (I.2) determine the coupling of the technigluons to the $Sp(2N)$-currents $\mathcal{J}^{\mu I}_\psi$ and $\mathcal{J}^{\mu I}_X$, that transform in the adjoint representation $\square\square$,

$$\mathcal{L}_{UV} = g_{HC}\left(\mathcal{J}^{\mu I}_\psi + \mathcal{J}^{\mu I}_X\right)\mathcal{G}_{\mu I} \ , \tag{I.4}$$

where

$$\mathcal{J}^{\mu I}_\psi = \psi\left(\Omega T^I\right)\sigma^\mu\overline{\psi} \ , \qquad \mathcal{J}^{\mu I}_X = 2\ \mathrm{Tr}\left[X\left(\Omega T^I\right)\sigma^\mu\overline{X}\Omega\right] \ . \tag{I.5}$$

Here Ω_{ij} is the $Sp(2N)$ invariant tensor, the trace is taken over $Sp(2N)$ indexes, and the expression of $\mathcal{J}^{\mu I}_X$ has been simplified using $\mathrm{Tr}\left[X\Omega\sigma^\mu\overline{X}\left(\Omega T^I\right)\right] = -\mathrm{Tr}\left[X\left(\Omega T^I\right)\sigma^\mu\overline{X}\Omega\right]$. It is understood that each fermion flavour ψ^a (X^F) behaves equally with respect to the $Sp(2N)$ dynamics, that is, the $Sp(2N)$ currents are flavour singlets. It will be useful to rearrange the fermion components X_{ij} as a vector $X^{\hat{I}}$, with one index $\hat{I}$ of the representation $\begin{smallmatrix}\square\\\square\end{smallmatrix}$,

$$X_{ij} = \sqrt{2}(T^{\hat{I}}\Omega)_{ij}X^{\hat{I}} \ , \qquad X^{\hat{I}} = -\sqrt{2}(\Omega T^{\hat{I}})_{ij}X_{ji} \ , \tag{I.6}$$

so that the second current in Eq. (I.5) can be written in terms of the generators in the representation $\begin{smallmatrix}\square\\\square\end{smallmatrix}$, that are given by $SU(2N)$ structure constants,

$$\mathcal{J}_X^{\mu I} = X^{\hat{I}}(T^I_{\begin{smallmatrix}\square\\\square\end{smallmatrix}})^{\hat{I}\hat{J}}\sigma^\mu\overline{X}^{\hat{J}} \ , \qquad (T^I_{\begin{smallmatrix}\square\\\square\end{smallmatrix}})^{\hat{I}\hat{J}} \equiv if^{\hat{I}I\hat{J}} = 2\mathrm{Tr}\left([T^{\hat{I}},T^I]T^{\hat{J}}\right) \ . \tag{I.7}$$

We assume that the confining strong dynamics can be described, in first approximation, by the exchange of one hypergluon which acquired a dynamical mass, that is the usual NJL assumption in QCD [56]. Then, the strong dynamics is supposed to generate, at leading order, $Sp(2N)$ current-current operators only,

$$\mathcal{L}_{eff} = \frac{\kappa_{UV}}{2N}\left[\mathcal{J}_\psi^{\mu I}\mathcal{J}^I_{\psi\mu} + \mathcal{J}_X^{\mu I}\mathcal{J}^I_{X\mu} + 2\mathcal{J}_\psi^{\mu I}\mathcal{J}^I_{X\mu}\right] \ , \tag{I.8}$$

where $\kappa_{UV}/(2N) \sim g^2_{HC}/\Lambda^2$ stands for the exchange of one 'massive' hypergluon. The large-N scaling of the gauge coupling is $g_{HC} \sim 1/\sqrt{2N}$, while κ_{UV} and Λ are N-independent. The operators in Eq. (I.8) are the product of fermion bilinears in the adjoint representation of $Sp(2N)$. In order to study physical resonances, that correspond to $Sp(2N)$-singlet fermion bilinears, we need to rewrite these operators by using Fierz transformations in the Lorentz, flavour and hypercolour spaces. Note that the last operator in Eq. (I.8) does not contribute to any meson resonance, because by a Fierz transformation one obtains only 'diquark-diquark' operators, such as $(\psi X)(\overline{\psi}\,\overline{X})$, that are not hypercolour singlets and therefore are not relevant for our analysis.

The Fierz transformations of Weyl indices are determined by the well-known identities

$$(\sigma^\mu)_{\alpha\dot\alpha}\,(\sigma_\mu)_{\beta\dot\beta} = -\,(\sigma^\mu)_{\alpha\dot\beta}\,(\sigma_\mu)_{\beta\dot\alpha} = 2\ \varepsilon_{\alpha\beta}\varepsilon_{\dot\alpha\dot\beta} \ . \tag{I.9}$$

The $SU(N)$ and $Sp(2N)$ Fierz transformations, relevant for flavour and hypercolour indexes respectively, are presented in sections I.3 and I.4 below.

I.2 General properties of Fierz transformations

In this section we derive general properties of the coefficients in Fierz transformations. For a given irreducible representation R of the symmetry group under consideration, let us construct the tensor products $\mathcal{R}\otimes\overline{\mathcal{R}} = \sum_{\mathcal{A}}\mathcal{R}_{\mathcal{A}}$ and $\mathcal{R}\otimes\mathcal{R} = \sum_{\mathcal{A}}\mathcal{R}_{\mathcal{A}}$, where the index $\mathcal{A}$ runs over the irreducible representations contained in the product. One can choose [310] a set of matrices $\{\Gamma^{\mathcal{A}}_a\}$ ($\{\tilde\Gamma^{\mathcal{A}}_a\}$), with $a = 1,\cdots,\dim\mathcal{R}_{\mathcal{A}}$, which form a basis of the vector space $\mathcal{R}\otimes\overline{\mathcal{R}}$ ($\mathcal{R}\otimes\mathcal{R}$). In the following, we will add a tilde wherever there is no conjugate in the tensor product. Such matrices have size $\dim\mathcal{R}\times\dim\mathcal{R}$ and satisfy the orthogonality relations

$$\mathrm{Tr}(\Gamma^{\mathcal{A}}_a\Gamma^{\mathcal{B}}_b) = \alpha\ \delta^{\mathcal{A}\mathcal{B}}g^{\mathcal{A}}_{ab} \ , \qquad \mathrm{Tr}(\tilde\Gamma^{\mathcal{A}}_a\tilde\Gamma^{\mathcal{B}\dagger}_b) = \alpha\ \delta^{\mathcal{A}\mathcal{B}}g^{\mathcal{A}}_{ab} \ , \tag{I.10}$$

where α is a normalisation constant and $g^{\mathcal{A}}_{ab}$ is a generic metric (in particular, $g^{\mathcal{A}}_{ab}g^{\mathcal{A}bc} = \delta^c_a$ and $\Gamma^{a\mathcal{A}} \equiv g^{\mathcal{A}ab}\Gamma^{\mathcal{A}}_b$). Any $\dim\mathcal{R}\times\dim\mathcal{R}$ matrix M can be decomposed on the basis $\{\Gamma^{\mathcal{A}}_a\}$ as

$$M = \sum_{\mathcal{A}}\sum_a c^{a\mathcal{A}}\Gamma^{\mathcal{A}}_a = \sum_{\mathcal{A}}^{\sim}\sum_a d^{a\mathcal{A}}\tilde\Gamma^{\mathcal{A}}_a \ , \qquad c^{a\mathcal{A}} = \frac{1}{\alpha}\mathrm{Tr}(\Gamma^{a\mathcal{A}}M) \ , \qquad d^{a\mathcal{A}} = \frac{1}{\alpha}\mathrm{Tr}(\tilde\Gamma^{a\mathcal{A}\dagger}M) \ . \tag{I.11}$$

Replacing the explicit form of $c^{a\mathcal{A}}$ and $d^{a\mathcal{A}}$ in M we obtain the completeness relations

$$\sum_{\mathcal{A}}\sum_a(\Gamma^{a\mathcal{A}})_{ij}(\Gamma^{\mathcal{A}}_a)_{kl} = \sum_{\mathcal{A}}^{\sim}\sum_a(\tilde\Gamma^{a\mathcal{A}})_{ij}(\tilde\Gamma^{\mathcal{A}\dagger}_a)_{kl} = \alpha\ \delta_{il}\delta_{kj} \ . \tag{I.12}$$

which are relevant to derive the Fierz coefficients.

Let us consider an interaction among four objects transforming as $(\mathcal{R}\otimes\overline{\mathcal{R}})_{\mathcal{A}}(\mathcal{R}\otimes\overline{\mathcal{R}})_{\mathcal{A}}$, where the subscripts indicate that each pair is contracted in the component $\mathcal{R}_{\mathcal{A}}$. Then, the Fierz transformations can be written as

$$\sum_a(\Gamma^{a\mathcal{A}})_{ij}(\Gamma^{\mathcal{A}}_a)_{kl} = \sum_{\mathcal{B}}C_{\mathcal{A}\mathcal{B}}\sum_b(\Gamma^{b\mathcal{B}})_{il}(\Gamma^{\mathcal{B}}_b)_{kj} = \sum_{\mathcal{B}}^{\sim}D_{\mathcal{A}\mathcal{B}}\sum_b(\tilde\Gamma^{b\mathcal{B}})_{ik}(\tilde\Gamma^{\mathcal{B}\dagger}_b)_{jl} \ , \tag{I.13}$$

where $C_{\mathcal{AB}}$ and $D_{\mathcal{AB}}$ are the Fierz coefficients for the channels $j \leftrightarrow l$ and $j \leftrightarrow k$, respectively. In terms of 'quarks' $\sim \mathcal{R}$ and 'antiquarks' $\sim \overline{\mathcal{R}}$, one can dub them the 'quark-antiquark' and the 'quark-quark' channels, respectively. Analogously, for the interaction $(\mathcal{R}\otimes\mathcal{R})_{\mathcal{A}}(\overline{\mathcal{R}}\otimes\overline{\mathcal{R}})_{\overline{\mathcal{A}}}$, the Fierz transformations read

$$\sum_a (\tilde{\Gamma}^{a\mathcal{A}})_{ij}(\tilde{\Gamma}^{\mathcal{A}\dagger}_a)_{kl} = \sum_{\mathcal{B}} \tilde{C}_{\mathcal{AB}} \sum_b (\Gamma^{b\mathcal{B}})_{il}(\Gamma^{\mathcal{B}T}_b)_{kj} = \sum_{\mathcal{B}} \tilde{D}_{\mathcal{AB}} \sum_b (\Gamma^{b\mathcal{B}})_{ik}(\Gamma^{\mathcal{B}}_b)_{jl} \ , \tag{I.14}$$

One can derive several, general constraints on the Fierz-coefficient matrices $C, D, \tilde{C}, \tilde{D}$. Applying twice a Fierz transformation on the same indexes the original contraction is recovered, therefore one obtains

$$\sum_{\mathcal{B}} C_{\mathcal{AB}} C_{\mathcal{BC}} = \delta_{\mathcal{AC}} \ , \qquad \sum_{\mathcal{B}}^{\sim} D_{\mathcal{AB}} \tilde{D}_{\mathcal{BC}} = \delta_{\mathcal{AC}} \ , \qquad \sum_{\mathcal{B}} \tilde{C}_{\mathcal{AB}} D_{\mathcal{BC}} = s_{\mathcal{A}} \delta_{\mathcal{AC}} \ , \qquad \sum_{\mathcal{B}} \tilde{D}_{\mathcal{AB}} D_{\mathcal{BC}} = \delta_{\mathcal{AC}} \ , \tag{I.15}$$

where $s_{\mathcal{A}} = +1$ (-1) when the representation $\mathcal{R}_{\mathcal{A}}$ belongs to the (anti-)symmetric part of the tensor product $\mathcal{R} \otimes \mathcal{R}$, and correspondingly the matrices $\tilde{\Gamma}^{\mathcal{A}}_a$ are (anti-)symmetric. Therefore, one has $C = C^{-1}$, while both $\tilde{C}$ and $\tilde{D}$ can be fully determined in terms of the matrix D. The contraction associated to the singlet representation, $\mathcal{R}_\bullet \subset \mathcal{R}\otimes\overline{\mathcal{R}}$, can be chosen as $\Gamma^\bullet_{ij} = \delta_{ij}\sqrt{\alpha/\mathrm{dim}\mathcal{R}}$. Therefore, Eq. (I.12) determines the first row of C and D,

$$C_{\bullet\mathcal{A}} = \frac{1}{\mathrm{dim}\mathcal{R}} \ , \quad \forall\ \mathcal{R}_{\mathcal{A}} \subset \mathcal{R}\otimes\overline{\mathcal{R}} \ , \qquad\qquad D_{\bullet\mathcal{A}} = \frac{s_{\mathcal{A}}}{\mathrm{dim}\mathcal{R}} \ , \quad \forall\ \mathcal{R}_{\mathcal{A}} \subset \mathcal{R}\otimes\mathcal{R} \ . \tag{I.16}$$

Indeed, from Eq. (I.13) one can obtain explicit expressions of the Fierz coefficients,

$$C_{\mathcal{AB}} = \frac{1}{\alpha^2}\sum_a \mathrm{Tr}[\Gamma^{a\mathcal{A}}\Gamma^{\mathcal{B}}_b\Gamma^{\mathcal{A}}_a\Gamma^{b\mathcal{B}}] \ , \qquad\qquad D_{\mathcal{AB}} = \frac{1}{\alpha^2}\sum_a \mathrm{Tr}[\Gamma^{a\mathcal{A}}(\tilde{\Gamma}^{\mathcal{B}}_b)^T(\Gamma^{\mathcal{A}}_a)^T\tilde{\Gamma}^{b\mathcal{B}\dagger}] \ , \tag{I.17}$$

which are valid for every b. The direct computation of such expressions, however, may be very complicated in practice. By summing over b the two identities in Eq. (I.17), one obtains quantities invariant under the exchanges $\mathcal{A} \leftrightarrow \mathcal{B}$ and $C \leftrightarrow C^{-1}$ $(D \leftrightarrow D^{-1})$, therefore one concludes that

$$C_{\mathcal{AB}}\ \mathrm{dim}\mathcal{R}_{\mathcal{B}} = C_{\mathcal{BA}}\ \mathrm{dim}\mathcal{R}_{\mathcal{A}} \ , \qquad\qquad D_{\mathcal{AB}}\ \mathrm{dim}\mathcal{R}_{\mathcal{B}} = (D^{-1})_{\mathcal{BA}}\ \mathrm{dim}\mathcal{R}_{\mathcal{A}} \ . \tag{I.18}$$

In particular, Eq. (I.16) implies $C_{\mathcal{A}\bullet} = C_{\bullet\mathcal{A}}\ \mathrm{dim}\mathcal{R}_{\mathcal{A}} = \mathrm{dim}\mathcal{R}_{\mathcal{A}}/\mathrm{dim}\mathcal{R}$.

In the special case of a (pseudo-)real representation $\mathcal{R}$, taking $\psi \sim \mathcal{R}$ and $\psi^\dagger \sim \overline{\mathcal{R}}$, one has $\overline{\psi}_i \equiv \psi^\dagger_j(\Omega_\epsilon)_{ji} \sim \mathcal{R}$, where Ω_ϵ is the invariant tensor establishing the equivalence of $\mathcal{R}$ and $\overline{\mathcal{R}}$, that is symmetric $(\epsilon = +1)$ or antisymmetric $(\epsilon = -1)$ in the case of real or pseudoreal representations, respectively. Therefore, the set of matrices $\{\Gamma^{\mathcal{A}}_a\}$ and $\{\tilde{\Gamma}^{\mathcal{A}}_a\}$ can be identified, according to $\tilde{\Gamma}^{\mathcal{A}}_a = \Gamma^{\mathcal{A}}_a\Omega_\epsilon$. In addition, the equality $\Omega_\epsilon\tilde{\Gamma}^{\mathcal{A}\dagger}_a = \epsilon\tilde{\Gamma}^{\mathcal{A}}_a\Omega_\epsilon$ holds, that implies in particular $(\psi\tilde{\Gamma}^{\mathcal{A}}_a\psi)^\dagger = \epsilon\overline{\psi}\tilde{\Gamma}^{\mathcal{A}}_a\overline{\psi}$. Then, it is convenient to rewrite the Fierz transformations in Eq. (I.13) [or, equivalently, Eq. (I.14)] in terms of the interaction $(\mathcal{R}\otimes\mathcal{R})_{\mathcal{A}}(\mathcal{R}\otimes\mathcal{R})_{\mathcal{A}}$,

$$\sum_a (\tilde{\Gamma}^{a\mathcal{A}})_{ij}(\tilde{\Gamma}^{\mathcal{A}}_a)_{kl} = \sum_{\mathcal{B}}^{\sim} C_{\mathcal{AB}} \sum_b (\tilde{\Gamma}^{b\mathcal{B}})_{il}(\tilde{\Gamma}^{\mathcal{B}}_b)_{kj} = \epsilon \sum_{\mathcal{B}}^{\sim} D_{\mathcal{AB}} \sum_b (\tilde{\Gamma}^{b\mathcal{B}})_{ik}(\tilde{\Gamma}^{\mathcal{B}}_b)_{jl} \ . \tag{I.19}$$

It follows immediately that the two sets of Fierz coefficients are related as

$$\epsilon D_{\mathcal{AB}} = s_{\mathcal{A}} C_{\mathcal{AB}} s_{\mathcal{B}} \ , \tag{I.20}$$

where $s_{\mathcal{A},\mathcal{B}} = \pm 1$ denotes, once again, the (anti-)symmetry of $\mathcal{R}_{\mathcal{A},\mathcal{B}}$ within $\mathcal{R}\otimes\mathcal{R}$. In this (pseudo-)real case the singlet contraction corresponds to $\tilde{\Gamma}^\bullet_{ij} = (\Omega_\epsilon)_{ij}\sqrt{\alpha/\mathrm{dim}\mathcal{R}}$, therefore $s_\bullet = \epsilon$, and one recovers Eq. (I.16).

I.3 $SU(N)$ Fierz transformations

Let us derive the Fierz transformations associated to the fundamental representation of $SU(N)$ (see e.g. [59]). In our model they are relevant for the flavour indexes, as the fermions ψ^a and X^f transform in the fundamental of $SU(4)$ and $SU(6)$, respectively.

In the 'quark-antiquark' channel, $(\overline{N}_a N^b)(\overline{N}_c N^d) \to (\overline{N}_a N^d)(\overline{N}_c N^b)$, one can employ the completeness relation of Eq. (I.12) for $\overline{N} \otimes N$,

$$\sum_{I=1}^{N^2-1} (T^I)^a{}_b (T^I)^c{}_d + (T^0)^a{}_b (T_0)^c{}_d = \frac{1}{2}\delta^a{}_d \delta^c{}_b \ , \tag{I.21}$$

where T^I are the (N^2-1) generators of $SU(N)$, $T^0 \equiv \mathbb{1}/\sqrt{2N}$, and $\alpha = \ell(N)/2 = \ell(\overline{N})/2 = 1/2$ as we adopted the normalisation $\mathrm{Tr}(T^I T^J) = \delta^{IJ}/2$. The first row of the Fierz-coefficient matrix $C_{\mathcal{AB}}$ is simply obtained by reshuffling the indexes in Eq. (I.21),

$$(T^0)^a{}_b (T^0)^c{}_d = \frac{1}{N}(T^0)^a{}_d (T^0)^c{}_b + \frac{1}{N}\sum_I (T^I)^a{}_d \, (T^I)^c{}_b \ , \tag{I.22}$$

The second row can be determined by imposing $C^2 \equiv \mathbb{1}$, as follows from Eq. (I.15). Thus, one concludes that

$$\begin{pmatrix} (T^0)^a{}_b (T^0)^c{}_d \\ \sum_I (T^I)^a{}_b \, (T^I)^c{}_d \end{pmatrix} = C \begin{pmatrix} (T^0)^a{}_d (T^0)^c{}_b \\ \sum_I (T^I)^a{}_d \, (T^I)^c{}_b \end{pmatrix} = \begin{pmatrix} \frac{1}{N} & \frac{1}{N} \\ \frac{N^2-1}{N} & -\frac{1}{N} \end{pmatrix} \begin{pmatrix} (T^0)^a{}_d (T^0)^c{}_b \\ \sum_I (T^I)^a{}_d \, (T^I)^c{}_b \end{pmatrix} \ . \tag{I.23}$$

In the 'quark-quark' channel, $(\overline{N}_a N^b)(\overline{N}_c N^d) \to (\overline{N}_a \overline{N}_c)(N^b N^d)$, one needs also the completeness relation for $N \otimes N$, that involves $N(N+1)/2$ symmetric matrices Γ^I_S, and $N(N-1)/2$ antisymmetric matrices Γ^I_A,

$$\sum_{I=1}^{N(N+1)/2} (\Gamma^{I\dagger}_S)^{ab} (\Gamma^I_S)_{cd} + \sum_{I=1}^{N(N-1)/2} (\Gamma^{I\dagger}_A)^{ab} (\Gamma^I_A)_{cd} = \frac{1}{2}\delta^a{}_d \delta^b{}_c \ . \tag{I.24}$$

A convenient basis of (anti-)symmetric matrices is provided by $\Gamma^0 \equiv \Sigma_\epsilon T^0$, $\Gamma^I \equiv \Sigma_\epsilon T^I$, and $\Gamma^{\hat{I}} \equiv \Sigma_\epsilon T^{\hat{I}}$, where $(\Sigma_\epsilon)_{ab}$ is the invariant tensor of a maximal $SU(N)$ subgroup, that is $SO(N)$ in the case $\epsilon = +1$, and $Sp(N)$ in the case $\epsilon = -1$ (present only for N even). Here the index I runs over the subgroup generators only, and the index $\hat{I}$ spans the coset. When $\epsilon = +1(-1)$, Σ_ϵ is a symmetric (antisymmetric) matrix and, according to Eq. (8.1.2), Γ^0 and $\Gamma^{\hat{I}}$ are symmetric (antisymmetric), while Γ^I are antisymmetric (symmetric). Using this basis for the matrices $\Gamma^I_{S,A}$, one can construct explicitly the Fierz-coefficient matrix $D_{\mathcal{AB}}$,

$$\begin{pmatrix} (T^0)^a{}_b (T^0)^c{}_d \\ \sum_I (T^I)^a{}_b \, (T^I)^c{}_d \end{pmatrix} = D \begin{pmatrix} \sum_I (\Gamma^{I\dagger}_S)^{ac} (\Gamma^I_S)_{bd} \\ \sum_I (\Gamma^{I\dagger}_A)^{ac} (\Gamma^I_A)_{bd} \end{pmatrix} = \begin{pmatrix} \frac{1}{N} & -\frac{1}{N} \\ \frac{N-1}{N} & \frac{N+1}{N} \end{pmatrix} \begin{pmatrix} \sum_I (\Gamma^{I\dagger}_S)^{ac} (\Gamma^I_S)_{bd} \\ \sum_I (\Gamma^{I\dagger}_A)^{ac} (\Gamma^I_A)_{bd} \end{pmatrix} \ . \tag{I.25}$$

For example, the first row of $D_{\mathcal{AB}}$ can be obtained from Eq. (I.22) by contracting with $(\Sigma_\epsilon)^{dd'} (\Sigma_\epsilon)_{c'c}$, and inverting appropriate pairs of (anti-)symmetrised indexes: the result agrees with Eq. (I.16). The second row is determined e.g. by Eq. (I.18), up to an overall sign, that can be fixed once again by (anti-)symmetrising over appropriate indexes.

I.4 $Sp(2N)$ Fierz transformations

Let us derive the Fierz transformations associated to the hypercolour representations of the fermions ψ_i and X_{ij}, that is, $\square$ and $\begin{smallmatrix}\square\\\square\end{smallmatrix}$ respectively. The group $Sp(2N)$ is a subgroup of $SU(2N)$, corresponding to the vacuum direction $\Sigma_- \equiv \Omega$, defined in Eq. (8.2.3). Taking advantage of Eq. (8.1.2), one

can decompose the $U(2N)$ completeness relation (I.21) in two parts, corresponding to the $Sp(2N)$ subalgebra and its coset,

$$\sum_{I=1}^{N(2N+1)} (T^I)_{ij}\,(T^I)_{kl} \;=\; \frac{1}{4}(\delta_{il}\delta_{kj}-\Omega_{ik}\Omega_{jl}) \;:\qquad Sp(2N)\;, \tag{I.26}$$

$$\sum_{\hat{I}=1}^{(2N+1)(N-1)} (T^{\hat{I}})_{ij}\,(T^{\hat{I}})_{kl}+(T^0)_{ij}\,(T^0)_{kl} \;=\; \frac{1}{4}(\delta_{il}\delta_{kj}+\Omega_{ik}\Omega_{jl}) \;:\qquad U(2N)/Sp(2N)\;. \tag{I.27}$$

The product of two fundamental representations of $Sp(2N)$ reads

$$\square\times\square = \bullet_a \;+\; \square\!\square_s \;+\; \begin{array}{l}\square\!\square\\ \square\end{array}_a\;, \tag{I.28}$$

where the bullet stands for the singlet and the subscripts indicate whether the contraction is symmetric or antisymmetric under the exchange of the two factors. These representations have dimensions

$$d\,(\square)=2N\;,\qquad d\,(\bullet)=1\;,\qquad d\,(\square\!\square)=N(2N+1)\;,\qquad d\left(\begin{array}{l}\square\!\square\\ \square\end{array}\right)=N(2N-1)-1=(2N+1)(N-1)\;. \tag{I.29}$$

The two indexes in $\square_i\square_j$ are contracted by an appropriate set of (anti-)symmetric matrices $\tilde{\Gamma}^a_{\mathcal{A}}$, that can be conveniently chosen as

$$\tilde{\Gamma}_\bullet \equiv \Omega T^0=\frac{\Omega}{\sqrt{4N}}\;,\qquad \tilde{\Gamma}^I_{\square\!\square}\equiv\Omega T^I\;,\qquad \tilde{\Gamma}^{\hat{I}}_{\begin{array}{l}\square\!\square\\ \square\end{array}}\equiv\Omega T^{\hat{I}}\;, \tag{I.30}$$

in one-to-one correspondence with the generators of $U(2N)$. Multiplying (I.26) and (I.27) by $\Omega_{mi}\Omega_{nk}$ one obtains useful equalities to determine the Fierz transformations of $(\square_i\square_j)(\square_k\square_l)$. Thus, the matrix of Fierz coefficients for the channel $(il)(kj)$, $C_{\mathcal{AB}}$, can be fully determined in agreement with the general results of section I.2:

$$\begin{pmatrix} (\Omega T^0)_{ij}(\Omega T^0)_{kl} \\ \sum_I (\Omega T^I)_{ij}(\Omega T^I)_{kl} \\ \sum_{\hat{I}} (\Omega T^{\hat{I}})_{ij}(\Omega T^{\hat{I}})_{kl} \end{pmatrix} = \begin{pmatrix} \frac{1}{2N} & \frac{1}{2N} & \frac{1}{2N} \\ \frac{2N+1}{2} & -\frac{1}{2} & \frac{1}{2} \\ \frac{(2N+1)(N-1)}{2N} & \frac{N-1}{2N} & -\frac{N+1}{2N} \end{pmatrix} \begin{pmatrix} (\Omega T^0)_{il}(\Omega T^0)_{kj} \\ \sum_I (\Omega T^I)_{il}(\Omega T^I)_{kj} \\ \sum_{\hat{I}} (\Omega T^{\hat{I}})_{il}(\Omega T^{\hat{I}})_{kj} \end{pmatrix}\;, \tag{I.31}$$

According to Eq. (I.20), the Fierz coefficients in the channel $(ik)(jl)$ are given by $D_{\mathcal{AB}}=-C_{\mathcal{AB}}$ when both $\mathcal{A}$ and $\mathcal{B}$ are (anti-)symmetric contractions, and $D_{\mathcal{AB}}=C_{\mathcal{AB}}$ otherwise.

We can now determine the coefficients $\kappa_{A,C,D}$ of the four-fermion operators in the ψ-sector, which are defined by Eqs. (8.2.14) and (8.2.30), assuming that the dynamics is well approximated by the ψ-sector current-current operator of Eq. (I.8), with coefficient κ_{UV}. Note that the 't Hooft operator with coefficient κ_B, defined by the second line of Eq. (8.2.14), is not generated by the current-current interaction, as the latter preserves the anomalous $U(1)_\psi$ symmetry, therefore the size of κ_B is unrelated to κ_{UV}. On the contrary, the size of κ_A (of $\kappa_{C,D}$) can be related to κ_{UV} by performing the pertinent set of Fierz transformations over Lorentz, $SU(4)$ flavour, and $Sp(2N)$ hypercolour indexes. Naively, with this procedure the current-current operator is recast into a sum over several operators: those with two hypercolour-singlet fermion bilinears, that correspond to physical meson states, plus those with two hypercolour-non-singlet fermion bilinears. The former operators receive a coefficient

$$\kappa_A=\kappa_C=\kappa_D=\frac{2N+1}{4N}\kappa_{UV}\;. \tag{I.32}$$

However, the latter operators could also contribute to these couplings, by further Fierz transformations, therefore, the above equalities cannot be firmly established on this basis. Fortunately, there exists a unique way to express the current-current operator in terms of hypercolour-singlet fermion bilinears only, by using the identity

$$\sum_I \left(\Omega T^I\right)_{ij}\left(\Omega T^I\right)_{kl}=\frac{1}{4}\left(\Omega_{il}\Omega_{kj}-\Omega_{ik}\Omega_{jl}\right)\;, \tag{I.33}$$

that is obtained e.g. by considering the first row of Eq. (I.31) and symmetrising over the indexes (il), or equivalently by multiplying the $Sp(2N)$ completeness relation (I.26) by $\Omega_{i'i}\Omega_{k'k}$. Employing this relation we obtain

$$\kappa_A = \kappa_C = \kappa_D = \frac{1}{2}\kappa_{UV} \ . \tag{I.34}$$

Therefore, in the current-current approximation, the scalar coupling κ_A and the vector couplings $\kappa_{C,D}$ are equal and N-independent when N becomes large, as κ_{UV} is. Notice that the naive relations in Eq. (I.32) were correct al leading order in $1/N$. The equality between vector and scalar couplings is common with the standard NJL model for QCD [259].

Let us now analyse the product of two $Sp(2N)$ two-index traceless antisymmetric representations $\square\!\!\square$, that is relevant for the colour sector of our model. The tensor product,

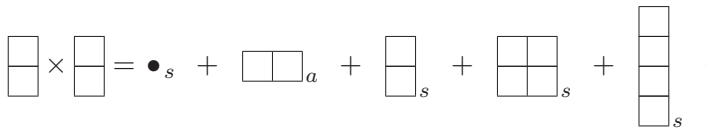

(I.35)

contains three four-index representations, of dimension

$$d\left(\square\!\square\,\square\!\square\right) = \frac{N}{3}\left(4N^3-7N+3\right),\ d\left(\begin{array}{c}\square\\\square\\\square\end{array}\right) = \frac{N}{6}\left(4N^3-12N^2-N+3\right),\ d\left(\begin{array}{cc}\square\!\square\\\square\!\square\end{array}\right) = \frac{1}{2}\left(4N^4-4N^3-9N^2+N+2\right). \tag{I.36}$$

These numbers can be derived taking into account the symmetry properties of each representation in Eq. (I.35), and subtracting the dimensions of the smaller representations, obtained by taking traces, as given in Eq. (I.29). The indexes in $\square\!\square_{ij}\,\square\!\square_{kl}$ are contracted into the representation $\mathcal{R}$ by a set of tensors $(\tilde{\Gamma}^a_{\mathcal{R}})_{ijkl}$, with $a = 1,\ldots,\dim\mathcal{R}$. Equivalently, one can use a single index running over the $(2N+1)(N-1)$ components of $\square\!\square$,

$$X_{li}(\tilde{\Gamma}^a_{\mathcal{R}})_{ijkl}X_{jk} = X_{\hat{I}}(\tilde{\Gamma}^a_{\mathcal{R}})_{\hat{I}\hat{J}}X_{\hat{J}} \ . \tag{I.37}$$

where X_{ij} and $X_{\hat{I}}$ are related by Eq. (I.6). In this notation, the completeness relation reads

$$\sum_{\mathcal{R}}\sum_{a}(\tilde{\Gamma}^a_{\mathcal{R}})_{\hat{I}\hat{J}}(\tilde{\Gamma}^a_{\mathcal{R}})_{\hat{K}\hat{L}} = \frac{1}{2}\ell(\square\!\square)\delta_{\hat{I}\hat{L}}\delta_{\hat{K}\hat{J}} = (N-1)\delta_{\hat{I}\hat{L}}\delta_{\hat{K}\hat{J}} \ , \qquad \mathcal{R} = \bullet, \square\!\square, \square\!\square\!\square, \square\!\square\,\square\!\square, \begin{array}{c}\square\!\square\\\square\end{array}, \begin{array}{cc}\square\!\square\\\square\!\square\end{array} \ . \tag{I.38}$$

In fact, the set of matrices $\{\tilde{\Gamma}^a_{\mathcal{R}}\}$ corresponds to the generators of the group $U\left[(2N+1)(N-1)\right]$, normalised as $\mathrm{Tr}[\tilde{\Gamma}^a_{\mathcal{R}}\tilde{\Gamma}^b_{\mathcal{R}'}] = \frac{1}{2}\ell(\square\!\square)\delta_{\mathcal{R}\mathcal{R}'}\delta^{ab}$. Let us provide the explicit form of these matrices for the smallest representations. The singlet contraction is given by

$$(\tilde{\Gamma}_\bullet)_{ijkl} = \frac{1}{\sqrt{2N+1}}\Omega_{ij}\Omega_{kl} \ , \qquad (\tilde{\Gamma}_\bullet)_{\hat{I}\hat{J}} = \frac{1}{\sqrt{2N+1}}\delta_{\hat{I}\hat{J}} \ . \tag{I.39}$$

The adjoint contraction, already employed in section I.1, is given by

$$(\tilde{\Gamma}^K_{\square\!\square})_{ijkl} = (\Omega T^I)_{ij}\Omega_{kl} - \Omega_{ij}(\Omega T^I)_{kl} \ , \qquad (\tilde{\Gamma}^K_{\square\!\square})_{\hat{I}\hat{J}} = -if^{\hat{I}\hat{J}K} = -2\mathrm{Tr}([T^{\hat{I}},T^{\hat{J}}]T^K) \ . \tag{I.40}$$

The two-index antisymmetric contraction has a similar structure, with the unbroken generators T^I replaced by the broken ones $T^{\hat{I}}$,

$$(\tilde{\Gamma}^{\hat{K}}_{\begin{array}{c}\square\\\square\end{array}})_{ijkl} = (\Omega T^{\hat{K}})_{ij}\Omega_{kl} + \Omega_{ij}(\Omega T^{\hat{K}})_{kl} \ , \qquad (\tilde{\Gamma}^{\hat{K}}_{\begin{array}{c}\square\\\square\end{array}})_{\hat{I}\hat{J}} = d^{\hat{I}\hat{J}\hat{K}} = 2\mathrm{Tr}(\{T^{\hat{I}},T^{\hat{J}}\}T^{\hat{K}}) \ . \tag{I.41}$$

One can easily check that the symmetry properties of the contractions in Eqs. (I.39), (I.40) and (I.41) agree with those indicated in Eq. (I.35).

The singlet Fierz coefficients in the channel $(\hat{I}\hat{L})(\hat{K}\hat{J})$, $C_{\bullet\mathcal{R}}$, are easily determined from the completeness relation (I.38), in agreement with Eq. (I.16). The coefficients $C_{\mathcal{R}\bullet}$ are determined in turn by Eq. (I.18). Thus, we can write

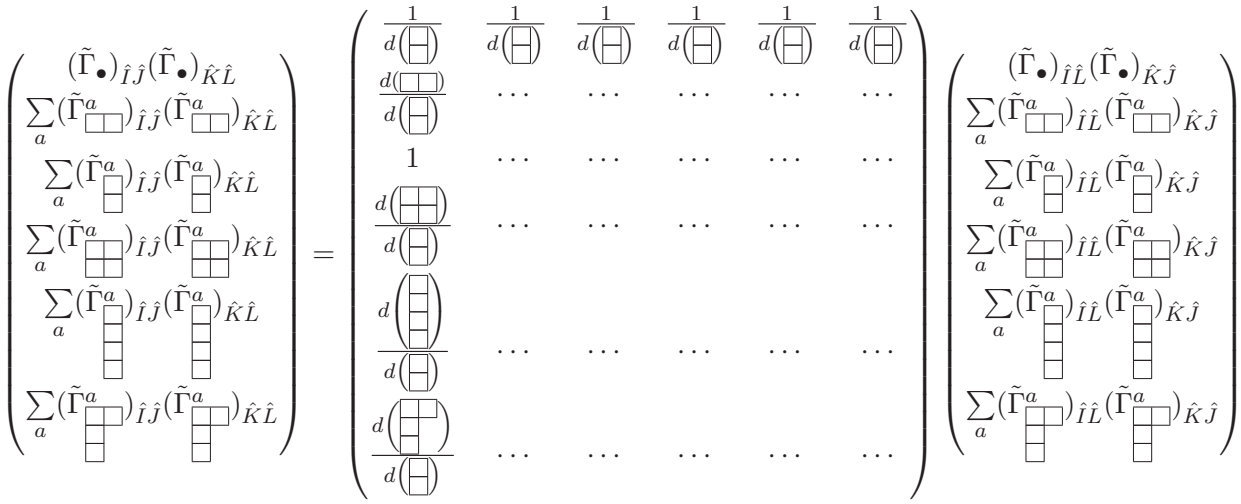

(I.42)

One needs further algebraic manipulations to determine the non-singlet Fierz coefficients, that are not needed for our purposes. The Fierz coefficients $D_{\mathcal{R}\mathcal{R}'}$ in the channel $(\hat{I}\hat{K})(\hat{J}\hat{L})$ are determined by Eq. (I.20), with $\epsilon = +1$ as $\square$ is a real representation. Since we aim to rewrite the X-sector current-current operator of Eq. (I.8) in terms of hypercolur-singlet fermion bilinears, the relevant Fierz coefficients are

$$C_{\square\square\,\bullet} = -D_{\square\square\,\bullet} = \frac{N}{N-1} \ . \tag{I.43}$$

In analogy with the above procedure in the ψ-sector, one can try to determine the coefficients $\kappa_{A6,C6,D6}$ of the four-fermion operators in the X-sector, which are defined by Eqs. (9.2.1) and (9.2.20). If one applies a pertinent Fierz transformation, over Lorentz, $SU(6)$ and $Sp(2N)$ indexes, to the X-sector current-current operator in Eq. (I.8), one obtains

$$\kappa_{A6} = \kappa_{C6} = \kappa_{D6} = \kappa_{UV} \ . \tag{I.44}$$

This indicates that the scalar and vector operators of the coloured sector receive the same coefficient, that is twice as large as for the corresponding operators of the electroweak sector, see Eq. (I.34). However, at the same time κ_{UV} also contributes to other operators, that involve hypercolour-non-singlet fermion bilinears, therefore the above relations are ambiguous, as they rely on a specific recasting of the current-current operator, that is not unique. Another possible recasting is obtained by anti-symmetrising Eq. (I.38), with respect to the pair of indexes $(\hat{K}\hat{L})$, to remove the symmetric components of Eq. (I.35),

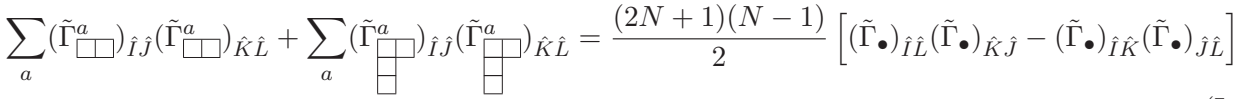

(I.45)

Contrary to the case of $\square\times\square$, this procedure does not allow to express the current-current contraction in terms of singlet-singlet contractions only. This is because the product $\square\times\square$ contains another antisymmetric representation, besides the adjoint. If one neglects, somehow arbitrarily, the second term on the left-hand side of Eq. (I.45), the relation between the current-current operator and the singlet-singlet operators becomes

$$\kappa_{A6} = \kappa_{C6} = \kappa_{D6} = \frac{(2N+1)(N-1)^2}{2N}\kappa_{UV} \ . \tag{I.46}$$

Note that these couplings can be much larger than those in Eq.(I.44), when N is large. The problem is that the current-current operator contains terms leading in $1/N$, that cannot be written as singlet-singlet contractions only.

We conclude that the strength of the coloured-sector couplings cannot be fixed in terms of κ_{UV}, and we treat it as a free parameter. In particular, κ_{A6} is independent from the strength of the electroweak-sector coupling κ_A: in our phenomenological analysis we take $\kappa_{A6} \sim \kappa_A$, such that the domain of validity of the NJL calculations is similar in the two sectors, and the NJL predictions can be compared. On the other hand, the equality between the scalar and vector couplings in each sector is a solid prediction of the current-current approximation, that holds independently from their absolute size. Finally, we remind that all predictions discussed in this appendix depend on the validity of the effective Lagrangian of Eq. (I.8), that relies on the 'ladder' approximation for the hypercolour dynamics, therefore departures from these predictions may be significant.

J Running of the SM gauge couplings

In this appendix, we present the running of the SM gauge couplings within the UV completion presented in chapters 8 and 9. The one-loop running of a generic coupling g from the scale μ to the scale μ' is given by

$$g^2(\mu') = \frac{g^2(\mu)}{1+\beta_0 g^2(\mu)\ln\frac{\mu'^2}{\mu^2}} \ , \qquad \beta(g) = \frac{dg}{d\ln\mu} = -\beta_0 g^2 + \cdots \tag{J.1}$$

where the general expression of the one-loop β-function is

$$\beta_0 = \frac{1}{16\pi^2}\left[\frac{11}{3}C(\mathbf{Ad}) - \frac{2}{3}\sum_{f_i} C(\mathbf{R}_{f_i})n_{f_i} - \frac{1}{3}\sum_{s_i} C(\mathbf{R}_{s_i})n_{s_i}\right] \ . \tag{J.2}$$

The first contribution in the above expression of β_0 comes from the gauge bosons while the second and third ones from generic Weyl fermions f_i and scalar s_i with multiplicity n_{f_i} and n_{s_i}.

We assume for simplicity that the condensation scale is around 10 TeV such that, above this scale the fundamental fermions ψ and X contribute to the SM β functions. This is a naive estimation of the running because we neglect the contributions of the composite resonances below Λ. However, this crude approximation gives a first guess of the constraints that originate from the SM gauge couplings. The fundamental fermions transform as $\psi \sim 2_0 + 1_{\pm 1/2}$ and $X \sim 3_{2/3} + \overline{3}_{-2/3}$ respectively under $SU(2)_L \times U(1)_Y$ and $SU(3)_c \times U(1)_Y$. Then from the dimension of the hypercolour representation [$2N$ and $(2N+1)(N-1)$ for ψ and X respectively] and from Eq. (J.2) we get

$$\beta_0^Y = \frac{1}{16\pi^2}\left[-\frac{20}{3} - \frac{2}{3}\left(\frac{8}{3}(2N+1)(N-1)+N\right)\right] \ , \tag{J.3}$$

$$\beta_0^{EW} = \frac{1}{16\pi^2}\left[\frac{10}{3} - \frac{2N}{3}\right] \ , \tag{J.4}$$

$$\beta_0^{QCD} = \frac{1}{16\pi^2}\left[7 - \frac{2}{3}(2N+1)(N-1)\right] \ , \tag{J.5}$$

for $U(1)_Y$, $SU(2)_L$ and $SU(3)_c$ respectively. The first contribution come from the SM particles [6] while the second one from the hypercolour fermions.

The running of the corresponding gauge couplings are displayed in figure 9 for different values of the number of hypercolour N. Depending on N, Landau poles may develop, possibly too close to

[6] Note that we have to remove the contribution of the SM Higgs doublet which is of course not present in composite Higgs model. In the SM we rather have

$$\beta_0^Y\big|_{SM} = -\frac{1}{16\pi^2}\frac{41}{6} \ , \tag{J.6}$$

$$\beta_0^{EW}\big|_{SM} = \frac{1}{16\pi^2}\frac{19}{6} \ , \tag{J.7}$$

$$\beta_0^{QCD}\big|_{SM} = \frac{7}{16\pi^2} \ , \tag{J.8}$$

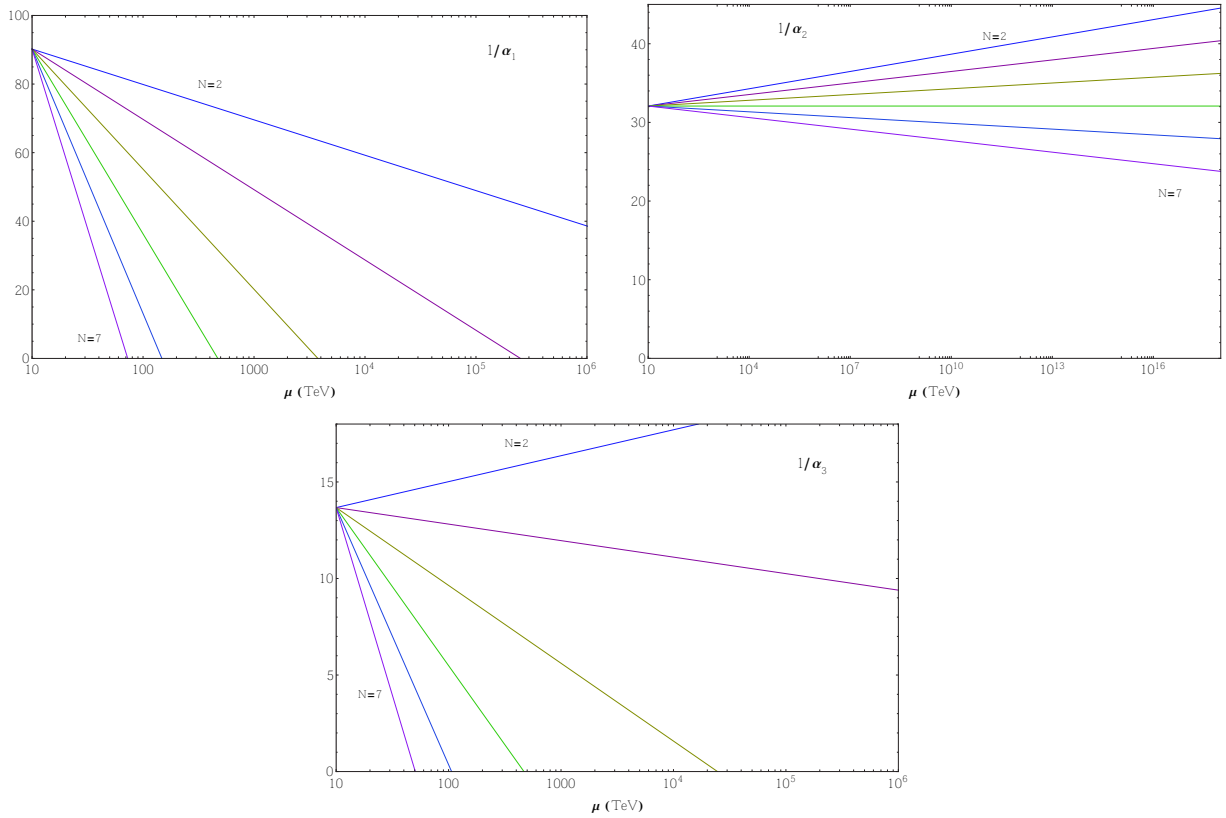

Figure 9: Running of the SM gauge coupling at one-loop, in presence of the EW and coloured hyperfermions ψ and X for a fixed number of hypercolours $N = 2$ to $N = 7$. From the upper to the lower panels: running of the hypercharge coupling $(1/\alpha_1)$, $SU(2)_L$ coupling $(1/\alpha_2)$ and $SU(3)_c$ coupling $(1/\alpha_3)$. The condensation scale Λ is assume to be at 10 TeV and the contribution of the composite resonances below Λ is neglected for simplicity.

the condensation scale of the strong sector. The naive one-loop estimation of the running of the SM gauge couplings in presence of the hypercolour fermions, as described above, leads to the appearance of Landau poles around 100 (500) TeV for $N = 6$ (5) while for $N = 4$, the Landau poles appear above $4 \cdot 10^3$ TeV. Then, a more reasonable interval for the number of hypercolours is $2 \leq N \leq 6$ and for the numerical illustration, we take the conservative value $N = 4$ in chapters 8 and 9.

Chapter 10

Conclusion and outlooks about the UV completions of CHMs

In the two precedent chapters, we have considered a particular UV realisation of the composite Higgs paradigm. The latter belongs to the class of VL theories and is based on a new $Sp(2N)$ gauge interaction that is supposed to condensate at low energy. Two species of fundamental fermions (hyperfermions), ψ and X, charged under the new strong dynamics are introduced. They respectively transform in the fundamental ($\psi_i \sim \square$, $i = 1, \cdots, 2N$) representation and in the two index antisymmetric ($X_{ij} = -X_{ji} \sim \begin{smallmatrix}\square\\\square\end{smallmatrix}$) and traceless ($X_{ij}\Omega_{ji} = 0$) representation of $Sp(2N)$. The number of hypercolours is constrained by $2 \leq N \leq 18$, where the lower bound comes from the existence of the representation $\begin{smallmatrix}\square\\\square\end{smallmatrix}$ while the upper bound comes from the preservation of asymptotic freedom in the UV. The latter bound is crucial as an asymptotically free gauge theory is expected to become strongly coupled in the IR as it is required in CHMs.

Below the condensation scale, the hypercolour confines and only hypercolour invariant bound states of $Sp(2N)$ are dynamical degrees of freedom. Restricting to the composite mesonic resonances, there are two sectors in the theory: the EW sector and the coloured sector. The first one contains the resonances constructed from fermions ψ while the second one the resonances constructed from fermions X. In order for the strong dynamics to realised the two main ingredients of CHMs, that is, to generate a pNGB Higgs and top partners (baryons with opposite quantum number under the SM gauge group than the top quark multiplets), the minimal flavour structure requires four fermions ψ^a ($a = 1, \cdots, 4$) and six fermions X^f ($f = 1, \cdots, 6$). This leads to a $SU(4)$ and a $SU(6)$ global symmetry respectively in the EW sector and in the coloured sector.

The SM gauge symmetry is embedded inside the global symmetries in such a way that, the EW sector contains the Higgs doublet while the coloured sector contains top partners. More precisely, $SU(2)_L \times U(1)_Y$ is embedded inside $SU(4)$ and after condensation, the $SU(4)$ global symmetry is supposed to be spontaneously broken down to $Sp(4)$, leading to a pNGB Higgs doublet that belongs to the coset space $SU(4)/Sp(4)$. In the hypothesis that $SU(4)$ is spontaneously broken, the above pattern of symmetry breaking is a direct consequence of the VL nature of the theory and of the pseudo-reality of the fundamental representation of $Sp(2N)$. Note that, the custodial symmetry is also embedded inside the global symmetry of the EW sector which protects the theory from large tree-level corrections to the T parameter. In a similar way, the gauge $SU(3)_c \times U(1)_Y$ symmetry is embedded inside $SU(6)$. As the coloured fermions X are in a real representation of $Sp(2N)$, if the global symmetry is spontaneously broken, the residual subgroup is $SO(6)$. However, contrary to the EW sector, there is no restriction of spontaneous symmetry breaking in that case and the $SU(6)$ symmetry could be broken or remain unbroken and still provides top partners with the right quantum numbers. Note that in any cases, the SM gauge group is embedded in the unbroken subgroups $Sp(4)$ and $SO(6)$ such that, the condensation of the strong dynamics does not break the EW symmetry as required in CHMs. On the contrary, the SM group is only partly embedded inside $SU(4)$ and $SU(6)$ such that, gauging the latter explicitly breaks the global symmetries and generates a potential for the pNGBs. In CHMs, this explicit breaking source does not destabilise the Higgs potential. Then, another source of explicit breaking should be introduced to drive the spontaneous breaking of the EW

symmetry. The latter comes from the linear couplings between the top quarks and its partners.

Starting from the above picture, we have studied in details the two mesonic sectors of the above UV completion. The analysis mostly divides in two parts: (i) general results about the strong dynamics and (ii) non-perturbative computations using techniques of the NJL model. In this chapter, we first summarise in section 10.1 the main results of the two precedent chapters. We present for instance, the results of the 't Hooft anomaly matching and the spectrum of the mesonic resonances in the EW and in the coloured sectors. We also discuss what remains to be done in more details in these mesonic sectors and the modifications that could be explored if some resonances are observed in the future.

In section 10.2, we list few interesting outlooks for the UV completions of CHMs in general. For instance, the study of other UV completions within the NJL framework, the use of other non-perturbative techniques to estimate the masses of the resonances and the introduction of the linear couplings between the top and its partners in order to drive the EWSB.

Finally, we present in subsection 10.2.1 some outlooks for the baryonic resonances of the UV completions. In particular, we focus on the UV completion discussed in chapters 8 and 9 and present how the top partner masses can be estimated within the NJL framework.

10.1 Summary of the mesonic sector of the minimal UV completion of CHM

The general idea of a composite, Nambu-Goldstone Higgs particle provides a very attractive effective theory for the EWSB. We have considered in chapters 8 and 9 an asymptotically-free gauge theory confining at the multi-TeV scale, that has the potential to provide a self-consistent, ultraviolet-complete framework to study the composite Higgs phenomenology.

The minimal model features four flavours of constituent fermions ψ^a, which condense as the hypercolour interaction becomes strong. The first, remarkable result is that, unavoidably, the corresponding $SU(4)$ flavour symmetry breaks spontaneously to $Sp(4)$, as required to generate a NGB Higgs. This follows from general results on vector-like gauge theories, reviewed in sections 8.1.1-8.1.2. Furthermore, such dynamical symmetry breaking is successfully described by a four-fermion operator, à la NJL: when the four-fermion coupling exceeds a critical value, a non-zero mass gap develops, as shown in section 8.2.1. The meson resonances are described by two-point correlators of fermion bilinears. The meson spin (zero or one) and its representation under the flavour group are determined by the quantum numbers of the associated hypercolour-singlet fermion bilinear. Following the standard NJL approach, we computed all the relevant two-point correlators, resummed at leading order in the number of hypercolours N: the meson mass is determined by the correlator pole, while the residue at the pole fixes the meson decay constant. In section 8.2.5 we have shown that the NGB decay constant f is almost ten times smaller than the cutoff of the constituent fermion loops, therefore our effective theory is well under control up to meson masses of order $\sim 10f$. Recall that electroweak precision measurements require $f \gtrsim 1$ TeV and fine-tuning in the composite Higgs potential is proportional to the ratio v^2/f^2. In order to correlate the various meson masses, we made the hypothesis that the hypercolour dynamics is dominated by current-current interactions, see appendix I.1, and we used Fierz transformations to relate the different four-fermion operators. In particular, in section I.4 we derived some $Sp(2N)$ Fierz identities which, to the best of our knowledge, were not available in the literature.

In section 8.2.6 we illustrated our results for the mass spectrum of electroweak mesons: for a reasonably small number of hypercolours, say $2N \lesssim 10$, the spin-one mesons are always heavier than $5f$, while the spin-zero mesons can be as light as f, and therefore accessible to the LHC, in the following special cases. The singlet scalar mass M_σ vanishes when the four-fermion coupling approaches its critical value, that is, when the condensate vanishes. The singlet pseudoscalar mass $M_{\eta'}$ is induced by the axial anomaly: the anomalous contribution is expected to scale as $M_{\eta'}^2 \sim 1/N$, but we did not attempt to quantify its absolute size. Therefore, we cannot exclude a very light value for $M_{\eta'}$. Note that these results for σ and η' hold for the electroweak sector in isolation: the effects of the mixing with the singlets of the colour sector are summarised below. The non-singlet scalar S

can also be light if both σ and η' are, as $M_S^2 \simeq M_\sigma^2 + M_{\eta'}^2$. In addition, one should keep in mind that the set of NGB is formed by the Higgs doublet plus a SM singlet η; their masses arise only from SM loops, that we did not study here, and are expected to lie at or below the scale f. In section 8.2.7 we perform an important test of the accuracy of our methods, by comparing our results with spectral sum rules, that have to be satisfied by the exact two-point correlators. We thus identified the values of the four-fermion coupling that better reproduce the sum rules. Conversely, our results in the effective NJL approximation depart significantly from the sum rules, when the continuum part of the spectral function becomes sizable. We also compared our results with available lattice simulations for $N = 1$, finding a fair agreement within the large error bars, with a preference for certain values of the four-fermion couplings; however our methods are expected to be more accurate when N is large.

In order to provide composite partners for the top quark, one needs to introduce additional constituent fermions X^f, in a different hypercolour representation, such that fermion trilinear baryons can be formed, with the quantum numbers of the top quark. A gauge theory with fermions in two different representations presents qualitatively new features, such as one non-anomalous $U(1)$ flavour symmetry, with an associated Nambu-Goldstone meson η_0. In section 9.1.2 we showed that this implies two additional sum rules, as well as a mixing between the singlet scalars and pseudoscalars of the two sectors. In addition, the axial anomaly may only generate operators that respect the non-anomalous $U(1)$ symmetry. As a consequence, we demonstrated in section 9.1.3 that the effect of the anomaly is described by a very large-dimension operator, involving $4 + 12(N - 1)$ fermions. Our analysis of this operator correctly takes into account all the symmetries of the model, and thus provides fully coherent results, and its large dimension may indicate that the effects of the anomaly are suppressed in such a scenario. On the other hand, we cannot exclude that such suppression is an artefact of our approximation of the true dynamics, in terms of fermionic operators only.

The dynamics of spontaneous flavour symmetry breaking also complicates in the presence of two sectors. Our analysis of anomaly matching in section 9.1.1 shows that the condensate $\langle \psi\psi \rangle$ necessarily forms, with the possible exception of the case when N is a multiple of 8, however the condensate $\langle XX \rangle$ may not form in the presence of light, coloured baryons. Indeed, in section 9.2.1 we showed that the system of two coupled mass-gap equations is very sensitive to the relative size of four-fermion couplings in the two sectors. As the NJL techniques can provide information on the spectrum of coloured mesons only in the case of a non-vanishing mass gap, we focused on the region of parameters where a non-zero $\langle XX \rangle$ develops as well. Let us remark that the solution of the gap equations corresponds to a stable minimum of the effective potential only for some range of the four-fermion couplings, and of course meson masses are under control only within this range. In the present case, it turns out the potential is stable (no tachyons) as long as the operators induced by the axial anomaly are suppressed with respect to the others, by a factor of ten to one hundred, as described in section 9.2.5. Therefore, we concentrated on the mass spectrum in this region of parameters.

We computed the masses of coloured mesons with the same techniques described for the electroweak sector. The results are illustrated in section 9.2.4. Once again, spin-one are extremely heavy, above $\sim 5f$. The situation is much more interesting for the coloured NGBs G_c, a real QCD octet and a complex sextet, that are massless in the chiral limit. We computed the contribution to their masses from gluon loops, and we found $M_{G_c} \gtrsim 1.5f$, as long as $2N \lesssim 10$. This may be sufficiently large to comply with present collider searches. Therefore, contrary to common lore, it is not strictly necessary to introduce an explicit mass term $m_X XX$. Nonetheless, we studied also the case $m_X \neq 0$, as some qualitative features of the mass gap and of the meson spectrum are very sensitive to this parameter. In particular, the singlet pseudoscalar η_0 is an exact NGB in the chiral limit, therefore its mass is controlled by the size of m_X (and by the size of the couplings to external SM fermions), as discussed in section 9.2.5. A prominent opportunity for the discovery of composite NGBs at the LHC is offered by their anomalous couplings to two SM gauge bosons, determined by the Wess-Zumino-Witten term. We provided the general formula for these couplings, and we specially discussed its phenomenological consequences for the η_0 state. The mass of the other singlet pseudoscalar η' is extremely sensitive to the effective anomaly coefficient: one may have $M_{\eta'} \lesssim f$ for $\kappa_B/\kappa_A \ll 0.01$, but as soon as $\kappa_B/\kappa_A \sim 0.1$ this state decouples, $M_{\eta'} \gtrsim 10f$. Finally, the heaviest singlet scalar σ' always lies in the multi-TeV range, while the lightest singlet scalar σ_0 may be as light as f. Indeed, we

already remarked that the vacuum provided by the mass-gap equations is stable only within specific ranges for the effective four-fermion couplings. Whenever the latter are close to the boundary of the stability region, M_{σ_0} vanishes.

We presented the first thorough analysis of the spectrum of meson resonances, in a confining gauge theory with fermions in two different representations of the gauge group. The main limitation of this study is the absence of interactions with external fermion fields. The interest of such interactions is twofold: to generate Yukawa couplings between the composite Higgs and the SM fermions, and to induce radiatively a Higgs potential that realizes EWSB. As a matter of fact, the colour sector of the model is engineered to contain fermion-trilinear bound states, which may mix linearly with the SM fermions. The mass spectrum of these baryons and their couplings to the mesons can be computed by generalising the techniques used in the above chapters. Indeed, in the QCD literature, several analytical predictions for the masses and couplings of baryons are consistent with experiments and with lattice simulations. Thus, one may predict the properties of composite top quark partners, that reside in definite representations of the flavour group, and then compute the Higgs effective potential induced by the top sector loops. Such theory has less free parameters than a generic composite Higgs model with no specific ultraviolet completion, therefore the challenge will be to reproduce the Higgs mass with a minimal amount of fine tuning of the parameters. The NJL techniques applied to the baryon sector of the theory will be presented briefly in the following section.

Finally, let us comment on the work that remains to be done but also on some outlooks for the particular UV completion under study. First, we have presented the anomalous couplings between the pNGBs and the SM gauge bosons but we did not explore yet the corresponding phenomenological consequences. Indeed, these anomalous couplings could be an interesting way to discover some of the composite resonances and it could be relevant to compute in details the associated cross-sections. Note also that we have derived the sum rules of the coloured sector as well as the ones attached to $\Pi^{\psi X}_{S^0}$ and $\Pi^{\psi X}_{P^0}$. However, we have not yet studied their realisations in the NJL approximation contrary to the sum rules of the EW sector and it could be interesting to do that.

In addition, if some of the composite resonances are discovered in a near future, it could be interesting to look at the model in more details. For instance, the first thing that we could explore is to consider another link between the couplings of the EW and coloured four-fermion interactions, that is, $\kappa_A \neq \kappa_{A6}$. Indeed, the relation $\kappa_A = \kappa_{A6}$ is not fixed from the UV gauge theory or equivalently by the current-current hypothesis as we rather assume this relation for simplicity and for phenomenological reasons. Furthermore, one could go beyond and explore a departure from the relation between the scalar and vector couplings, that is, $\kappa_A \neq \kappa_{C,D}$ and similarly for the coloured couplings.

Another possibility to explore, is the breaking of the vector symmetries. Indeed, for instance in the coloured sector, the explicit breaking mass m_X could be a matrix in the $SU(6)$ flavour space. In this way, the components of the $Sp(6)$ multiplets would not be degenerated anymore. In the same spirit, one could also consider the mixing between the axial-vector singlets a^μ and a_c^μ Finally, we have neglected the tensor channels in our analysis. However, for some dynamical reasons, the latter could be light and it could be relevant to compute the masses of the corresponding spin one resonances with the NJL techniques.

10.2 Some outlooks for the UV completions of CHMs

In this section, we present some interesting outlooks for the UV completions of CHMs in general. The first thing that we can think of is to repeat the analysis of chapters 8 and 9 for other UV completions of CHMs. In particular, it could be interesting to systematically apply the 't Hooft anomaly matching to all of the other UV completions listed in table 7.3. In this way, one could identify the most promising UV completions from a dynamical point of view, that is, one can possibly proof that the spontaneous symmetry breaking occurs in the EW sector and that a pNGB Higgs is present in the spectrum. One can also compute the masses of the mesonic resonances in other UV completions within the NJL framework. The computations will be relatively similar but the final results can differ in two points: (i) the constraints on the number of hypercolours N will be different and (ii) the form of the 't Hooft term that links the EW and the coloured sectors will be modified. In addition, the global symmetries

and the patterns of symmetry breaking will change such that, the number of light resonances can be drastically modified as well as their quantum numbers under the SM gauge group (see section 7.4). These two features are crucial from a collider point of view and could discard some UV completions if composite resonances are discovered in the future.

Another interesting outlook could be to use other non-perturbative techniques of calculations than the NJL ones. For instance one could use the techniques described in Ref. [311] for QCD and compare them with the NJL predictions. We have already discussed a bit the comparison between the NJL predictions and the lattice computations, it could then provide a third comparison.

Next, one could introduce explicitly the spontaneous breaking of the EW symmetry. Indeed, we have just studied some of its consequences by gauging the SM group inside the unbroken global symmetries. In this way, we have computed the radiative corrections to the pNGBs masses as well as their anomalous couplings to the SM gauge fields. Then, a further step could be to introduce the linear couplings between the top quark and its partners. As discussed in section 6.3, the minimal way to generate such coupling is through a four-fermion interaction between the top quark multiplets and three hyperfermions. In this way, one could compute the form factors involved in Higgs potential as well as the Higgs mass itself. Then, we would have additional parameters, that is, the linears couplings but also an additional constraint coming from the Higgs mass.

Finally, within the NJL framework, one can compute strong quantities like the form factors present in the effective approach to CHMs (see chapter 6). Then, one could compute the tree-level contribution from the composite spin-one resonances to the S parameters and more generally, the contributions to S and T parameters from the strong dynamics.

10.2.1 Baryonic masses in CHMs

Let us now briefly present another important outlooks which has not been mentioned above, that is, the estimation of the baryonic masses in the NJL approximation. As we have seen, the baryons and in particular the top partners are a crucial ingredient of CHMs. Then, it is primordial to have a prediction for their masses as in addition, top partners are expected to be the lightest baryons in the spectrum. We consider QCD with two flavours as an example and then generalise to the case of CHMs. As we have seen, the two flavours case is simpler (see subsection) as there is no explicit reaking of the $SU(2)_V$ vector symmetry.

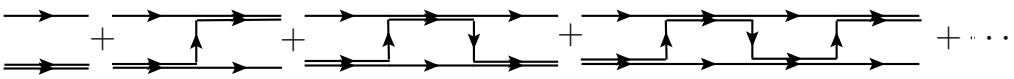

Figure 10.1: Interpretation of a baryon as a bound state of a quark and a diquark which are bounded by the exchange of a quark.

In QCD, the baryons are bound states of three (anti)quarks. Then, it is not possible to directly apply the Bethe-Salpether equation to the baryons as this equation is intrinsically valid for a two-body system. To apply the NJL formalism introduced previously, one should use a simplify description of the baryons. As a first approximation, the baryons can be interpreted as bound states of a quark and a diquark (bound state of two quarks) [309]. In this way, one can apply a generalisation of the Bethe-Salpether equation, the so-called Fadeev equation, to the quark-diquark system. This system is bounded by the exchange of a quark as it is depicted in figure 10.1. A further approximation is to neglect the momentum dependence of the exchanged quark. This approximation is called the static approximation and leads to effective "four-fermion" interactions between two quarks and two diquarks as it is illustrated in figure 10.2. In the static approximation, one can then compute an effective four-point interaction and sum the infinite number of corresponding one-loop diagrams as usual with the Bethe-Salpether equation.

The first step is to identify the diquarks channels and to compute their masses. Let us consider the following products of representation in QCD

$$3 \times \overline{3} = 1 + 8_{adj} \ , \qquad 3 \times 3 = \overline{3}_a + 6_s \ . \tag{10.2.1}$$

The first product stands for the mesonic resonances while the second for the diquarks. Note that, for the mesons, we have not considered the octets as they are coloured and the colour confines at low energy. In the same way, for the diquarks which are by definition coloured as they form a colour invariant when contracted with a quark, we have only the possibility $\overline{3}$. The above arguments on the diquark representation may not be applied to CHMs as several representations could a priori be allowed in a more general case than QCD. Then, let us present a way to discriminate between the possible representations.

This way is called the maximal attractive channel (MAC) [45] and it allows to identify the representations of the bound states which are more likely to form. Let us consider the product $R_i \times R_j = \sum_k R_k$ of two irreducible representations R_i and R_j of a gauge symmetry. The potential between the two states charged under the gauge symmetry is

$$V \sim T^a_{R_i} T^a_{R_j} = \frac{1}{2}[C_2(R_k) - C_2(R_i) - C_2(R_j)] \ . \tag{10.2.2}$$

If $V < 0$ (> 0), the potential is attractive (repulsive). Using table 7.1 and Eq. (A.3) we obtain

$$C_2(1) = 0 \ , \qquad C_2(3) = C_2(\overline{3}) = \frac{4}{3} \ , \qquad C_2(6) = \frac{10}{3} \ , \qquad C_2(8) = 3 \ . \tag{10.2.3}$$

Then, for the mesonic channel we have $V(3 \times \overline{3} = 1) = -4/3 < 0$ which is well attractive as expected. On the other hand, for the octet channel, the potential is repulsive as $V(3 \times \overline{3} = 8) = 5/6 < 0$. It is consequently justified to not consider this channel for the QCD bound states [1]. In the same way, for the diquark channels we have $V(3 \times 3 = \overline{3}) = -2/3 < 0$ and $V(3 \times 3 = 6) = 1/3 > 0$. As mentioned above, the (attractive) diquark channel is then unique and corresponds to the anti-triplet contraction. Note that, the mesonic channel is more attractive than the diquark channel and in general, channels with more quarks are expected to be less attractive. Similarly, for the CHM that we have studied, the relevant product of representations are

(10.2.4)

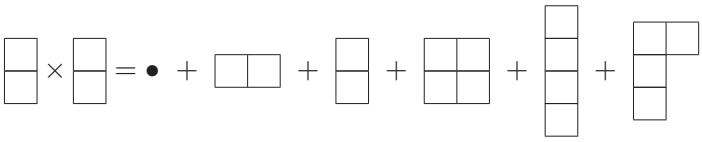

(10.2.5)

From table 7.1, we extract the relevant Casimir coefficients

$$C_2(\bullet) = 0 \ , \qquad C_2(\square) = \frac{2N+1}{4} \ , \qquad C_2(\square\square) = N+1 \ , \qquad C_2(\begin{smallmatrix}\square\\\square\end{smallmatrix}) = N \ . \tag{10.2.6}$$

For the mesonic channels $(\psi\psi)$ and (XX) we have

$$V(\square \times \square = \bullet) = -\frac{(2N+1)}{4} \ , \qquad V(\begin{smallmatrix}\square\\\square\end{smallmatrix} \times \begin{smallmatrix}\square\\\square\end{smallmatrix} = \bullet) = -N \ , \tag{10.2.7}$$

and the mesons made of two X fermions are more bounded than the ones with two ψ. This is expected as the fermions X are in a higher dimensional representation of $Sp(2N)$ than the fermions ψ. In the same way, the potentials becomes more attractive when the number of hypercolours increase. There is of course no mesonic channel (ψX) as this product does not contain a singlet contraction. For the baryonic states with three fundamental fermions we have two possibilities to form an $Sp(2N)$ invariant: $(\psi\psi X)$ and (XXX). The other possible 3 fermions states $(\psi\psi\psi)$ and (ψXX) do not

[1] This conclusion is trivial for the mesons which are made of a quark and an antiquark but relevant for instance for tetraquarks (bound states of two quarks and two antiquarks) as a priori, a colour singlet is possible by contracting two colour octets.

contain a gauge singlet as there is an odd number of gauge indices and the invariant tensor of $Sp(2N)$ is Ω_{ij}. Then, for the diquark channels we have three possibilities

$$V(\square \times \square = \begin{smallmatrix}\square\\\square\end{smallmatrix}) = -\frac{1}{4} \ , \qquad V(\square \times \begin{smallmatrix}\square\\\square\end{smallmatrix} = \square) = -\frac{N}{2} \ , \tag{10.2.8}$$

$$V(\begin{smallmatrix}\square\\\square\end{smallmatrix} \times \begin{smallmatrix}\square\\\square\end{smallmatrix} = \begin{smallmatrix}\square\\\square\end{smallmatrix}) = -\frac{N}{2} \ , \tag{10.2.9}$$

where the two first diquarks are attached to the baryons $(\psi\psi X)$ while the third one is attached to (XXX). Note that contrary to QCD, there are two possible gauge representations for the diquarks of the baryons $(\psi\psi X)$. However, from the MAC, we expect that the diquark (ψX) is more attractive than the diquark $(\psi\psi)$ as $N \geq 2$. Consequently, as a first approximation, one can simply consider the diquark (ψX) such that the exchanged hyperfermion is X. This is interesting as contrary to the fermions ψ, one has introduced an explicit breaking term m_X for the fermions X and one can increase the mass of the latter such that the static approximation becomes more justified. For the baryons (XXX), there is only one possible diquark which leads to a singlet contraction and is attractive.

Now we have identified the diquark states, one can compute their masses as the latter are relevant to compute the baryonic masses as we will see. Taking the example of QCD, one has the following four-fermion interaction

$$\mathcal{L}_{diquark} = G_S^d(\overline{\Psi}\Lambda_\alpha\Psi^c)(\overline{\Psi}^c\Lambda^\alpha\Psi) \ , \tag{10.2.10}$$

where $\Psi^c = C\overline{\Psi}^T$, $\overline{\Psi}^c = \Psi^T C$ ($C = i\gamma^2\gamma^0$) and the colour, flavour and Dirac contractions are encoded in $\Lambda_\alpha = i\epsilon^I/\sqrt{2}T^A\Gamma_\alpha$. The colour anti-triplet contraction is antisymmetric and obtained from the generators of the $\overline{3}_A$ expressed in term of the Levi-Civita tensor $(\epsilon^I)_{JK}$. The flavour contraction is given by the generators T^a of $U(N)$ where $a = 0, \cdots, N^2-1$. Finally, the Dirac contractions are given by $\Gamma_\alpha = \{\mathbb{1}, i\gamma_5, i\gamma^\mu/\sqrt{2}, i\gamma^\mu\gamma_5/\sqrt{2}\}$. Note that, the above Lagrangian has been obtained from the current-current hypothesis such that, the Fierz identities (see subsection 3.2.3) relate the mesonic and the diquark sector as follow $G_S = G_S^d$. Note also that the Γ_α contractions have been conveniently normalised to take into account the relative strength between the scalar and vector diquark channels which is the same than in the mesonic sector that is $G_S^d = -2G_V^d$. Also, the singlet and non-singlet channels have the same four-fermion coupling. From the Lagrangian in Eq. (10.2.10), one can compute the one-loop two-point functions associated to the diquark channels. The latter are given by

$$\Pi_{S/P}^d(p^2) = \frac{1}{N_c}\Pi_{P/S}(p^2) \ , \qquad \Pi_{V/A}^d(p^2) = \frac{1}{N_c}\Pi_{A/V}(p^2) \ , \tag{10.2.11}$$

where the two-point functions $\Pi_{S/P}$ and $\Pi_{V/A}$ correspond to the mesonic channels and are given in appendix B. The interactions in the diquarks channels are a factor $1/N_c$ weaker than the ones in the mesonic channel. This behaviour comes from the colour traces which are $Tr[\mathbb{1}_{N_c}] = N_c$ in the mesonic sector and $Tr[i\epsilon^I/\sqrt{2}i\epsilon^J/\sqrt{2}] = -(-1/2)2\delta^{IJ} = \delta^{IJ}$ in the diquarks channels. Then, the one-loop functions are the same than in the mesonic sector but the charge conjugation matrix C present in the Dirac traces exchange scalar with pseudo-scalar and vector with axial-vector. Inserting the four-fermion interactions of Eq. (10.2.10) and the one-loop function of Eq. (10.2.11) in the Bethe-Salpeter equation, it is easy to derive the diquark masses. For instance, in the two flavours case and in the limit where the 't Hooft term coupling H is set to zero, we have

$$M_{d_\sigma} = M_\pi \ , \qquad M_{d_\pi} = M_\sigma \ , \qquad M_{d_V} = M_A \ , \qquad M_{d_A} = M_V \ , \tag{10.2.12}$$

and similarly for the singlet masses. Note that, by definition, the mesons are real while the diquarks are complex fields. Then, the residue of the resumed two-point functions differ by a factor two between the mesonic and diquark channels but this difference has no influence on the position of the poles.

Similarly for the composite Higgs model of chapters 8 and 9, one has for the diquark channels

$$\mathcal{L}_{diquark} = \frac{\kappa_A^d}{(2N)}(\psi^a X^f)_i\Omega_{ij}(\overline{\psi}_a\overline{X}_f)_j + \frac{\kappa_D^d}{(2N)}(\psi^a\overline{\sigma}^\mu\overline{X}_f)_i\Omega_{ij}(\overline{\psi}_a\sigma_\mu X^f)_j \ , \tag{10.2.13}$$

where the gauge contraction of the diquarks is underlying ie $(\psi X)_i = \psi_j \Omega_{jk} X_{ki}$. To compute the diquark masses, one can follow the same procedure than in QCD. However, in that case, the two point functions contain two different mass eigenstates and one should generalise the expression of the one-loop functions as discussed in subsection 3.2.4.

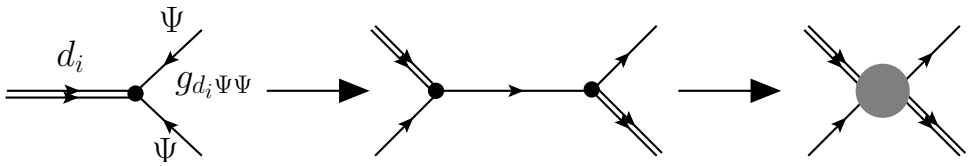

Figure 10.2: Graphical illustration of the effective "four-fermion" interaction between two diquarks d_i and two quarks Ψ. On the left, the effective interaction between a diquark and two quarks with a coupling $g_{d_i\Psi\Psi}$. On the center, the tree-level exchange of a quark constructed from the precedent interaction. On the right, the effective "four-fermion" interaction between two diquarks and two quarks obtained from integrated out the exchange quark of the precedent diagram. This effective interaction is of the order of $g^2_{d_i\Psi\Psi}/M$ where M is teh dynamical mass of the quarks.

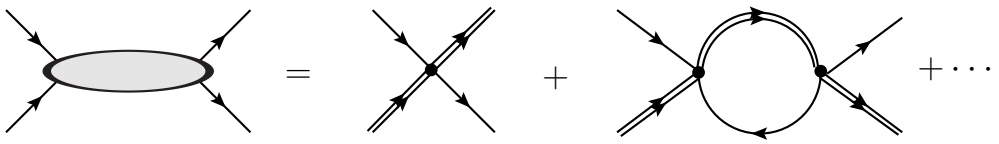

Figure 10.3: Diagrammatic illustration of the Bethe-Salpether equation in the Baryonic case.

Finally, starting from the above derivations, we now present schematically how we can evaluate the baryonic masses in the context of the NJL model. As mentioned above, let us assume that a baryon can be weel approximated as a bound state of one fermion and one diquark. Using the static approximation [309], one can integrated out the exchanged fermions such that, one obtains a system of two state: the quark and the diquark. From the effective coupling between the diquark state and the two fundamental quarks, one can construct an effective "four-fermion" interaction involving two diquarks and two quarks. This is illustrated in figure 10.2. Note that the coupling $g_{d_i\Psi\Psi}$ between the diquark state and the two quarks is obtained from the resumed T-matrix as discussed in appendix H. From this effective four-point interaction, one computes as usual with the Bethe-Salpether equation, the masses of the resonances which are this time the baryons. The latter is diagrammatically displayed in figure 10.3. Note that the diquark mass is different from the dynamical mass of the fermion such that again, one needs to generalise the expressions of the one-loop two point functions to the case of two different masses. In the CHM case, one follows the same procedure. As the relevant baryons are $(\psi\psi X)$ and (XXX), the exchange fermion in the static approximation is the fermion X and the four-point interaction is of the order of $g^2_{d\psi X}/M_X$.

Chapter 11

Conclusions

Despite its impressive success, the SM has some missing pieces and shortcomings intrinsic to its formulation. Indeed, as we have seen in chapter 1, there are some evidences that call for new physics at a higher scale and consequently, the SM should rather be viewed as an effective theory valid up to a scale Λ_{SM}. In this manuscript, we have followed two different approaches to introduce new physics above Λ_{SM}.

In the first one, we have considered minimal extensions of the SM where we extend the latter with only few new states at the EW scale. These new states are assumed to be the lightest ones while other possible states are integrated out and are decoupled from the EW scale. This is a minimal and mostly phenomenological approach which can be viewed as a low energy manifestation of a more fundamental theory. However, this approach is clearly model independent as there are no constraints coming for instance from the symmetry of the underlying UV theory. As a particular extensions, we have focused on fermions coupled to the Higgs sector. Indeed, the Higgs couplings are now measured and will be measured with higher accuracy in the future such that, it is relevant to isolate what model is still viable. In chapter 4, we have first considered the minimal fermionic extensions coupled to the SM Higgs sector. We have classified all of the possibilities and studied the impact on the EWPT as well as on the Higgs couplings. Then, in chapter 5, we have extended the Higgs sector with a second Higgs doublet and we have focussed on a particular kind of new fermions coupled to the Higgs sector, that is, on VL fermions. In this way, we have tried to explain two LHC anomalies: the diphoton excess at 750 GeV and the LFV decay $h \to \tau\mu$.

The second approach to new physics is more theoretical and based on a well-motivated UV completion of the SM like for instance supersymmetry or composite Higgs models. The purpose of this approach is to cure some shortcomings of the SM. In this manuscript, we have focused on composite Higgs models that aim to solve the hierarchy problem of the EW scale. More precisely, we have presented the effective approach to composite Higgs models in chapter 6 and outlined its limitations. Then, in chapter 7, we have presented a classification of the minimal UV completions of CHMs. The latter are a particular UV realisation of the composite Higgs paradigm in term of fundamental fermions charged under a new gauge symmetry called hypercolour. We have isolated the most promising UV completion based on $Sp(2N)$ gauge symmetry with a pattern of symmetry breaking $SU(4) \times SU(6)/Sp(4) \times SO(6)$. This UV completions has been studied within the NJL framework, presented in chapter 3 in the QCD context, in term of four-fermion interactions. We have also derived few exact results concerning the strong dynamics like for instance the sum rules, the 't Hooft anomaly matching and the anomalous couplings which have been introduced in the QCD context in chapter 2.

Let us summarise the main results attached to the phenomenological approach of new physics where only few new states are added to the SM. We first undertook a systematic analysis of new fermions interacting with the SM Higgs sector. Their properties are significantly more constrained after the measurement of the Higgs mass and couplings. Then, it is interesting to identify the few extensions that are still allowed. We have first presented a complete classification of all the possible sets of n chiral fermions interacting with the Higgs, for $n \leq 4$. Larger sets of new fermions, with $n \geq 5$, do not allow for qualitatively different phenomena, as all the possible building blocks of a

fermion mass matrix already appeared in the classification. These sets of new fermions emerge from a non-trivial interplay between several self-consistency conditions: cancellation of gauge anomalies, absence of charged massless components, non-zero Yukawa coupling to the SM Higgs doublet. In the classification, we recovered the fermionic content of some well-motivated BSM theories, such as the seesaw, supersymmetry, or partial compositeness. These cases have been studied in a more general context, by considering the most general Lagrangian for the new fermions, not restricted by additional theoretical considerations. Indeed, if a new particle could emerge from data, one should explore the full parameter space, before restricting to a particular model. Then, we argue that the phenomenological approach is necessary before turning to a specific model. In our analysis, we paid a special attention to the relative contribution of the new fermions to $h \to \gamma\gamma$ and $h \to \gamma Z$, as the former rate is already constrained to be close to the SM prediction, while the latter could still depart strongly from the SM prediction. It is commonly believed that new physics cannot provide a large correction to the γZ channel without affecting $\gamma\gamma$ as well. However, as these two processes are loop-induced, the rates involve the sum over all fermions mass eigenstates. These sums can lead to a cancellation in the signal strength $\mu_{\gamma\gamma}$ and not in $\mu_{\gamma Z}$. In addition, $h\gamma Z$ receives additional contributions from loops involving two fermions mass eigenstates, with off-diagonal couplings to both h and Z. We encountered a few scenarios where $\delta\mu_{\gamma Z} \gg \delta\mu_{\gamma\gamma}$. For instance, some mechanisms allow to reach few times the SM prediction and even, to saturate the present upper bound on $\mu_{\gamma Z}$.

As a second work on the phenomenological approach to new physics, we have tried to explain two LHC anomalies at the same time. In particular, we have considered the diphoton excess at 750 GeV and the LFV $h \to \tau\mu$ decay. Despite the former excess has now disappeared, we have assumed for the exercise that it is still there. A minimal way to introduce flavour violating Higgs couplings and extra bosons to the SM is to add a second Higgs doublet. In this way, the neutral scalars H and A can play the role of the diphoton resonance. As the cross section of the diphoton excess was significantly larger than the one expected in the 2HDM alone, we have taken this as a hint that additional states close to the TeV scale are present. The latter should have large Yukawa couplings to the second Higgs doublet in order to reproduce the diphoton excess. We have shown that a pair of VL fermions is sufficient to reproduce the right cross-section and respect all other constraints. It is not a trivial task and in order to comply with te $h\gamma\gamma$ coupling, we have used the mechanism of chapter 4. However, the new VL fermions must have charges larger than the SM fermions and large Yukawa couplings. Alternatively, several pairs of fermions have to be introduced. To explain the LFV decay $h \to \tau\mu$, the heavy Higgses must interact with $\tau\mu$ and a mixing is required between h and H such that both excess require a particular value of the mixing. The framework that we have presented is general enough to be applied in a broader context. For instance, it can be generalised to a diphoton resonance with a larger mass than 750 Gev and with a smaller cross section. The latter point would relax a lot of constraints such that our model appears as a benchmark as it proves that it is possible to induce a large $\gamma\gamma$ cross section and still respect all of the constraints. If a new diphoton excess is observed in the future, it could be an interesting possibility. Also, one should not forget that it explains the $h \to \tau\mu$ decay independently of the diphoton excess.

Let us now turn to the results on the UV completions of CHMs. In general, CHMs are studied from an effective point of view. However, in that case, a lot of informations about the underlying strong dynamics are missing. Then, there is a necessity to go beyond this approach. In this manuscript, we have considered UV completions of CHMs and in particular, one possible realisation in term of a new gauge symmetry with fundamental fermions charged under the strong dynamics. The latter is supposed to condensates at low energy and to break a global symmetry leading to the emergence of a Higgs as a pNGB. The most promising UV completion that we have studied, is based on a $Sp(2N)$ gauge symmetry with a pattern of symmetry breaking $SU(4) \times SU(6)/Sp(4) \times SO(6)$.

As a first interesting result, using the 't Hooft anomaly matching, we have demonstrate that the global symmetry of the EW sector, that is, $SU(4)$ must be spontaneously broken down to $Sp(4)$. However, there is no such argument for the coloured sector where the $SU(6)$ symmetry could be broken down to $SO(6)$ or remain unbroken.

Using the NJL techniques, we have computed the dynamical masses M_ψ and M_X, respectively

attached to the fermions ψ and X and generated by the strong interactions. Assuming that the current-current hypothesis holds, there are only three free parameters in our analysis: the number of hypercolours N, the four-fermion coupling κ_A and the coupling of the 't Hooft term parametrised by κ_B/κ_A. In addition, there is also the scale f which fixes the scale of the UV completions and is experimentally roughly constrained to be larger than 1 TeV. Then, we have derived the expressions for the masses of the lightest mesonic resonances present in the spectrum. Few points are interesting to note. In the EW sector, the masses belong to the multi-TeV range if $f = 1$ TeV and $N = 18$. In particular, the mass of the η, when the EW sector is in isolation, is directly proportional to κ_B and can be very light as when $\kappa_B = 0$, the pseudo-scalar η is a NGB. The scalar quintuplet $S^{\hat{A}}$ is always heavier than the scalar singlet σ. In the same way, the vector decuplet V_μ^A is lighter than the axial vector quintuplet $A_\mu^{\hat{A}}$. However, the vector can be lighter than the σ mass depending on the strength of the four-fermion interaction, that is, depending on the parameter $\xi = \Lambda^2(\kappa_A + \kappa_B)/(4\pi^2)$. In some cases, the vector can even be lighter than the pseudo-scalar singlet η, that is, the lightest state in the spectrum if one excludes the NGBs $G^{\hat{A}}$. Note that, if one decreases the number of hypercolours from the maximal allowed value of $N = 18$ down to $N = 2$, as f scale like $\sqrt{N}$, all of the resonances would be rescaled in the same way and would be heavier than what is described above.

Let us now consider the complete model with the coloured sector. The main consequence is that, with the two sectors, there is one combination of the anomalous $U(1)_\psi$ and $U(1)_X$ symmetries which is non-anomalous. Then, we have derived the 't Hooft term that parametrises the explicit breaking of the anomalous $U(1)$ symmetry but preserves the non-anomalous combination. We have then derived the corresponding effective four-fermion interactions and computed the expressions of the masses. As a consequence, the two sectors are linked in a rather non-trivial way as the dynamical masses M_ψ and M_X are determined by a system of two coupled equations. Note that, in the coloured sector, the spectrum is quite similar to the one in the EW sector. However, there are two different points which are relevant to outline. First, we have introduced an explicit breaking mass m_X such that, the pseudo-scalar non-singlet $G_c^{\hat{F}}$ of the coloured sector are pNGBs when $m_X \neq 0$. Second, some resonances of the coloured sector are charged under QCD and receive non-negligible radiative corrections to their masses. Then, the coloured pNGBs can respect the lower experimental bounds on their masses in two cases: (i) only with the QCD radiative corrections if f is larger than 1 TeV and (ii) if the explicit breaking mass term m_X is sufficiently large. For instance, taking $f = 1.7$ TeV, the coloured pNGBs are above 1 TeV and comply with the direct searches limits. If one consider in addition the explicit breaking $m_X = 0.1\ f$ one obtains for the pNGBs a mass of the order of 3 TeV for $f = 1$ TeV. Then, one can avoid the presence of an explicit breaking term with an unknown origin but the price to paid is to increase f and then to increase every masses in the EW and in the coloured sector. On the contrary, if m_X is introduced, one increases the masses of all of the coloured resonances but not the ones of the EW sector.

Finally, in the complete model, the singlet sectors are more involved. Indeed, when the two sectors are considered, there is a non-trivial mixing between the singlets of the EW sector and the ones of the coloured sector. This mixing leads to a strong bound on the parameter κ_B/κ_A. As a general prediction, the η_0 can be very light, of the order of 100 GeV (1 TeV) if $N = 18$ ($N = 2$). Similarly, close to the maximal allowed value of κ_B/κ_A, the σ_0 can be light as well, even below 1 TeV in some cases.

Then, in addition to the Higgs boson, we expect other light or even very light SM singlets: $G^{\hat{3}}$ which is part of the EW pNGBs and η_0 which is the pNGB associated to the non-anomalous $U(1)$ symmetry. In addition, the coloured pNGBs can be as light as the experimental bounds, around 1 TeV and in some cases, the vectors of the EW sector could be the next lightest states. Interestingly, the spectrum in the EW and in coloured sectors are really particular and can be tested at colliders if some resonances are observed in a near future.

As discussed in chapter 10, there are several interesting outlooks about the UV completions of CHMs and a lot of work remain to be done. In particular, the most pressing issue is to introduce the linear couplings between the top quark and its partners in order to drive the EWSB as for the moment, the Higgs is a pure NGB in our first approximation.

The two approaches that we have followed to introduce new physics give interesting and complementary results. In particular, they lead to different ways to look and to discover new physics. In the first one, as expected, we mainly obtain constraints at low energy, that is, constraints on the deviations in the SM couplings. In particular, we have outlined the possibility to increase significantly the Higgs couplings to γZ. In the second approach, we rather obtain predictions on the masses of new heavy states. In particular, we have outlined the resonances that can be light in the UV completions of CHMs.

For the moment, there are no significant signs of new physic and all the measurements are SM-like or compatible with the SM predictions. Then, new physics seems to behave differently than we could expect at first glance. Maybe the first evidence of new physics is hiding in very particular processes not explored yet or maybe it is simply at a higher energy scale. Consequently, it is crucial to explore all the available possibilities in order to discard them or to isolate the most relevant ones. This can be done by doing systematic analysis of simple and mostly phenomenological extensions of the SM or by studying deeper well-motivated UV theories. Indeed, up to now, only few systematic analysis like the one presented in chapter 4 have been done as most of the works have focused on one or few very specific phenomenological extensions of the SM. Also, even if the idea of CHMs is not recent, the study of their UV completions presented in chapters 8, 9 and 10 is rather soon. In any case, if nature care about naturalness, new physics should be present close to the TeV scale. However, our understanding of naturalness is maybe not complete and what appears to be unatural is maybe due to our present limited knowledges. Thus, let's hope that nature understand the naturalness principle as our, such that new physics will be accessible at the LHC and will be discovered soon.

Acknowledgements

First I would like to thank my girl friend and future wife Marie who was always present to support me during my PhD and even before during my studies. It was not an easy task at the end and a great part of my motivation in the last year is due to his understanding and his patience. I sincerely think that I would not have done the same work without his unconditional support.

Of course, I also thanks my family and all of my friends. In particular, I would like to thank Steeven and Thibault who were very present in the difficult moments.

I can not forget in these acknowledgements my PhD supervisor Michele Frigerio. He always gave me very good advices for the PhD but also for my future career. He is really a good supervisor and his involvement in all of our projects was impressive. In my opinion, a PhD thesis needs a good student (I hope it was the case with me) but also a good supervisor and I feel that within his supervision, he taught me the proper way to do research in physics.

Also, I would like to thank my two other PhD supervisors Jean-Loïc Kneur and Marc Knecht. They were very patient with me and taught me a lot of complementary things. In particular, I am very grateful to Jean-Loïc because I did my first internship in a research laboratory with him.

Finally, I would like to thank all of the IFAC team in Montpellier who host me during the PhD. In particular, Gilbert Moultaka and Cyril Hugonie who were always there to answer my questions or to get involved in my thesis. It was a long and difficult work before I get here to write these few lines but I feel it was worth it as I am not the same person that I was three years ago.

Bibliography

[1] **Gfitter Group** Collaboration, M. Baak et al., *The global electroweak fit at NNLO and prospects for the LHC and ILC*, *Eur.Phys.J.* **C74** (2014) 3046, [arXiv:1407.3792]. v, 105, 106

[2] M. Ciuchini, E. Franco, S. Mishima, and L. Silvestrini, *Electroweak Precision Observables, New Physics and the Nature of a 126 GeV Higgs Boson*, *JHEP* **1308** (2013) 106, [arXiv:1306.4644]. v, 108, 109

[3] T. A. collaboration, *Search for resonances decaying to photon pairs in 3.2 fb^{-1} of pp collisions at $\sqrt{s}$ = 13 TeV with the ATLAS detector*, . vi, 120, 121, 127

[4] **CMS** Collaboration, C. Collaboration, *Search for new physics in high mass diphoton events in proton-proton collisions at 13TeV*, . vi, 120, 121, 127

[5] **CMS Collaboration** Collaboration, S. Chatrchyan et al., *Searches for long-lived charged particles in pp collisions at $\sqrt{s}$=7 and 8 TeV*, *JHEP* **1307** (2013) 122, [arXiv:1305.0491]. ix, 71, 74

[6] L. Di Luzio, R. Grober, J. F. Kamenik, and M. Nardecchia, *Accidental matter at the LHC*, arXiv:1504.00359. ix, 61, 64, 71, 73, 74

[7] **ATLAS** Collaboration, G. Aad et al., *Search for heavy long-lived multi-charged particles in pp collisions at $\sqrt{s}$ = 8 TeV using the ATLAS detector*, arXiv:1504.04188. ix, 74

[8] **ATLAS** Collaboration, G. Aad et al., *Search for Massive Long-lived Highly Ionising Particles with the ATLAS Detector at the LHC*, *Phys.Lett.* **B698** (2011) 353–370, [arXiv:1102.0459]. ix, 74

[9] **CMS** Collaboration, *Projected Performance of an Upgraded CMS Detector at the LHC and HL-LHC: Contribution to the Snowmass Process*, arXiv:1307.7135. ix, 118, 119

[10] G. Ferretti and D. Karateev, *Fermionic UV completions of Composite Higgs models*, *JHEP* **03** (2014) 077, [arXiv:1312.5330]. ix, 145, 146, 149, 150, 151, 152, 153, 165, 175

[11] N. Bizot and M. Frigerio, *Fermionic extensions of the Standard Model in light of the Higgs couplings*, *JHEP* **01** (2016) 036, [arXiv:1508.01645]. 3, 41, 122

[12] N. Bizot, S. Davidson, M. Frigerio, and J. L. Kneur, *Two Higgs doublets to explain the excesses $pp \to \gamma\gamma(750\ \text{GeV})$ and $h \to \tau^{\pm}\mu^{\mp}$*, *JHEP* **03** (2016) 073, [arXiv:1512.08508]. 3

[13] M. K. J.-L. K. N. Bizot, M. Frigerio, *Non-perturbative analysis of the spectrum of meson resonances in an ultraviolet-complete composite-Higgs model*, . 3

[14] S. L. Glashow, *Partial Symmetries of Weak Interactions*, *Nucl. Phys.* **22** (1961) 579–588. 6, 7

[15] S. Weinberg, *A Model of Leptons*, *Phys. Rev. Lett.* **19** (1967) 1264–1266. 6, 7

[16] A. Salam and J. C. Ward, *Weak and electromagnetic interactions*, *Nuovo Cim.* **11** (1959) 568–577. 6, 7

[17] S. L. Glashow, J. Iliopoulos, and L. Maiani, *Weak Interactions with Lepton-Hadron Symmetry*, *Phys. Rev.* **D2** (1970) 1285–1292. 6, 7

[18] **ATLAS** Collaboration, G. Aad et al., *Observation of a new particle in the search for the Standard Model Higgs boson with the ATLAS detector at the LHC*, *Phys.Lett.* **B716** (2012) 1–29, [arXiv:1207.7214]. 6, 63

[19] **CMS** Collaboration, S. Chatrchyan et al., *Observation of a new boson at a mass of 125 GeV with the CMS experiment at the LHC*, *Phys. Lett.* **B716** (2012) 30–61, [arXiv:1207.7235]. 6

[20] F. Englert and R. Brout, *Broken Symmetry and the Mass of Gauge Vector Mesons*, *Phys. Rev. Lett.* **13** (1964) 321–323. 9

[21] P. W. Higgs, *Broken symmetries, massless particles and gauge fields*, *Phys. Lett.* **12** (1964) 132–133. 9

[22] P. W. Higgs, *Broken Symmetries and the Masses of Gauge Bosons*, *Phys. Rev. Lett.* **13** (1964) 508–509. 9

[23] G. S. Guralnik, C. R. Hagen, and T. W. B. Kibble, *Global Conservation Laws and Massless Particles*, *Phys. Rev. Lett.* **13** (1964) 585–587. 9

[24] P. W. Higgs, *Spontaneous Symmetry Breakdown without Massless Bosons*, *Phys. Rev.* **145** (1966) 1156–1163. 9

[25] T. W. B. Kibble, *Symmetry breaking in nonAbelian gauge theories*, *Phys. Rev.* **155** (1967) 1554–1561. 9

[26] M. D. Schwartz, *Quantum Field Theory and the Standard Model*. Cambridge University Press, 2014. 9, 15

[27] N. Cabibbo, *Unitary Symmetry and Leptonic Decays*, *Phys. Rev. Lett.* **10** (1963) 531–533. [,648(1963)]. 11

[28] M. Kobayashi and T. Maskawa, *CP Violation in the Renormalizable Theory of Weak Interaction*, *Prog. Theor. Phys.* **49** (1973) 652–657. 11

[29] B. Pontecorvo, *Mesonium and anti-mesonium*, *Sov. Phys. JETP* **6** (1957) 429. [Zh. Eksp. Teor. Fiz.33,549(1957)]. 11

[30] Z. Maki, M. Nakagawa, and S. Sakata, *Remarks on the unified model of elementary particles*, *Prog. Theor. Phys.* **28** (1962) 870–880. 11

[31] B. Pontecorvo, *Neutrino Experiments and the Problem of Conservation of Leptonic Charge*, *Sov. Phys. JETP* **26** (1968) 984–988. [Zh. Eksp. Teor. Fiz.53,1717(1967)]. 11

[32] R. Barbieri, *Ten Lectures on the ElectroWeak Interactions*. 2007. 14

[33] G. Bertone, D. Hooper, and J. Silk, *Particle dark matter: Evidence, candidates and constraints*, *Phys. Rept.* **405** (2005) 279–390, [hep-ph/0404175]. 17

[34] R. D. Peccei and H. R. Quinn, *CP Conservation in the Presence of Instantons*, *Phys. Rev. Lett.* **38** (1977) 1440–1443. 17

[35] R. D. Peccei and H. R. Quinn, *Constraints Imposed by CP Conservation in the Presence of Instantons*, *Phys. Rev.* **D16** (1977) 1791–1797. 17

[36] R. Contino, L. Da Rold, and A. Pomarol, *Light custodians in natural composite Higgs models*, *Phys. Rev.* **D75** (2007) 055014, [hep-ph/0612048]. 21, 96, 141, 144

[37] S. Scherer and M. R. Schindler, *A Primer for Chiral Perturbation Theory*, *Lect. Notes Phys.* **830** (2012) pp.1–338. 31

[38] C. Vafa and E. Witten, *Restrictions on Symmetry Breaking in Vector-Like Gauge Theories*, *Nucl. Phys.* **B234** (1984) 173–188. 32, 169

[39] G. 't Hooft, *Naturalness, chiral symmetry, and spontaneous chiral symmetry breaking*, *NATO Sci. Ser. B* **59** (1980) 135. 33, 170

[40] J. S. Bell and R. Jackiw, *A PCAC puzzle: pi0 –¿ gamma gamma in the sigma model*, *Nuovo Cim.* **A60** (1969) 47–61. 33, 170

[41] S. L. Adler, *Axial vector vertex in spinor electrodynamics*, *Phys. Rev.* **177** (1969) 2426–2438. 33, 170

[42] S. L. Adler and W. A. Bardeen, *Absence of higher order corrections in the anomalous axial vector divergence equation*, *Phys. Rev.* **182** (1969) 1517–1536. 33, 170

[43] Y. Frishman, A. Schwimmer, T. Banks, and S. Yankielowicz, *The Axial Anomaly and the Bound State Spectrum in Confining Theories*, *Nucl. Phys.* **B177** (1981) 157. 33, 170

[44] S. R. Coleman and B. Grossman, *'t Hooft's Consistency Condition as a Consequence of Analyticity and Unitarity*, *Nucl. Phys.* **B203** (1982) 205. 33, 170

[45] S. Raby, S. Dimopoulos, and L. Susskind, *Tumbling Gauge Theories*, *Nucl. Phys.* **B169** (1980) 373–383. 34, 248

[46] T. Appelquist and J. Carazzone, *Infrared Singularities and Massive Fields*, *Phys. Rev.* **D11** (1975) 2856. 36

[47] S. Weinberg, *Precise relations between the spectra of vector and axial vector mesons*, *Phys. Rev. Lett.* **18** (1967) 507–509. 36, 171

[48] T. Das, G. S. Guralnik, V. S. Mathur, F. E. Low, and J. E. Young, *Electromagnetic mass difference of pions*, *Phys. Rev. Lett.* **18** (1967) 759–761. 41, 174

[49] J. Wess and B. Zumino, *Consequences of anomalous Ward identities*, *Phys. Lett.* **B37** (1971) 95–97. 41, 175

[50] E. Witten, *Global Aspects of Current Algebra*, *Nucl. Phys.* **B223** (1983) 422–432. 41, 175

[51] C.-S. Chu, P.-M. Ho, and B. Zumino, *NonAbelian anomalies and effective actions for a homogeneous space G/H*, *Nucl. Phys.* **B475** (1996) 484–504, [hep-th/9602093]. 41, 175

[52] Y. Nambu and G. Jona-Lasinio, *Dynamical Model of Elementary Particles Based on an Analogy with Superconductivity. 1.*, *Phys. Rev.* **122** (1961) 345–358. 43, 175, 178, 179, 182, 183

[53] Y. Nambu and G. Jona-Lasinio, *Dynamical model of elementary particles based on an analogy with superconductivity. II*, *Phys. Rev.* **124** (1961) 246–254. 43, 175

[54] G. 't Hooft, *A Planar Diagram Theory for Strong Interactions*, *Nucl. Phys.* **B72** (1974) 461. 43

[55] E. Witten, *Baryons in the 1/n Expansion*, *Nucl. Phys.* **B160** (1979) 57–115. 43

[56] S. P. Klevansky, *The Nambu-Jona-Lasinio model of quantum chromodynamics*, *Rev. Mod. Phys.* **64** (1992) 649–708. 44, 49, 175, 177, 178, 179, 182, 183, 184, 186, 235

[57] U. Vogl and W. Weise, *The Nambu and Jona Lasinio model: Its implications for hadrons and nuclei*, *Prog. Part. Nucl. Phys.* **27** (1991) 195–272. 44

[58] V. Dmitrasinovic, *Composite antisymmetric tensor Nambu-Goldstone bosons in a four fermion interaction model and the Higgs mechanism*, *Eur. Phys. J.* **C14** (2000) 179–184, [hep-th/9911121]. 45, 46

[59] M. Buballa, *NJL model analysis of quark matter at large density*, *Phys. Rept.* **407** (2005) 205–376, [hep-ph/0402234]. 52, 237

[60] S. Klimt, M. F. M. Lutz, U. Vogl, and W. Weise, *Generalized SU(3) Nambu-Jona-Lasinio Model. Part. 1. mesonic modes*, *Nucl. Phys.* **A516** (1990) 429–468. 52, 53, 54, 55, 56, 175, 176, 179, 183, 186, 234

[61] U. Vogl, M. F. M. Lutz, S. Klimt, and W. Weise, *Generalized SU(3) Nambu-Jona-Lasinio Model. Part 2. From Current to Constituent Quarks*, *Nucl. Phys.* **A516** (1990) 469–495. 53

[62] C. Biggio and M. Bordone, *Minimal muon anomalous magnetic moment*, *JHEP* **02** (2015) 099, [arXiv:1411.6799]. 61

[63] C. Biggio, M. Bordone, L. Di Luzio, and G. Ridolfi, *Massive vectors and loop observables: the $g-2$ case*, arXiv:1607.07621. 61

[64] P. Bamert, C. Burgess, J. M. Cline, D. London, and E. Nardi, *R(b) and new physics: A Comprehensive analysis*, *Phys.Rev.* **D54** (1996) 4275–4300, [hep-ph/9602438]. 61, 108

[65] M. Cirelli, N. Fornengo, and A. Strumia, *Minimal dark matter*, *Nucl.Phys.* **B753** (2006) 178–194, [hep-ph/0512090]. 61, 64, 76

[66] E. Del Nobile, R. Franceschini, D. Pappadopulo, and A. Strumia, *Minimal Matter at the Large Hadron Collider*, *Nucl. Phys.* **B826** (2010) 217–234, [arXiv:0908.1567]. 61, 64

[67] H. Flacher, M. Goebel, J. Haller, A. Hocker, K. Monig, et al., *Revisiting the Global Electroweak Fit of the Standard Model and Beyond with Gfitter*, *Eur.Phys.J.* **C60** (2009) 543–583, [arXiv:0811.0009]. 63

[68] **ALEPH, DELPHI, L3, OPAL, LEP Electroweak** Collaboration, S. Schael et al., *Electroweak Measurements in Electron-Positron Collisions at W-Boson-Pair Energies at LEP*, *Phys.Rept.* **532** (2013) 119–244, [arXiv:1302.3415]. 63

[69] **Particle Data Group** Collaboration, K. Olive et al., *Review of Particle Physics*, *Chin.Phys.* **C38** (2014) 090001. 63, 77, 108

[70] M. Raidal et al., *Flavour physics of leptons and dipole moments*, *Eur. Phys. J.* **C57** (2008) 13–182, [arXiv:0801.1826]. 63

[71] G. Isidori, Y. Nir, and G. Perez, *Flavor Physics Constraints for Physics Beyond the Standard Model*, *Ann.Rev.Nucl.Part.Sci.* **60** (2010) 355, [arXiv:1002.0900]. 63

[72] D. Toback and L. Ivkovi, *Review of Physics Results from the Tevatron: Searches for New Particles and Interactions*, *Int.J.Mod.Phys.* **A30** (2015), no. 06 1541007, [arXiv:1409.4910]. 63

[73] **Particle Data Group** Collaboration, K. Nakamura et al., *Review of particle physics*, *J. Phys.* **G37** (2010) 075021. 63

[74] **ATLAS** Collaboration, https://twiki.cern.ch/twiki/bin/view/AtlasPublic. 63

[75] **CMS** Collaboration, http://cms-results.web.cern.ch/cms-results/public-results/publications/. 63

[76] **CMS** Collaboration, S. Chatrchyan et al., *Observation of a new boson at a mass of 125 GeV with the CMS experiment at the LHC*, *Phys.Lett.* **B716** (2012) 30–61, [arXiv:1207.7235]. 63

[77] **CMS** Collaboration, V. Khachatryan et al., *Precise determination of the mass of the Higgs boson and tests of compatibility of its couplings with the standard model predictions using proton collisions at 7 and 8 TeV*, arXiv:1412.8662. 63, 118

[78] **ATLAS, CMS** Collaboration, G. Aad et al., *Combined Measurement of the Higgs Boson Mass in pp Collisions at $\sqrt{s} = 7$ and 8 TeV with the ATLAS and CMS Experiments*, arXiv:1503.07589. 63, 118

[79] **ATLAS** Collaboration, G. Aad et al., *Measurements of the Higgs boson production and decay rates and coupling strengths using pp collision data at $\sqrt{s} = 7$ and 8 TeV in the ATLAS experiment*, arXiv:1507.04548. 63, 118

[80] **ALEPH, DELPHI, L3, OPAL, SLD, LEP Electroweak Working Group, SLD Electroweak Group, SLD Heavy Flavour Group** Collaboration, S. Schael et al., *Precision electroweak measurements on the Z resonance*, *Phys.Rept.* **427** (2006) 257–454, [hep-ex/0509008]. 63

[81] D. B. Kaplan, *Flavor at SSC energies: A New mechanism for dynamically generated fermion masses*, *Nucl.Phys.* **B365** (1991) 259–278. 64, 84, 138, 204

[82] R. Contino and A. Pomarol, *Holography for fermions*, *JHEP* **11** (2004) 058, [hep-th/0406257]. 64, 204

[83] I. Picek and B. Radovcic, *Nondecoupling of terascale isosinglet quark and rare K- and B-decays*, *Phys. Rev.* **D78** (2008) 015014, [arXiv:0804.2216]. 64

[84] G. Cacciapaglia, A. Deandrea, L. Panizzi, N. Gaur, D. Harada, et al., *Heavy Vector-like Top Partners at the LHC and flavour constraints*, *JHEP* **1203** (2012) 070, [arXiv:1108.6329]. 64, 89

[85] C. Han, A. Kobakhidze, N. Liu, L. Wu, and B. Yang, *Constraining Top partner and Naturalness at the LHC and TLEP*, *Nucl. Phys.* **B890** (2014) 388–399, [arXiv:1405.1498]. 64, 94

[86] E. Witten, *An SU(2) Anomaly*, *Phys. Lett.* **B117** (1982) 324–328. 66, 146

[87] O. Eberhardt, G. Herbert, H. Lacker, A. Lenz, A. Menzel, et al., *Impact of a Higgs boson at a mass of 126 GeV on the standard model with three and four fermion generations*, *Phys.Rev.Lett.* **109** (2012) 241802, [arXiv:1209.1101]. 70, 72

[88] A. Azatov, O. Bondu, A. Falkowski, M. Felcini, S. Gascon-Shotkin, et al., *Higgs boson production via vector-like top-partner decays: Diphoton or multilepton plus multijets channels at the LHC*, *Phys.Rev.* **D85** (2012) 115022, [arXiv:1204.0455]. 71

[89] M. Montull, F. Riva, E. Salvioni, and R. Torre, *Higgs Couplings in Composite Models*, *Phys.Rev.* **D88** (2013) 095006, [arXiv:1308.0559]. 71

[90] T. Flacke, J. H. Kim, S. J. Lee, and S. H. Lim, *Constraints on composite quark partners from Higgs searches*, *JHEP* **1405** (2014) 123, [arXiv:1312.5316]. 71

[91] C.-Y. Chen, S. Dawson, and I. Lewis, *Top Partners and Higgs Boson Production*, *Phys.Rev.* **D90** (2014), no. 3 035016, [arXiv:1406.3349]. 71

[92] O. Matsedonskyi, G. Panico, and A. Wulzer, *On the Interpretation of Top Partners Searches*, *JHEP* **1412** (2014) 097, [arXiv:1409.0100]. 71

[93] **ATLAS Collaboration** Collaboration, G. Aad et al., *Searches for heavy long-lived sleptons and R-Hadrons with the ATLAS detector in pp collisions at $\sqrt{s} = 7$ TeV*, *Phys.Lett.* **B720** (2013) 277–308, [arXiv:1211.1597]. 71

[94] **ATLAS** Collaboration, G. Aad et al., *Searches for heavy long-lived charged particles with the ATLAS detector in proton-proton collisions at $\sqrt{s} = 8$ TeV*, *JHEP* **1501** (2015) 068, [arXiv:1411.6795]. 71, 100

[95] M. Fairbairn, A. C. Kraan, D. A. Milstead, T. Sjostrand, P. Z. Skands, and T. Sloan, *Stable massive particles at colliders*, *Phys. Rept.* **438** (2007) 1–63, [hep-ph/0611040]. 71, 74

[96] *Measurements of the Higgs boson production and decay rates and constraints on its couplings from a combined ATLAS and CMS analysis of the LHC pp collision data at $\sqrt{s} = 7$ and 8 TeV*, Tech. Rep. ATLAS-CONF-2015-044, CMS-PAS-HIG-15-002, CERN, Geneva, Sep, 2015. 72, 73, 118

[97] S. Banerjee, M. Frank, and S. K. Rai, *Higgs data confronts Sequential Fourth Generation Fermions in the Higgs Triplet Model*, *Phys. Rev.* **D89** (2014), no. 7 075005, [arXiv:1312.4249]. 73

[98] A. Alves, E. Ramirez Barreto, D. A. Camargo, and A. G. Dias, *A Model with Chiral Quarks of Electric Charges -4/3 and 5/3*, *JHEP* **07** (2013) 129, [arXiv:1306.1275]. 73

[99] D. Wyler and L. Wolfenstein, *Massless Neutrinos in Left-Right Symmetric Models*, *Nucl. Phys.* **B218** (1983) 205. 75

[100] R. N. Mohapatra and J. W. F. Valle, *Neutrino Mass and Baryon Number Nonconservation in Superstring Models*, *Phys. Rev.* **D34** (1986) 1642. 75

[101] M. C. Gonzalez-Garcia and J. W. F. Valle, *Fast Decaying Neutrinos and Observable Flavor Violation in a New Class of Majoron Models*, *Phys. Lett.* **B216** (1989) 360. 75

[102] S. S. C. Law and K. L. McDonald, *Generalized inverse seesaw mechanisms*, *Phys. Rev.* **D87** (2013), no. 11 113003, [arXiv:1303.4887]. 75

[103] A. de Gouvea, *GeV seesaw, accidentally small neutrino masses, and Higgs decays to neutrinos*, arXiv:0706.1732. 75

[104] J.-H. Chen, X.-G. He, J. Tandean, and L.-H. Tsai, *Effect on Higgs Boson Decays from Large Light-Heavy Neutrino Mixing in Seesaw Models*, *Phys.Rev.* **D81** (2010) 113004, [arXiv:1001.5215]. 75

[105] P. Bhupal Dev, R. Franceschini, and R. Mohapatra, *Bounds on TeV Seesaw Models from LHC Higgs Data*, *Phys.Rev.* **D86** (2012) 093010, [arXiv:1207.2756]. 75

[106] C. G. Cely, A. Ibarra, E. Molinaro, and S. Petcov, *Higgs Decays in the Low Scale Type I See-Saw Model*, *Phys.Lett.* **B718** (2013) 957–964, [arXiv:1208.3654]. 75

[107] S. Antusch and O. Fischer, *Testing sterile neutrino extensions of the Standard Model at future lepton colliders*, *JHEP* **05** (2015) 053, [arXiv:1502.05915]. 75

[108] **ATLAS Collaboration** Collaboration, *Search for Majorana neutrino production in pp collisions at sqrt(s)=7 TeV in dimuon final states with the ATLAS detector*, Tech. Rep. ATLAS-CONF-2012-139, CERN, Geneva, Sep, 2012. 75

[109] **ATLAS** Collaboration, G. Aad et al., *Search for heavy Majorana neutrinos with the ATLAS detector in pp collisions at $\sqrt{s} = 8$ TeV*, arXiv:1506.06020. 75

[110] **CMS Collaboration** Collaboration, S. Chatrchyan et al., *Search for heavy Majorana neutrinos in $\mu^+\mu^+[\mu^-\mu^-]$ and $e^+e^+[e^-e^-]$ events in pp collisions at $\sqrt{s} = 7$ TeV*, *Phys.Lett.* **B717** (2012) 109–128, [arXiv:1207.6079]. 75

[111] **CMS Collaboration** Collaboration, V. Khachatryan et al., *Search for heavy Majorana neutrinos in $\mu^{\pm}\mu^{\pm}$+jets events in proton-proton collisions at $\sqrt{s} = 8$ TeV*, arXiv:1501.05566. 75

[112] A. Abada, C. Biggio, F. Bonnet, M. Gavela, and T. Hambye, *mu e gamma and tau l gamma decays in the fermion triplet seesaw model*, *Phys.Rev.* **D78** (2008) 033007, [arXiv:0803.0481]. 76

[113] A. Abada, C. Biggio, F. Bonnet, M. Gavela, and T. Hambye, *Low energy effects of neutrino masses*, *JHEP* **0712** (2007) 061, [arXiv:0707.4058]. 76

[114] R. Franceschini, T. Hambye, and A. Strumia, *Type-III see-saw at LHC*, *Phys.Rev.* **D78** (2008) 033002, [arXiv:0805.1613]. 76, 77

[115] **L3 Collaboration** Collaboration, P. Achard et al., *Search for heavy neutral and charged leptons in e^+e^- annihilation at LEP*, *Phys.Lett.* **B517** (2001) 75–85, [hep-ex/0107015]. 76, 78

[116] **CMS Collaboration** Collaboration, S. Chatrchyan et al., *Search for heavy lepton partners of neutrinos in proton-proton collisions in the context of the type III seesaw mechanism*, *Phys.Lett.* **B718** (2012) 348–368, [arXiv:1210.1797]. 76

[117] **ATLAS** Collaboration, G. Aad et al., *Search for type-III Seesaw heavy leptons in pp collisions at $\sqrt{s} = 8$ TeV with the ATLAS Detector*, arXiv:1506.01839. 76

[118] A. Falkowski, D. M. Straub, and A. Vicente, *Vector-like leptons: Higgs decays and collider phenomenology*, *JHEP* **1405** (2014) 092, [arXiv:1312.5329]. 79

[119] W. Altmannshofer, M. Bauer, and M. Carena, *Exotic Leptons: Higgs, Flavor and Collider Phenomenology*, *JHEP* **1401** (2014) 060, [arXiv:1308.1987]. 79

[120] T. Ma, B. Zhang, and G. Cacciapaglia, *Doubly Charged Lepton from an Exotic Doublet at the LHC*, *Phys. Rev.* **D89** (2014), no. 9 093022, [arXiv:1404.2375]. 79

[121] A. Delgado, C. Garcia Cely, T. Han, and Z. Wang, *Phenomenology of a lepton triplet*, *Phys. Rev.* **D84** (2011) 073007, [arXiv:1105.5417]. 79

[122] T. Ma, B. Zhang, and G. Cacciapaglia, *Triplet with a doubly-charged lepton at the LHC*, *Phys. Rev.* **D89** (2014), no. 1 015020, [arXiv:1309.7396]. 79

[123] **ATLAS** Collaboration, G. Aad et al., *Evidence for the Higgs-boson Yukawa coupling to tau leptons with the ATLAS detector*, *JHEP* **04** (2015) 117, [arXiv:1501.04943]. 80

[124] **CMS Collaboration** Collaboration, S. Chatrchyan et al., *Evidence for the 125 GeV Higgs boson decaying to a pair of τ leptons*, arXiv:1401.5041. 80

[125] **ATLAS** Collaboration, G. Aad et al., *Search for lepton-flavour-violating $H \to \mu\tau$ decays of the Higgs boson with the ATLAS detector*, arXiv:1508.03372. 80, 121

[126] **CMS** Collaboration, V. Khachatryan et al., *Search for lepton-flavour-violating decays of the Higgs boson*, arXiv:1502.07400. 80, 120, 124

[127] **ATLAS Collaboration** Collaboration, G. Aad et al., *Search for the Standard Model Higgs boson decay to $\mu^+\mu^-$ with the ATLAS detector*, arXiv:1406.7663. 80

[128] **CMS** Collaboration, V. Khachatryan et al., *Search for a standard model-like Higgs boson in the μ^+ μ and e^+ e decay channels at the LHC*, *Phys. Lett.* **B744** (2015) 184–207, [arXiv:1410.6679]. 80

[129] K. Agashe, R. Contino, L. Da Rold, and A. Pomarol, *A Custodial symmetry for Zb anti-b*, *Phys.Lett.* **B641** (2006) 62–66, [hep-ph/0605341]. 81, 96

[130] F. del Aguila, A. Carmona, and J. Santiago, *Tau Custodian searches at the LHC*, *Phys.Lett.* **B695** (2011) 449–453, [arXiv:1007.4206]. 81

[131] A. Carmona and F. Goertz, *Custodial Leptons and Higgs Decays*, *JHEP* **1304** (2013) 163, [arXiv:1301.5856]. 81

[132] L. G. Almeida, E. Bertuzzo, P. A. Machado, and R. Z. Funchal, *Does $H \to \gamma\gamma$ Taste like vanilla New Physics?*, *JHEP* **1211** (2012) 085, [arXiv:1207.5254]. 82

[133] J. Kearney, A. Pierce, and N. Weiner, *Vectorlike Fermions and Higgs Couplings*, *Phys. Rev.* **D86** (2012) 113005, [arXiv:1207.7062]. 84

[134] A. Joglekar, P. Schwaller, and C. E. M. Wagner, *Dark Matter and Enhanced Higgs to Di-photon Rate from Vector-like Leptons*, *JHEP* **12** (2012) 064, [arXiv:1207.4235]. 84

[135] M. Redi, *Leptons in Composite MFV*, *JHEP* **1309** (2013) 060, [arXiv:1306.1525]. 85

[136] S. P. Martin, *A Supersymmetry primer*, *Adv.Ser.Direct.High Energy Phys.* **21** (2010) 1–153, [hep-ph/9709356]. 88

[137] H. K. Dreiner, J. S. Kim, and O. Lebedev, *First LHC Constraints on Neutralinos*, *Phys. Lett.* **B715** (2012) 199–202, [arXiv:1206.3096]. 88

[138] B. Ananthanarayan, J. Lahiri, P. Pandita, and M. Patra, *Invisible decays of the lightest Higgs boson in supersymmetric models*, *Phys.Rev.* **D87** (2013), no. 11 115021, [arXiv:1306.1291]. 88

[139] J. A. Casas, J. M. Moreno, K. Rolbiecki, and B. Zaldivar, *Implications of light charginos for Higgs observables, LHC searches and dark matter*, *JHEP* **1309** (2013) 099, [arXiv:1305.3274]. 88

[140] B. Batell, S. Jung, and C. E. Wagner, *Very Light Charginos and Higgs Decays*, *JHEP* **1312** (2013) 075, [arXiv:1309.2297]. 88

[141] F. del Aguila, M. Perez-Victoria, and J. Santiago, *Observable contributions of new exotic quarks to quark mixing*, *JHEP* **09** (2000) 011, [hep-ph/0007316]. 89

[142] J. Aguilar-Saavedra, *Identifying top partners at LHC*, *JHEP* **0911** (2009) 030, [arXiv:0907.3155]. 89, 92

[143] G. Cacciapaglia, A. Deandrea, D. Harada, and Y. Okada, *Bounds and Decays of New Heavy Vector-like Top Partners*, *JHEP* **1011** (2010) 159, [arXiv:1007.2933]. 89, 92

[144] S. Gopalakrishna, T. Mandal, S. Mitra, and R. Tibrewala, *LHC Signatures of a Vector-like b'*, *Phys. Rev.* **D84** (2011) 055001, [arXiv:1107.4306]. 89

[145] Y. Okada and L. Panizzi, *LHC signatures of vector-like quarks*, *Adv.High Energy Phys.* **2013** (2013) 364936, [arXiv:1207.5607]. 89

[146] J. Aguilar-Saavedra, R. Benbrik, S. Heinemeyer, and M. Prez-Victoria, *Handbook of vectorlike quarks: Mixing and single production*, *Phys.Rev.* **D88** (2013), no. 9 094010, [arXiv:1306.0572]. 89

[147] S. Gopalakrishna, T. Mandal, S. Mitra, and G. Moreau, *LHC Signatures of Warped-space Vectorlike Quarks*, *JHEP* **08** (2014) 079, [arXiv:1306.2656]. 92, 100

[148] T. A. collaboration, *Search for production of vector-like quark pairs and of four top quarks in the lepton plus jets final state in pp collisions at $\sqrt{s} = 8$ TeV with the ATLAS detector*, . 93, 94

[149] **CMS** Collaboration, V. Khachatryan et al., *Search for vector-like T quarks decaying to top quarks and Higgs bosons in the all-hadronic channel using jet substructure*, *JHEP* **06** (2015) 080, [arXiv:1503.01952]. 93

[150] **ATLAS** Collaboration, G. Aad et al., *Search for vector-like B quarks in events with one isolated lepton, missing transverse momentum and jets at $\sqrt{s} = 8$ TeV with the ATLAS detector*, arXiv:1503.05425. 94

[151] **ATLAS Collaboration** Collaboration, G. Aad et al., *Search for pair and single production of new heavy quarks that decay to a Z boson and a third-generation quark in pp collisions at $\sqrt{s} = 8$ TeV with the ATLAS detector*, arXiv:1409.5500. 94

[152] **CMS** Collaboration, C. Collaboration, *Search for vector-like quarks in final states with a single lepton and jets in pp collisions at $\sqrt{s} = 8$ TeV*, . 94

[153] **CMS** Collaboration, C. Collaboration, *Search for pair-produced vector-like quarks of charge -1/3 decaying to bH using boosted Higgs jet-tagging in pp collisions at $\sqrt{s} = 8$ TeV*, . 94

[154] **CMS** Collaboration, C. Collaboration, *Search for pair-produced vector-like quarks of charge -1/3 in lepton+jets final state in pp collisions at $\sqrt{s} = 8$ TeV*, . 94

[155] **CMS** Collaboration, V. Khachatryan et al., *Search for vector-like charge 2/3 T quarks in proton-proton collisions at $\sqrt{s} = 8$ TeV*, arXiv:1509.04177. 94

[156] A. Pomarol and J. Serra, *Top Quark Compositeness: Feasibility and Implications*, *Phys. Rev.* **D78** (2008) 074026, [arXiv:0806.3247]. 96, 100

[157] E. Bertuzzo, P. A. Machado, and R. Zukanovich Funchal, *Can New Colored Particles Illuminate the Higgs?*, *JHEP* **1302** (2013) 086, [arXiv:1209.6359]. 97

[158] O. Matsedonskyi, F. Riva, and T. Vantalon, *Composite Charge 8/3 Resonances at the LHC*, *JHEP* **04** (2014) 059, [arXiv:1401.3740]. 99

[159] G. Cacciapaglia, A. Deandrea, N. Gaur, D. Harada, Y. Okada, et al., *Interplay of vector-like top partner multiplets in a realistic mixing set-up*, arXiv:1502.00370. 99

[160] M. Gillioz, *A Light composite Higgs boson facing electroweak precision tests*, *Phys. Rev.* **D80** (2009) 055003, [arXiv:0806.3450]. 100

[161] A. Azatov and J. Galloway, *Light Custodians and Higgs Physics in Composite Models*, *Phys. Rev.* **D85** (2012) 055013, [arXiv:1110.5646]. 100

[162] J. Elias-Mir, J. Espinosa, E. Masso, and A. Pomarol, *Renormalization of dimension-six operators relevant for the Higgs decays $h \to \gamma\gamma, \gamma Z$*, *JHEP* **1308** (2013) 033, [arXiv:1302.5661]. 102

[163] M. E. Peskin and T. Takeuchi, *A New constraint on a strongly interacting Higgs sector*, *Phys.Rev.Lett.* **65** (1990) 964–967. 104

[164] G. Altarelli and R. Barbieri, *Vacuum polarization effects of new physics on electroweak processes*, *Phys.Lett.* **B253** (1991) 161–167. 104

[165] M. E. Peskin and T. Takeuchi, *Estimation of oblique electroweak corrections*, *Phys.Rev.* **D46** (1992) 381–409. 104, 105

[166] R. Barbieri, A. Pomarol, R. Rattazzi, and A. Strumia, *Electroweak symmetry breaking after LEP-1 and LEP-2*, *Nucl.Phys.* **B703** (2004) 127–146, [hep-ph/0405040]. 104, 105

[167] S. Gori, J. Gu, and L.-T. Wang, *The Zbb Couplings at Future e^+e^- Colliders*, arXiv:1508.07010. 108

[168] J. R. Ellis, M. K. Gaillard, and D. V. Nanopoulos, *A Phenomenological Profile of the Higgs Boson*, *Nucl.Phys.* **B106** (1976) 292. 113

[169] M. A. Shifman, A. Vainshtein, M. Voloshin, and V. I. Zakharov, *Low-Energy Theorems for Higgs Boson Couplings to Photons*, *Sov.J.Nucl.Phys.* **30** (1979) 711–716. 113

[170] B. A. Kniehl and M. Spira, *Low-energy theorems in Higgs physics*, *Z.Phys.* **C69** (1995) 77–88, [hep-ph/9505225]. 113

[171] M. Carena, I. Low, and C. E. M. Wagner, *Implications of a Modified Higgs to Diphoton Decay Width*, *JHEP* **08** (2012) 060, [arXiv:1206.1082]. 113

[172] M. Gillioz, R. Grober, C. Grojean, M. Muhlleitner, and E. Salvioni, *Higgs Low-Energy Theorem (and its corrections) in Composite Models*, *JHEP* **1210** (2012) 004, [arXiv:1206.7120]. 113

[173] M. B. Voloshin, *CP Violation in Higgs Diphoton Decay in Models with Vectorlike Heavy Fermions*, *Phys. Rev.* **D86** (2012) 093016, [arXiv:1208.4303]. 113

[174] M. Gavela, G. Girardi, C. Malleville, and P. Sorba, *A Nonlinear R(xi) Gauge Condition for the Electroweak SU(2) X U(1) Model*, *Nucl.Phys.* **B193** (1981) 257. 113

[175] R. Cahn, M. S. Chanowitz, and N. Fleishon, *Higgs Particle Production by Z H Gamma*, *Phys.Lett.* **B82** (1979) 113. 114

[176] L. Bergstrom and G. Hulth, *Induced Higgs Couplings to Neutral Bosons in e^+e^- Collisions*, *Nucl.Phys.* **B259** (1985) 137. 114

[177] G. Passarino and M. Veltman, *One Loop Corrections for e+ e- Annihilation Into mu+ mu- in the Weinberg Model*, *Nucl.Phys.* **B160** (1979) 151. 117, 231

[178] D. Y. Bardin and G. Passarino, *The standard model in the making: Precision study of the electroweak interactions*, . 117

[179] A. Denner, *Techniques for calculation of electroweak radiative corrections at the one loop level and results for W physics at LEP-200*, *Fortsch.Phys.* **41** (1993) 307–420, [arXiv:0709.1075]. 117

[180] A. Djouadi, V. Driesen, W. Hollik, and J. Rosiek, *Associated production of Higgs bosons and a photon in high-energy e+ e- collisions*, *Nucl.Phys.* **B491** (1997) 68–102, [hep-ph/9609420]. 117

[181] A. Djouadi, V. Driesen, W. Hollik, and A. Kraft, *The Higgs photon - Z boson coupling revisited*, *Eur.Phys.J.* **C1** (1998) 163–175, [hep-ph/9701342]. 117

[182] J. Cao, L. Wu, P. Wu, and J. M. Yang, *The Z+photon and diphoton decays of the Higgs boson as a joint probe of low energy SUSY models*, *JHEP* **1309** (2013) 043, [arXiv:1301.4641]. 117

[183] *Projections for measurements of Higgs boson signal strengths and coupling parameters with the ATLAS detector at a HL-LHC*, Tech. Rep. ATL-PHYS-PUB-2014-016, CERN, Geneva, Oct, 2014. 118, 119

[184] **ATLAS Collaboration** Collaboration, G. Aad et al., *Search for Higgs boson decays to a photon and a Z boson in pp collisions at $\sqrt{s}$=7 and 8 TeV with the ATLAS detector*, *Phys.Lett.* **B732** (2014) 8–27, [arXiv:1402.3051]. 118

[185] **CMS Collaboration** Collaboration, S. Chatrchyan et al., *Search for a Higgs boson decaying into a Z and a photon in pp collisions at $\sqrt{s}$ = 7 and 8 TeV*, *Phys.Lett.* **B726** (2013) 587–609, [arXiv:1307.5515]. 118

[186] *Search for an Invisibly Decaying Higgs Boson Produced via Vector Boson Fusion in pp Collisions at $\sqrt{s} = 8$ TeV using the ATLAS Detector at the LHC*, Tech. Rep. ATLAS-CONF-2015-004, CERN, Geneva, Mar, 2015. 118

[187] **CMS** Collaboration, S. Chatrchyan et al., *Search for invisible decays of Higgs bosons in the vector boson fusion and associated ZH production modes*, *Eur.Phys.J.* **C74** (2014) 2980, [arXiv:1404.1344]. 118

[188] J. R. Espinosa, C. Grojean, M. Muhlleitner, and M. Trott, *First Glimpses at Higgs' face*, *JHEP* **12** (2012) 045, [arXiv:1207.1717]. 118

[189] D. Carmi, A. Falkowski, E. Kuflik, T. Volansky, and J. Zupan, *Higgs After the Discovery: A Status Report*, *JHEP* **10** (2012) 196, [arXiv:1207.1718]. 118, 122

[190] G. Cacciapaglia, A. Deandrea, G. D. La Rochelle, and J.-B. Flament, *Higgs couplings beyond the Standard Model*, *JHEP* **03** (2013) 029, [arXiv:1210.8120]. 118

[191] A. Azatov and J. Galloway, *Electroweak Symmetry Breaking and the Higgs Boson: Confronting Theories at Colliders*, *Int. J. Mod. Phys.* **A28** (2013) 1330004, [arXiv:1212.1380]. 118

[192] A. Falkowski, F. Riva, and A. Urbano, *Higgs at last*, *JHEP* **11** (2013) 111, [arXiv:1303.1812]. 118

[193] P. P. Giardino, K. Kannike, I. Masina, M. Raidal, and A. Strumia, *The universal Higgs fit*, *JHEP* **05** (2014) 046, [arXiv:1303.3570]. 118

[194] A. Djouadi and G. Moreau, *The couplings of the Higgs boson and its CP properties from fits of the signal strengths and their ratios at the 7+8 TeV LHC*, *Eur. Phys. J.* **C73** (2013), no. 9 2512, [arXiv:1303.6591]. 118

[195] G. Belanger, B. Dumont, U. Ellwanger, J. F. Gunion, and S. Kraml, *Global fit to Higgs signal strengths and couplings and implications for extended Higgs sectors*, *Phys. Rev.* **D88** (2013) 075008, [arXiv:1306.2941]. 118

[196] G. Moreau, *Constraining extra-fermion(s) from the Higgs boson data*, *Phys. Rev.* **D87** (2013), no. 1 015027, [arXiv:1210.3977]. 118

[197] G. C. Branco, P. M. Ferreira, L. Lavoura, M. N. Rebelo, M. Sher, and J. P. Silva, *Theory and phenomenology of two-Higgs-doublet models*, *Phys. Rept.* **516** (2012) 1–102, [arXiv:1106.0034]. 121

[198] A. Djouadi, *The Anatomy of electro-weak symmetry breaking. I: The Higgs boson in the standard model*, *Phys.Rept.* **457** (2008) 1–216, [hep-ph/0503172]. 121

[199] A. Djouadi, *The Anatomy of electro-weak symmetry breaking. II. The Higgs bosons in the minimal supersymmetric model*, *Phys.Rept.* **459** (2008) 1–241, [hep-ph/0503173]. 121

[200] J. F. Gunion, H. E. Haber, G. L. Kane, and S. Dawson, *The Higgs Hunter's Guide*, *Front. Phys.* **80** (2000) 1–404. 121

[201] J. D. Bjorken and S. Weinberg, *A Mechanism for Nonconservation of Muon Number*, *Phys. Rev. Lett.* **38** (1977) 622. 121, 124

[202] S. Davidson and G. J. Grenier, *Lepton flavour violating Higgs and tau to mu gamma*, *Phys. Rev.* **D81** (2010) 095016, [arXiv:1001.0434]. 121, 123, 125

[203] R. A. Diaz, R. Martinez, and J. A. Rodriguez, *Phenomenology of lepton flavor violation in 2HDM(3) from (g-2)(μ) and leptonic decays*, *Phys. Rev.* **D67** (2003) 075011, [hep-ph/0208117]. 121

[204] A. Arhrib, *Top and Higgs flavor changing neutral couplings in two Higgs doublets model*, *Phys. Rev.* **D72** (2005) 075016, [hep-ph/0510107]. 121

[205] S. Kanemura, T. Ota, and K. Tsumura, *Lepton flavor violation in Higgs boson decays under the rare tau decay results*, *Phys. Rev.* **D73** (2006) 016006, [hep-ph/0505191]. 121

[206] P. Paradisi, *Higgs-mediated $e \to \mu$ transitions in II Higgs doublet model and supersymmetry*, *JHEP* **08** (2006) 047, [hep-ph/0601100]. 121

[207] A. Crivellin, A. Kokulu, and C. Greub, *Flavor-phenomenology of two-Higgs-doublet models with generic Yukawa structure*, *Phys. Rev.* **D87** (2013), no. 9 094031, [arXiv:1303.5877]. 121

[208] R. Harnik, J. Kopp, and J. Zupan, *Flavor Violating Higgs Decays*, *JHEP* **1303** (2013) 026, [arXiv:1209.1397]. 121

[209] A. Dery, A. Efrati, Y. Nir, Y. Soreq, and V. Susi, *Model building for flavor changing Higgs couplings*, *Phys. Rev.* **D90** (2014) 115022, [arXiv:1408.1371]. 121

[210] D. Aristizabal Sierra and A. Vicente, *Explaining the CMS Higgs flavor violating decay excess*, *Phys. Rev.* **D90** (2014), no. 11 115004, [arXiv:1409.7690]. 121

[211] J. Heeck, M. Holthausen, W. Rodejohann, and Y. Shimizu, *Higgs in Abelian and non-Abelian flavor symmetry models*, *Nucl. Phys.* **B896** (2015) 281–310, [arXiv:1412.3671]. 121

[212] A. Crivellin, G. D'Ambrosio, and J. Heeck, *Explaining $h \to \mu^\pm\tau^\mp$, $B \to K^*\mu^+\mu^-$ and $B \to K\mu^+\mu^-/B \to Ke^+e^-$ in a two-Higgs-doublet model with gauged $L_\mu - L_\tau$*, *Phys. Rev. Lett.* **114** (2015) 151801, [arXiv:1501.00993]. 121

[213] L. de Lima, C. S. Machado, R. D. Matheus, and L. A. F. do Prado, *Higgs Flavor Violation as a Signal to Discriminate Models*, *JHEP* **11** (2015) 074, [arXiv:1501.06923].

[214] I. Dorner, S. Fajfer, A. Greljo, J. F. Kamenik, N. Konik, and I. Niandic, *New Physics Models Facing Lepton Flavor Violating Higgs Decays at the Percent Level*, *JHEP* **06** (2015) 108, [arXiv:1502.07784]. 121

[215] A. Angelescu, A. Djouadi, and G. Moreau, *Scenarii for interpretations of the LHC diphoton excess: two Higgs doublets and vector-like quarks and leptons*, *Phys. Lett.* **B756** (2016) 126–132, [arXiv:1512.04921]. 121

[216] R. S. Gupta, S. Jger, Y. Kats, G. Perez, and E. Stamou, *Interpreting a 750 GeV Diphoton Resonance*, *JHEP* **07** (2016) 145, [arXiv:1512.05332]. 121

[217] M. Badziak, *Interpreting the 750 GeV diphoton excess in minimal extensions of Two-Higgs-Doublet models*, *Phys. Lett.* **B759** (2016) 464–470, [arXiv:1512.07497]. 121

[218] S. Di Chiara, L. Marzola, and M. Raidal, *First interpretation of the 750 GeV diphoton resonance at the LHC*, *Phys. Rev.* **D93** (2016), no. 9 095018, [arXiv:1512.04939]. 121

[219] T.-F. Feng, X.-Q. Li, H.-B. Zhang, and S.-M. Zhao, *The LHC 750 GeV diphoton excess in supersymmetry with gauged baryon and lepton numbers*, arXiv:1512.06696. 121

[220] X.-F. Han and L. Wang, *Implication of the 750 GeV diphoton resonance on two-Higgs-doublet model and its extensions with Higgs field*, *Phys. Rev.* **D93** (2016), no. 5 055027, [arXiv:1512.06587]. 121

[221] R. Ding, L. Huang, T. Li, and B. Zhu, *Interpreting 750 GeV Diphoton Excess with R-parity Violating Supersymmetry*, arXiv:1512.06560. 121

[222] W.-C. Huang, Y.-L. S. Tsai, and T.-C. Yuan, *Gauged Two Higgs Doublet Model confronts the LHC 750 GeV diphoton anomaly*, *Nucl. Phys.* **B909** (2016) 122–134, [arXiv:1512.07268]. 121

[223] S. Moretti and K. Yagyu, *750 GeV diphoton excess and its explanation in two-Higgs-doublet models with a real inert scalar multiplet*, *Phys. Rev.* **D93** (2016), no. 5 055043, [arXiv:1512.07462]. 121

[224] M. Backovic, A. Mariotti, and D. Redigolo, *Di-photon excess illuminates Dark Matter*, *JHEP* **03** (2016) 157, [arXiv:1512.04917]. 121

[225] Y. Mambrini, G. Arcadi, and A. Djouadi, *The LHC diphoton resonance and dark matter*, *Phys. Lett.* **B755** (2016) 426–432, [arXiv:1512.04913]. 121

[226] Y. Bai, J. Berger, and R. Lu, *750 GeV dark pion: Cousin of a dark G -parity odd WIMP*, *Phys. Rev.* **D93** (2016), no. 7 076009, [arXiv:1512.05779]. 121

[227] E. Gabrielli, K. Kannike, B. Mele, M. Raidal, C. Spethmann, and H. Veerme, *A SUSY Inspired Simplified Model for the 750 GeV Diphoton Excess*, *Phys. Lett.* **B756** (2016) 36–41, [arXiv:1512.05961]. 121

[228] X.-J. Bi, Q.-F. Xiang, P.-F. Yin, and Z.-H. Yu, *The 750 GeV diphoton excess at the LHC and dark matter constraints*, *Nucl. Phys.* **B909** (2016) 43–64, [arXiv:1512.06787]. 121

[229] H. Han, S. Wang, and S. Zheng, *Scalar Explanation of Diphoton Excess at LHC*, *Nucl. Phys.* **B907** (2016) 180–186, [arXiv:1512.06562]. 121

[230] C. Han, H. M. Lee, M. Park, and V. Sanz, *The diphoton resonance as a gravity mediator of dark matter*, *Phys. Lett.* **B755** (2016) 371–379, [arXiv:1512.06376]. 121

[231] U. K. Dey, S. Mohanty, and G. Tomar, *750 GeV resonance in the dark leftright model*, *Phys. Lett.* **B756** (2016) 384–389, [arXiv:1512.07212]. 121

[232] P. S. B. Dev and D. Teresi, *Asymmetric dark matter in the Sun and diphoton excess at the LHC*, *Phys. Rev.* **D94** (2016), no. 2 025001, [arXiv:1512.07243]. 121

[233] H. Davoudiasl and C. Zhang, *750 GeV messenger of dark conformal symmetry breaking*, *Phys. Rev.* **D93** (2016), no. 5 055006, [arXiv:1512.07672]. 121

[234] M. Bauer and M. Neubert, *Flavor anomalies, the 750 GeV diphoton excess, and a dark matter candidate*, *Phys. Rev.* **D93** (2016), no. 11 115030, [arXiv:1512.06828]. 121

[235] F. Wang, L. Wu, J. M. Yang, and M. Zhang, *750 GeV diphoton resonance, 125 GeV Higgs and muon g 2 anomaly in deflected anomaly mediation SUSY breaking scenarios*, *Phys. Lett.* **B759** (2016) 191–199, [arXiv:1512.06715]. 121

[236] C. W. Murphy, *Vector Leptoquarks and the 750 GeV Diphoton Resonance at the LHC*, *Phys. Lett.* **B757** (2016) 192–198, [arXiv:1512.06976]. 121

[237] R. Franceschini, G. F. Giudice, J. F. Kamenik, M. McCullough, A. Pomarol, R. Rattazzi, M. Redi, F. Riva, A. Strumia, and R. Torre, *What is the $\gamma\gamma$ resonance at 750 GeV?*, *JHEP* **03** (2016) 144, [arXiv:1512.04933]. 121, 125, 126

[238] S. Knapen, T. Melia, M. Papucci, and K. Zurek, *Rays of light from the LHC*, *Phys. Rev.* **D93** (2016), no. 7 075020, [arXiv:1512.04928]. 121

[239] R. Benbrik, C.-H. Chen, and T. Nomura, *Higgs singlet boson as a diphoton resonance in a vectorlike quark model*, *Phys. Rev.* **D93** (2016), no. 5 055034, [arXiv:1512.06028]. 121

[240] D. Aloni, K. Blum, A. Dery, A. Efrati, and Y. Nir, *On a possible large width 750 GeV diphoton resonance at ATLAS and CMS*, *JHEP* **08** (2016) 017, [arXiv:1512.05778]. 121

[241] J. F. Gunion and H. E. Haber, *The CP conserving two Higgs doublet model: The Approach to the decoupling limit*, *Phys. Rev.* **D67** (2003) 075019, [hep-ph/0207010]. 121, 123

[242] N. Bonne and G. Moreau, *Reproducing the Higgs boson data with vector-like quarks*, *Phys. Lett.* **B717** (2012) 409–419, [arXiv:1206.3360]. 122

[243] K. Harigaya and Y. Nomura, *Composite Models for the 750 GeV Diphoton Excess*, *Phys. Lett.* **B754** (2016) 151–156, [arXiv:1512.04850]. 123

[244] S. Davidson and H. E. Haber, *Basis-independent methods for the two-Higgs-doublet model*, *Phys. Rev.* **D72** (2005) 035004, [hep-ph/0504050]. [Erratum: Phys. Rev.D72,099902(2005)]. 123

[245] **BaBar** Collaboration, B. Aubert et al., *Searches for Lepton Flavor Violation in the Decays $\tau^{\pm} \to e^{\pm}\gamma$ and $\tau^{\pm} \to \mu^{\pm}\gamma$*, *Phys. Rev. Lett.* **104** (2010) 021802, [arXiv:0908.2381]. 124

[246] **Belle** Collaboration, K. Hayasaka et al., *New search for $\tau \to \mu\gamma$ and $\tau \to e\gamma$ decays at Belle*, *Phys. Lett.* **B666** (2008) 16–22, [arXiv:0705.0650]. 124

[247] D. Chang, W. S. Hou, and W.-Y. Keung, *Two loop contributions of flavor changing neutral Higgs bosons to $\mu \to e\gamma$*, *Phys. Rev.* **D48** (1993) 217–224, [hep-ph/9302267]. 124

[248] M. Baak, M. Goebel, J. Haller, A. Hoecker, D. Ludwig, et al., *Updated Status of the Global Electroweak Fit and Constraints on New Physics*, *Eur.Phys.J.* **C72** (2012) 2003, [arXiv:1107.0975]. 125

[249] **LHC Higgs Cross Section Working Group** Collaboration, S. Dittmaier et al., *Handbook of LHC Higgs Cross Sections: 1. Inclusive Observables*, arXiv:1101.0593. 125

[250] J. F. Owens, A. Accardi, and W. Melnitchouk, *Global parton distributions with nuclear and finite-Q^2 corrections*, *Phys. Rev.* **D87** (2013), no. 9 094012, [arXiv:1212.1702]. 125

[251] R. Contino, *The Higgs as a Composite Nambu-Goldstone Boson*, in *Physics of the large and the small, TASI 09, proceedings of the Theoretical Advanced Study Institute in Elementary Particle Physics, Boulder, Colorado, USA, 1-26 June 2009*, pp. 235–306, 2011. arXiv:1005.4269. 132, 134, 135, 136, 140, 141, 146

[252] G. Panico and A. Wulzer, *The Composite Nambu-Goldstone Higgs*, *Lect. Notes Phys.* **913** (2016) pp.1–316, [arXiv:1506.01961]. 132, 182, 183

[253] S. Weinberg, *Implications of Dynamical Symmetry Breaking*, *Phys. Rev.* **D13** (1976) 974–996. 133

[254] L. Susskind, *Dynamics of Spontaneous Symmetry Breaking in the Weinberg-Salam Theory*, *Phys. Rev.* **D20** (1979) 2619–2625. 133

[255] K. Agashe, R. Contino, and A. Pomarol, *The Minimal composite Higgs model*, *Nucl. Phys.* **B719** (2005) 165–187, [hep-ph/0412089]. 133

[256] B. Gripaios, A. Pomarol, F. Riva, and J. Serra, *Beyond the Minimal Composite Higgs Model*, *JHEP* **04** (2009) 070, [arXiv:0902.1483]. 133, 149, 175

[257] D. Ghosh, M. Salvarezza, and F. Senia, *Extending the Analysis of Electroweak Precision Constraints in Composite Higgs Models*, arXiv:1511.08235. 136

[258] M. E. Peskin, *The Alignment of the Vacuum in Theories of Technicolor*, *Nucl. Phys.* **B175** (1980) 197–233. 148, 169, 174, 229

[259] J. Barnard, T. Gherghetta, and T. S. Ray, *UV descriptions of composite Higgs models without elementary scalars*, *JHEP* **02** (2014) 002, [arXiv:1311.6562]. 148, 167, 175, 177, 179, 186, 188, 204, 206, 223, 239

[260] G. Cacciapaglia, H. Cai, A. Deandrea, T. Flacke, S. J. Lee, and A. Parolini, *Composite scalars at the LHC: the Higgs, the Sextet and the Octet*, *JHEP* **11** (2015) 201, [arXiv:1507.02283]. 149, 153, 211, 218

[261] N. Yamatsu, *Finite-Dimensional Lie Algebras and Their Representations for Unified Model Building*, arXiv:1511.08771. 153, 154, 207

[262] H. K. Dreiner, H. E. Haber, and S. P. Martin, *Two-component spinor techniques and Feynman rules for quantum field theory and supersymmetry*, *Phys. Rept.* **494** (2010) 1–196, [arXiv:0812.1594]. 153, 232

[263] G. Ferretti, *UV Completions of Partial Compositeness: The Case for a SU(4) Gauge Group*, *JHEP* **06** (2014) 142, [arXiv:1404.7137]. 169

[264] Ya. I. Kogan, M. A. Shifman, and M. I. Vysotsky, *Spontaneous breaking of chiral symmetry for real fermions and N=2 SUSY Yang-Mills theory*, *Sov. J. Nucl. Phys.* **42** (1985) 318. [Yad. Fiz.42,504(1985)]. 169

[265] D. Weingarten, *Mass Inequalities for QCD*, *Phys. Rev. Lett.* **51** (1983) 1830. 170, 171

[266] E. Witten, *Some Inequalities Among Hadron Masses*, *Phys. Rev. Lett.* **51** (1983) 2351. 170, 174

[267] S. Nussinov, *Baryon meson mass inequality*, *Phys. Rev. Lett.* **51** (1983) 2081. 170, 171

[268] D. Espriu, M. Gross, and J. F. Wheater, *Rigorous Inequalities in Vector - Like Gauge Theories*, *Phys. Lett.* **B146** (1984) 67. 170, 171

[269] S. Nussinov and B. Sathiapalan, *Mass and Scattering Length Inequalities in QCD and QCD Like Theories*, *Nucl. Phys.* **B256** (1985) 285. 170, 171

[270] S. Nussinov and M. A. Lampert, *QCD inequalities*, *Phys. Rept.* **362** (2002) 193–301, [hep-ph/9911532]. 171

[271] C. W. Bernard, A. Duncan, J. LoSecco, and S. Weinberg, *Exact Spectral Function Sum Rules*, *Phys. Rev.* **D12** (1975) 792. 171

[272] K. G. Wilson, *Nonlagrangian models of current algebra*, *Phys. Rev.* **179** (1969) 1499–1512. 171

[273] M. A. Shifman, A. I. Vainshtein, and V. I. Zakharov, *QCD and Resonance Physics: Applications*, *Nucl. Phys.* **B147** (1979) 448–518. 171

[274] J. Preskill, *Subgroup Alignment in Hypercolor Theories*, *Nucl. Phys.* **B177** (1981) 21–59. 174

[275] M. Knecht and E. de Rafael, *Patterns of spontaneous chiral symmetry breaking in the large N(c) limit of QCD - like theories*, *Phys. Lett.* **B424** (1998) 335–342, [hep-ph/9712457]. 174

[276] H. Georgi, *SU(2) X U(1) breaking, compositeness and flavor*, . [Conf. Proc.C850701,339(1985)]. 174

[277] E. Katz, A. E. Nelson, and D. G. E. Walker, *The Intermediate Higgs*, *JHEP* **08** (2005) 074, [hep-ph/0504252]. 175

[278] M. Frigerio, A. Pomarol, F. Riva, and A. Urbano, *Composite Scalar Dark Matter*, *JHEP* **07** (2012) 015, [arXiv:1204.2808]. 175

[279] T. A. Ryttov and F. Sannino, *Ultra Minimal Technicolor and its Dark Matter TIMP*, *Phys. Rev.* **D78** (2008) 115010, [arXiv:0809.0713]. 175

[280] J. Galloway, J. A. Evans, M. A. Luty, and R. A. Tacchi, *Minimal Conformal Technicolor and Precision Electroweak Tests*, *JHEP* **10** (2010) 086, [arXiv:1001.1361]. 175

[281] G. Cacciapaglia and F. Sannino, *Fundamental Composite (Goldstone) Higgs Dynamics*, arXiv:1402.0233. 175

[282] T. Hatsuda and T. Kunihiro, *QCD phenomenology based on a chiral effective Lagrangian*, *Phys. Rept.* **247** (1994) 221–367, [hep-ph/9401310]. 175, 177, 178, 179, 183

[283] G. 't Hooft, *Symmetry Breaking Through Bell-Jackiw Anomalies*, *Phys. Rev. Lett.* **37** (1976) 8–11. 176

[284] G. 't Hooft, *Computation of the Quantum Effects Due to a Four-Dimensional Pseudoparticle*, *Phys. Rev.* **D14** (1976) 3432–3450. [Erratum: Phys. Rev.D18,2199(1978)]. 176

[285] G. 't Hooft, *How Instantons Solve the U(1) Problem*, *Phys. Rept.* **142** (1986) 357–387. 176

[286] D. Diakonov, *Chiral quark - soliton model*, in *Nonperturbative quantum field physics. Proceedings, Advanced School, Peniscola, Spain, June 2-6, 1997*, 1997. hep-ph/9802298. 176

[287] S. R. Coleman and E. J. Weinberg, *Radiative Corrections as the Origin of Spontaneous Symmetry Breaking*, *Phys. Rev.* **D7** (1973) 1888–1910. 177

[288] J. Bijnens, E. de Rafael, and H.-q. Zheng, *Low-energy behavior of two point functions of quark currents*, *Z. Phys.* **C62** (1994) 437–454, [hep-ph/9306323]. 179, 191

[289] M. Takizawa, K. Kubodera, and F. Myhrer, *Novel feature of the vector meson solution in the Nambu-Jona-Lasinio model*, *Phys. Lett.* **B261** (1991) 221–228. 180

[290] S. P. Klevansky and R. H. Lemmer, *Spectral density functions and their sum rules in an effective chiral field theory*, hep-ph/9707206. 180, 191

[291] E. Witten, *Current Algebra Theorems for the U(1) Goldstone Boson*, *Nucl. Phys.* **B156** (1979) 269. 182

[292] R. Contino, *The Higgs as a Composite Nambu-Goldstone Boson*, in *Physics of the large and the small, TASI 09, proceedings of the Theoretical Advanced Study Institute in Elementary Particle Physics, Boulder, Colorado, USA, 1-26 June 2009*, pp. 235–306, 2011. arXiv:1005.4269. 182, 183

[293] J. Bijnens, C. Bruno, and E. de Rafael, *Nambu-Jona-Lasinio like models and the low-energy effective action of QCD*, *Nucl. Phys.* **B390** (1993) 501–541, [hep-ph/9206236]. 183

[294] R. Arthur, V. Drach, M. Hansen, A. Hietanen, C. Pica, and F. Sannino, *SU(2) Gauge Theory with Two Fundamental Flavours: a Minimal Template for Model Building*, arXiv:1602.06559. 190

[295] R. Arthur, V. Drach, A. Hietanen, C. Pica, and F. Sannino, *SU(2) Gauge Theory with Two Fundamental Flavours: Scalar and Pseudoscalar Spectrum*, arXiv:1607.06654. 190

[296] T. DeGrand, Y. Liu, E. T. Neil, Y. Shamir, and B. Svetitsky, *Spectroscopy of SU(4) gauge theory with two flavors of sextet fermions*, *Phys. Rev.* **D91** (2015) 114502, [arXiv:1501.05665]. 191

[297] T. DeGrand and Y. Liu, *Lattice study of large N_c QCD*, *Phys. Rev.* **D94** (2016), no. 3 034506, [arXiv:1606.01277]. 191

[298] V. Dmitrasinovic, S. P. Klevansky, and R. H. Lemmer, *Weinberg sum rules in an effective chiral field theory*, *Phys. Lett.* **B386** (1996) 45–49. 191

[299] S. Peris, M. Perrottet, and E. de Rafael, *Matching long and short distances in large N(c) QCD*, *JHEP* **05** (1998) 011, [hep-ph/9805442]. 193, 195, 197

[300] R. F. Dashen, *Chiral SU(3) x SU(3) as a symmetry of the strong interactions*, *Phys. Rev.* **183** (1969) 1245–1260. 207

[301] I. I. Kogan, A. Kovner, and M. A. Shifman, *Chiral symmetry breaking without bilinear condensates, unbroken axial Z(N) symmetry, and exact QCD inequalities*, *Phys. Rev.* **D59** (1999) 016001, [hep-ph/9807286]. 207

[302] G. Cacciapaglia and A. Parolini, *Light 't Hooft Top Partners*, arXiv:1511.05163. 207

[303] S. R. Coleman, *The Uses of Instantons*, *Subnucl. Ser.* **15** (1979) 805. Reprinted in S. Coleman, *Aspects of Symmetries*, Cambridge University Press (1985). 209

[304] D. I. Olive, S. Sciuto, and R. J. Crewther, *Instantons in field theory*, *Riv. Nuovo Cim.* **2N8** (1979) 1–117. 209

[305] S. Vandoren and P. van Nieuwenhuizen, *Lectures on instantons*, arXiv:0802.1862. 209

[306] A. I. Vainshtein and V. I. Zakharov, *CALCULATION OF THE FERMION DETERMINANT IN CHIRAL AND SUPERSYMMETRICAL THEORIES*, *JETP Lett.* **35** (1982) 323–326. [Pisma Zh. Eksp. Teor. Fiz.35,258(1982)]. 209

[307] A. Belyaev, G. Cacciapaglia, H. Cai, T. Flacke, A. Parolini, and H. Serdio, *Singlets in Composite Higgs Models in light of the LHC di-photon searches*, arXiv:1512.07242. 228

[308] A. O. Bouzas, *Mixing renormalization for scalar fields*, *Int. J. Mod. Phys.* **A18** (2003) 3695–3734, [hep-ph/0305110]. [Int. J. Mod. Phys.A21,1157(2006)]. 229

[309] A. Buck, R. Alkofer, and H. Reinhardt, *Baryons as bound states of diquarks and quarks in the Nambu-Jona-Lasinio model*, *Phys. Lett.* **B286** (1992) 29–35. 234, 247, 250

[310] T. Brauner, *Fierz transformations*, *http://gemma.ujf.cas.cz/~brauner/files/Fierz_transform.pdf*. 235

[311] J. L. Kneur and A. Neveu, *Quark Condensate from Renormalization Group Optimized Spectral Density*, *Nucl. Part. Phys. Proc.* **270-272** (2016) 98–102, [arXiv:1512.03406]. 247